THE UNIVERSITY
of EDINBURGH

This thesis has been submitted in fulfilment of the requirements for a postgraduate degree (e.g. PhD, MPhil, DClinPsychol) at the University of Edinburgh. Please note the following terms and conditions of use:

This work is protected by copyright and other intellectual property rights, which are retained by the thesis author, unless otherwise stated.
A copy can be downloaded for personal non-commercial research or study, without prior permission or charge.
This thesis cannot be reproduced or quoted extensively from without first obtaining permission in writing from the author.
The content must not be changed in any way or sold commercially in any format or medium without the formal permission of the author.
When referring to this work, full bibliographic details including the author, title, awarding institution and date of the thesis must be given.

PUNCHING SHEAR OF FLAT REINFORCED-CONCRETE SLABS UNDER FIRE CONDITIONS

HOLLY KATE MCLEOD SMITH

Doctor of Philosophy

The University of Edinburgh

2016

Holly Kate McLeod Smith: *Punching Shear of Flat Reinforced-Concrete Slabs Under Fire Conditions,* Doctor of Philosophy, © 2016

In memory of my grandfather, Alexander William McLeod Short

DECLARATION

I hereby declare that this thesis and the work reported herein was composed and originated entirely by myself, under the supervision of Dr. Tim Stratford in the School of Engineering at The University of Edinburgh.

The following conference publications are as a result of the research conducted for this thesis, which has not been submitted for any other degree or professional qualification. They can be found online at The University of Edinburgh Research Explorer (www.research.ed.ac.uk) by searching the reference ID listed.

- Smith, H. K. M., Stratford, T. J., and Bisby, L. A. Deflection response of reinforced concrete slabs tested in punching shear in fire. In *Proceedings of the 4th International Conference on Applications of Structural Fire Engineering*, 2015. Web ID 21887313.
- Smith, H. K. M., Stratford, T., and Bisby, L. Punching shear of reinforced concrete slabs under fire conditions: experimental vs. design. In *Proceedings of the 1st International Conference on Structural Safety under Fire and Blast*, 2015. Web ID 21599178.
- Smith, H. K. M., Stratford, T., and Bisby, L. The punching shear mechanism in reinforced-concrete slabs under fire conditions. In *Proceedings of the 5th International Workshop on Performance, Protection and Strengthening of Structures under Extreme Loading*, 2015. Web ID 22046177.
- Smith, H. K. M,, Stratford, T. J., and Bisby, L. A. Punching shear of restrained reinforced concrete slabs under fire conditions. In *Proceedings of the 8th International Conference on Structures in Fire*, 2014. Web ID 15533789.
- Smith, H. K. M., Reid, E. R. E., Beatty, A. A., Stratford, T. J., and Bisby, L. A. Shear strength of concrete at elevated temperature. In *Proceedings of the Applications of Structural Fire Engineering*, 2011. Web ID 4123024.

Edinburgh, 2016

Holly Kate McLeod Smith

ABSTRACT

This thesis examines punching shear response of reinforced-concrete flat slabs under fire conditions. The shear behaviour of concrete in fire is relatively poorly understood compared to its flexural response. Failures such as the Gretzenbach car park failure in Switzerland (2004) have prompted concerns over the punching shear capacity of flat slabs in fire. The shear behaviour of reinforced-concrete in fire depends on degradation of the individual material properties with temperature, their interaction, and more recently recognised, the effects of restrained thermal expansion. Through experimental testing this thesis aims to build a foundation understanding of the punching shear behaviour of flat reinforced-concrete slabs in fire conditions.

A series of shear blocks, tested after exposure to elevated temperature (realistic fire temperature), were used to develop an understanding of the effects of elevated temperature on the shear transfer performance of reinforced-concrete. These tests allowed the complex interplay of shear-carrying mechanisms at ambient temperature to be extended to the case of post-elevated temperature.

Fifteen slab-column punching shear specimens were tested under both applied load and extreme heating. In particular, the effects of restrained thermal expansion were experimentally investigated by altering the support conditions of the slab-column specimens. A purpose-built restraint frame allowed the boundary support conditions to be either fully restrained or unrestrained. This experimental series is the only series to have tested restrained specimens at elevated temperatures, though previous researchers have simulated the thermal restraint effects and reported the importance of restrained thermal expansion and curvature on the behaviour of punching shear. Parameters of slab thickness and reinforcement ratio were also varied to investigate their respective impacts on punching shear behaviour at elevated temperature.

The thicker 100 mm reinforced slabs failed in punching shear, whereas the 50 mm and 75 mm thick slabs failed in flexure-shear mechanisms and the unreinforced slabs failed in flexure. Clear behavioural differences were observed between specimens with different support conditions. Unrestrained 100 mm thick slabs under sustained load failed soon after heating began, whereas none of the corresponding restrained specimens failed during heating. One restrained, heavily reinforced specimen failed during cooling, whilst under sustained load. This is the first recorded punching shear failure during the cooling phase of an elevated temperature test and may also be the first recorded test specimen ever to have failed during the cooling phase of an elevated temperature test.

This failure highlights the unknown and potentially unsafe behaviour of structures during the cooling phase. Further structural investigation of the cooling behaviour of concrete flat slabs after exposure to fire, needs to be undertaken.

Most of the specimens' central deflection was away from the heat source (in the direction of loading) during the whole test, irrespective of support condition. The test setup was assessed to investigate the unusual slab-column deflection away from the heat source, however the complex behaviour observed during the tests cannot currently be explained. It is assumed that the degradation in concrete properties and non-linear material behaviour dominates over the thermal expansion of the slabs.

Quantitative and qualitative comparisons are presented, though the quantitative data is impacted by size effect, non-repeatable heating application between tests and jack friction influences on specimens with low capacities.

Eurocode 2 punching shear prescriptive elevated temperature design, extends the ambient temperature equation for elevated temperature use, by degrading the temperature-dependant parameters by factors. Support conditions are not considered, with the code specifically telling the designer not to consider in-plane thermal expansion effects, therefore consequently ignoring the premature punching shear failure that can occur. Furthermore, the ambient temperature equation is based on the regression of available experimental data at the time and does not consider the reinforcement as a shear transfer mechanism.

The experimental capacities of the 100 mm thick, reinforced slabs that failed in pure punching shear mechanism were similar to the Eurocode 2 punching shear prescriptive design capacity, when directly compared. The unrestrained support condition was shown to be consistently, not conservatively predicted by Eurocode 2, whereas the restrained support condition capacities were conservatively predicted. It is comforting to know that the Eurocode 2 design predicts the restrained supported slabs conservatively, as real buildings are more likely to have supports closer to the restrained condition rather than the unrestrained support condition.

A sensitivity analysis of the Eurocode 2 prescriptive design equation shows it is highly sensitive to the concrete strength degradation and not the variable, σ_{cp}, which was used to make a support condition comparison in this thesis. This indicates how the Eurocode 2 equation for punching shear capacity lacks in its consideration of whole structural behaviour.

The Critical Shear Crack Theory has been proposed as the background to a harmonised shear design approach, called Model Code 2010. The Critical Shear Crack Theory was safe in predicting the experimental punching shear capacities. There were large variances for the 100 mm thick slabs, however they are consistent with the original model comparison to test data. An expansion

of the Critical Shear Crack Theory for elevated temperature requires further validation with experimental restrained thermal expansion tests, such as those presented in this thesis.

Finally, a digital image correlation technique has been proven to be a reliable method to measure structural displacements of concrete at elevated temperatures. Digital image correlation allowed the crack locations and slab rotation angles to be visualized throughout testing. No other measurement techniques are able to provide similar versatility in fire testing such as that presented herein.

LAY SUMMARY

This thesis examines punching shear response of reinforced-concrete flat slabs in fire conditions. Punching shear failure is when a structural column punches through the floor slab it is supporting, producing a cone crack pattern of reinforced-concrete. The failure of an underground car park in Gretzenbach, Switzerland (2004) prompted concerns over the understanding of punching shear failure in fire.

The behaviour of reinforced-concrete in fire to transfer shear depends on degradation of the concrete and steel with temperature, the material interaction at high temperature (realistic fire temperature), and more recently recognised, the effects of restrained thermal expansion. Through experimental testing this thesis aims to build a foundation understanding of the punching shear behaviour of reinforced-concrete in fire conditions.

A series of reinforced-concrete blocks were tested in shear, after having been cooled from elevated temperatures. This series was used to develop an understanding of the effects of elevated temperature on the shear transfer performance of reinforced-concrete.

Fifteen reinforced-concrete specimens of portions of slab with a small column stub, were tested in punching shear at both ambient (room) and elevated temperature. In particular, the method by which the edges of the slab portion were supported, were compared to investigate the impact of restrained thermal expansion. The edges of the slab portion were supported either: by resting the slab on a roller bar and the edges not touching the testing frame (unrestrained) or by clamping the slab edges between solid pieces of steel and them butting up against the testing frame (restrained). The unrestrained support condition allows the slab to rotate and expand at elevated temperatures. The restrained support condition clamps the edges of the slab to stop rotation and expansion at ambient and elevated temperatures. A purpose-built testing frame allowed the boundary support conditions to be either fully restrained or unrestrained.

This experimental series is the only series to have tested restrained punching shear specimens at elevated temperatures, though previous researchers have modelled the effects. The slab thickness and steel reinforcement quantity were also varied to investigate their respective impacts on punching shear behaviour at elevated temperature.

The thicker 100 mm reinforced slabs were seen to fail in punching shear. Clear behavioural differences were observed between specimens with different support conditions. Unrestrained 100 mm thick slabs under sustained load

failed soon after heating began, whereas none of the corresponding restrained specimens failed during heating. One restrained, heavily reinforced specimen failed during cooling, whilst under sustained load. This is the first recorded punching shear failure during the cooling phase of an elevated temperature test and may also be the first recorded test specimen ever to have failed during the cooling phase of an elevated temperature test. This failure highlights the unknown and potentially unsafe behaviour of structures during the cooling phase. Further structural investigation of the cooling behaviour of concrete flat slabs after exposure to fire, needs to be undertaken.

Most of the specimens central movement was away from the heat source (in the direction of loading) during the whole test, irrespective of support condition. The test setup was assessed to investigate the unusual specimen movement away from the heat source, however the complex behaviour observed during the tests cannot currently be explained. It is assumed that the degradation in the concrete and non-linear material behaviour dominates over the thermal expansion of the slabs.

Quantitative and qualitative comparisons are presented, though the quantitative data is impacted by the experimental specimens not being life size, the heating application not being repeatable between tests and the load application being impacted by friction.

The current structural reinforced-concrete design method (Eurocode 2) for punching shear is shown to be deficient. It uses a simple method to design for elevated temperature and does not consider support conditions. The experimental punching shear failure loads of the 100 mm thick, reinforced slabs at elevated temperature, were similar to those predicted by the code. The unrestrained slabs were consistently not conservatively predicted, whereas the restrained support condition failure loads were conservatively predicted. It is comforting to know that the code design predicts the restrained supported slabs conservatively, as real buildings are more likely to have supports closer to the restrained condition rather than the unrestrained support condition.

A harmonised design approach for shear, called Critical Shear Crack Theory has been proposed in Model Code 2010. The Critical Shear Crack Theory was safe in predicting the experimental punching shear failure loads. There were large differences for the 100 mm thick slabs, however they are consistent with the original model comparison to test data. An expansion of the Critical Shear Crack Theory for elevated temperature requires further validation with experimental restrained thermal expansion tests, such as those presented in this thesis.

ACKNOWLEDGMENTS

This project was supported by funding from the Engineering and Physical Sciences Research Council (EPSRC), together with additional follow-up funding provided by EPSRC and AECOM.

Untold thanks to my supervisor Dr. Tim Stratford for his patient guidance, experience and sharing of scribbled notes on scrap paper. Many thanks to my second supervisor, Prof. Luke Bisby for his advice and encouragement throughout my thesis.

For all the laboratory assistance, I thank Derek Jardine, Jim Hutcheson, Kevin Tierney and Michal Krajcovic.

Thanks to my husband, Dr. Craig Warren for putting up with me and moreover for helping me keep things in perspective. Many thanks to my parents for their patience and my friends and family for all their support.

CONTENTS

1 INTRODUCTION 1
1.1 Motivation . . . 1
1.2 Research aims . . . 2
1.3 Thesis overview . . . 2

2 BACKGROUND TO PUNCHING SHEAR IN REINFORCED-CONCRETE IN FIRE 5
2.1 Shear at ambient temperature . . . 6
2.1.1 Shear transfer mechanisms at ambient temperature . . . 8
2.1.2 Shear in beams . . . 15
2.2 Punching shear in slabs at ambient temperature . . . 18
2.2.1 Critical Shear Crack Theory . . . 23
2.2.2 Experimental slab-column research . . . 30
2.3 Shear at elevated temperature . . . 34
2.3.1 Effects of elevated temperature on material properties . . . 34
2.4 Punching shear in slabs at elevated temperature . . . 39
2.4.1 Experimental research . . . 39
2.4.2 Modelling research . . . 44
2.4.3 Research review . . . 48
2.5 Eurocode reinforced-concrete shear design . . . 49
2.5.1 Ambient temperature . . . 49
2.5.2 Elevated temperature . . . 51
2.6 Summary . . . 56

3 BACKGROUND TO DIGITAL IMAGE CORRELATION 59
3.1 Technique development . . . 59
3.2 Validation . . . 60
3.3 Structural testing application . . . 61

4 SHEAR BLOCK EXPERIMENTS 63
4.1 Design philosophy . . . 63
4.2 Specimen design . . . 64
4.3 Electric furnace heating . . . 64
4.4 Hydraulic loading . . . 67
4.5 Displacement instrumentation . . . 67
4.6 Results and analysis . . . 68
4.6.1 Strength variation with temperature . . . 68

4.6.2 Load-displacement response 70
4.6.3 Crack opening width development 71
4.7 Summary 71

5 PUNCHING SHEAR SLAB-COLUMN EXPERIMENTAL DESIGN AND METHODOLOGY 73
5.1 Design philosophy 74
5.2 Specimen 78
5.2.1 Design 78
5.2.2 Dimensions 78
5.2.3 Steelwork 80
5.2.4 Concrete 80
5.2.5 Fabrication 83
5.3 Structural reaction frame 84
5.4 Radiant panel heating 87
5.4.1 Calibration 89
5.5 Insulation 92
5.6 Hydraulic loading 94
5.7 Instrumentation 95
5.7.1 Strain gauges 95
5.7.2 Thermocouples 96
5.7.3 Displacement measurement 96

6 PUNCHING SHEAR SLAB-COLUMN EXPERIMENTAL RESULTS 103
6.1 Ambient tests 105
6.1.1 Failure crack patterns 105
6.1.2 Load-deflection behaviours and failure modes 114
6.1.3 Capacity comparison to Muttoni's Critical Shear Crack Theory (CSCT) 115
6.2 50 mm thick, 0.8% reinforced tests 118
6.2.1 Test overview 119
6.2.2 Temperature curves 119
6.2.3 Temperature profiles through the slab thickness 120
6.2.4 Failure crack patterns 124
6.2.5 Heated load-deflection behaviour and failure modes . . . 129
6.2.6 Displacement measurement comparison for HR50-0.8 test 130
6.2.7 Summary 132
6.3 75 mm thick, 0.8% reinforced tests 133
6.3.1 Test overview 133
6.3.2 Temperature curves 133
6.3.3 Temperature profiles through the slab thickness 134

6.3.4 Failure crack patterns 134
6.3.5 Heated load-deflection behaviour and failure modes . . . 142
6.3.6 Summary 142
6.4 100 mm thick, 0.8% reinforced tests 143
6.4.1 Test overview 143
6.4.2 Temperature curves 144
6.4.3 Temperature profiles through the slab thickness 144
6.4.4 Failure crack patterns 149
6.4.5 Heated load-deflection behaviour and failure modes . . . 153
6.4.6 Summary 153
6.5 100 mm thick, 1.5% reinforced tests 154
6.5.1 Test overview 155
6.5.2 Temperature curves 155
6.5.3 Temperature profiles through the slab thickness 157
6.5.4 Failure crack patterns 157
6.5.5 Heated load-deflection behaviour and failure modes . . . 164
6.5.6 Summary 164
6.6 100 mm thick, 0% reinforced tests 165
6.6.1 Test overview 165
6.6.2 Temperature curves 166
6.6.3 Temperature profiles through the slab thickness 166
6.6.4 Failure crack patterns 166
6.6.5 Heated load-deflection behaviour and failure modes . . . 174
6.6.6 Summary 174
6.7 Residual tests 176
6.7.1 50 mm thick, 0.8% reinforced tests 176
6.7.2 75 mm thick, 0.8% reinforced tests 177
6.7.3 100 mm thick, 0.8% reinforced tests 177
6.7.4 100 mm thick, 0% reinforced tests 178
6.8 Deflection history of heated 0.8% reinforced slabs 178
6.9 Test observations of heated 0.8% reinforced slabs 181
6.10 Deflection history of heated 100 mm thick slabs 181
6.11 Test observations of heated 100 mm thick slabs 183
6.12 Slab-column reaction forces and moments on the reaction frame 186
6.12.1 Ambient example 50 mm thick, 0.8% reinforced tests . . 186
6.12.2 Heated example 50 mm thick, 0.8% reinforced tests . . . 186
6.13 Strength of material specimens 192
6.13.1 Concrete 192
6.13.2 Steel 192
6.14 Summary 195

7 ANALYSIS AND DISCUSSION 201
7.1 Experiment methodology verification 201
7.1.1 Specimen dimensional tolerances 201
7.1.2 Heat application reproducibility 203
7.1.3 Friction in 600 kN jack 206
7.1.4 Vertical displacement instrumentation 208
7.1.5 In-plane reaction force and moment accuracy 214
7.1.6 Specimen support condition functionality 215
7.1.7 Summary 219
7.2 Deflection profiles across the slab-column specimens 220
7.2.1 50 mm thick, 0.8% reinforced 221
7.2.2 75 mm thick, 0.8% reinforced 223
7.2.3 100 mm thick, 0.8% reinforced 225
7.2.4 100 mm thick, 1.5% reinforced 227
7.2.5 100 mm thick, 0% unreinforced 227
7.2.6 Summary 231
7.3 Punching shear failure comparison to shear design 232
7.3.1 Material properties at elevated temperature 232
7.3.2 Eurocode 2 (EC2) ambient and elevated temperature . . 234
7.3.3 Critical Shear Crack Theory (CSCT) ambient and elevated temperature 250
7.3.4 Summary 256

8 CONCLUSIONS AND FURTHER WORK 259
8.1 Experimental methodology verification 260
8.2 Support condition impact 260
8.3 Displacement behaviour 261
8.4 Cooling behaviour 261
8.5 Assessment of the current punching shear design methods . . . 262
8.5.1 Eurocode 2 design shortcomings 262
8.5.2 Comparison to experimental tests 262
8.5.3 Critical Shear Crack Theory punching shear design . . . 263
8.6 Digital Image Correlation technique for structural fire testing . 263
8.7 Further work 264

REFERENCES 265

A HEALTH AND SAFETY CONSIDERATIONS 273

B CONCRETE MOISTURE CONTENT WITH TIME 325

C SLAB CONCRETE DESIGN CERTIFICATE 327

D OPTIMUM MIX VALVE SETTINGS FOR THE RADIANT PANELS 331

E STRAIN GAUGE CALIBRATION 333

F POST-PROCESSING MATLAB SCRIPT FOR HU75-0.8 343

G CAMERA TEST SETTINGS 347

H SLAB-COLUMN TEST SCHEDULE 349
H.1 Structural reaction frame 349
H.2 Specimen 349
H.3 Radiant panel heating 350
H.4 Cameras 350

I SLAB-COLUMN REACTION FORCES AND MOMENTS ON THE REACTION FRAME 351
I.1 50 mm thick, 0.8% reinforced tests 351
I.1.1 Ambient unrestrained test 351
I.1.2 Heated unrestrained test 355
I.1.3 Heated restrained test 359
I.2 75 mm thick, 0.8% reinforced tests 363
I.2.1 Ambient unrestrained test 363
I.2.2 Heated unrestrained test 367
I.2.3 Heated restrained test 371
I.3 100 mm thick, 0.8% reinforced tests 375
I.3.1 Ambient unrestrained test 375
I.3.2 Heated unrestrained test 379
I.3.3 Heated restrained test 383
I.4 100 mm thick, 1.5% reinforced tests 387
I.4.1 Ambient unrestrained test 387
I.4.2 Heated unrestrained test 391
I.4.3 Heated restrained test 395
I.5 100 mm thick, 0% reinforced tests 399
I.5.1 Ambient unrestrained test 399
I.5.2 Heated unrestrained test 403
I.5.3 Heated restrained test 407

J POST-FAILURE MEASURED THERMOCOUPLE DEPTHS FROM THE HEATED SURFACE 411

K OVERVIEW OF THE COLUMN NET AXIAL FORCE AND MOMENT DATA FOR EACH TEST 413
K.1 Ambient 415

K.2 50 mm thick, 0.8% reinforced 418
K.3 75 mm thick, 0.8% reinforced 419
K.4 100 mm thick, 0.8% reinforced 420
K.5 100 mm thick, 1.5% reinforced 421
K.6 100 mm thick, 0% reinforced 422

LIST OF FIGURES

Figure 1.1	Punching shear in Reinforced-Concrete (RC)	2
Figure 2.1	RC ambient failure modes	6
Figure 2.2	RC beam ambient shear failure modes	7
Figure 2.3	Shear transfer actions, adapted from Stratford and Burgoyne (2003)	8
Figure 2.4	Compressive and tensile stress trajectories in RC beam	9
Figure 2.5	Compressive force path, adapted from Kotsovos (1988)	9
Figure 2.6	Typical reinforcement types, reproduced from Hertz (1982)	10
Figure 2.7	Ribbed reinforcement in concrete	11
Figure 2.8	Simplified pre-cracked push-off specimen, reproduced from Mohamed Ali et al. (2008)	13
Figure 2.9	Typical Mattock style shear block specimen, reproduced from Hofbeck et al. (1969)	14
Figure 2.10	Crack surface structure, adapted from Vecchio and Collins (1986)	14
Figure 2.11	Truss analogy with fixed 45° struts, adapted from Mörsch (1909)	16
Figure 2.12	Modified compressive-field theory element, adapted from Vecchio and Collins (1986)	17
Figure 2.13	One-way spanning slab design, reproduced from Stratford (2007)	19
Figure 2.14	Two-way spanning slab design, reproduced from Stratford (2007)	20
Figure 2.15	Flat slab design, reproduced from Stratford (2007)	21
Figure 2.16	Shear strength comparison in one- and two-way slabs subjected to concentrated loads, reproduced from Sigrist (2010)	22
Figure 2.17	Shear force concentrations in slabs, reproduced from Sigrist (2010)	24
Figure 2.18	Typical punching shear failure, reproduced from Fernández Ruiz and Muttoni (2010)	25
Figure 2.19	Slab behaviour with and without shear reinforcement, reproduced from Fernández Ruiz and Muttoni (2010)	25
Figure 2.20	Muttoni's critical shear crack position, adapted from Sigrist (2010)	26

Figure 2.21 Calculation of the punching shear capacity by CSCT, reproduced from Bamonte et al. (2012) 27
Figure 2.22 Circular isolated slab-column element, adapted from Guandalini (2005) 28
Figure 2.23 Comparison of 99 experimental test results to Muttoni's CSCT simplified failure criterion, reproduced from Sigrist (2010) 29
Figure 2.24 Comparison of CSCT with tests of inner columns with moment transfer from Anis (1970), Elstner and Hognestad (1956), Hawkins et al. (1989), Kruger (1999) and Moe (1961), reproduced from Sigrist (2010) 30
Figure 2.25 Punching shear specimen setup types 31
Figure 2.26 Effect of edge restraint on the punching shear capacity, reproduced from Kuang and Morley (1993) 33
Figure 2.27 Portland cement concrete thermometer of physicochemical processes undertaken at elevated temperatures, reproduced from Bailey and Khoury (2011) 35
Figure 2.28 Environmental factors that influence concrete at high temperatures, reproduced from Naus (2005) 36
Figure 2.29 Comparison between normalised average concrete residual and elevated temperature compressive strengths, reproduced from Li and Franssen (2011) 37
Figure 2.30 Comparison of cooling technique on normalised average residual strength specimens, reproduced from Li and Franssen (2011) 38
Figure 2.31 Graphical representation of Load Induced Thermal Strains (LITS), reproduced from Law and Gillie (2008) 38
Figure 2.32 Non-dimensional residual tensile strength, reproduced from Neves et al. (1996) 40
Figure 2.33 Kordina test set-up, adapted from Bamonte and Felicetti (2009) (dimensions in mm) 42
Figure 2.34 Plan and three-dimensional views of modelled structure, reproduced from Annerel et al. (2013) 46
Figure 2.35 Impact of indirect actions on the structural behaviour of a flat slab in a fire, reproduced from Bamonte et al. (2012) 47
Figure 2.36 Compressed concrete stress-strain relationships at elevated temperature, reproduced from BS EN 1992-1-2:2004 (2010) 54

Figure 2.37 Reinforcing and pre-stressing steel stress-strain relationships at elevated temperature, reproduced from BS EN 1992-1-2:2004 (2010) 55
Figure 4.1 Shear block test setup 65
Figure 4.2 Schematic of the shear block reinforcement 66
Figure 4.3 Temperature curves in the furnace and within the concrete blocks 67
Figure 4.4 Effect of temperature upon the residual strength of the shear block, and upon the residual concrete compressive and tensile strengths 70
Figure 4.5 Effect of temperature upon the residual load-displacement response of shear blocks 71
Figure 4.6 Effect of temperature upon the residual crack opening width development of shear blocks 72
Figure 5.1 Evolution of specimen design 75
Figure 5.2 Elevation of the slab-column test setup 77
Figure 5.3 Reinforcement schedule for 50 mm / 75 mm thick slabs with 0.8% 81
Figure 5.4 Reinforcement schedule for 100 mm thick slabs with 0.8% / 1.5% 82
Figure 5.5 Slab dehumidified curing environment 83
Figure 5.6 Dimensioned elevation of the structural reaction frame 85
Figure 5.7 Plan of the structural reaction frame 86
Figure 5.8 Elevation showing the two slab-column boundary support conditions 86
Figure 5.9 Schematic of propane gas radiant panel array 88
Figure 5.10 Radiant panel array improvements 90
Figure 5.11 Plan showing the heat flux measurement location used in Figure 5.12 91
Figure 5.12 Heat flux with time near the approximated punching shear perimeter 92
Figure 5.13 Elevation of the insulation design 93
Figure 5.14 Schematic of hydraulic slab loading 94
Figure 5.15 Schematic of active and passive strain gauge positioning for a 100 mm thick slab 95
Figure 5.16 Thermocouple positions in the slabs 97
Figure 5.17 Photo of the positioning of two of the Digital Image Correlation (DIC) cameras 98
Figure 5.18 Geometry used to correct vertical displacement output from DIC analysis 99
Figure 5.19 DIC camera calibration board 100

Figure 5.20 Photo of the texture optimisation in ambient 100 mm thick, 0.8% reinforced: unrestrained test 101
Figure 6.1 Cross-sections of ambient, unrestrained slabs showing the post-failure crack patterns 106
Figure 6.2 Ambient 50 mm thick, 0.8% reinforced: unrestrained slab showing the plan post-failure crack patterns . . . 107
Figure 6.3 Ambient 75 mm thick, 0.8% reinforced: unrestrained slab showing the plan post-failure crack patterns . . . 108
Figure 6.4 Ambient 100 mm thick, 0.8% reinforced: unrestrained slab showing the plan post-failure crack patterns . . . 110
Figure 6.5 Ambient 100 mm thick, 1.5% reinforced: unrestrained slab showing the plan post-failure crack patterns . . . 111
Figure 6.6 Flexural failure mechanism of 100 mm thick, 0% slab . 112
Figure 6.7 Ambient 100 mm thick, 0% reinforced: unrestrained slab showing the plan post-failure crack patterns . . . 113
Figure 6.8 Load-deflection behaviour of ambient tests 114
Figure 6.9 Ambient 100 mm thick, 1.5% reinforced: unrestrained test, support channel section photos 115
Figure 6.10 Test observations for all ambient unrestrained slabs . . 116
Figure 6.11 Experimental and design failure load comparison . . . 118
Figure 6.12 Temperature curves for 50 mm thick, 0.8% slabs 121
Figure 6.13 North temperature profile through 50 mm thickness, 0.8%: unrestrained slab 122
Figure 6.14 South temperature profile through 50 mm thickness, 0.8%: unrestrained slab 122
Figure 6.15 West temperature profile through 50 mm thickness, 0.8%: unrestrained slab 123
Figure 6.16 Thermocouple tree temperature profile comparison at 110 minutes and 200 minutes after ignition (50 mm thick, 0.8%: unrestrained slab) 123
Figure 6.17 North temperature profile through 50 mm thickness, 0.8%: restrained slab 124
Figure 6.18 South temperature profile through 50 mm thickness, 0.8%: restrained slab 125
Figure 6.19 West temperature profile through 50 mm thickness, 0.8%: restrained slab 125
Figure 6.20 Cross-sections of 50 mm thick, 0.8% reinforced slabs showing the post-failure crack patterns 126
Figure 6.21 Heated 50 mm thick, 0.8% reinforced: unrestrained slab showing the plan post-failure crack patterns 127

Figure 6.22 Heated 50 mm thick, 0.8% reinforced: restrained slab showing the plan post-failure crack patterns 128
Figure 6.23 Load-deflection behaviour of 50 mm thick, 0.8% slabs . 129
Figure 6.24 Vertical deflection comparison of 30 mm Displacement Transducer (LP) and DIC average for 50 mm thick, 0.8%: restrained slab 131
Figure 6.25 DIC patch location on heated 50 mm thick, 0.8% reinforced: restrained slab relative to calibration board . . 131
Figure 6.26 Temperature curves for 75 mm thick, 0.8% slabs 135
Figure 6.27 North temperature profile through 75 mm thickness, 0.8%: unrestrained slab 136
Figure 6.28 South temperature profile through 75 mm thickness, 0.8%: unrestrained slab 136
Figure 6.29 West temperature profile through 75 mm thickness, 0.8%: unrestrained slab 137
Figure 6.30 North temperature profile through 75 mm thickness, 0.8%: restrained slab 137
Figure 6.31 South temperature profile through 75 mm thickness, 0.8%: restrained slab 138
Figure 6.32 East temperature profile through 75 mm thickness, 0.8%: restrained slab 138
Figure 6.33 Cross-sections of 75 mm thick, 0.8% reinforced slabs showing the post-failure crack patterns 139
Figure 6.34 Heated 75 mm thick, 0.8% reinforced: unrestrained slab showing the plan post-failure crack patterns 140
Figure 6.35 Heated 75 mm thick, 0.8% reinforced: restrained slab showing the plan post-failure crack patterns 141
Figure 6.36 Load-deflection behaviour of 75 mm thick, 0.8% slab . 142
Figure 6.37 Temperature curves for 100 mm thick, 0.8% slabs . . . 145
Figure 6.38 South temperature profile through 100 mm thickness, 0.8%: unrestrained slab 146
Figure 6.39 West temperature profile through 100 mm thickness, 0.8%: unrestrained slab 146
Figure 6.40 East temperature profile through 100 mm thickness, 0.8%: unrestrained slab 147
Figure 6.41 South temperature profile through 100 mm thickness, 0.8%: restrained slab 147
Figure 6.42 West temperature profile through 100 mm thickness, 0.8%: restrained slab 148
Figure 6.43 East temperature profile through 100 mm thickness, 0.8%: restrained slab 148

Figure 6.44 Cross-sections of 100 mm thick, 0.8% reinforced slabs showing the post-failure crack patterns 149
Figure 6.45 Catastrophic punching shear failure of 0.8% reinforced heated slab, 100 mm thickness: unrestrained 150
Figure 6.46 Heated 100 mm thick, 0.8% reinforced: unrestrained slab showing the plan post-failure crack patterns . . . 151
Figure 6.47 Heated 100 mm thick, 0.8% reinforced: restrained slab showing the plan post-failure crack patterns 152
Figure 6.48 Load-deflection behaviour of 100 mm thick, 0.8% slabs 154
Figure 6.49 Temperature curves for 100 mm thick, 1.5% slabs . . . 156
Figure 6.50 South temperature profile through 100 mm thickness, 1.5%: unrestrained slab 158
Figure 6.51 West temperature profile through 100 mm thickness, 1.5%: unrestrained slab 158
Figure 6.52 East temperature profile through 100 mm thickness, 1.5%: unrestrained slab 159
Figure 6.53 South temperature profile through 100 mm thickness, 1.5%: restrained slab 159
Figure 6.54 West temperature profile through 100 mm thickness, 1.5%: restrained slab 160
Figure 6.55 East temperature profile through 100 mm thickness, 1.5%: restrained slab 160
Figure 6.56 Cross-sections of 100 mm thick, 1.5% reinforced slabs showing the post-failure crack patterns 161
Figure 6.57 Heated 100 mm thick, 1.5% reinforced: unrestrained slab showing the plan post-failure crack patterns . . . 162
Figure 6.58 Heated 100 mm thick, 1.5% reinforced: restrained slab showing the plan post-failure crack patterns 163
Figure 6.59 Load-deflection behaviour of 100 mm thick, 1.5% slabs 164
Figure 6.60 Temperature curves for 100 mm thick, 0% slabs 167
Figure 6.61 North temperature profile through 100 mm thickness, 0%: unrestrained slab 168
Figure 6.62 West temperature profile through 100 mm thickness, 0%: unrestrained slab 168
Figure 6.63 East temperature profile through 100 mm thickness, 0%: unrestrained slab 169
Figure 6.64 North temperature profile through 100 mm thickness, 0%: restrained slab 169
Figure 6.65 West temperature profile through 100 mm thickness, 0%: restrained slab 170

Figure 6.66 East temperature profile through 100 mm thickness, 0%: restrained slab 170
Figure 6.67 Cross-section of the ambient 100 mm thick, unreinforced slab showing the post-failure crack patterns . . . 171
Figure 6.68 Heated 100 mm thick, 0% reinforced: unrestrained slab showing the plan post-failure crack patterns 172
Figure 6.69 Heated 100 mm thick, 0% reinforced: restrained slab showing the plan post-failure crack patterns 173
Figure 6.70 Load-deflection behaviour of 100 mm thick, 0% slabs . 175
Figure 6.71 Residual load-deflection behaviour of 50 mm thick, 0.8% slabs 176
Figure 6.72 Residual load-deflection behaviour of 75 mm thick, 0.8% slabs 177
Figure 6.73 Residual load-deflection behaviour of 100 mm thick, 0.8% slabs 178
Figure 6.74 Residual load-deflection behaviour of 100 mm thick, 0% slabs 179
Figure 6.75 Behaviour with time for 0.8% reinforced slabs 180
Figure 6.76 Test observations for 0.8% reinforced slabs 182
Figure 6.77 Views of the lifted corners of the heated 75 mm thick, 0.8% reinforced: unrestrained slab 183
Figure 6.78 Behaviour with time for 100 mm thick slabs 184
Figure 6.79 Test observations for 100 mm thick slabs 185
Figure 6.80 East reaction frame net axial force, N and moment, M for ambient 50 mm thick, 0.8% reinforced: unrestrained slab 187
Figure 6.81 South reaction frame net axial force, N and moment, M for ambient 50 mm thick, 0.8% reinforced: unrestrained slab 188
Figure 6.82 West reaction frame net axial force, N and moment, M for ambient 50 mm thick, 0.8% reinforced: unrestrained slab 189
Figure 6.83 North reaction frame net axial force, N and moment, M for ambient 50 mm thick, 0.8% reinforced: unrestrained slab 190
Figure 6.84 Column WS net axial force, N and moment, M for heated 50 mm thick, 0.8% reinforced slabs 191
Figure 6.85 Concrete compressive and tensile strength 192
Figure 6.86 Stages in steady-state reinforcement tensile testing, reproduced from Batson (2013) 194

Figure 7.1 Flexural reinforcement spacing: design and measured (with one standard deviation) 202
Figure 7.2 Flexural concrete cover: design and measured (with one standard deviation) 203
Figure 7.3 Column concrete cover: design and measured (with one standard deviation) 204
Figure 7.4 Temperature curves at different frame positions, for approximately the same slab depth 205
Figure 7.5 Temperature curves for approximately similar slab depths of 31 mm to 36 mm from the heated surface of the 50 mm and 100 mm thick slabs 206
Figure 7.6 Load comparison during hydraulic friction test 208
Figure 7.7 East camera DIC vertical displacement across the heated 75 mm thick, 0.8% reinforced: unrestrained slab 209
Figure 7.8 South camera DIC vertical displacement across the heated 75 mm thick, 0.8% reinforced: unrestrained slab 209
Figure 7.9 West camera DIC vertical displacement across the heated 75 mm thick, 0.8% reinforced: unrestrained slab 210
Figure 7.10 Comparison of West and East cameras, DIC vertical displacement across the heated 75 mm thick, 0.8% reinforced: unrestrained slab 210
Figure 7.11 Vertical deflection comparison of LP and DIC average for 50 mm thick, 0.8% reinforced slabs 211
Figure 7.12 Vertical deflection comparison of LP and DIC average for 75 mm thick, 0.8% reinforced slabs 212
Figure 7.13 Vertical deflection comparison of LP and DIC average for 100 mm thick, 0.8% reinforced slabs 212
Figure 7.14 Vertical deflection comparison of LP and DIC average for 100 mm thick, 1.5% reinforced slabs 213
Figure 7.15 Vertical deflection comparison of LP and DIC average for 100 mm thick, 0% reinforced slabs 213
Figure 7.16 Vertical deflection difference between LP and DIC with time 214
Figure 7.17 Impact of eccentricity correction on net average in-plane force and moment unrestrained test graphs . . . 216
Figure 7.18 Net average in-plane reaction force in the unrestrained ambient and heated tests 217
Figure 7.19 Ambient unrestrained tests, net average in-plane reaction force with applied load 217
Figure 7.20 Restrained ambient and heated test reactions 218

Figure 7.21 DIC vertical displacement across the ambient 50 mm thick, 0.8% reinforced: unrestrained slab at 10 minute intervals 221
Figure 7.22 DIC vertical displacement across the heated 50 mm thick, 0.8% reinforced: unrestrained slab at 10 minute intervals 222
Figure 7.23 DIC vertical displacement across the heated 50 mm thick, 0.8% reinforced: restrained slab at 10 minute intervals 222
Figure 7.24 DIC vertical displacement across the ambient 75 mm thick, 0.8% reinforced: unrestrained slab at 10 minute intervals 224
Figure 7.25 DIC vertical displacement across the heated 75 mm thick, 0.8% reinforced: unrestrained slab at 10 minute intervals 224
Figure 7.26 DIC vertical displacement across the heated 75 mm thick, 0.8% reinforced: restrained slab at 10 minute intervals 225
Figure 7.27 DIC vertical displacement across the ambient 100 mm thick, 0.8% reinforced: unrestrained slab at 10 minute intervals 226
Figure 7.28 DIC vertical displacement across the heated 100 mm thick, 0.8% reinforced: unrestrained slab at 10 minute intervals 226
Figure 7.29 DIC vertical displacement across the heated 100 mm thick, 0.8% reinforced: restrained slab at 10 minute intervals 227
Figure 7.30 DIC vertical displacement across the ambient 100 mm thick, 1.5% reinforced: unrestrained slab at 10 minute intervals 228
Figure 7.31 DIC vertical displacement across the heated 100 mm thick, 1.5% reinforced: unrestrained slab at 10 minute intervals 228
Figure 7.32 DIC vertical displacement across the heated 100 mm thick, 1.5% reinforced: restrained slab at 10 minute intervals 229
Figure 7.33 DIC vertical displacement across the ambient 100 mm thick, 0% reinforced: unrestrained slab at 10 minute intervals 229

Figure 7.34 DIC vertical displacement across the heated 100 mm thick, 0% reinforced: unrestrained slab at 10 minute intervals . . . 230
Figure 7.35 DIC vertical displacement across the heated 100 mm thick, 0% reinforced: restrained slab at 10 minute intervals 230
Figure 7.36 Class X values for either hot rolled or cold worked steel stress-strain relationships at elevated temperature, reproduced from BS EN 1992-1-2:2004 (2010) . . . 234
Figure 7.37 Elevated temperature reduction factors from experimental values and EC2 class N and X . . . 235
Figure 7.38 EC2 ambient square column, punching shear crack diameter and perimeter, adapted from BS EN 1992-1-1:2004 (2008) . . . 237
Figure 7.39 Punching shear failure load compared to EC2 . . . 241
Figure 7.40 Ratio of EC2 design shear capacity to experimental punching shear capacity . . . 241
Figure 7.41 EC2 punching shear failure load sensitivity to concrete strength degradation for 50 mm thick, 0.8% reinforced slabs . . . 243
Figure 7.42 EC2 punching shear failure load sensitivity to concrete strength degradation for 75 mm thick, 0.8% reinforced slabs . . . 243
Figure 7.43 EC2 punching shear failure load sensitivity to concrete strength degradation for 100 mm thick, 0.8% reinforced slabs . . . 244
Figure 7.44 EC2 punching shear failure load sensitivity to concrete strength degradation for 100 mm thick, 1.5% reinforced slabs . . . 244
Figure 7.45 Punching shear crack diameter on heated and unheated surfaces compared to EC2 . . . 245
Figure 7.46 Theoretical stress profiles in the heated slab-column specimens . . . 246
Figure 7.47 EC2 ambient circular column, punching shear crack diameter and perimeter, adapted from BS EN 1992-1-1:2004 (2008) . . . 247
Figure 7.48 Sensitivity of EC2 punching shear capacity to the perimeter variable, as a ratio of the experimental punching shear capacity . . . 249
Figure 7.49 Punching shear crack angle on the North and South frame sides . . . 250

Figure 7.50 CSCT punching shear capacity for the unrestrained slab-column parameters 254
Figure 7.51 Punching shear failure load compared to CSCT 255
Figure 7.52 Punching shear slab rotation compared to CSCT 256
Figure B.1 Graph of slab-column concrete moisture content 326
Figure C.1 Tarmac readymix concrete receipt 327
Figure C.2 Tarmac readymix design certificate 328
Figure C.3 Tarmac concrete product data sheet 329
Figure D.1 Schematic of the radiant panel array from plan view . 332
Figure E.1 Plan view schematic of strain gauge calibration setup . 334
Figure E.2 N–S strain gauge calibration graphs 335
Figure E.3 N–S strain gauge calibration graphs 336
Figure E.4 E–W strain gauge calibration graphs 337
Figure E.5 E–W strain gauge calibration graphs 338
Figure E.6 Unrestrained test setup with applied load eccentric to the strain gauges 342
Figure I.1 East reaction frame net axial force, N and moment, M for ambient 50 mm thick, 0.8% reinforced: unrestrained slab 351
Figure I.2 South reaction frame net axial force, N and moment, M for ambient 50 mm thick, 0.8% reinforced: unrestrained slab 352
Figure I.3 West reaction frame net axial force, N and moment, M for ambient 50 mm thick, 0.8% reinforced: unrestrained slab 353
Figure I.4 North reaction frame net axial force, N and moment, M for ambient 50 mm thick, 0.8% reinforced: unrestrained slab 354
Figure I.5 East reaction frame net axial force, N and moment, M for heated 50 mm thick, 0.8% reinforced: unrestrained slab 355
Figure I.6 South reaction frame net axial force, N and moment, M for heated 50 mm thick, 0.8% reinforced: unrestrained slab 356
Figure I.7 West reaction frame net axial force, N and moment, M for heated 50 mm thick, 0.8% reinforced: unrestrained slab 357
Figure I.8 North reaction frame net axial force, N and moment, M for heated 50 mm thick, 0.8% reinforced: unrestrained slab 358

Figure I.9 East reaction frame net axial force, N and moment, M for heated 50 mm thick, 0.8% reinforced: restrained slab 359
Figure I.10 South reaction frame net axial force, N and moment, M for heated 50 mm thick, 0.8% reinforced: restrained slab 360
Figure I.11 West reaction frame net axial force, N and moment, M for heated 50 mm thick, 0.8% reinforced: restrained slab 361
Figure I.12 North reaction frame net axial force, N and moment, M for heated 50 mm thick, 0.8% reinforced: restrained slab 362
Figure I.13 East reaction frame net axial force, N and moment, M for ambient 75 mm thick, 0.8% reinforced: unrestrained slab 363
Figure I.14 South reaction frame net axial force, N and moment, M for ambient 75 mm thick, 0.8% reinforced: unrestrained slab 364
Figure I.15 West reaction frame net axial force, N and moment, M for ambient 75 mm thick, 0.8% reinforced: unrestrained slab 365
Figure I.16 North reaction frame net axial force, N and moment, M for ambient 75 mm thick, 0.8% reinforced: unrestrained slab 366
Figure I.17 East reaction frame net axial force, N and moment, M for heated 75 mm thick, 0.8% reinforced: unrestrained slab 367
Figure I.18 South reaction frame net axial force, N and moment, M for heated 75 mm thick, 0.8% reinforced: unrestrained slab 368
Figure I.19 West reaction frame net axial force, N and moment, M for heated 75 mm thick, 0.8% reinforced: unrestrained slab 369
Figure I.20 North reaction frame net axial force, N and moment, M for heated 75 mm thick, 0.8% reinforced: unrestrained slab 370
Figure I.21 East reaction frame net axial force, N and moment, M for heated 75 mm thick, 0.8% reinforced: restrained slab 371
Figure I.22 South reaction frame net axial force, N and moment, M for heated 75 mm thick, 0.8% reinforced: restrained slab 372
Figure I.23 West reaction frame net axial force, N and moment, M for heated 75 mm thick, 0.8% reinforced: restrained slab 373

Figure I.24 North reaction frame net axial force, N and moment, M for heated 75 mm thick, 0.8% reinforced: restrained slab 374
Figure I.25 East reaction frame net axial force, N and moment, M for ambient 100 mm thick, 0.8% reinforced: unrestrained slab 375
Figure I.26 South reaction frame net axial force, N and moment, M for ambient 100 mm thick, 0.8% reinforced: unrestrained slab 376
Figure I.27 West reaction frame net axial force, N and moment, M for ambient 100 mm thick, 0.8% reinforced: unrestrained slab 377
Figure I.28 North reaction frame net axial force, N and moment, M for ambient 100 mm thick, 0.8% reinforced: unrestrained slab 378
Figure I.29 East reaction frame net axial force, N and moment, M for heated 100 mm thick, 0.8% reinforced: unrestrained slab 379
Figure I.30 South reaction frame net axial force, N and moment, M for heated 100 mm thick, 0.8% reinforced: unrestrained slab 380
Figure I.31 West reaction frame net axial force, N and moment, M for heated 100 mm thick, 0.8% reinforced: unrestrained slab 381
Figure I.32 North reaction frame net axial force, N and moment, M for heated 100 mm thick, 0.8% reinforced: unrestrained slab 382
Figure I.33 East reaction frame net axial force, N and moment, M for heated 100 mm thick, 0.8% reinforced: restrained slab383
Figure I.34 South reaction frame net axial force, N and moment, M for heated 100 mm thick, 0.8% reinforced: restrained slab 384
Figure I.35 West reaction frame net axial force, N and moment, M for heated 100 mm thick, 0.8% reinforced: restrained slab385
Figure I.36 North reaction frame net axial force, N and moment, M for heated 100 mm thick, 0.8% reinforced: restrained slab 386
Figure I.37 East reaction frame net axial force, N and moment, M for ambient 100 mm thick, 1.5% reinforced: unrestrained slab 387

Figure I.38 South reaction frame net axial force, N and moment, M for ambient 100 mm thick, 1.5% reinforced: unrestrained slab 388
Figure I.39 West reaction frame net axial force, N and moment, M for ambient 100 mm thick, 1.5% reinforced: unrestrained slab 389
Figure I.40 North reaction frame net axial force, N and moment, M for ambient 100 mm thick, 1.5% reinforced: unrestrained slab 390
Figure I.41 East reaction frame net axial force, N and moment, M for heated 100 mm thick, 1.5% reinforced: unrestrained slab 391
Figure I.42 South reaction frame net axial force, N and moment, M for heated 100 mm thick, 1.5% reinforced: unrestrained slab 392
Figure I.43 West reaction frame net axial force, N and moment, M for heated 100 mm thick, 1.5% reinforced: unrestrained slab 393
Figure I.44 North reaction frame net axial force, N and moment, M for heated 100 mm thick, 1.5% reinforced: unrestrained slab 394
Figure I.45 East reaction frame net axial force, N and moment, M for heated 100 mm thick, 1.5% reinforced: restrained slab395
Figure I.46 South reaction frame net axial force, N and moment, M for heated 100 mm thick, 1.5% reinforced: restrained slab 396
Figure I.47 West reaction frame net axial force, N and moment, M for heated 100 mm thick, 1.5% reinforced: restrained slab397
Figure I.48 North reaction frame net axial force, N and moment, M for heated 100 mm thick, 1.5% reinforced: restrained slab 398
Figure I.49 East reaction frame net axial force, N and moment, M for ambient 100 mm thick, 0% reinforced: unrestrained slab 399
Figure I.50 South reaction frame net axial force, N and moment, M for ambient 100 mm thick, 0% reinforced: unrestrained slab 400
Figure I.51 West reaction frame net axial force, N and moment, M for ambient 100 mm thick, 0% reinforced: unrestrained slab 401

Figure I.52 North reaction frame net axial force, N and moment, M for ambient 100 mm thick, 0% reinforced: unrestrained slab 402
Figure I.53 East reaction frame net axial force, N and moment, M for heated 100 mm thick, 0% reinforced: unrestrained slab 403
Figure I.54 South reaction frame net axial force, N and moment, M for heated 100 mm thick, 0% reinforced: unrestrained slab 404
Figure I.55 West reaction frame net axial force, N and moment, M for heated 100 mm thick, 0% reinforced: unrestrained slab 405
Figure I.56 North reaction frame net axial force, N and moment, M for heated 100 mm thick, 0% reinforced: unrestrained slab 406
Figure I.57 East reaction frame net axial force, N and moment, M for heated 100 mm thick, 0% reinforced: restrained slab 407
Figure I.58 South reaction frame net axial force, N and moment, M for heated 100 mm thick, 0% reinforced: restrained slab 408
Figure I.59 West reaction frame net axial force, N and moment, M for heated 100 mm thick, 0% reinforced: restrained slab 409
Figure I.60 North reaction frame net axial force, N and moment, M for heated 100 mm thick, 0% reinforced: restrained slab 410
Figure K.1 Percentage ratio between net axial force and applied load for all columns in the ambient 50 mm thick, 0.8% reinforced: unrestrained test 415
Figure K.2 Percentage ratio between net axial force and applied load for all columns in the ambient 75 mm thick, 0.8% reinforced: unrestrained test 415
Figure K.3 Percentage ratio between net axial force and applied load for all columns in the ambient 100 mm thick, 0.8% reinforced: unrestrained test 416
Figure K.4 Percentage ratio between net axial force and applied load for all columns in the ambient 100 mm thick, 1.5% reinforced: unrestrained test 416
Figure K.5 Percentage ratio between net axial force and applied load for all columns in the ambient 100 mm thick, 0% reinforced: unrestrained test 417

Figure K.6 Percentage ratio between net axial force and applied load for all columns in the heated 50 mm thick, 0.8% reinforced: unrestrained test 418
Figure K.7 Percentage ratio between net axial force and applied load for all columns in the heated 50 mm thick, 0.8% reinforced: restrained test 418
Figure K.8 Percentage ratio between net axial force and applied load for all columns in the heated 75 mm thick, 0.8% reinforced: unrestrained test 419
Figure K.9 Percentage ratio between net axial force and applied load for all columns in the heated 75 mm thick, 0.8% reinforced: restrained test 419
Figure K.10 Percentage ratio between net axial force and applied load for all columns in the heated 100 mm thick, 0.8% reinforced: unrestrained test 420
Figure K.11 Percentage ratio between net axial force and applied load for all columns in the heated 100 mm thick, 0.8% reinforced: restrained test 420
Figure K.12 Percentage ratio between net axial force and applied load for all columns in the heated 100 mm thick, 1.5% reinforced: unrestrained test 421
Figure K.13 Percentage ratio between net axial force and applied load for all columns in the heated 100 mm thick, 1.5% reinforced: restrained test 421
Figure K.14 Percentage ratio between net axial force and applied load for all columns in the heated 100 mm thick, 0% reinforced: unrestrained test 422
Figure K.15 Percentage ratio between net axial force and applied load for all columns in the heated 100 mm thick, 0% reinforced: restrained test 422

LIST OF TABLES

Table 4.1 Shear block test programme and key results 69
Table 5.1 Test specimen details 79
Table 6.1 Slab-column summary test results 104
Table 6.2 Ambient experimental failure loads and calculated applied loads for heated tests 117
Table 6.3 Slab-column specimen concrete strength 193
Table 6.4 Steel reinforcement properties 194
Table 6.5 Steel reinforcement properties, reproduced from Batson (2013) 196
Table 6.6 Yield strength, $f_{sy,\theta}$ and Young's modulus, $E_{s,\theta}$ reduction factors from experimental values 197
Table 6.7 Yield strength, $f_{sy,\theta}$ reduction factors from EC2 linearly interpolated class N and X 198
Table 6.8 Young's modulus, $E_{s,\theta}$ reduction factors from EC2 linearly interpolated class N and X 199
Table 7.1 Approximate observation time the propane gas flow rate decreased during testing 207
Table 7.2 Horizontal structural frame stiffness, reproduced from Fox (2013) 219
Table 7.3 DIC central slab-column vertical displacement at the end of testing 220
Table 7.4 DIC central slab-column vertical displacement at ignition 221
Table 7.5 Siliceous concrete material parameters at elevated temperature 233
Table 7.6 Reinforcing steel material parameters at elevated temperature 236
Table 7.7 EC2 punching shear resistance parameters 238
Table 7.8 Further EC2 punching shear resistance parameters . . . 239
Table 7.9 Experimental punching shear loads and EC2 punching shear capacity, calculated with different perimeters . . 248
Table 7.10 CSCT failure criterion parameters 252
Table 7.11 CSCT load-rotation parameters 253
Table D.1 Slab testing optimum mix valve settings 331
Table E.1 Calibration factor (kN) for N–S frame strain gauges in each slab test (NA specified where no gauge data was recorded) 340

Table E.2 Calibration factor (kN) for E–W frame strain gauges in each slab test (NA specified where no gauge data was recorded) 341
Table E.3 Lever arm distances for the moment calculation of different slab thicknesses 342
Table G.1 Camera test settings 347
Table J.1 Post-failure measured thermocouple depths from the heated surface 412
Table K.1 Overview of strain gauge column net axial force and moment data assessment 414

ABBREVIATIONS

CMA Compressive Membrane Action

CSCT Critical Shear Crack Theory

DIC Digital Image Correlation

DSLR Digital Single-Lens Reflex

EC Eurocode

EC2 Eurocode 2

EPSRC Engineering and Physical Sciences Research Council

FE Finite Element

fib fédération internationale du béton

FRP Fibre-Reinforced Polymer

HSC High Strength Concrete

LITS Load Induced Thermal Strains

LoA Levels of Approximation

LP Displacement Transducer

NSC Normal Strength Concrete

PIV Particle Image Velocimetry

RC Reinforced-Concrete

Sign convention used throughout is:

- tension is positive
- compression is negative

1 INTRODUCTION

1.1 MOTIVATION

Reinforced-concrete members can fail in either flexural or shear mechanisms. Neither failure is desirable, however flexural failure is preferred over shear because it is a ductile failure and gives warning of impending failure, with visual tensile cracks forming. Shear failure is a brittle failure and occurs with little displacement or visible crack warning signs. Shear has been researched extensively and yet current understanding is not complete.

Punching shear failure is when a column punches through the slab it is supporting, shown in Figure 1.1, producing a cone crack pattern of reinforced-concrete. The three-dimensional punching shear at ambient temperature is a complex phenomenon and continues to be the subject of research. The addition of elevated temperature in a fire, makes the problem of punching shear even more challenging.

Structural fire research has focussed more on steel and steel-concrete composites than on concrete, due to concrete's beneficial properties of low thermal conductivity and non-combustibility. The shear behaviour of reinforced-concrete in fire is poorly understood compared to its flexural response, and the Gretzenbach car park failure in Switzerland in 2004 prompted concerns over the lack of understanding of punching shear response of reinforced-concrete in fire. Punching shear in reinforced-concrete at elevated temperature is dependent upon the effects of: steel and concrete properties with elevated temperature, differential material thermal expansion effects, combined with the whole structural effects of: in-plane actions that result from restrained thermal expansion, and large deflection load-carrying mechanisms.

The shear capacity of concrete at ambient temperature is known to be affected by the presence of in-plane membrane forces. During fire, membrane forces result from restrained thermal actions, and the prior work has identified that premature punching shear failure could consequently result from restrained thermal action. There has not, however, been an experimental investigation into the effect of restraint conditions upon the punching shear response of reinforced-concrete in fire, and these effects are not included in current code provisions.

This thesis addresses the need for further fundamental understanding of punching shear behaviour in flat reinforced-concrete slabs in fire conditions.

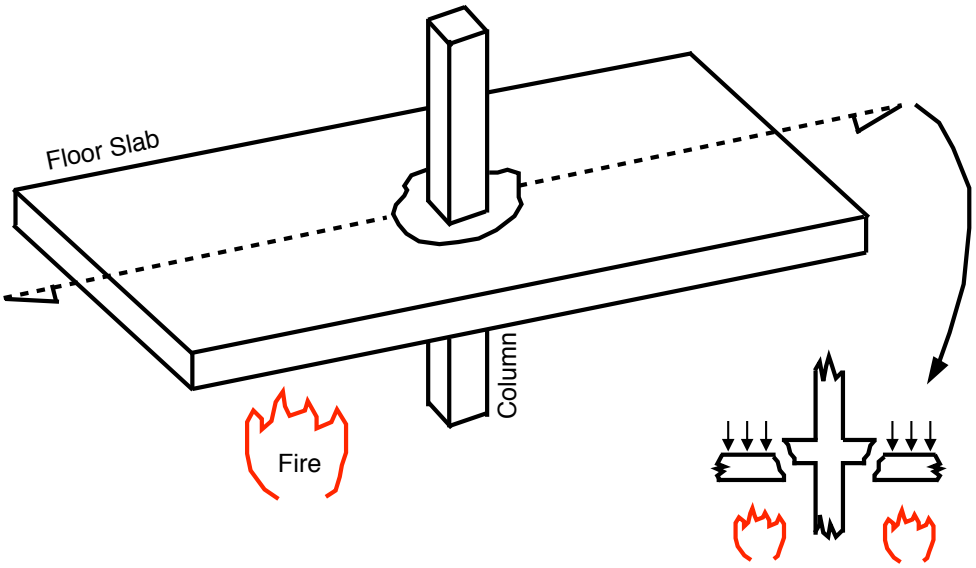

Figure 1.1: Punching shear in RC

In particular, the effects of restrained thermal expansion were experimentally investigated by altering the support conditions of slab-column specimens.

1.2 RESEARCH AIMS

This research aims to provide:

- Insight into the fundamental understanding of the transfer of shear between the concrete and steel in reinforced-concrete at both ambient and elevated temperatures.
- A series of slab-column experiments tested in punching shear at both ambient and elevated temperature, in order to investigate the behaviour of punching shear failure in fire.
  - Investigate the effect of support condition on punching shear failure by restrained thermal expansion.
  - Research the influence of slab thickness and reinforcement ratio on the punching shear failure in fire conditions.

1.3 THESIS OVERVIEW

At the beginning of each individual chapter is an overview of what is presented in the chapter and at the end is a summary of the main points and conclusions. The following is intended to give an overview of the thesis structure and

content.

Chapter 1 introduces punching shear failure of flat reinforced-concrete slabs. Shear and flexural failure of reinforced-concrete members are outlined and the requirement for fundamental understanding highlighted. The added complexity that elevated temperature (as experienced during a fire) brings to punching shear failure is presented, along with the recognition that in particular, support conditions need to be considered.

Chapter 2 focuses on the current research and theory of punching shear in reinforced-concrete at both ambient and elevated temperatures. The chapter begins with ambient temperature (room temperature) research of shear transfer mechanisms, shear in beams and punching shear. The limited research of shear transfer mechanisms at elevated temperature is presented, along with the impact of elevated temperature on the properties of concrete and steel. The experimental and modelling punching shear research at elevated temperature, done by six research groups, is presented in depth. The Eurocode 2 punching shear design at both ambient and elevated temperature is described, as well as its shortcomings.

Chapter 3 presents the current research application of Digital Image Correlation as an instrument to optically measure displacement and strain distributions during experiments.

Chapter 4 discusses the design, methodology and results of the preliminary Mattock style shear block experiments.

Chapter 5 presents the design and methodology of the large punching shear slab-column test series. The design philosophy of the test series, specimen design, test arrangement and instrumentation used is outlined.

Chapter 6 focuses on the results of the slab-column experimental punching shear test series. The experimental results presented includes: failure loads and time to failure, slab-column load-deflection behaviours, slab temperature curve plots, slab temperature through thickness profiles, failure crack patterns, slab-column deflection history, slab-column in-plane reaction forces and moments, and material specimen strengths.

Chapter 7 presents a comparative analysis and discussion of the slab-column results. The experimental methodology is assessed to outline strengths, weaknesses and future test design considerations. Digital image correlation is used

to present displacement profiles of the slabs. The experimental results are compared to both current Eurocode 2 design predictions and a proposed harmonised shear design approach, called Critical Shear Crack Theory.

Chapter 8 summarises the conclusions and provides recommendations for further research.

2

BACKGROUND TO PUNCHING SHEAR IN REINFORCED-CONCRETE IN FIRE

This chapter describes the current research and theory of punching shear in Reinforced-Concrete (RC) both at ambient and at elevated temperature, as experienced during a fire.

The chapter begins with ambient temperature (room temperature) research, reviewing the shear failure modes and actions through which shear is transferred in RC. Elevated temperature response cannot be understood until the ambient temperature behaviour has been established. Section 2.1.1 presents the individual transfer mechanisms: compressive force paths, tension zone concrete, concrete-steel bond, shear reinforcement, flexural reinforcement, dowel action, and aggregate interlock. Though the mechanisms are discussed separately, it is the combination of them that transfers shear in RC.

Section 2.1.2 describes one-way shear in beams with and without shear reinforcement and Section 2.2 presents the three-dimensional failure mode of flat slab punching shear. A mechanical-based design approach for both beam shear and punching shear, Critical Shear Crack Theory (CSCT), is outlined in Section 2.2.1. Ambient temperature experimental slab-column testing of punching shear is presented in Section 2.2.2. The support condition and membrane action implications of the test setups are assessed.

The complexity of shear at ambient temperature is great and increases at elevated temperatures. Section 2.3 presents shear in RC research at elevated temperature. Structural fire research has focussed more on steel and steel-concrete composites than on concrete, due to concrete's beneficial properties of low thermal conductivity and non-combustibility. Shear understanding at high temperature has been less researched, even though there is a good acknowledgement that further investigation into shear at high temperature is needed Bamonte et al. (2009); Ghoreishi et al. (2015).

Shear transfer mechanisms at elevated temperature are not well understood. The limited pull-out and beam tests of shear transfer mechanisms at elevated temperature are presented. Researchers have separately investigated the impact of elevated temperature on the properties of concrete and steel. Section 2.3.1 gives a brief outline. Six research groups have done research into punching shear at elevated temperature, presented in Section 2.4. The experimental (Section 2.4.1) and modelling research (Section 2.4.2) are discussed.

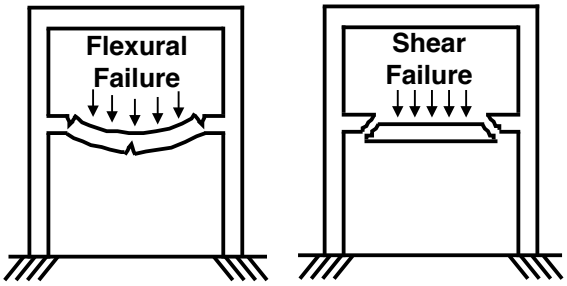

(a) Flexural failure (b) Shear failure

Figure 2.1: RC ambient failure modes

Two state-of-the-art reviews of punching shear work at elevated temperature are presented in Section 2.4.3.

Section 2.5 presents the Eurocode 2 (EC2) punching shear design at ambient (Section 2.5.1) and elevated (Section 2.5.2) temperature and describes shortcomings.

Chapter 2 thus establishes the state-of-the-art, which is built upon in the reminder of this thesis.

2.1 SHEAR AT AMBIENT TEMPERATURE

Ambient failure of RC members can be (a) flexural or (b) shear failure as shown in Figure 2.1. Often it is difficult to define failure as decisively one type, as it is often a combination of both. Obviously, neither failure is desirable, but flexural failure is preferred over shear because it is a ductile failure and gives warning of impending failure, with visual tensile cracks forming. Ductile failure allows yielding of the steel, which gives occupants time for escape. Shear failure is a brittle failure and occurs with little displacement or visible warning of failure. Shear failure is characterised by a sudden and catastrophic failure. This section will describe the understanding of shear in RC at ambient temperature.

Due to the complexity of shear carrying mechanisms in concrete, understanding of shear is first established for a simply supported RC beam without shear reinforcement, before examining the three dimensional, punching shear, case. There are three observed modes of shear failure in a RC beam: shear-compression failure (Figure 2.2a), diagonal-tension failure (Figure 2.2b) and deep beam failure:

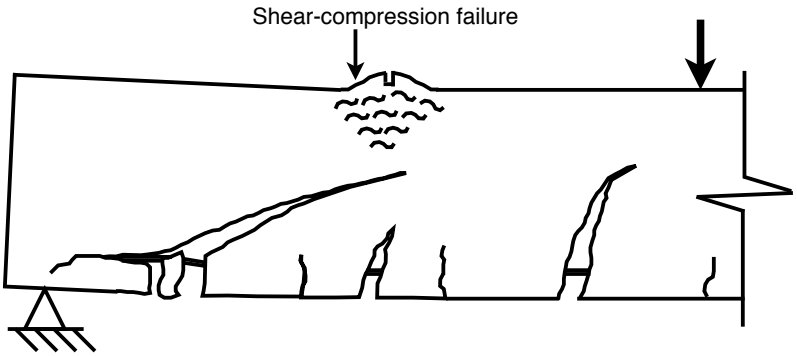

(a) Shear-compression failure

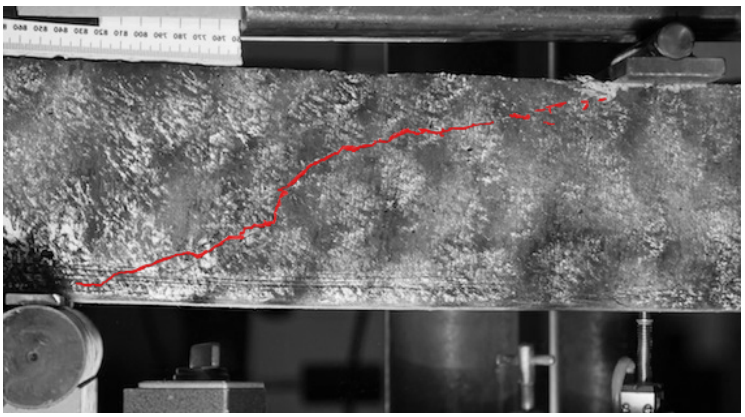

(b) Diagonal-tension failure

Figure 2.2: RC beam ambient shear failure modes

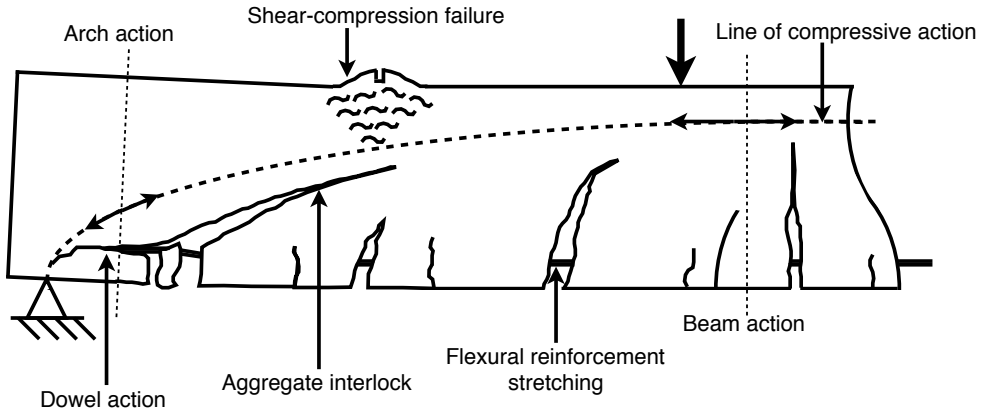

Figure 2.3: Shear transfer actions, adapted from Stratford and Burgoyne (2003)

2.1.1 *Shear transfer mechanisms at ambient temperature*

Shear is carried in RC through the interactions of the following shear transfer actions or mechanisms (Sigrist, 2010):

- compressive force paths within the concrete;
- tension zone concrete;
- tensile crack bridging by the reinforcing steel (relying upon concrete-steel bond);
- flexural reinforcement in tension;
- dowel action in the reinforcing steel;
- friction across cracked surfaces due to aggregate interlock; and
- shear reinforcement.

Understanding the complex interplay of these transfer mechanisms is difficult even at ambient temperature. The relative contribution of the transfer mechanisms to the shear capacity of a section (whether with or without shear reinforcement) has been under investigation for many years. The load sustained by a RC beam without shear reinforcement is transferred between load points and support by the transfer mechanisms shown in Figure 2.3. Each transfer mechanism will be considered separately here; however, it is the combination of these mechanisms that transfers shear in RC.

Compressive force path

A compressive force path forms along the theoretical compressive principal stress trajectories between the load point and support, as shown in Figures 2.3

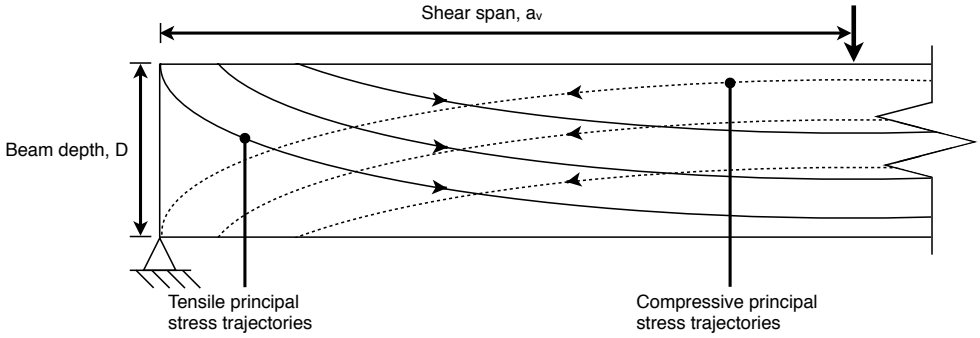

Figure 2.4: Compressive and tensile stress trajectories in RC beam

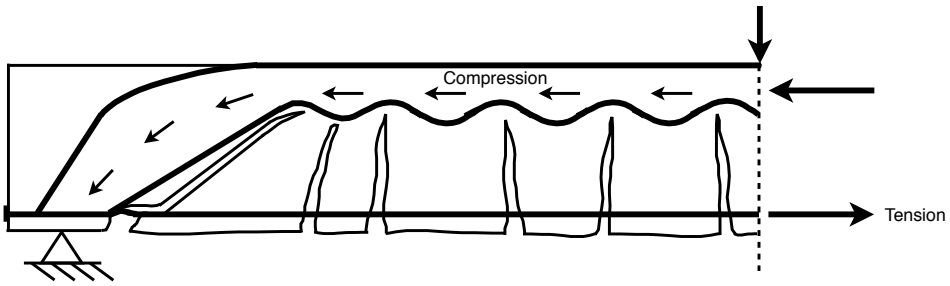

Figure 2.5: Compressive force path, adapted from Kotsovos (1988)

and 2.4. Kotsovos and Pavlović (1999) show in Figure 2.5 that the compressive force path is a horizontal narrow strip in the upper section of the beam which then changes direction towards the support. The force path changes direction and forms a diagonal strip where the uncracked end of the beam joins the upper narrow strip.

Tension zone concrete

Concrete in tension has a small strength capacity. It is only a minor contributor to shear transfer.

Size effect states that as the slab size increases, the nominal shear stress decreases (Bažant and Cao, 1987). Testing scaled down test specimens can lead to unrealistic high strengths. For example, two identical beams of different sizes, have the same length of the tension-zone at the end of a propagating crack. Proportionally however, the tension-zone is large in a small beam, therefore the load carried by the tension-zone is large in comparison to the total load. Correspondingly, the load carried by the tension-zone in the large beam is small in comparison to the total load.

Concrete-steel bond

Both the concrete and reinforcement is required in a RC beam to carry shear. It is transferred between the two materials at their interface, by the concrete-

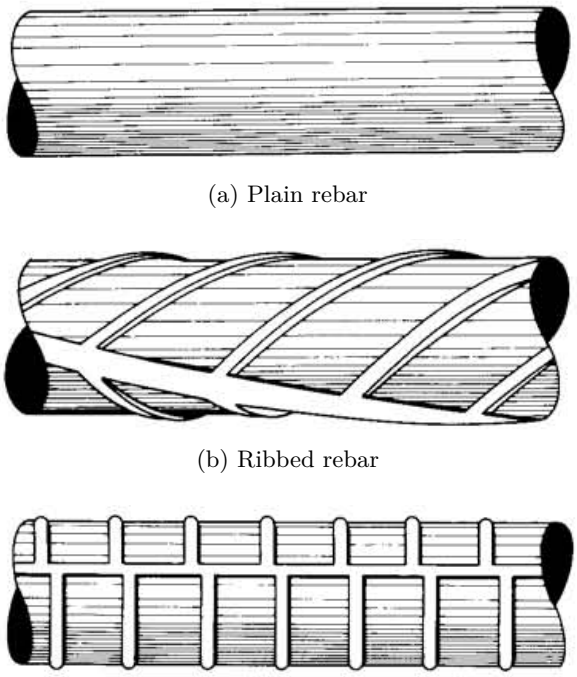

(a) Plain rebar

(b) Ribbed rebar

(c) Ribbed rebar

Figure 2.6: Typical reinforcement types, reproduced from Hertz (1982)

steel bond. *"The bond of reinforcement in concrete is the critical feature of reinforced-concrete that makes the use of concrete as a structural material possible"*(Tepfers, 2000). Ferguson (1966); Tepfers (1979) are early state-of-the-art papers on the bond behaviour for plain and ribbed bars.

The smooth surfaces of plain reinforcing bars, shown in Figure 2.6a, are bonded to concrete by chemical adhesion and friction. Figure 2.6b and Figure 2.6c show reinforcement with surface deformations, referred to as ribbed reinforcement in this thesis. Concrete-steel bond between concrete and ribbed reinforcement is produced by a combination of (Stratford, 2001; Tepfers, 1979, 2000):

- chemical adhesion: chemical bond formed between the cement paste and reinforcement during the concrete hydration process;
- mechanical interlock: surface profile of the reinforcement, interlocks with the concrete; and
- friction: residual frictional bond stresses.

Tepfers (2000) discusses in detail the factors that influence the performance of concrete-steel bond:

- flexural reinforcement surface geometry of lugs (Figure 2.7);
- concrete;

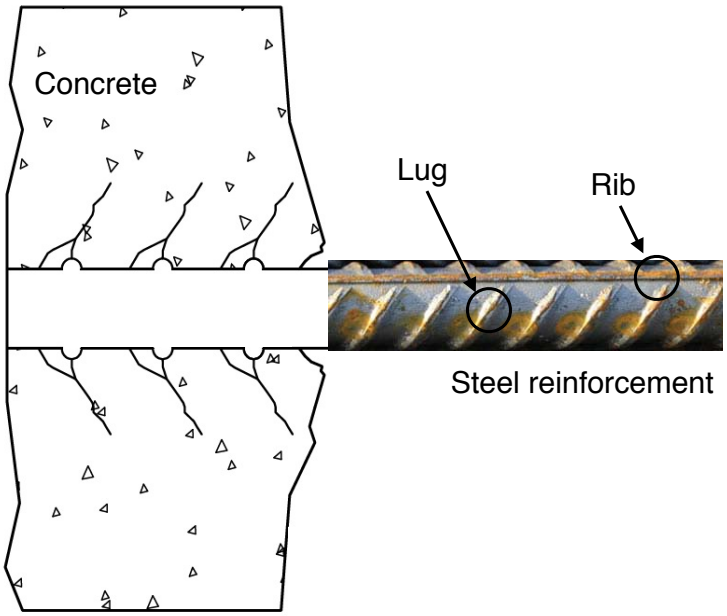

Figure 2.7: Ribbed reinforcement in concrete

  - strength
  - maximum aggregate size
  - mix quality (meaning less trapped water micro-bubbles produces better concrete)

- environmental effects; and
  - reinforcement corrosion, for example rusting
  - temperature effects (discussed in Section 2.3)

- load-time history.

Flexural reinforcement

Reinforcement stretches and slips where the critical shear crack forms. Figure 2.3 shows the flexural reinforcement stretching at a flexural crack. Unbonded reinforcement is where there is no concrete-steel bond. Unbonded reinforcement stretches and starts to yield, whereas bonded reinforcement can slip relative to the surrounding concrete. Reinforcement slip is negligible relative to stretching.

The reinforcement, within the shear span, (a_v) shown in Figure 2.4, can pull-out or be debonded from the surrounding concrete if the bond is weak. If debonding occurs, the RC section must transfer load via other actions, so flexural cracks propagate further into the compression-zone of the beam. If crack propagation continues, the beam can fail by either shear-compression

or diagonal-tension. Debonding of the reinforcement can be increased by local cracking of the concrete nearby the steel. The length of debonded reinforcement can be much greater than the flexural crack width.

Dowel action

Dowel action is the shearing and flexure of the reinforcement across a crack, as seen in Figure 2.3. Millard and Johnson (1984) investigated the shear transfer mechanisms of aggregate interlock and dowel action using push-off specimens. Enclosing the flexural reinforcement with shear reinforcement can allow dowel action to occur.

Simplified push-off specimens like those shown in Figure 2.8 have been used by many researchers to investigate shear transfer mechanisms. Hofbeck et al. (1969) investigated dowel action as a shear transfer action by using a simplified push-off specimen, similar to a Mattock shear block, shown in Figure 2.9. Hofbeck et al. (1969) found that dowel action did not contribute greatly to the shear capacity of uncracked specimens.

Aggregate interlock

Aggregate interlock is one of the shear transfer mechanisms acting across the propagating cracks, shown in Figure 2.3. Along both sides of the cracked concrete interface there are protruding pieces of aggregate and hardened cement paste. Figure 2.10 shows that as the two concrete bodies move past each other, the protruding pieces catch on each other, causing aggregate interlock.

There have been various experimental investigations using push-off specimens to research aggregate interlock (Hamadi and Regan, 1980; Mattock and Hawkins, 1972; Mattock et al., 1975; Millard and Johnson, 1984, 1985; Sagaseta and Vollum, 2011; Walraven, 1981).

Shear reinforcement

Shear reinforcement produces concrete confinement, which increases the ductility of a RC beam. Additionally, it increases the shear-capacity, by confining the compression-zone. Confinement can be produced both actively or passively, though active confinement is more effective than passive. Shear reinforcement and concrete cover produce a passive confinement, whereas active confinement is particularly effective in enabling dowel action and is produced either directly from a support or from the continuity of a column in a beam-column joint (Tepfers, 2000). Stratford and Burgoyne (2003) state that shear reinforcement can prevent dowel action, though it needs to enclose the flexural reinforcement.

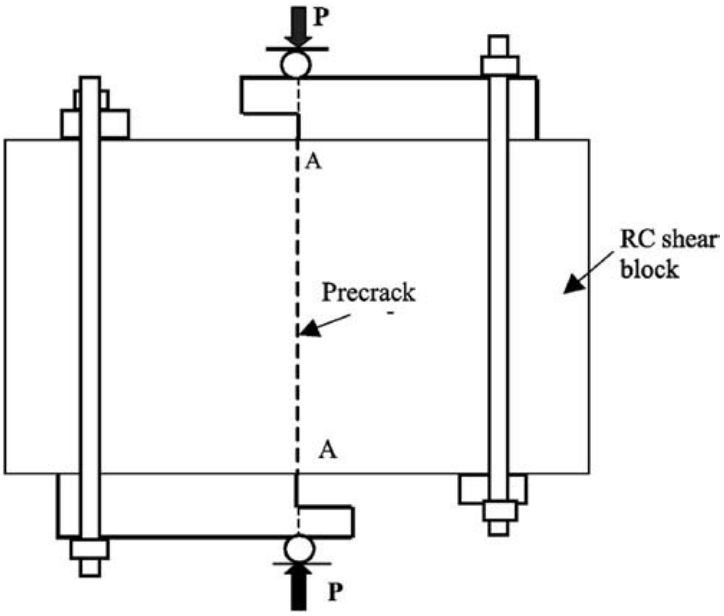

(a) Simplified push-off specimen test setup

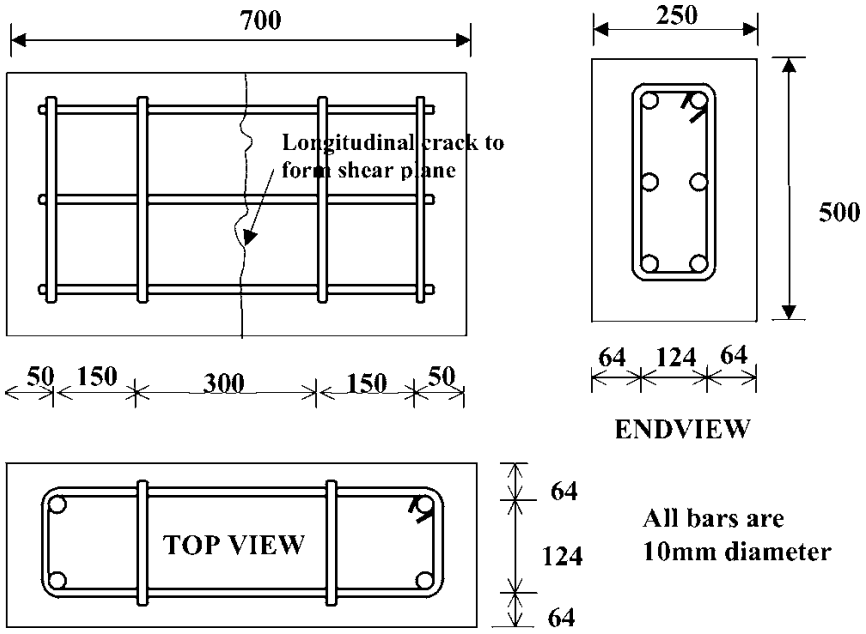

(b) Reinforcement details of simplified push-off specimen

Figure 2.8: Simplified pre-cracked push-off specimen, reproduced from Mohamed Ali et al. (2008)

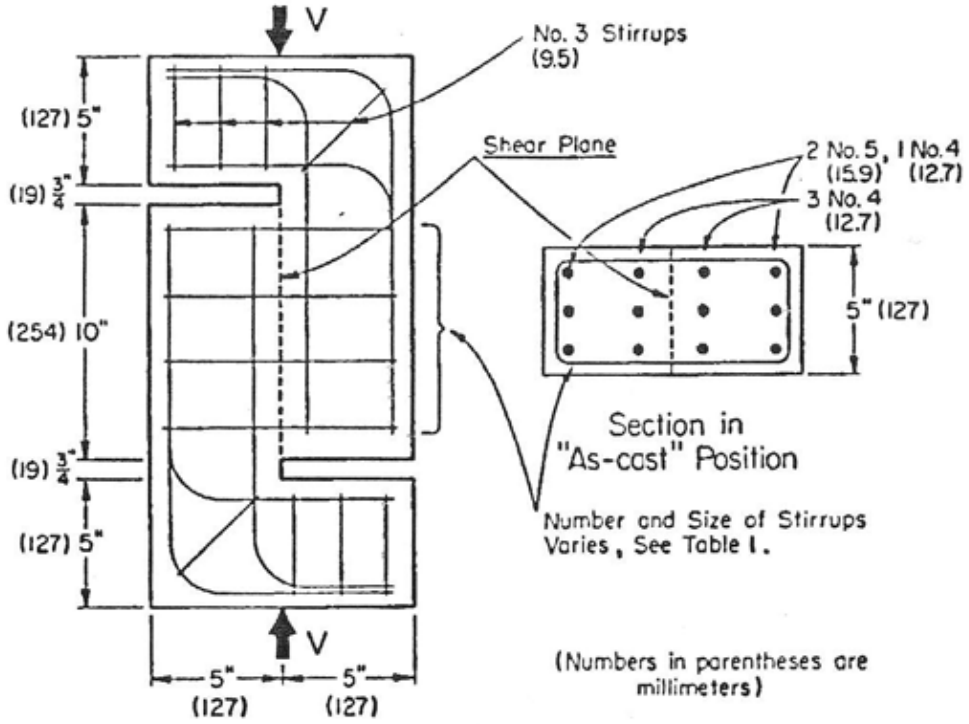

Figure 2.9: Typical Mattock style shear block specimen, reproduced from Hofbeck et al. (1969)

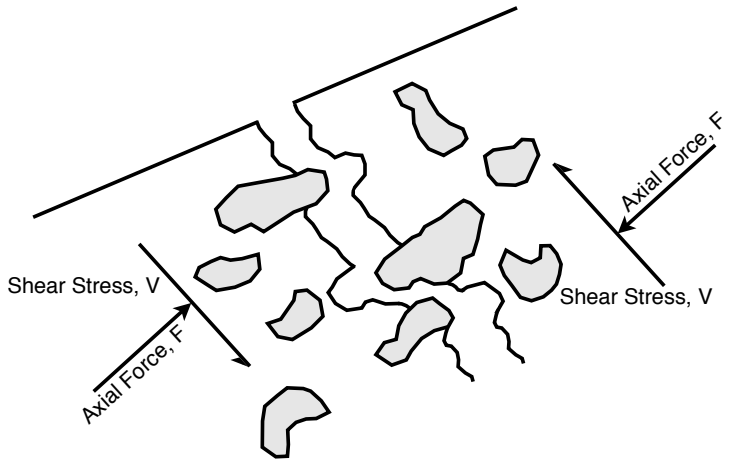

Figure 2.10: Crack surface structure, adapted from Vecchio and Collins (1986)

Shear reinforcement supports the flexural reinforcement and in turn, it gets support from the flexural reinforcement, forming a reinforcement cage. The crack propagation shape is different in a RC beam with shear reinforcement in comparison to one without, it is shorter and wider (Stratford and Burgoyne, 2003).

2.1.2 *Shear in beams*

The current understanding of shear in RC beams has developed from extensive research, outlined in state-of-the-art papers by Collins et al. (1996); Kotsovos and Pavlović (1999); Regan (1993).

Beam behaviour without shear reinforcement

Figure 2.3 shows that stresses are transferred within the concrete of the RC beam jointly by beam and arch action. Beam action occurs both in the compression zone concrete and the concrete near the flexural reinforcement. Beam action transfers the stresses induced from load in a cracked concrete beam through the concrete 'teeth' of the beam between the cracks. For beam action to transfer stresses it relies on concrete-steel bond (discussed in Section 2.1.1). Once the concrete-steel bond is lost in diagonal-tension failure, beam action no longer occurs.

Arch action occurs in the uncracked concrete section near the end of a beam, along a compressive strut. A compressive strut transfers the load from the compression-zone below the load point to the beam support (discussed in Section 2.1.1). The vertical component of the resolved strut force is transferred to the beam support, while the horizontal component is in equilibrium with the tensile flexural reinforcement.

The propagation of cracks in the beam determine how the beam and arch actions carry the shear load. Across cracks, stresses are transferred by flexural reinforcement, concrete-steel bond, dowel action and aggregate interlock (discussed in Section 2.1.1). The contribution of dowel action as a transfer action depends on the strength of the concrete surrounding the flexural reinforcement. Dowel action becomes more significant with high amounts of flexural reinforcement. Shear transfer across the crack interface is mainly due to aggregate interlock.

Many researchers have developed the understanding of shear in RC beams without shear reinforcement (Fenwick and Paulay, 1968; Hamadi and Regan, 1980; Hillerborg et al., 1976; Kani, 1964; Kim and White, 1991; Kotsovos, 1983; Mörsch, 1909).

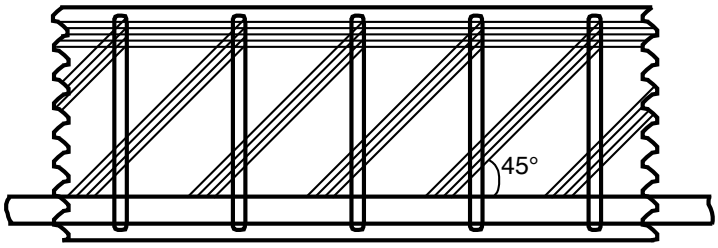

Figure 2.11: Truss analogy with fixed 45° struts, adapted from Mörsch (1909)

Beam behaviour with shear reinforcement

The shear transfer mechanisms in RC beams without shear reinforcement are changed with the addition of shear reinforcement (discussed in Section 2.1.1). Methods for modelling shear transfer in beams include: truss analogies, compressive-field theories, and the compressive force path.

Truss analogies

Ritter (1899) proposed that a RC beam after diagonal cracking could be described by a truss. Shortly after, Mörsch (1909) developed the truss analogy further. Mörsch (1909) assumed that a beam with shear stirrups must also have similar stresses in the concrete rib between two cracks, as one without, because of the similarity in the inclined cracks near the support. Mörsch (1909) visualised a RC beam as a parallel truss arrangement with the lower reinforcing rods in tension, upper concrete being a compressive chord, stirrups acting as the vertical tension members, and fixed 45° diagonal inclined concrete layers as the compression members (Figure 2.11).

Nielsen et al. (1978) adapted the truss analogy approximately 50 years later to consider varied compressive strut angles. Rather than compatibility conditions, the lower bound theorem of plasticity was used to derive the modified truss analogy. The modified truss analogy of Nielsen et al. (1978) considered the possibility of aggregate interlock as a shear transfer action.

The truss analogies do not describe what actually happens in a RC beam, by considering the shear transfer mechanisms. Rather truss analogies simplify the problem into a truss.

Compressive-field theories

Mitchell and Collins (1974); Vecchio and Collins (1986) simplify the complex RC beam behaviour into a simple square RC element, with the diagonal compression field theory. Three resistant forces balance the applied load in the modified compressive-field theory element:

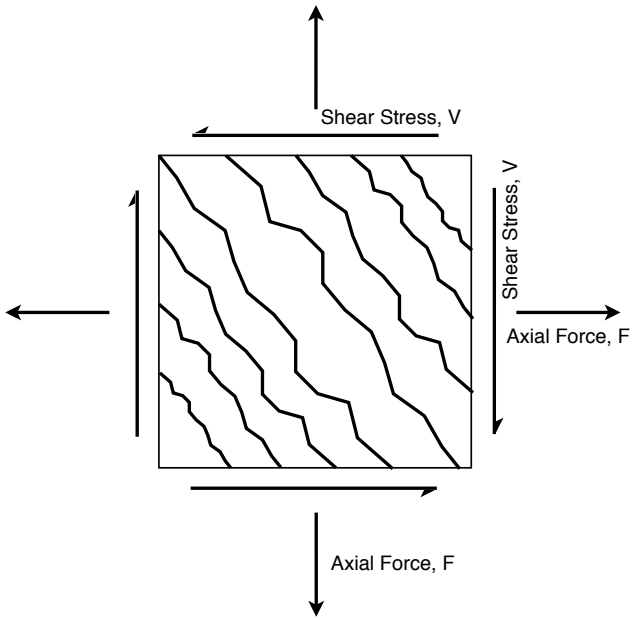

Figure 2.12: Modified compressive-field theory element, adapted from Vecchio and Collins (1986)

1. Stress in the reinforcement can vary along the length, with the highest stress at cracks

2. Aggregate interlock transmits shear and compression at contact locations

3. Tensile stress exists between the concrete bodies at cracks

A simple square element, shown in Figure 2.12 cannot be used to idealise the complex RC beam behaviour with all the shear transfer mechanisms and describe their interaction. To model the element as part of a beam, simplifications are made that rely on stress-redistribution, including a uniform shear stress assumed through the depth of the beam (Collins et al., 1996).

Compressive-field theories calculate the shear-capacity from a critical vertical section. The shear force in a beam under two-point loading is constant in the shear span, which leads to all the sections in the shear span being critical according to the theory. Experiments show failure to be due to a single critical crack, proving there are limitations with the compressive-field theories (Stratford and Burgoyne, 2003).

Compressive force path method

Kotsovos (1983) looks at the shear problem as a whole and agrees with Kani (1964), that shear forces are only part of the cause of shear failure. Kotsovos (1983) proposed that there is no single cause of shear failure, and that the various mechanisms of shear failure are linked to *"the shape of the path along which*

the compressive force is transmitted to the support", rather than Kani (1964) consideration of the stress conditions in the region of the concrete cantilevers.

The experimental research of Kotsovos (1983) highlighted that although current shear design procedures *"may be successful in preventing shear failure within the shear span, a_v, they may lead to 'brittle' types of structural collapse outside this span due to failure of concrete in localized regions subjected to uniaxial compression"*.

Having brought to light various inadequacies with design codes, Kotsovos (1988) presented the compressive force path concept as a model on which the design of RC beams should be based. Figure 2.5 shows that Kotsovos visualises the beam with a 'flow' of compressive stresses within a path, that act perpendicular to the path direction, joining the support to the loading point. The basis for the compressive force path is that, RC beam failure is caused by the development of tensile stresses within the compressive force path. The compressive force path concept of Kotsovos (1988) identifies the shear transfer mechanisms (described in Section 2.1), which may cause the development of the tensile stresses and agrees with fundamental concrete properties.

The compressive force path concept has been developed for both simply supported beams with and without shear reinforcement and has also been extended to consider punching shear at ambient temperature.

2.2 PUNCHING SHEAR IN SLABS AT AMBIENT TEMPERATURE

One-way or two-way spanning RC slabs are supported by beams (shown in Figures 2.13 and 2.14, respectively), which in turn transfer the load to columns. Figure 2.15 shows that flat RC slabs are supported directly onto columns without beams. The design of flat slabs is often similar to that of two-way spanning slabs, however the high forces transferred from the slab to the column at the slab-column joint requires punching shear to be considered.

Shear action in one-way slabs is similar to that in beams (discussed in Section 2.1.2), as the main flexural reinforcement in the spanning direction is similar to that in RC beams. Shear action in two-way slabs may be assumed to be the same as one-way slabs acting in both x- and y-directions. The transfer of punching shear is a complex three-dimensional interaction of the shear transfer mechanisms, discussed in Section 2.1.1. Figure 2.16 compares the shear force per unit length for a beam and a two-way slab and indicates how complex the two-way slab interaction may be. The shear force distribution increases to a maximum at the column for two-way slabs, whereas it is constant for beams, when the self weight of the beam is not considered.

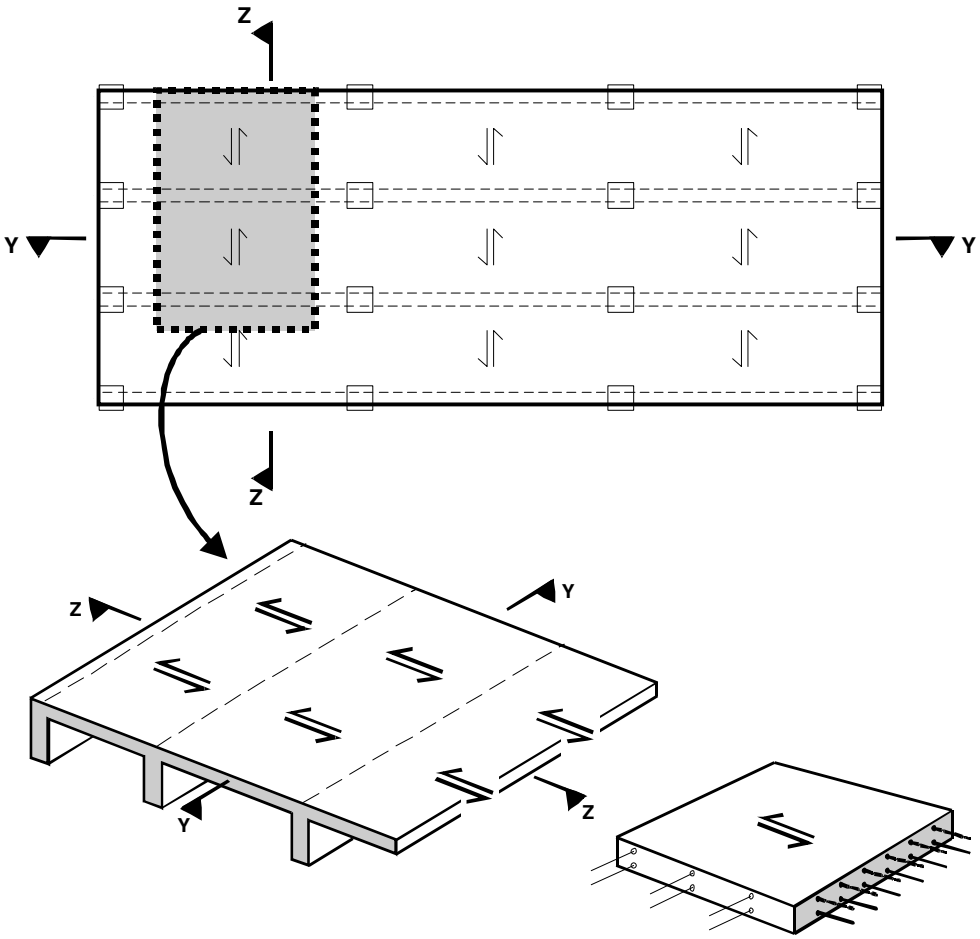

Figure 2.13: One-way spanning slab design, reproduced from Stratford (2007)

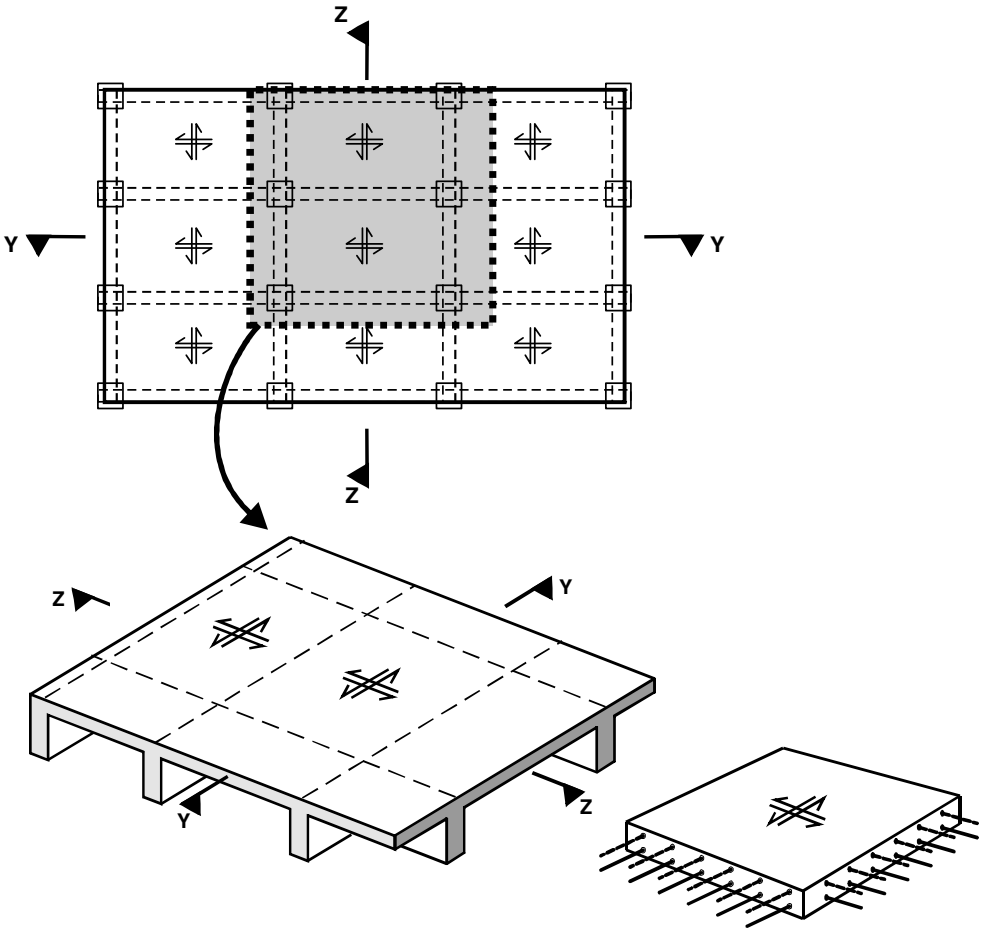

Figure 2.14: Two-way spanning slab design, reproduced from Stratford (2007)

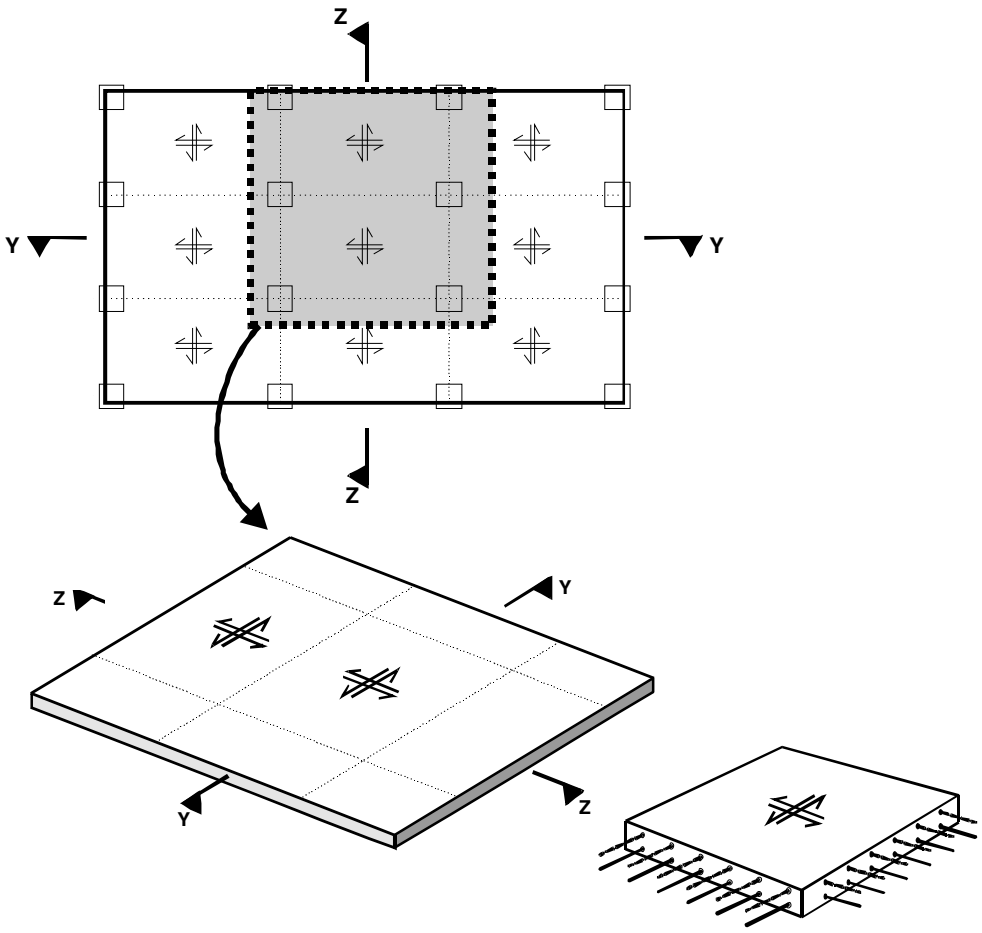

Figure 2.15: Flat slab design, reproduced from Stratford (2007)

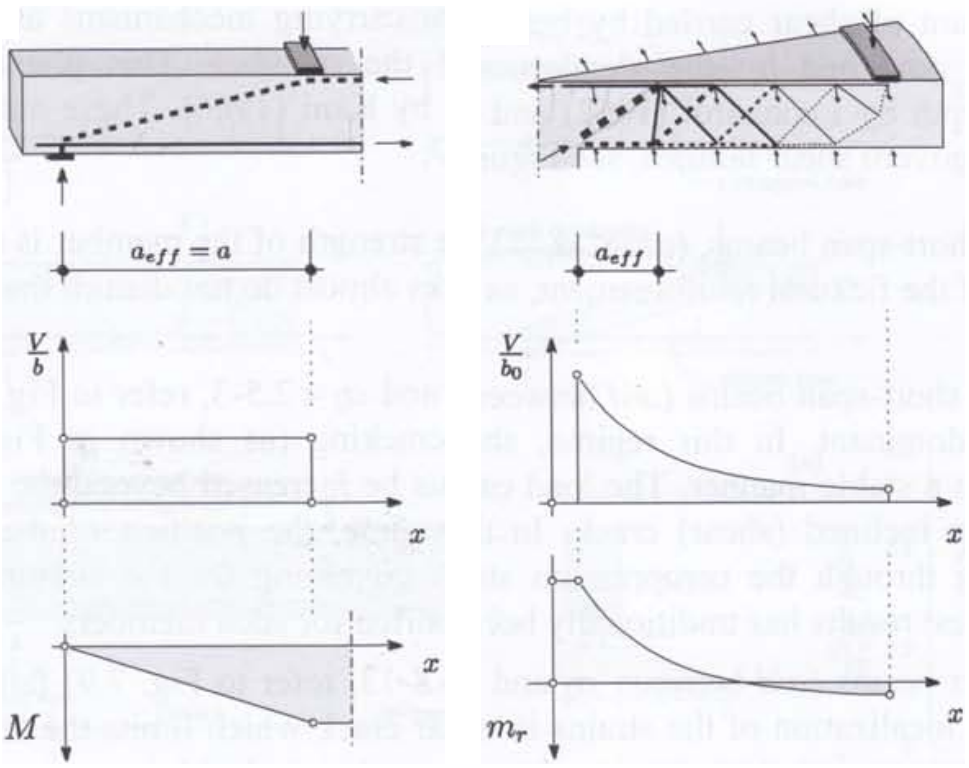

(a) Unitary shear force and bending moments for a beam or one-way slab

(b) Unitary shear force and bending moments for a two-way slab

Figure 2.16: Shear strength comparison in one- and two-way slabs subjected to concentrated loads, reproduced from Sigrist (2010) where a_{eff} = effective shear span (mm), b = control perimeter from the face of the column (mm) and d = effective depth of the member (mm)

Shear failure of slabs can occur at either point loads (Figure 2.17a), wall-slab joints (Figure 2.17b shows one-way slab) or column-slab joints (Figure 2.17c). Punching shear failure of flat slabs at slab-column joints at ambient temperature is the focus of Section 2.2 and the shear force concentration type used to test slabs in this thesis.

Punching shear failure of slabs requires a three dimensional consideration to visualise the failure mode. Figure 2.18 shows the cross-section of punching shear failure, where a column punches through the slab it is supporting, producing a cone crack pattern of RC. The failure surface in plan view, from above and below the column is a circle (assuming a circular column cross-section). The warning signs for punching shear failure are limited to very small defections and cracks that open on the slab above the column, which are often hidden by floor coverings.

Figure 2.19 shows that punching shear failure is less brittle and therefore more ductile, when shear reinforcement is included. A small amount of shear reinforcement can change the failure mode substantially. Traditional shear design is divided into two approaches: with and without shear reinforcement. The experimental work in this thesis only covers punching shear without shear reinforcement.

Ghoreishi et al. (2013); Reineck (2001); Sigrist (2010) give state-of-the-art reviews of punching shear in RC. The fédération internationale du béton (fib) Working Group 4.2 was tasked with harmonising different shear design approach ideas into draft Model Code 2010, reported in Sigrist (2010). One main outcome of the group discussions was to use a similar design approach for beam shear and punching shear, which considers both the reinforcement and concrete contribution to shear transfer. Critical Shear Crack Theory (CSCT) was proposed as the background to the draft Model Code 2010. CSCT was used as a basis for the design of the experimental work presented in this thesis.

2.2.1 *Critical Shear Crack Theory*

CSCT is a mechanical model which gives consistent and compact design formulations for shear and punching shear in members with and without shear reinforcement, as well as non-symmetrical loading conditions (Muttoni, 2008; Muttoni and Fernández Ruiz, 2008). CSCT is based on a critical crack that penetrates through an inclined concrete compressive strut, which transfers the load on the slab to the column, as shown in Figure 2.20.

The fundamental assumption of the CSCT is that for members without shear reinforcement, the shear strength is governed by the critical shear crack width

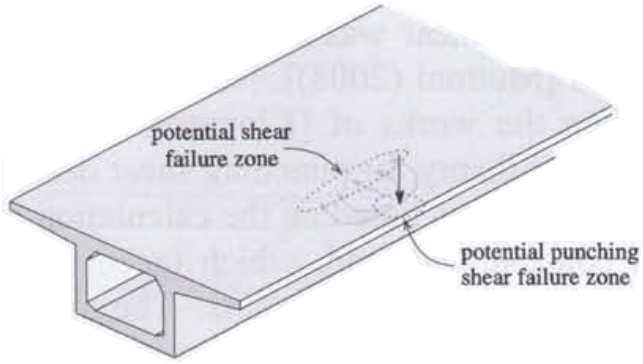

(a) Concentrated loading on a deck slab of a bridge

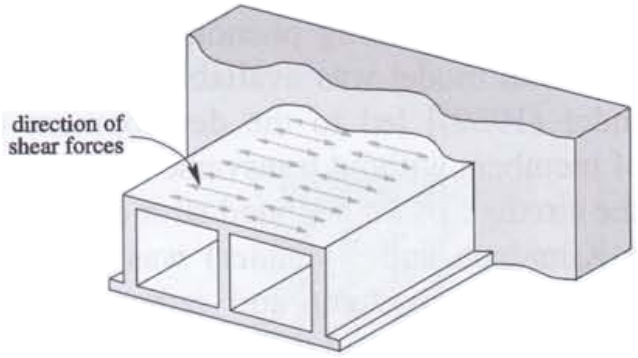

(b) Roof slab of an earth-covered structure

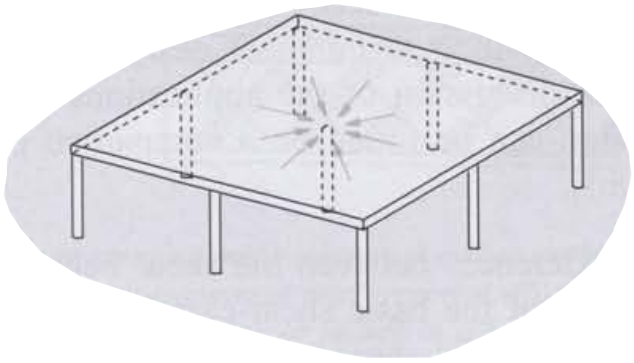

(c) Shear force directions near the inner column of a flat slab

Figure 2.17: Shear force concentrations in slabs, reproduced from Sigrist (2010)

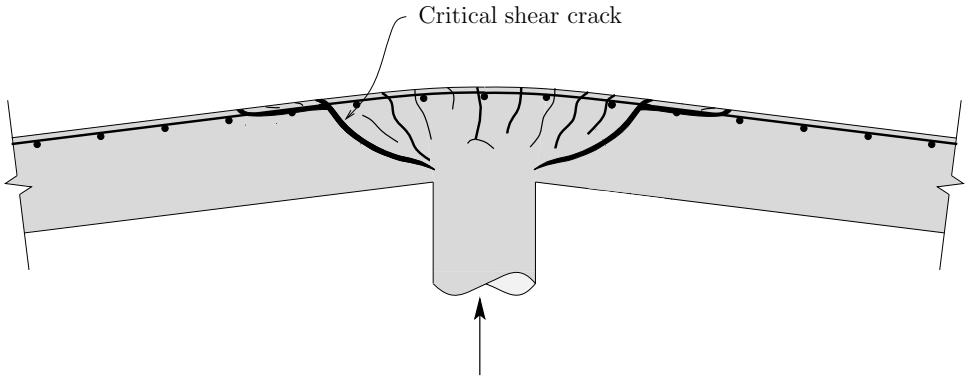

Figure 2.18: Typical punching shear failure, reproduced from Fernández Ruiz and Muttoni (2010)

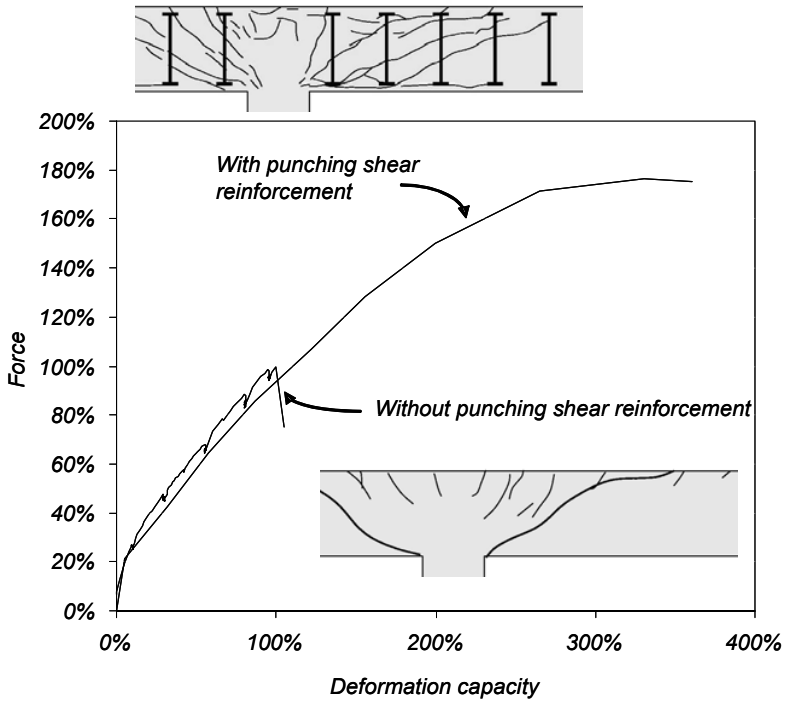

Figure 2.19: Slab behaviour with and without shear reinforcement, reproduced from Fernández Ruiz and Muttoni (2010)

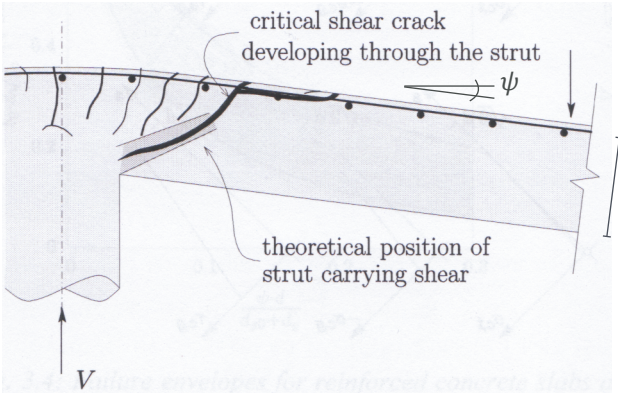

Figure 2.20: Muttoni's critical shear crack position, adapted from Sigrist (2010) where crack width, w, is defined as proportional to the slab rotation, ψ, multiplied by the effective depth of the slab, d

and roughness of the shear crack that develops through the inclined compressive strut carrying shear.

The model is based on kinematic equilibrium equations at failure of the free-body rotation of the slab, relative to the column. These kinematics allow both tensile stresses and aggregate interlock induced stresses to develop along the critical shear crack. The shear strength calculation therefore considers both the concrete in tension and aggregate interlock contribution, along the critical shear crack failure surface. Dowel action is neglected from the shear transfer mechanisms considered, as it is assumed spalling of the concrete cover over the flexural reinforcement may occur.

When the rotation angle increases, there is a point when the contribution of concrete in tension is no longer significant and the behaviour is dominated by aggregate interlock. The punching shear strength is therefore plotted as a function of slab rotation.

In two-way spanning slabs, the critical shear crack width is assumed to be proportional to the slab rotation multiplied by the effective depth of the slab. The failure criterion for members without shear reinforcement is calculated with Equation 2.1 (Lips et al., 2012).

$$\frac{V_R}{b_0 \cdot d_v \cdot \sqrt{f_c}} = \frac{3/4}{1 + 15\frac{\psi \cdot d}{d_{g0} + d_g}} \tag{2.1}$$

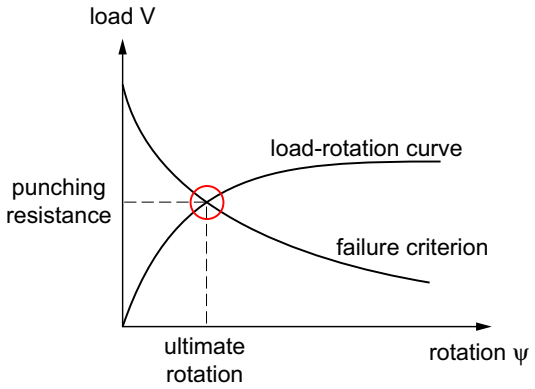

Figure 2.21: Calculation of the punching shear capacity by CSCT, reproduced from Bamonte et al. (2012)

where:

V_R = shear strength (N)

b_0 = control perimeter set at $\frac{d}{2}$ of the border of the support region and circular at the corners (mm)

d_v = shear-resisting effective depth (mm) (distance between the centroid of the flexural reinforcement and the surface at which the slab is supported)

f_c = average compressive cylinder strength of concrete (MPa)

d_{g0} = reference aggregate size (16 mm)

d_g = maximum aggregate size (mm)

Assuming:

$w = \psi \cdot d$

w = critical shear crack width (mm)

ψ = slab rotation (radians)

d = effective depth of the member (mm)

The CSCT punching shear strength circled in Figure 2.21, is found at the intersection between the failure criterion and the load-rotation curve. The load-rotation curve for an ambient simply-supported circular slab, as shown in Figure 2.22, is given by Equation 2.2 (Muttoni, 2008). The load-rotation curve gives a relationship for the slab-column behaviour governed by flexural capacity of the slab specimen, steel and concrete properties, and slab rotation angle. The shear strength of the slab is considered to be directly related to the flexural capacity.

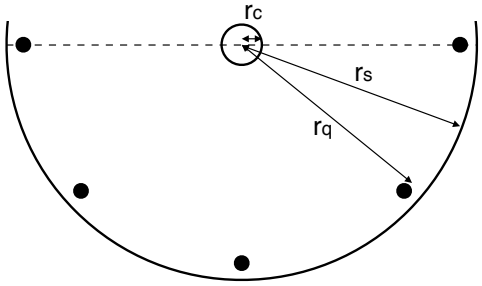

Figure 2.22: Circular isolated slab-column element, adapted from Guandalini (2005)

$$V = V_{flex}\left(\frac{\psi}{1.5}\frac{d}{r_s}\frac{E_s}{f_y}\right)^{\frac{2}{3}} \tag{2.2}$$

where:

$$\begin{aligned} V_{flex} &= 2\pi m_R \frac{r_s}{r_q - r_c} \\ m_R &= \rho f_y d^2 \left(1 - \frac{\rho f_y}{2 f_c}\right) \end{aligned} \tag{2.3}$$

where:

V = shear failure load (N)
V_{flex} = shear force associated with flexural capacity of slab specimen (N)
m_R = nominal moment capacity per unit width (N.mm per mm)
ρ = flexural reinforcement ratio
f_y = flexural reinforcement yield strength (MPa)
d = distance from extreme compression fibre to the centroid of the longitudinal tensile reinforcement (mm)
f_c = average compressive cylinder strength of concrete (MPa)
r_s = radius of circular isolated slab element (mm)
r_q = radius of the load introduced at the perimeter (mm)
r_c = radius of circular column (mm)
ψ = slab rotation
E_s = flexural reinforcement Young's modulus (MPa)

Muttoni and Fernàndez Ruiz (Sigrist, 2010) comment that *"developing suitable moment-curvature and axial force in-plane strains provides a general frame to investigate some phenomena like the increase of the punching shear*

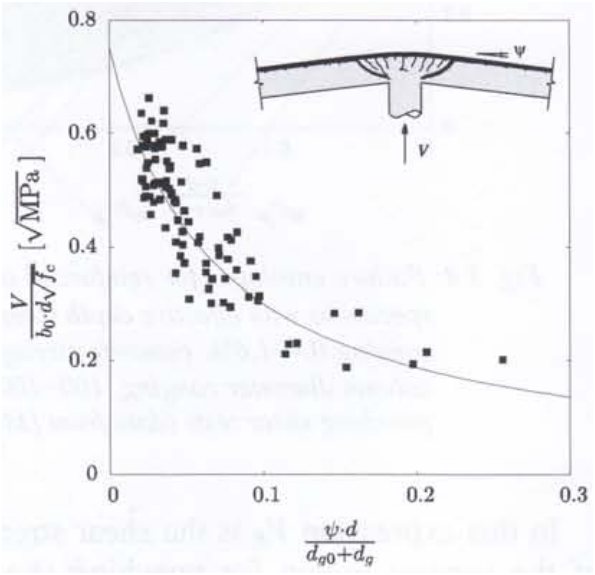

Figure 2.23: Comparison of 99 experimental test results to Muttoni's CSCT simplified failure criterion, reproduced from Sigrist (2010)

strength in slabs with restricted horizontal expansion ..., the behaviour and strength of flat slabs under fire conditions ..., or the increase of the punching shear strength for slabs transferring large column loads". Muttoni and Fernàndez Ruiz describe how the CSCT method could be applied to more complex situations by developing standard load-rotation curves.

The CSCT is supported by 146 actual size punching shear tests, which have been undertaken over the past 10 years. Slab-column specimens are supported by the column stub and loaded at points, a fixed distance from the column stub, with consideration for the effective perimeter. Figure 2.23 shows that there is good agreement between the model and 99 experimental test results. Guandalini et al. (2009) presents 11 fully restrained punching shear slab tests without shear reinforcement. These half-size slabs (dimensions 1500×1500 mm and height 125 mm) were used to guide the design of the slabs in this thesis.

Figure 2.24 shows a good agreement between experimental results for an inner column transferring moments and CSCT analysis, where the four Levels of Approximation (LoA) for shear analysis options relate to (Sigrist, 2010):

Level I = simplest and most conservative
Level II = intermediate complexity and accuracy
Level III = provides the most accurate and general predictions, at the cost of high computational complexity
Level IV = use of tools such as nonlinear finite element analysis and generalised stress-field approaches

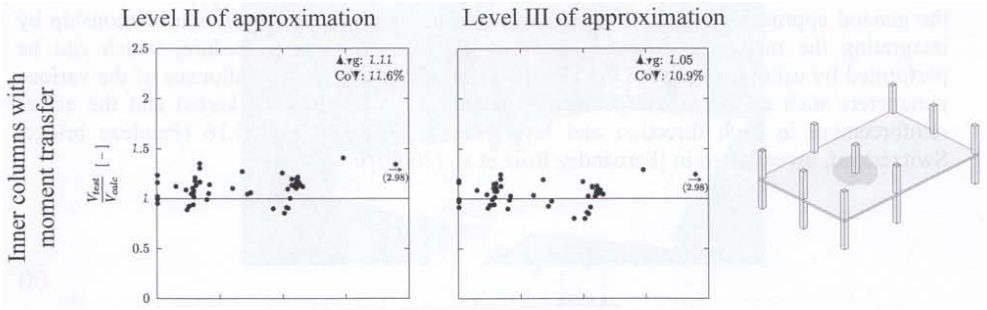

Figure 2.24: Comparison of CSCT with tests of inner columns with moment transfer from Anis (1970), Elstner and Hognestad (1956), Hawkins et al. (1989), Kruger (1999) and Moe (1961), reproduced from Sigrist (2010)

2.2.2 *Experimental slab-column research*

Punching shear experimental research has been undertaken with two setup types: isolated slab-columns and full slab sub-systems, similar to those shown in Figure 2.25. Isolated slab-column tests consist of a portion of slab with a column stub, which is focused on here as it is the specimen type tested in this thesis. The isolated slab-column (referred to as slab-column) specimen is more economical, which allows a parameter comparison. Additionally, specimens can be tested at full scale, eliminating size effects.

Slab-column specimens have been tested either as slabs supported along the boundary and load applied to the column stub or the reverse, as slabs supported by the column stub and loads applied at a fixed distance from the column stub. Figure 2.25a shows the typical calculation of the slab dimensions for slab-column tests, which are often chosen to model the points of contra flexure or zone of negative moments of a real slab.

Shear capacity is influenced by the distance between the loaded area and the support, shear span (a_v). The support interferes with the failure surface at low values of a_v. Gardner (1990) recommended that a_v needed to be at least $3d$ to ensure punching shear failure occurred and that bond failure would result. Otherwise, the slab diameter would not be sufficient to allow the slab steel to be effective.

The main disadvantage of isolated slab-column tests is that only an element of the structure and not the whole structural behaviour is assessed. Long and Bond (1967) recognised that the early slab-column testing needed to consider the specimen as a part of a whole structural system. Long and Bond (1967) presented a correction factor to consider the stiffening effect of the slab portion beyond the supports.

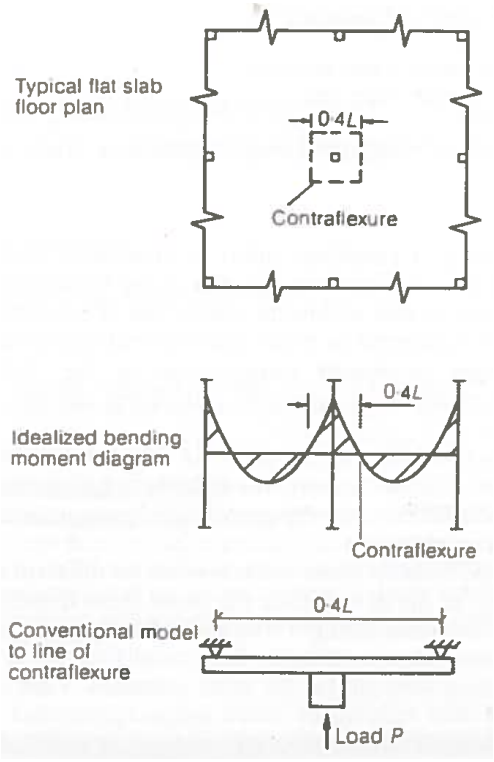

(a) Typical isolated slab-column specimen setup, reproduced from Rankin and Long (1987)

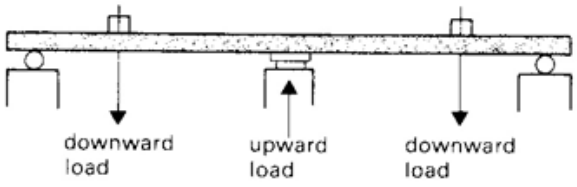

(b) Full panel slab-column specimen setup, reproduced from Regan (1986)

Figure 2.25: Punching shear specimen setup types

Support conditions

The known factors that are often not assessed with slab-column tests, include: support conditions, confinement, load re-distribution, and in-plane restraint forces (which can also lead to membrane action). Elstner and Hognestad (1956) undertook early simply supported slab-column tests to investigate support conditions, however reported local failure near the supports rather than punching shear failure. Alexander and Simmonds (1992) showed that rotational restraint without any in-plane restraint increased the shear capacity of the isolated slab-column section.

Taylor and Hayes (1965) compared unrestrained and restrained support conditions of slab-column specimens. Taylor and Hayes (1965) conclude that the restraint of the edges of the slabs increased the punching shear capacity by *"24–60% when the corresponding simply supported slabs were near to flexural failure at collapse, but only 0–16% when the corresponding simply supported slabs were not near to flexural failure at collapse"*.

Compressive Membrane Action (CMA) can increase the punching shear capacity. Regan (1986) investigated the impact of membrane action on punching shear with full panel specimens, shown in Figure 2.25b. Regan (1986) found, *"the strength rises with increasing restraining moments, but it is uncertain whether the cause is really the moment or the lateral restraint provided by the uncracked concrete at the edges of the 1.73 m square."*

Kuang and Morley (1993) vary the support restraint of slab-column specimens and show the punching shear capacity is increased with an increase in stiffness of the lateral restraint (Figure 2.26). They proved that CMA was produced in the tests, by measuring lateral bowing and a sharp load-deflection increase after initial cracking in the edge beams. Further similar testing was undertaken by Alam et al. (2009).

Reineck (2001) details the work done on CMA by Masterson and Long (1974); Rankin and Long (1987). Sigrist (2010) references further tests on inner columns with moment transfer, including Anis (1970); Hawkins et al. (1989); Moe (1961), though a copy of Anis (1970); Moe (1961) work could not be found. Hawkins et al. (1989) undertook 36 slab-column tests to investigate the moment and shear transfer. Thorough results of crack patterns, crack widths, deflections, steel and concrete strains and failure loads were presented. Hawkins et al. (1989) conclude that the ACI 318-83 design methods are conservative for reinforcement ratio's greater than 0.7% and not below.

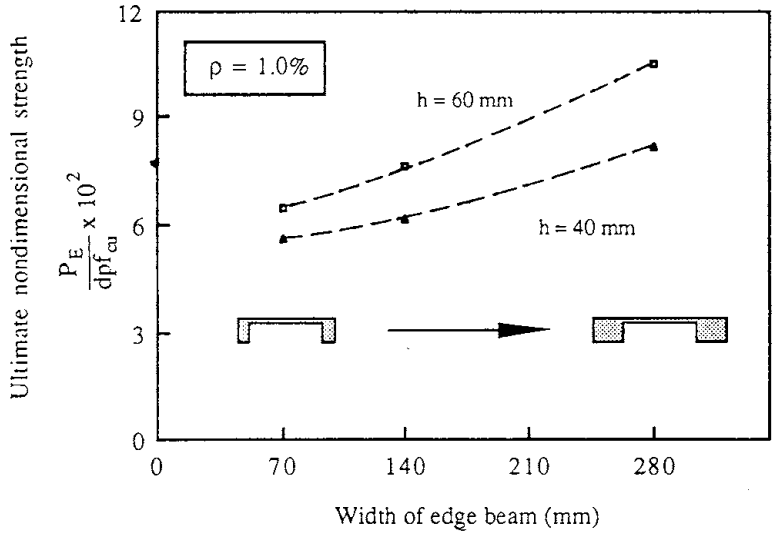

(a) Effect for different slab thicknesses

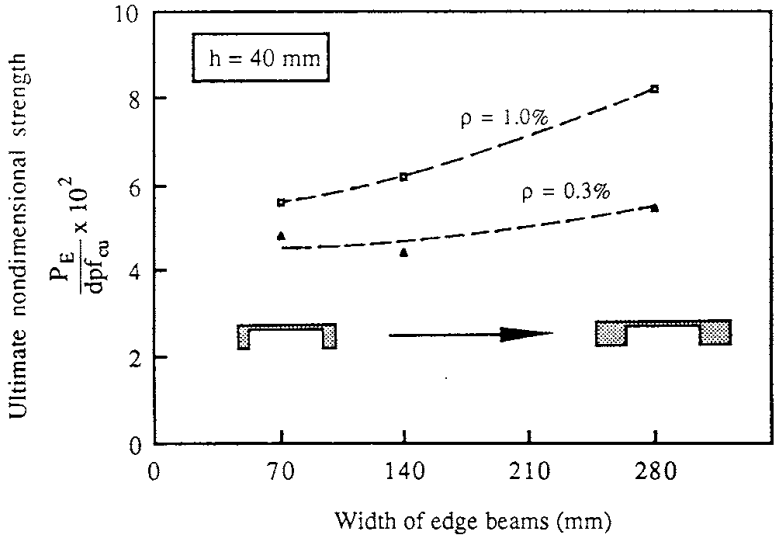

(b) Effect for different slab reinforcement ratios

Figure 2.26: Effect of edge restraint on the punching shear capacity, reproduced from Kuang and Morley (1993) where: non-dimensional punching shear capacity is calculated as the ultimate punching shear capacity divided by the product of the compressive concrete strength and the distance of the critical surface, located at half the effective depth away from the perimeter of the load

2.3 SHEAR AT ELEVATED TEMPERATURE

The expression 'elevated temperature' is used to refer to realistic fire temperatures. Shear failure at ambient temperature is not well understood and temperature gradient effects through the RC section add complexity. The ambient temperature shear failure modes of RC are used as a foundation to understand the following impacts of elevated temperature:

1. the steel and concrete individually degrade with time, inducing strength and stiffness losses;
2. the shear transfer mechanisms change with time, as the elevated temperature heat front penetrates through the member;
3. internal, self-equilibrating thermal restraint affects the shear transfer mechanisms and
4. external thermal restraint actions from the whole structural response.

Shear transfer mechanisms at elevated temperatures are not well understood. Elevated temperature pull-out tests have been undertaken to research concrete-steel bond only. Grauers et al. (1994); Morley and Royles (1980) present a state-of-the-art on concrete-steel bond at elevated temperature, including work done by Diederichs and Schneider (1981); Hertz (1982). Morley and Royles (1983) undertook pull-out tests and presented bond stress-slip curves.

There have been various RC beam investigations at elevated temperatures, with Grauers et al. (1994); Sigrist (2010) presenting state-of-the-art reviews. However, few tests have investigated the shear transfer mechanisms in beams at elevated temperature.

Beam tests were undertaken at elevated temperature by Khan and Royles (1986) to investigate concrete-steel bond and Khan et al. (2010) researching dowel action. Research by El-Hawary et al. (1997); Ellingwood and Lin (1991) focussed more on beam shear behaviour at elevated temperature. Ellingwood and Lin (1991) state that the behaviour of RC beams in fire depends on *"thermal properties of the steel and concrete, strength and stiffness properties of the concrete and steel at elevated temperatures, and the ability of the structure to redistribute internal forces during the course of the fire"*.

2.3.1 *Effects of elevated temperature on material properties*

A brief description of the effects of elevated temperature on the material properties of Normal Strength Concrete (NSC) and steel are given here. Concrete spalling is mentioned, however the impact of spalling on punching shear is not considered in the scope of this work.

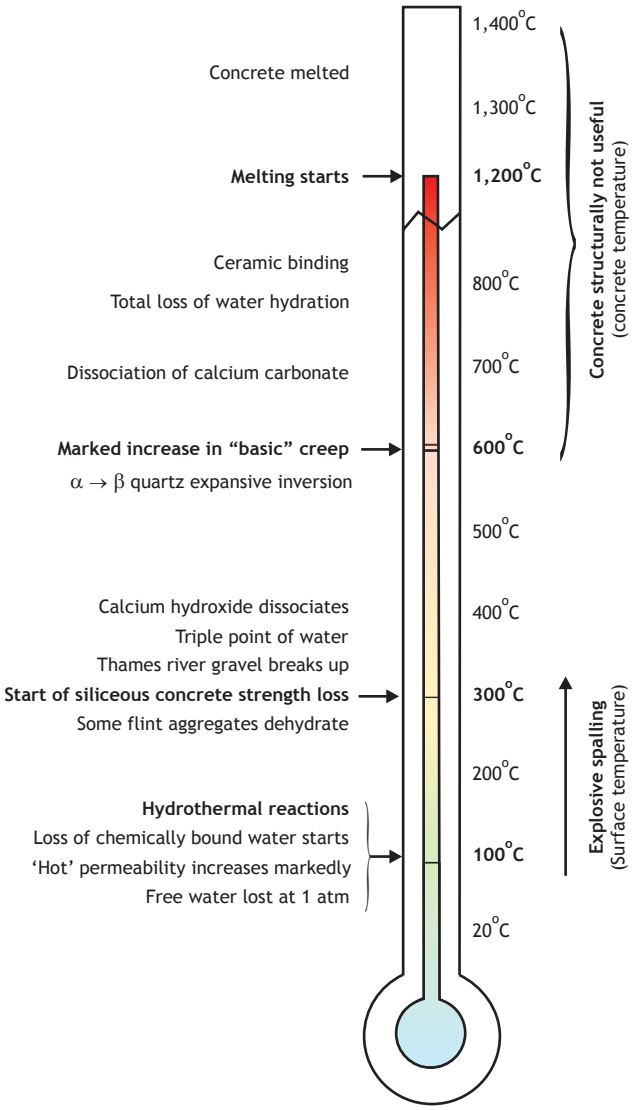

Figure 2.27: Portland cement concrete thermometer of physicochemical processes undertaken at elevated temperatures, reproduced from Bailey and Khoury (2011)

Concrete

Figure 2.27 shows a thermometer which details the physicochemical processes Portland cement concrete undergoes. The constituents of concrete react differently to elevated temperature. The cement paste shrinks with temperature increase, whereas the aggregate expands. This difference causes high stresses within the concrete, which cause cracks and a subsequent decrease in strength. The aggregate type (for example, calcareous, siliceous, etc...) changes the thermal conductivity and coefficient of thermal expansion of the concrete.

Naus (2005) presents a state-of-the-art review of the impact of elevated temperature on concrete, showing that many factors are involved, listed in Figure 2.28. Naus (2005) shows that crack development decreases at elevated

Factor	Influence	Comment
Temperature Level	***	• Chemical-physical structure (see Chapter 2) & most properties (see Chapters 6-14).
	**	• The properties of some concrete (e.g. compressive strength and modulus of elastcicity) when heated under 20-30% load can vary less with temperature - up to about 500°C - than if heated without load (see Chapters 6 & 14).
Heating Rate	**	• *< 2°C/min:* Second order influence.
	***	• *> about 5°C/min:* Becomes significant ⇒ explosive spalling.
Cooling Rate	*	• *< 2°C/minute:* Negligible influence.
	**	• *> 2°C/minute:* Cracking could occur.
	***	• *Quenching*: Very significant influence.
Thermal Cycling	**	• *Unsealed Concrete:* Significant influence mainly during first cycle to given temperature.
	**	• *Sealed concrete*: Influence in so far as it allows longer duration at temperature for hydrothermal transformations to develop.
Duration at Temperature	**	• *Unsealed concrete*: Only significant at early stages while transformations decay.
	***	• *Sealed concrete*: Duration at temperature above 100°C ⇒ Continuing hydrothermal transformations.
Load-Temp. Sequence	***	• Very important - not usually appreciated
Load Level	***	• < 30%: Linear influence on Transient Creep (Chapter 9) at least in range up to 30% cold strength.
	***	• >50%: Failure could occur during heating at high load levels.
Moisture Level	**	• *Unsealed*: Small influence on thermal strain and transient creep particularly above 100°C.
	***	• *Sealed*: Very significant influence on the structure of cement paste and properties of concrete above 100°C.

*** First order influence. ** Second order influence. * First order influence.

Figure 2.28: Environmental factors that influence concrete at high temperatures, reproduced from Naus (2005)

temperature when concrete is loaded. This highlights the importance of assessing the structure as a whole, by also considering structural regions that are less stressed and potentially more susceptible to elevated temperatures.

Li and Franssen (2011) review approximately 400 elevated temperature and 1500 residual, concrete compressive strength tests. Residual testing refers to testing once the specimen has been heated to a target temperature and cooled to ambient temperature. Li and Franssen (2011) show in Figure 2.29 the average residual concrete capacity is less than the capacity at elevated temperature, making the residual strength the critical case.

Among other comparisons, Li and Franssen (2011) show that water cooling technique decreases the residual strength more than air cooling (Figure 2.30).

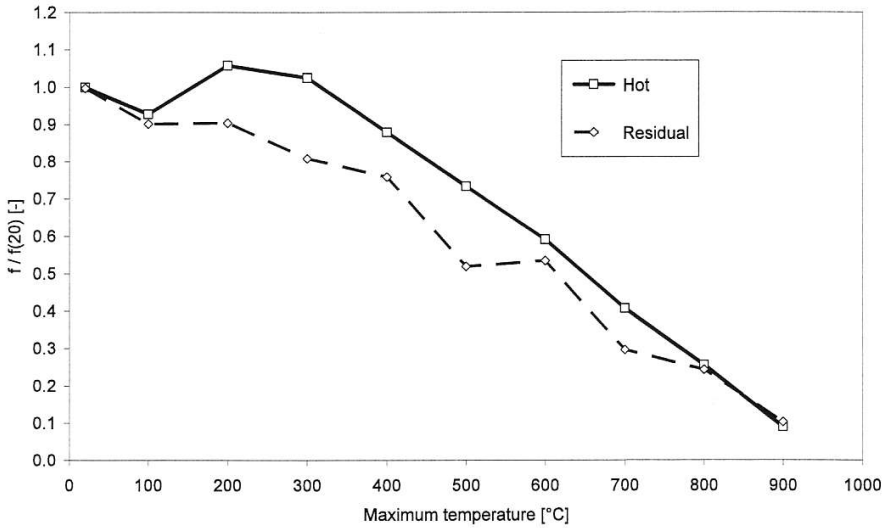

Figure 2.29: Comparison between normalised average concrete residual and elevated temperature compressive strengths, reproduced from Li and Franssen (2011)

A real structure would experience this water cooling thermal shock when fire fighters are tackling a fire, proving that further research where a specimen is cooled in a structural fire test with water is required.

Concrete spalling

Spalling of concrete is the explosive breaking of concrete. This behaviour has been seen to occur in concrete at elevated temperature. The main impact of spalling in the context of this work, is the reduction in section and increase in flexural reinforcement temperature, which are both caused by the loss of concrete cover. Figure 2.27 shows that spalling can occur at any surface temperature above approximately 100°C.

Load Induced Thermal Strains

"Load Induced Thermal Strains (LITS) is defined as the difference between the free thermal expansion of concrete when it is heated, and the net thermal expansion when the same concrete is heated under a level of pre-stress" (Law and Gillie, 2008). Concrete can shrink at elevated temperatures, when under high levels of pre-stress, contrary to the understanding that concrete expands when heated (Khoury, 2000). Figure 2.31 shows graphically the importance of Load Induced Thermal Strains (LITS) on structural behaviour at elevated temperatures. The main contributors of LITS (but not all) are non-recoverable, therefore the effects of LITS are only seen on first-time heating and the strains are irrecoverable during cooling.

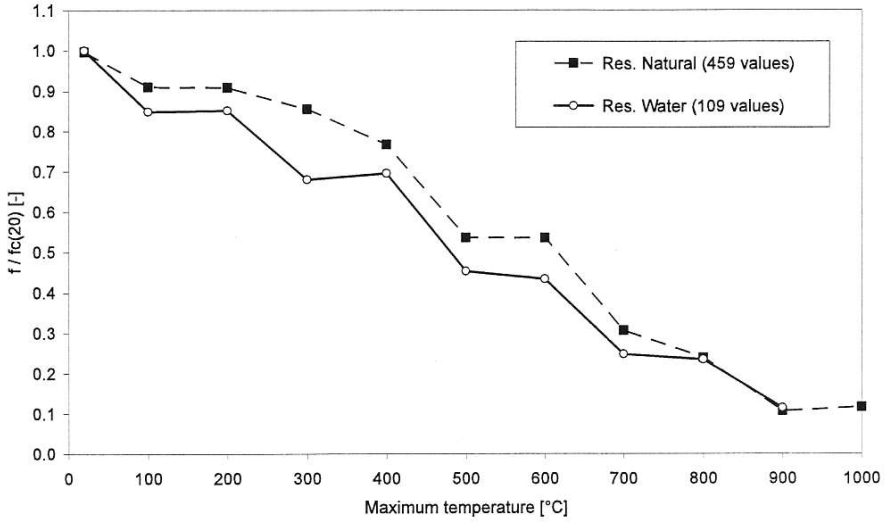

Figure 2.30: Comparison of cooling technique on normalised average residual strength specimens, reproduced from Li and Franssen (2011)

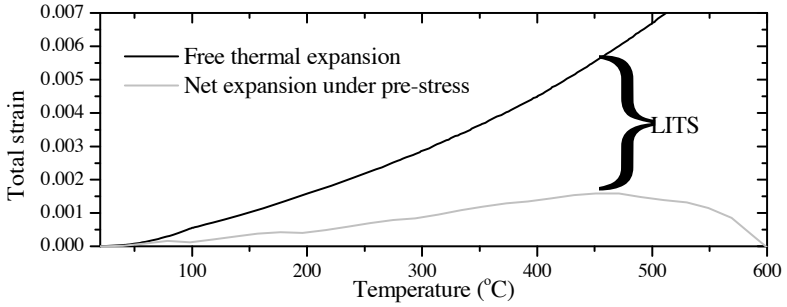

Figure 2.31: Graphical representation of Load Induced Thermal Strains (LITS), reproduced from Law and Gillie (2008)

Steel

Figure 2.32 shows how the residual tensile steel strength varies with maximum temperature for different cooling regimes.

2.4 PUNCHING SHEAR IN SLABS AT ELEVATED TEMPERATURE

Section 2.4.1 describes the limited experimental slab-column punching shear tests at elevated temperature. A total of 51 elevated temperature punching shear specimens have been tested, with 30 of them having been residually tested at ambient temperature. There are no recorded elevated temperature punching shear tests that vary the support conditions, though the impact of restrained thermal curvature by fixed supports is critical for many redundant structures (Bamonte et al., 2009).

Section 2.4.2 presents the punching shear modelling at elevated temperature. In addition to the material properties degradation, modelling was used to investigate the global structural analysis. Research focussed on the impact of in-plane axial forces and moments caused by restrained thermal expansion of the slab and column.

The tragic underground collapse of a car park in Gretzenbach Switzerland, on 27 November 2004 had a large influence on the direction of elevated temperature punching shear research and catalysed much of the experimental and modelling research done to date. Muttoni et al. (2005) report their opinion of the cause of the car park collapse, which took the lives of seven fire fighters. Investigations found design and execution errors that led to a reduced punching shear design safety factor, which became critical under fire. For example, soil layer thickness was larger than design allowed for, upper reinforcement was positioned lower than designed, and the column top was partially in the slab (Annerel et al., 2011a, 2012).

2.4.1 *Experimental research*

Kordina (1997) conducted some of the first punching shear tests in fire. Figure 2.33b shows the 10 isolated slab-column full-scale specimens he tested at elevated temperature, for the German Research Association. Kordina (1997) presented and analysed the results, including 4 similar tests that were undertaken previously in 1986 at the Technical University of Braunschweig. Kordina (1997) considered the following parameters important:

- flexural reinforcement ratio;
- shear reinforcement;

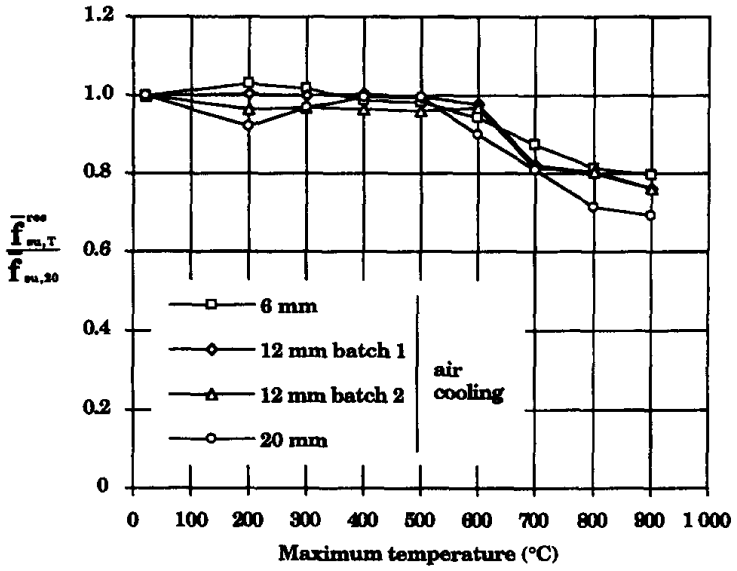

(a) For air cooling

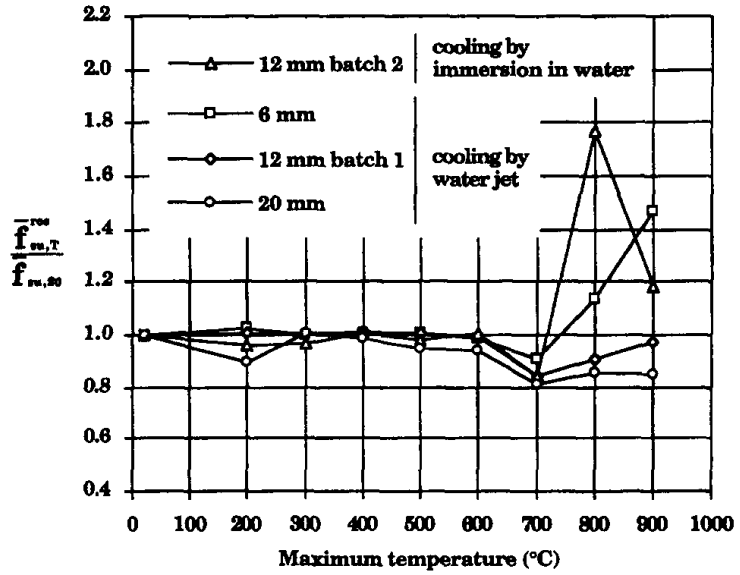

(b) Comparing immersion and jet water cooling

Figure 2.32: Non-dimensional residual tensile strength, reproduced from Neves et al. (1996)

- thermal restraint effects, simulated by increasing the service load during the first 30 minutes of the ISO-834 fire; and
- punching cone crack pattern formation.

Kordina (1997) designed his simply-supported slabs according to EC2 (1992 version) and considered the previous tests with which he also wanted to compare his results. The slabs were loaded upwards through the column stub, to 70% of their ambient ultimate design punching shear resistance, prior to fire being applied via an ISO-834 fire curve.

Kordina (1997) reported that all the tests deflected downwards, towards the fire and opposite from the loading direction. The 4 earlier tests only recorded this behaviour during the first 30 minutes of the fire, after which the deflection reversed.

Ghoreishi et al. (2013) conducted 6 RC slab-column tests, 3 at ambient temperature and 3 at elevated temperature. Ghoreishi et al. (2015) give the experimental results from the 6 simply-supported tests with specimen dimensions, 1000×1000 mm and thickness 120 mm. A furnace with three infrared radiant heating elements was used to apply the elevated temperature. The slab-columns were heated until a steady temperature was reached and thereafter monotonically loaded through the column stub until failure.

The Ghoreishi et al. (2013) experiments show reinforcement ratio to have an impact on the punching shear capacity and urgently recommend the flexural reinforcement ratio be included in the calculation of the punching shear capacity in the Canadian Standard (CSA) code provisions.

Gretzenbach failure experimental work

Annerel et al. (2011a,b) reported an experimental series of 6 large scale slabs, with dimensions 3200×3500 mm and thickness 400 mm. These 2 ambient temperature and 4 elevated temperature tests were the first to follow the Kordina (1997) tests and were based on an underground parking garage situation, similar to the Gretzenbach tragedy. Annerel et al. (2011b) outlined four main contributing actions in the case of a fire in an underground parking garage:

1. temperature induced losses of strength and stiffness;
2. restraint of the thermal expansion of the slabs;
3. restraint of the thermal expansion of the column; and
4. a possible car explosion.

The large scale simply-supported slab-column specimens avoided impacts of size effect. The distribution of the support points was slightly adapted from

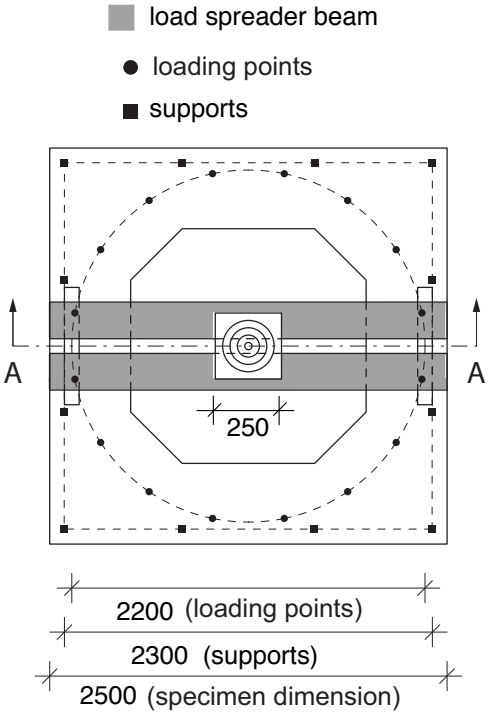

(a) Plan view

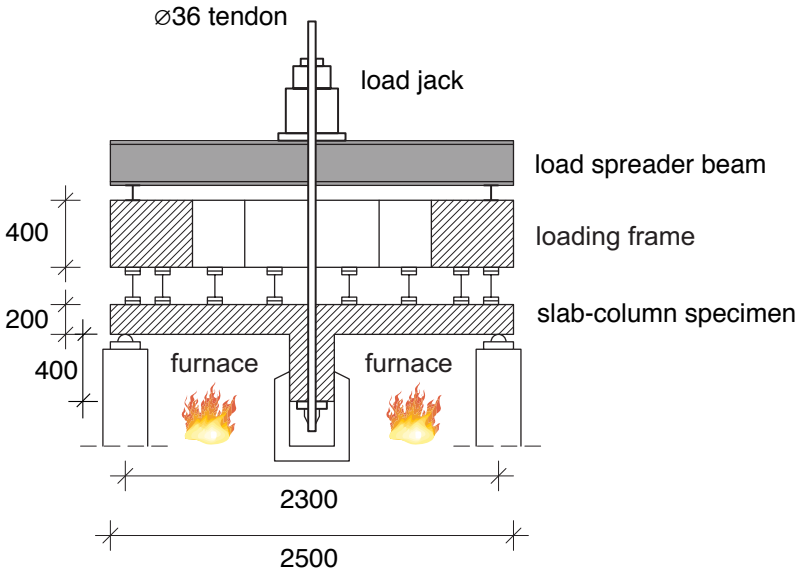

(b) Cross-section A-A

Figure 2.33: Kordina test set-up, adapted from Bamonte and Felicetti (2009) (dimensions in mm)

Kordina (1997) setup. The ambient tests were loaded until failure, whereas the heated tests were loaded until the service load (calculated from the ultimate design resistance, EN1992-1-1) and then heated according to a two hour ISO-834 fire curve with the load held constant. The tests that didn't fail during two hours of heating, were thereafter loaded until failure.

The experimental tests presented in Annerel et al. (2011b) analysed the contribution of the first action only, due to furnace and setup limitations. Annerel et al. (2011b) reported having accidentally overloaded a slab, which subsequently failed in punching shear after 20 minutes of ISO-834 fire. This failure highlighted a gap in knowledge of, restrained thermal elongations and curvatures increasing the axial load on a column. Annerel et al. (2011a,b) report the need to consider thermal restraints to understand the global structural response of underground parking structures.

Annerel et al. (2012) give full results and expand the discussion of the 6 punching shear slab tests presented in Annerel et al. (2011b). Annerel et al. (2012) reinforce that the tests only consider the impacts of their first listed consideration on punching shear strength, *"Because of limitations of the fire testing infrastructure, the supporting edges of the slabs are not restrained and only a short column stub of about 650 mm is provided"*. However, the safety factors (punching shear failure loads with respect to the service loads) show agreement with those found from Bamonte and Felicetti (2009) global structural modelling, which considered the effect of thermal curvature restraint (described in Section 2.4.2).

Residual ambient temperature testing after heated to elevated temperatures

Felicetti and Gambarova (2000) present 16 circular High Strength Concrete (HSC) punching shear, residual slab tests. Both unreinforced and reinforced slabs were tested residually after being cooled from elevated temperatures of 105, 250 and 400°C. Further details of the Felicetti and Gambarova (2000) testing is not given as the structural behaviour of HSC and residual ambient temperature testing varies greatly from the testing presented in this thesis.

Salem et al. (2012) present an experimental series of 14 residually tested RC slabs with dimensions, 1100×1100 mm and a depth of 100 mm. Comparative cooling methods of water and air were tested, as well as varying the concrete cover to investigate the sensitivity of punching shear to construction detailing.

During testing, the slabs were supported in an inverted orientation with roller supports along the sides of the square slab. The slabs were loaded downwards through the column stub and heated from below, on the tension slab face, with an oven. Salem et al. (2012) propose the critical punching shear failure in fire is when the main flexural reinforcement (tensile reinforcement)

degrades and loses strength. And that a greater decrease in punching shear capacity occurs when the fire impacts the column-slab connection from above the slab.

The thermal shock of water cooling compared to air causes larger crack widths, spalling and a 25% reduction in residual punching shear capacity. Salem et al. (2012) heating on the tension slab face causes the resulting behaviour to be different from the other research examined in this thesis.

2.4.2 *Modelling research*

Gretzenbach failure modelling

Bamonte and Felicetti (2009) used information available about the Gretzenbach failure, to question if the loss of punching shear capacity of an underground parking garage was dependant mainly on material decay or structural behaviour at high temperature. Bamonte and Felicetti (2009); Bamonte et al. (2009) detail a Finite Element (FE) structural model coupled with a fire zone-model. Bamonte et al. (2009) state that using only the standard fire curves (Eurocode 1) for analysis of underground parking garages is not sufficient as punching shear failure is much more complicated due to, *"thermal damage in the materials and redistribution of the internal forces"*.

Bamonte et al. (2009) build their analysis by considering:

- support conditions (simply supported and perfect rotational restraints, both with axial restraint);
- temperature distribution within the parking garage (modelled at a single compartment or 15 compartments); and
- two incremental non-linear analyses take account of the decay of the concrete elastic material modulus.
    1. concrete is considered as a linear elastic, uncracked section and the elastic modulus is temperature dependent
    2. concrete is a cracked section, again with the elastic modulus as temperature dependent

Bamonte et al. (2009) show that the thermal field from the natural fire is not as severe as the standard fire, because the 100 minutes natural fire duration is equivalent to 45 minutes ISO-834 fire. This in turn causes the material mechanical decay to be small, with a 10% decrease in shear capacity after 100 minutes. The redistribution of internal forces causes an increase of 30-60% in the punching force, making the structural behaviour critical. Bamonte et al. (2009) conclude that for the case presented there is great importance

in analysing the indirect actions caused by natural fires correctly, which the Eurocode (EC) generally under-evaluates by using a standard fire to assess the structural behaviour. The 'indirect actions' which the authors discuss, are not clearly outlined.

Bamonte et al. (2009) show that the axially restrained support conditions play a negligible role here, due to the columns limiting the vertical displacement of the slab. Furthermore if the external walls were fully restrained (axially and vertically), the displacements would be further reduced causing the critical column's vertical load to be *"hardly affected by the fire"*. However, while the support conditions play a limited role for this case, it is stressed that safety margins will be paramount for many redundant structures, where the thermal curvature is restrained by fixed supports.

Annerel et al. (2013) state their motivation at the beginning of the abstract as, *"Underground concrete structures composed of flat slab-column connections are sensitive to punching failure at ambient temperatures. During fire, however, due to the restraint of thermal curvatures an increase of the punching load can occur, possibly leading to premature collapse"*. Annerel et al. (2013) present a global structural analysis to investigate the gap in knowledge of restrained thermal elongations and curvatures increasing the axial load on a column highlighted in Section 2.4.1 by Annerel et al. (2011b). The analysis approach was based on Bamonte et al. (2009).

A review of car park fires between 2002-2007 is presented. The structural dimension data is taken from the real structural collapse in fire, of an underground car park in Gretzenbach (Muttoni et al., 2005). The columns are modelled as point supports with no transfer of bending moments or shear forces between the slab or column. The walls around the slab support are modelled as linear roller supports that provide no rotational or horizontal restraint. Annerel et al. (2013) assume that the deflection of the slab due to the thermal curvature will be much larger than that due to the elongation of the column, therefore the thermal elongation of the columns is ignored. Additionally, the slab is relatively thin compared to the columns of the underground car park.

Three fire scenarios are compared by varying; the sequence in which the cars ignite, time it takes for the fire to spread between adjacent cars, HRR standard fire curves for single car fires, and calculation methods. The fire scenario comparison shows the critical slab-column joints, are those at the corner of the fire, exposed to fire on 2-sides only (Figure 2.34a). The fire scenario where car 3 ignites first and the fire spreads to the other cars in Figure 2.34b causes the greatest increase on the column axial load.

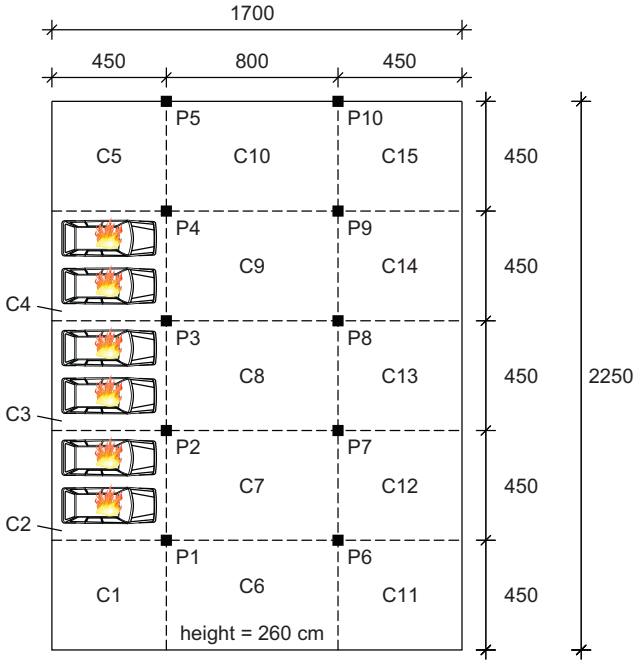

(a) Plan view geometry of the structure

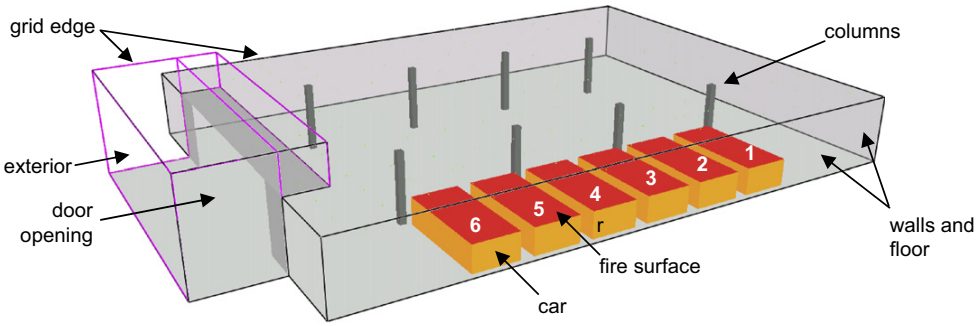

(b) Three-dimensional schematic of the numerical model

Figure 2.34: Plan and three-dimensional views of modelled structure, reproduced from Annerel et al. (2013)

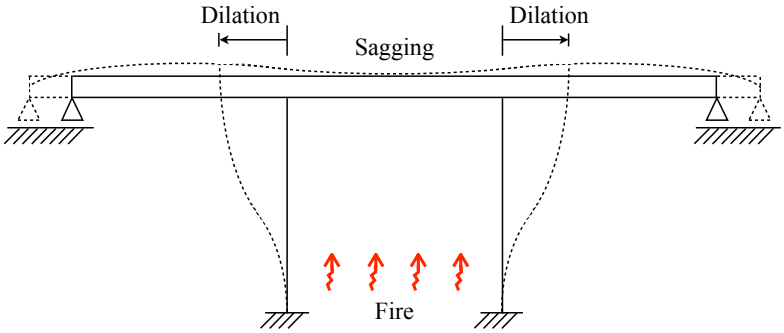

(a) Temperature induced displacements

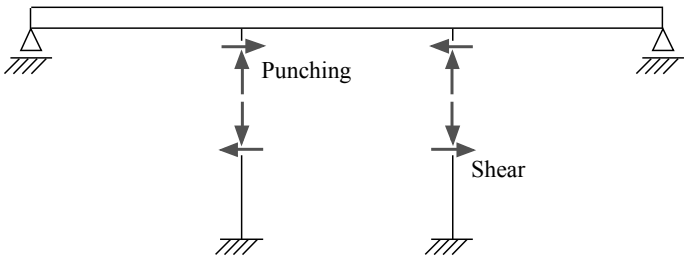

(b) Indirect actions

Figure 2.35: Impact of indirect actions on the structural behaviour of a flat slab in a fire, reproduced from Bamonte et al. (2012)

Critical Shear Crack Theory modelling

Punching shear failure in RC in fire is a combination of both a decrease in mechanical material properties, mainly strength and stiffness and indirect actions (Bamonte, 2011; Bamonte et al., 2012). Bamonte (2011); Bamonte et al. (2012) build on Bamonte et al. (2009) and outlines the indirect actions of thermal dilation and curvature, which impact the structure behaviour of a flat slab in a fire (Figure 2.35).

Bamonte et al. (2012) build on the mechanical-based approach of CSCT. The fundamental assumption of the CSCT is held true, *"diagonal shear crack forms at early loading stages and influences the behaviour of the whole slab-column assembly"*. The two backbone curves used in the CSCT, namely failure criterion and load-deformation curve (described in Section 2.2.1) are altered to consider the effects of elevated temperature. Similarly as with ambient temperature applications of the CSCT, the intersection of the two curves defines the elevated temperature punching shear failure load.

Equation 2.4 shows the total slab displacement is uncoupled into two displacement components of:

$$w_{tot} = w_{load} + w_{th}, \tag{2.4}$$

where:

$$w_{tot} = \text{total slab displacement (mm)}$$
$$w_{load} = \text{load-induced displacement (mm)}$$
$$w_{th} = \text{thermal displacement (mm)}$$

w_{load} accounts for material decay effects, mainly stiffness decrease, leading to a decrease in the ultimate strength for long fire durations. Whereas, w_{th} accounts for the thermal dilation of the hot layers of material, causing thermal curvature along the thickness of the slab. These are then summed and used in the calculation of both curves. Bamonte et al. (2012) introduce two assumptions:

1. *"outside the diagonal crack, the load-induced rotation* Ψ *is constant: therefore, the load-induced displacement* w_{load} *is a linear function of the radial coordinate, outside the diagonal crack"* and
2. *"the thermal displacement* w_{th} *is a* 2^{nd}*-order parabola of the radial coordinate"*

Bamonte et al. (2012) find a good comparison between limited experimental data from (Kordina, 1997) and their proposed adapted CSCT. Bamonte et al. (2012) clearly state that further experimental tests are needed to validate the adapted theory further, including experimental studies that consider the role of membrane stresses in structures that are restrained against thermal elongation.

2.4.3 *Research review*

Annerel et al. (2012) present a review of computational and experimental research of punching shear failure in fire. The impact on the punching shear capacity of a RC structure in fire is discussed, with three main considerations:

1. decrease in constitutive material strength and stiffness due to the elevated temperature, causing a lower punching shear capacity;
2. the concrete layers closer to the fire will expand more than the inner layers, causing a thermal curvature towards the fire. This curvature is restrained at the column-slab connection, which increases the support moment and therefore decreases the punching shear capacity; and
3. restraining the thermal expansion of the column can increase the axial load at the support. Moreover the restraint of thermal expansion of a column is considered not to impact the column's capacity if the axial load

can be redistributed to the surrounding structure via the slab-column connection. However, this redistribution may be reduced for flat slabs considering the connection punching shear capacity.

Ghoreishi et al. (2013) also present a state-of-the-art review of punching shear in RC flat slabs at ambient and elevated temperatures. Ghoreishi et al. (2013) report an extensive 215 ambient experimental tests of punching shear behaviour, which vastly outnumber the 37 tests at elevated temperature.

Ghoreishi et al. (2013) graph the influence of elevated temperature on the punching shear capacity for Annerel et al. (2012); Felicetti and Gambarova (2000); Ghoreishi et al. (2013); Kordina (1997). There is limited correlation, mainly due to the few test results available, however the one undeniable conclusion for the simply-supported tests presented, is that the punching shear capacity decreases with elevated temperature.

Ghoreishi et al. (2013) highlight the lack of experimental research of punching shear at elevated temperature and attribute this to the difficulty and high cost associated with high temperature punching shear test setups. Ghoreishi et al. (2013) state that the current research shows the punching shear capacity reduces by 20–30% (depending on reinforcement ratio) at elevated temperatures reaching 300°C, for a period of an hour or more.

2.5 EUROCODE REINFORCED-CONCRETE SHEAR DESIGN

The current state and shortcomings of the EC punching shear design are discussed. Section 2.5.1 presents the ambient RC EC2 shear design. Section 2.5.2 presents the prescriptive and performance elevated temperature EC2 shear design approaches and their shortcomings.

Different design codes for both ambient and elevated temperature punching shear design are outlined by Ghoreishi et al. (2013).

2.5.1 *Ambient temperature*

The current EC2 design code (BS EN 1992-1-1:2004, 2008) uses the truss analogy, outlined in Section 2.1.2, for shear design of beams. The punching shear design is based on semi-empirical relationships, outlined in Section 2.2. The EC2 ambient temperature punching shear stress design resistance of slabs without shear reinforcement is given by Equation 2.5 (BS EN 1992-1-1:2004, 2008).

$$v_{Rd,c} = C_{Rd,c} k (100 \rho_l f_{ck})^{1/3} + k_1 \sigma_{cp} \geq (v_{min} + k_1 \sigma_{cp}) \tag{2.5}$$

where:

$$\begin{aligned} C_{Rd,c} &= \frac{0.18}{\gamma_c} \\ k &= 1 + \sqrt{\frac{200}{d}} \leq 2.0 \\ \rho_l &= \sqrt{\rho_{ly} \cdot \rho_{lz}} \leq 0.02 \\ \sigma_{cp} &= \frac{(\sigma_{c,y} + \sigma_{c,z})}{2} \\ \sigma_{c,y} &= \frac{N_{Ed,y}}{A_{c,y}} \text{ and } \sigma_{c,z} = \frac{N_{Ed,z}}{A_{c,z}} \\ v_{min} &= 0.035 k^{3/2} f_{ck}^{1/2} \end{aligned} \tag{2.6}$$

where:

$v_{Rd,c}$ = design punching shear resistance of a slab without punching shear reinforcement along the control section (MPa)

$C_{Rd,c}$ = Country National Annex specific factor, as in (National Annex to BS EN 1992-1-1:2004, 2009)

γ_c = partial factor for concrete

d = effective depth of the slab (mm)

ρ_{ly}, ρ_{lz} = relate to the bonded tension steel in y- and z-directions, respectively. The values should be calculated as mean values taking into account a slab width equal to the column width plus $3d$ each side.

f_{ck} = characteristic compressive cylinder strength of concrete at 28 days (MPa)

k_1 = Country National Annex specific factor considering the effects of axial forces on the stress distribution, as in (National Annex to BS EN 1992-1-1:2004, 2009)

$\sigma_{c,y}, \sigma_{c,z}$ = normal concrete stresses in the critical section in y- and z-directions (MPa, positive in compression)

$N_{Ed,y}, N_{Ed,z}$ = longitudinal forces across the full bay for internal columns and the longitudinal force across the control section for edge columns. The force may be from a load or prestressing action. (N)

$A_{c,y}, A_{c,z}$ = area of the concrete according to the definition of N_{Ed} (mm^2)

2.5.2 *Elevated temperature*

The EC2 fire design of concrete structures allows for two approaches: prescriptive design or performance-based design.

Prescriptive design

Prescriptive design is the traditional method of designing the concrete cover to be sufficient so the reinforcement is insulated from the elevated temperature. The EC2 prescriptive shear resistance design of a RC cross-section in fire

can be applied via either the 500°C Isotherm or Zone method, as detailed in BS EN 1992-1-2:2004 (2010). These two methods use different approaches to decrease the cross-sectional geometry according to the temperature penetration of the fire. Additionally, they consider elevated temperature degradation by a reduction in the concrete compression and tensile strength (Figure 2.36) and steel tensile strength (Figure 2.37). The material strength reductions and reduced cross-sections are then assessed using the ambient shear design to find the shear capacity.

Prescriptive design shortcomings

The current EC2 punching shear design approach has been criticised. Bamonte (2011) highlight the current code limitations in designing for punching shear at elevated temperatures (CEN, European Committee for Standardisation. EN 1992-1-1), *"code equations were obtained on a semi-empirical basis, by operating a regression of the available experimental data: an immediate extension of these expressions to the case of fire is, therefore, highly questionable, to say the least."* Bamonte et al. (2012) suggest that understanding punching shear in fire requires a rational approach in the form of the physical-based CSCT model (discussed in Section 2.2.1 and Section 2.4.2).

There is no specific elevated temperature punching shear equation, rather the ambient equation is used and the temperature-dependant parameters are reduced according to factors. The only temperature-dependant parameter in Equation 2.5 is the characteristic compressive cylinder concrete strength at 28 days, f_{ck}. It is important to note that the reinforcement capacity is not considered in the calculation of the punching shear capacity, therefore its interaction in carrying shear is not considered.

The EC2 punching shear resistance calculation requires the check for k, shown in Equation 2.6. This stipulation indicates that EC2 design codes are written assuming an effective depth of flat slab equal or greater than 200 mm. This 200 mm slab thickness requirement is prevalent in EC2 design in both serviceability limit state design of crack control, and detailing of member and particular rules for solid slabs.

Anderberg et al. (2004) present background documentation to (BS EN 1992-1-2:2004, 2010) for concrete structural fire design. The only shear design alteration detailed in the documentation is the reduction in minimum slab thickness requirement from 200 mm to 180 mm for the fire resistance class of 60 minutes fire exposure for load-bearing, integrity and insulation criterion (REI 60). The alteration is justified by a reference to Kordina (1997) (tests outlined in Section 2.4.1). This change to EC2 design approach was accepted with the knowledge that Kordina (1997) testing did not consider the impact of in-plane

lateral restraint. Anderberg et al. (2004) reference Kordina summarising, *"The test arrangements were on the safe side, because there was no restraint for longitudinal expansion (in practice it increases shear capacity), neither membrane effect".*

EC2 tells the designer not to consider in-plane thermal expansion effects and consequently ignores the premature failure that can potentially occur (see Chapter 6) Ghoreishi et al. (2013). EC2 states that *"(4) Only the effects of thermal deformations resulting from thermal gradients across the cross-section need be considered. The effects of axial or in-plane thermal expansions may be neglected. (5) The support conditions at supports and ends of member, applicable at time $t = 0$, are assumed to remain unchanged throughout the fire exposure"* (BS EN 1992-1-2:2004, 2010).

The strength of the flexural steel at elevated temperature is reduced, however shear reinforcement strength is not considered. One of the shear reinforcement functions is to provide confinement (outlined in Section 2.1.1). Shear stirrups achieve this by being tied around the outside of the flexural reinforcement. Shear reinforcement decreases in strength at elevated temperatures and hence reduces its ability to transfer shear.

Performance-based design

Performance-based design is more commonplace, however requires a fundamental understanding of the behaviour in order to design. The approach often utilises modelling techniques, which make a full structural analysis more feasible. Analysing the whole structure ensures that the structural interaction in a fire environment is considered.

However, recent performance-based design has focussed on large displacement mechanisms and membrane action. Large deflections of steel in fire are feasible because it is a ductile material, however the brittle failure of punching shear failure does not require large deflections. This thesis aims to provide a fundamental understanding of punching shear at elevated temperature.

Material properties

Figure 2.36a shows the stress-strain relationship given in EC2 for uniaxial concrete in compression for different elevated temperatures, where adjustments are made for siliceous and calcareous aggregates. The tensile strength of concrete is ignored in EC2 design. Figure 2.37a shows the steel stress-strain relationship given in EC2 for different elevated temperatures, where adjustments are made for hot rolled and cold worked steel.

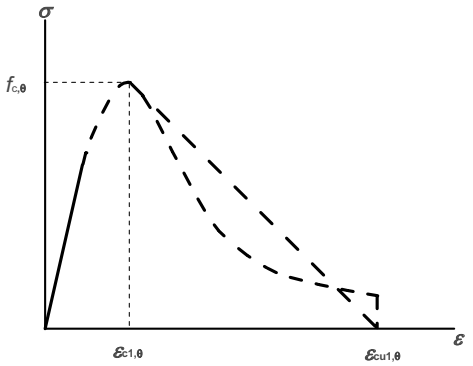

Range	Stress $\sigma(\theta)$
$\varepsilon \leq \varepsilon_{c1,\theta}$	$\frac{3\varepsilon f_{c,\theta}}{\varepsilon_{c1,\theta}\left(2+\left(\frac{\varepsilon}{\varepsilon_{c1,\theta}}\right)^3\right)}$
$\varepsilon_{c1(\theta)} < \varepsilon \leq \varepsilon_{cu1,\theta}$	For numerical purposes a descending branch should be adopted. Linear or non-linear models are permitted.

(a) Stress-strain variation at elevated temperature

Concrete temp.θ	Siliceous aggregates			Calcareous aggregates		
	$f_{c,\theta}/f_{ck}$	$\varepsilon_{c1,\theta}$	$\varepsilon_{cu1,\theta}$	$f_{c,\theta}/f_{ck}$	$\varepsilon_{c1,\theta}$	$\varepsilon_{cu1,\theta}$
[°C]	[-]	[-]	[-]	[-]	[-]	[-]
1	2	3	4	5	6	7
20	1,00	0,0025	0,0200	1,00	0,0025	0,0200
100	1,00	0,0040	0,0225	1,00	0,0040	0,0225
200	0,95	0,0055	0,0250	0,97	0,0055	0,0250
300	0,85	0,0070	0,0275	0,91	0,0070	0,0275
400	0,75	0,0100	0,0300	0,85	0,0100	0,0300
500	0,60	0,0150	0,0325	0,74	0,0150	0,0325
600	0,45	0,0250	0,0350	0,60	0,0250	0,0350
700	0,30	0,0250	0,0375	0,43	0,0250	0,0375
800	0,15	0,0250	0,0400	0,27	0,0250	0,0400
900	0,08	0,0250	0,0425	0,15	0,0250	0,0425
1000	0,04	0,0250	0,0450	0,06	0,0250	0,0450
1100	0,01	0,0250	0,0475	0,02	0,0250	0,0475
1200	0,00	-	-	0,00	-	-

(b) Normal weight concrete with either siliceous or calcareous aggregates

Figure 2.36: Compressed concrete stress-strain relationships at elevated temperature, reproduced from BS EN 1992-1-2:2004 (2010)

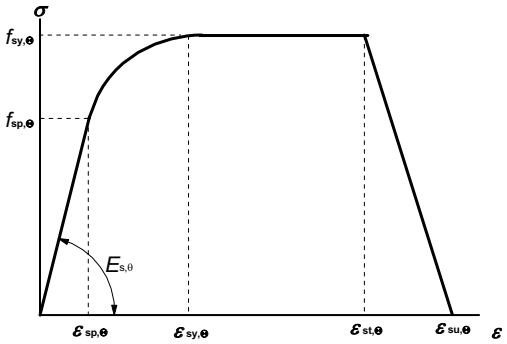

Range	Stress $\sigma(\theta)$	Tangent modulus
$\varepsilon_{sp,\theta}$	$\varepsilon E_{s,\theta}$	$E_{s,\theta}$
$\varepsilon_{sp,\theta} \le \varepsilon \le \varepsilon_{sy,\theta}$	$f_{sp,\theta} - c + (b/a)[a^2 - (\varepsilon_{sy,\theta} - \varepsilon)^2]^{0,5}$	$\frac{b(\varepsilon_{sy,\theta} - \varepsilon)}{a\left[a^2 - \left(\varepsilon - \varepsilon_{sy,\theta}\right)^2\right]^{0,5}}$
$\varepsilon_{sy,\theta} \le \varepsilon \le \varepsilon_{st,\theta}$	$f_{sy,\theta}$	0
$\varepsilon_{st,\theta} \le \varepsilon \le \varepsilon_{su,\theta}$	$f_{sy,\theta}\,[1-(\varepsilon - \varepsilon_{st,\theta})/(\varepsilon_{su,\theta} - \varepsilon_{st,\theta})]$	-
$\varepsilon = \varepsilon_{su,\theta}$	0,00	-
Parameter *)	$\varepsilon_{sp,\theta} = f_{sp,\theta} / E_{s,\theta}$ $\varepsilon_{sy,\theta} = 0,02$ $\varepsilon_{st,\theta} = 0,15$ $\varepsilon_{su,\theta} = 0,20$ Class A reinforcement: $\varepsilon_{st,\theta} = 0,05$ $\varepsilon_{su,\theta} = 0,10$	
Functions	$a^2 = (\varepsilon_{sy,\theta} - \varepsilon_{sp,\theta})(\varepsilon_{sy,\theta} - \varepsilon_{sp,\theta} + c/E_{s,\theta})$ $b^2 = c\,(\varepsilon_{sy,\theta} - \varepsilon_{sp,\theta})\,E_{s,\theta} + c^2$ $c = \frac{(f_{sy,\theta} - f_{sp,\theta})^2}{(\varepsilon_{sy,\theta} - \varepsilon_{sp,\theta})E_{s,\theta} - 2(f_{sy,\theta} - f_{sp,\theta})}$	

*) Values for the parameters $\varepsilon_{pt,\theta}$ and $\varepsilon_{pu,\theta}$ for prestressing steel may be taken from Table 3.3. Class A reinforcement is defined in Annex C of EN 1992-1-1.

(a) Stress-strain variation at elevated temperature

Steel Temperature	$f_{sy,\theta} / f_{yk}$		$f_{sp,\theta} / f_{yk}$		$E_{s,\theta} / E_s$	
θ [°C]	hot rolled	cold worked	hot rolled	cold worked	hot rolled	cold worked
1	2	3	4	5	6	7
20	1,00	1,00	1,00	1,00	1,00	1,00
100	1,00	1,00	1,00	0,96	1,00	1,00
200	1,00	1,00	0,81	0,92	0,90	0,87
300	1,00	1,00	0,61	0,81	0,80	0,72
400	1,00	0,94	0,42	0,63	0,70	0,56
500	0,78	0,67	0,36	0,44	0,60	0,40
600	0,47	0,40	0,18	0,26	0,31	0,24
700	0,23	0,12	0,07	0,08	0,13	0,08
800	0,11	0,11	0,05	0,06	0,09	0,06
900	0,06	0,08	0,04	0,05	0,07	0,05
1000	0,04	0,05	0,02	0,03	0,04	0,03
1100	0,02	0,03	0,01	0,02	0,02	0,02
1200	0,00	0,00	0,00	0,00	0,00	0,00

(b) Class N values for either hot rolled or cold worked steel

Figure 2.37: Reinforcing and pre-stressing steel stress-strain relationships at elevated temperature, reproduced from BS EN 1992-1-2:2004 (2010) (notations: p =prestressing, s =reinforcing steel)

2.6 SUMMARY

This section summarises the main shear in RC background at both ambient and elevated temperature from Chapter 2:

- The shear transfer mechanisms of: compressive force paths, tension zone concrete, concrete-steel bond, shear reinforcement, flexural reinforcement, dowel action, and aggregate interlock and their interaction in a RC beam have been extensively researched at ambient temperature. Whereas the transfer of shear at elevated temperature is not well understood and there have been limited pull-out and beam specimen tests.
- The shear capacity is influenced by size effect, therefore when scaling down test specimens this must be considered.
- The Critical Shear Crack Theory (CSCT) is a mechanical model which considers punching shear failure to be caused by a critical crack that penetrates through an inclined concrete compressive strut, transferring the load on the slab to the column. The rotation of the slab section relative to the column is used to find the capacity when the critical crack, and hence punching shear failure, is caused. Developing load-rotation relationships for restrained slabs would allow the influence of support conditions to be investigated numerically. CSCT was used as a basis of the experimental work presented in this thesis.
- Isolated slab-column tests are often undertaken to investigate punching shear behaviour, however they often do not assess the factors: support condition, confinement, load re-distribution, and in-plane restraint forces. Isolated slab-column specimen type was tested in this thesis.
- When investigating shear behaviour, it is critical to understand the whole structural behaviour and not just the isolated slab-column behaviour.
- Shear at ambient temperature is not well understood and temperature gradient effects through the RC section add complexities of:
    1. the steel and concrete individually degrade with time, inducing strength and stiffness losses;
    2. the shear transfer mechanisms change with time, as the elevated temperature heat front penetrates through the member;
    3. internal, self-equilibrating thermal restraint affects the shear transfer mechanisms; and
    4. external thermal restraint actions from the whole structural response.

- A total of 51 elevated temperature punching shear tests have been undertaken, where 30 of them were residually tested to failure at ambient temperature.

- Kordina (1997) reported that all the tests had deflections towards the fire and opposite from the loading direction. The 4 earlier tests only recorded this behaviour during the first 30 minutes of the fire, after which the deflection reversed.

- No elevated temperature punching shear testing has varied the support conditions, though the impact of restrained thermal curvature by fixed supports is critical for many redundant structures Bamonte et al. (2009).
  - Annerel et al. (2011b) reported having accidentally overloaded a slab, which subsequently failed in punching shear after 20 minutes of ISO-834 fire. This failure highlighted a gap in knowledge of, restrained thermal elongations and curvatures increasing the axial load on a column. Annerel et al. (2011a,b) report the need to consider thermal restraints to understand the global structural response of underground parking structures.
  - Bamonte et al. (2009) state that using only the standard fire curves (Eurocode 1) for analysis of underground parking garages is not sufficient as punching shear failure is much more complicated due to, *"thermal damage in the materials and redistribution of the internal forces"*.

- Bamonte et al. (2012) build on the mechanical-based approach of CSCT and consider the elevated temperature implications, though state that experimental tests are needed to validate the adapted theory.

- EC2 elevated temperature prescriptive, RC punching shear design has been criticised by Bamonte (2011), *"code equations were obtained on a semi-empirical basis, by operating a regression of the available experimental data: an immediate extension of these expressions to the case of fire is, therefore, highly questionable, to say the least."*

- EC2 tells the designer not to consider in-plane thermal expansion effects and consequently ignores the premature failure that can potentially occur Ghoreishi et al. (2013).

- The reinforcement capacity is not considered in the calculation of the punching shear capacity in EC2 design, therefore its interaction in carrying shear is not considered.

- EC2 performance-based design often utilises modelling techniques, which make the whole structural interactions feasible to analyse. Performance-based design requires a fundamental understanding of the behaviour, which is what this thesis aims to provide for punching shear at elevated temperature.

3

BACKGROUND TO DIGITAL IMAGE CORRELATION

This chapter describes the current research application of Digital Image Correlation (DIC) as an instrument to optically measure displacement and strain distributions during experiments. DIC was used in both the shear block and slab-column experimental series to measure displacement only.

Off the shelf Digital Single-Lens Reflex (DSLR) cameras were used in the experiments to take high-resolution photos of the specimen surface, at regular intervals throughout testing. The photo stream was then post-processed using software to calculate the movement of pre-defined regions in the images. The post-processing technique is named Digital Image Correlation (DIC). The pre-defined regions of interest are called patches and are defined on the first image to be analysed and are then tracked in subsequent defined images. The post-processing output gives the pixel patch co-ordinates in each image analysed. The calculated displacement needs to be converted from a pixel measurement to object space mm measurement, via a conversion factor. The factor is found as a ratio of a known predefined length in a photo taken prior to testing, to the measured pixel length in the image.

The whole specimens surface requires a unique visual texture to allow the patches selected to be tracked within the defined search zone. The visual texture is therefore an important test variable to optimise, as it impacts patch size and hence computation time. The visual texture can be optimised by varying the intensity and distribution of pixel colours.

A bespoke post-processing software called geoPIV8 (White and Take, 2005b) was used to track the motion of selected patches from image to image. GeoPIV8 uses a normalised cross-correlation to calculate the co-ordinates of the patches and runs within MATLAB®. The patch size, image order, etc. are all defined in the program commands.

3.1 TECHNIQUE DEVELOPMENT

The technique of Particle Image Velocimetry (PIV) named here as DIC, was initially developed in the field of experimental fluid mechanics to measure velocity (Adrian, 1991). It was originally implemented to analyse images of a region of flow to calculate local velocities. The flow was seeded with particles to allow features for the image processing to track. White et al. (2003b) modified and tested PIV to measure soil deformations in geotechnical experiments. Sand

provided not only a natural texture with different coloured grains to track, but illuminating the sand grains caused further features of light and shadow. Seeding became obsolete for the geotechnical sand grade application. When using PIV for planes of clay, the addition of coloured flock material or dyed sand was required for texture. Flock is mainly finely cut natural or synthetic fibres, which are dispersed onto a surface to produce a texture and reduce the surfaces reflectivity.

3.2 VALIDATION

White et al. (2003a) undertook DIC validation experiments that showed the distances measured by DIC have an accuracy of a tenth of a pixel. The application of DIC in geotechnics used the assumption that a single scale conversion factor can be used to convert pixel coordinates to object plane coordinates. The validity of the assumption depends on the camera behaviour conforming to; the pinhole model, the object plane is parallel to the plane of the camera and the pixels are square. However, these assumptions are rarely all satisfied for short focal length digital images, therefore image distortion is caused. Image distortion is the spatial variation in the image scale. White et al. (2003a) identified several sources of image distortion:

- the practical experimental assembly means that only approximate parallel alignment of the object plane and camera plane can be achieved;
  - Slight misalignment of the planes causes a relatively large error compared to that of the precision of DIC. A rigid body motion corresponding to 10 *pixels* in the centre of the image would therefore be seen as 10.03 and 9.97 *pixels* at the edges.
- radial and tangential lens distortion; and
  - Radial distortion is caused by light rays that are deflected radially from the normal to the lens, also known as fisheye.
  - Tangential lens distortion causes de-centring distortion, which has both a radial and tangential component. Tangential distortion is caused by light being refracted because the centres of curvature of the lens surfaces are not collinear.
- camera pixels are non-square.
  - This is only a small correction and is easily implemented by a linear scaling factor in the pixel to object-space co-ordinate conversion, constantly across the image.

DIC was first used in structural engineering for taking strain measurements in Fibre-Reinforced Polymer (FRP) confined concrete columns (Bisby et al., 2007). Bisby and Take (2009) gives a validation of the DIC technique applied to structures.

3.3 STRUCTURAL TESTING APPLICATION

The digital image analysis technique has only recently become realistic for the small displacements that are important for structural engineering research, and as a consequence there remain a number of challenges in its use. For example, for very small displacements pincushion lens distortion can mask the measurements. There are further image distortion unknown effects relating to the application, for example when the images are taken through the window in a furnace or oven, high temperatures are present during fire testing. Gales et al. (2012) demonstrated that implementing DIC on a case-by-case basis is an effective method of recording displacement without the difficulties inherent in traditional contact methods of measurement at high temperatures.

The DIC measurement technique is sensitive to errors, which requires certain considerations when using DIC for structural testing applications:

- protect camera from mechanical damage, e.g. heat application or broken concrete pieces;
- stable camera mounting;
- lighting of the measurement surface;
  - lighting in-front of the camera lens, to avoid the camera equipment from over heating and causing image distortion
  - balanced lighting to limit shadows being projected onto the object plane
  - opposite symmetrical lighting must not be visible in the testing images
- texture application of the measurement surface;
  White and Take (2005a) give practical guidance for the use of artificial textures: If colour is imparted onto material, it should be of maximum contrast to the underlying material. Additionally, *"texture should be fine enough to give a high spatial brightness frequency, but not so fine that the contrast between the texture and the soil is lost, giving a uniform brightness across the image. The focus should be sharp in order that high frequency texture is not lost by blurring"*.

  - must be unique to decrease post-processing errors
    White et al. (2003b) states that errors can occur with DIC, *"If the correct correlation peak is drowned by random noise on the correlation plane an incorrect, or 'wild', vector will be recorded. To eliminate this possibility, the 'initial' image, in which the test patches are established, is updated at intervals during the analysis"*.
  - continuous texture of matt shades to reduce reflection
  - paint colour deterioration with high temperature must be considered

- accurate measurement of camera orientation relative to measurement surface (to assist in further post-processing analysis);
- camera body and lens combination needs to suit the test and measurement requirements;
- camera and lens settings (turn off autofocus and image stabilisation, as they can cause automatic lens and focus adjustments between images, which leads to post-processing errors); and
- sources of image distortion were mentioned in Section 3.2.

Furthermore Smith (2010) highlighted errors caused by lens distortion for structural testing applications, which can be corrected by post-processing.

4

SHEAR BLOCK EXPERIMENTS

This chapter presents the design, methodology and results of the preliminary Mattock style shear block experiments. Chapter 2 described the importance of transfer mechanisms in understanding the fundamental behaviour of shear. The shear block tests were undertaken to build a fundamental understanding of the shear transfer mechanisms and their interactions in RC after being exposed to elevated temperature. The simplified pure shear behaviour in the block tests allow for the mechanisms to be investigated in isolation to the complex three dimensional punching shear interactions.

4.1 DESIGN PHILOSOPHY

The design concept was similar to the shear blocks tested by Mattock and Hawkins (1972), however a modified geometry was adopted, based upon that used by Mohamed Ali et al. (2008), shown in Figure 2.8. Shear blocks are designed to load a RC section in pure shear, and hence fail by cracking along the central shear plane, shown in Figure 2.8. The behaviour of this crack is characterised by the shear mechanisms of aggregate interlock, concrete-steel bond and dowel action, and is particularly relevant to the shear failure of columns where aggregate interlock is mobilised due to the confinement provided by the axial force in the column.

The shear block dimensions were governed by the physical size and thermal mass that could be effectively heated in the available electric furnace.

The shear block tests were undertaken residually, hence the specimens were tested to failure once they had cooled to ambient temperature. This is supported by Naus (2005) concrete testing, which showed that residual quartz aggregate concrete yields conservative compressive strengths in comparison to testing at high temperature.

Concrete compression and tension tests were conducted in accordance to BS EN 12390-3:2002 (2009) and BS EN 12390-6:2000 (2004), respectively. A cylinder compression and split-cylinder tension test accompanied each shear block test.

4.2 SPECIMEN DESIGN

A series of sixteen shear blocks were constructed and tested with dimensions 100×160×320 mm. Twelve shear blocks were heated to the target temperatures: 112, 188, 390, 475 and 622°C to expose the specimens to a wide range of elevated temperatures, starting at 112°C when vaporisation of water in the concrete has been initiated, to above 390°C as the residual compressive strength starts to decrease much more. Figure 2.27 shows the physicochemical processes undertaken in concrete at elevated temperature. The heated specimens were tested after cooling to find their residual strength. Four unheated specimens were tested at ambient temperature as a baseline.

Figure 4.1 shows the dimensions and test setup for the shear block experiments. The specimens were reinforced with 6 mm diameter smooth mild steel bars with an ambient yield strength of 415 MPa. Figure 4.2 shows that four pieces of reinforcement crossed the shear failure plane, with additional reinforcement to provide anchorage and to prevent failure of the concrete away from the shear plane. The concrete was supplied by a local ready-mix supplier with a maximum aggregate size of 10 mm, an average ambient compressive strength, f_c of 29 MPa (based upon cube tests), and an average ambient tensile strength, f_t of 1.8 MPa (based upon split-cylinder tests).

After removal from the moulds, the specimens were cured in a water tank for one week, followed by seven weeks in a controlled low humidity environment. To reduce the moisture content of the specimens and hence minimise the likelihood of spalling, the specimens were pre-dried at 90°C for seven days. Two standard 100 mm cylinder specimens were cast for each shear block, and these were conditioned in the same way.

4.3 ELECTRIC FURNACE HEATING

The electric furnace used could accommodate one shear block and two cylinders at a time. They were heated to target temperatures of 112, 188, 390, 475 and 622°C. Figure 4.2 shows that a thermocouple was placed at the centre of the shear block to record the internal temperature. A second thermocouple was inserted into the furnace to record its temperature. The specimens were heated as fast as the furnace was capable, with a temperature increase rate ranging from 5–15°C/min. After the initial heating, the furnace was controlled manually to achieve the required temperature inside the concrete. All specimens were heated for 120 minutes, except for those at the highest temperature, for which it was necessary to increase the heating duration to 165 minutes.

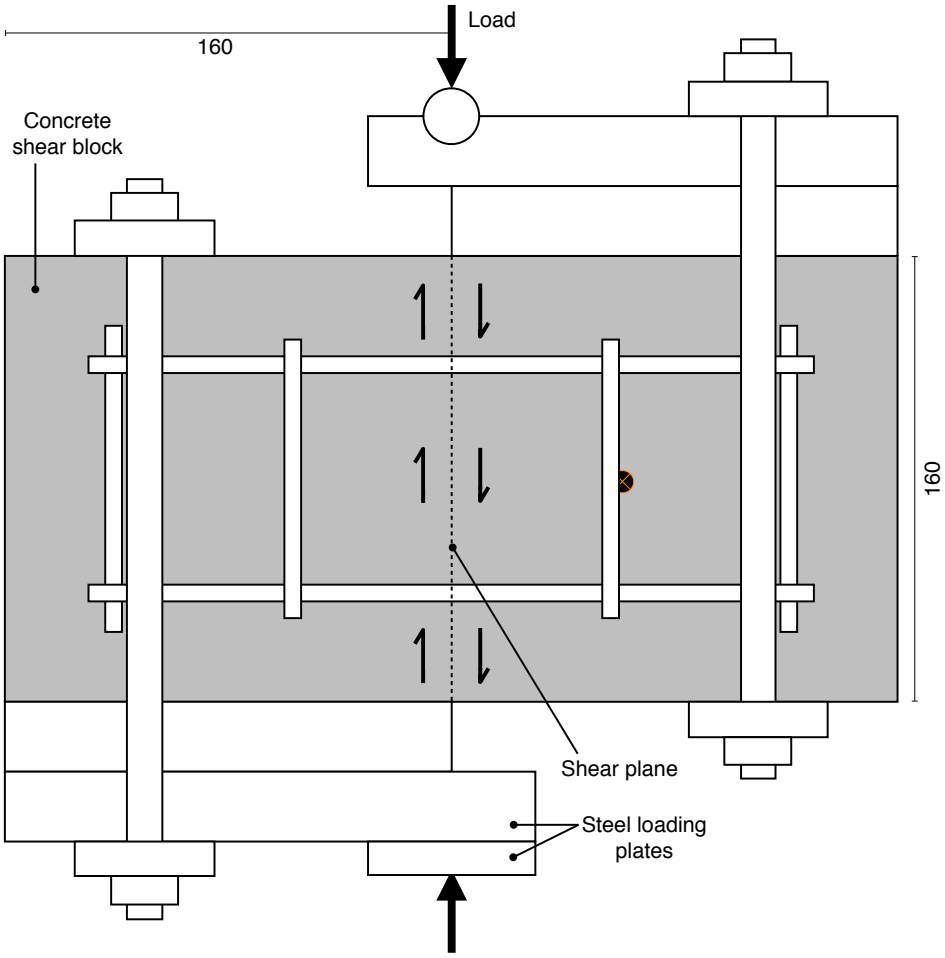

(a) Side view schematic

(b) Photo prior to testing

Figure 4.1: Shear block test setup

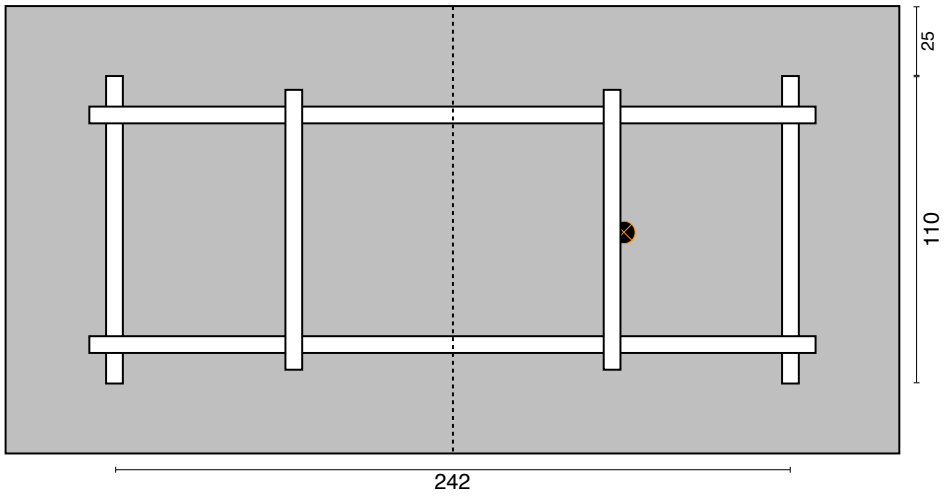

(a) Side view

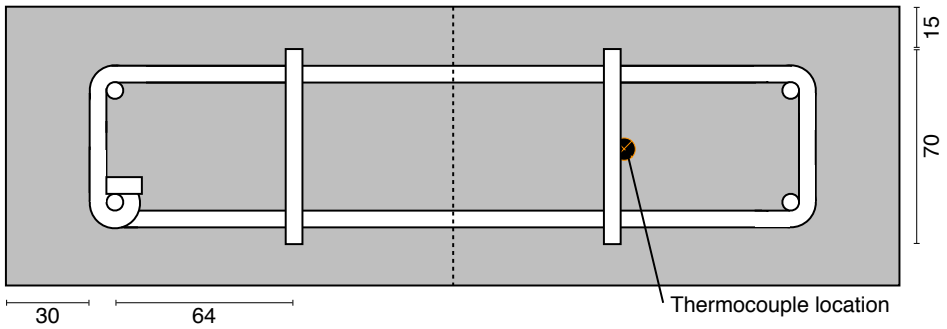

(b) Plan view

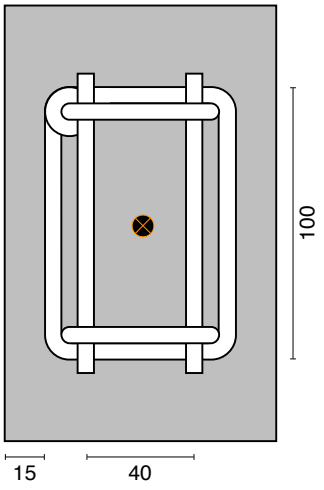

(c) End view

Figure 4.2: Schematic of the shear block reinforcement

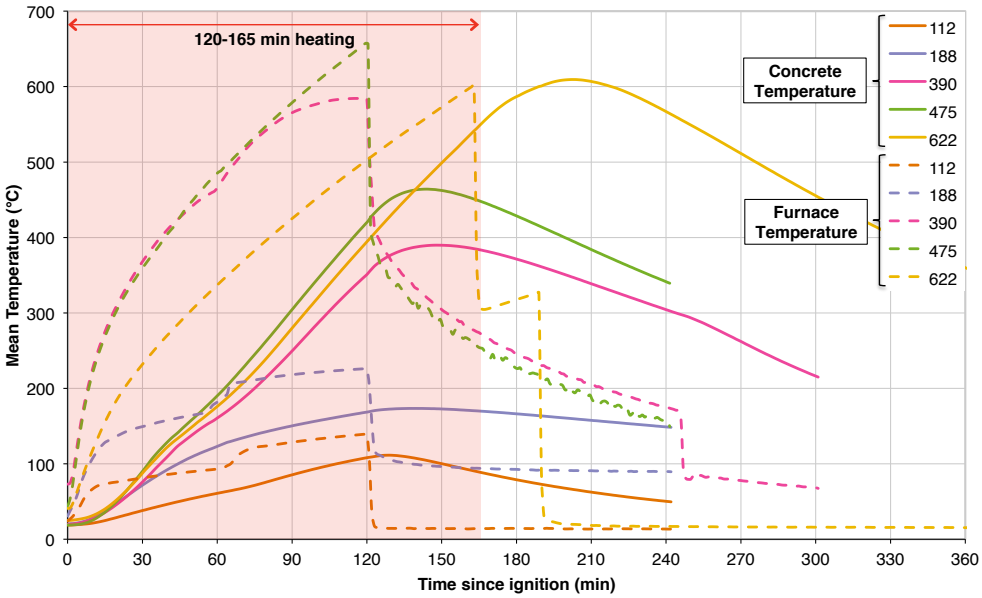

Figure 4.3: Temperature curves in the furnace and within the concrete blocks

After heating, the specimens were left in the furnace to cool, and each shear block was left for seven days before it was tested to failure.

Figure 4.3 shows the heating and cooling temperatures recorded within the furnace and the concrete blocks.

4.4 HYDRAULIC LOADING

Figure 4.1 shows that steel loading plates were attached to the shear block to force shear failure. The specimens were loaded using a hydraulic universal test machine at an initial rate of 20 kN/min, with the applied load recorded using a load cell.

4.5 DISPLACEMENT INSTRUMENTATION

DIC was used to obtain the specimen displacements from a sequence of 21 megapixel photographs taken at a frequency of 0.2 Hz. The specimen surface was painted with a high-contrast black and white speckle pattern prior to testing, and geoPIV8 (White and Take, 2005b) was used for post-processing. The resolution of DIC for this application was of the order of 0.006 mm.

DIC was chosen for these tests rather than a traditional displacement measurement technique because it allows:

- positions at which displacements are measured to be selected after the test;

- relative displacements to be measured within the concrete (hence avoiding the effects of local crushing at the supports);
- both the shear displacement and crack opening displacement to be measured across the cracked surface; and
- variations in displacement along the crack surface to be observed.

4.6 RESULTS AND ANALYSIS

Smith et al. (2011) outlines in detail the shear block experimental results, which include:

- strength variation with temperature;
- load-displacement response; and
- crack opening width development.

Section 4.6.1 presents the variation in compressive and tensile strength of the concrete cylinder strength specimens, which accompanied each shear block. The average concrete strength is compared to the shear block failure load at elevated temperature. Section 4.6.2 presents the behaviour of the load against shear displacement measured across the crack. Section 4.6.3 presents the DIC crack opening widths that developed as the shear blocks were loaded. Table 4.1 gives an overview of the test programme and key results.

4.6.1 *Strength variation with temperature*

Figure 4.4 compares the residual concrete compressive and tensile strengths for different maximum elevated temperatures. The concrete strengths are normalised by the ambient temperature strength and the average strength variation has been shown. The concrete strength reduces with elevated temperature as expected, but it should be noted that some of the specimens were impacted by poor compaction.

The shear block strength with elevated temperature is also plotted for comparison in Figure 4.4. The shear strength follows a similar trend to the concrete strength variation. The reduction in shear strength at high temperatures is less pronounced, because the shear block strength is dependent upon the strengths of both the concrete and steel.

SPECIMEN ID	HEATING DURATION (MIN)	TARGET INTERNAL TEMPERATURE (°C)	ACHIEVED PEAK INTERNAL TEMPERATURE (°C)	COMPRESSIVE CONCRETE STRENGTH (MPA)	TENSILE CONCRETE STRENGTH (MPA)	SHEAR FAILURE LOAD (KN)	FRICTIONAL SHEAR STRESS (MPA)
17-1			17.2			100.5	-
17-2			17.0			93.7	-
17-3	-	17	17.1	25.1	4.1	110.5	3.5
17-4			17.5			119.2	2.6
112-1			102.7			103.5	2.9
112-2	120	112	109.2	26.9	3.7	97.5	3.9
112-3			122.6			102.0	2.7
188-1			178.1			93.0	2.4
188-2	120	188	191.2	27.8	3.9	88.5	3.6
188-3			196.1			106.3	3.3
390-1			379.9			91.0	1.9
390-2	120	390	399.8	19.3	2.5	95.0	3.3
475-1			464.1			79.8	-
475-2	120	475	486.5	17.5	2.2	81.8	1.5
622-1			619.9			71.8	1.8
622-2	165	622	624.4	12.6	1.8	67.9	1.8

Table 4.1: Shear block test programme and key results

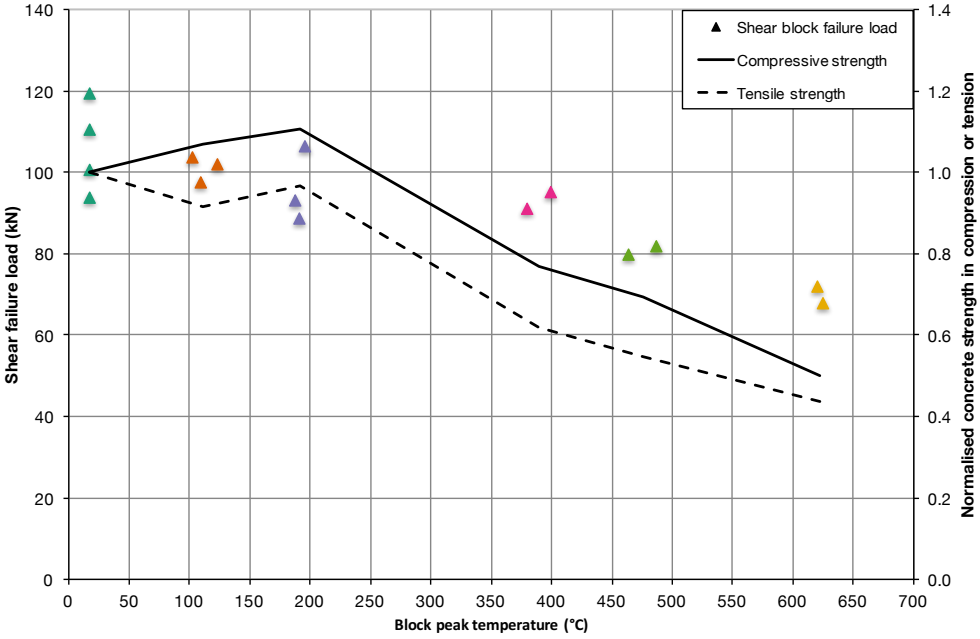

Figure 4.4: Effect of temperature upon the residual strength of the shear block, and upon the residual concrete compressive and tensile strengths

4.6.2 *Load-displacement response*

Figure 4.5 shows the applied load versus shear displacement, measured across the crack. For clarity, one load-displacement has been plotted for each temperature; these were chosen to be a good representation of the full set of results; other responses were similar. The load-deflection response of the shear blocks has an initial peak load, at which point the shear crack fully forms and the shear capacity drops to a frictional value that is governed by aggregate interlock, confinement by the reinforcement, and reinforcement dowel action. The initial stiffness and the peak strength of the specimen reduced with temperature, whereas the displacement corresponding to the peak strength increased with temperature.

The post-peak frictional shear strength was also affected by temperature, with two clear groups apparent: the lowest three temperatures carried a frictional shear of 50 kN; the highest three temperatures carried a frictional shear of 25 kN. At the three lower temperatures, diagonal tension cracks initially formed at an angle to the shear plane, which coalesced into a single shear crack. The reinforcement sheared across the crack, and caused some separation of the cover concrete.

At the three higher temperatures, the straight shear crack formed immediately. Cover concrete bursting was far more extensive, and this allowed the reinforcement to debond and reduced confinement of the shear crack. The aggregate could also be heard to "snap" during the higher temperature residual

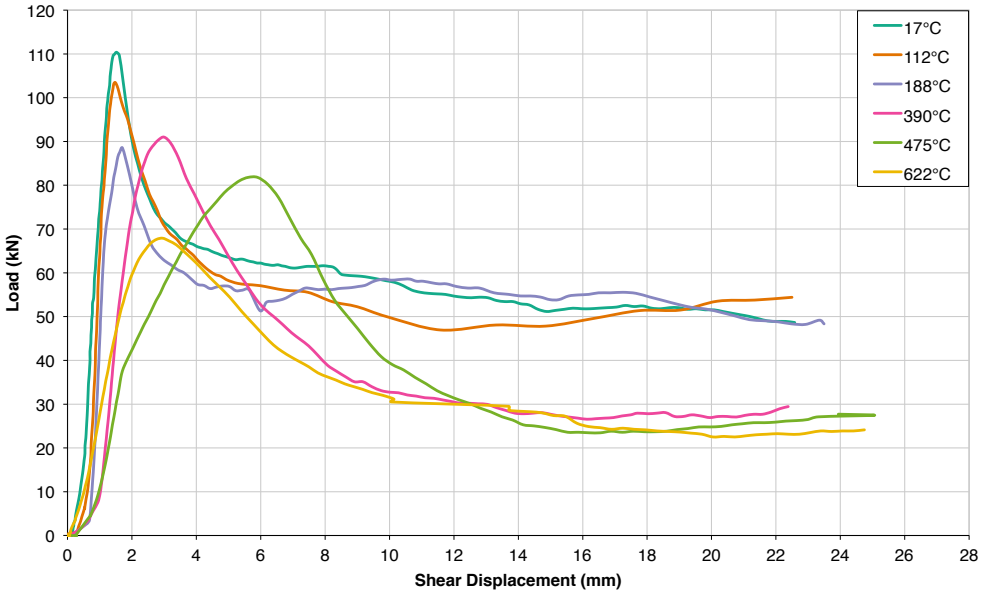

Figure 4.5: Effect of temperature upon the residual load-displacement response of shear blocks

tests. Consequently, the performance of the shear blocks was governed by a combination of the residual strength of the concrete, the residual strength of the reinforcement and the complex interaction between the two.

4.6.3 *Crack opening width development*

DIC was used to determine the crack opening widths that developed as the load was applied, and these are shown in Figure 4.6. The response is again split into two groups, with the three higher temperatures characterised by larger crack opening displacements, even prior to the peak load being reached.

4.7 SUMMARY

These bullet points summarize the key findings from the preliminary Mattock style shear block experiments:

- The residual shear strength of RC is reduced by elevated temperature.
- The reduction in shear performance depends upon the interaction of the concrete and the reinforcing steel.
- The initial shear block stiffness and peak strength reduced with elevated temperature, whereas the shear displacement corresponding to the peak strength increased with elevated temperature.

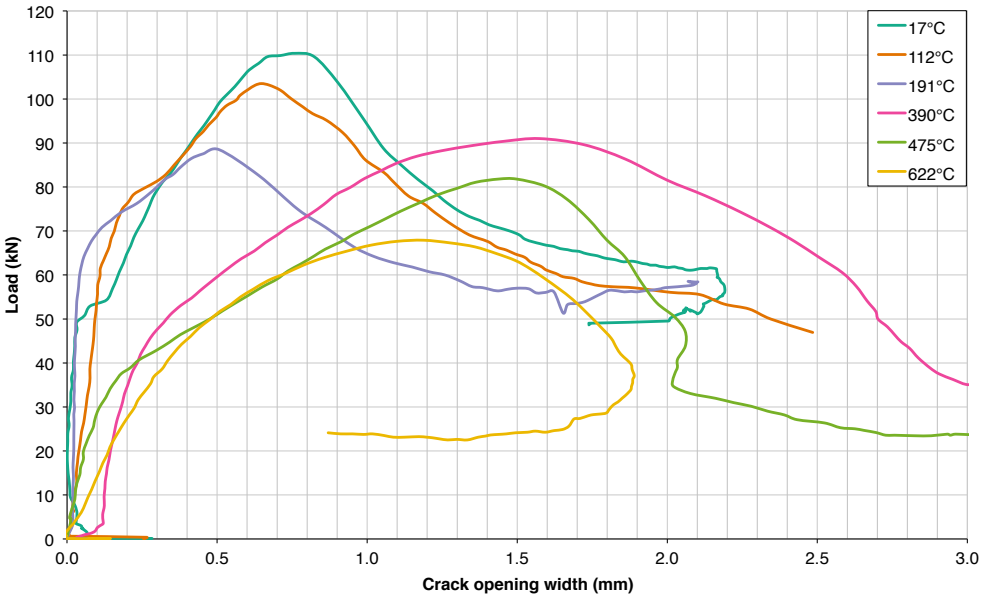

Figure 4.6: Effect of temperature upon the residual crack opening width development of shear blocks

- The post-peak frictional shear strength was clearly impacted by elevated temperature. There were two load-displacement responses. Specimen subjected to elevated temperatures up to 188°C carried a post-peak frictional shear of 50 kN, whereas those subjected to temperature above that and up to 622°C carried 25 kN.

- The DIC measured crack opening width was again split into the same two behavioural groups. The specimens subjected to elevated temperatures in the range 188°C to 622°C had larger crack opening displacements even prior to the peak load having been reached, in comparison to the lower temperature group.

5

PUNCHING SHEAR SLAB-COLUMN EXPERIMENTAL DESIGN AND METHODOLOGY

This chapter presents the design and methodology of a large punching shear slab-column test series. Fifteen isolated slab-column specimens were tested at ambient and elevated temperature to investigate the punching shear behaviour within a whole structure. This test series increases the current recorded elevated temperature, RC flat slab punching shear tests by 50%.

Chapter 2 highlighted the lack of knowledge regarding the impact of restraint on the behaviour of punching shear failure. A purpose built reaction frame allowed the support conditions of the specimens to be varied as either simply supported or fully restrained. These three-dimensional tests allow the affects of: in-plane actions that result from restrained thermal expansion, large deflection load-carrying mechanisms and degradation of material properties on punching shear in fire to be investigated.

The ambient tests were conducted using a displacement rate of 2 mm/min to determine their ultimate capacity. These ambient tests results were first used to calibrate a capacity model using Guandalini et al. (2009) approach (recognising the inherent variability of the small number of ambient test results). This model was used to calculate the sustained load to be applied during the heated tests, which was taken to be 70% of the ambient capacity (in accordance with BS EN 1992-1-2:2004 (2010)). Note that the same load was applied to both the restrained and unrestrained slabs because, according to EC ambient design methods the punching shear capacity is not influenced by the edge restraint.

Similarly to the ambient tests, the elevated temperature test slabs were loaded at a displacement rate of 2 mm/min up to 70% ambient slab capacity. This load was held constant as the slabs were heated for 120 minutes using the gas radiant panels or until slab failure occurred. These tests did not attempt to follow a standard fire curve. The radiant panels applied a nominal heat flux at slab surface of approximately 50 kW/m^2. For the slabs that did not fail during the 120 minutes of heating, the applied load was maintained whilst the slabs cooled until temperatures dropped below 150°C throughout their depth, and then the load was removed at a displacement rate of 2 mm/min. Residual strength tests were conducted the following day to those specimens that did not fail during heating.

A detailed test schedule can be found in Appendix H.

Concrete compression and tension tests were conducted in accordance to BS EN 12390-3:2002 (2009) and BS EN 12390-6:2000 (2004), respectively. Throughout the slab-column specimen testing (detailed in Table 6.3), cylinder and cube compression and split-cylinder tension tests were undertaken.

The chapter details the design philosophy of the test series, specimen design, test arrangement and instrumentation used. All instrumentation calibration is presented. Health and safety considerations including; laboratory induction, machinery and gas safety training and project specific paperwork were undertaken prior to the laboratory work commencing. Project specific safe systems of work, risk assessments and control of substances hazardous to human health were completed in accordance with The University of Edinburgh health and safety policies (Appendix A).

5.1 DESIGN PHILOSOPHY

The specimen design evolved from one-way slab or half an isolated slab-column specimen (Figure 5.1a) to a whole two-way slab-column specimen (Figure 5.1b). The one-way slab choice would not have allowed flat slab punching shear transfer actions to be investigated as it was only one- rather than two-way spanning. The half isolated slab-column design was difficult to implement, because the complex shear and moment interactions between the slab and column stub would have had to be externally simulated along the open cross-section. However, the visible cross-section allowed the advantage of visualising shear transfer mechanisms and the crack pattern development within the specimen during testing. It would also have allowed DIC measurements to be utilised. However, restraining the open cross-section while also being able to keep a line of sight of the cross-section, caused extensive design difficulties. Figure 5.1b type was chosen for the specimen design.

Figure 5.2 shows the reaction frame with integrated six radiant panel array, which was modified for punching shear and used for the slab-column specimens presented herein. All the slab-column test Figures in Chapter 5 show the restrained support condition on the right hand half and the unrestrained support condition on the left hand half. It is important to note that both support conditions would not be applied to the same slab, rather either one or the other.

Fox (2013) details the original design of the reaction frame with radiant panel array, which allowed a slab specimen to be tested under variable restraint conditions at elevated temperature. The slabs were supported in the structural reaction frame in an inverted orientation, with the column stub above the slab. The gas radiant panels heated the slabs from above and hydraulic jack loaded

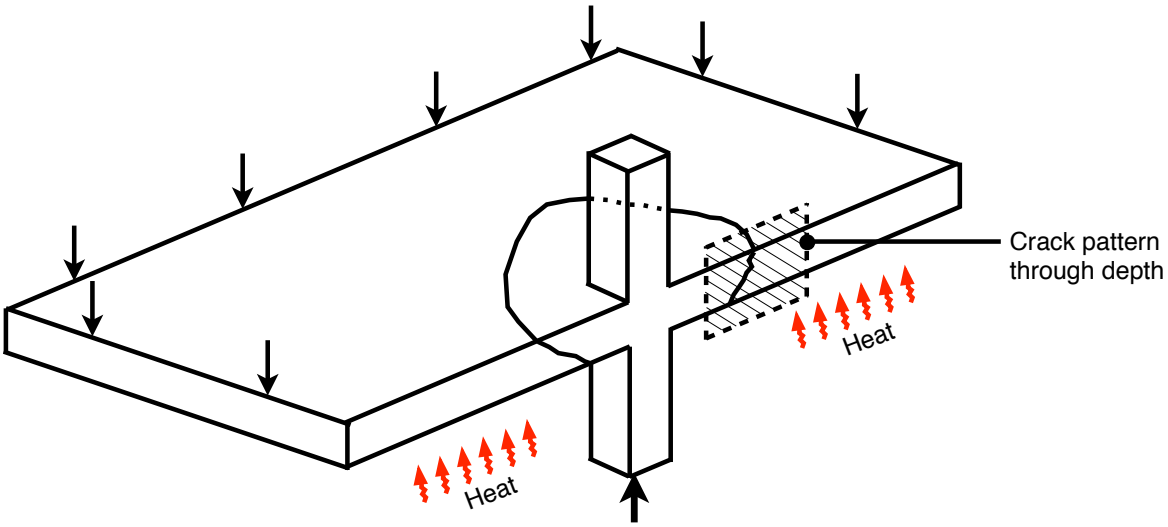

(a) Half isolated slab-column specimen

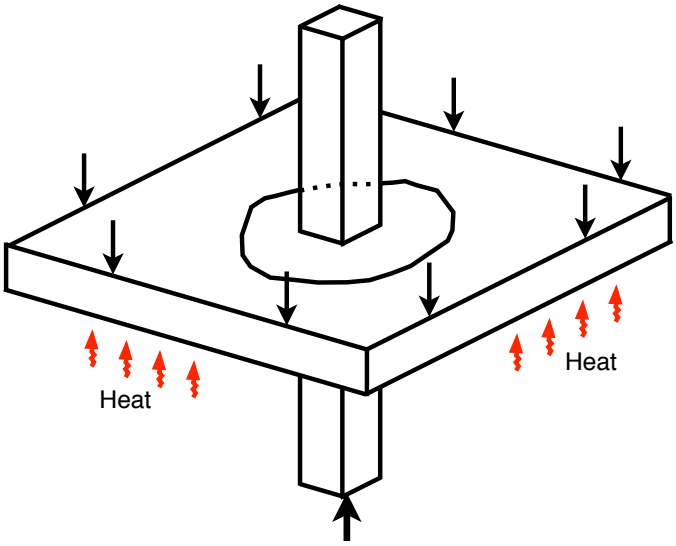

(b) Two-way slab-column specimen

Figure 5.1: Evolution of specimen design

the slab through the column stub from below. The traditional test setup was inverted to allow:

- reduced risk of broken concrete pieces damaging the delicate and expensive radiant panels;
- the specimen to be heated by radiation and convective currents. The reaction frame was insulated from conductive heat transfer and convective hot gases were directed away; and
- the laboratory strong floor to be used to react the tensile hydraulic jack against.

A disadvantage of the inverted test setup is the additional load of the specimens' self weight under gravity, which acts in the opposite direction. It is calculated as negligible (2–4%) compared to the slabs' shear capacity (ignoring the unreinforced slabs).

The test variables chosen were:

- restraint condition;
  - As described in Sections 2.4, there have been no studies investigating the impact of different restraint conditions on punching shear at elevated temperature. This experimental series is the first to directly compare the impact of restraint condition on punching shear at elevated temperature.
- slab thickness (mm); and
  - By varying the slab thickness, it was possible to indirectly investigate fire intensity. However, it was not intended to control the heat flux, Q applied to the specimens, rather that the resulting temperature profile through the slab was measured. Radiant panels were used, therefore the resulting heat flux, Q could not be directly varied.
- reinforcement ratio (%).
  - Finally, reinforcement ratio was chosen as a parameter as it has a large impact on punching shear and was adjustable within the limitations of the experimental design.

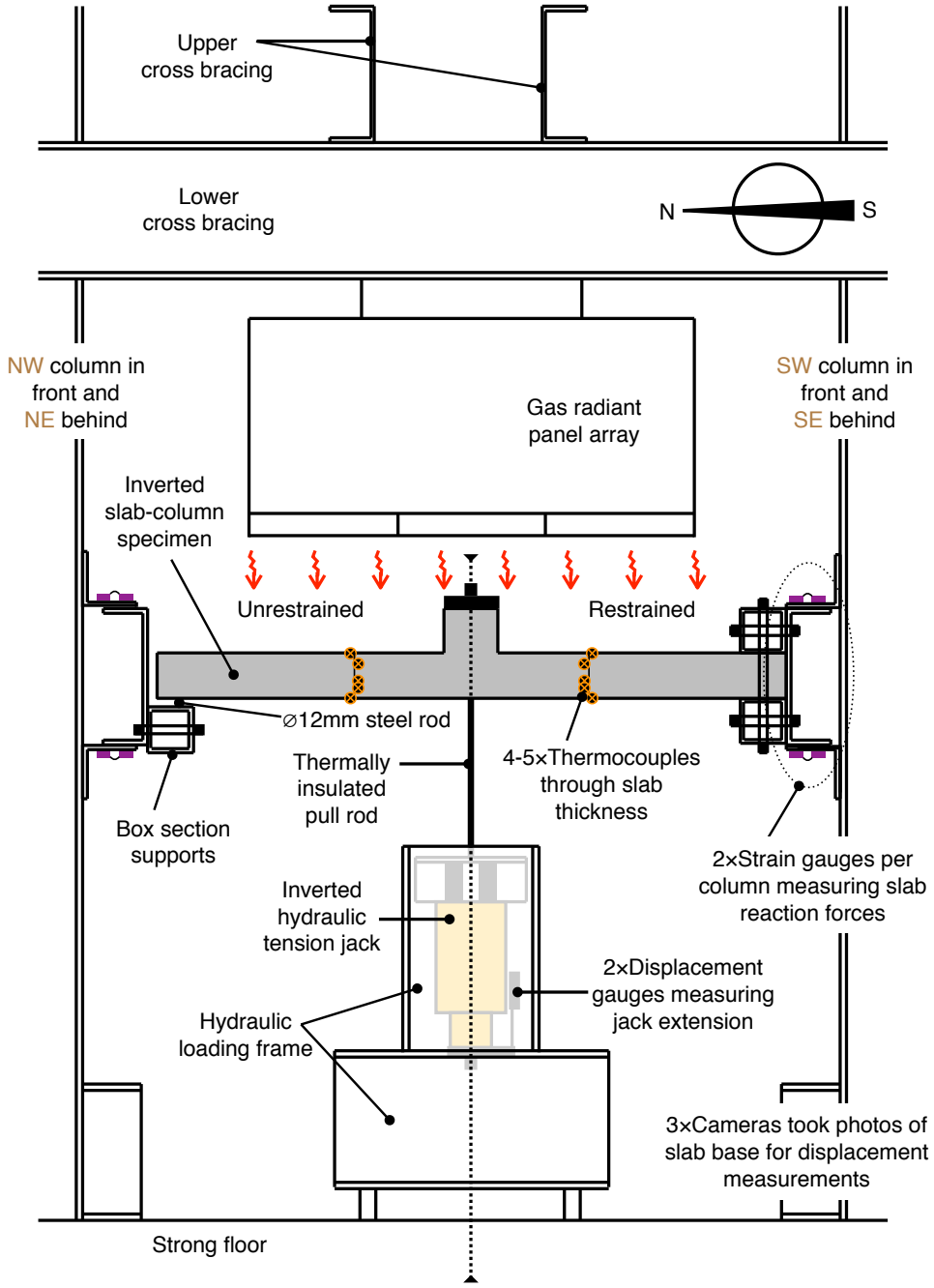

Figure 5.2: Elevation of the slab-column test setup

5.2 SPECIMEN

5.2.1 *Design*

The series consisted of fifteen slab-column test specimens, as in Figure 5.2 with dimensions of 1400×1400 mm and a central column stub of 120×120×100 mm. All the slabs had the same dimensions except for the slab thickness. The slabs are not full size, therefore size effect will impact the results. The slabs were all cast from the same concrete batch and tested within the age of approximately 420-745 days after casting. Appendix B shows that the slabs had a similar moisture content of 4% at the time of testing. There was no shear reinforcement, and the flexural reinforcement had varying diameters to achieve a reinforcement ratio comparison.

Table 5.1 gives the test specimen details and identifiers (tests will be referred to by specimen ID). Three types of tests were performed: ambient tests without edge restraint (AU), heated tests without edge restraint (HU), and restrained heated tests (HR). Five specimens were tested for each of these conditions. Three thicknesses of slab (50, 75, 100 mm) with a 0.8% reinforcement ratio were tested, and a further two 100 mm thick slabs were tested with 0 and 1.5% reinforcement ratio.

5.2.2 *Dimensions*

The slab-column specimen dimensions were governed by:

- slab plan dimensions were set at 1400×1400 mm to utilise the existing reaction frame; and
- slab thickness was limited to 100 mm to ensure the radiant panel array produced an effective heat gradient through the slabs' thickness, comparable to that of a real fire and to satisfy the load capacity of the frame.

The slab-column specimen design was based on ambient testing by Muttoni and Fernàndez Ruiz (Guandalini et al., 2009) (discussed in Section 2.2), in order to ensure the failure mode was punching shear. The slab dimensions satisfy the above limitations, but also approximately match the reinforcement, column stub and slab thickness of low reinforcement tests conducted by Guandalini et al. (2009).

SPECIMEN ID	FIRE SCENARIO	SUPPORT TYPE	SLAB THICKNESS (MM)	FLEXURAL REINFORCEMENT RATIO (%)	REINFORCEMENT DIAMETER & SPACING (MM)
AU50-0.8	Ambient	Unrestrained	50	0.8	ø6 at 114
AU75-0.8	Ambient	Unrestrained	75	0.8	ø6 at 65
AU100-0	Ambient	Unrestrained	100	0	-
AU100-0.8	Ambient	Unrestrained	100	0.8	ø6 at 42
AU100-1.5	Ambient	Unrestrained	100	1.5	ø8 at 42
HU50-0.8	Heated	Unrestrained	50	0.8	ø6 at 114
HU75-0.8	Heated	Unrestrained	75	0.8	ø6 at 65
HU100-0	Heated	Unrestrained	100	0	-
HU100-0.8	Heated	Unrestrained	100	0.8	ø6 at 42
HU100-1.5	Heated	Unrestrained	100	1.5	ø8 at 42
HR50-0.8	Heated	Restrained	50	0.8	ø6 at 114
HR75-0.8	Heated	Restrained	75	0.8	ø6 at 65
HR100-0	Heated	Restrained	100	0	-
HR100-0.8	Heated	Restrained	100	0.8	ø6 at 42
HR100-1.5	Heated	Restrained	100	1.5	ø8 at 42

Table 5.1: Test specimen details

5.2.3 *Steelwork*

Orthogonal flexural reinforcement was placed on the lower, tension face, using the bar diameters and spacing given in Table 5.1. Every second mesh overlap was tied with steel wire according to the reinforcement schedule seen in Figures 5.3 and 5.4. Eurocode requirements for flexural reinforcement at internal columns were not implemented as the panel width either side of the column is not representative of a real building. Rather the slab reinforcement was analysed using the ambient design methods of Guandalini et al. (2009). For the 50 mm and 75 mm thick restrained slabs, the bar spacing at the slab edges were adjusted to ensure there was one bar out with the restraining tubes, in order to provide anchorage (shown in Figure 5.3). Shear reinforcement was not provided as we wanted to ensure shear failure.

A 2.5×2.5 mm galvanised steel mesh was used to increase the column stub capacity and ensure the column did not crush prior to slab failure. The column mesh was raised off the tension face by either the flexural reinforcement or spacers. The column stub did not fail prior to slab failure in any test.

Two additional bars were placed in each direction in the compression area to tie the column stub to the slab in accordance with BS EN 1992-1-1:2004 (2008). The two bars passed through the column mesh to tie the column into the slab and prevent unzipping of the reinforcement during failure. The two bars spanned in the same direction as the orientation of the flexural reinforcement in all the slabs, except for the 50 mm thick slabs. The only steel in the three unreinforced slabs was mesh to reinforce the column stub.

All reinforcement steel used came from the same reel, therefore the metallurgy is assumed to be the same. Both 6 mm and 8 mm diameter reinforcement were ribbed, and were cold worked and hot rolled, respectively.

5.2.4 *Concrete*

Ready-mix concrete was used so that all the slab-column and concrete strength specimens could be cast from the same batch. A concrete grade of RC40/50 and maximum aggregate size of 10 mm was specified. Appendix C gives the ready-mix concrete receipt (Figure C.1), design certificate (Figure C.2) and product data sheet (Figure C.3). The product data sheet states the typical chemical analysis of the aggregate, which shows it to be siliceous aggregate. The measured slump was 130 mm. Concrete spacers, 15 mm thick were placed below the inner spanning flexural reinforcement, therefore the concrete cover varied from 9–7 mm for slabs with ø6–8 mm rebar, respectively.

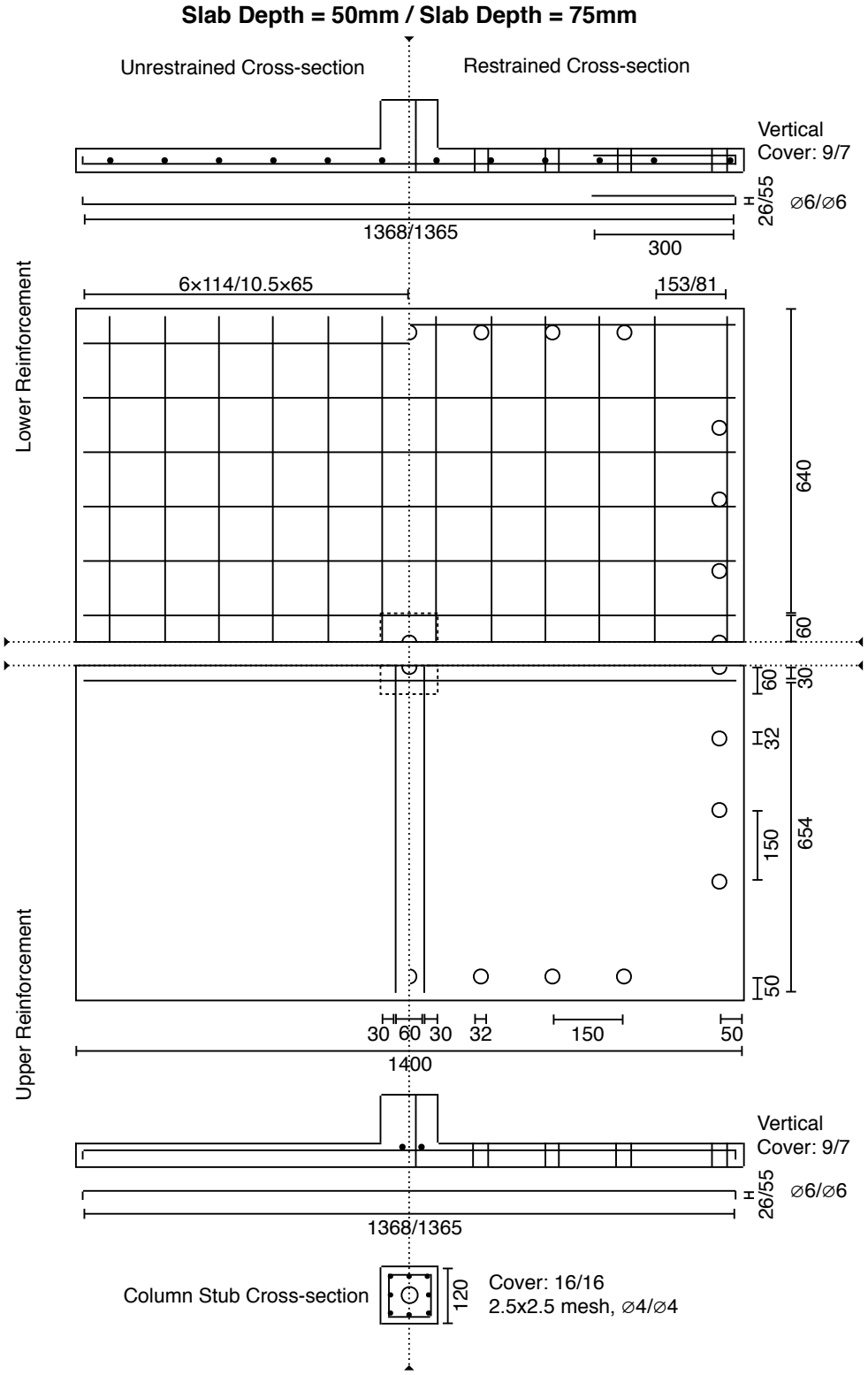

Figure 5.3: Reinforcement schedule for 50 mm / 75 mm thick slabs with 0.8%

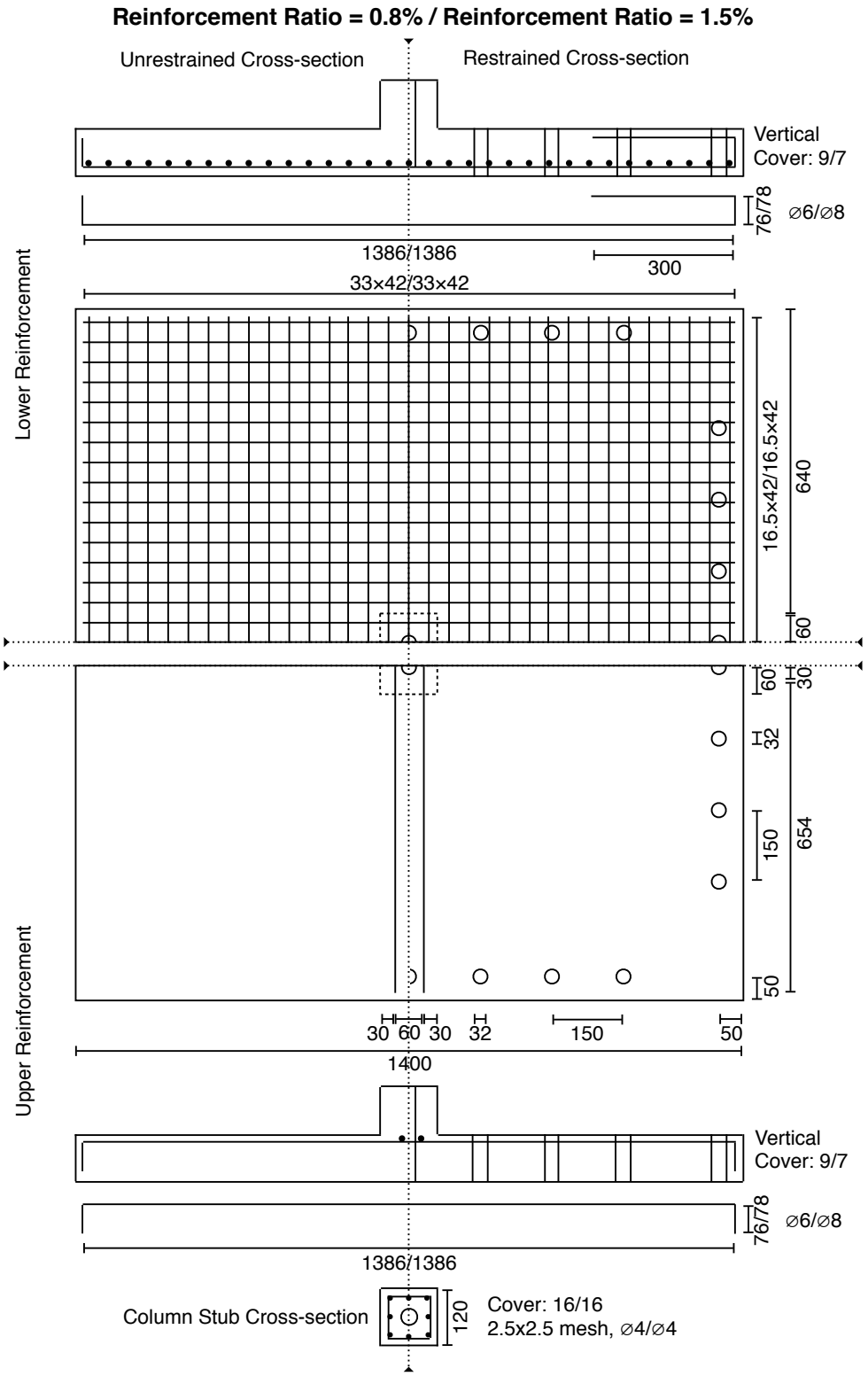

Figure 5.4: Reinforcement schedule for 100 mm thick slabs with 0.8% / 1.5%

Figure 5.5: Slab dehumidified curing environment

5.2.5 *Fabrication*

The column stub was cast directly into the slab centre to ensure a single slab-column specimen. Column stub compaction was manually undertaken, because using a vibrating poker on the column concrete would have caused it to settle down into the slab rather than cure in the column formwork. Eight cube and fifty-four concrete cylinder strength specimens were cast to monitor the ambient and elevated temperature strength. The slab, cube and cylinder specimens were cured dry, but kept well hydrated with damp towels under polyethylene sheeting. De-moulding the slabs was undertaken 7–8 days post-casting. Honeycombing was visible on the column stubs, to the extent that the steel mesh was exposed. The column stub honeycombing was patched with mortar 78 days post-casting.

Figure 5.5 shows the slab-column specimens stacked and cured in a dehumidified environment for over 16 months. The slabs were well cured to reduce their moisture content and hence potential for spalling. Stacks of slabs were moved from the dehumidified environment and into the testing laboratory in three stages, as testing progressed. Graphs of the moisture content variation with time for both the dehumidified environment and laboratory are included in Appendix B.

5.3 STRUCTURAL REACTION FRAME

A detailed description of the original design and construction of the reaction frame with integrated radiant panel heating is provided by Fox (2013). Extensive upgrading and modification was undertaken for these tests to both the reaction frame and radiant panel heating array. Section 5.3 presents the alterations to the reaction frame, with Section 5.4 detailing the radiant panel heating modifications.

The structural reaction frame was constructed of a general purpose meccano reaction frame system on the laboratory strong floor. The pieces of channel section vary in length with 305×102 mm cross-sections. Figures 5.6 and 5.7 show an elevation and plan view of the structural reaction frame, respectively.

The slabs were mounted into the frame with 100 mm box section supports along all four sides in a square. Each of the frame sides had two columns to ensure rigidity. Figure 5.6 shows that the slabs were positioned approximately half the distance between the strong floor and lower frame cross bracing to ensure they were symmetrically supported. Testing by Fox (2013) used a distance of 260 mm between the surface of the slab and the radiant panel array. This distance was fixed to ensure the radiant panels worked effectively and allowed for the combined 150 mm height of: column stub, loading plate and pull rod nut, to fit beneath. Slot holes, 60 mm long, in the support box sections allowed the slab support height to be varied between tests of different slab thicknesses. The height below the slab had to be sufficient to fit the hydraulic loading frame and not be too far for the 1000 mm length pull rod to extend from below the inverted tension jack to above the loading plate. Additionally, the cross brace location used in Fox (2013) was modified by raising both lower and upper cross brace pairs by 152.4 mm. The upper and lower cross brace pairs were not bolted together, only to the columns.

The modified reaction frame was designed to allow the boundary support conditions to be altered. The slab supports were either:

- restrained (fixed against in-plane expansion and edge moment)
- unrestrained (allowed to expand, and free to rotate)

The right hand side of Figure 5.8 shows the restrained condition was achieved by vertically and horizontally bolting the box sections above and below the slab. The restrained slabs were cast with seven ø32 mm metal tubes along each edge (1 mm wall thickness). The tubes passed through the depth of the respective slabs and provided a sleeve for the vertical ø30 mm bolts to pass through. Additionally, the tubes ensured there was no local concrete crushing

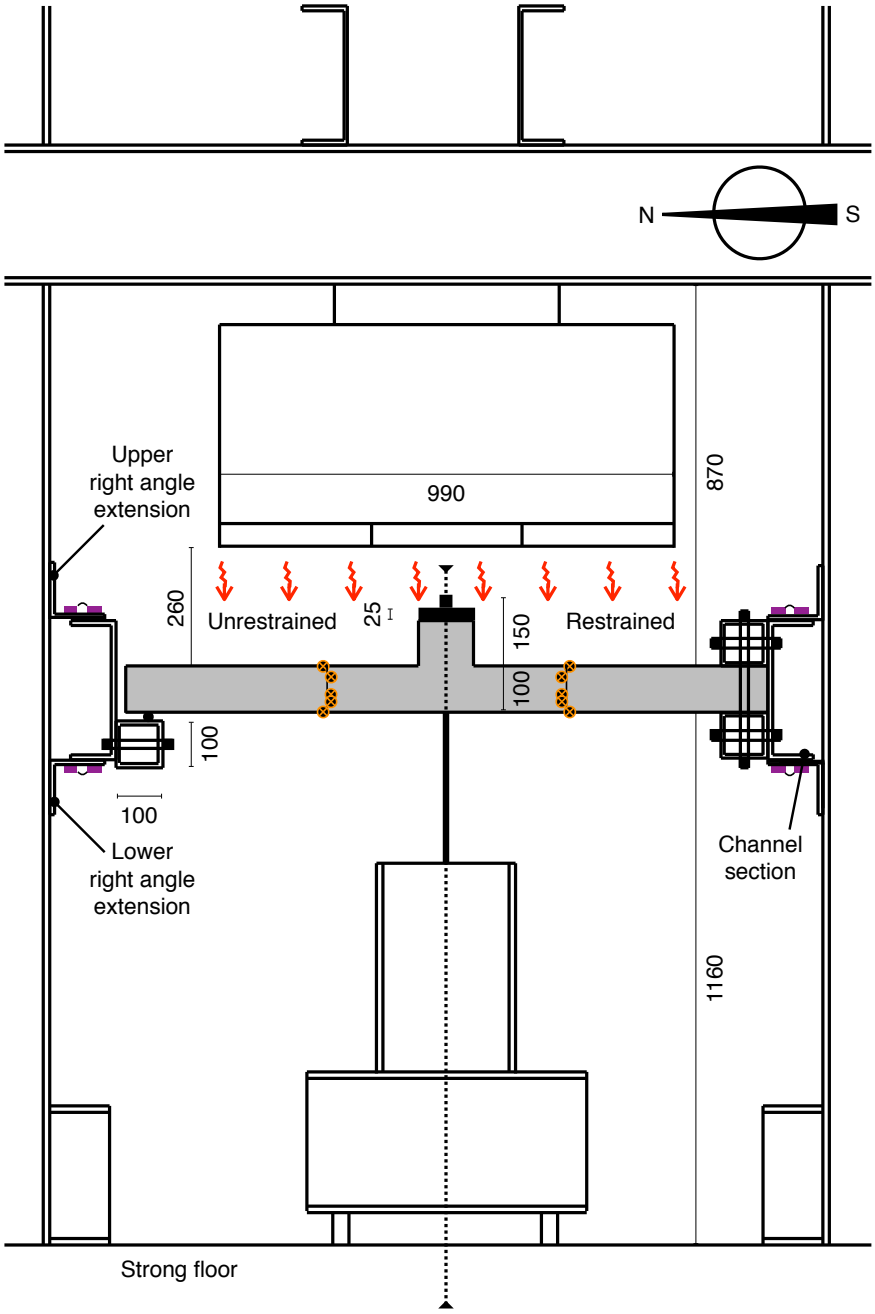

Figure 5.6: Dimensioned elevation of the structural reaction frame

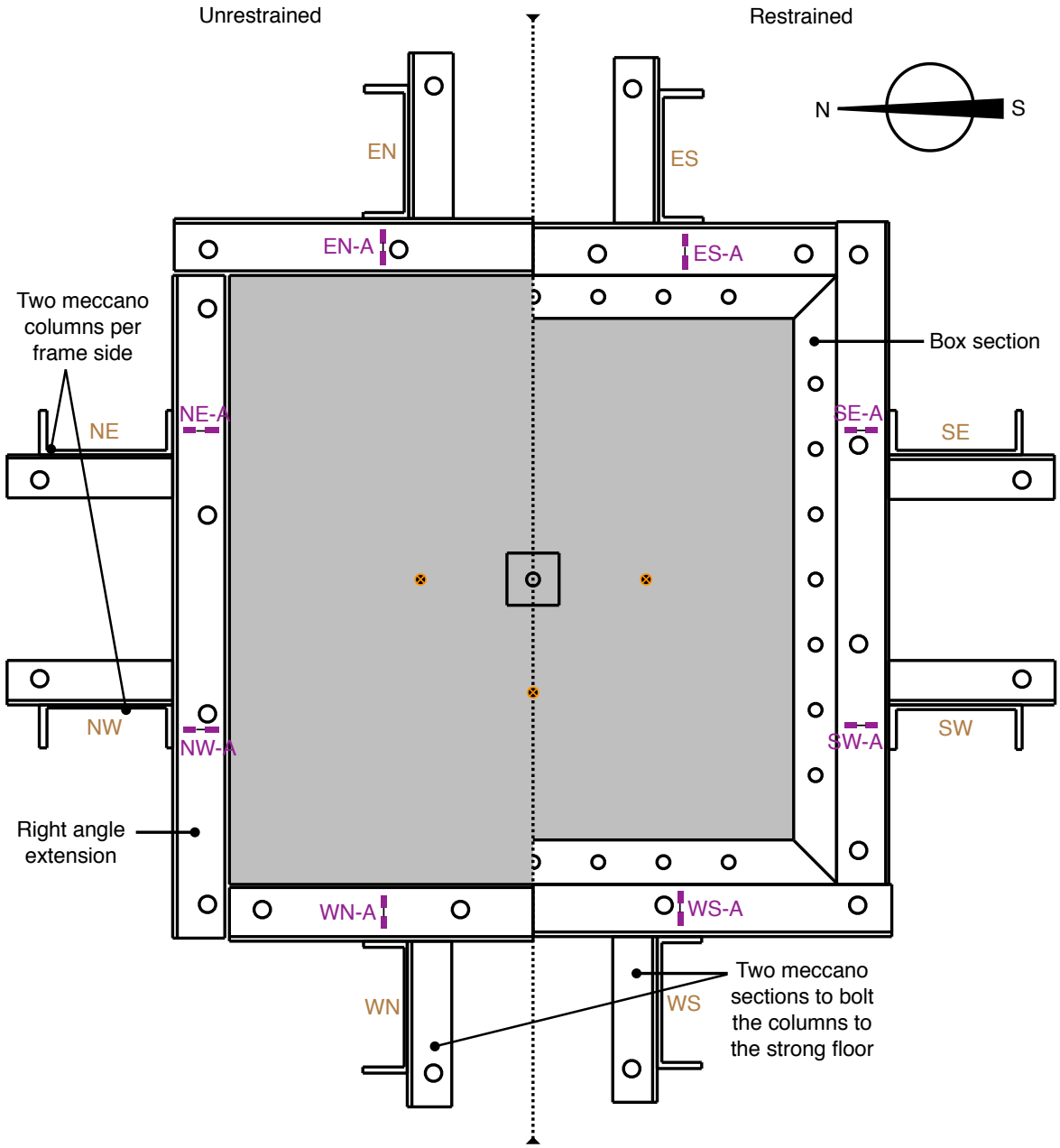

Figure 5.7: Plan of the structural reaction frame

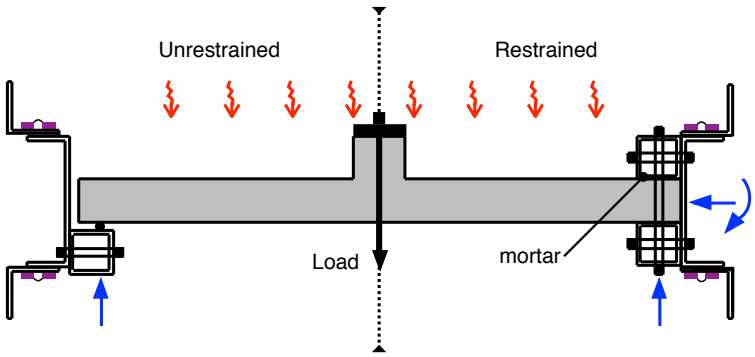

Figure 5.8: Elevation showing the two slab-column boundary support conditions

at the supports, caused by the bolt thread. The upper, heated slab surface was slightly uneven due to it having been hand skimmed, therefore mortar was used to ensure a sound bedding of the upper box sections to the surface of the slabs.

The left hand side of Figure 5.8 shows the unrestrained condition was achieved by supporting the slab on a 6 mm diameter steel rod. The rod was temporarily held in place with Blu-tack on the box section, which was horizontally bolted to the structural reaction frame. An approximate 5 mm gap between the slab edge and structural reaction frame was created to allow the slab to freely rotate and expand. The gap was produced by moving the channel sections back towards the columns (shown in Figure 5.6), as they were designed with slot holes to allow horizontal adjustment.

The stiffness of the structural reaction frame is investigated in Section 7.1.6, in order to assess the effectiveness of the restrained support condition in providing in-plane and vertical restraint.

5.4 RADIANT PANEL HEATING

Figure 5.9 shows elevations of the 960×990 mm array of six individual propane gas radiant panels, used to heat the slabs from above. The radiant panel array was modified from previous testing by Fox (2013). The main aims of the modifications were to:

- increase even application of heat flux
- decrease the danger of flashback
- improve health and safety of the propane gas supply

The radiant panel array was improved to avoid the flashback phenomena, which is where *"fuel burns inside the plenum chamber"* (Robertson, 1982) and the array is required to be turned off for safety. During the testing there were no incidents of flashback, though the heating of two tests (HR100-0 and HR100-1.5) had to be ended early to avoid flashback.

Improvements to the radiant panel array required it to be completely disassembled, cleaned, two damaged panels replaced, and then re-assembled with copper piping (Figures 5.10a and 5.10b). Additions to the system included: an air manifold, a propane gas manifold, and a 0.2 m^3/s capacity fan. Figure 5.10c shows the manifolds were integrated into the pipework to evenly distribute the air and propane between the radiant panels, so that an even heat flux could be achieved. The fan was attached directly to the air manifold to decrease friction losses and evenly distribute the air to the six panels. The

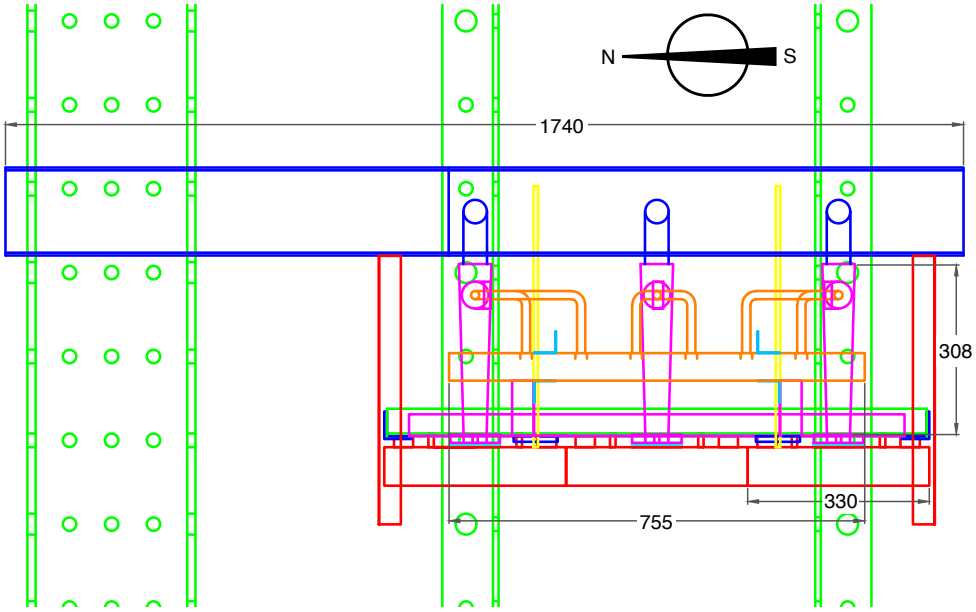

(a) N–S elevation

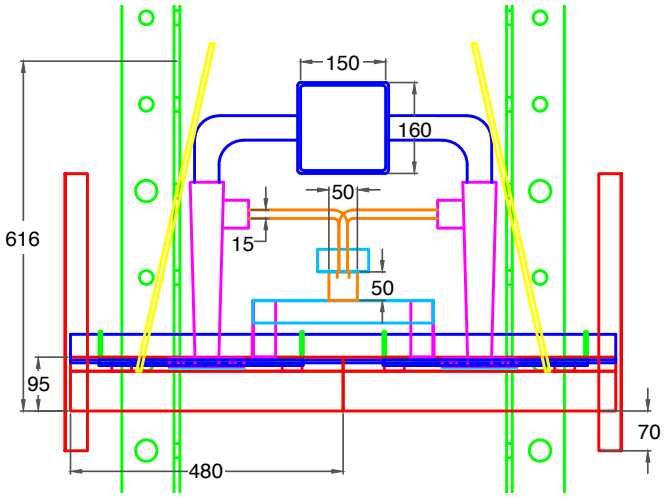

(b) E–W elevation

Figure 5.9: Schematic of propane gas radiant panel array

fan was supported on rubber insulation and vibration reducing washers from the lower cross bracing, out with the North columns of the structural frame.

5.4.1 *Calibration*

The radiant panels were calibrated to find the optimum setup to ensure 120 minutes of operation. Factors that impact the operation of the radiant panels include the:

- temperature of the surrounding environment;
- air flow around the panels;
- proximity and chemical characteristics of materials surrounding the panels;
- mixing efficiency of the propane and air;
- volumetric capacity of the propane supply (lack of capacity led to variable flow rates);
- temperature of propane supply (cooling resulted in a decreased flow rate); and
- pipe friction losses (decreased propane and air flow rates).

The parameters that were varied during the visual calibration were propane and air flow rates, and mix valve orifice aperture. These three parameters were varied by trial-and-error until the optimum combination, producing a even progression of panel colour with time, was reached. The optimum propane flow rate for this setup was 2.5 g/sec and maximum air fan volume flow rate of 0.2 m^3/s. Appendix D shows the optimum mix valve settings, which were used for all tests (range: 1–8). The heat flux distribution could have been improved by installing a mesh in front of the radiant panel array and this would have also protected the panels from damage, however insufficient height between the radiant panel array and slab surface prevented this.

The calibration highlighted that using a single fan attached to one end of the air manifold caused an imbalance in air and gas distribution. A further improvement in heat flux distribution could have been achieved by using two fans symmetrically about the manifolds, however this was not possible due to physical space and cost limitations.

A measurement of the heat flux of the radiant panel array throughout a standard test was undertaken. Two spare slabs of 50 mm thickness, with dimensions 1400×700 mm were inserted side-by-side into the structural reaction

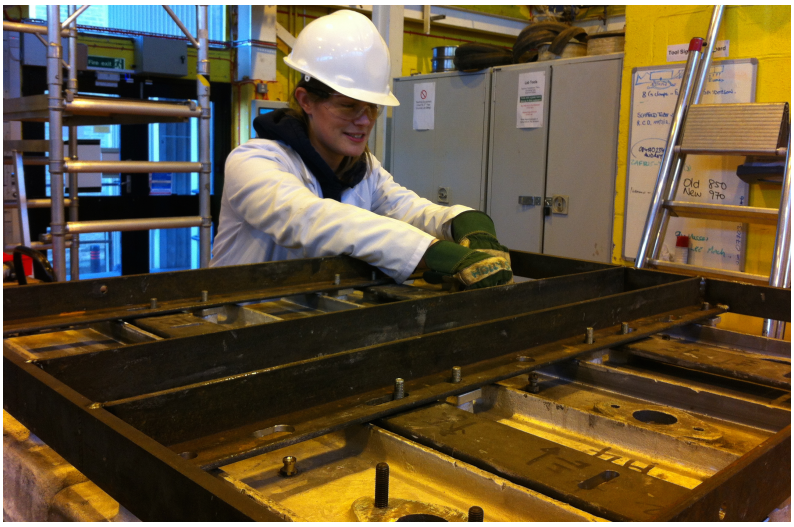

(a) Base re-assemblement

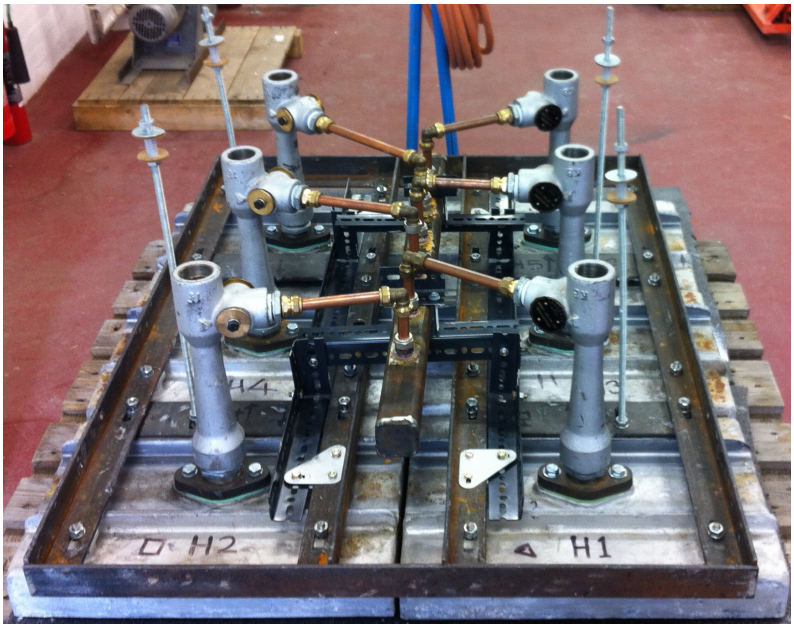

(b) Back of the panels showing the copper piping joining the individual mix valves to the gas manifold

(c) N–S elevation, showing the air manifold and fan at the top

Figure 5.10: Radiant panel array improvements

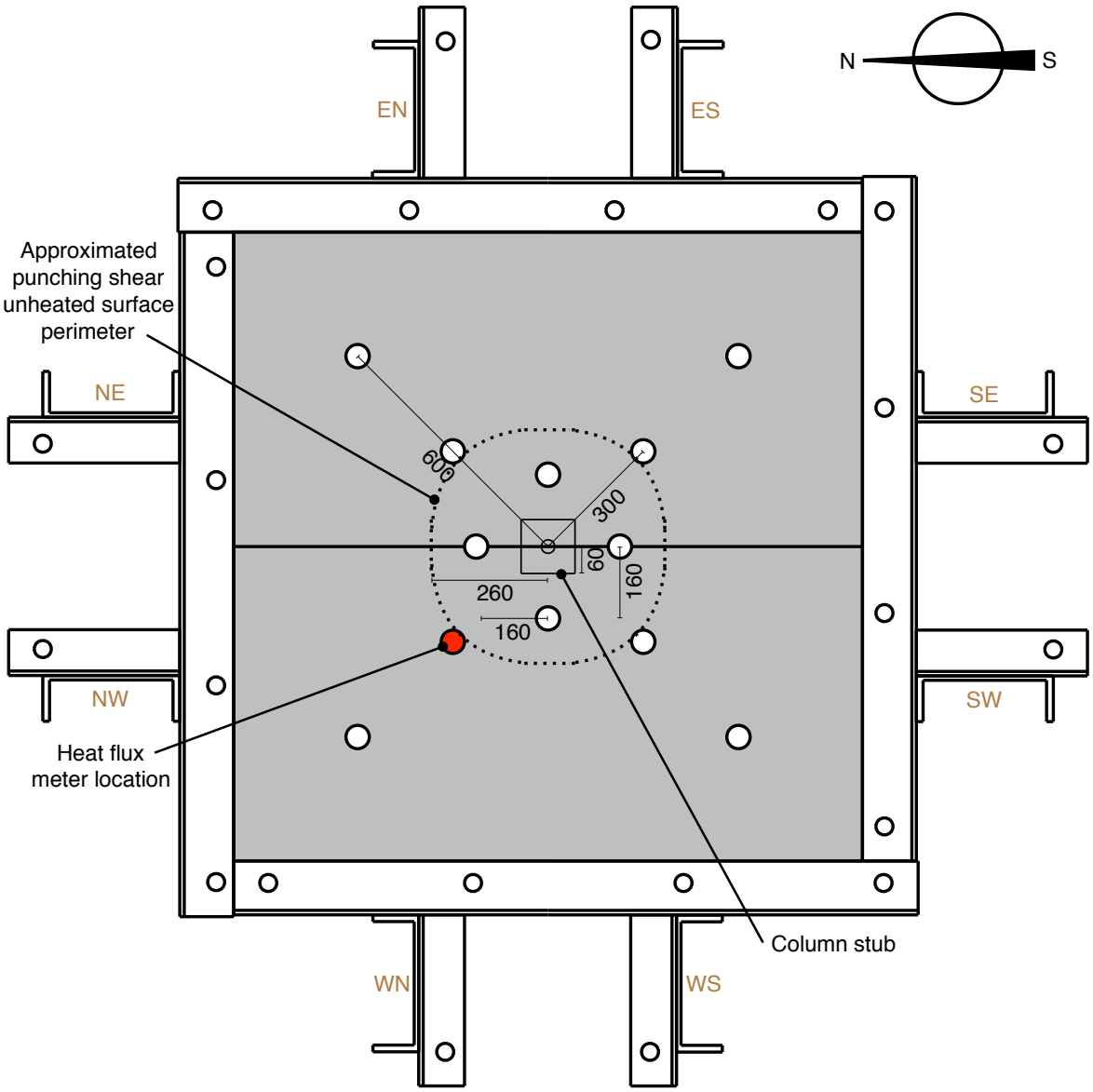

Figure 5.11: Plan showing the heat flux measurement location used in Figure 5.12

frame, 260 mm below the radiant panel surface to replicate a real slab test. A ø52 mm diamond core drill was used to drill 12 holes through the depth of the slabs to allow measurements with a heat flux meter to be taken. Figure 5.11 shows the positioning of the heat flux meter as close to the EC2 approximated 100 mm thick slab, unheated surface punching shear perimeter, as possible. Measurements of variation of heat flux with position were planned, however during the test it was not possible to move the meter. The black line in Figure 5.12 shows the moving average of the recorded heat flux with time, measured at the location highlighted in Figure 5.11.

Figure 5.12 shows the radiant panel array reached a nominal heat flux at slab level of approximately 50 kW/m^2. The fluctuations of heat flux are attributed

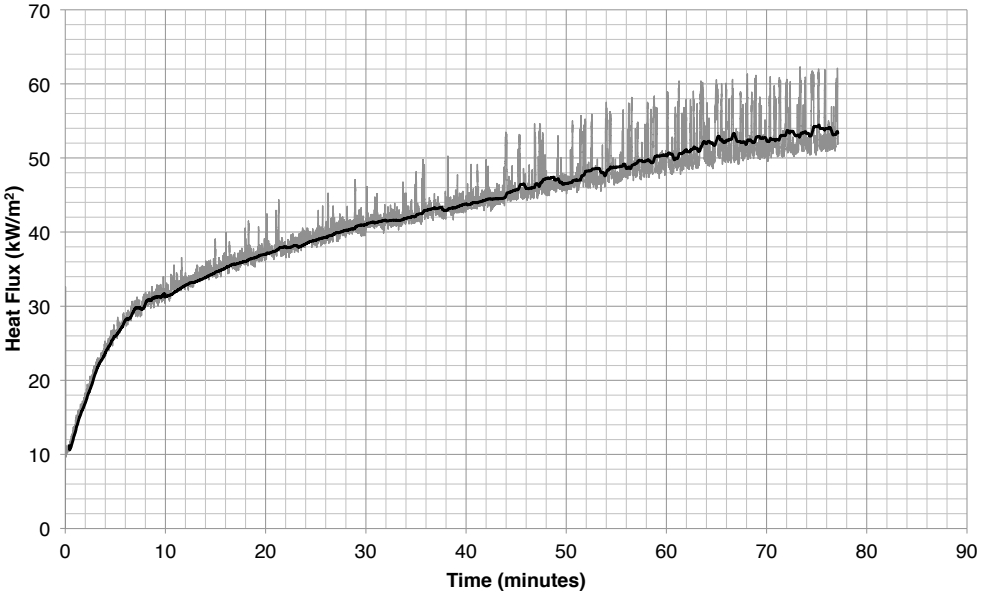

Figure 5.12: Heat flux with time near the approximated punching shear perimeter

to the heat flux meter not being positioned flush with the concrete slab surface. The heat flux meter is sensitive to re-radiation and convection currents in this setup. The experimental elevated temperature measurement was recorded with thermocouples through the slab thickness, as detailed in Section 5.7.2.

5.5 INSULATION

Insulation was applied to cover all elements of the setup exposed to heat from the radiant panels, to ensure the structural frame was not impacted by expansion due to heat and hence falsely impact the test results. The insulation is highlighted in green in Figure 5.13, dark green represents Econicboard (Duncryne, 2014) and light green represents Ceraboard (SiG, 2013) insulation types. The radiant panel array was enclosed within Econicboard (magnesium oxide insulation board), which ended at the panel surface on W and E frame sides. It extended 70 mm further down on the N and S frame sides to vent hot gases away from the propane and air manifolds. The manifolds and copper piping were heavily insulated to shield the gases from a temperature increase, which would have caused unwanted decreases in flow rates, and posed a health and safety hazard. Gaps in insulation were filled with VITCAS (VITCAS, 2011) square glass fibre thermal rope and strips of Ceraboard insulation.

Ceraboard was bolted below the cross brace sections and vertically to the frame columns. It was carefully positioned between the N frame side columns to restrict hot gases from venting near to the fan intake. The loading plate, pull rod and bolt were thermally-insulated by a double thickness of Ceraboard.

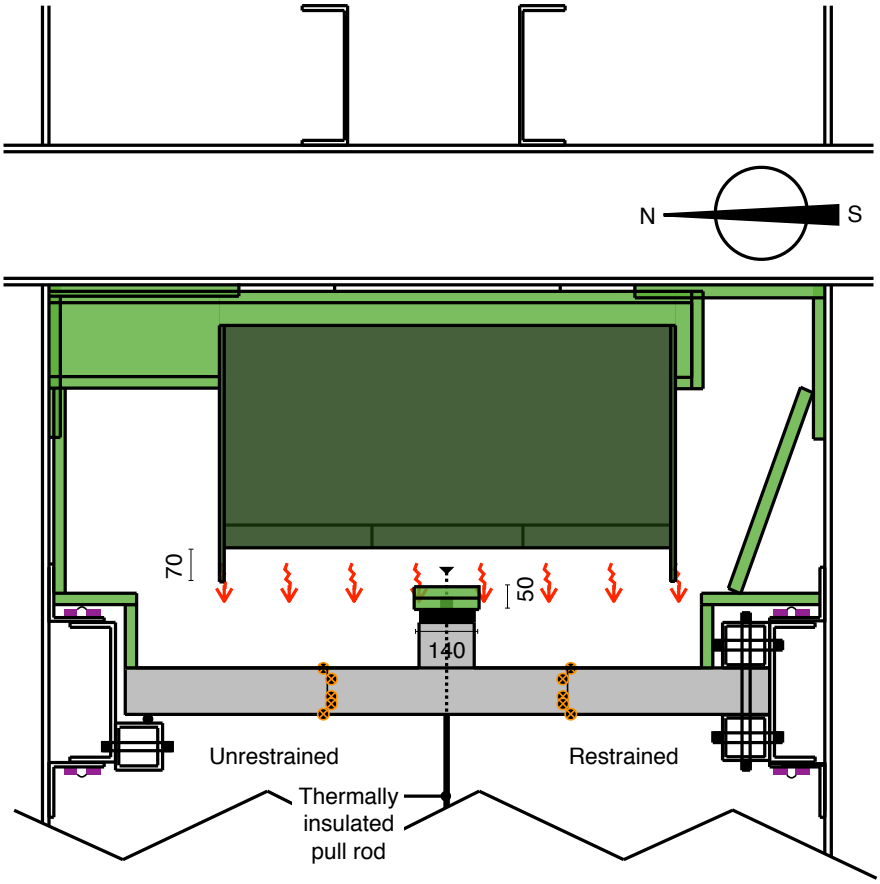

Figure 5.13: Elevation of the insulation design

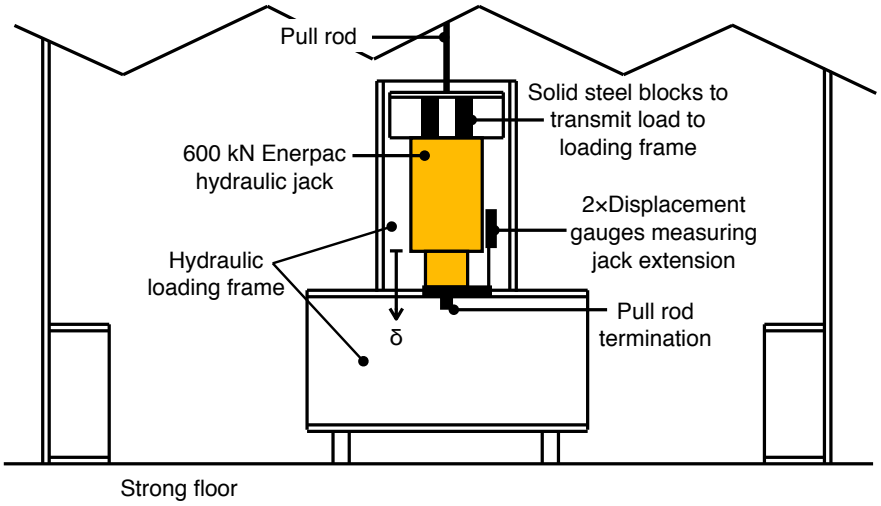

Figure 5.14: Schematic of hydraulic slab loading

5.6 HYDRAULIC LOADING

The inverted test orientation required a downwards force to be applied to the column stub. The limited space above the slab and elevated temperature meant that the load had to be applied from below the slab. Figure 5.14 shows an inverted Enerpac 600 kN hollow jack (Enerpac, 2014) below the slab. The jack loaded the slab via a pull rod through the column stub. Two steel blocks transmitted the jack load to the loading frame, which was bolted to the laboratory strong floor.

The pull rod was attached to a 25 mm thick steel loading plate to distribute the load evenly to the 120×120 mm column stub surface. The 1000 mm high strength steel, pull rod was attached with hand tightened nuts at either end.

The hollow loading jack was connected to a second 600 kN Enerpac jack (latterly a 250 kN jack), which in turn was loaded using a servo-hydraulic controlled, bi-axial Instron 8800 actuator system giving precise control of the load and displacement. Displacement and load readings were digitally output and recorded by a datalogger.

A pressure transducer with a range of 0-10,000 psi was connected into the hydraulic pipe line close to the 600 kN hollow jack. Data was logged from the pressure transducer and Instron load cell to ensure redundancy. The Omegadyne Inc. manufacturer's calibration of 1.9964 psi/mV was used for the pressure transducer.

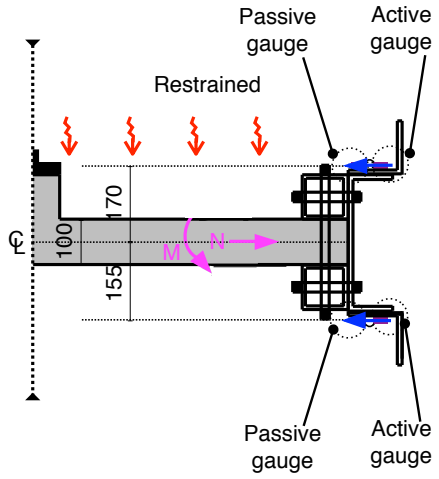

Figure 5.15: Schematic of active and passive strain gauge positioning for a 100 mm thick slab

5.7 INSTRUMENTATION

The structural reaction frame and slab-column specimens were instrumented with a combination of strain gauges, thermocouples, a pressure transducer, Displacement Transducer (LP), and DIC using cameras.

5.7.1 *Strain gauges*

The reaction frame was instrumented with bonded strain gauges to measure in-plane reaction forces and moments imparted by the slab on the four sides of the reaction frame. Strain gauge pairs were attached onto the upper and lower right angled extension sections, which were above and below the slab level. Figure 5.7 shows 8 gauge pairs were bonded just outside the slab boundary, in line with each of the 8 columns. Each gauge pair is identified by the columns they were near to and designated as A or B if the pairs were above or below the slab level, respectively. Figure 5.7 annotates the identification of the columns (brown) and above slab level strain gauges (purple).

Temperature resistant strain gauges were wired as half bridges with one active and one passive gauge. The remaining half of the bridge was provided by the data logger. Figure 5.15 shows how the active gauge was bonded between the support bolt and column to take strain readings. A paired passive gauge was bonded immediately next to the edge of the angle, where the strain was zero. Readings from the passive gauge corrected the active gauge for temperature. The gauges were protected from damage and elevated temperature by applying silicone sealant on top of them.

All the calibration information for the strain gauges can be found in Appendix E.

5.7.2 *Thermocouples*

Temperature was recorded using 12–15 thermocouples within each heated slab, with 4 thermocouples in 50 mm thick slabs and 5 thermocouples distributed through the depth of the 75 and 100 mm thick slabs. Figure 5.16 shows the respective thermocouple depths from the heated surface of the slabs and where the 3 thermocouple trees were positioned, at 150 mm beyond $D/2$ (where D = slab thickness) from the column of each respective slab. The thermocouple wires were designed to come out of the concrete at 120 mm from the slab edges, just outwith the area of the restrained upper box section.

5.7.3 *Displacement measurement*

Two LP, capable of measuring maximum displacements of 30 and 100 mm, were attached to the 600 kN hollow jack, as shown in Figure 5.14. They measured the jack extension, which was assumed to be equal to the column stub displacement (discussed further in Section 7.1.4).

In addition to the LP, Digital Image Correlation (DIC) was used to take measurements of vertical displacement at any retrospectively chosen location on the lower (unheated) surface of the slabs (as presented in Chapter 3). The resolution of DIC for this application was calculated for W camera only and was of the approximate order of 0.015 mm and 0.026 mm in the N–S and E–W frame direction, respectively.

The common positioning of the cameras perpendicular to the object plane was not possible as the hydraulic loading frame had to be positioned directly below the slab centre. Additionally, there was a high risk that broken concrete pieces would damage the camera equipment. The limited space around the structural reaction frame and heating implications from the radiant panels, lead to inverted cameras positioned between the columns on the E, S and W frame sides. Figure 5.17 shows the positioning of the cameras mounted on scaffolding, at angles to the bottom (unheated) slab surface, just out with the structural reaction frame columns.

Positioning the cameras at angles to the bottom slab surface required further post-processing to calculate the corrected vertical displacement from the output DIC analysis. Simple geometry, shown in Figure 5.18 was used to calculate the corrected vertical displacement. Appendix F presents an example

100 mm thickness

Designed thermocouple depth from heated surface (mm)
0
23
62
77
100

75 mm thickness

Designed thermocouple depth from heated surface (mm)
15
21
39
54
75

50 mm thickness

Designed thermocouple depth from heated surface (mm)
15
21
35
50

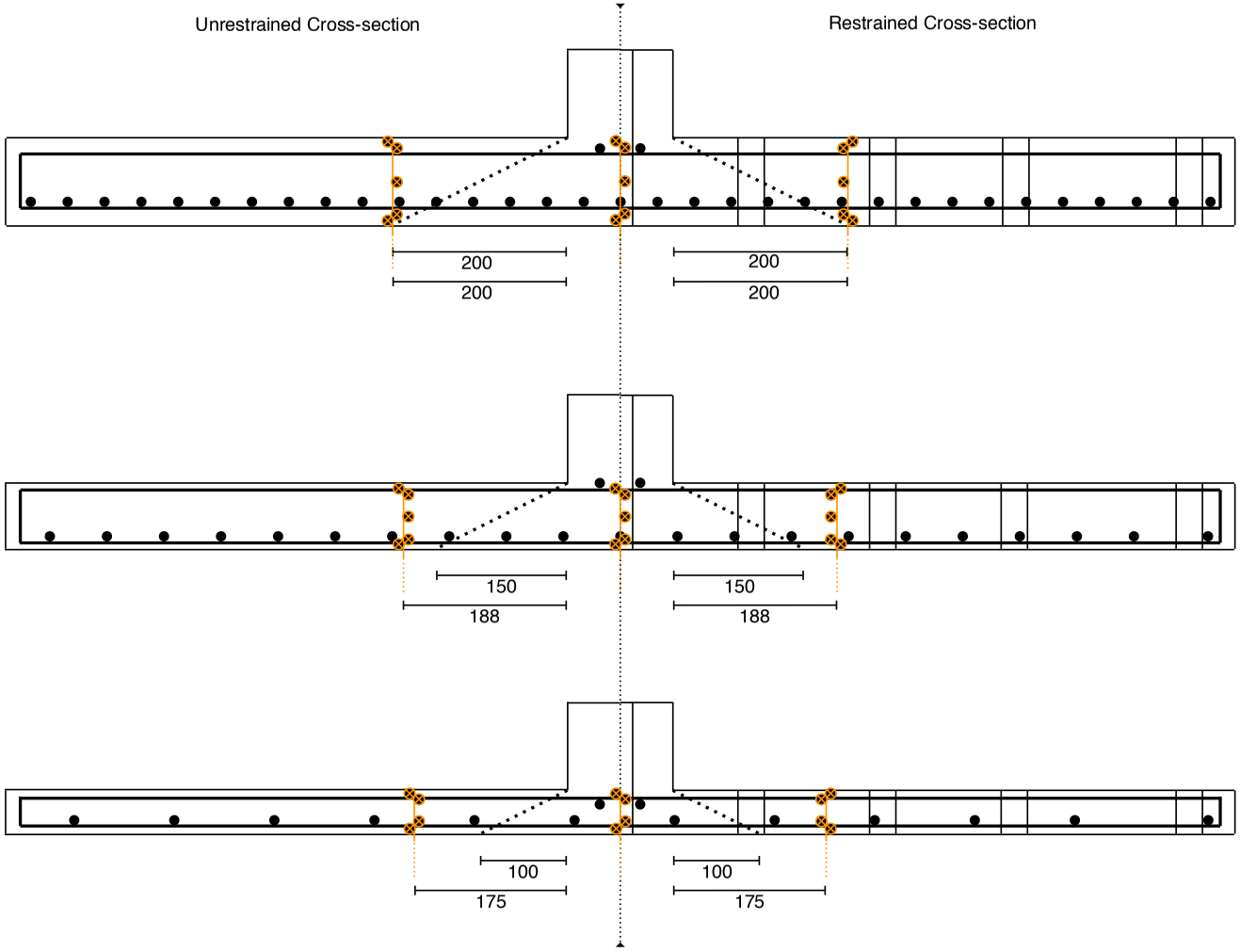

Figure 5.16: Thermocouple positions in the slabs

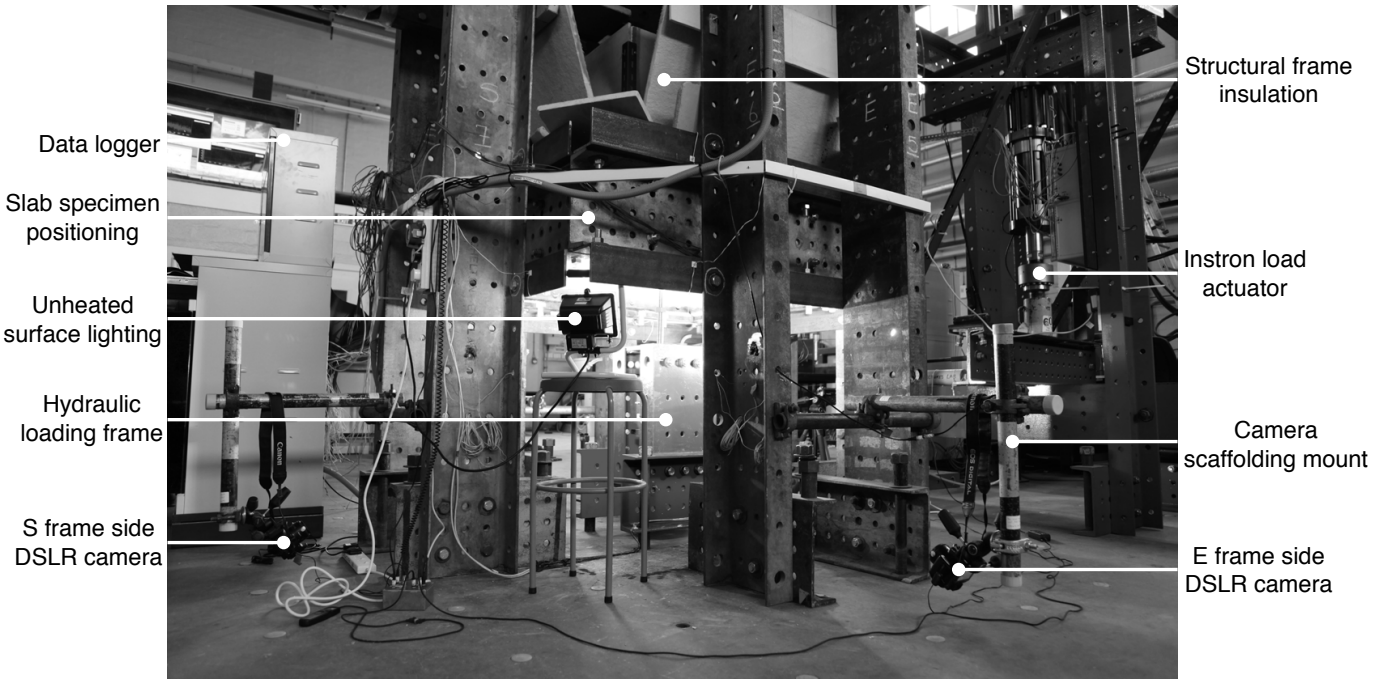

Figure 5.17: Photo of the positioning of two of the DIC cameras

MATLAB® script written to calculate the corrected vertical displacements for the unrestrained 75 mm thick, 0.8% reinforced slab.

Three cameras were used for vertical displacement measurement as it allowed more of the slab's unheated surface to be captured for post-processing and provided redundancy in case of camera failure. Canon cameras were used, with twin 650D models positioned at the S and W frame sides and a 450D model positioned at the E frame side. The cameras were setup for testing using the camera settings listed in Appendix G. After test setup, a photograph from each camera was taken with a calibration board, to allow slab surface points between cameras to be correlated. The two piece calibration board consisted of a grid of black dots on a white background for maximum contrast, shown in Figure 5.19. The calibration board was wedged flush against the slab unheated surface with wooden stays. A Geocentroid analysis script was run within MATLAB® on the calibration board images, which allowed the centroid of the dots to be found.

Optimisation

The optimum horizontal and vertical field of view for the respective cameras was calculated to find the horizontal and vertical distance from the centre of the slabs, unheated surface to position each camera.

The visual texture imparted on the slab surface was optimised with image analysis from the first slab-column test (AU100-0.8). Patches with different

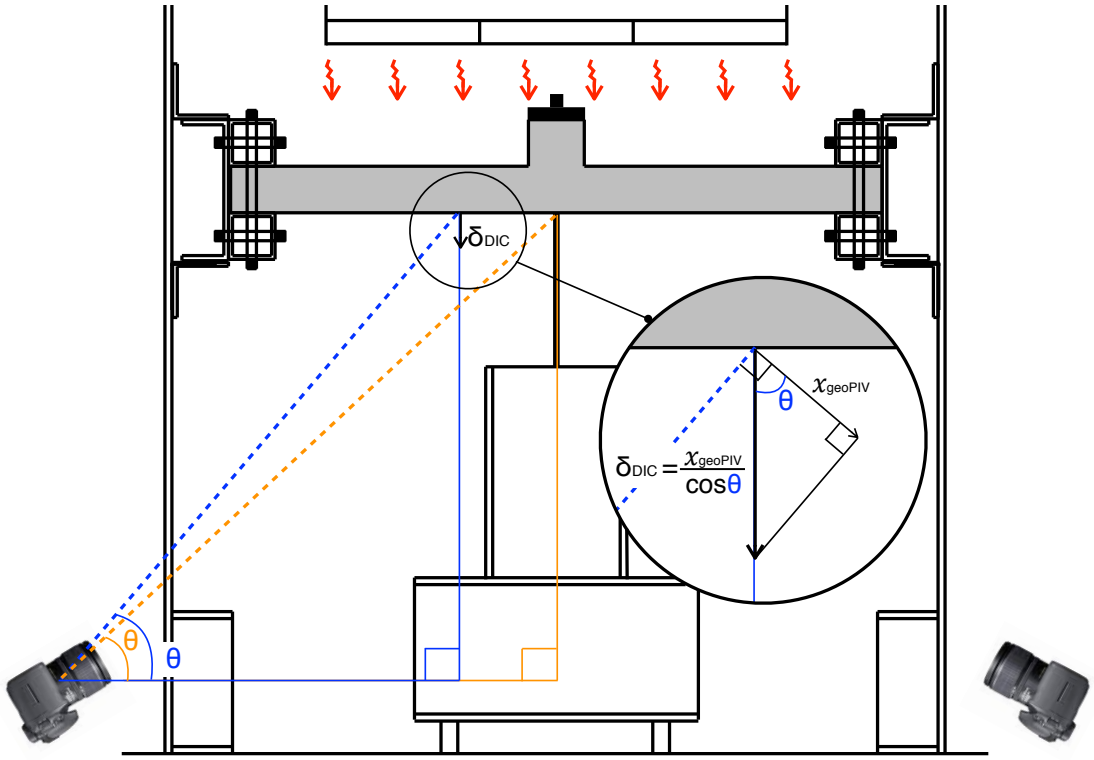

Figure 5.18: Geometry used to correct vertical displacement output from DIC analysis

texture were tracked with DIC and the number of analysis errors was much less when tracking the patches on the black spray paint, speckled with white dots (seen in the bottom right of Figure 5.20).

Initial image analysis showed that the cameras focus lens ring moved during testing, probably due to the inverted camera orientation. Blu-tack was therefore attached to the focus lens ring during each test setup to remove this error.

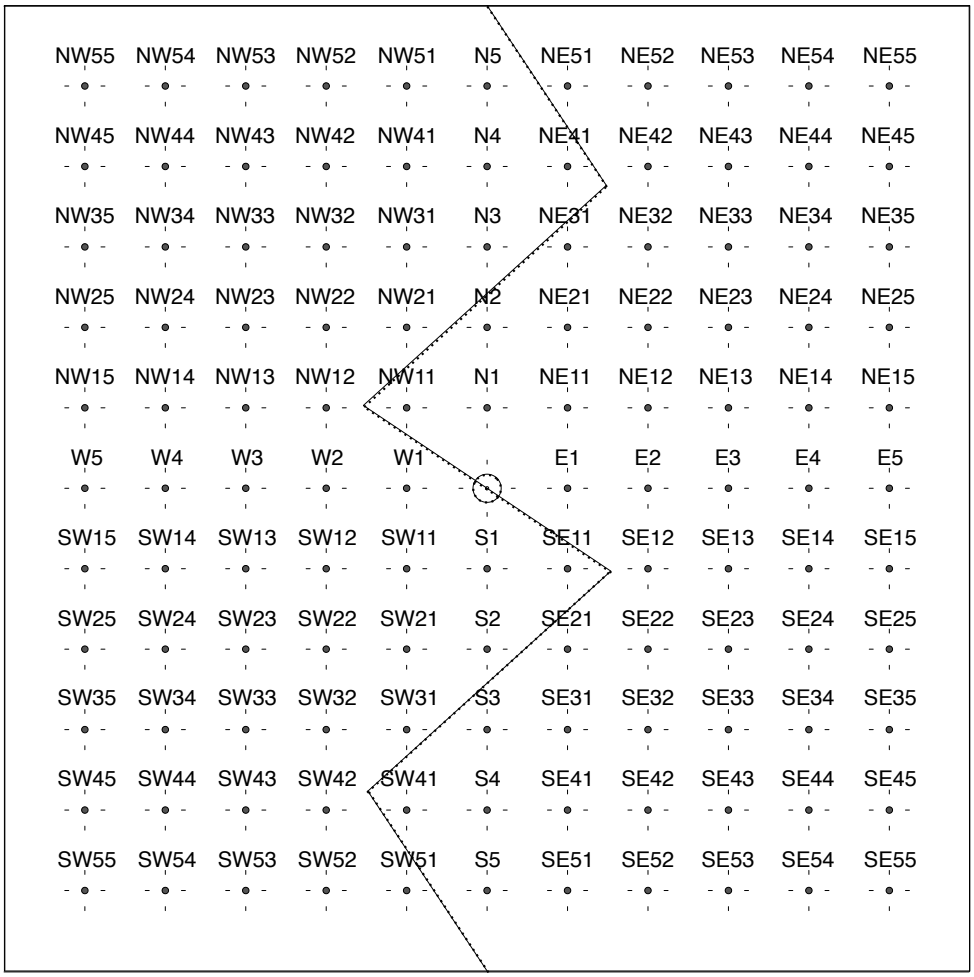

Figure 5.19: DIC camera calibration board

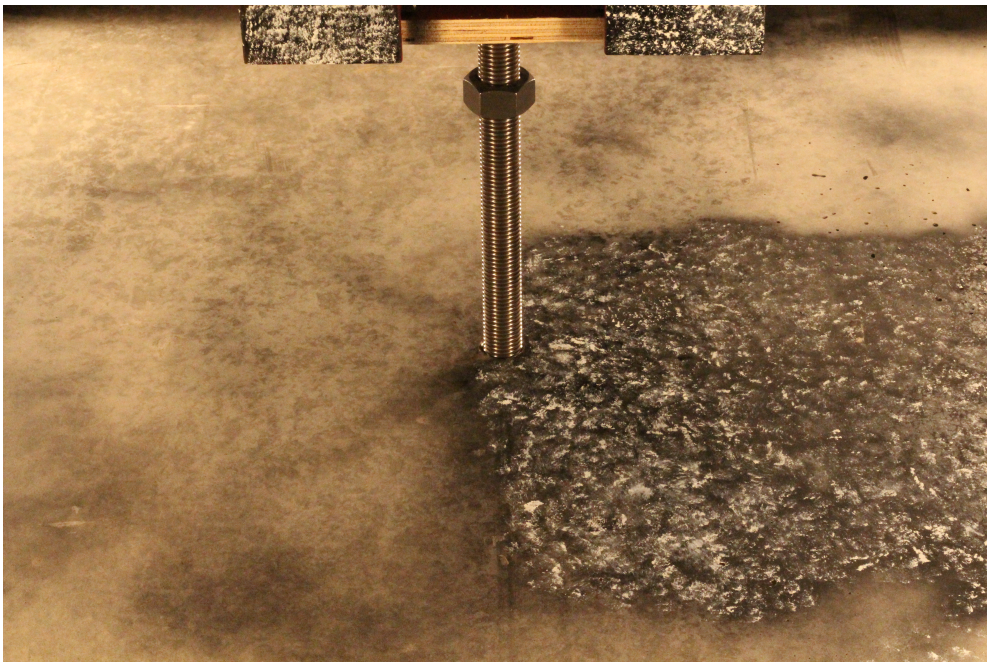

Figure 5.20: Photo of the texture optimisation in ambient 100 mm thick, 0.8% reinforced: unrestrained test

6

PUNCHING SHEAR SLAB-COLUMN EXPERIMENTAL RESULTS

This chapter presents the results of the experimental investigation of the punching shear slab-column experiments. The slab-column experimental data includes:

- failure loads and time to failure;
- slab-column load-deflection behaviours;
- slab temperature curve plots;
- slab temperature through thickness profiles;
- failure crack patterns;
- slab-column deflection history, annotated with test observations;
- axial in-plane reaction forces transferred by the slab-column onto the reaction frame;
- slab-column moments on the reaction frame; and
- material specimen strengths.

Section 6.1 presents the ambient test results, as the capacity of the unheated specimens was used to set the load applied to the heated slab-column tests. Sections 6.2 – 6.6 present the heated test results for the 50 mm, 75 mm and 100 mm thick 0.8% reinforced, 100 mm thick 1.5% reinforced and 100 mm unreinforced slab, respectively. Section 6.7 presents the residual strength tests undertaken on the slab-column specimens that did not fail during 120 minutes heating and subsequent cooling to 150°C throughout the slab thickness. Table 6.1 gives an initial overview of the test results. The deflection history and test observations of heated 0.8% reinforced slabs are presented in Sections 6.8 and 6.9, respectively. Similarly, the 100 mm thick slabs deflection history and test observations are presented in Sections 6.10 and 6.11, respectively. Section 6.12 presents the results of the strain gauge data, as slab-column reaction forces and moments on the reaction frame. The concrete and steel specimen strengths are presented in Section 6.13.

SPECIMEN ID	LOAD APPLIED DURING HEATING (KN)	FAILURE LOAD (KN)	RESIDUAL CAPACITY (KN)	DISPLACEMENT AT FAILURE LOAD (MM)	HEATING PHASE DURATION (MIN)
AU50-0.8	-	54.2	-	69.6	-
AU75-0.8	-	101.4	-	31.8	-
AU100-0	-	43.8	-	18.3	-
AU100-0.8	-	226.3	-	62.4	-
AU100-1.5	-	279.7	-	38.7	-
HU50-0.8	25.5	-	55.7	40.3	120
HU75-0.8	82.8	-	90.7	17.7	121
HU100-0	30.0	38.9	-	2.2	6
HU100-0.8	174.6	174.8	-	30.8	4
HU100-1.5	234.0	237.0	-	28.5	14
HR50-0.8	26.4	-	64.4	29.4	121
HR75-0.8	82.0	-	115.5	20.0	120
HR100-0	33.1	-	82.2	28.2	99
HR100-0.8	166.5	-	245.1	20.7	120
HR100-1.5	232.7	233.2	-	21.2	105

Table 6.1: Slab-column summary test results

6.1 AMBIENT TESTS

This section presents the results of the five ambient unrestrained slab-column experiments, as given in Table 5.1; 50 mm with 0.8% steel (AU50-0.8), 75 mm with 0.8% steel (AU75-0.8), 100 mm with 0.8% steel (AU100-0.8), 100 mm with no flexural reinforcement (AU100-0) and 100 mm with 1.5% steel (AU100-1.5). The ultimate capacities of the ambient specimens were used to calculate the sustained load to be applied during the heated tests.

6.1.1 *Failure crack patterns*

Figure 6.1 shows the failure cross-sectional crack patterns of all the ambient tested slab-column specimens. The direction, N–S of the frame in Figure 6.1, depicts which cross-sectional half is presented. The column stub was cut off prior to cutting the cross-sections, in order to make it easier to cut them. The blue arrows indicate the reaction forces acting on the slabs, whereas the load applied is shown with black arrows.

The crack patterns of the 50 mm and 75 mm thick slabs have many cracks rather than the 100 mm thick slabs, which have a clear critical shear crack. Additionally, the thinner slabs have vertical cracks through the slab depth, where the column stub joins the slab. These two specimens failed in flexure-shear mechanisms, as shown in the plan view Figures 6.2 and 6.3. The crack patterns are marked in red on the top and bottom slab surfaces, with the reinforcement positioning superimposed in the background. The crack developments on the bottom surface can be seen to align with the flexural reinforcement. The top surface crack pattern in Figure 6.2 shows a ductile failure mechanism with concentric cones formed.

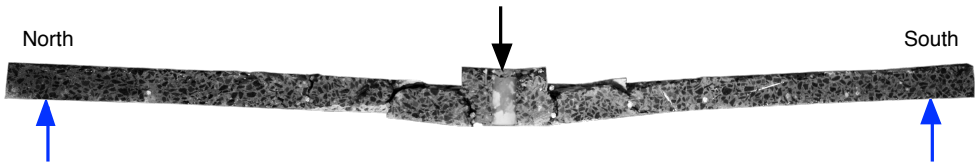

(a) 50 mm thick, 0.8% reinforced

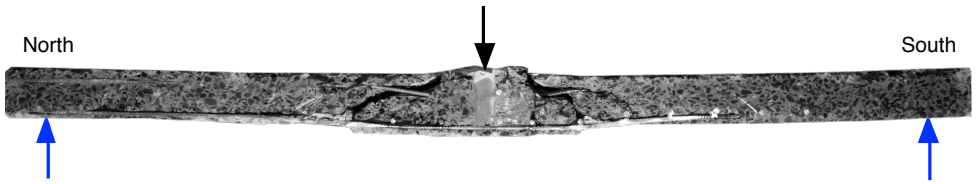

(b) 75 mm thick, 0.8% reinforced

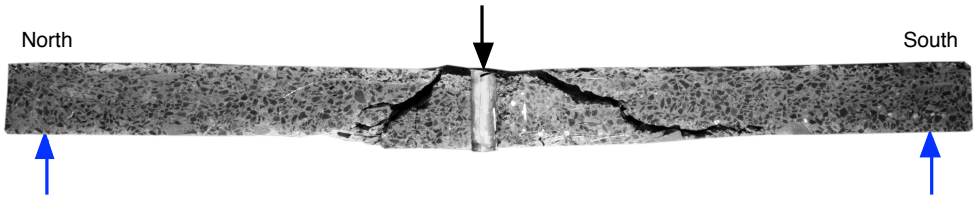

(c) 100 mm thick, 0.8% reinforced

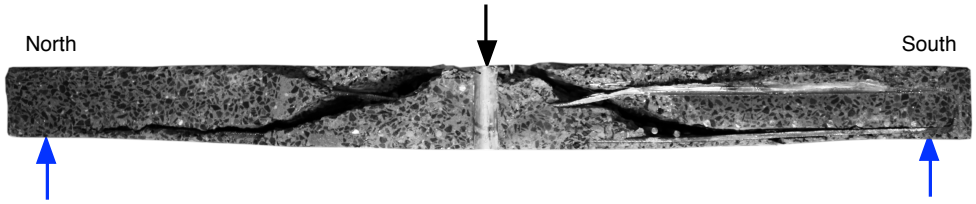

(d) 100 mm thick, 1.5% reinforced

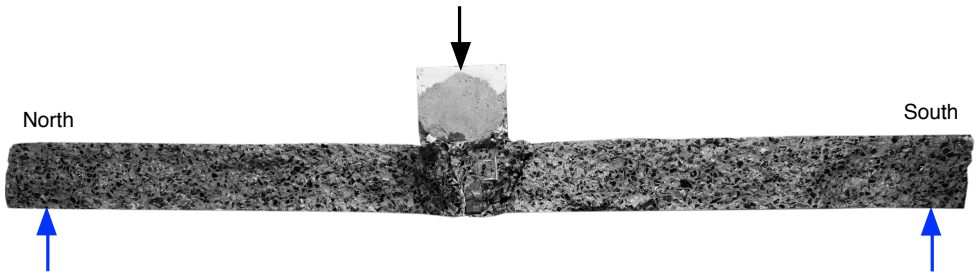

(e) 100 mm thick, unreinforced

Figure 6.1: Cross-sections of ambient, unrestrained slabs showing the post-failure crack patterns

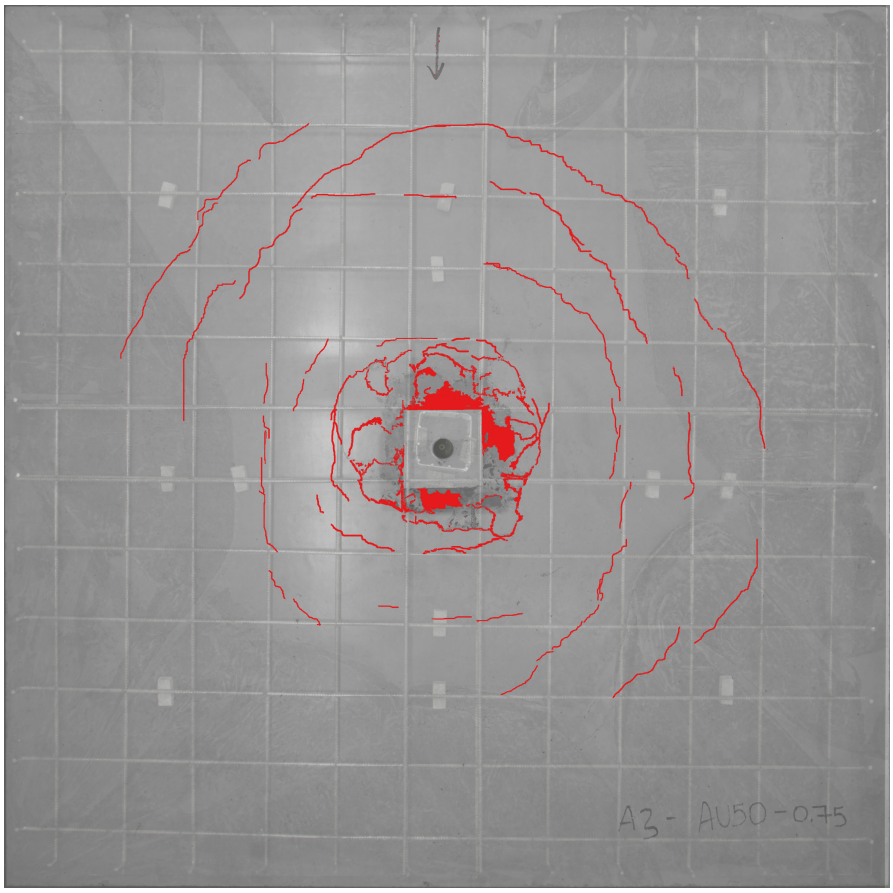

(a) Top surface

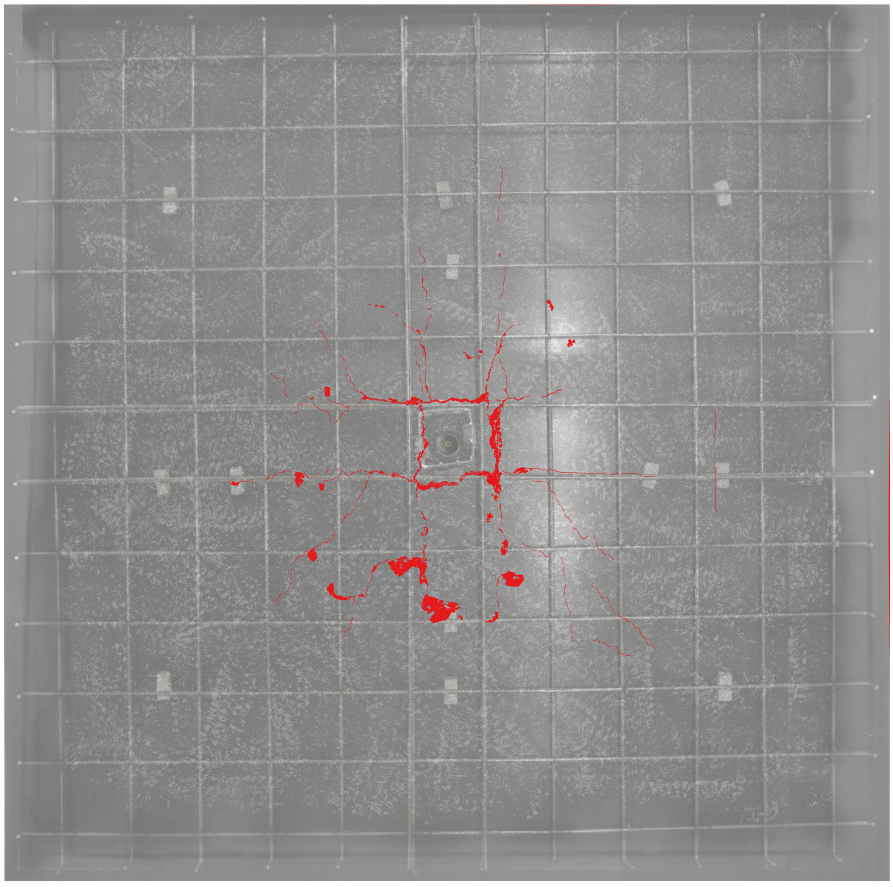

(b) Bottom surface

Figure 6.2: Ambient 50 mm thick, 0.8% reinforced: unrestrained slab showing the plan post-failure crack patterns

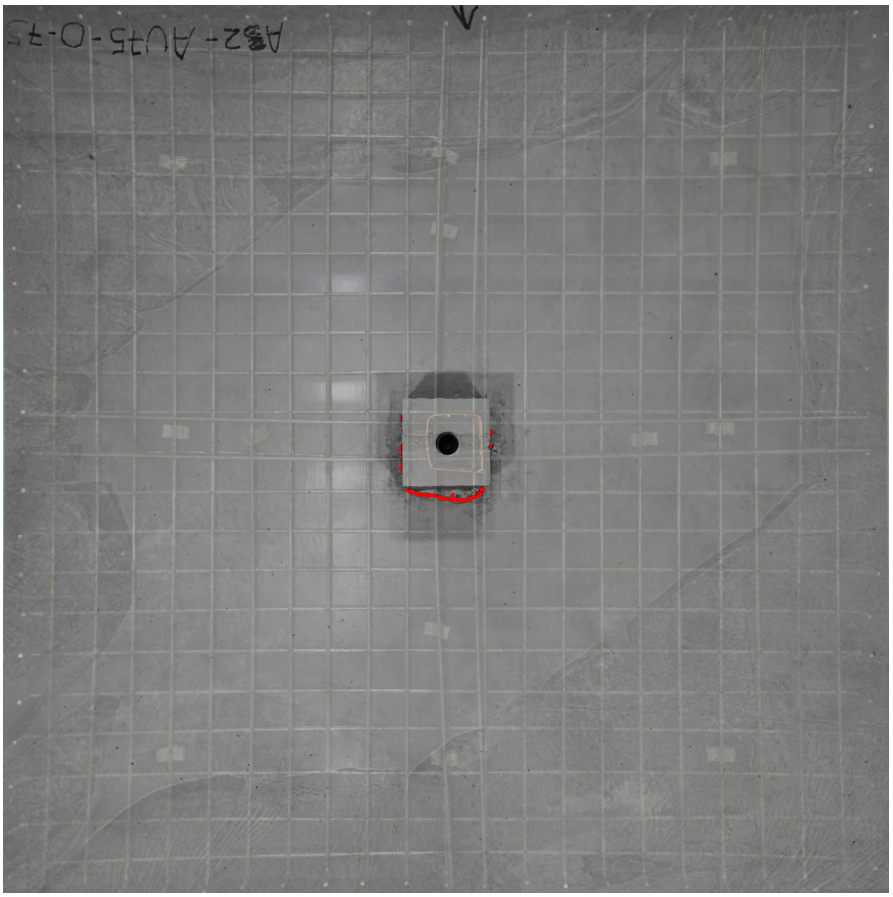

(a) Top surface

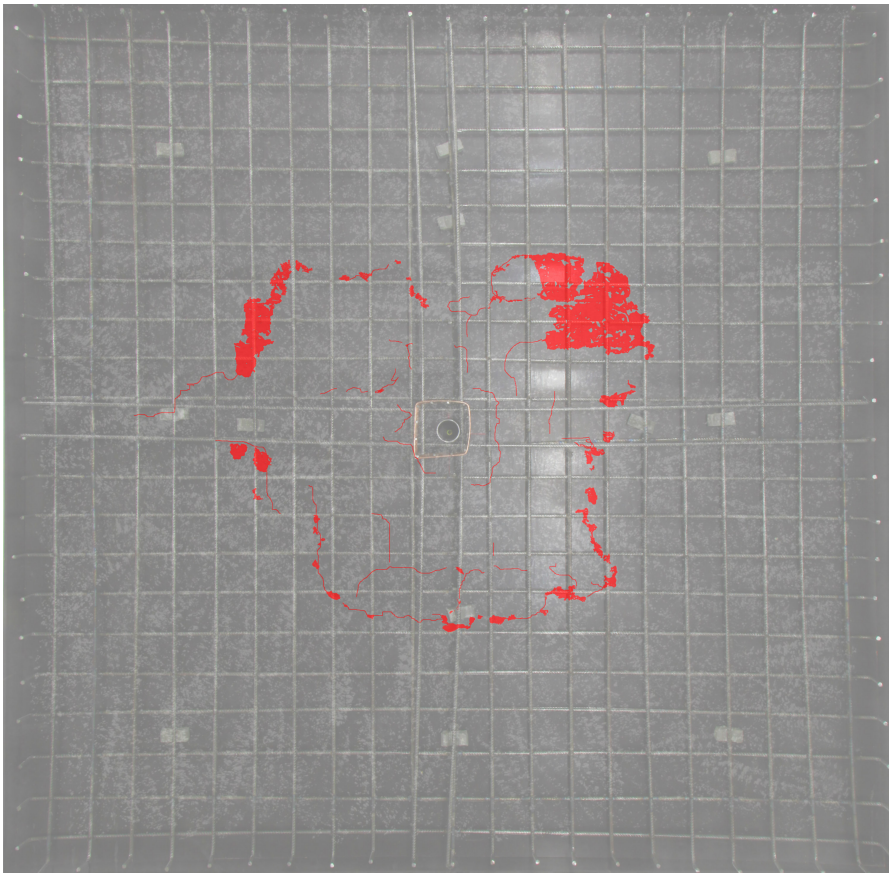

(b) Bottom surface

Figure 6.3: Ambient 75 mm thick, 0.8% reinforced: unrestrained slab showing the plan post-failure crack patterns

The cross-sections in Figures 6.1c and 6.1d show critical shear cracks formed in both the 100 mm thick reinforced slabs. As expected the increase in slab depth caused a larger punching shear cone to form in these pure shear failure mechanisms. The plan crack patterns shown in Figures 6.4 and 6.5, respectively do not clearly show the pure punching shear failure, as seen in the cross-sections. The critical shear crack is shown to form from around the loaded column stub at the top surface in both the 100 mm thick reinforced slabs. The bottom surface has many cracks in Figure 6.4, which was less reinforced (0.8%) then Figure 6.5, with fewer cracks (1.5%).

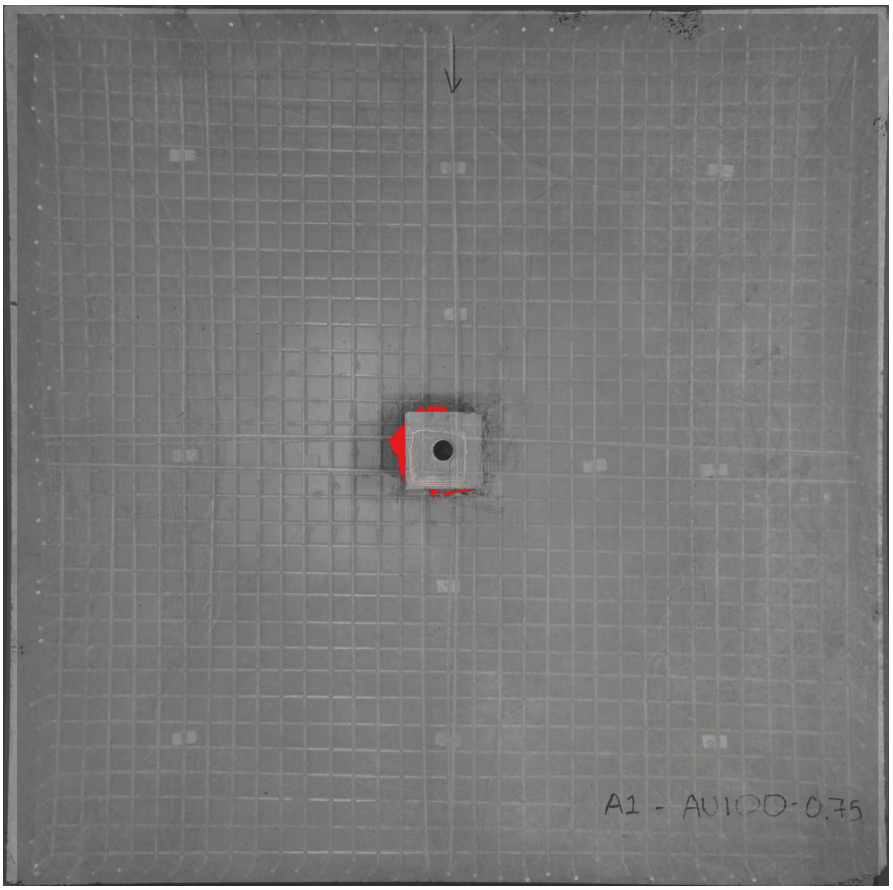

(a) Top surface

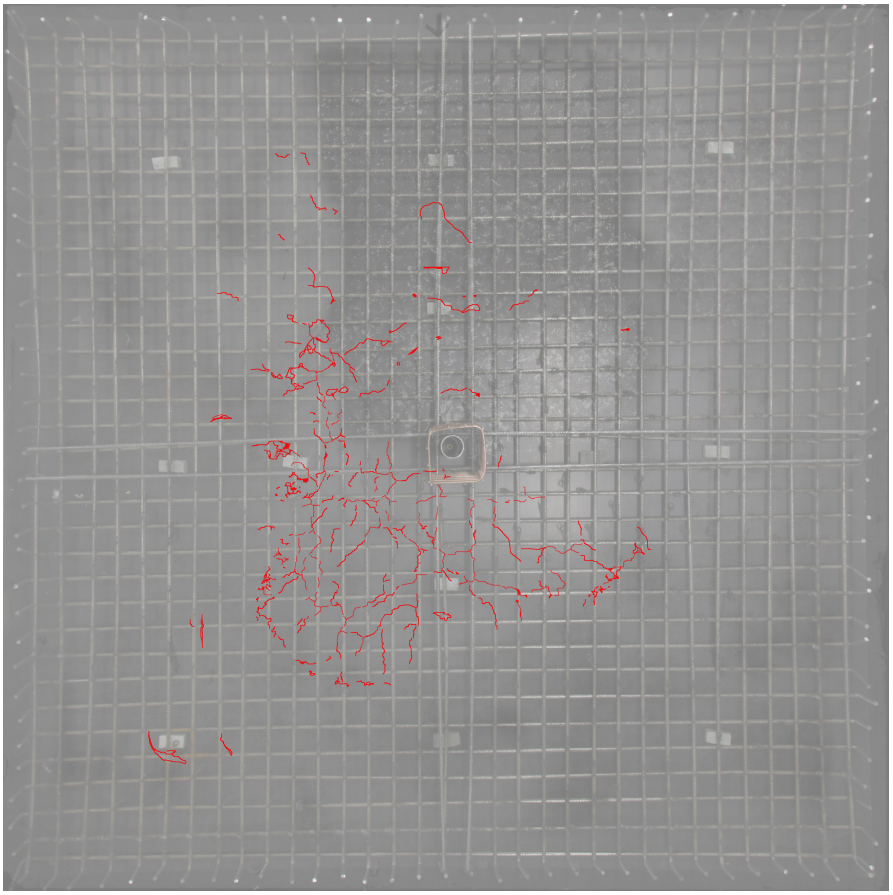

(b) Bottom surface

Figure 6.4: Ambient 100 mm thick, 0.8% reinforced: unrestrained slab showing the plan post-failure crack patterns

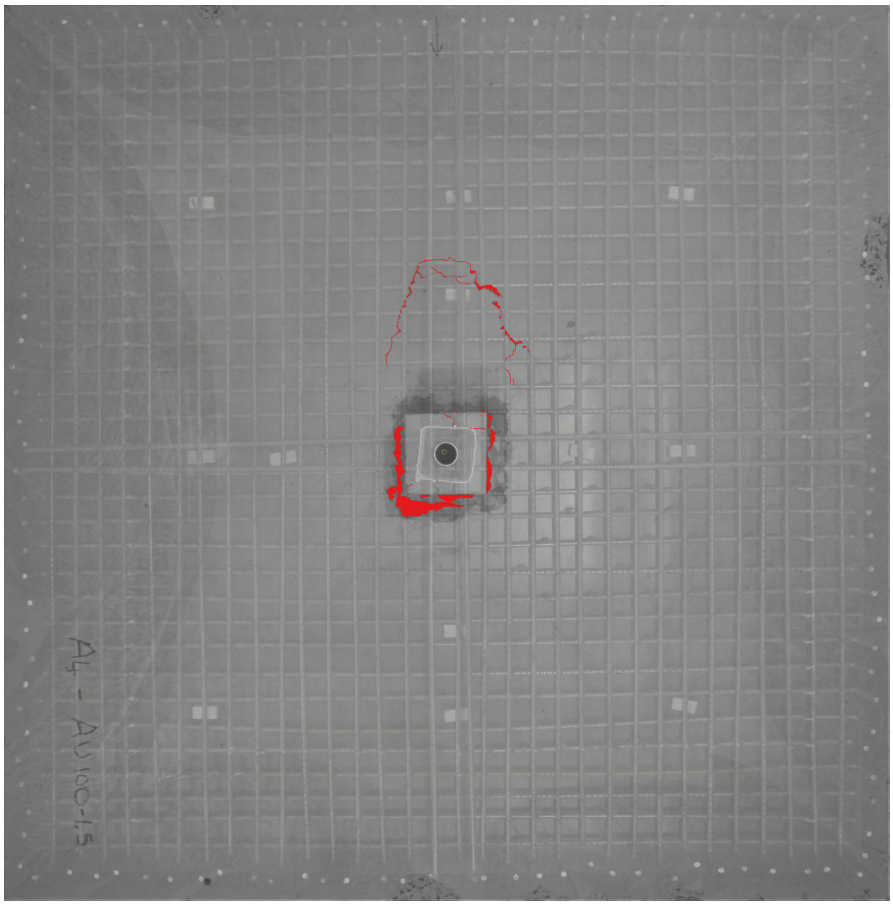

(a) Top surface

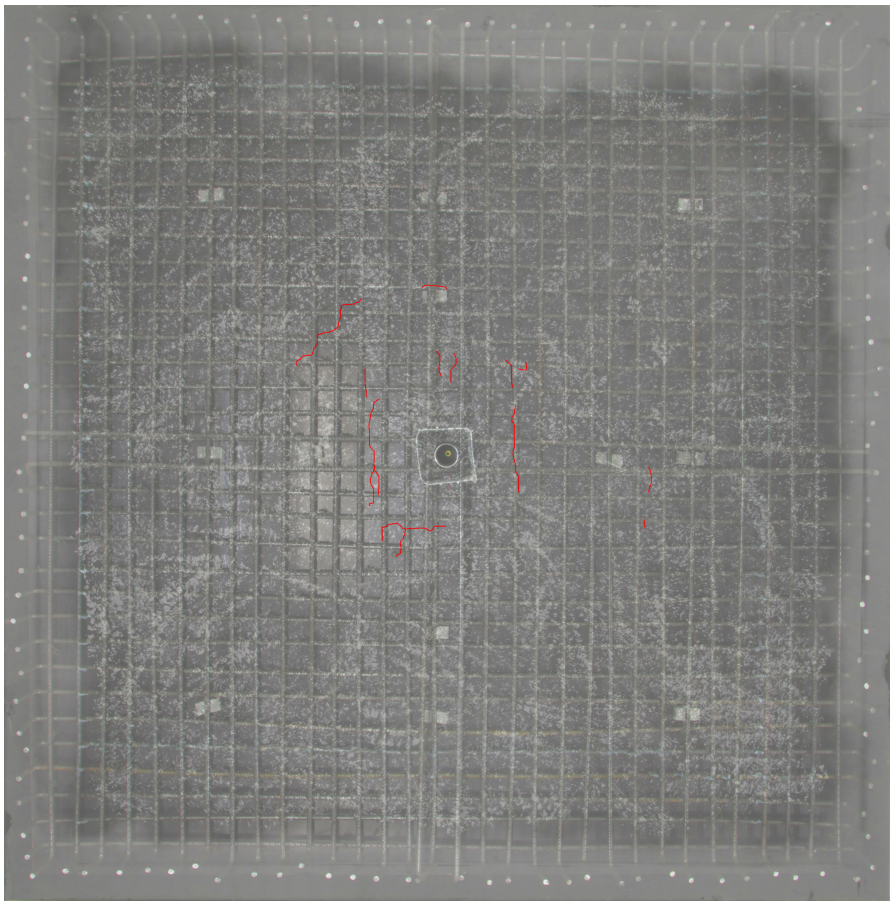

(b) Bottom surface

Figure 6.5: Ambient 100 mm thick, 1.5% reinforced: unrestrained slab showing the plan post-failure crack patterns

Figure 6.6: Flexural failure mechanism of 100 mm thick, 0% slab

The unreinforced 100 mm thick slab failed in flexure with Figures 6.6 and 6.7 showing the sagging yield lines that formed.

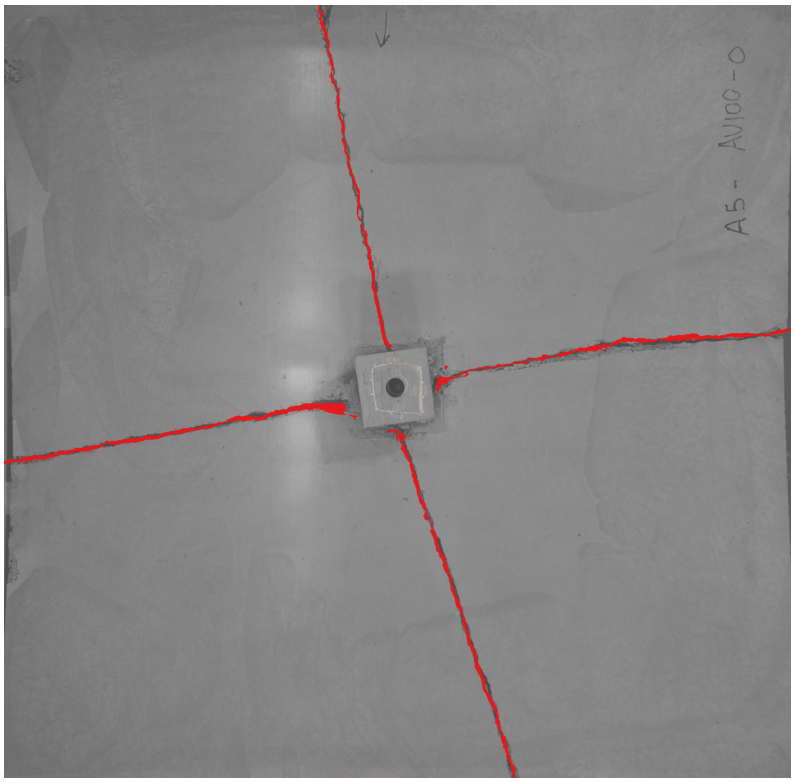

(a) Top surface

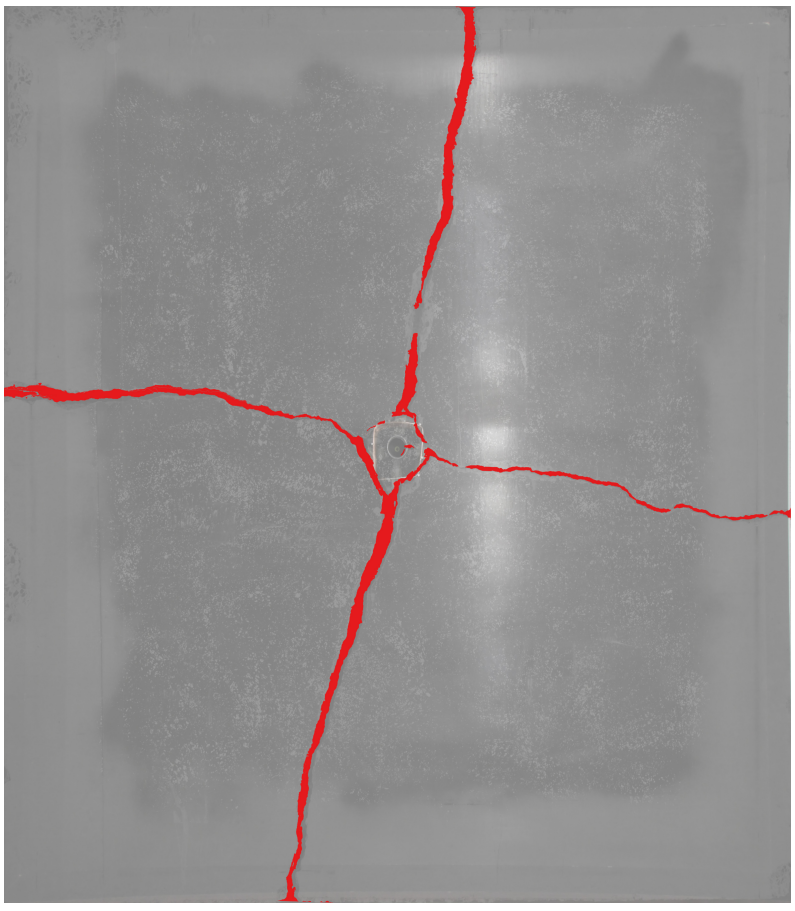

(b) Bottom surface

Figure 6.7: Ambient 100 mm thick, 0% reinforced: unrestrained slab showing the plan post-failure crack patterns

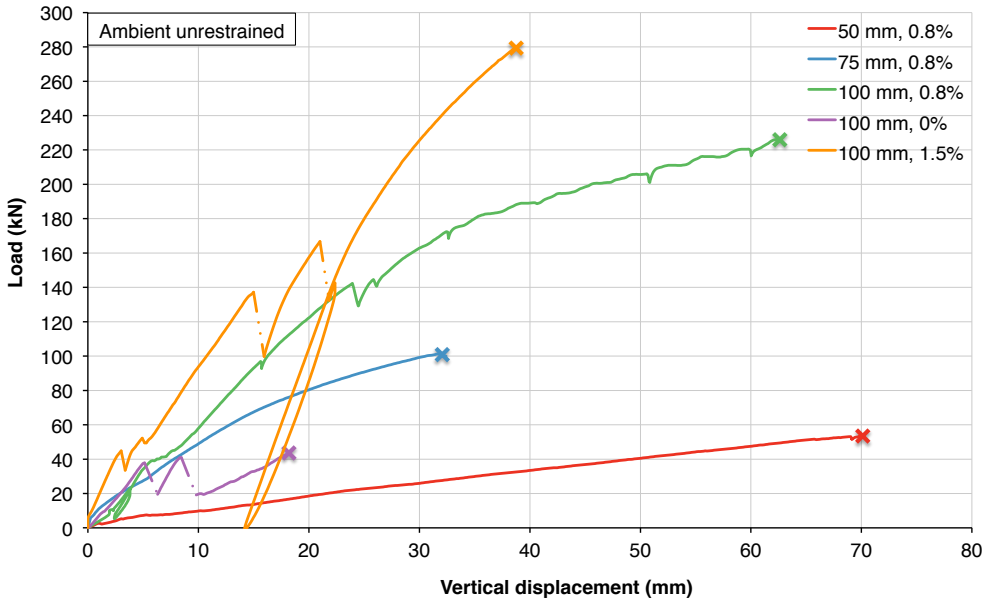

Figure 6.8: Load-deflection behaviour of ambient tests

6.1.2 *Load-deflection behaviours and failure modes*

Figure 6.8 shows the load-deflection behaviours for the five ambient slab-column tests. The load plotted is the calibrated pressure transducer load, measured in the hydraulic jack pipeline near the slab. The vertical displacement plotted is the central deflection measured by the LP, positive in the downwards direction (i.e. in the direction of loading). The load-deflection behaviours in this work consistently present the pressure transducer load and LP vertical displacement. Where there are no data points, a dashed-dotted line joins the load-deflection curve.

The slabs were loaded at a rate of 2 mm/min until failure (annotated with a cross). The experimental failure loads varied greatly. As expected, an increase in slab thickness, increases the capacity of the 0.8% reinforced slabs. The unreinforced, 100 mm thick slab failed at a low load, similar to the 50 mm, 0.8% reinforced specimen. The most heavily reinforced, 100 mm thick slab had the greatest capacity of all the specimens.

The load applied in AU100-1.5 drops and recovers at approximately 137 kN and again at 167 kN. These load drops were caused by the channel sections rotating under load, as seen by the comparison in Figure 6.9. After the second drop in load, the slab was unloaded for safety and it was re-loaded to failure. The only other ambient test where there was channel section movement was AU100-0.8 at approximately 141 kN, the S support channel section rotated and banged into the W section.

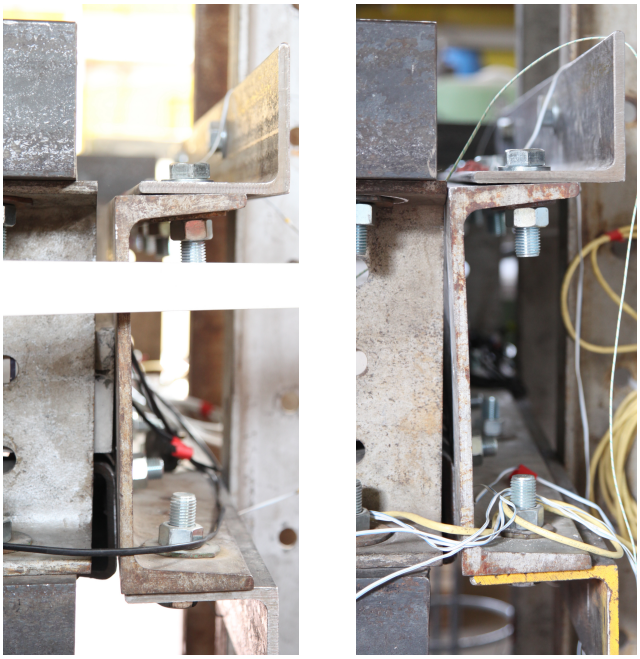

(a) Unrotated E support channel section

(b) Rotated S support channel section

Figure 6.9: Ambient 100 mm thick, 1.5% reinforced: unrestrained test, support channel section photos

Figure 6.10 shows test observations with deflection history for all the ambient tested slabs.

6.1.3 *Capacity comparison to Muttoni's CSCT*

As the ambient experimental failure loads had a high variability, the load applied to the heated specimens was factored by taking Muttoni's CSCT (Guandalini et al., 2009) predictions into consideration. This sustained load to be applied during the heated tests was taken as 70% of the ambient capacity (in accordance with BS EN 1992-1-2:2004 (2010)). Table 6.2 compares the designed Muttoni failure loads with the experimental failure loads. Table 6.2 shows that excluding the 50 mm thick slab, the failure load percentage difference between the CSCT design and experimental measured loads had some consistency considering the small test sample.

No CSCT prediction could be calculated for the unreinforced specimen, as this would not be applicable in a real building. The design failure load for the unreinforced slab, AU100-0 was back calculated using the average percentage difference of the other four tests, which was 68%.

Figure 6.11 shows graphically how the calculated applied load for the heated tests compares to the experimental ambient temperature failure load.

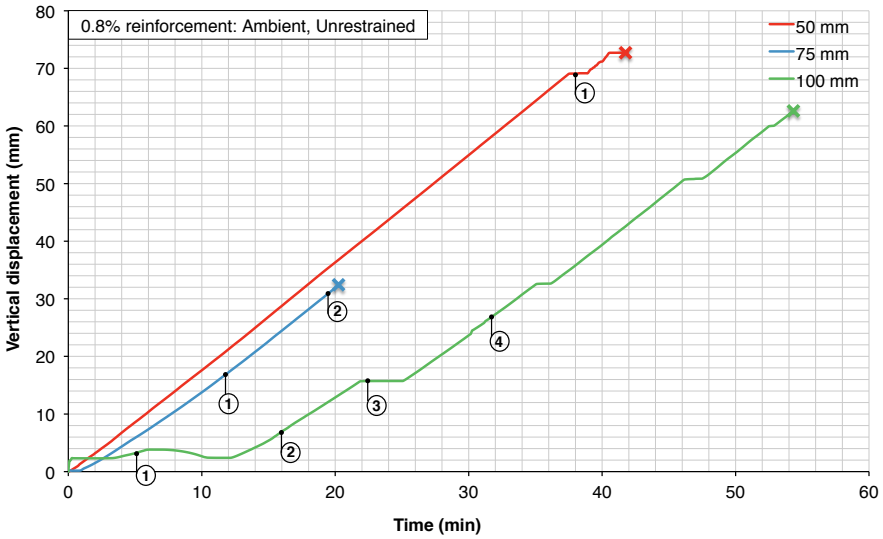

① required further jack extension, so hand pump used

① cracks form
② frame noise prior to slab failure

① noise from concrete bedding in
② top surface cracks near supports and diagonal into centre
③ loading pause to change actuator settings
④ S frame C-section rotate and bang into W frame C-section

(a) 0.8% reinforced

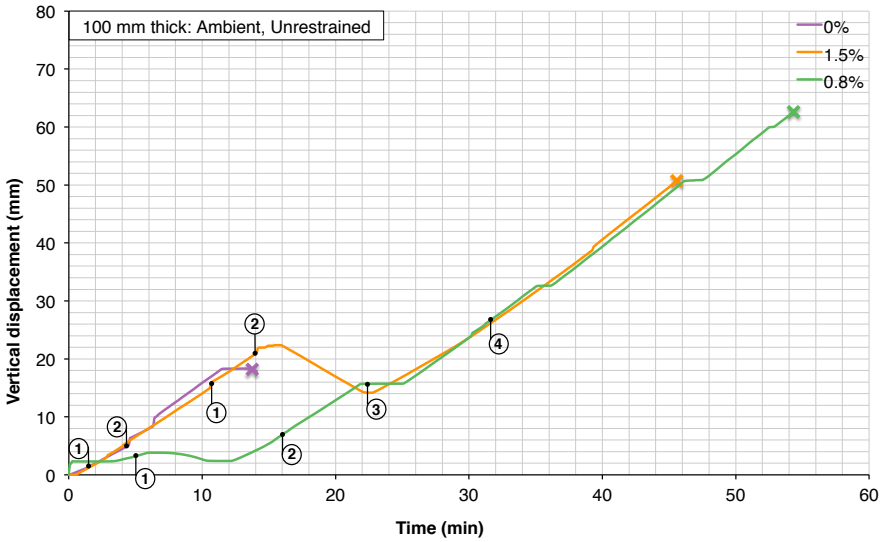

① noise from concrete bedding in
② crack forming

① S and W frame C-sections rotate and bang into W and N frame C-sections, respectively
② E frame C-section rotate and bang into S frame C-section

① noise from concrete bedding in
② top surface cracks near supports and diagonal into centre
③ loading pause to change actuator settings
④ S frame C-section rotate and bang into W frame C-section

(b) 100 mm thick

Figure 6.10: Test observations for all ambient unrestrained slabs

Specimen ID	Column 1 Experimental failure load (kN)	Column 2 Muttoni design failure load (kN)	Column 3 Failure load difference (%)	Column 4 Factored Muttoni design load (kN)	Column 5 Applied load for heated test (kN)
AU50-0.8	54.2	24	126	40	28
AU75-0.8	101.4	72	41	121	85
AU100-0	43.8	26	68	44	31
AU100-0.8	226.3	144	57	242	169
AU100-1.5	279.7	190	47	319	223
		Average	68		

$$\text{Column 3} = 100 * \frac{(\text{Column 1} - \text{Column 2})}{\text{Column 2}} \tag{6.1}$$

$$\text{Column 4} = \text{Column 2} * \left(1 + \frac{\text{Column 3 Average}}{100}\right) \tag{6.2}$$

$$\text{Column 5} = 0.7 * \text{Column 4} \tag{6.3}$$

Table 6.2: Ambient experimental failure loads and calculated applied loads for heated tests

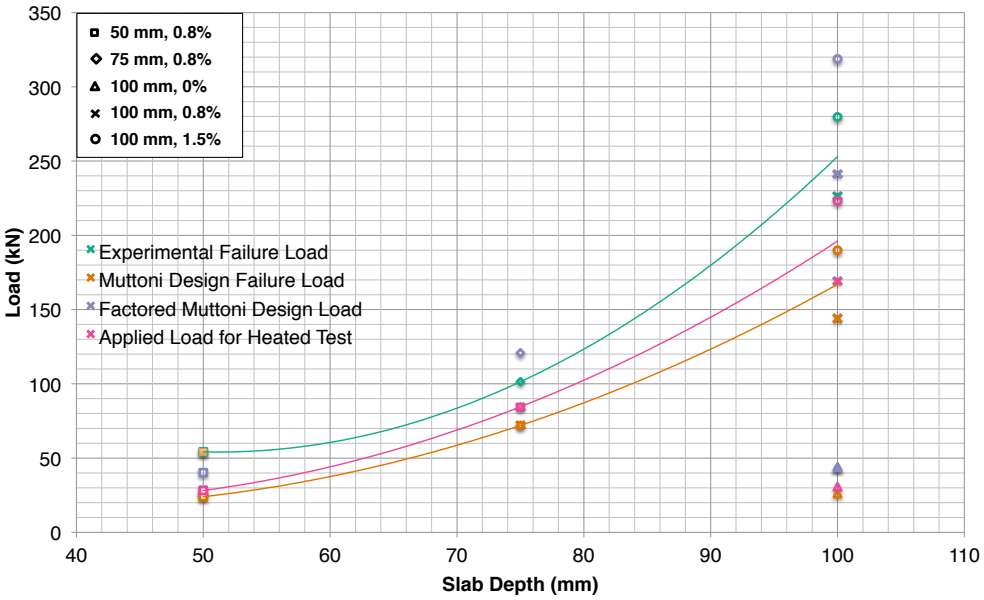

Figure 6.11: Experimental and design failure load comparison

The subsequent sections describe each of the heated slab tests:

- Section 6.2: 50 mm with 0.8% reinforcement ratio: the ambient unrestrained (AU50-0.8), the heated unrestrained (HU50-0.8) and the heated restrained (HR50-0.8);
- Section 6.3: 75 mm with 0.8% reinforcement ratio: the ambient unrestrained (AU75-0.8), the heated unrestrained (HU75-0.8) and the heated restrained (HR75-0.8);
- Section 6.4: 100 mm with 0.8% reinforcement ratio: the ambient unrestrained (AU100-0.8), the heated unrestrained (HU100-0.8) and the heated restrained (HR100-0.8);
- Section 6.5: 100 mm with 1.5% reinforcement ratio: the ambient unrestrained (AU100-1.5), the heated unrestrained (HU100-1.5) and the heated restrained (HR100-1.5); and
- Section 6.6: 100 mm unreinforced: the ambient unrestrained (AU100-0), the heated unrestrained (HU100-0) and the heated restrained (HR100-0).

Spalling of the concrete did not occur during any of the heated tests.

6.2 50 mm thick, 0.8% reinforced tests

This section presents the results of the three slab-column experiments that were 50 mm thick with 0.8% reinforcement ratio, as given in Table 5.1: the

ambient unrestrained (AU50-0.8), the heated unrestrained (HU50-0.8) and the heated restrained (HR50-0.8).

6.2.1 *Test overview*

The key 50 mm thick slab-column test outcomes are summarised in bullet points here:

- Both elevated temperature tests were heated for 120 minutes approximately;
- The propane gas flow rate was noted to decrease towards the end of the heating phase in both tests, at 75 minutes in the unrestrained test and 112 minutes in the restrained test;
- The maximum concrete temperature near the heated surface was approximately 500°C in the unrestrained slab and 630°C in the restrained slab;
- The flexural steel at an effective depth of 31 mm, reached a maximum temperature during the cooling phase, of an approximate average of 350°C for the unrestrained slab and 445°C for the restrained slab;
- Neither heated slab failed during the punching shear test, therefore they were both residually tested (described in Section 6.7.1);
- All heated slabs failed residually in flexure-shear mechanisms;
- The ambient temperature tested slab had a capacity of 54.2 kN. The sustained loads of 25.5 kN and 26.4 kN were applied during heating in the unrestrained and restrained tests, respectively; and
- The applied load increased during the cooling phase of the HU50-0.8 test due to the actuator having reached its maximum travel length.

6.2.2 *Temperature curves*

Figure 6.12 shows the temperature curves for the heated tests, with heating and cooling periods annotated. The thermocouple depths were measured from the heated surface downwards after failure. The variance in temperature curves within each test is assumed to be caused by the difference in the thermocouple measured depths and different positioning of the thermocouple trees in the slabs relative to the radiant panel array in the frame (discussed further in Chapter 7). The temperature curves for the unrestrained and restrained tests

attain a different peak temperature, which is a further indication that the two tests had different heating curves.

At 75 minutes after ignition of the unrestrained test and 112 minutes after ignition of the restrained test, the propane gas flow rate was noted to decrease continuously until the end of the heating phase. This caused the different maximum temperature attained and it being reached prior to the full 120 minutes heating. A temperature of 500°C was recorded at 1 mm from the surface (S side thermocouple) in the unrestrained case (Figure 6.12a) compared to the approximate 630°C measured at the same thermocouple location and depth in the restrained test (Figure 6.12b). In the unrestrained test, the W thermocouples at depths 15, 35 and 40 mm from the surface are comparable with the N and S location thermocouple readings. This singles out the N thermocouple at 7 mm as likely to have incorrect readings. The cooling phase lasted 92 minutes in the restrained test, whereas it was only 69 minutes in the unrestrained test, due to lower peak temperatures having been attained.

6.2.3 *Temperature profiles through the slab thickness*

Figures 6.13 – 6.15 show the temperature profiles through the thickness of the slab, for the unrestrained test thermocouple trees are positioned in the N, S and W of the frame, respectively. Curved lines join the data points together to represent profiles at 10 minute time intervals throughout the test. Note that the heated slab surface is at the top of the plot due to the inverted test setup. The red continuous lines correspond to the heating phase and the dashed blue lines, the cooling phase. The three thermocouple trees show slightly different spatial variations in extrapolated profiles, even though the radiant panels were visually calibrated to produce an even heat flux (as described in Section 5.4.1).

Plotting all three thermocouple profiles on the same plot is not realistic, however Figure 6.16 shows the difference in the profiles for the unrestrained slab heating time steps, 110 and 200 minutes after ignition. The temperature near the slab surface measured by thermocouples in the N, S and W of the reaction frame have a large difference of up to approximately 100°C, at 110 minutes after ignition. This shows the radiant panel array did not produce a perfectly even heat flux across the upper slab surface. The measured effective depth of the flexural steel after failure was 31 mm down from the heated surface in both the unrestrained and restrained slabs. Figure 6.16 shows that the three thermocouple trees record similar temperatures at 110 minutes after ignition, at approximately the flexural steel depth and below. The 200 minute test interval profiles of all three thermocouple trees in Figure 6.16, are similar.

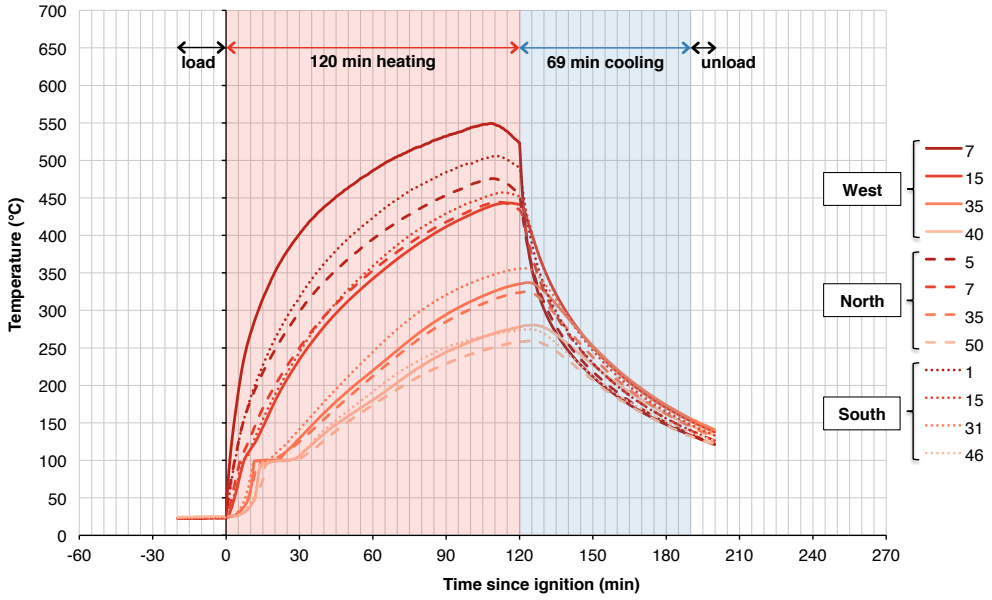

(a) Heated Unrestrained

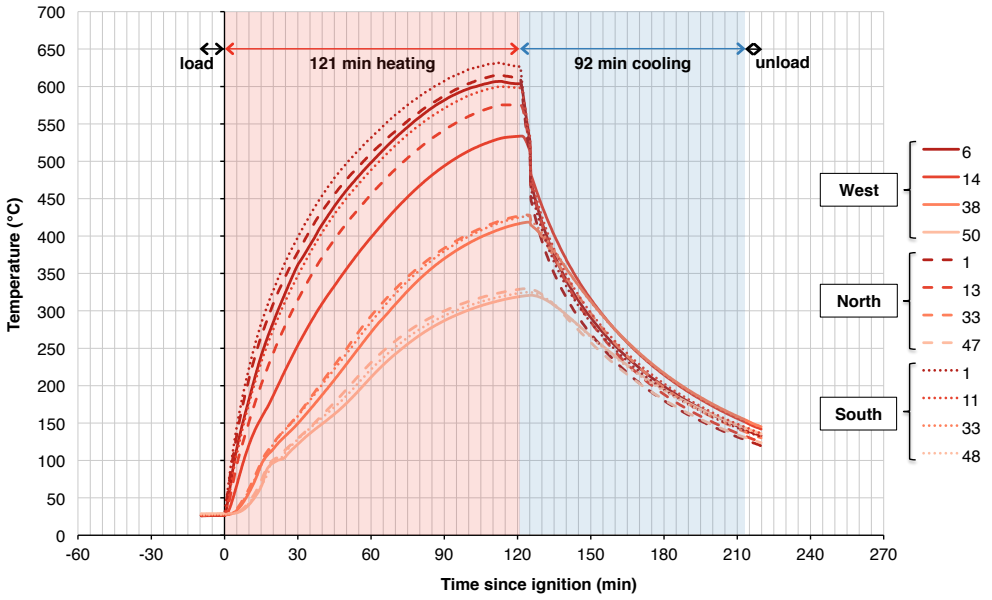

(b) Heated Restrained

Figure 6.12: Temperature curves for 50 mm thick, 0.8% slabs

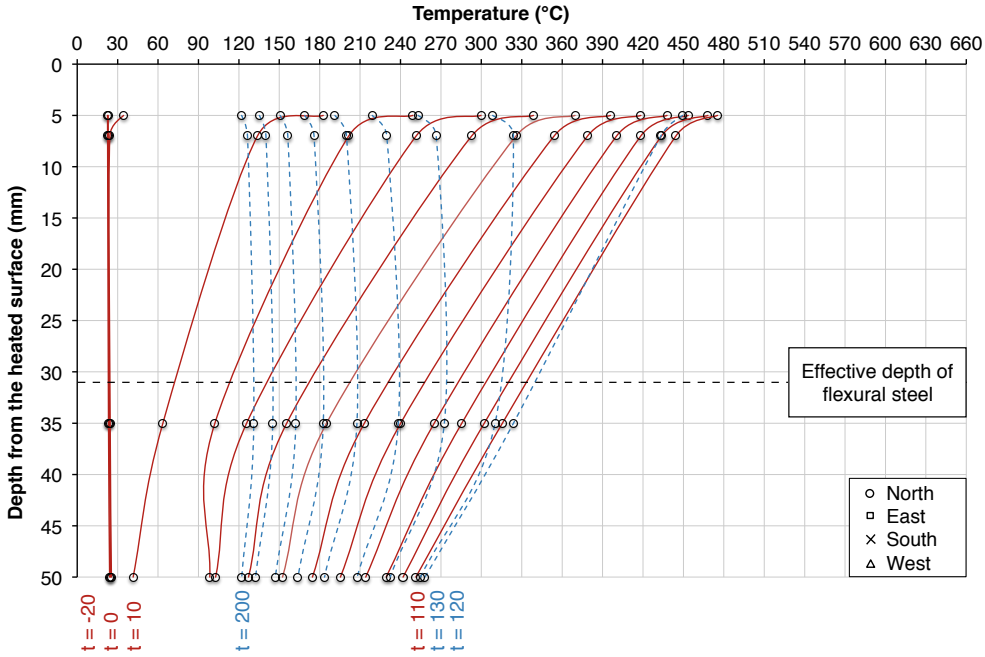

Figure 6.13: North temperature profile through 50 mm thickness, 0.8%: unrestrained slab

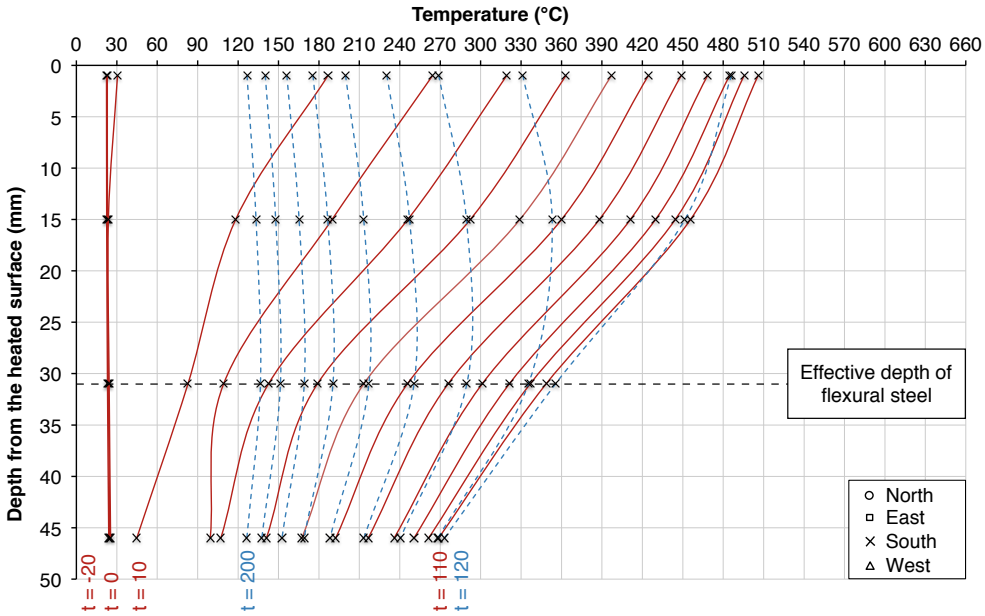

Figure 6.14: South temperature profile through 50 mm thickness, 0.8%: unrestrained slab

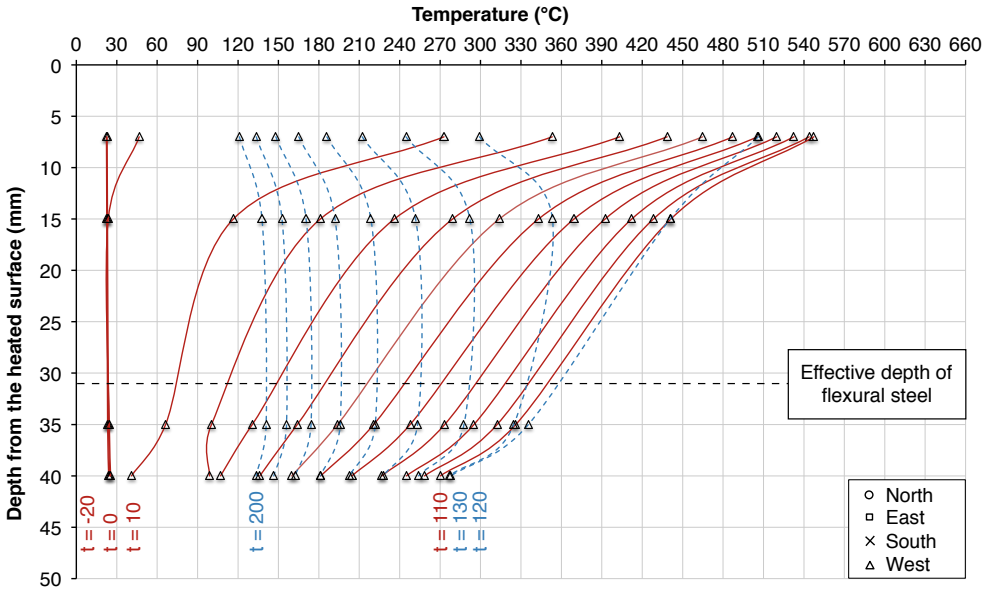

Figure 6.15: West temperature profile through 50 mm thickness, 0.8%: unrestrained slab

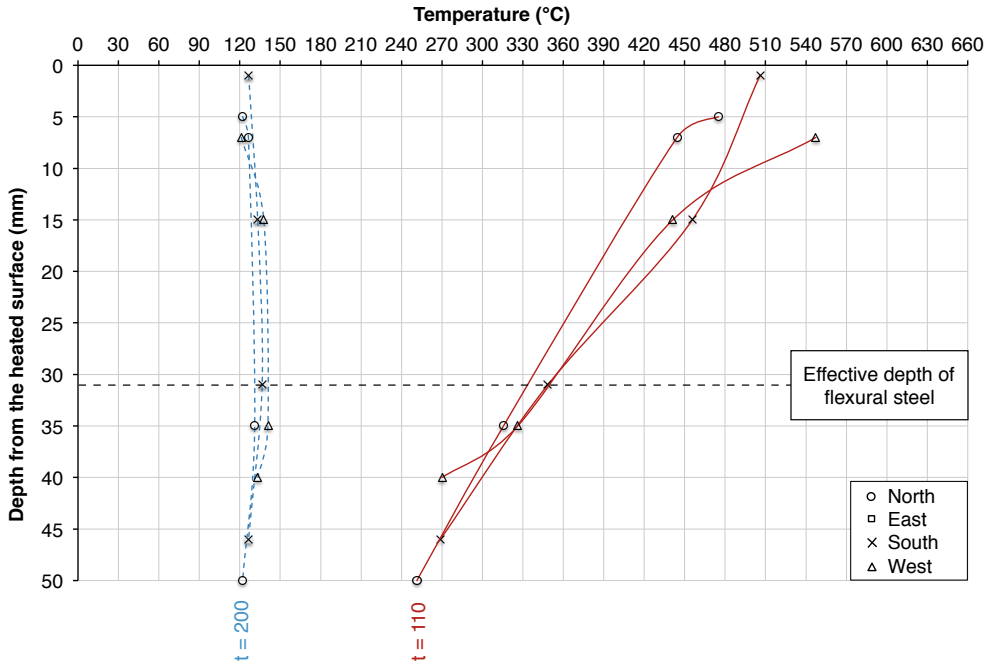

Figure 6.16: Thermocouple tree temperature profile comparison at 110 minutes and 200 minutes after ignition (50 mm thick, 0.8%: unrestrained slab)

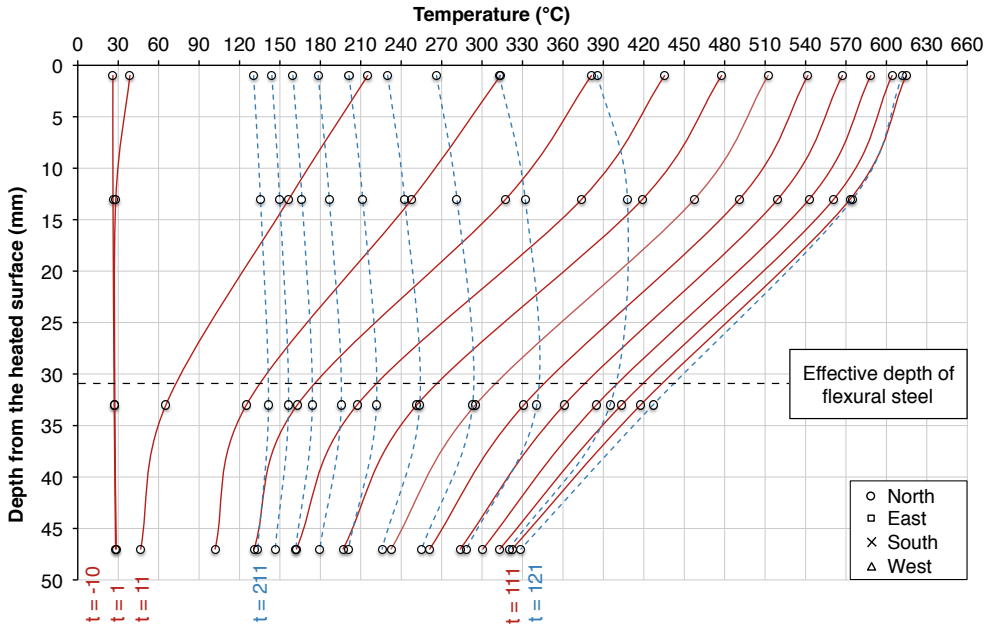

Figure 6.17: North temperature profile through 50 mm thickness, 0.8%: restrained slab

The comparable temperature profiles for the restrained test are shown in Figures 6.17 – 6.19. The unrestrained and restrained test profiles are similar at the three thermocouple tree locations, however the heat front penetrates into the restrained slab more efficiently than the unrestrained slab. The near surface temperatures are greater soon after ignition, which caused the temperature gradient through the slab thickness to be greater and the profile hence more curved.

The maximum surface temperature is reached in both tests, at all thermocouple locations at approximately 110 minutes after ignition. The temperatures on the unheated surface of both slabs reaches a maximum during the cooling phase, as the heat front penetrates the slab. The flexural steel at a depth of 31 mm, reached a maximum temperature during the cooling phase of an approximate average of 350°C for the unrestrained slab and 445°C for the restrained slab. The rate of temperature increase towards the end of the unrestrained heating (80-110 minutes time intervals) starts to decrease in comparison to the restrained. This can be seen in the unrestrained temperature profiles by the 10 minute time interval profiles getting closer together.

6.2.4 *Failure crack patterns*

These thinner, three specimens failed in a flexure-shear mode. Figure 6.20 shows the failure cross-sections through the 50 mm thick slab-column specimens, from N–S of the frame. The red arrows indicate the action of heat

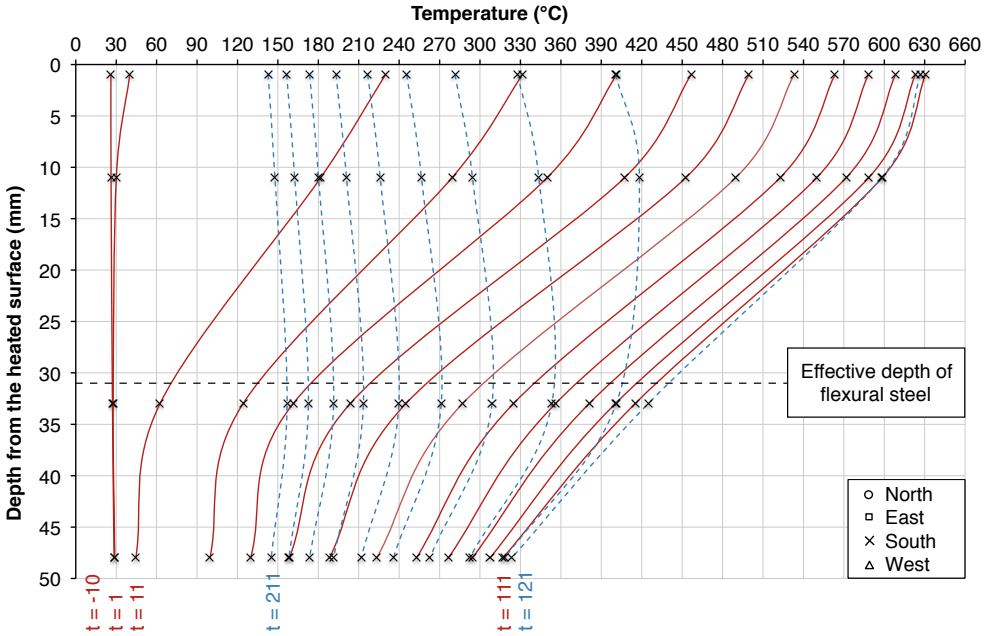

Figure 6.18: South temperature profile through 50 mm thickness, 0.8%: restrained slab

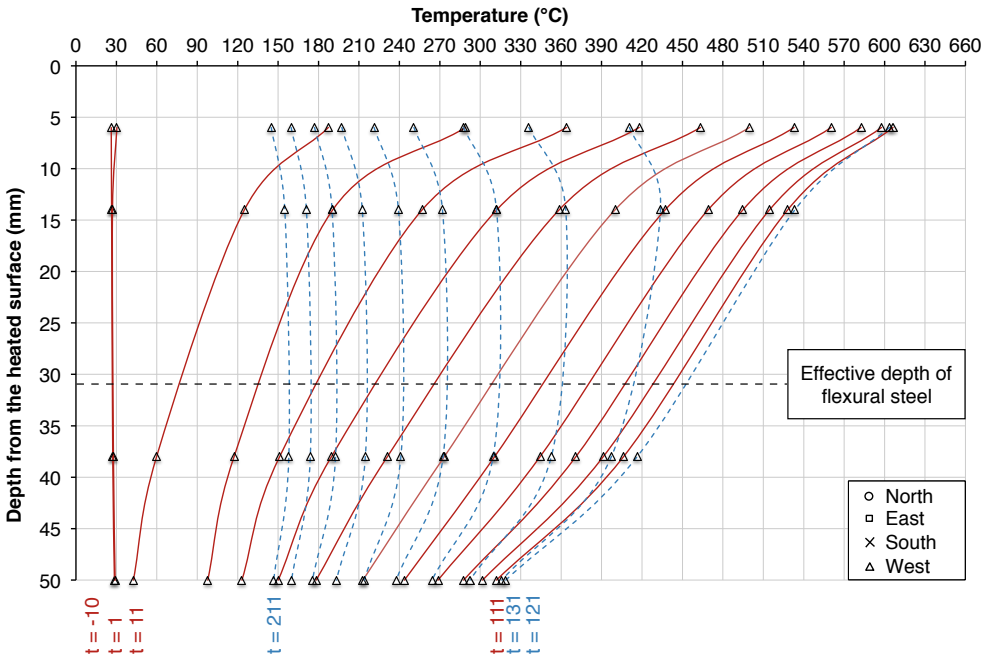

Figure 6.19: West temperature profile through 50 mm thickness, 0.8%: restrained slab

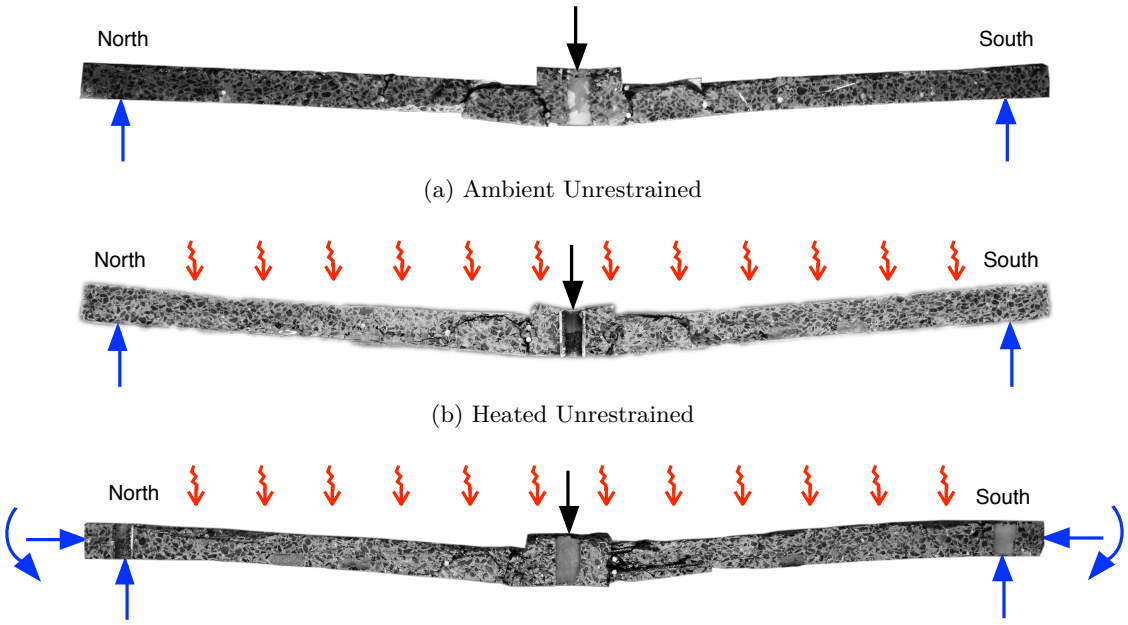

(a) Ambient Unrestrained

(b) Heated Unrestrained

(c) Heated Restrained

Figure 6.20: Cross-sections of 50 mm thick, 0.8% reinforced slabs showing the post-failure crack patterns

applied during the heated tests. The cracks are all within the central quarter of the slab width. All the slabs have vertical cracks through the slab depth where the column stub joins the slab and shear cone cracks which formed from the edge of the column stub on the upper, heated surface joining with the unheated surface approximately 100 mm out with the column stub. The curved shear crack shows that arching action occurred during loading of all the 50 mm thick slabs.

The cross-sectional crack patterns show the unrestrained slab has a bowl shape, whereas the restrained slab has a curved deflected shape only in the centre third due to the edges having been rigidly restrained. The corresponding ambient, unrestrained slab failure cross-section shown in Figure 6.20a looks more of a linear deflected shape beyond the failure cracks. The impact of the restraint condition on the heated slabs, is not clear in Figures 6.20b and 6.20c, however is shown more clearly in the post-failure, plan view crack patterns, Figures 6.21 and 6.22 (discussed further in Section 7.2.1).

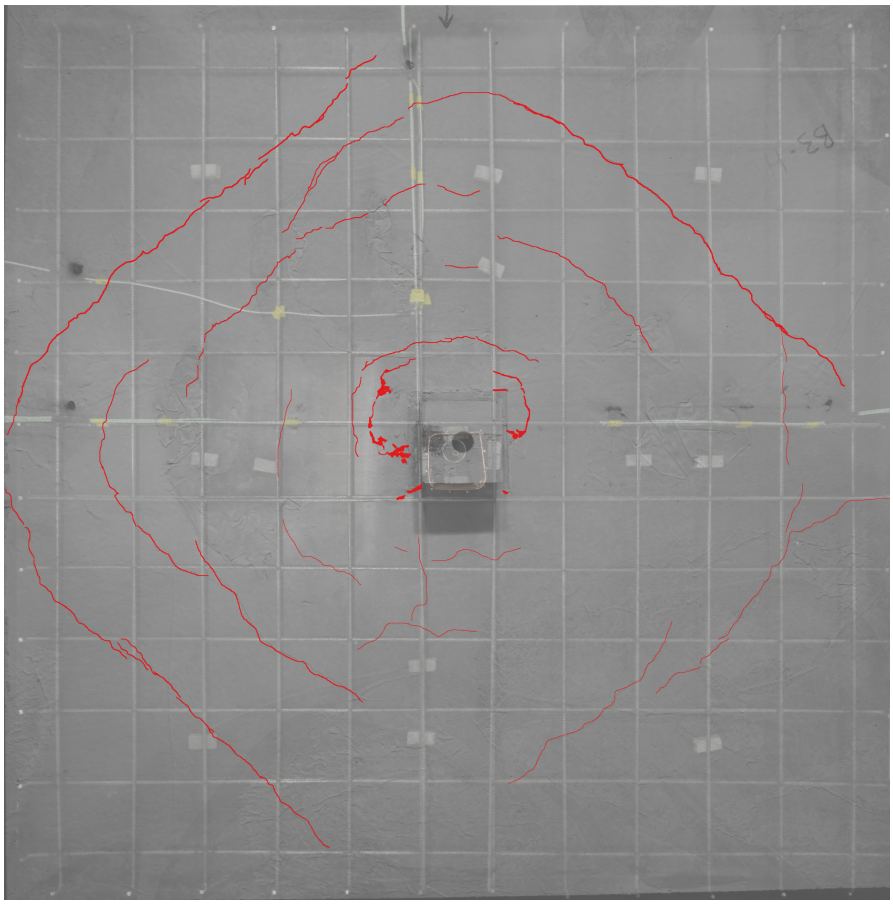

(a) Top surface

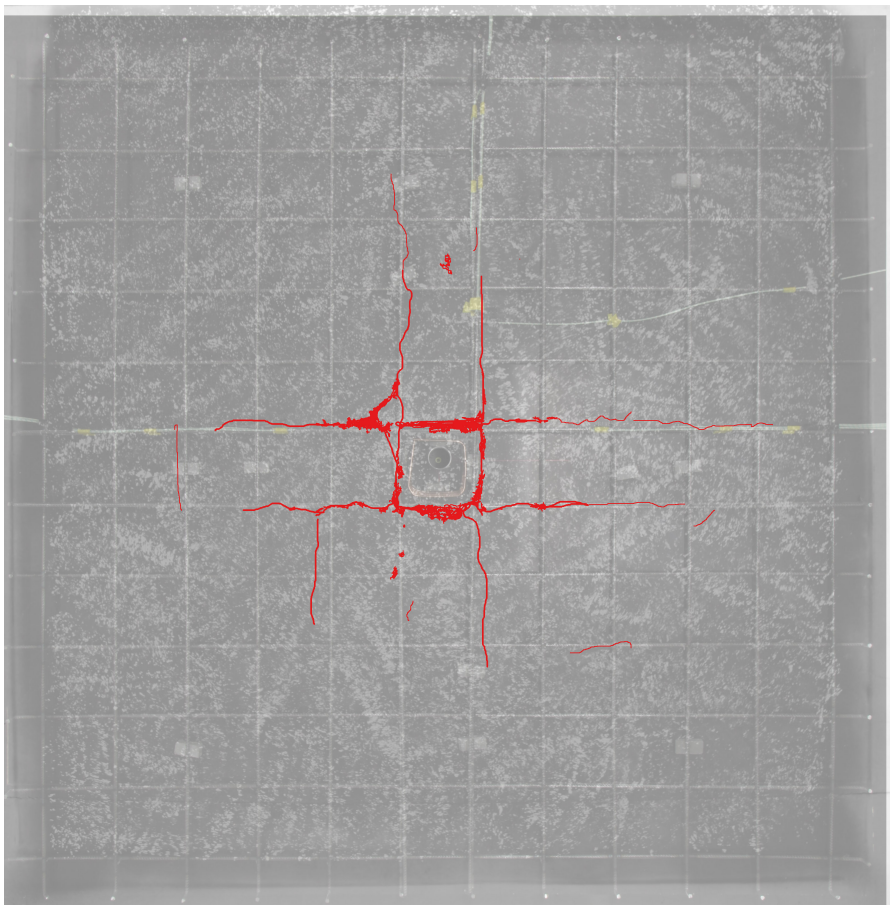

(b) Bottom surface

Figure 6.21: Heated 50 mm thick, 0.8% reinforced: unrestrained slab showing the plan post-failure crack patterns

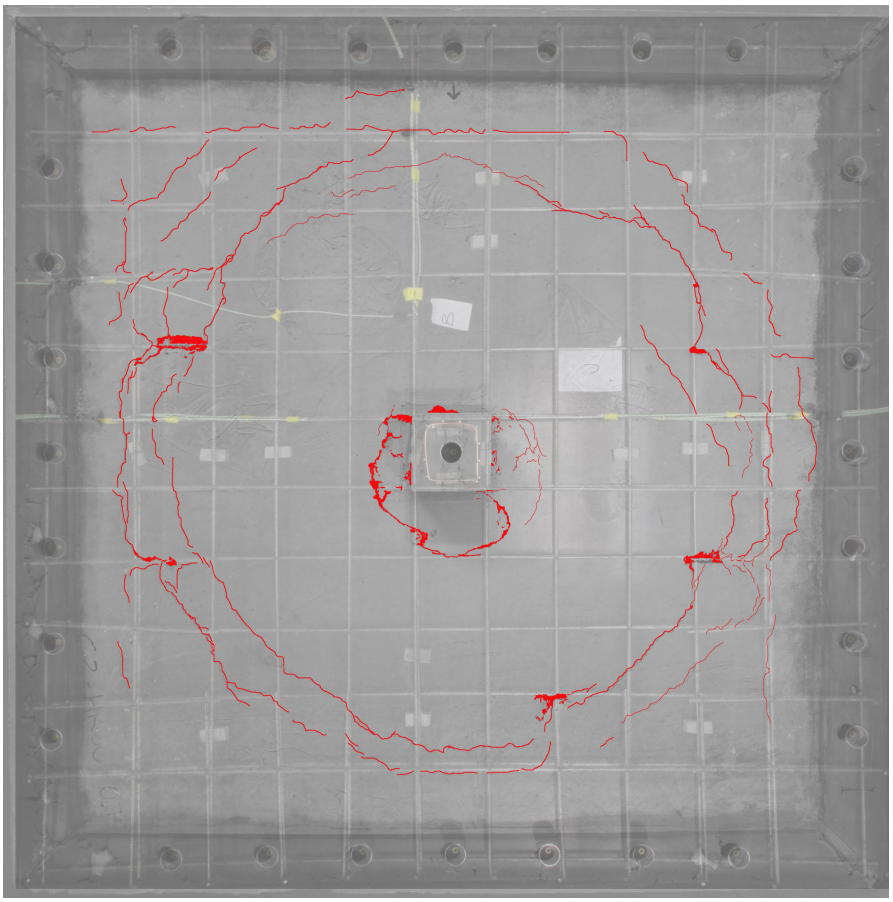

(a) Top surface

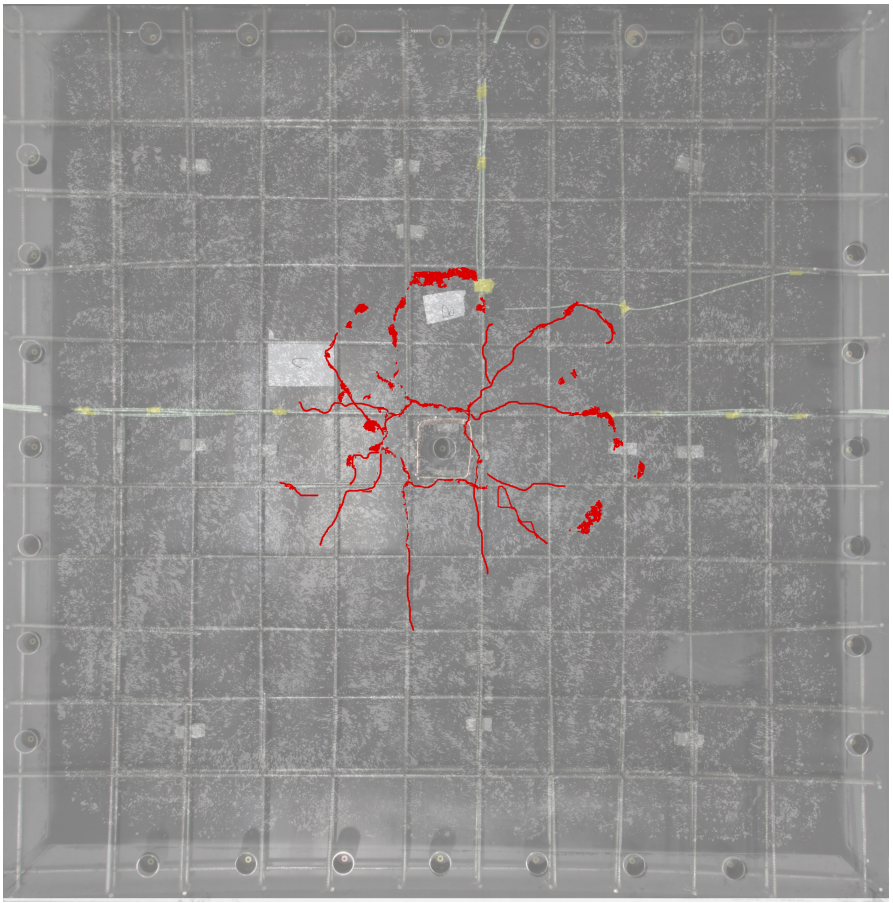

(b) Bottom surface

Figure 6.22: Heated 50 mm thick, 0.8% reinforced: restrained slab showing the plan post-failure crack patterns

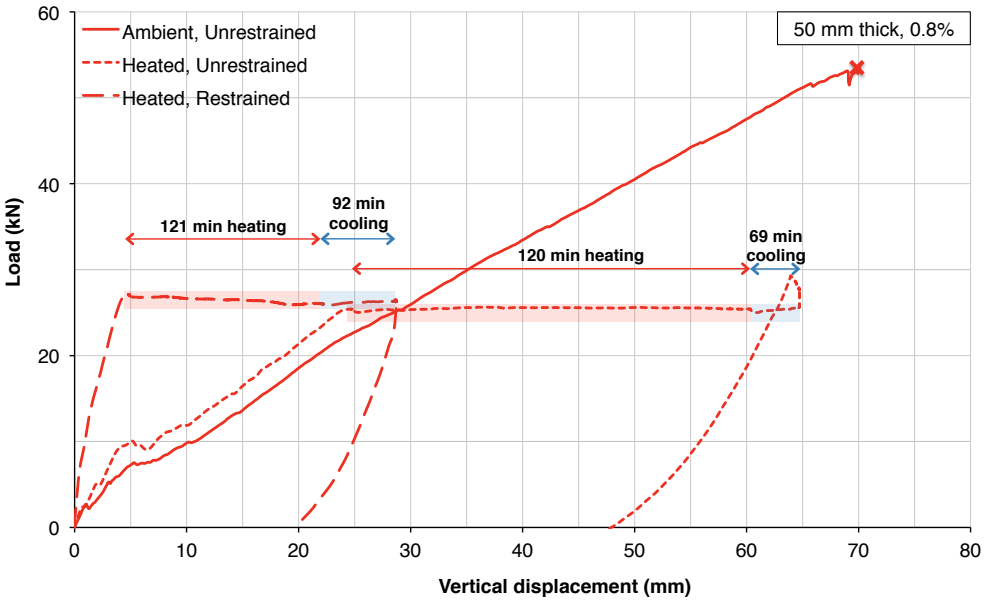

Figure 6.23: Load-deflection behaviour of 50 mm thick, 0.8% slabs

The restrained test has more extensive cracking than the unrestrained, however they have similar patterns. In both support conditions, the top surface cracks are symmetrical and radiate out from just outside the loaded column stub. They are flexure-shear mechanism crack patterns. The restrained top surface cracks are more circular than the unrestrained and both radiate out to the edge of the slab (the restrained slab edge is inside the support box sections). The bottom surface cracks follow the flexural reinforcement passing through the column stub, in both support conditions. The restrained test bottom surface cracks also radiating out from the column stub at 45° between the orthogonal flexural steel cracks.

6.2.5 *Heated load-deflection behaviour and failure modes*

Figure 6.23 shows the load-deflection behaviour of the 50 mm, 0.8% reinforced slab-column specimens. As before, the vertical displacement is measured as positive in the downwards direction, away from the heat source and in the direction of loading. Both AU50-0.8 and HU50-0.8 deflections were plotted from the 100 mm LP, however it failed during the HR50-0.8 test.

The 50 mm LP had insufficient travel for the full HR50-0.8 test displacement and the reading was falsely impacted by loading rod thermal extension. Accidentally during the HR50-0.8 test, the top of the column stub and loading rod was not insulated from the radiant heat panels throughout the whole test. The plotted vertical displacement for HR50-0.8 in Figure 6.23 was measured by DIC.

Figure 6.23 shows both the heated tests were heated for approximately 120 minutes once the 70% of the ambient capacity load was applied and held constant. Neither of the heated tests failed during the 120 minutes of heating or subsequent cooling period and therefore were unloaded and their residual strength found after cooling. The unrestrained and restrained slabs required 69 and 92 minutes, respectively for their thermocouple readings to decrease to below 150°C throughout their depth. The slabs were then unloaded at the same rate as loading, 2 mm/min. The applied load increased during the cooling period for HU50-0.8, due to the actuator having reached its maximum travel length. Irrespective of the increase in applied load, the central deflection is shown to decrease during the cooling phase. The slab shows deflection towards the heat source during the cooling phase.

6.2.6 *Displacement measurement comparison for HR50-0.8 test*

This section presents the comparison of the LP and DIC displacement readings near the centre of the HR50-0.8 slab. The DIC displacement readings allow the full test displacement behaviour to be plotted and are not impacted by potential errors from the thermal extension of the loading rod. The vertical displacement plotted in any graph for the restrained heated, 50 mm thick slab, including Figure 6.23 is the average of all camera DIC analyses.

Figure 6.24 shows a comparison of the LP reading to the DIC vertical displacement at points 30 mm from the slab centre. The DIC displacement for both the W and E camera is an average of two positions at 30 mm from the slab centre, as shown in Figure 6.25. Whereas the S camera is a patch at 30 mm from the slab centre on the E side of the load rod only. The loading rod impeded DIC measurements to be taken directly at the centre of the slab, therefore it was measured at various points 30 mm away from the centre.

Zero time corresponds to the start of heating, with the negative time region corresponding to loading of the slabs prior to ignition. Throughout the remainder of the thesis, figures plotted against time will always be with ignition as zero time. The 30 mm LP can be seen to reach the end of its travel at approximately 29 mm displacement in Figure 6.24, which corresponds to 120 minutes after ignition.

The displacement trends in Figure 6.24 show good agreement, though the DIC measurements are consistently less than the LP. The author believes the difference is due to the LP readings being falsely affected by either column stub local concrete crushing, loading rod extension or reaction frame movements (analysed further in Section 7.1.4).

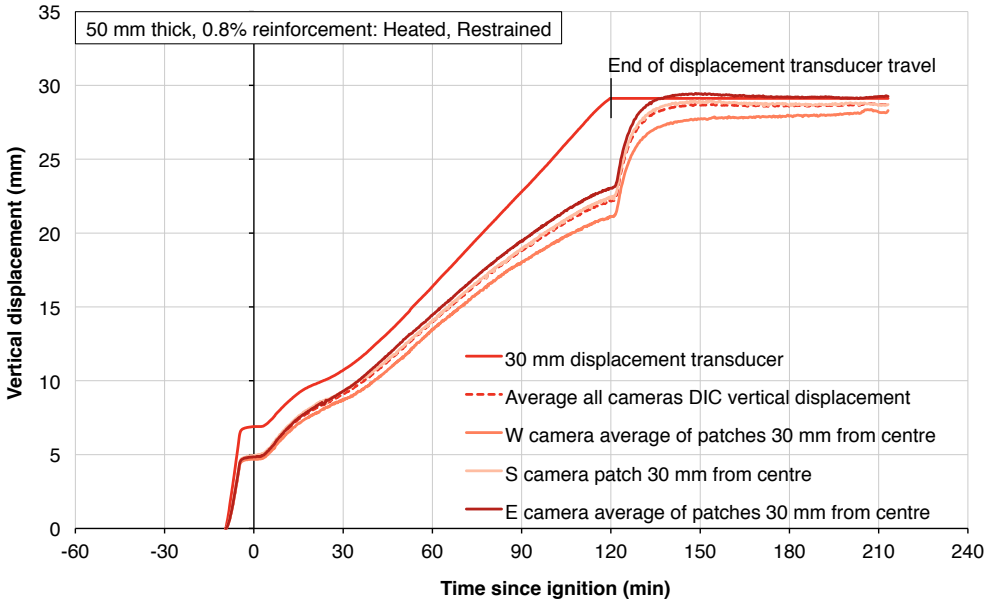

Figure 6.24: Vertical deflection comparison of 30 mm LP and DIC average for 50 mm thick, 0.8%: restrained slab

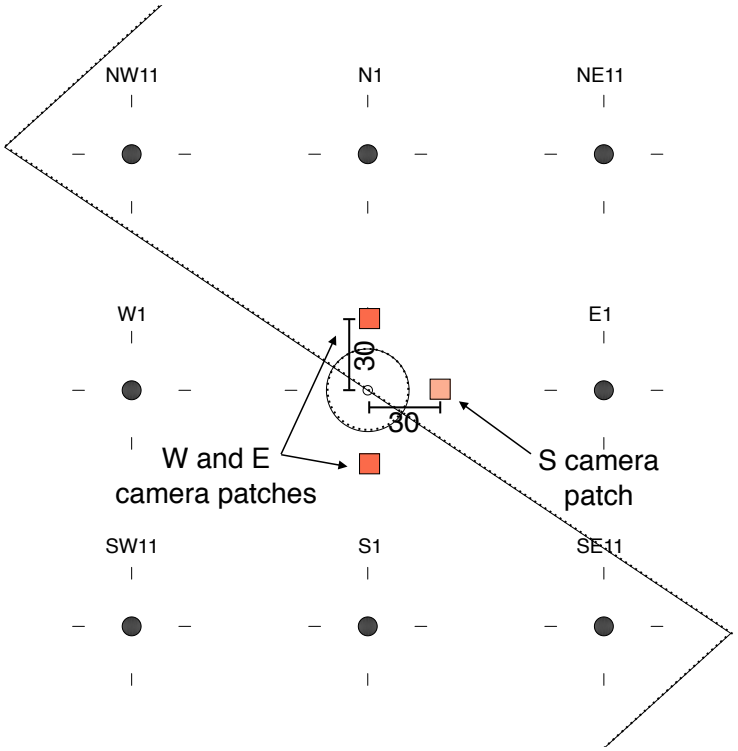

Figure 6.25: DIC patch location on heated 50 mm thick, 0.8% reinforced: restrained slab relative to calibration board

6.2.7 *Summary*

The main bullet points summarising the 50 mm thick slab-column results in Section 6.2, are presented here:

- The heating curves were different between comparative elevated temperature tests.
- A decrease in propane gas flow rate caused the unrestrained test to reach a lower, maximum near surface temperature of 500°C, compared to the approximate maximum temperature of 630°C measured in the restrained test.
- The temperature profiles through the slab thickness show the radiant panel array did not produce a perfectly even heat flux across the upper slab surface in the unrestrained test.
- At the measured effective depth of the flexural steel and below, the unrestrained test temperature profiles at the three thermocouple tree locations are similar.
- In contrast to the unrestrained test, the restrained test profiles are similar in the three thermocouple tree locations.
- The temperatures on the unheated surface of both slabs reached a maximum during the cooling phase, as the heat front penetrates the slab.
- The flexural steel at a depth of 31 mm, reached a maximum temperature during the cooling phase of an approximate average of 350°C for the unrestrained slab and 445°C for the restrained slab.
- Both heated 50 mm thick slabs failed residually in flexure-shear mechanisms.
- Irrespective of the increase in applied load towards the end of the HU50-0.8 test, the slab deflected towards the heat source during the cooling phase.
- Test HR50-0.8 vertical displacement was measured by DIC, as the 100 mm LP failed and the 30 mm LP ran out of travel.
- DIC and LP measurements were compared and shown to have good agreement, though the DIC measurements were consistently less than the LP. The author believes the difference is due to the LP readings being falsely affected by either column stub local concrete crushing, loading rod extension or with reaction frame movements (analysed further in Section 7.1.4).

6.3 75 mm thick, 0.8% reinforced tests

This section presents the results of the three slab-column experiments that were 75 mm thick with 0.8% reinforcement ratio: the ambient unrestrained (AU75-0.8), the heated unrestrained (HU75-0.8) and the heated restrained (HR75-0.8).

6.3.1 *Test overview*

The key 75 mm thick slab-column test outcomes are summarised in bullet points here:

- Both elevated temperature tests were heated for 120 minutes approximately;
- The propane gas flow rate was noted to decrease towards the end of the heating phase in both elevated temperature tests;
- The maximum concrete temperature near the heated surface was approximately 480°C in the unrestrained slab and 560°C in the restrained slab;
- The flexural steel at an effective depth of 58 mm in the unrestrained test and 55 mm in the restrained, reached an approximate average maximum temperature of 245°C and 290°C, respectively;
- Neither slab failed during the punching shear test, therefore they were both residually tested (described in Section 6.7.2);
- All heated slabs failed residually in flexure-shear mechanisms;
- The ambient temperature tested slab had a capacity of 101.4 kN. The sustained loads of 82.8 kN and 82.0 kN were applied during heating in the unrestrained and restrained tests, respectively; and
- The applied load increased during the cooling phase of the HU75-0.8 test, due to friction in the hydraulic loading jack.

6.3.2 *Temperature curves*

The temperature curves for the unrestrained and restrained heated, 75 mm thick slabs are shown in Figure 6.26. The maximum temperature recorded in the unrestrained slab was approximately 80°C less than that recorded in the restrained, measuring approximately 480°C rather than 560°C. As in the

50 mm thick slab tests, the propane gas flow rate decreased towards the end of the 120 minute heating phase for both 75 mm thick heated slab tests.

6.3.3 *Temperature profiles through the slab thickness*

Figures 6.27 – 6.29 show the unrestrained, 75 mm thick slab temperature profiles for the N, S and W thermocouple trees. The restrained slab temperature profiles are shown in Figures 6.30 – 6.32. The thermocouples trees in the restrained slab were located at the N, S and E of the frame.

All three unrestrained temperature profiles show similar trends of heat front penetration through the 75 mm slab depth. The three restrained temperature profiles are also similar to one another. The support condition is assumed to have a limited impact on the temperature profiles, however the restrained slab reached a greater maximum temperature than the unrestrained. This is assumed to be caused by the time difference after ignition at which the gas flow rate decreased in the unrestrained and restrained tests.

The effective depth of the flexural steel was 58 mm for the unrestrained test and 55 mm for the restrained, measured after failure from the heated surface down. The maximum measured steel temperature was an approximate average of 245°C for the unrestrained slab and 290°C for the restrained, both measured at 136 minutes after ignition.

6.3.4 *Failure crack patterns*

The failure cross-sections for all the 75 mm thick slab-column specimens are shown in Figure 6.33. The 75 mm thick slabs all failed in a flexure-shear mechanism. Similar to the 50 mm thick slabs, there are various cracks at different angles, fanning out from the column stub edge on the upper, heated surface. In both heated tests, the shear cone was larger on the N side than the S. This unsymmetrical failure may have been caused by imperfections in the specimens during construction.

Figures 6.34 and 6.35 show the post-failure, plan view crack patterns of the unrestrained and restrained slabs. The top surface cracks are different to those for the 50 mm thick slabs, with the restrained cracks forming a square with circular edges compared to a circular pattern in the unrestrained test. In both the tests, the top surface have cracks directly around the loaded column stub. There are many bottom surface cracks within the centre third of the slab, radiating out from the column stub.

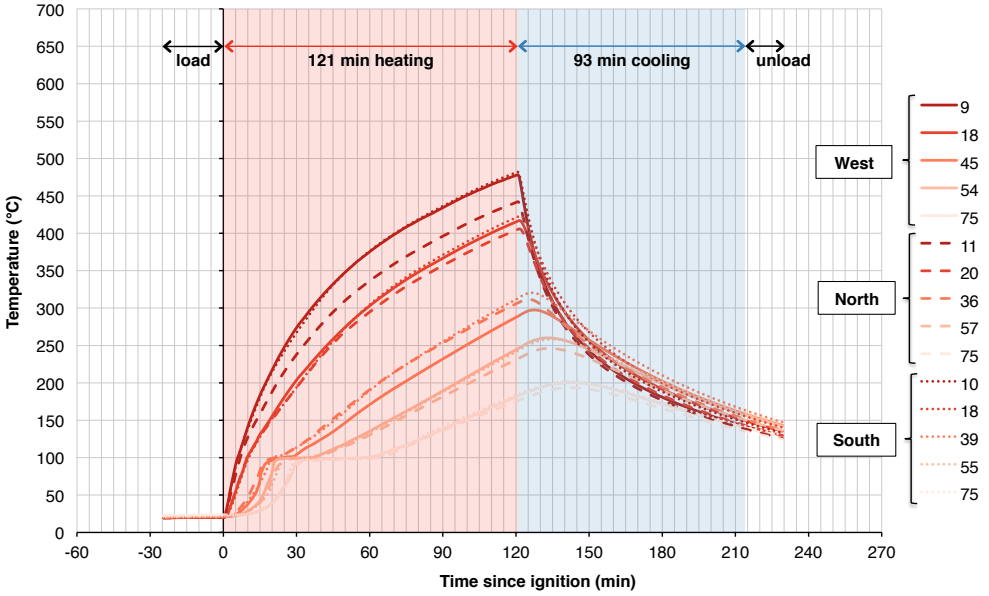

(a) Heated Unrestrained

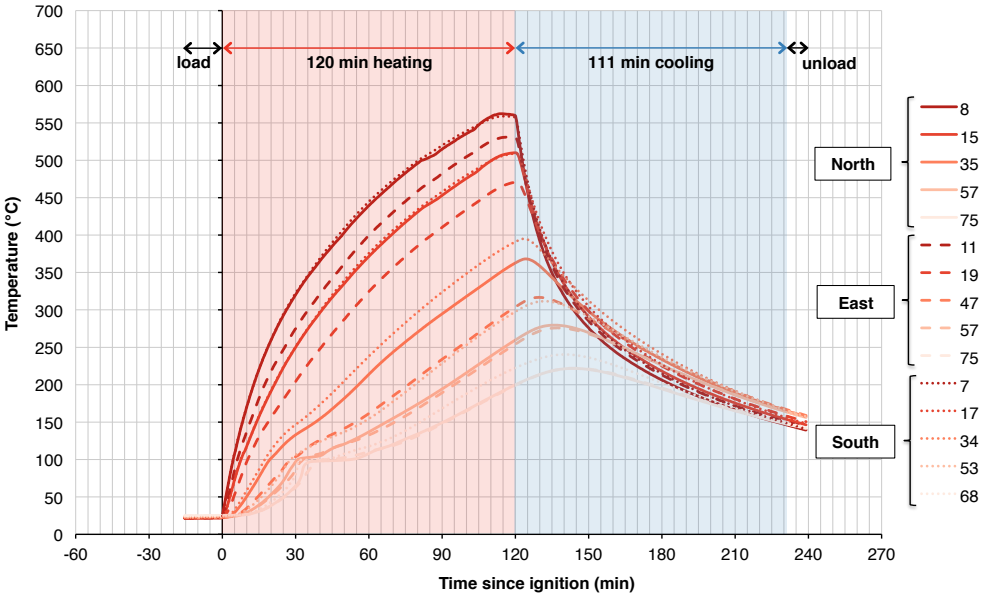

(b) Heated Restrained

Figure 6.26: Temperature curves for 75 mm thick, 0.8% slabs

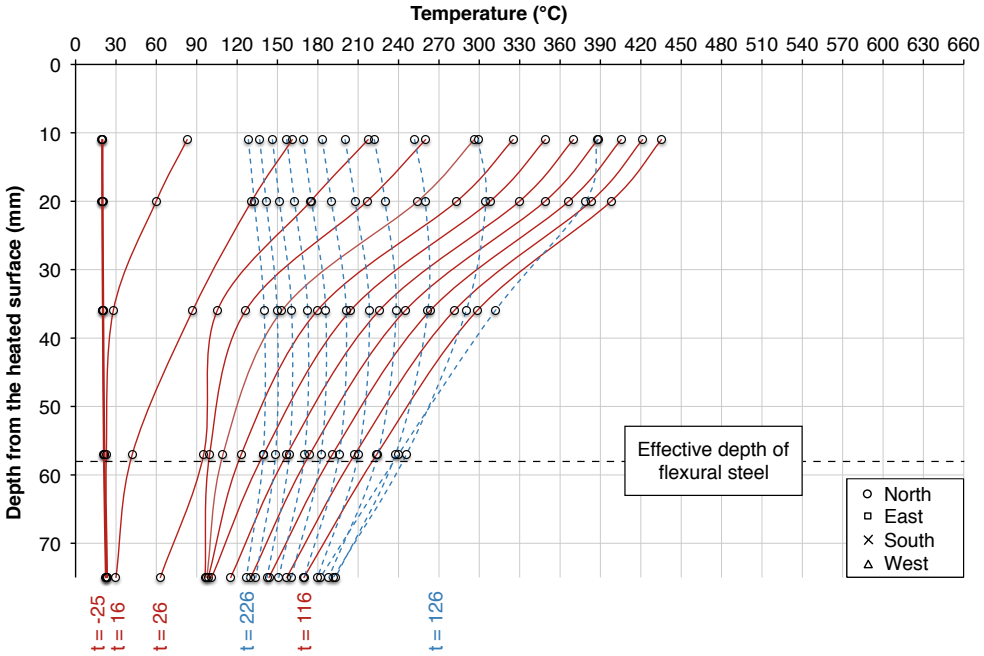

Figure 6.27: North temperature profile through 75 mm thickness, 0.8%: unrestrained slab

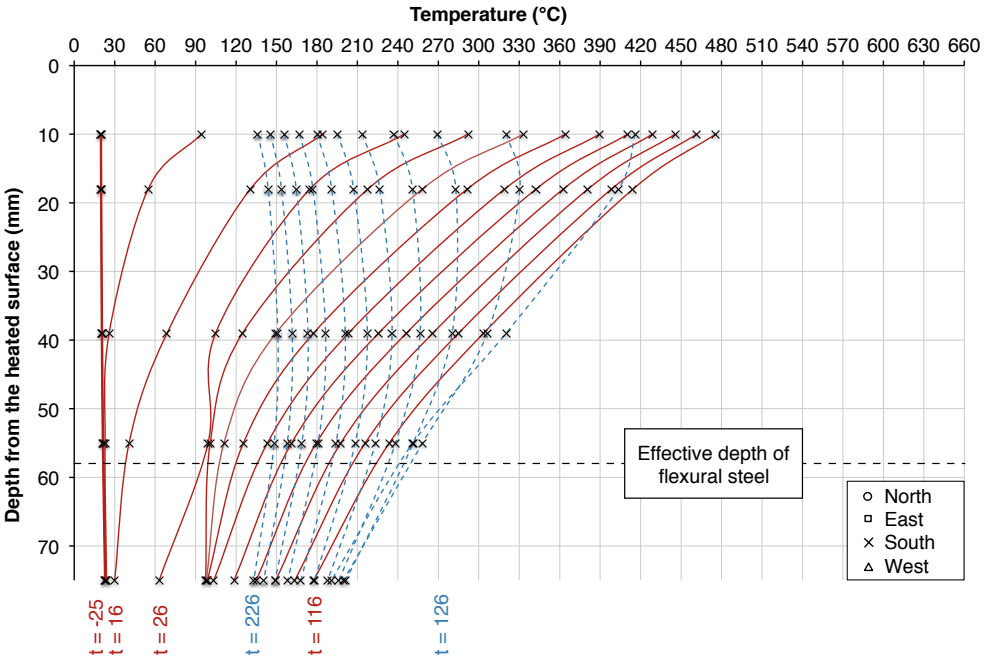

Figure 6.28: South temperature profile through 75 mm thickness, 0.8%: unrestrained slab

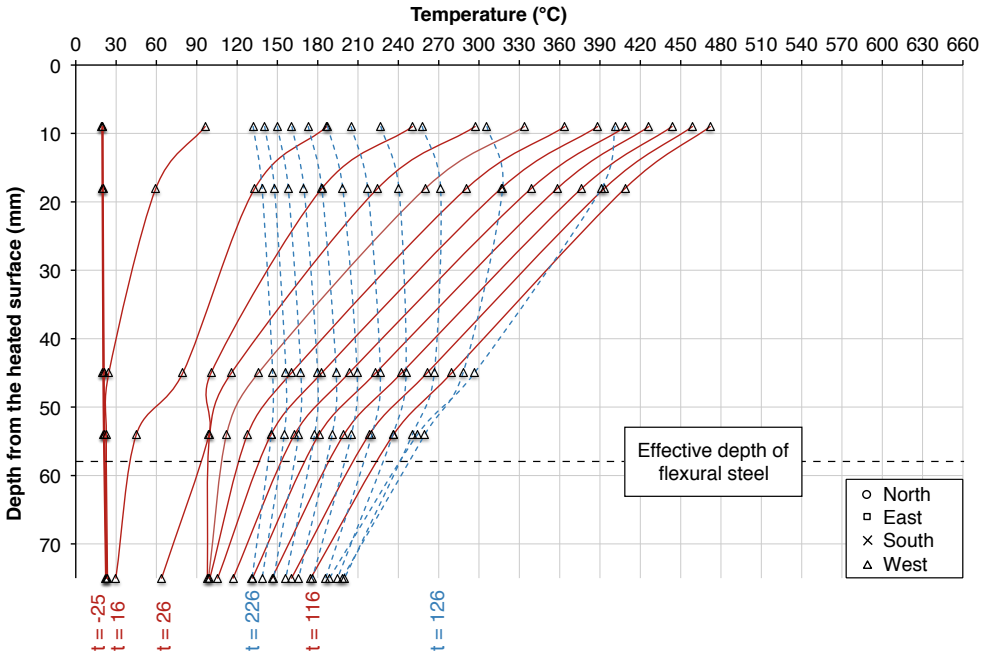

Figure 6.29: West temperature profile through 75 mm thickness, 0.8%: unrestrained slab

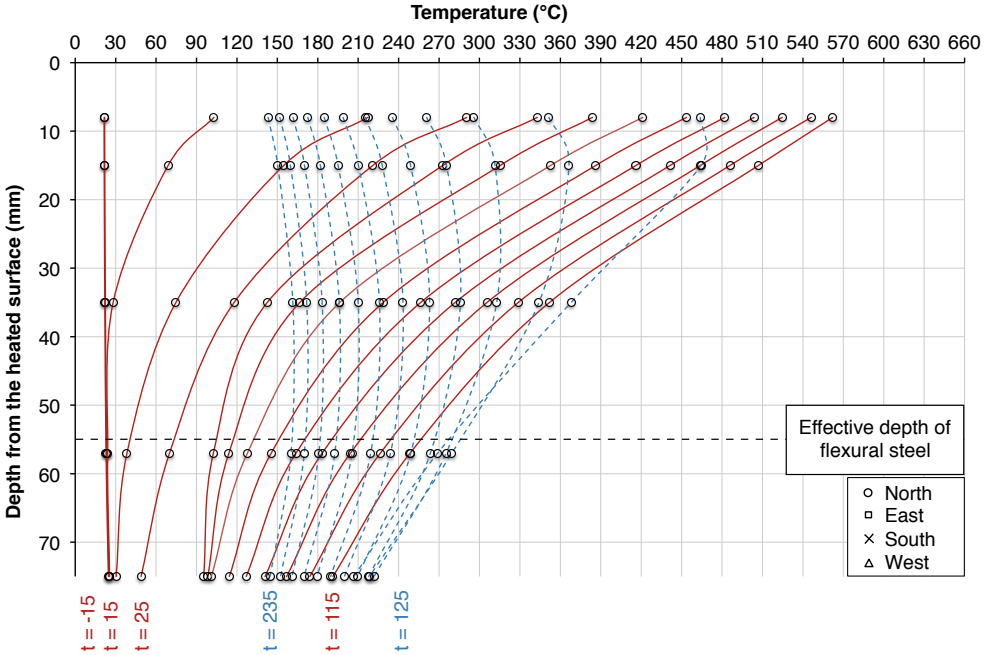

Figure 6.30: North temperature profile through 75 mm thickness, 0.8%: restrained slab

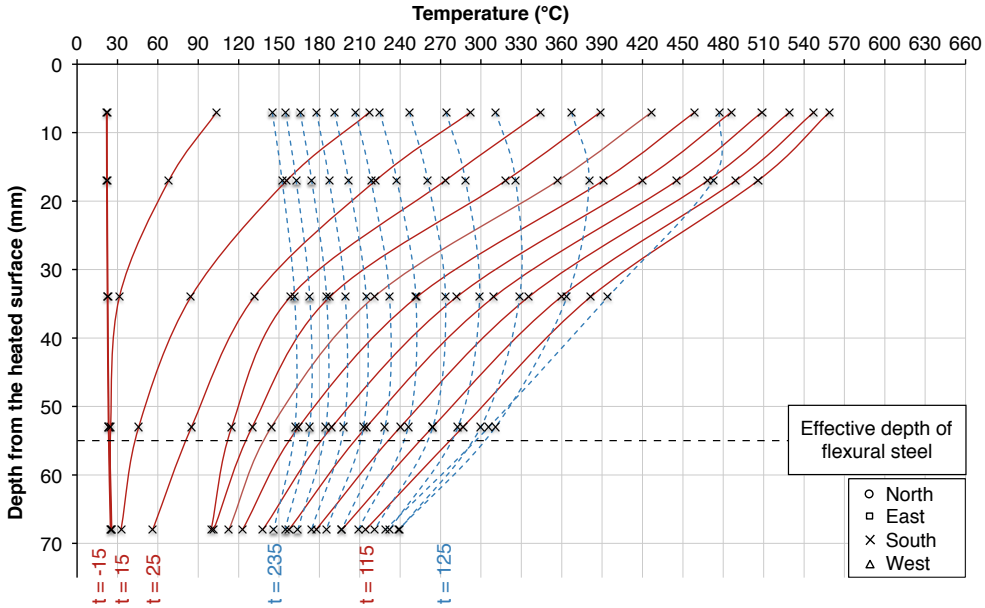

Figure 6.31: South temperature profile through 75 mm thickness, 0.8%: restrained slab

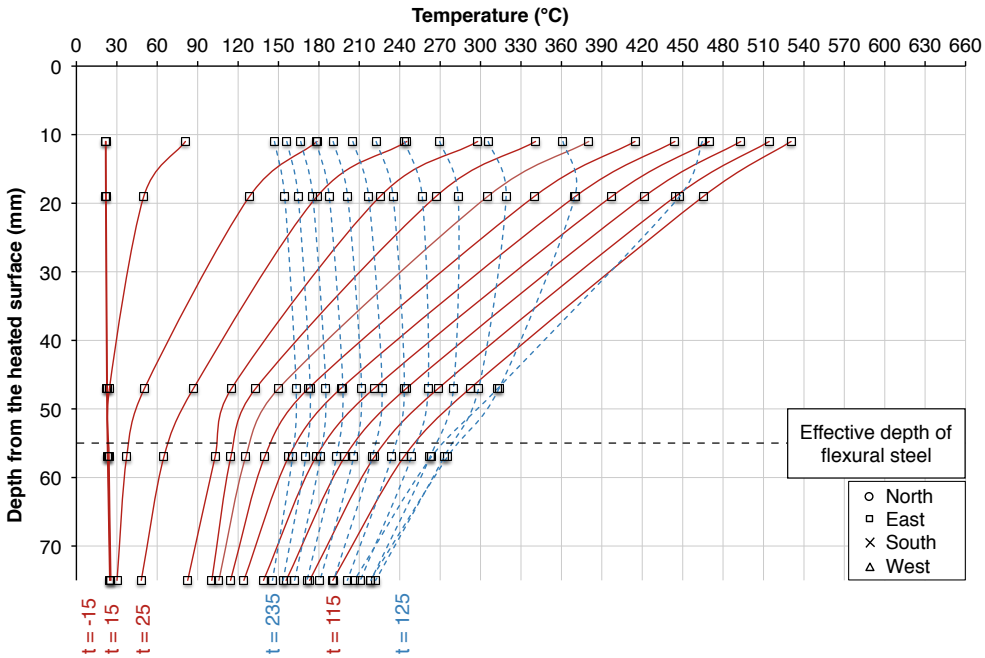

Figure 6.32: East temperature profile through 75 mm thickness, 0.8%: restrained slab

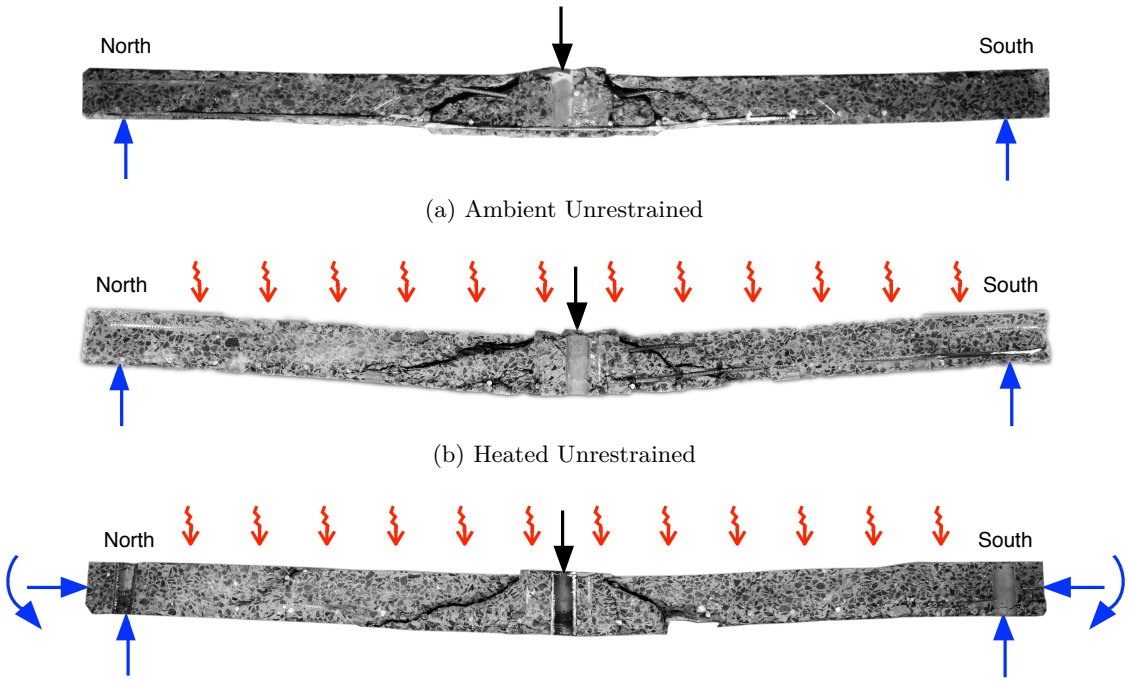

(a) Ambient Unrestrained

(b) Heated Unrestrained

(c) Heated Restrained

Figure 6.33: Cross-sections of 75 mm thick, 0.8% reinforced slabs showing the post-failure crack patterns

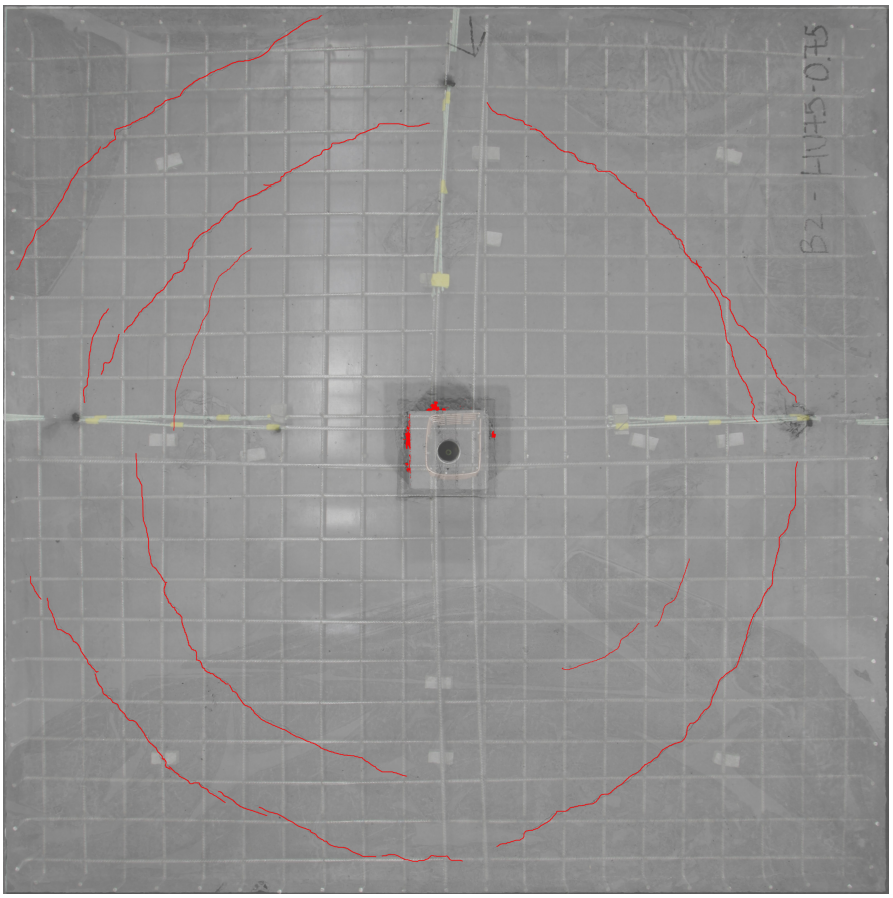

(a) Top surface

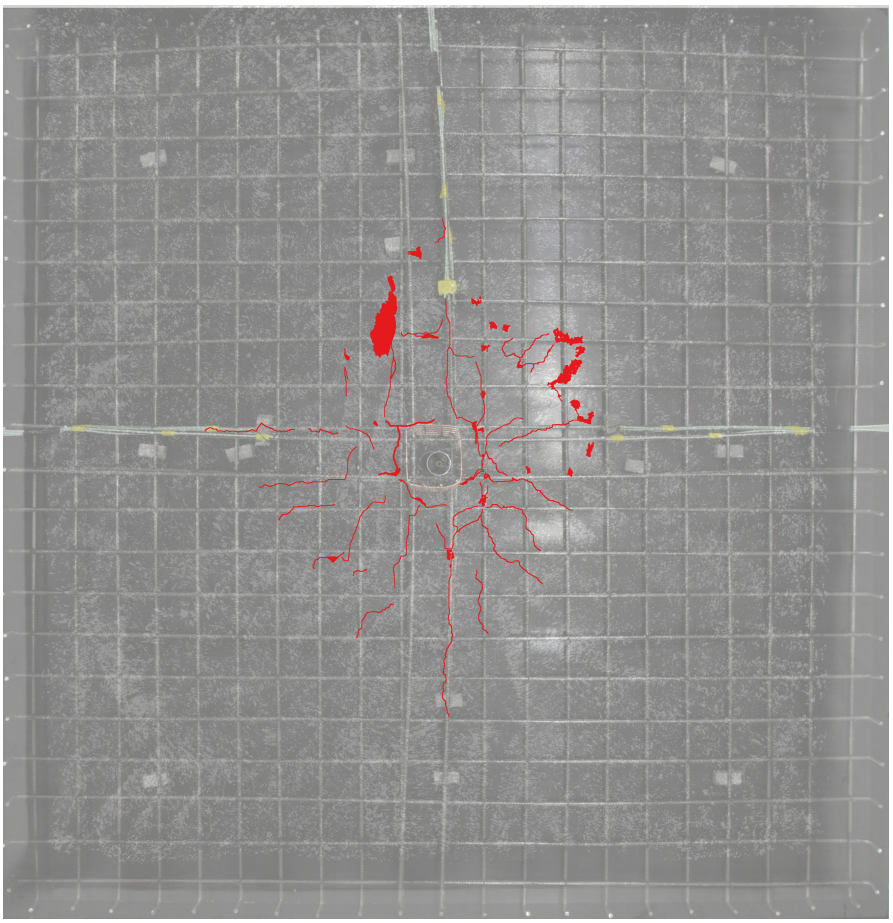

(b) Bottom surface

Figure 6.34: Heated 75 mm thick, 0.8% reinforced: unrestrained slab showing the plan post-failure crack patterns

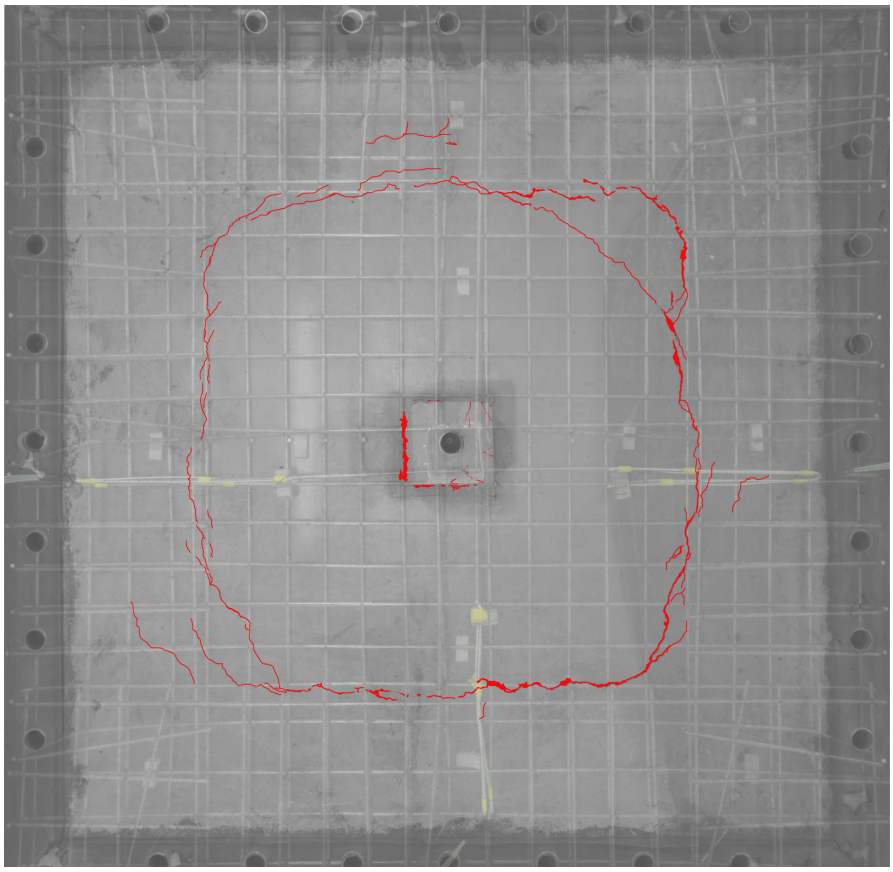

(a) Top surface

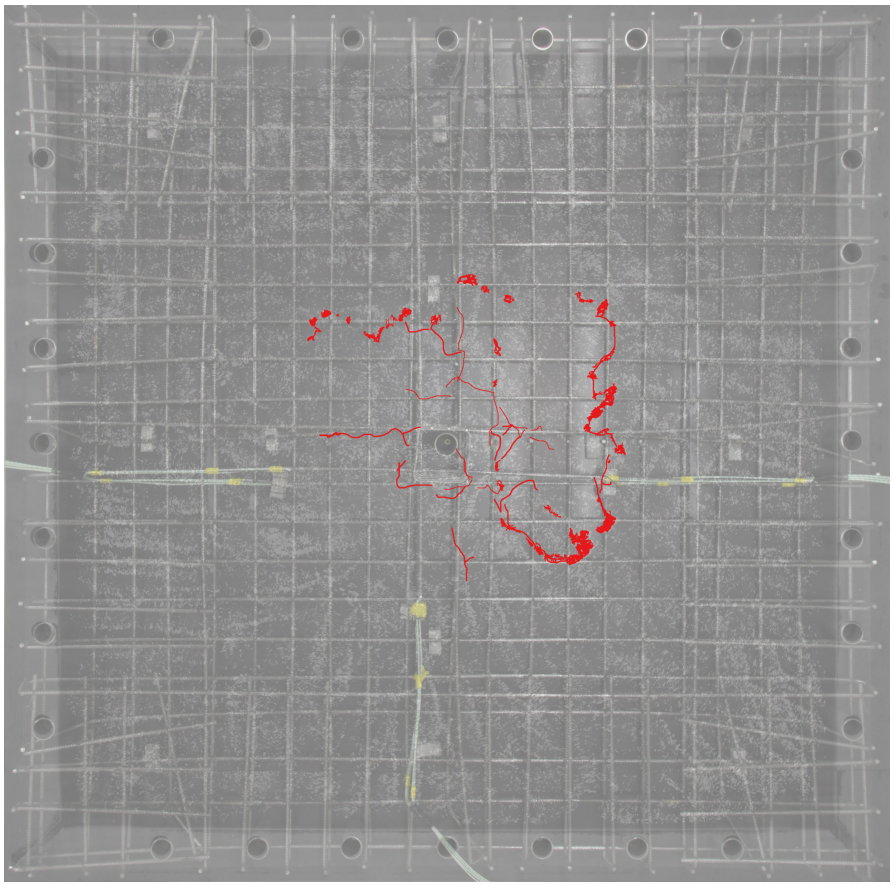

(b) Bottom surface

Figure 6.35: Heated 75 mm thick, 0.8% reinforced: restrained slab showing the plan post-failure crack patterns

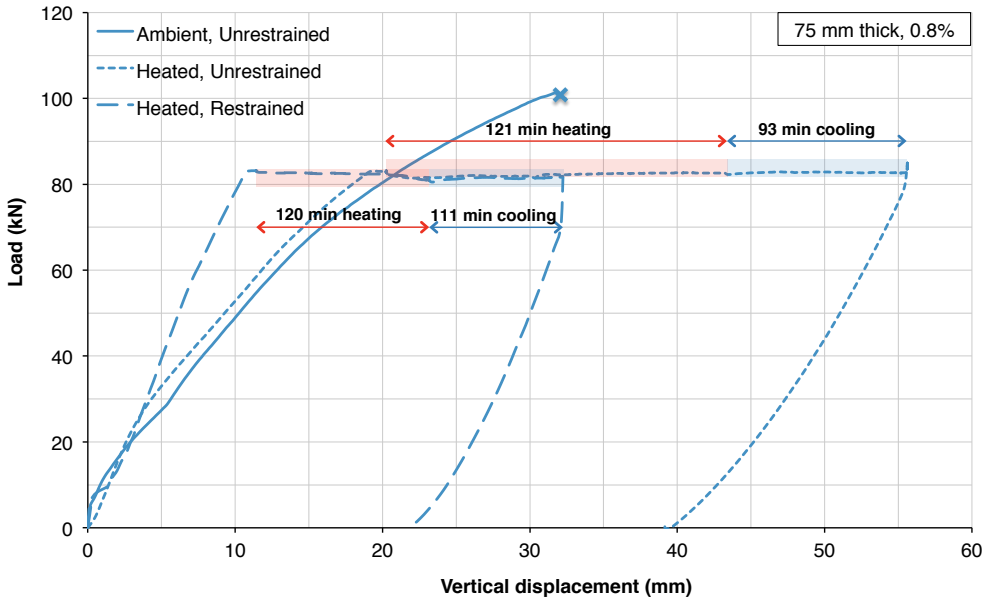

Figure 6.36: Load-deflection behaviour of 75 mm thick, 0.8% slab

6.3.5 *Heated load-deflection behaviour and failure modes*

Figure 6.36 shows the load-deflection behaviour of the 75 mm, 0.8% reinforced slab-column specimens. Both heated tests were heated for approximately 120 minutes and did not fail during the slab-column test, therefore were residually tested. The cooling phases lasted from 93 to 111 minutes for the unrestrained and restrained tests, respectively. Figure 6.36 shows the restrained slab was much stiffer than the unrestrained during loading and unloading. As for the HU50-0.8 test, the applied load increased at the end of the cooling period for HU75-0.8. A hydraulic friction test presented in Section 7.1.3, shows the increased applied load was caused by friction in the hydraulic loading jack.

6.3.6 *Summary*

The main bullet points summarising the 75 mm thick slab-column results in Section 6.3, are presented here:

- The heating curves were different between comparative elevated temperature tests.
- The support condition is assumed to have a limited impact on the temperature profile trends of the heat front penetration through the 75 mm thick slabs, however the restrained slab reached a greater maximum sur-

face temperature, which is assumed to be caused by the time difference after ignition, at which the gas flow rate decreased.

- A decrease in propane gas flow rate caused the unrestrained test to reach a lower, maximum near surface concrete temperature of 480°C, compared to the approximate maximum temperature of 560°C measured in the restrained test.
- The flexural steel at an effective depth of 58 mm in the unrestrained test and 55 mm in the restrained, reached an approximate average maximum temperature of 245°C and 290°C, respectively.
- Both heated 75 mm thick slabs failed residually in flexure-shear mechanisms.

6.4 100 mm thick, 0.8% reinforced tests

This section presents the results of the three slab-column experiments that were 100 mm thick with 0.8% reinforcement ratio: the ambient unrestrained (AU100-0.8), the heated unrestrained (HU100-0.8) and the heated restrained (HR100-0.8).

6.4.1 *Test overview*

The key 100 mm thick, 0.8% reinforced slab-column test outcomes are summarised in bullet points here:

- The unrestrained slab failed 4 minutes after ignition, which is in complete contrast to the restrained specimen which sustained the full 120 minutes of heating and was residually tested (described in Section 6.7.3);
- The propane gas flow rate was noted to decrease in the restrained test, therefore the maximum recorded temperature was prior to the end of the heating phase, at 100 minutes after ignition;
- The maximum approximate concrete temperature near the heated surface was 130°C in the unrestrained slab and 435°C in the restrained slab;
- The flexural steel at an effective depth of 81 mm in the unrestrained test and 82 mm in the restrained, reached an approximate average maximum temperature of 18°C and 170°C, respectively;
- All the slabs failed in punching shear mechanisms; and

- The ambient temperature tested slab had a capacity of 226.3 kN. The specimens were loaded to 174.6 kN and 166.5 kN during heating in the unrestrained and restrained slab-column tests, respectively.

6.4.2 *Temperature curves*

Figure 6.37 presents the temperature curves for the heated unrestrained and restrained 100 mm, 0.8% reinforced slabs. The difference caused by the support condition is shown in Figure 6.37. The unrestrained slab failed 4 minutes after ignition, whereas the restrained slab lasted the full 120 minutes of heating and was residually tested to failure.

The unrestrained slab failed after 4 minutes of heating with a maximum surface temperature of approximately 130°C, measured by a thermocouple on the E frame side. The maximum temperature of the restrained slab measured 10 mm from the surface was approximately 435°C at 100 minutes after ignition. The restrained slab temperature did not continue to increase for the full 120 minutes of heating, because the gas flow rate was recorded in test notes to decrease well before 107 minutes after ignition. The slab-column test was undertaken in November when the weather outside was very cold, which affected the temperature of the propane gas cylinders stored outside the laboratory.

6.4.3 *Temperature profiles through the slab thickness*

Figures 6.38 – 6.40 show the temperature profiles at 10 minute intervals through the 100 mm thick unrestrained slab, reinforced with 0.8% steel. Similarly, Figures 6.41 – 6.43 show the comparative restrained slab temperature profiles. The thermocouple trees were located at the same, S, W and E positions in the frame for both tests.

The unrestrained profiles all show similar trends. The restrained profiles also show similar trends, though the thermocouple tree located at the E side of the frame does not measure as high temperature, even though the thermocouple tree depth is approximately comparable to the others.

The effective depth of the flexural steel in the unrestrained and restrained 100 mm thick slabs, reinforced with 0.8% steel was measured after failure as 81 mm and 82 mm, respectively (measured from the heated surface down). The average flexural steel temperature measured at 6 minutes after ignition in the unrestrained test was 18°C, whereas the steel in the restrained slab reached almost 10 times a temperature, with an approximate average of 170°C.

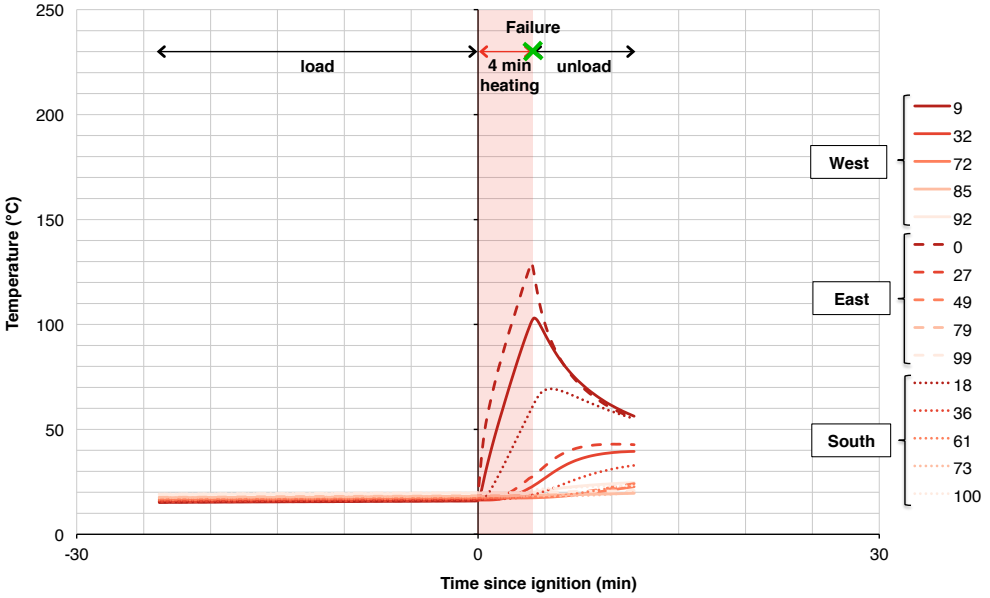

(a) Heated Unrestrained

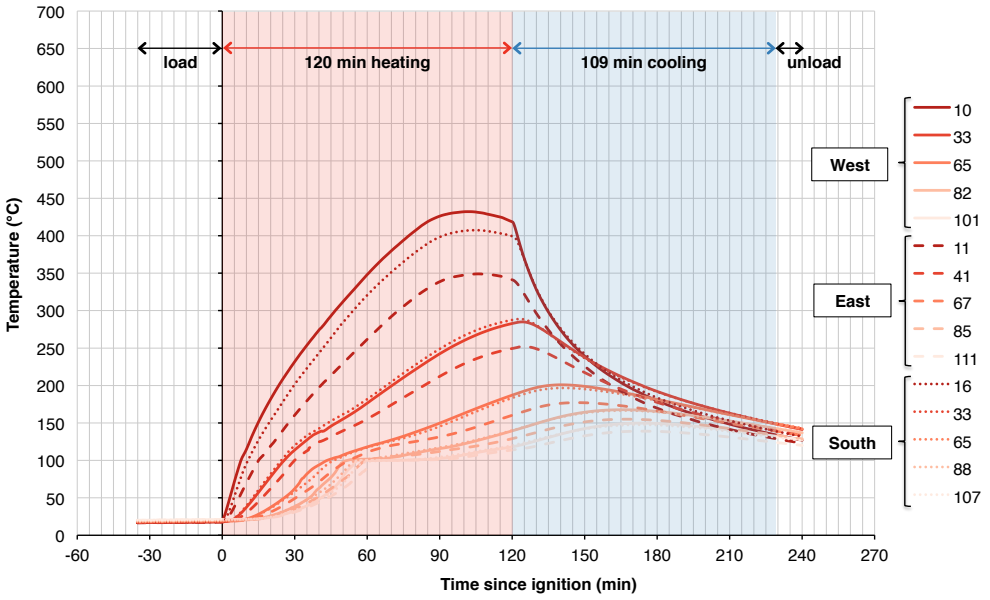

(b) Heated Restrained

Figure 6.37: Temperature curves for 100 mm thick, 0.8% slabs

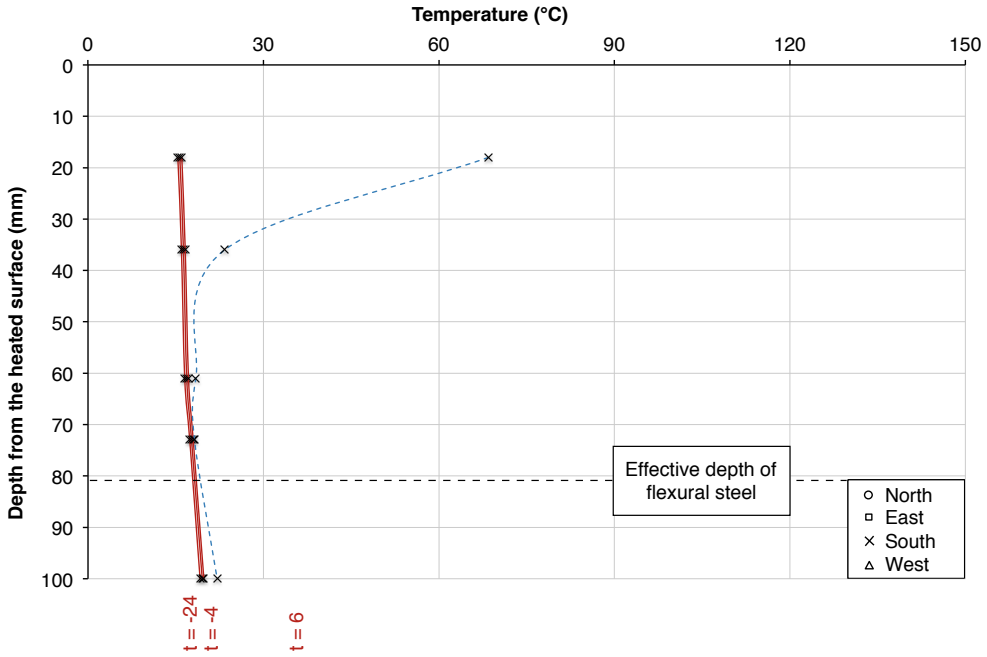

Figure 6.38: South temperature profile through 100 mm thickness, 0.8%: unrestrained slab

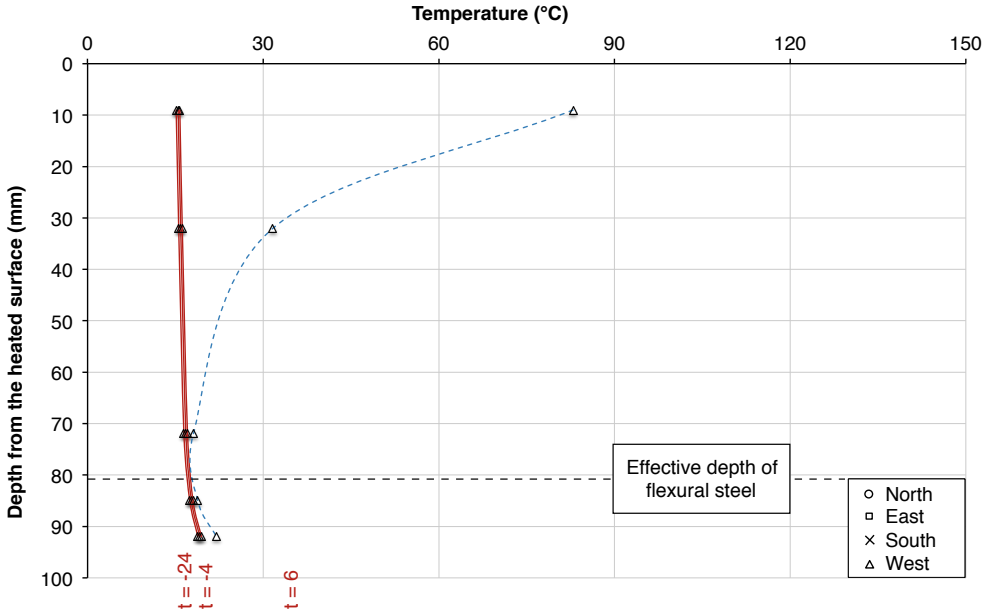

Figure 6.39: West temperature profile through 100 mm thickness, 0.8%: unrestrained slab

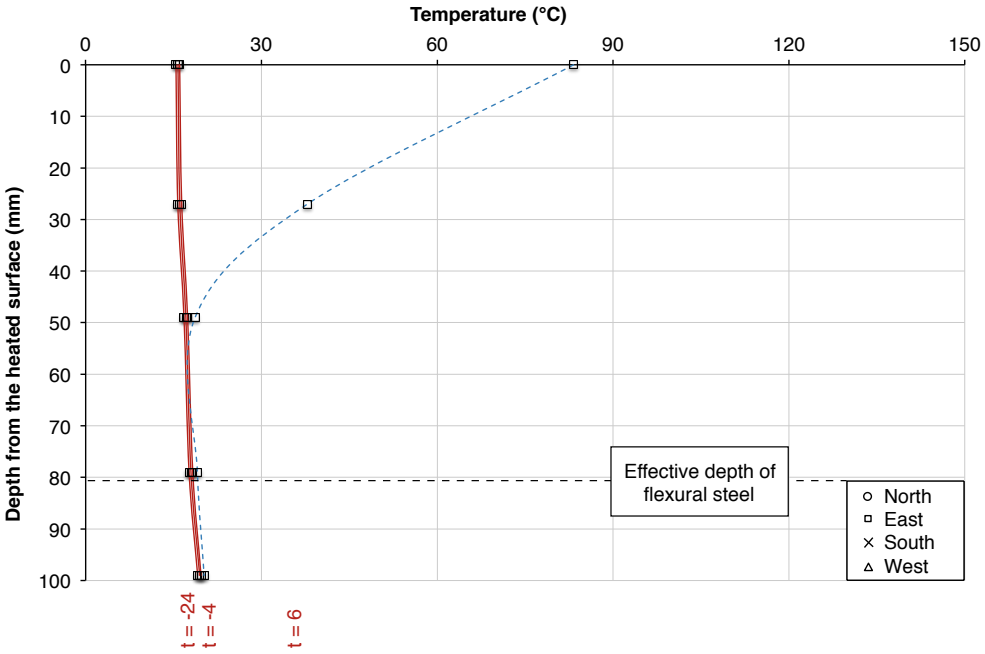

Figure 6.40: East temperature profile through 100 mm thickness, 0.8%: unrestrained slab

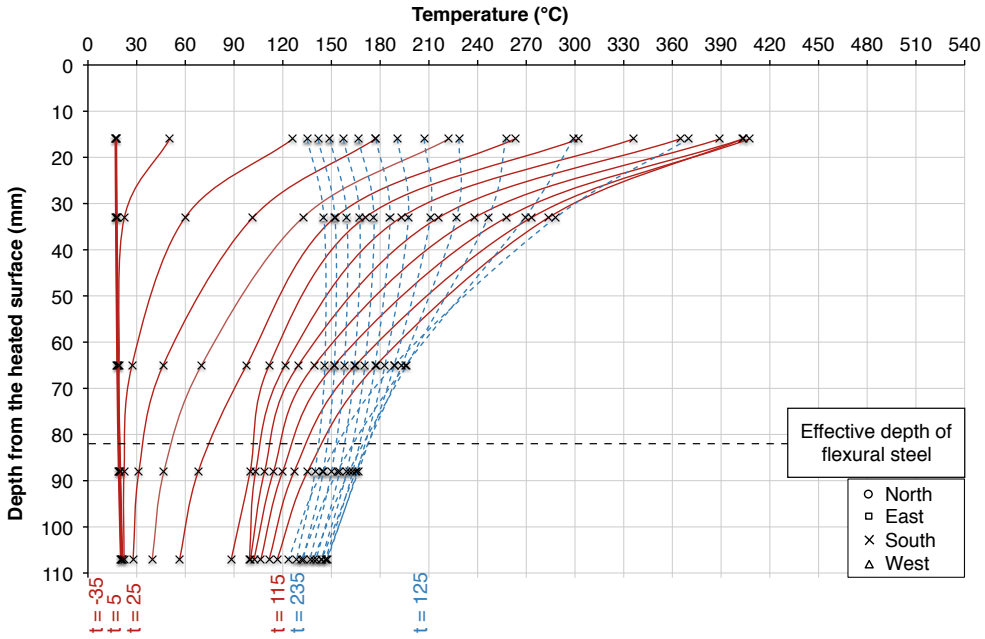

Figure 6.41: South temperature profile through 100 mm thickness, 0.8%: restrained slab

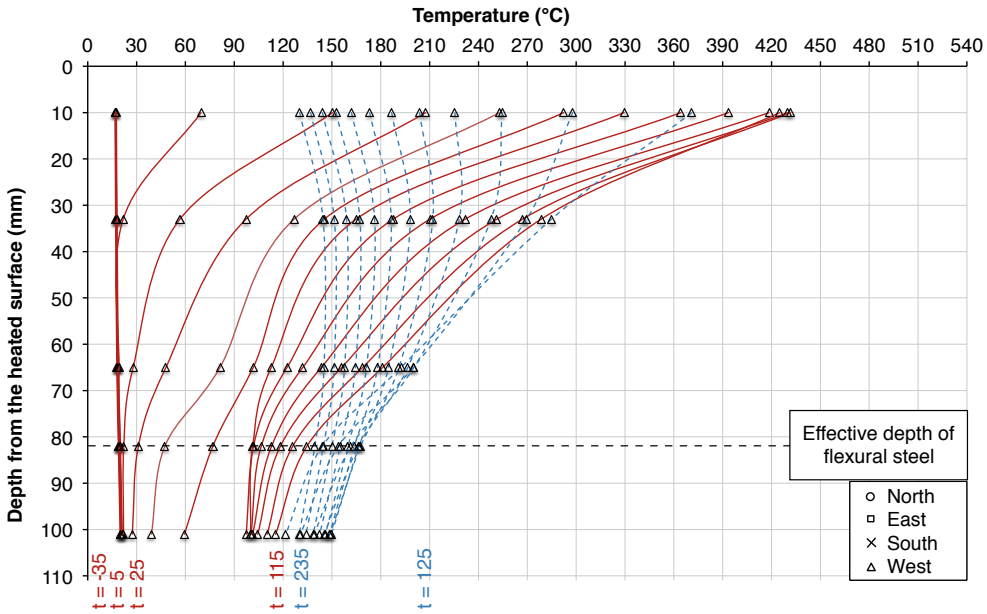

Figure 6.42: West temperature profile through 100 mm thickness, 0.8%: restrained slab

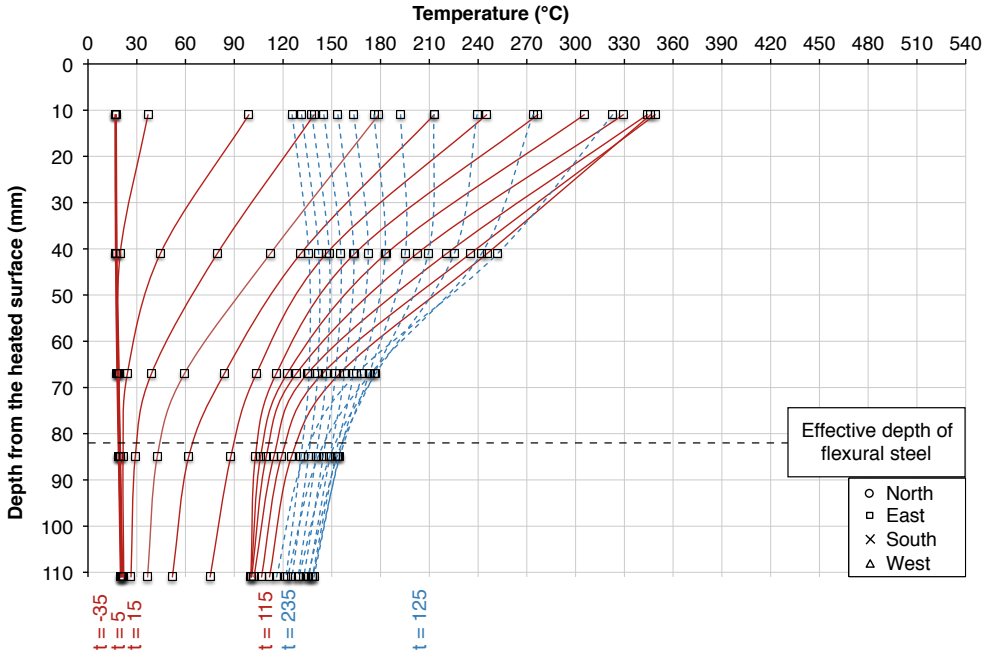

Figure 6.43: East temperature profile through 100 mm thickness, 0.8%: restrained slab

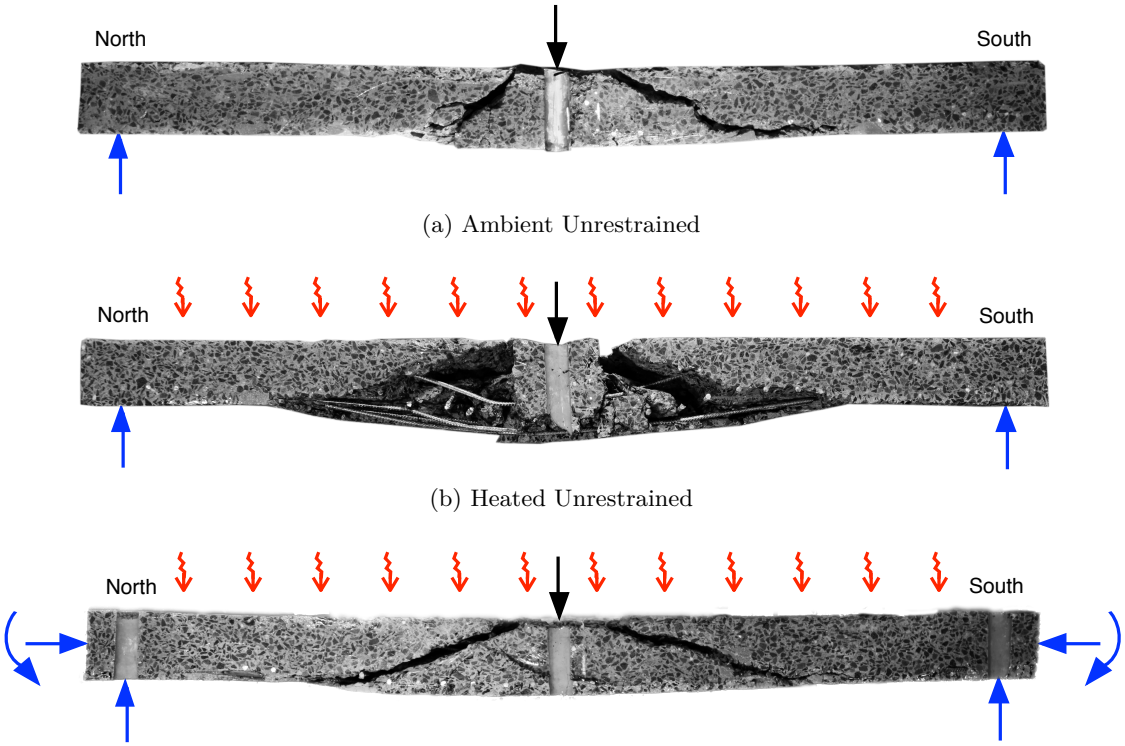

(a) Ambient Unrestrained

(b) Heated Unrestrained

(c) Heated Restrained

Figure 6.44: Cross-sections of 100 mm thick, 0.8% reinforced slabs showing the post-failure crack patterns

6.4.4 *Failure crack patterns*

Figure 6.44 presents the failure cross-sections for all the 0.8% reinforced, 100 mm thick slabs tested. All the reinforced, 100 mm thick slabs failed in punching shear, with larger shear cones than those that formed in the thinner 50 mm and 75 mm slabs. The ambient slab failure cone is unsymmetrical, biased towards the S frame side.

The heated slabs both formed similar sizes of punching shear cone diameters, though there was a lot of concrete crushing and aggregate loss in the unrestrained test compared to the restrained. Figures 6.45 and 6.46b show: the extensive aggregate loss, exposed flexural steel and catastrophic punching shear failure of the unrestrained, heated slab. The strength added by the restrained support condition caused there to be less aggregate loss during the restrained test compared to the corresponding unrestrained test.

Figure 6.45: Catastrophic punching shear failure of 0.8% reinforced heated slab, 100 mm thickness: unrestrained

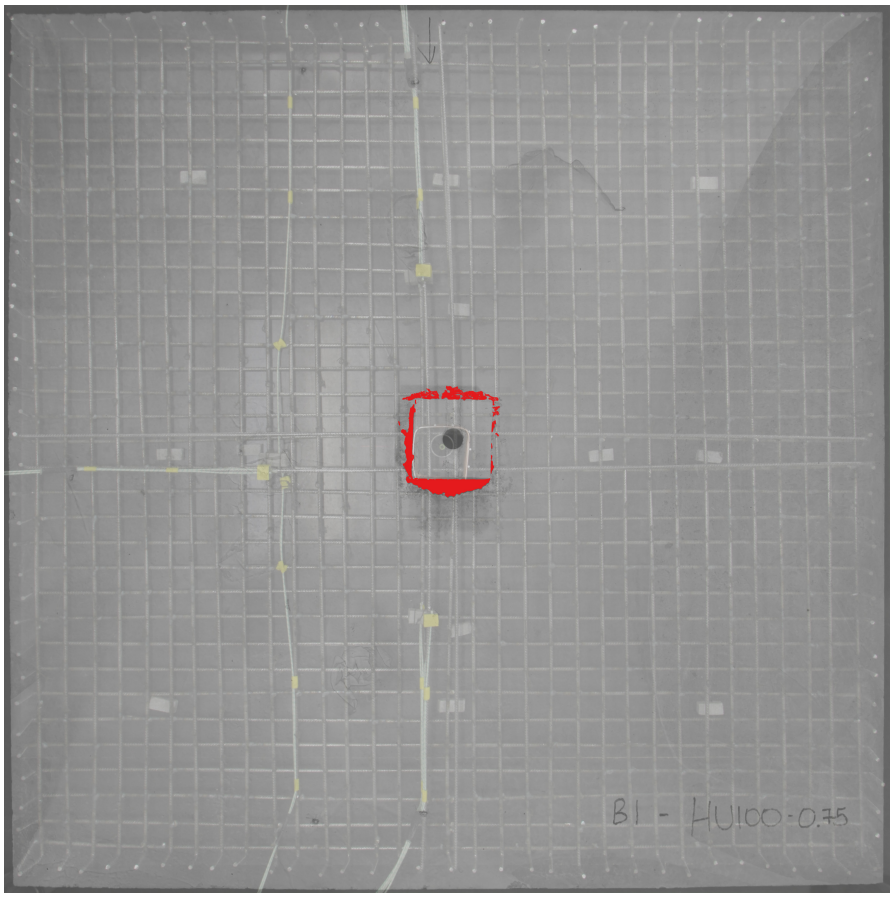

(a) Top surface

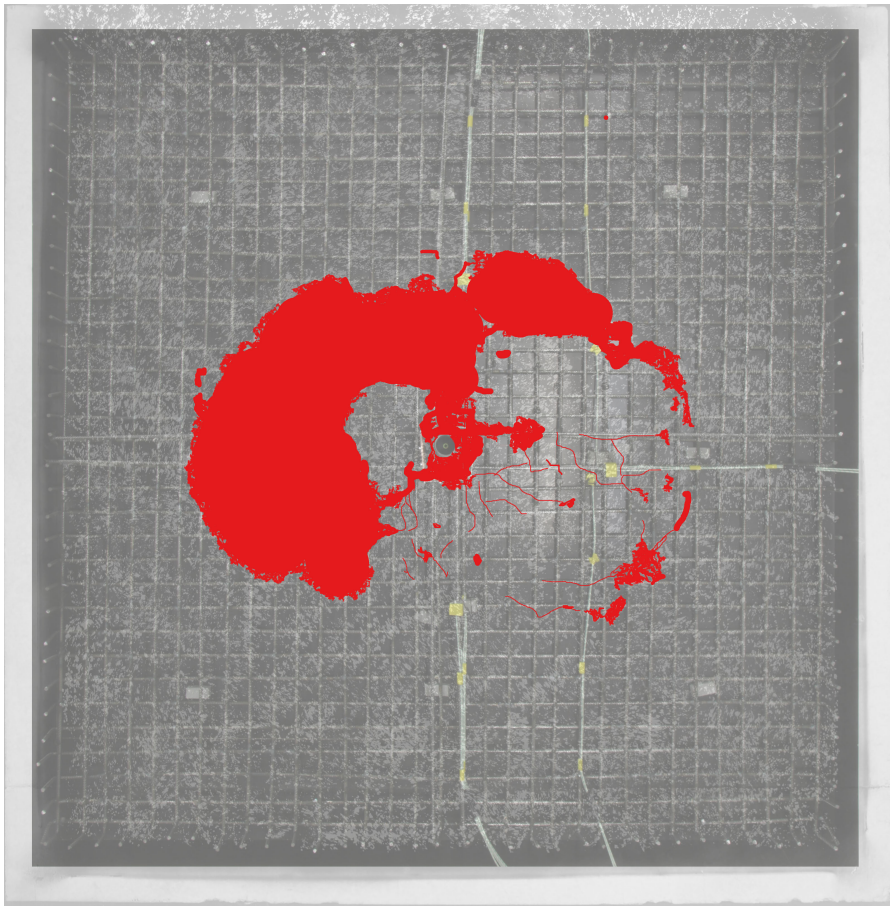

(b) Bottom surface

Figure 6.46: Heated 100 mm thick, 0.8% reinforced: unrestrained slab showing the plan post-failure crack patterns

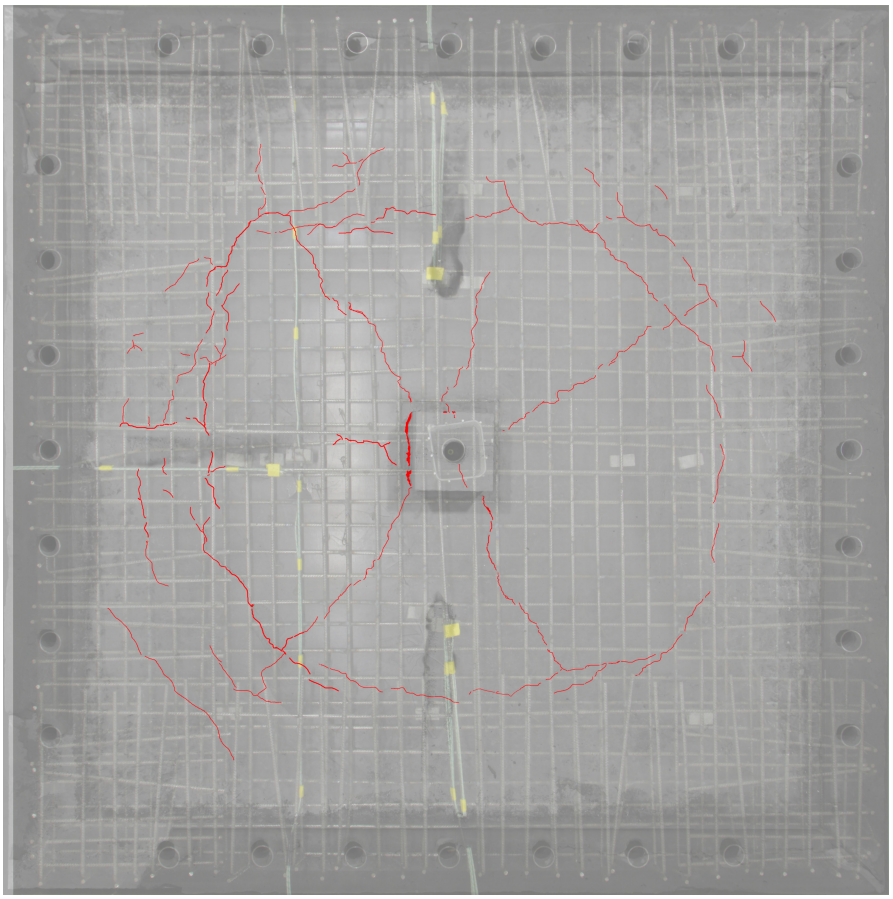

(a) Top surface

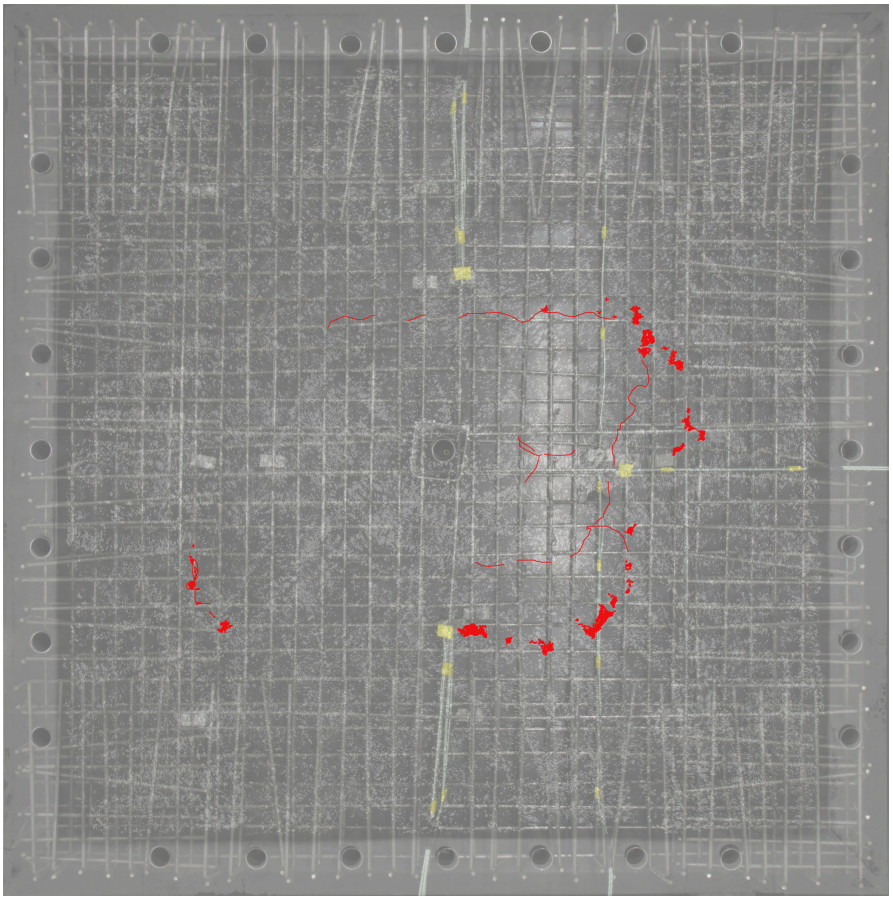

(b) Bottom surface

Figure 6.47: Heated 100 mm thick, 0.8% reinforced: restrained slab showing the plan post-failure crack patterns

Though a similar punching shear cone diameter was seen in both the heated unrestrained and restrained test, the heated restrained slab did not fail during heating, and the crack pattern in Figure 6.44c is from the residual strength test. If the restrained slab had failed during the heating, the punching shear cone might have been different.

There is a large difference when comparing the top surface crack patterns in the comparative support cases for 100 mm thick, 0.8% reinforced slabs, Figures 6.46a and 6.47a. The unrestrained slab top surface cracks emanate around the loaded column stub only, whereas the restrained slab top surface cracks radiate out from the column stub and join with a large circular crack. The restrained supported slab cracks show that the slab utilises membrane action.

Both bottom surface crack patterns, Figures 6.46b and 6.47b show unsymmetrical punching shear, with the cone diameter larger in the N-S cross-section rather than the E-W.

6.4.5 *Heated load-deflection behaviour and failure modes*

The load-deflection behaviour for the 100 mm thick, reinforced with 0.8% steel slab-column specimens is shown in Figure 6.48. Similar to the 50 mm and 75 mm thick, 0.8% reinforced slabs, both the restrained and unrestrained 100 mm thick slabs were stiffer during the loading phase compared to their corresponding ambient tested slabs. The heated, unrestrained slab failed in catastrophic punching shear, 4 minutes after ignition, whereas the heated, restrained slab was heated for 120 minutes and did not fail. The restrained slab was later residually tested, as described in Section 6.7.3.

6.4.6 *Summary*

The main bullet points summarising the 100 mm thick, 0.8% slab-column results in Section 6.4, are presented here:

- The support condition had a large impact on the failure of the 100 mm thick, 0.8% reinforced heated specimens. The unrestrained slab failed 4 minutes after ignition, whereas the restrained slab sustained the full 120 minutes of heating and was residually tested.
- The propane gas flow rate decreased in the restrained test only, causing the approximate maximum recorded near surface temperature to be 435°C, prior to the end of the test. As the unrestrained slab failed very

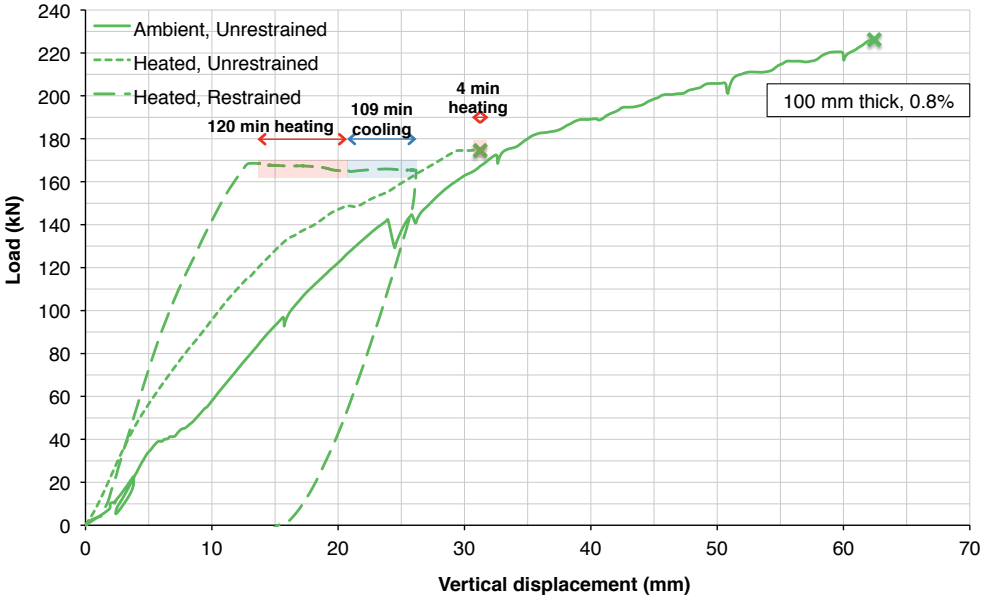

Figure 6.48: Load-deflection behaviour of 100 mm thick, 0.8% slabs

soon after ignition, its approximate maximum surface temperature was only 130°C.

- The unrestrained test flexural steel was at an effective depth of 81 mm and stayed at 18°C throughout the test. The restrained slab has a similar flexural steel effective depth of 82 mm and reached an approximate average maximum temperature of 170°C.
- The slabs all failed in a catastrophic punching shear mode.
- The comparative heated slabs formed similar sizes of punching shear cone diameter, even though the support condition varied. Though the heated restrained slab did not fail during heating and the crack pattern is from the residual strength test.
- If the restrained slab had failed during the heating, the punching shear cone might have been different.
- The added strength from the restrained support, caused there to be less aggregate loss on the unheated surface, compared to the unrestrained slab. The restrained heated surface cracks show that the slab utilises membrane action, compared the unrestrained case.

6.5 100 mm thick, 1.5% reinforced tests

This section presents the results of the three slab-column experiments that were 100 mm thick, reinforced with 1.5% steel (the most heavily reinforced

specimens): the ambient unrestrained (AU100-1.5), the heated unrestrained (HU100-1.5) and the heated restrained (HR100-1.5).

6.5.1 *Test overview*

The key 100 mm thick, 1.5% reinforced slab-column test outcomes are summarised in bullet points here:

- The approximate maximum concrete temperature near the heated surface was 208°C in the unrestrained slab and 510°C in the restrained slab;
- The propane gas flow rate was noted to decrease in the restrained test, and the heating phase was ended after 105 minutes due to radiant panel difficulties;
- The flexural steel at an effective depth of 86 mm in the unrestrained test and 82 mm in the restrained, reached an approximate average maximum temperature of 22°C and 148°C, respectively;
- Both the slabs failed in catastrophic punching shear mode, however their behaviour was very different. The unrestrained slab failed 14 minutes into the heating phase, whereas the restrained specimen sustained 105 minutes heating (radiant panel difficulties) and failed as the temperature was approximately 150°C throughout its thickness, in the cooling phase; and
- The ambient temperature tested slab had a capacity of 279.7 kN. Both the heated specimens had similar failure capacities. Their failure capacities were similar to the applied load during the heating phase of 234.0 kN and 232.7 kN in the unrestrained and restrained slab-column tests, respectively.

6.5.2 *Temperature curves*

Even though the heavily reinforced slab-column specimens had similar capacities when tested at elevated temperature, their behaviour and failure mode was very different. Both the slabs failed in a catastrophic punching shear mechanism; however, the restrained slab failed during the cooling phase of the experiment, whereas the unrestrained slab failed 14 minutes after ignition.

The temperature curve for the unrestrained heated test that failed 14 minutes after ignition, is shown in Figure 6.49a. Figure 6.49b shows the heating curve for the corresponding restrained slab.

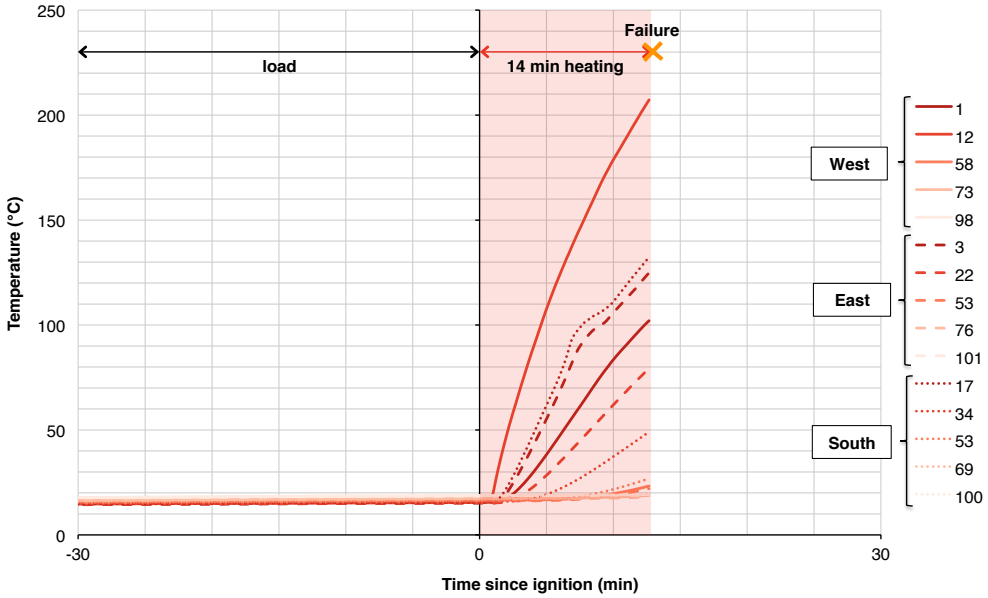

(a) Heated Unrestrained

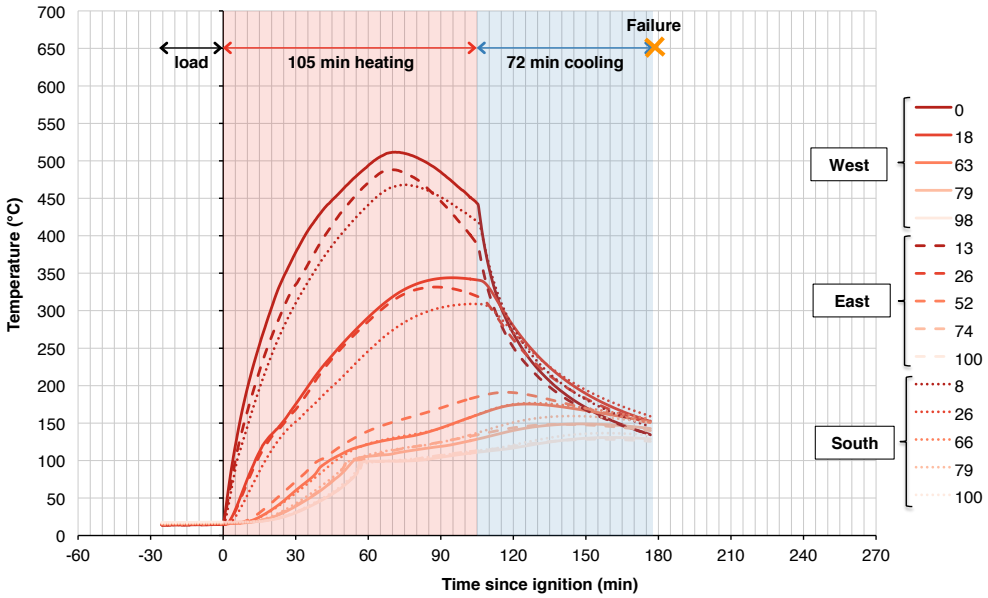

(b) Heated Restrained

Figure 6.49: Temperature curves for 100 mm thick, 1.5% slabs

The maximum temperature attained in the unrestrained slab was recorded as approximately 208°C at the W thermocouple, at a depth of 1 mm from the surface. The maximum approximate surface temperature of 510°C was attained in the restrained slab at 70 minutes after ignition, which was prior to when the radiant panels were turned off at 105 minutes.

The propane gas flow rate decreased at approximately 68 minutes after ignition in the restrained test and the heating phase was ended after 105 minutes due to radiant panel difficulties. Both the decrease in gas flow rate and shortened heating phase will have impacted the material degradation damage caused from the elevated temperature. Regardless of the elevated temperature impact, the restrained slab-column specimen failed during the cooling phase. This is the first recorded punching shear failure during the cooling phase of an elevated temperature test. As far as the author is aware, this may also be the first recorded high temperature test specimen that has failed during the cooling phase.

6.5.3 *Temperature profiles through the slab thickness*

The temperature profiles for the S, W and E thermocouple trees in the unrestrained 100 mm thick, reinforced with 1.5% steel slab, are shown in Figures 6.50 – 6.52. The corresponding restrained slab thermocouple positions are the same, relative to the reaction frame. Figures 6.53 – 6.55 show the restrained test temperature profiles.

The effective depth of the flexural steel in the 1.5% reinforced, 100 mm thick unrestrained slab was measured as 86 mm from the heated surface and 82 mm for the restrained slab. The flexural steel in the unrestrained test at 16 minutes after ignition was still at ambient temperature, an approximate average of 22°C. The maximum approximate average flexural steel temperature in the restrained test was 148°C, at 145 minutes after ignition or 40 minutes after the cooling phase started. The restrained slab-column failed as the temperature was approximately 150°C throughout its thickness.

6.5.4 *Failure crack patterns*

Figure 6.56 shows the failure cross-sections of all the 100 mm, 1.5% reinforced slab-column specimens tested. The punching shear cone formation of both the unrestrained tests, ambient and heated, have a similar path and change in angle. The change in crack angle corresponds approximately with the depth of the upper two bars of steel reinforcement, spanning through the column stub. The ambient unrestrained shear cone diameter is much greater than the

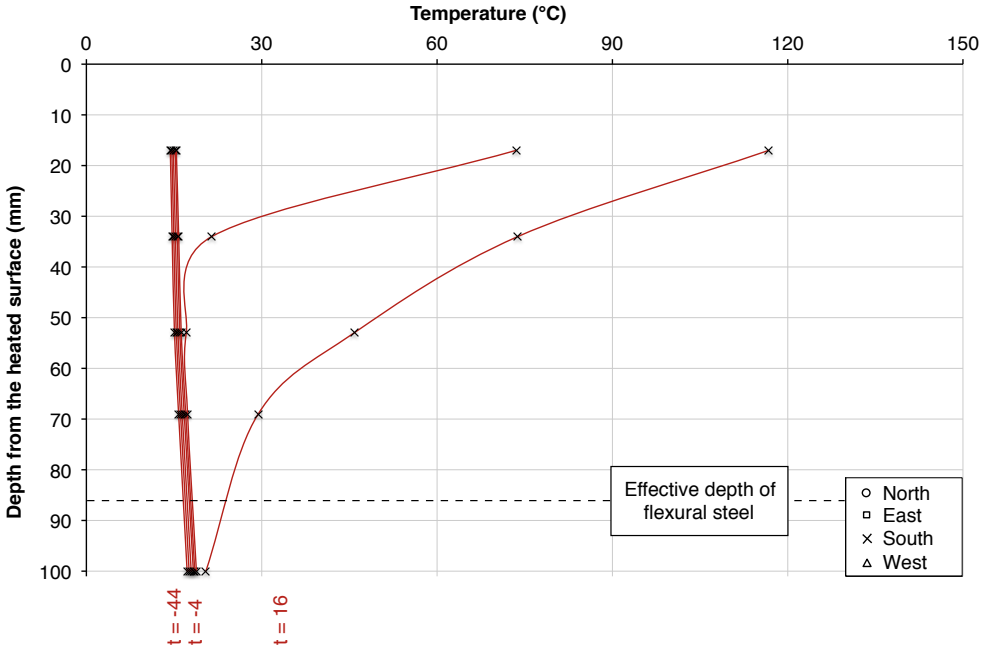

Figure 6.50: South temperature profile through 100 mm thickness, 1.5%: unrestrained slab

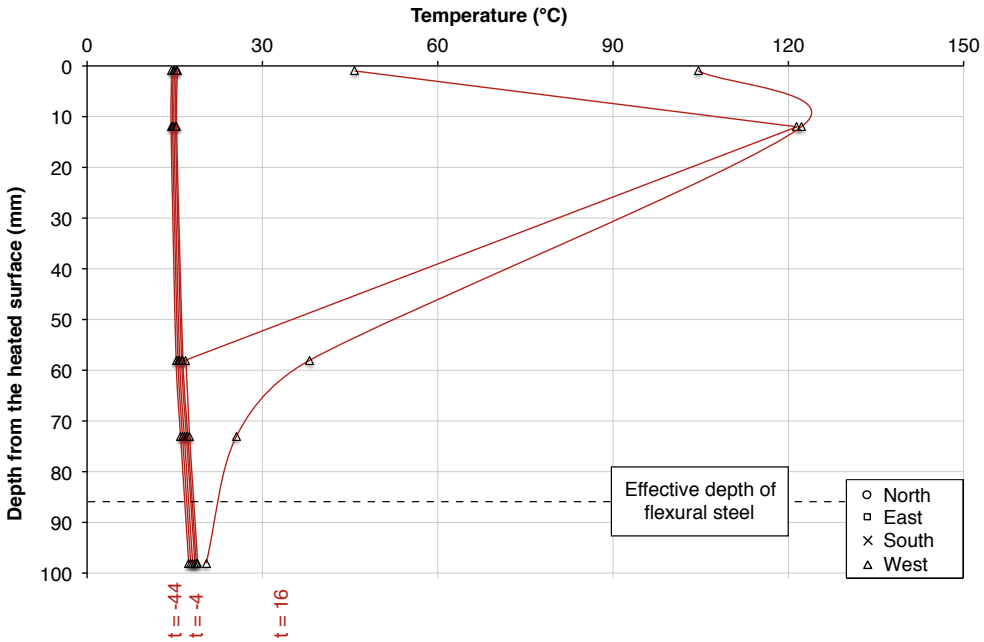

Figure 6.51: West temperature profile through 100 mm thickness, 1.5%: unrestrained slab

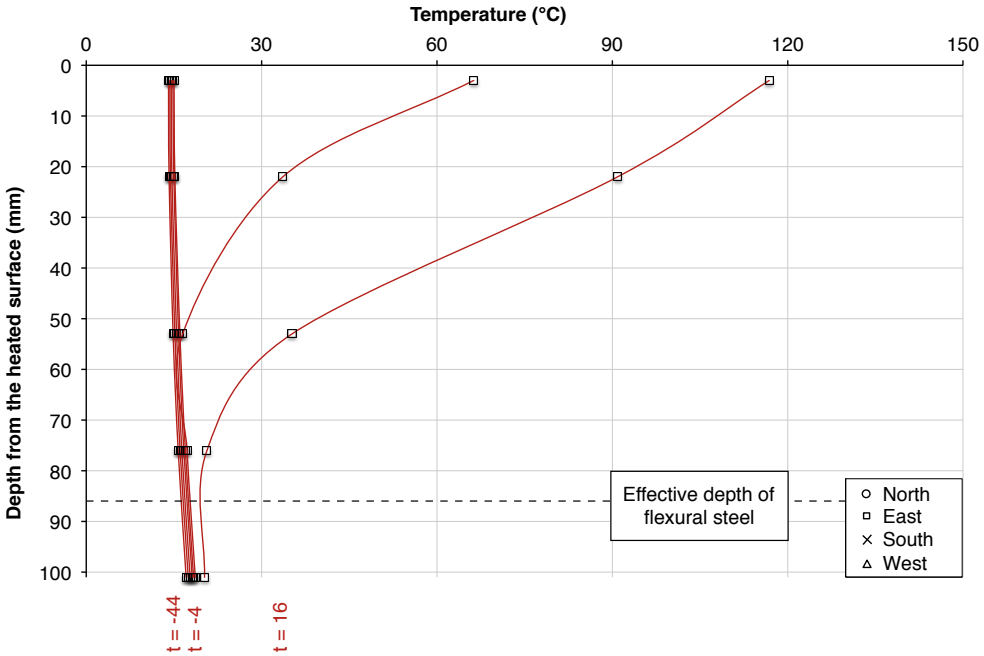

Figure 6.52: East temperature profile through 100 mm thickness, 1.5%: unrestrained slab

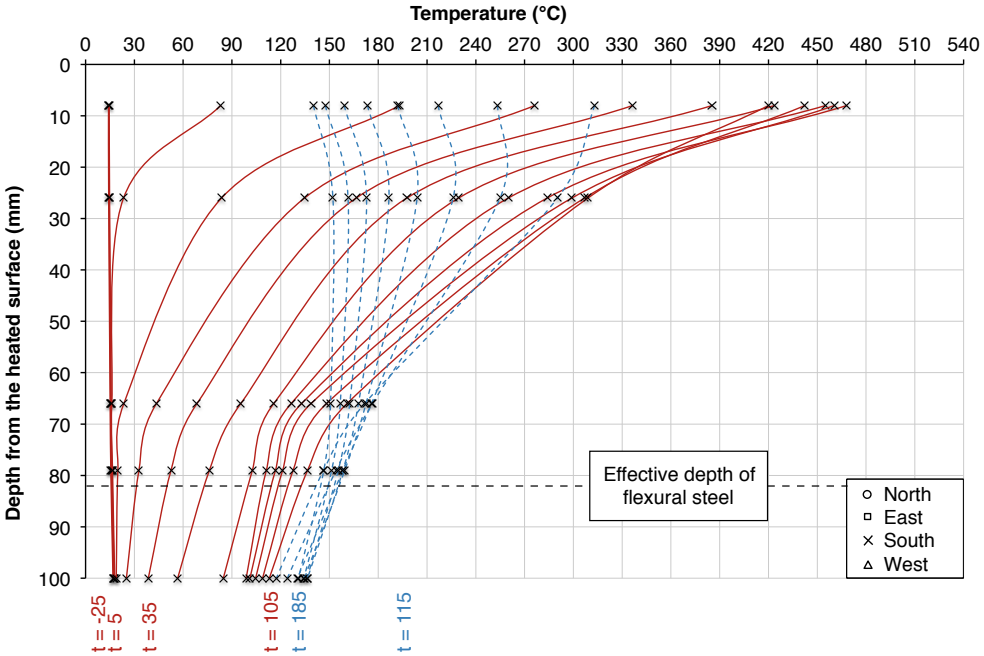

Figure 6.53: South temperature profile through 100 mm thickness, 1.5%: restrained slab

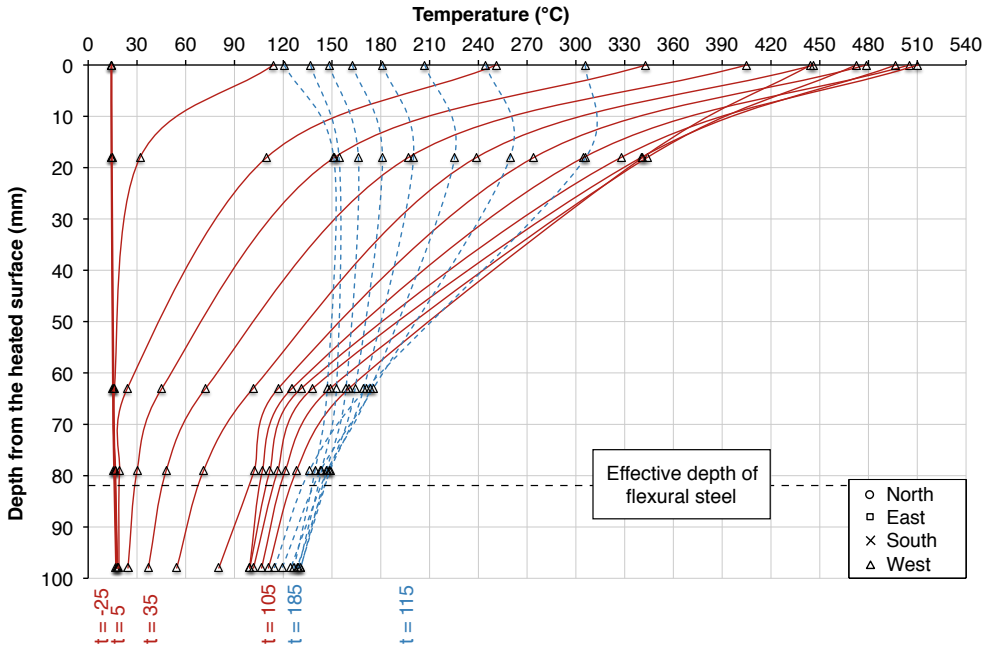

Figure 6.54: West temperature profile through 100 mm thickness, 1.5%: restrained slab

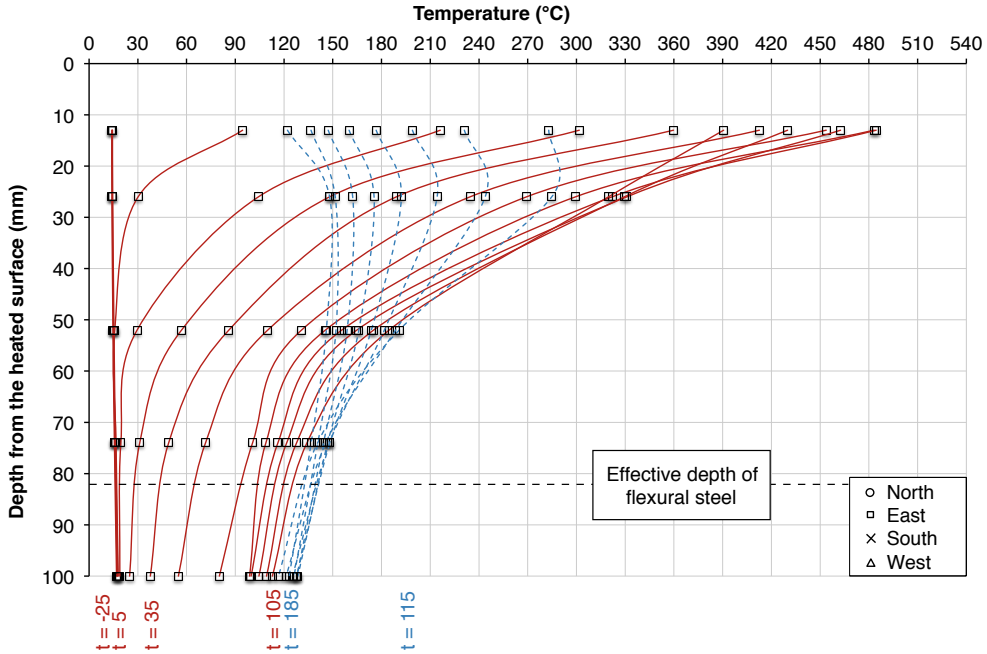

Figure 6.55: East temperature profile through 100 mm thickness, 1.5%: restrained slab

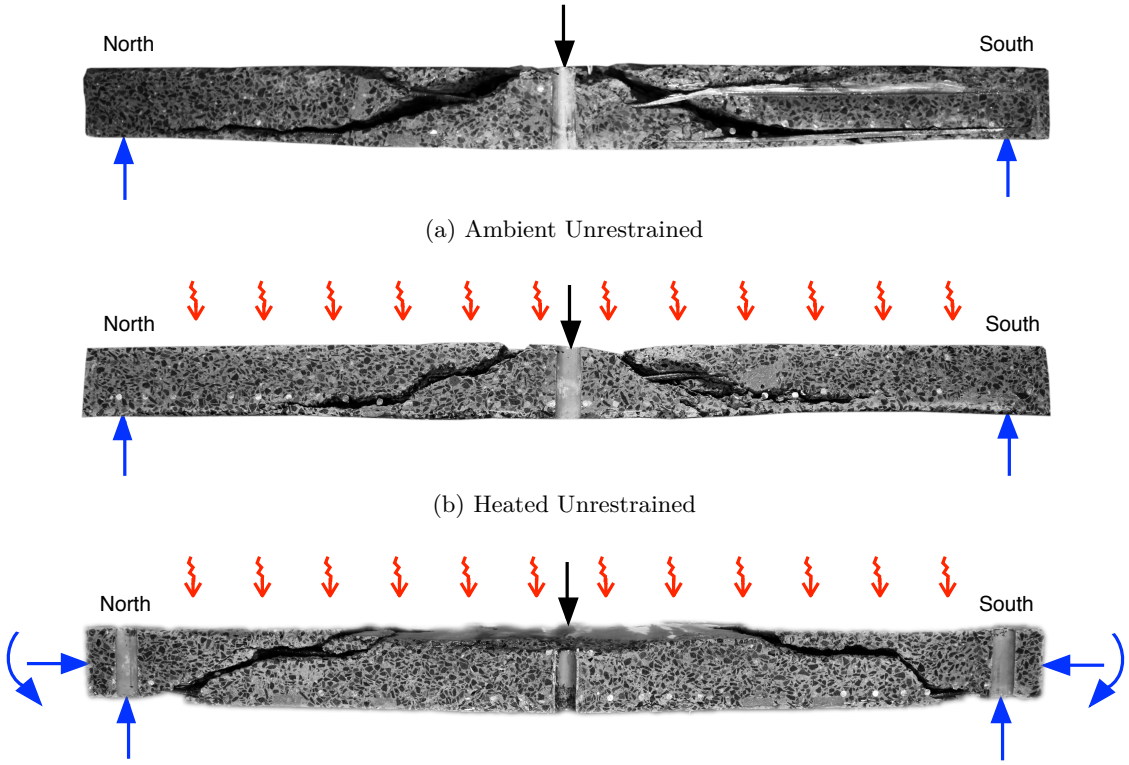

(a) Ambient Unrestrained

(b) Heated Unrestrained

(c) Heated Restrained

Figure 6.56: Cross-sections of 100 mm thick, 1.5% reinforced slabs showing the post-failure crack patterns

heated unrestrained diameter, as the crack forms along the flexural steel for a greater length. The flexural reinforcement here is unbonded and only frictional stresses are active in the concrete-steel bond.

The plan view crack patterns of the unrestrained and restrained, heated slabs are shown in Figures 6.57 and 6.58, respectively. The bottom surface cracks for the unrestrained slab, shown in Figure 6.57b were difficult to annotate post-failure.

(a) Top surface

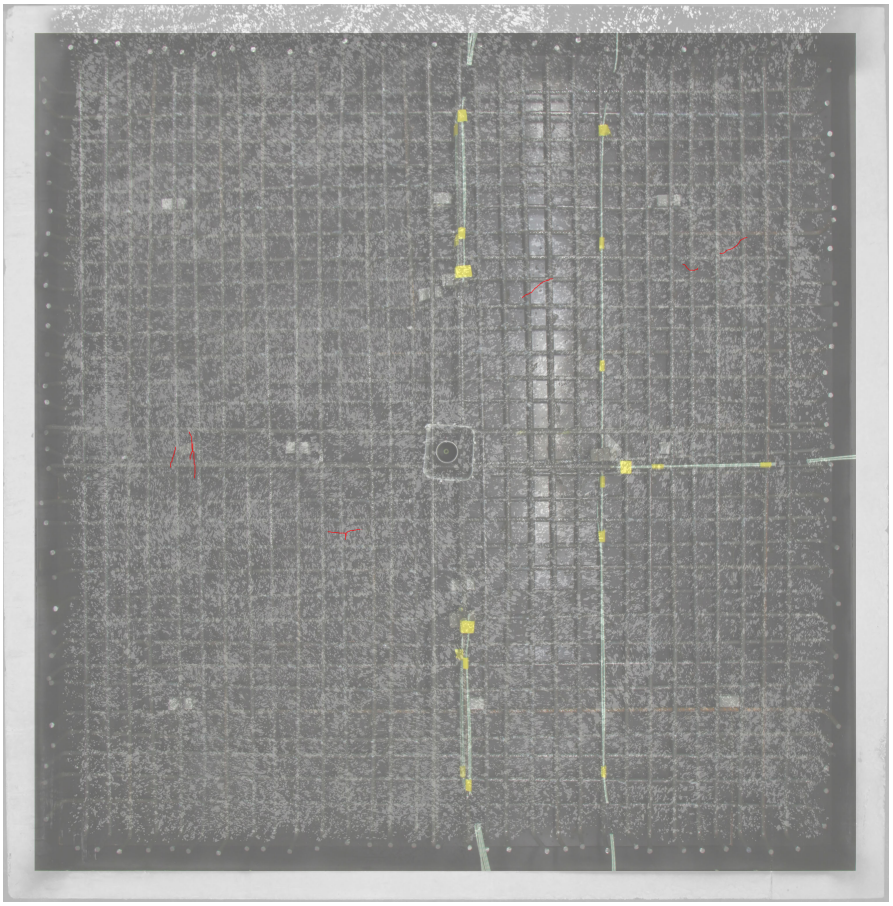

(b) Bottom surface

Figure 6.57: Heated 100 mm thick, 1.5% reinforced: unrestrained slab showing the plan post-failure crack patterns

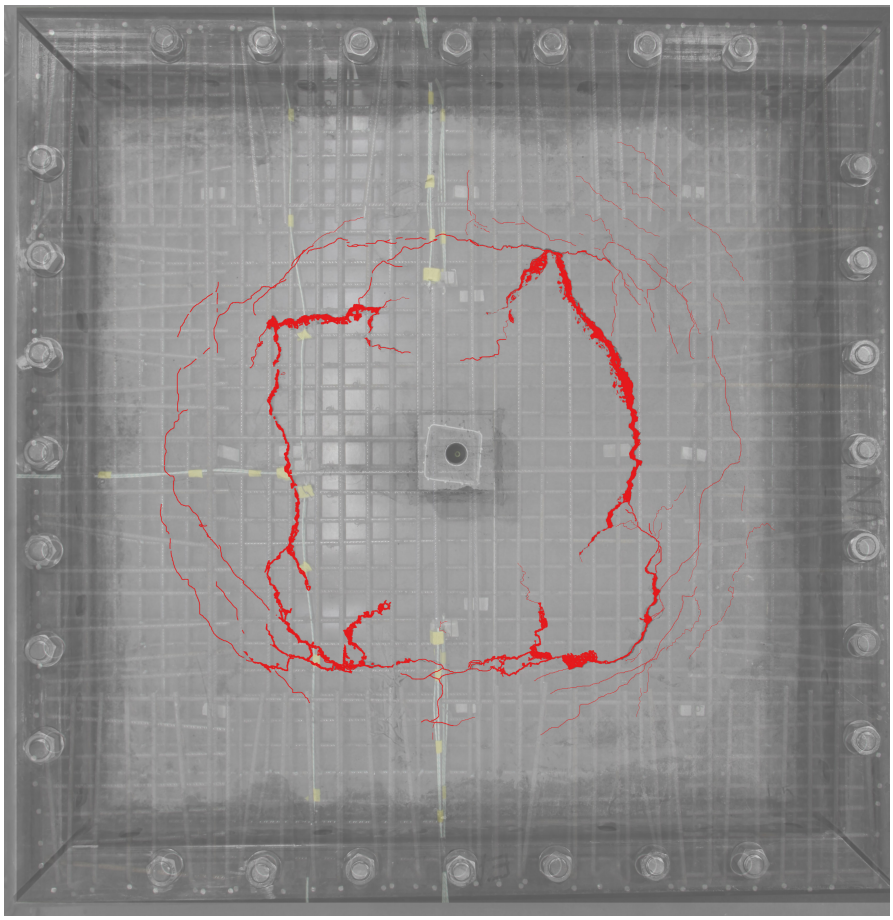

(a) Top surface

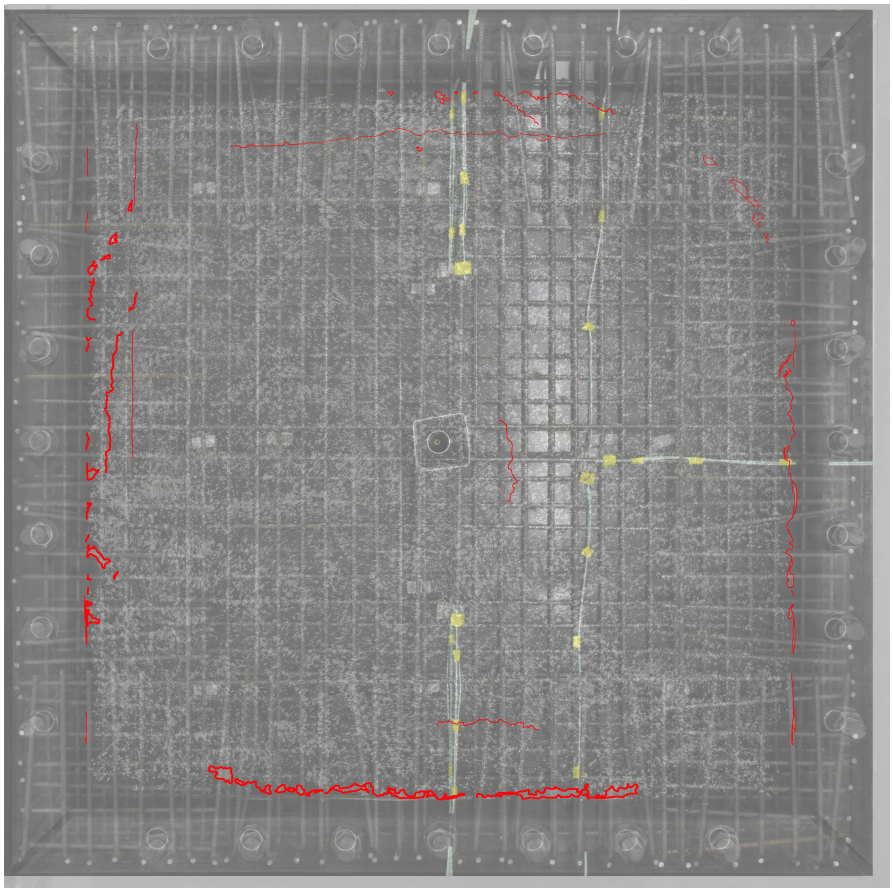

(b) Bottom surface

Figure 6.58: Heated 100 mm thick, 1.5% reinforced: restrained slab showing the plan post-failure crack patterns

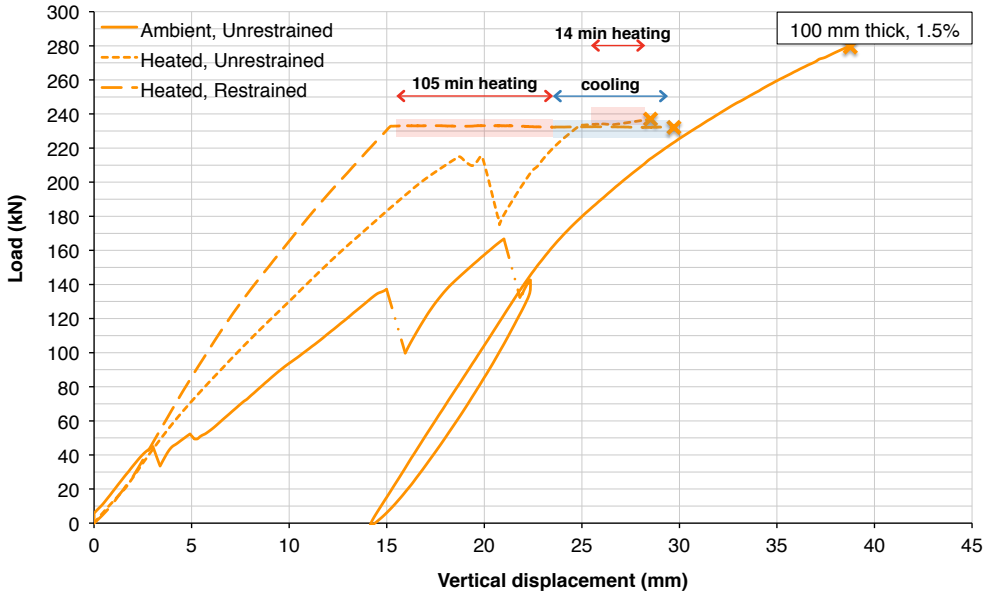

Figure 6.59: Load-deflection behaviour of 100 mm thick, 1.5% slabs

The punching shear cone in the heated, restrained slab-column is very different than any of the others seen during testing, shown by Figure 6.56c and Figure 6.58. This may be explained by the fact that the HR100-1.5 failed during the cooling phase, unlike any of the other tests. Both the top and bottom surface crack diameters are larger than all other tests. The restrained box sections may have limited the bottom surface crack diameter, as the cracks formed directly within the box sections, shown in Figure 6.58b. Figure 6.56c shows the crack propagated along the compression zone further than in all other tests.

6.5.5 *Heated load-deflection behaviour and failure modes*

Figure 6.59 shows the load-deflection behaviour for the 100 mm thick slabs, reinforced with 1.5% flexural steel. Both the heated slabs failed in punching shear during the slab-column testing, the unrestrained slab at 237.0 kN and the restrained failed at a slightly lower load of 233.2 kN. The failure capacities are similar to the load applied during the slab-column testing. The support condition therefore has no impact on the failure capacities of the heated 100 mm thick, 1.5% reinforced specimens.

6.5.6 *Summary*

The main bullet points summarising the 100 mm thick, 1.5% slab-column results in Section 6.5, are presented here:

- Both the heavily reinforced, heated specimens failed in punching shear, though the support condition had a large impact on the behaviour.
- The unrestrained test failed 14 minutes after ignition and the restrained specimen failed during the cooling phase. The restrained slab sustained 105 minutes heating (not 120 minutes due to radiant panel difficulties) and failed as the temperature throughout its thickness was approximately 150°C.
- HR100-1.5 is the first recorded punching shear failure during the cooling phase of an elevated temperature test. As far as the author is aware, this may also be the first recorded high temperature test specimen that has failed during the cooling phase.
- The restrained test sustained an approximate maximum near surface concrete temperature of 510°C and the flexural steel reached an average approximate maximum temperature of 148°C.
- The punching shear cone formation of both the ambient and heated, unrestrained tests, have a similar path and change in angle.
- The heated, restrained punching shear cone is very different from all the other tests. Both the top and bottom surface crack diameters are larger than all other tests. The crack propagates along the compression zone further than in all other tests.
- Both the heated specimens had similar failure capacities as they failed as the applied load was held constant during the slab-column test. The failure capacities do not represent the contrasting behaviour seen in the unrestrained and restrained, heated test.

6.6 100 mm thick, 0% reinforced tests

This section presents the results of the unreinforced, 100 mm thick slab-column specimens: the ambient unrestrained (AU100-0), the heated unrestrained (HU100-0) and the heated restrained (HR100-0).

6.6.1 *Test overview*

The key 100 mm thick, unreinforced slab-column test outcomes are summarised in bullet points here:

- The unrestrained slab failed 6 minutes after ignition, which is in contrast to the restrained specimen which sustained 99 minutes of heating

(120 minutes heating was not attainable due to radiant panel difficulties) and was residually tested (described in Section 6.7.4);

- The maximum approximate concrete temperature near the heated surface was 165°C in the unrestrained slab and 500°C in the restrained slab;
- All the slabs failed in flexure mechanisms; and
- Friction in the hydraulic jack caused the load to increase continuously during the heating phase, until the unrestrained specimen failed.

6.6.2 *Temperature curves*

The support condition had a large impact on the behaviour of the heated specimens. The unrestrained, heated slab failed 6 minutes after ignition, whereas the restrained, heated slab did not fail and had to be residually tested (described in Section 6.7.4).

Figure 6.60 presents the temperature curves for both the heated tests. The maximum approximate concrete temperature measured in the unrestrained slab was 165°C, measured on the N side, 3 mm below the surface. The N side thermocouple positioned 22 mm below the surface, measured the maximum temperature of 500°C in the restrained test.

At approximately 49 minutes after ignition of the restrained test, the gas flow rate was recorded to be decreased. This rate continued to decrease until the radiant panels had to be turned off at 99 minutes due to difficulties.

6.6.3 *Temperature profiles through the slab thickness*

Figures 6.61 – 6.63 show the temperature profiles for the N, W and E thermocouple trees in the unreinforced unrestrained, heated 100 mm thick slab. The comparative temperature profiles for the restrained slab are shown in Figures 6.64 – 6.66. The heat fronts were plotted as straight lines, otherwise the heat front was mis-represented as decreasing with time.

In both heated tests, the N temperature profiles show greater, near heated surface temperatures compared to the others. Differences may have been caused by uneven radiant panel array heating across the surface of the two specimens.

6.6.4 *Failure crack patterns*

Figure 6.67 shows the ambient failure cross-section for the unrestrained, unreinforced 100 mm thick test only. It was not possible to take cross-sectional

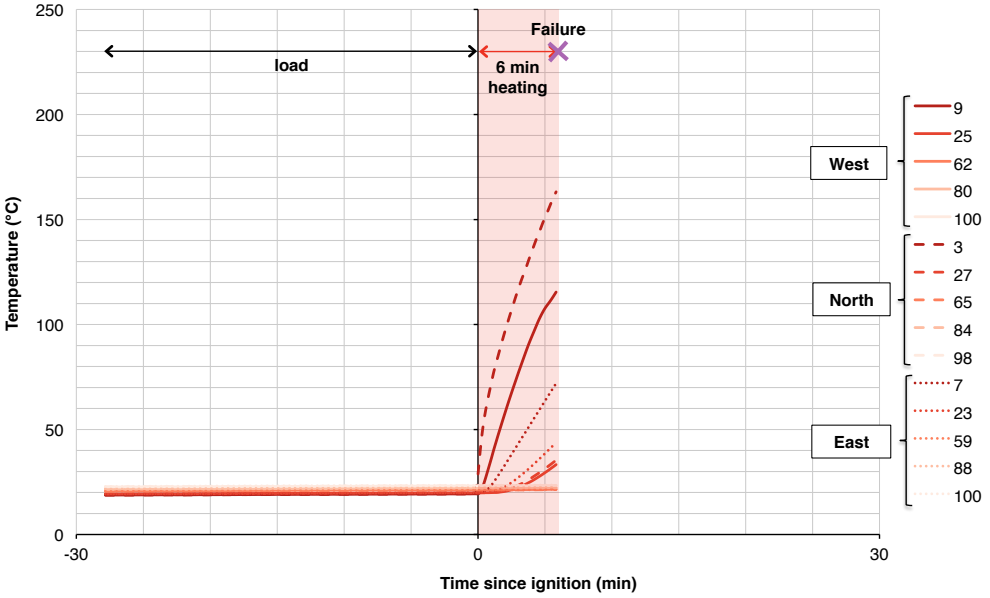

(a) Heated Unrestrained

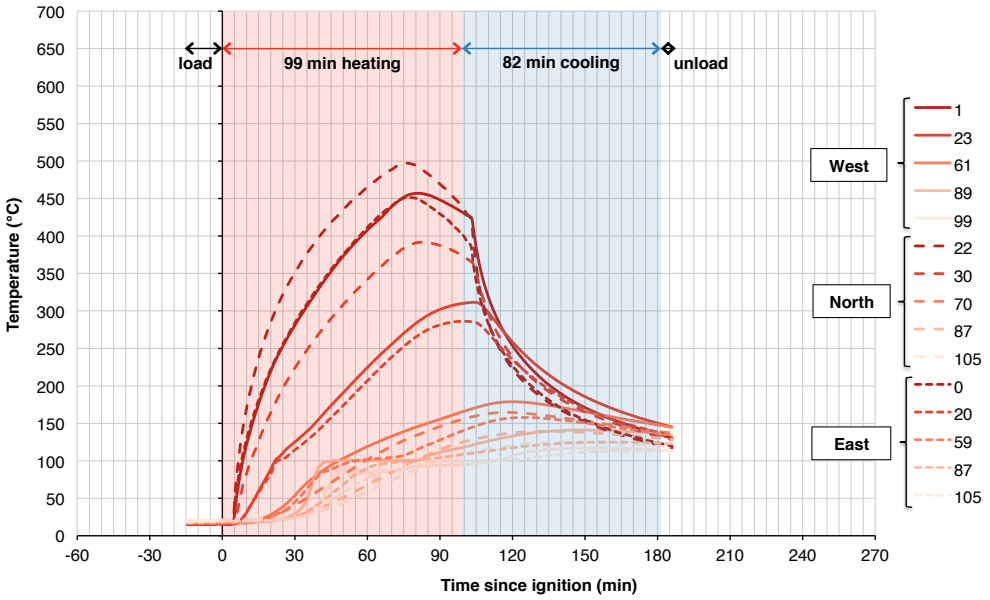

(b) Heated Restrained

Figure 6.60: Temperature curves for 100 mm thick, 0% slabs

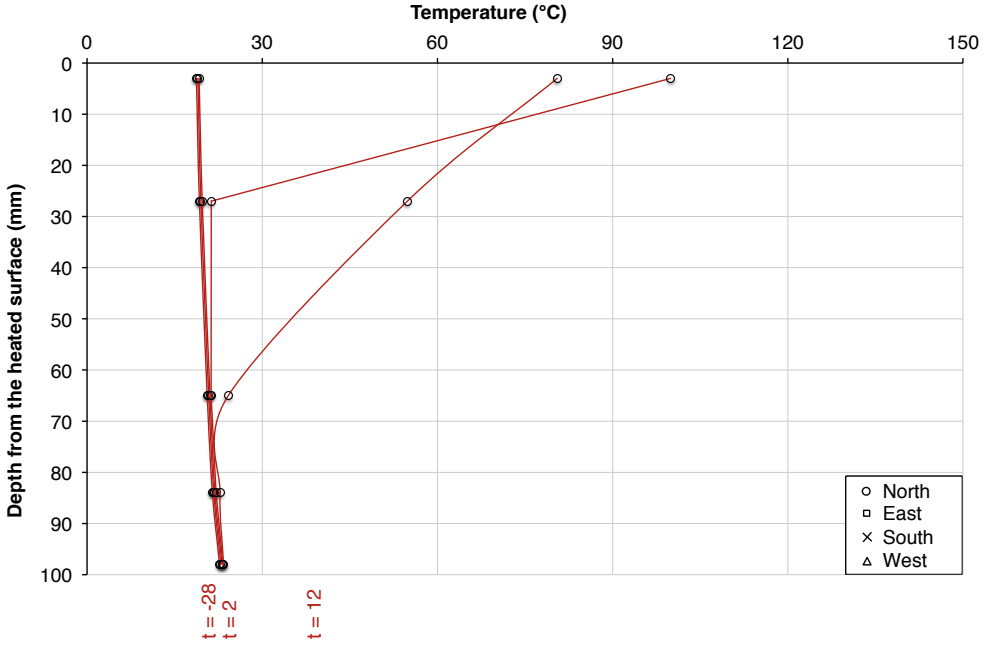

Figure 6.61: North temperature profile through 100 mm thickness, 0%: unrestrained slab

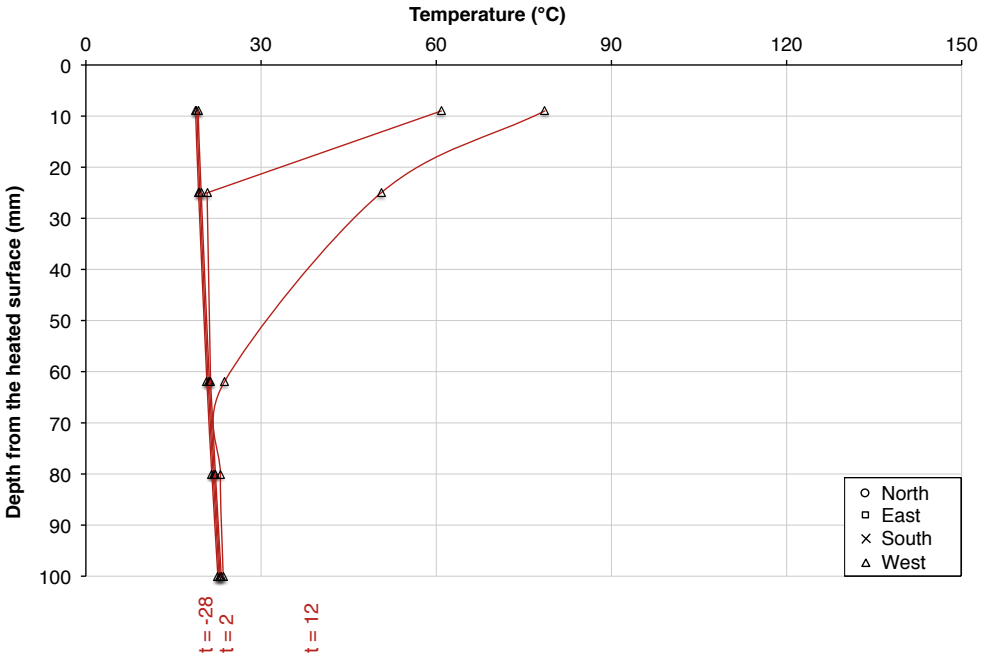

Figure 6.62: West temperature profile through 100 mm thickness, 0%: unrestrained slab

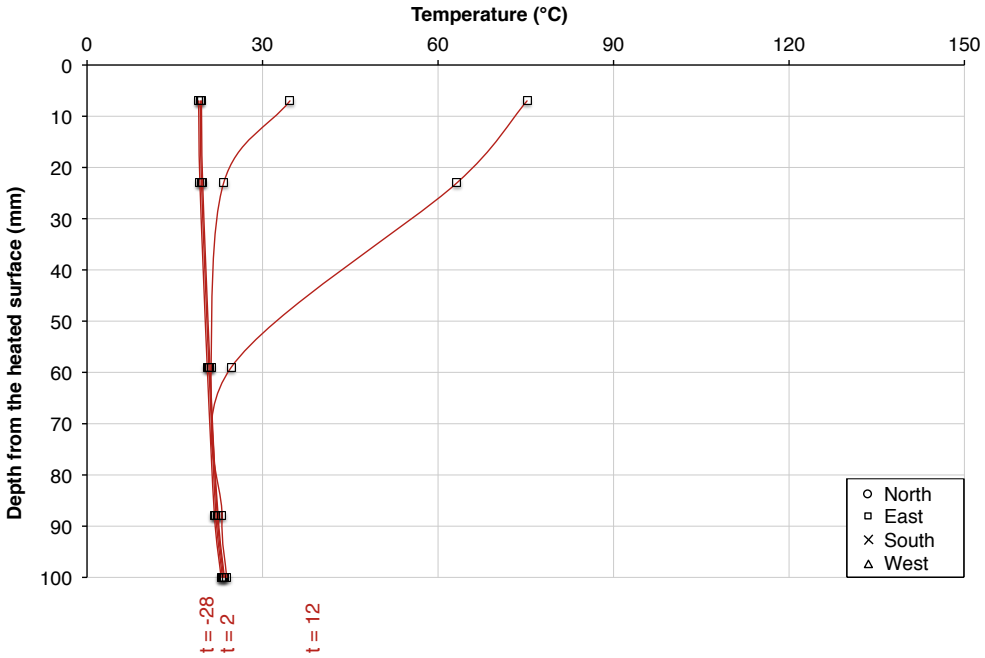

Figure 6.63: East temperature profile through 100 mm thickness, 0%: unrestrained slab

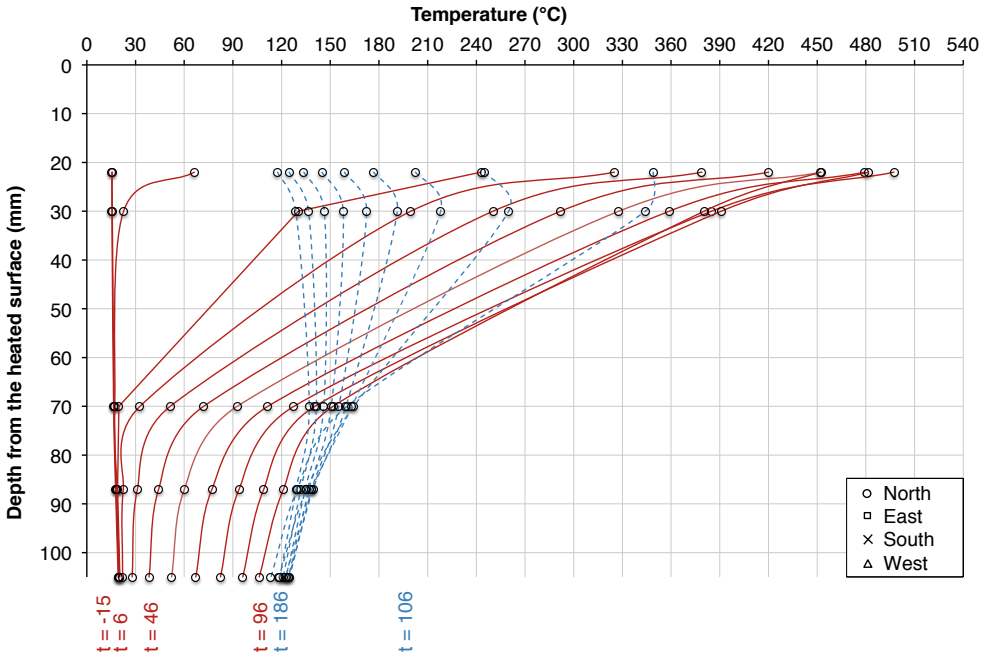

Figure 6.64: North temperature profile through 100 mm thickness, 0%: restrained slab

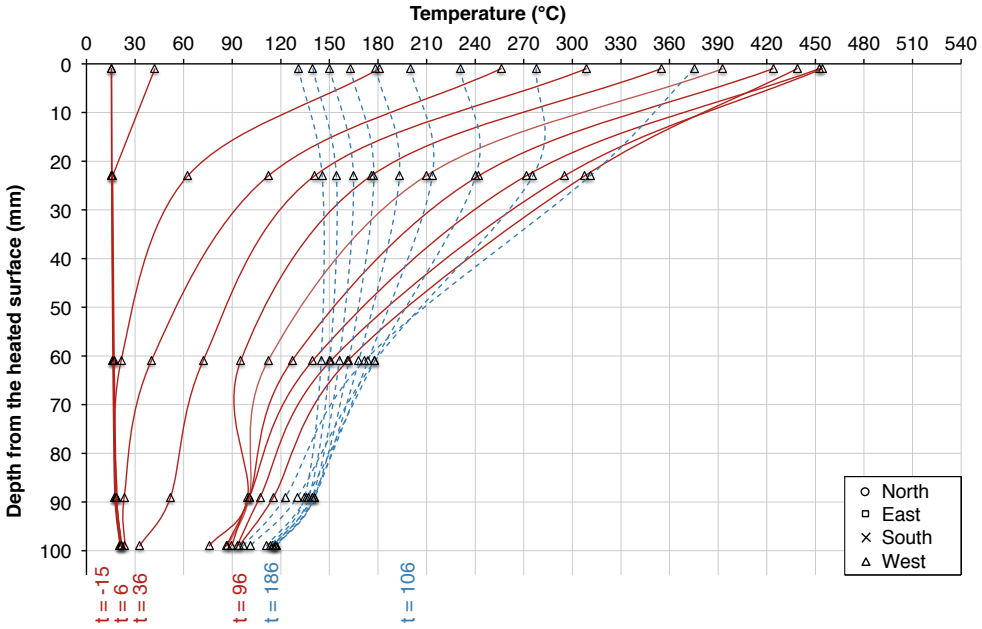

Figure 6.65: West temperature profile through 100 mm thickness, 0%: restrained slab

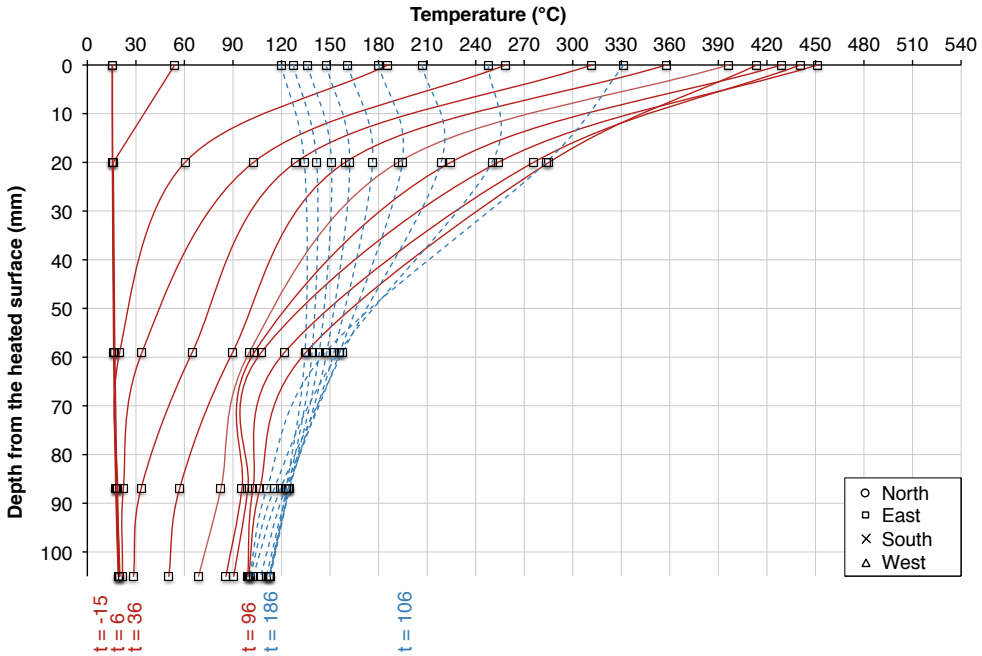

Figure 6.66: East temperature profile through 100 mm thickness, 0%: restrained slab

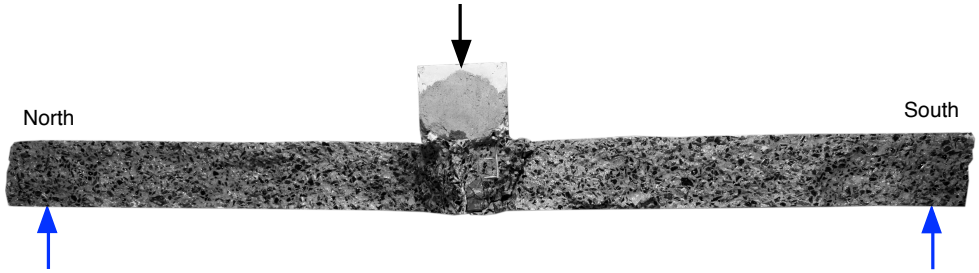

Figure 6.67: Cross-section of the ambient 100 mm thick, unreinforced slab showing the post-failure crack patterns

photos of either of the heated unreinforced failures, as they failed into too many pieces. The ambient failure cracks are at angles of approximately 117°, causing the direction to be opposite to that seen during the shear failure tests.

Figures 6.68 and 6.69 show the plan view crack patterns of the unrestrained and restrained, unreinforced heated slabs, respectively. All the unreinforced slabs failed in flexure with characteristic compression and tensile yield lines on the top (Figures 6.68a and 6.68b) and bottom (Figures 6.69a and 6.69b) surfaces, respectively.

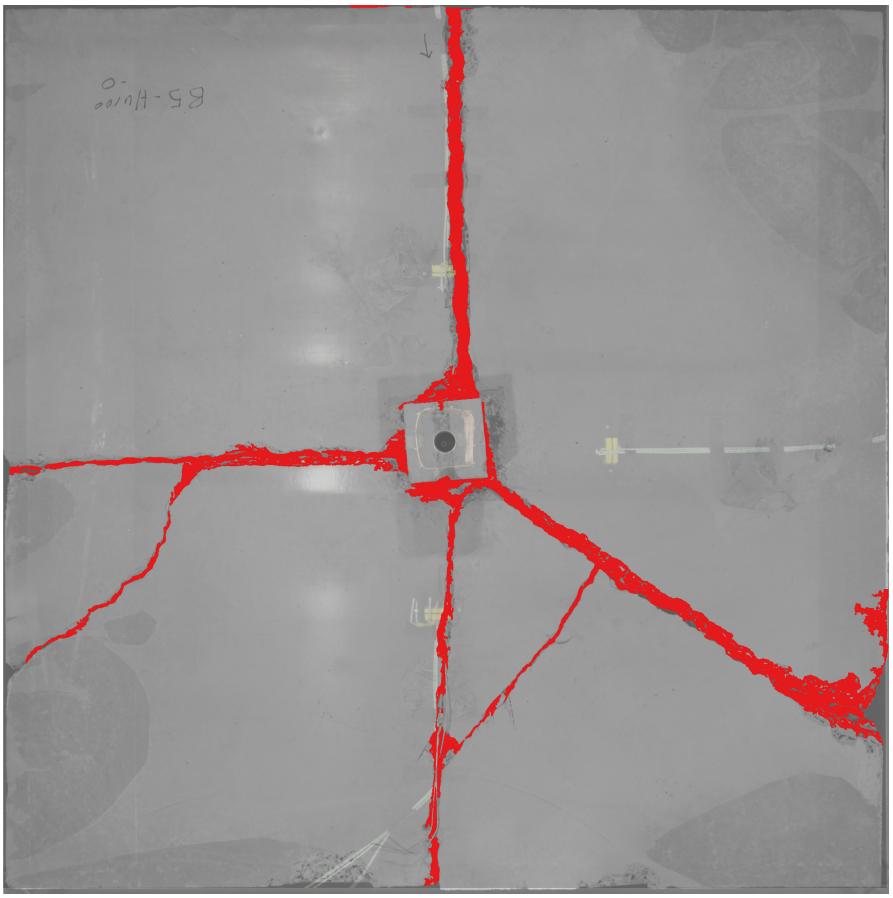

(a) Top surface

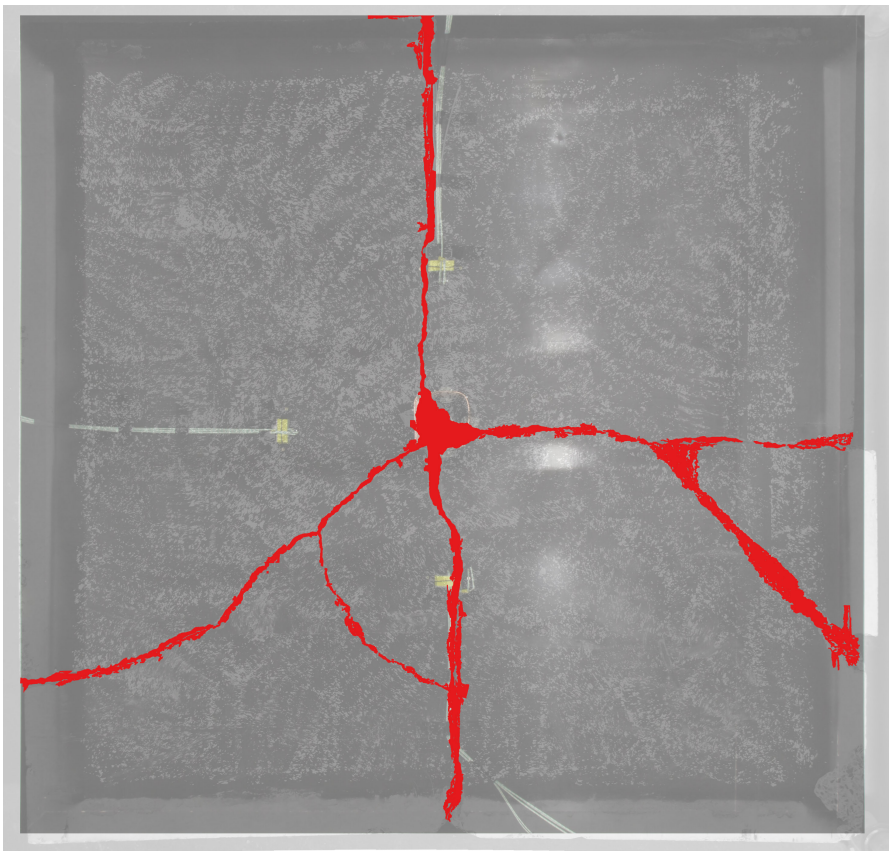

(b) Bottom surface

Figure 6.68: Heated 100 mm thick, 0% reinforced: unrestrained slab showing the plan post-failure crack patterns

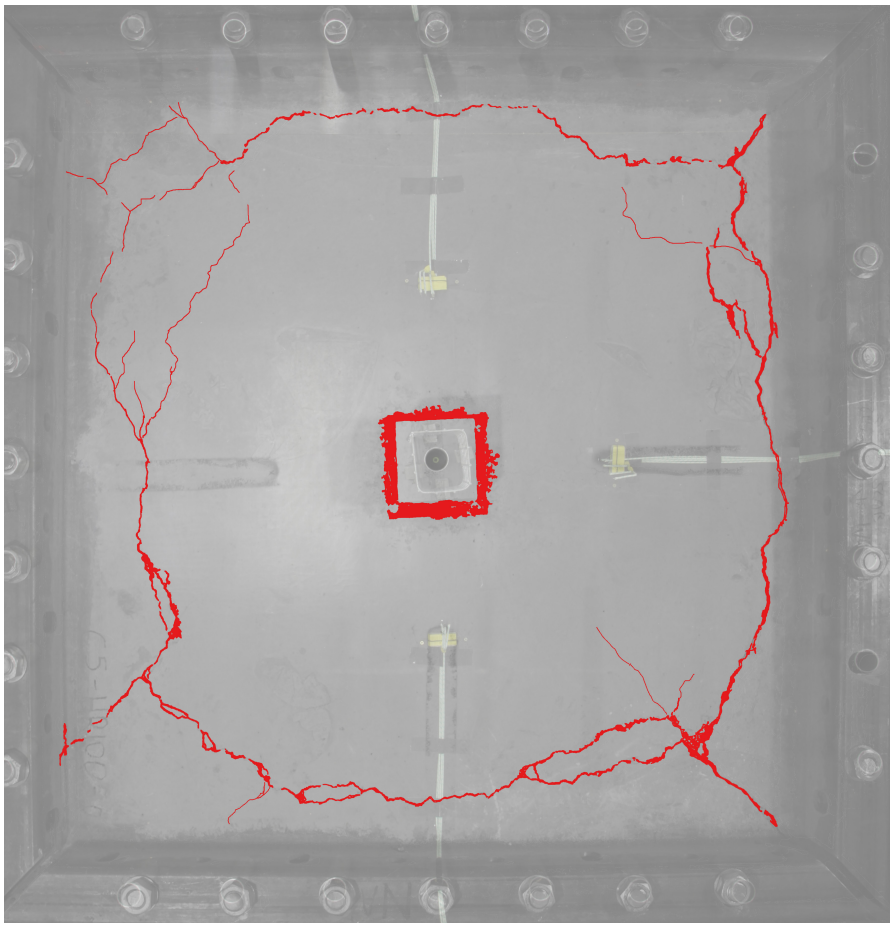

(a) Top surface

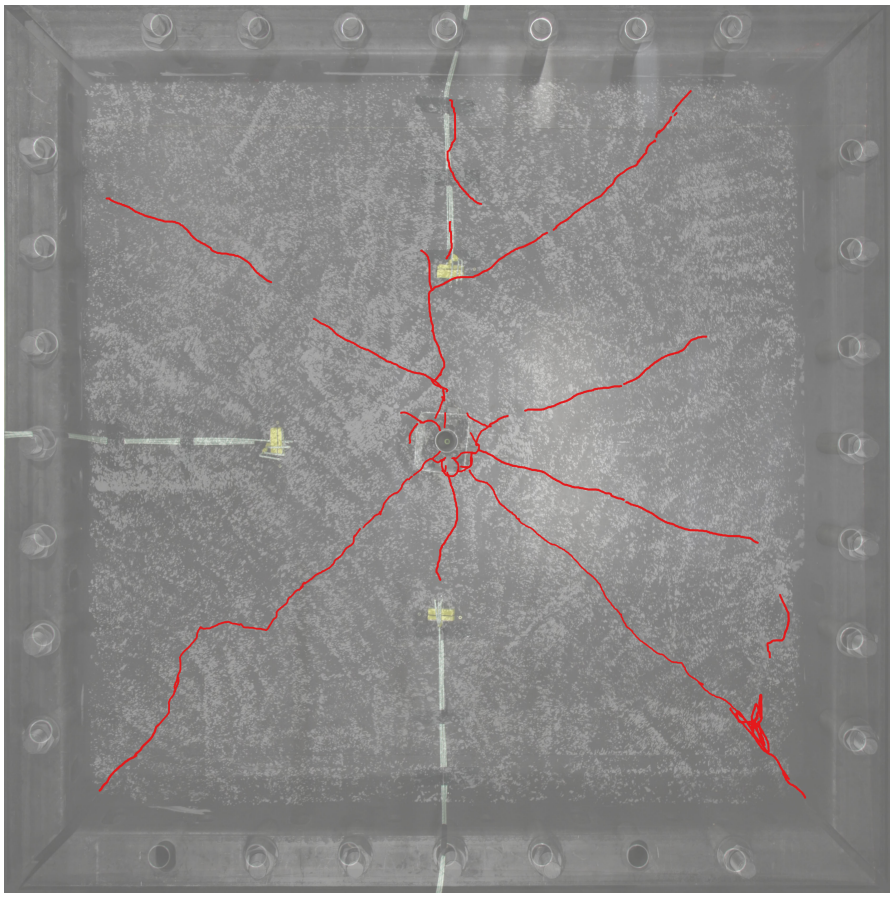

(b) Bottom surface

Figure 6.69: Heated 100 mm thick, 0% reinforced: restrained slab showing the plan post-failure crack patterns

6.6.5 *Heated load-deflection behaviour and failure modes*

Figure 6.70 shows the load-deflection behaviour for both the unrestrained and restrained tests compared to the ambient behaviour. Figure 6.70a shows the direct heat impact on the unrestrained unreinforced, 100 mm thick slabs. The failure capacities of both the slab-column specimens was similar with, 38.9 kN for the heated and 43.8 kN for the ambient. The heated specimen failed after 6 minutes of heating, with a central displacement of approximately 2.2 mm, much less than the ambient specimen's central displacement of approximately 18.2 mm.

Prior to heating the unrestrained specimen, the load was applied as usual, up to 30 kN. Figure 6.70a shows that once heating started, the load applied increased continuously until failure. This load increase was later found to be caused by friction in the hydraulic loading jack as presented in Section 7.1.3. The same friction was overcome and hence not recognised in all the reinforced specimen tests as the loads applied were greater. Even though the applied load on the unrestrained specimen increased until failure, it can be seen to deflect slightly towards the heat source after ignition.

The hydraulic jack friction was overcome in the restrained heated test, as the specimen was accidentally initially loaded above the 70% capacity, up to approximately 41 kN. After the accidental overload, the specimen was unloaded and checked for cracks. A crack in the centre of the slab, running from W to E, was observed. The slab-column specimen was re-loaded at a rate of 2mm/min up to 33.1 kN and while the load was held constant, the specimen was heated. Throughout the heating phase the initial crack extended and other cracks formed. The restrained, heated slab did not fail during the slab-column test, therefore it was residually tested to failure (presented in Section 6.7.4).

6.6.6 *Summary*

The main bullet points summarising the 100 mm thick, unreinforced slab-column results in Section 6.6, are presented here:

- The support condition had a large impact on the failure of the 100 mm thick, unreinforced heated specimens. The unrestrained slab failed 6 minutes after ignition, whereas the restrained slab sustained 99 minutes of heating (not 120 minutes due to radiant panel difficulties) and was residually tested.
- The maximum approximate concrete temperature near the heated surface was 165°C in the unrestrained slab and 500°C in the restrained slab.

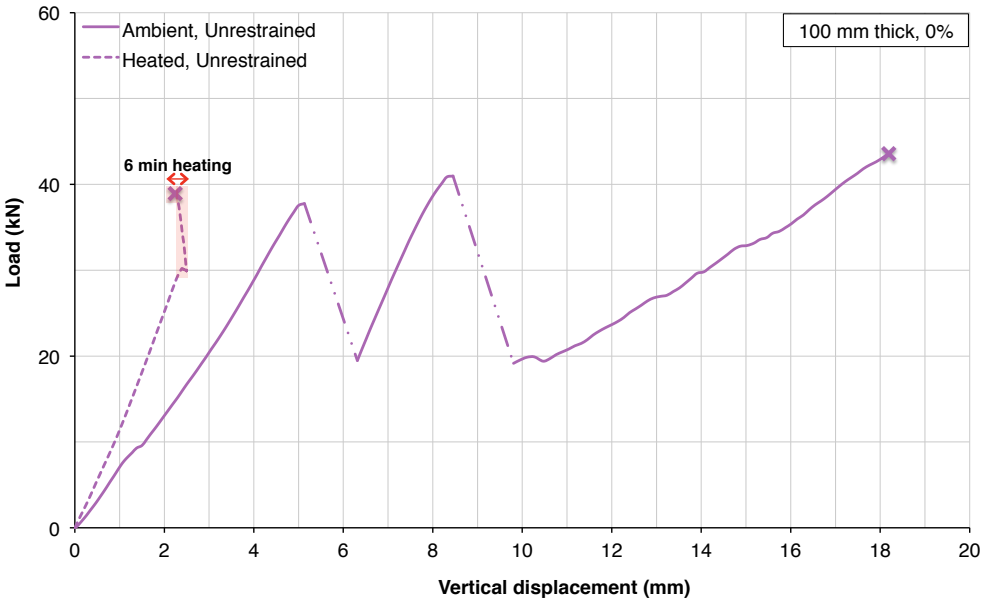

(a) Heated Unrestrained

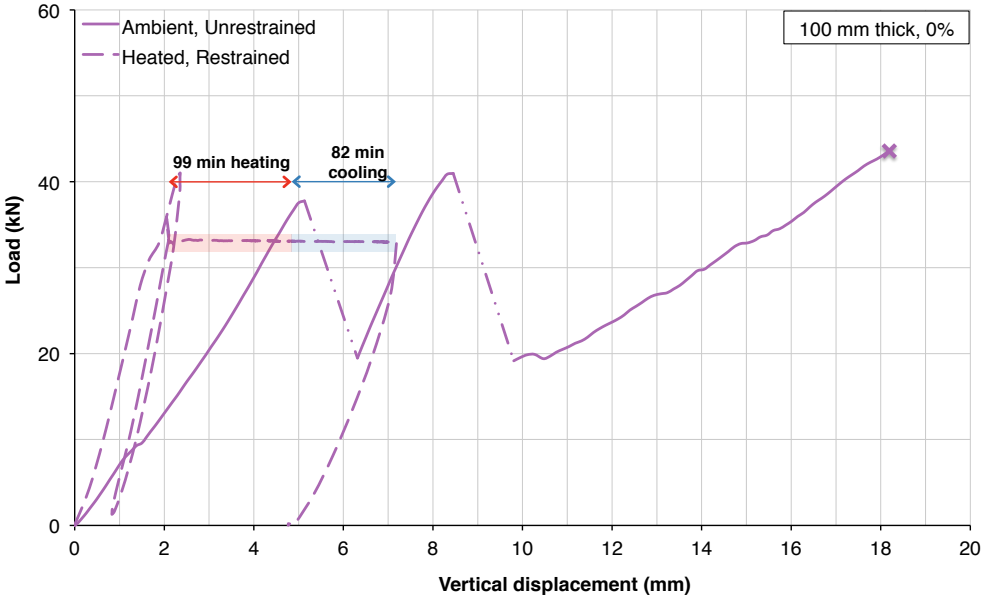

(b) Heated Restrained

Figure 6.70: Load-deflection behaviour of 100 mm thick, 0% slabs

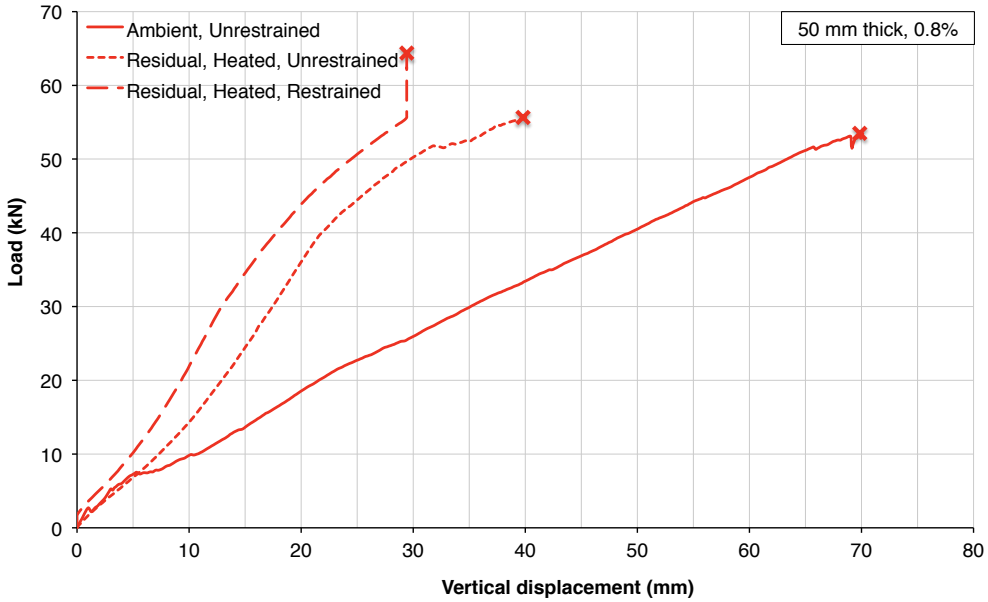

Figure 6.71: Residual load-deflection behaviour of 50 mm thick, 0.8% slabs

- All the unreinforced slabs failed in flexure with characteristic compressive and tensile yield lines on the top and bottom surfaces, respectively.
- Though hydraulic jack friction caused the load to increase on the unrestrained specimen during the heating phase, the central displacement can be seen to deflect slightly towards the heat source after ignition (analysed further in Section 7.2.5).

6.7 RESIDUAL TESTS

This section presents the residual test results for all the slabs that did not fail during the slab-column heated tests. The residual tests were undertaken the day following the slab-column test. The specimens were tested to failure to find their residual strength. For each respective residual test, the support conditions were the same as those used in the original slab-column testing.

6.7.1 *50 mm thick, 0.8% reinforced tests*

Both the unrestrained and restrained, 50 mm specimens did not fail during the heated slab-column test. The heated specimen's residual load-deflection behaviour is plotted in Figure 6.71 against the ambient behaviour to show the impact of elevated temperature.

A direct comparison of similar unrestrained, 50 mm slabs with 0.8% shows that elevated temperature has little impact on the capacity, with a slight in-

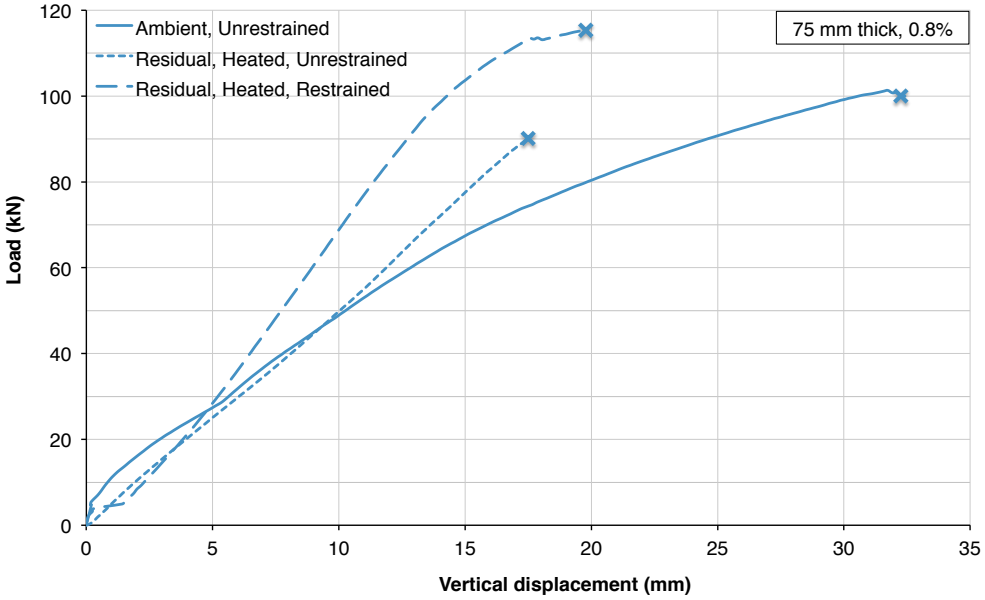

Figure 6.72: Residual load-deflection behaviour of 75 mm thick, 0.8% slabs

crease from 54.2 kN to 55.7 kN. The restrained support type increases the elevated temperature capacity by 14%, to 64.4 kN and decreased the central deflection.

6.7.2 *75 mm thick, 0.8% reinforced tests*

As with the 50 mm thick heated tests, both the 75 mm thick specimens also did not fail during the heated slab-column test. Figure 6.72 shows the residually tested behaviour of both heated tests compared to the ambient, unrestrained test.

The unrestrained heated slab failed residually at 90.7 kN, compared to the similar ambient unrestrained tested slab at 101.4 kN. The material degradation at elevated temperature led to a decrease of 10 kN capacity. The restrained support condition increased the capacity to 115.5 kN, which is approximately 21% greater than the comparative unrestrained heated slab. This direct comparison shows that the support condition alone is accountable for a large difference in slab-column capacity.

6.7.3 *100 mm thick, 0.8% reinforced tests*

The restrained 100 mm thick, 0.8% reinforced slab was residually tested to failure, as shown in Figure 6.73. The comparative failure loads of the two support types was 174.8 kN for the unrestrained (during slab-column test) and 245.1 kN for the restrained. The restrained support condition increased the

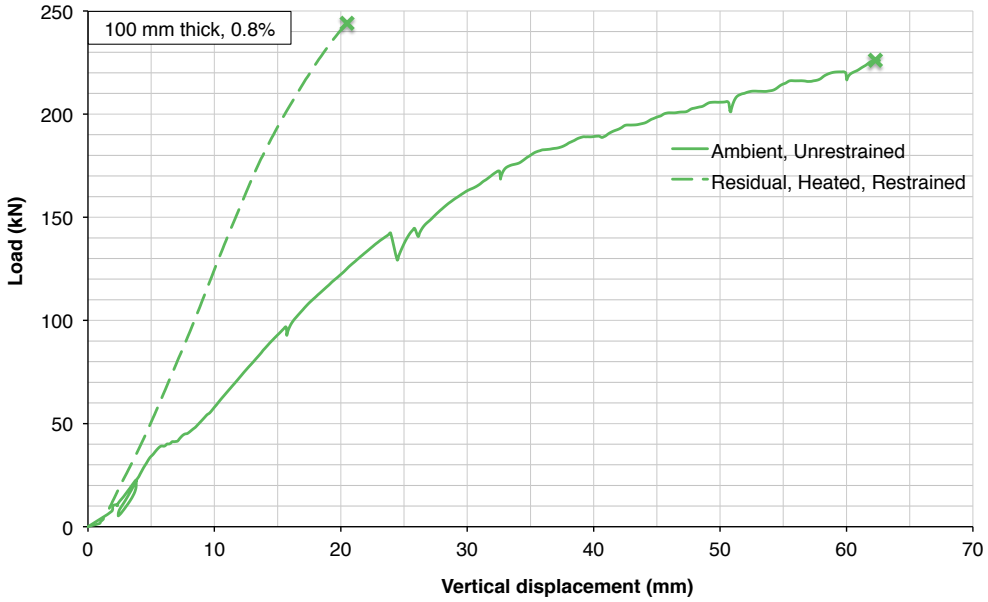

Figure 6.73: Residual load-deflection behaviour of 100 mm thick, 0.8% slabs

capacity by approximately 28% and sustained the full 120 minutes of elevated temperature, whereas the unrestrained failed 4 minutes after the slab-column test ignition.

6.7.4 *100 mm thick, 0% reinforced tests*

The restrained specimen did not fail during the slab-column testing, therefore it was residually tested to failure. Figure 6.74 shows the specimen failed at a residual load of 82.2 kN.

6.8 DEFLECTION HISTORY OF HEATED 0.8% REINFORCED SLABS

This section makes a comparison of all the slab-column specimens with 0.8% reinforcement. It investigates the impact the slab thickness parameter had on punching shear.

Figure 6.75a compares the vertical displacement for all the 0.8% reinforced slabs with varying thickness. The deflection readings are measured by LP and have been corrected for initial concrete bedding in. Zero time corresponds to the start of heating, with the negative time region corresponding to loading of the slabs prior to ignition. Positive deflection is downwards, in the direction of loading and away from the heat source. The flexural steel temperature has been plotted on the same x-axis in Figure 6.75b as a representation of the different heating curves the specimens sustained.

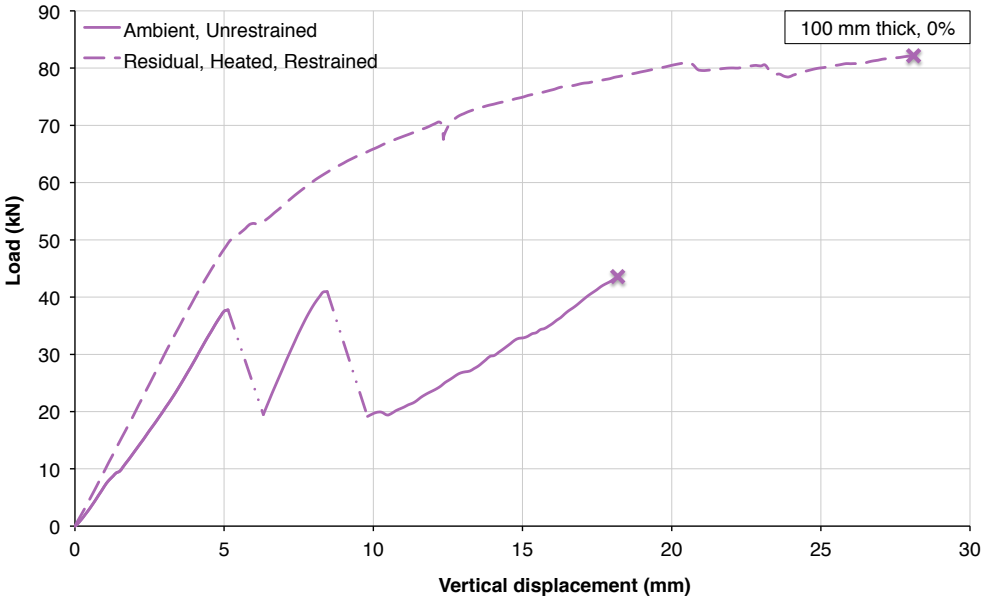

Figure 6.74: Residual load-deflection behaviour of 100 mm thick, 0% slabs

The three ambient tests (AU50-0.8, AU75-0.8 and AU100-0.8) are plotted with a start time of -60 minutes, but this count of time is arbitrary, as they were not heated. The similar slopes in the elastic range (prior to ignition), shows that the behaviour is identical when loaded. All the specimens were loaded at a displacement rate of 2 mm/min. This proves that even though the experimental test setup is complex, we have consistency between similar slab-column specimens.

All the 0.8% reinforced slabs were heated for approximately 120 minutes, with only HU100-0.8 failing soon after ignition, as shown by the cross in Figure 6.75a. The stiffness of the restrained support condition in comparison to the unrestrained can be seen by the grouping of restrained tests at low vertical displacement values and grouping of corresponding unrestrained tests at higher vertical displacements. The fully restrained support condition, significantly decreases the vertical displacement of the slab-column specimens.

It was assumed that the application of heat would cause thermal bowing towards the heat source (in the opposite direction to loading), as seen during experimental testing by Kordina (1997) and Annerel et al. (2012). During the heating phase the applied load was kept constant (70% factored ambient capacity), however the central displacement of all of the slabs, irrespective of support condition, increased continually away from the heat source. Kordina (1997) reports deflection away from the heat source, in the direction of loading for four initial (simply supported) tests after 30 minutes of heating.

This behaviour indicates that the degradation in concrete properties and non-linear material behaviour dominates over the expansion of the slabs due

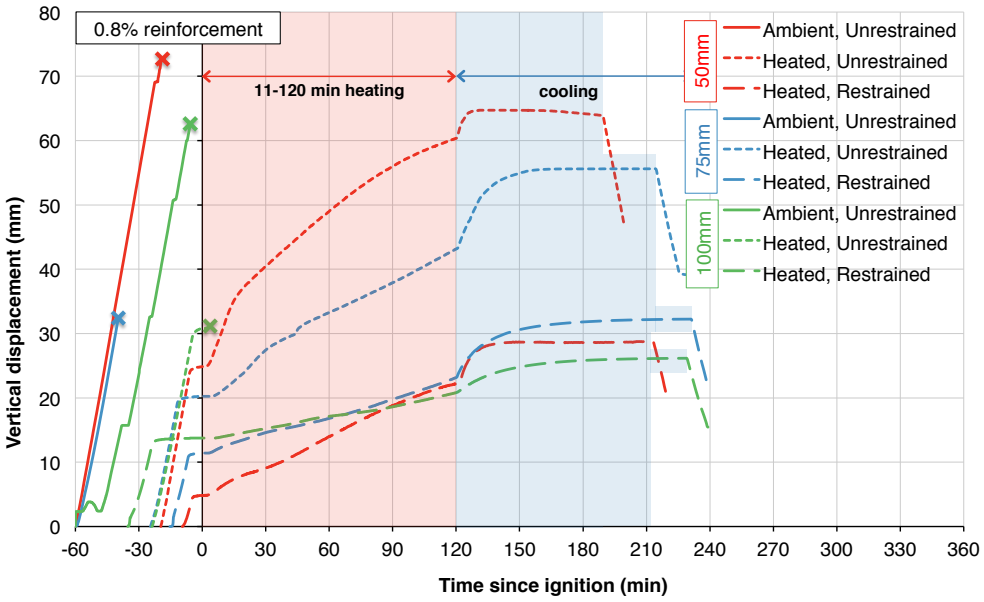

(a) Central displacement behaviour

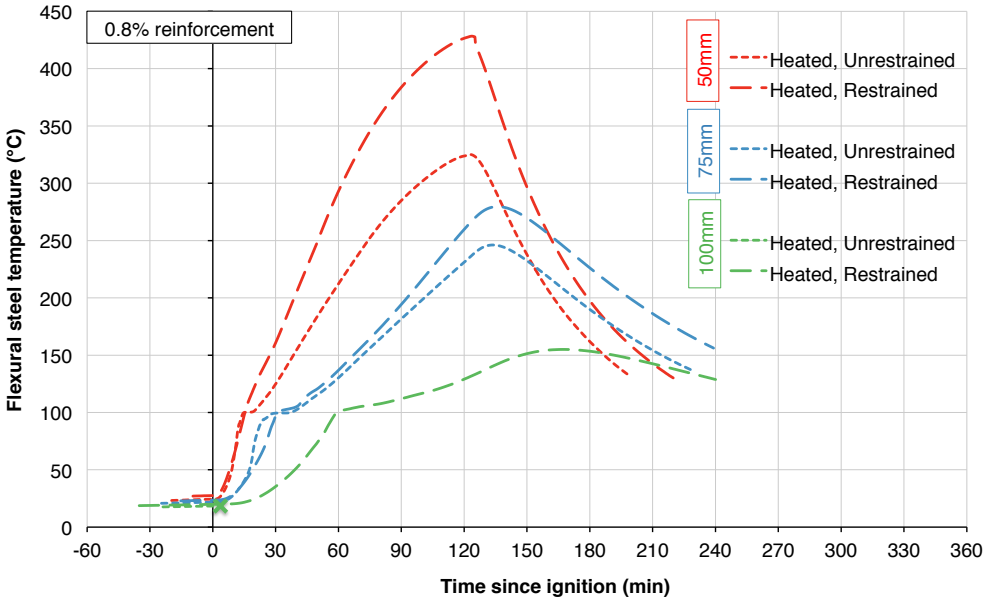

(b) Flexural steel temperature

Figure 6.75: Behaviour with time for 0.8% reinforced slabs

to heat (expansion varying through the slab depth). After ignition, the slab center continued to deflect away from the heat source for all the 0.8% reinforced specimens, during the heating and cooling phases. Only the lightly reinforced, unrestrained 50 mm thick, heated specimen (HU50-0.8), deflected toward the heat source at the end of the cooling phase.

Similar to the start of the heating phase, as the cooling phase initiated, there was a distinctive increase in the displacement rate. The sharp increase in deflection rate at the start of the cooling phase is consistent with the heated surface cooling down, whilst the heat front propagates deeper into the slab (as seen in all the temperature profiles, for example Figure 6.41). The difference in the slab cooling deflection rates are caused by the difference in the thickness of the slabs and impact of propane gas flow rate decrease at different times after ignition (discussed in Section 6.2.2).

6.9 TEST OBSERVATIONS OF HEATED 0.8% REINFORCED SLABS

This section compares the test notes taken during the tests with 0.8% reinforcement. Figure 6.76 shows test observations taken throughout all the heated, 0.8% reinforced tests. The propagation of cracks described in both Figures 6.76a and 6.76b is consistent with the flexure-shear failure modes of the thinner 50 mm and 75 mm slabs and pure punching shear failure of thicker 100 mm slabs.

The 50 mm and 75 mm unrestrained slabs are described to have their corners lift off of the roller supports at approximately 30 and 60 minutes after ignition, respectively. This lifting caused the bowl shape described in Section 6.2.4. Figure 6.77 shows different views of the unrestrained corners of the 75 mm thick, 0.8% reinforced slab during the heated test. The 100 mm thick slabs had limited cracks form during the testing (discussed further in Section 6.4.4), which is consistent with the brittle nature of punching shear failure.

6.10 DEFLECTION HISTORY OF HEATED 100 MM THICK SLABS

This section compares all the 100 mm thick slab-column specimens. It investigates the impact the flexural reinforcement ratio parameter had on punching shear. Figure 6.78a shows a comparison of the LP vertical displacement of all the 100 mm thick slabs with varying reinforcement ratios and Figure 6.78b presents a representation of the specimen heating curves with a plot of flexural steel temperature.

Figure 6.78a shows no trend with flexural reinforcement ratio. There is a clear difference behaviour with support condition. All the heated unrestrained

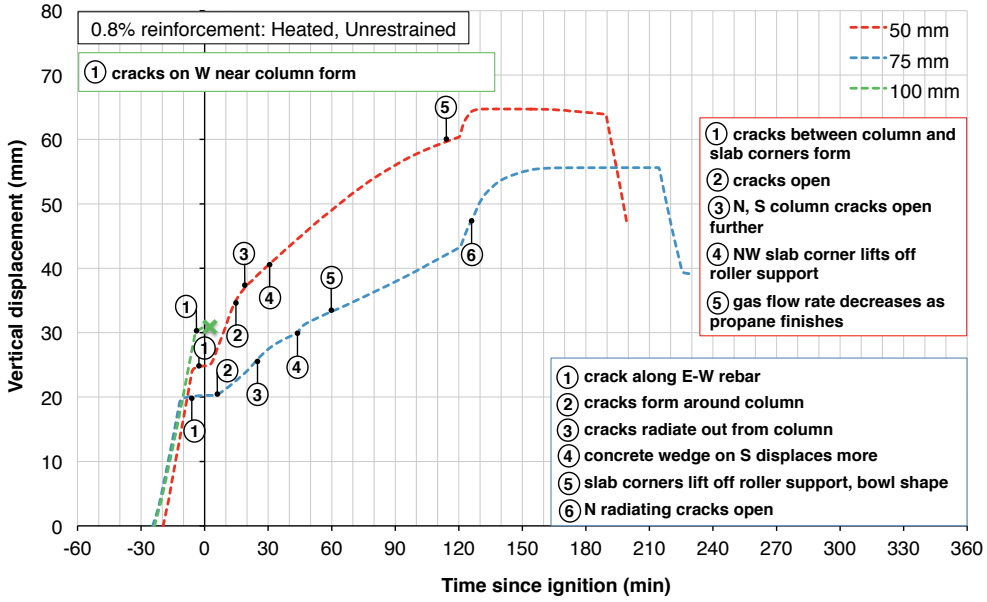

(a) Heated Unrestrained

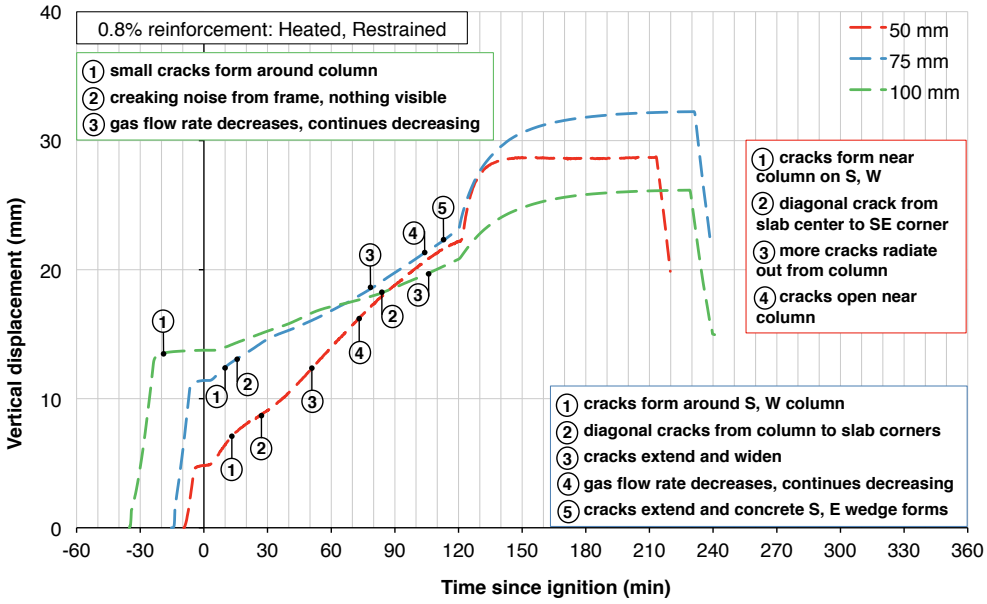

(b) Heated Restrained

Figure 6.76: Test observations for 0.8% reinforced slabs

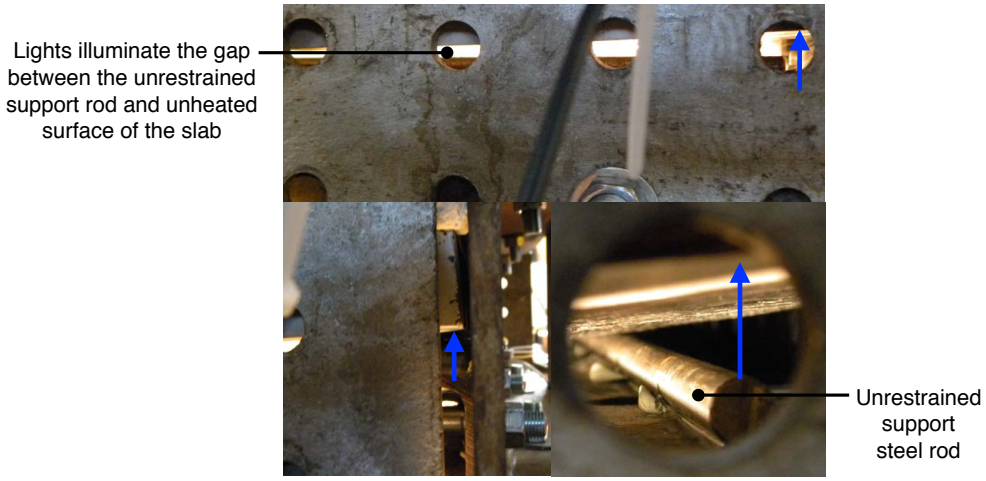

Figure 6.77: Views of the lifted corners of the heated 75 mm thick, 0.8% reinforced: unrestrained slab

slabs tested (HU100-0, HU100-0.8 and HU100-1.5) failed within 4-14 minutes after ignition. Two of the corresponding heated restrained slabs had higher capacities when they were residually tested (HR100-0 and HR100-0.8), whereas HR100-1.5 failed during the cooling phase of the slab-column test.

The increase in displacement rate (away from the heat source) with ignition was similar, but less pronounced with the 100 mm thick restrained slabs, compared to the thinner 50 mm and 75 mm. The thicker, 100 mm slabs retain the heat better than the thinner slabs, which causes the increase in displacement rate on the initiation of the cooling phase to be less pronounced with the 100 mm specimens. The heated unrestrained, unreinforced slab (HU100-0) was the only 100 mm thick specimen to slightly deflect towards the heat source, soon after ignition and prior to failure at 6 minutes.

6.11 TEST OBSERVATIONS OF HEATED 100 MM THICK SLABS

This section presents the test observations of all the 100 mm thick slab-column specimens. Figure 6.79 shows the test observations taken throughout the 100 mm thick slab tests. The absence of crack propagation during all the reinforced 100 mm thick slab tests is consistent with the pure punching shear failure modes seen. The failures were catastrophic and loud as they were brittle failure with limited cracks prior to failure.

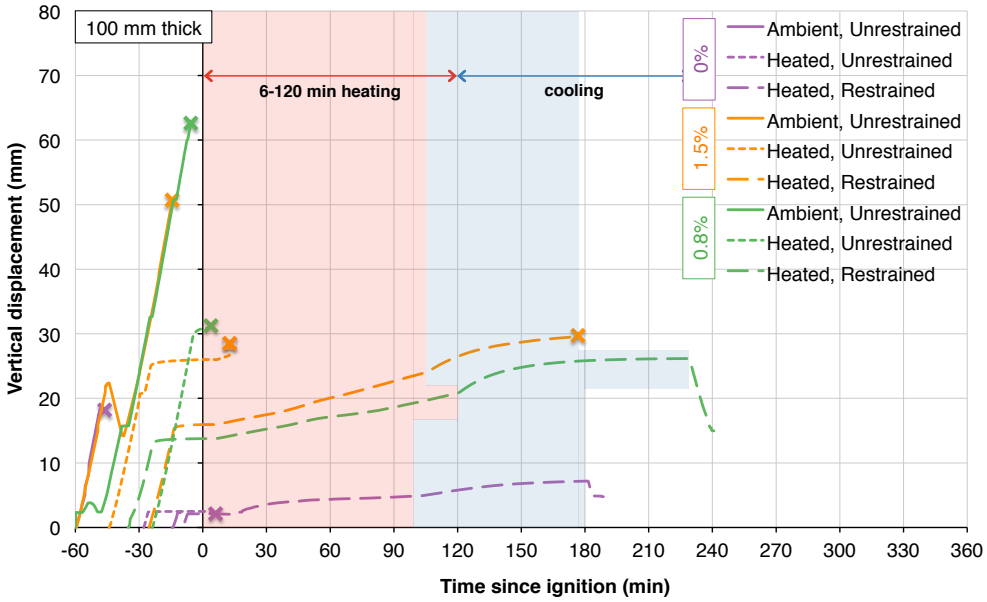

(a) Central displacement behaviour

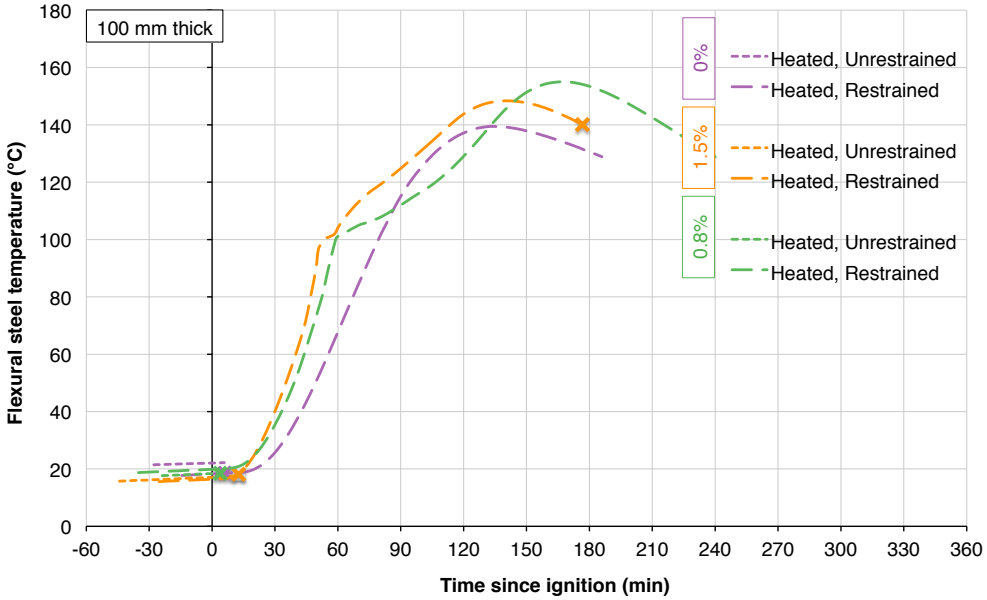

(b) Flexural steel temperature

Figure 6.78: Behaviour with time for 100 mm thick slabs

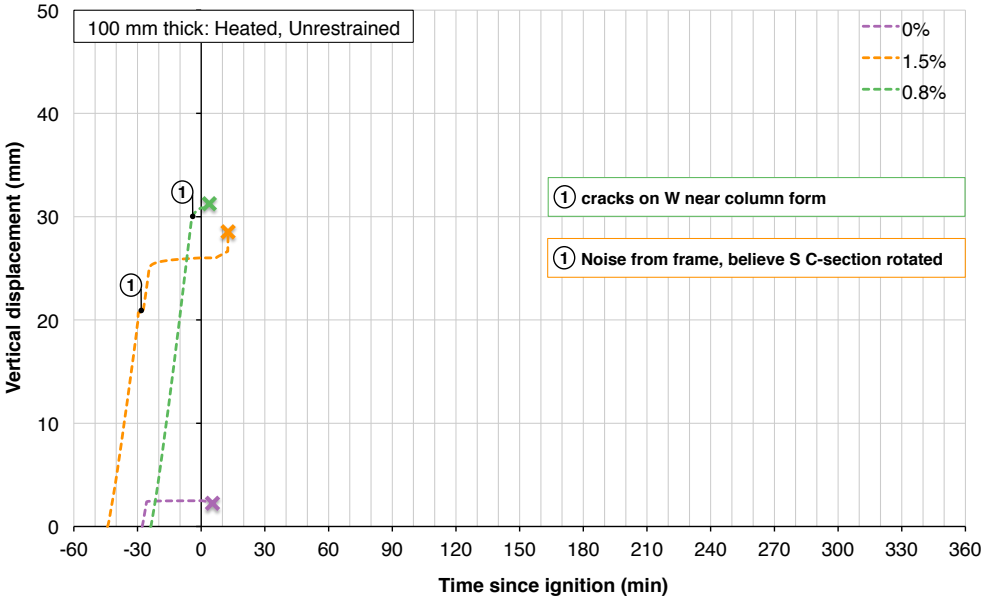

(a) Heated Unrestrained

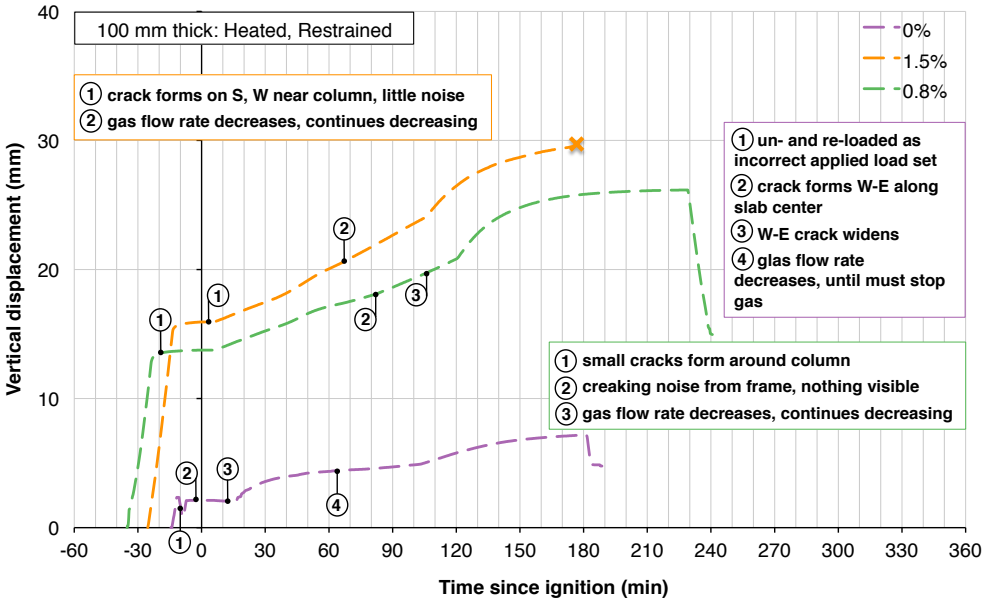

(b) Heated Restrained

Figure 6.79: Test observations for 100 mm thick slabs

6.12 SLAB-COLUMN REACTION FORCES AND MOMENTS ON THE REACTION FRAME

The in-plane reaction forces and moments imparted by the slab on the four sides of the reaction frame were intended to be measured with strain gauges (see Section 5.7.1). This section presents the net axial force and moment imparted by the 50 mm, 0.8% reinforced slab on each reaction frame column as a representative example. The result graphs for all the slab-column tests can be seen in Appendix I.

6.12.1 *Ambient example 50 mm thick, 0.8% reinforced tests*

This section presents the ambient test results for AU50-0.8 as a representative example. Figures 6.80 – 6.83 show the reaction frame net axial forces and moments imparted by the slab on the E, S, W and N columns in the ambient unrestrained 50 mm thick, 0.8% reinforced test, respectively.

The results in Figure 6.80b show that the readings from ES-A strain gauge (ES reaction frame column, above slab level gauge) are incorrect, thereby causing an error in the calculation of the net axial force and moment for column ES. This result has therefore been ignored during further analyses. The remaining seven column readings are consistent and have low values of net axial force and moment, as expected for an ambient, unrestrained test.

6.12.2 *Heated example 50 mm thick, 0.8% reinforced tests*

This section presents the heated test results for both the unrestrained (HU50-0.8) and restrained (HR50-0.8) slabs as representative examples. Figures 6.84a and 6.84b show the comparative column WS plots for the heated unrestrained and restrained tests of the 50 mm thick, 0.8% reinforced slabs, respectively. The other seven column test result graphs can be seen in Appendix I. Zero time corresponds to the start of heating, with the negative region corresponding to loading of the slabs prior to ignition. The vertical black line shows when the cooling phase was started in each of the heated tests.

Throughout the unrestrained test, shown in Figure 6.84a, the net axial force and moment is approximately zero, as expected. The restrained test shows the net axial force to increase greatly with ignition and continue to increase until cooling starts at 121 minutes. The sign convention is positive tension with respect to the slab-column, therefore the slab expanded during the heating phase, as it was in tension. The behaviour reverses during the cooling phase and the tension decreases. After 210 minutes the slab is unloaded as the tem-

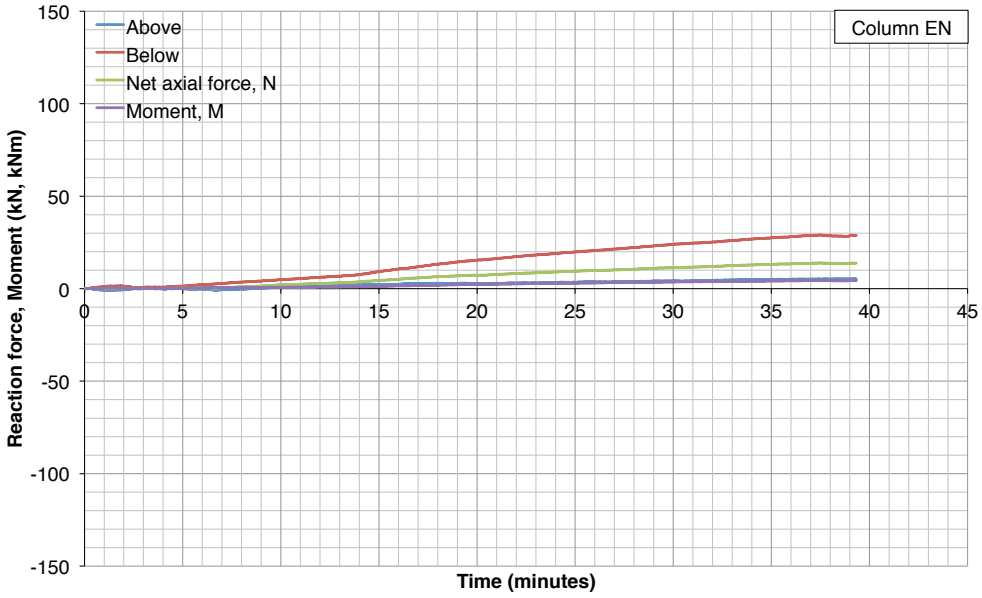

(a) Column EN

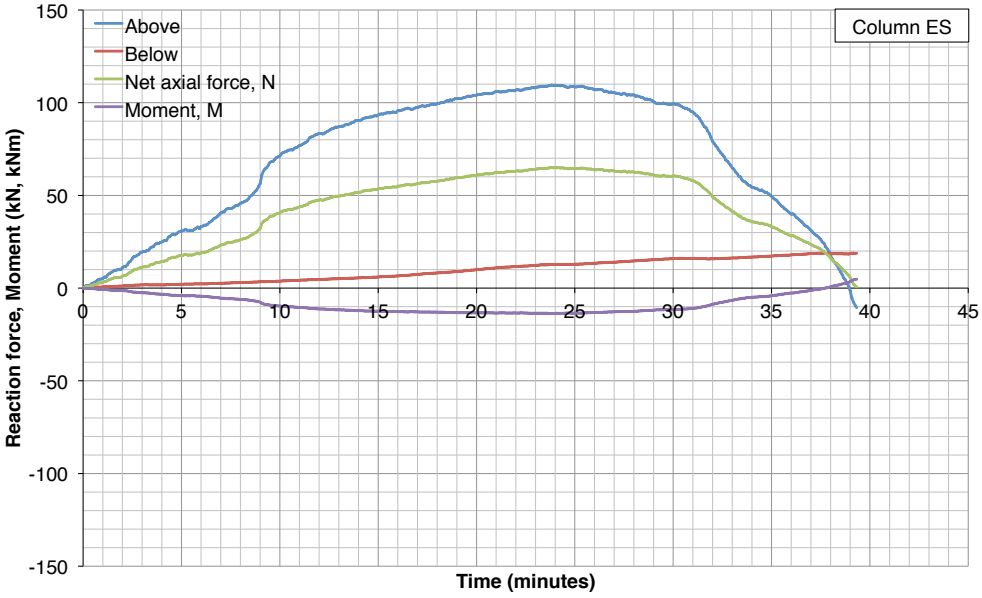

(b) Column ES

Figure 6.80: East reaction frame net axial force, N and moment, M for ambient 50 mm thick, 0.8% reinforced: unrestrained slab

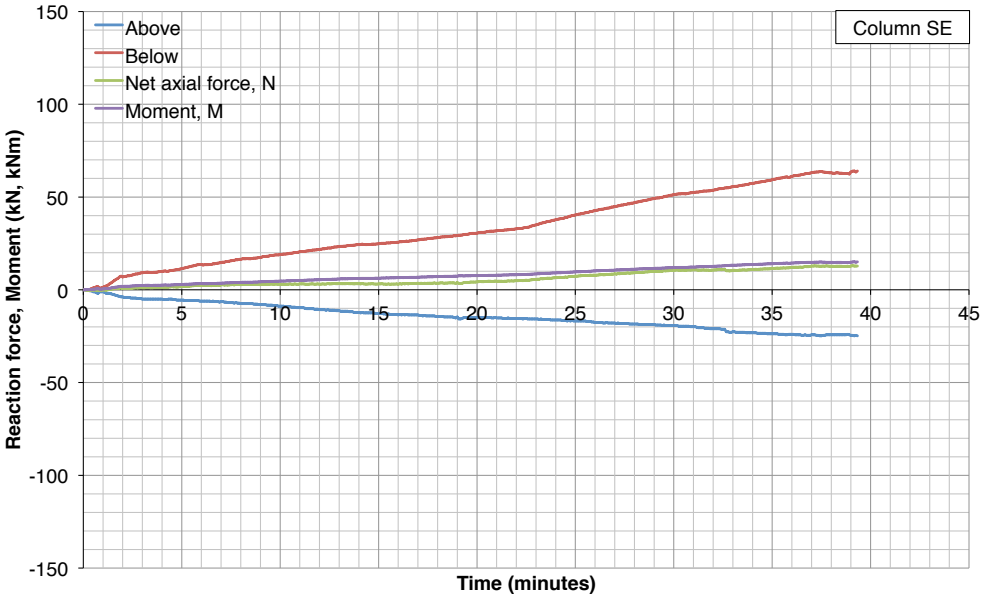

(a) Column SE

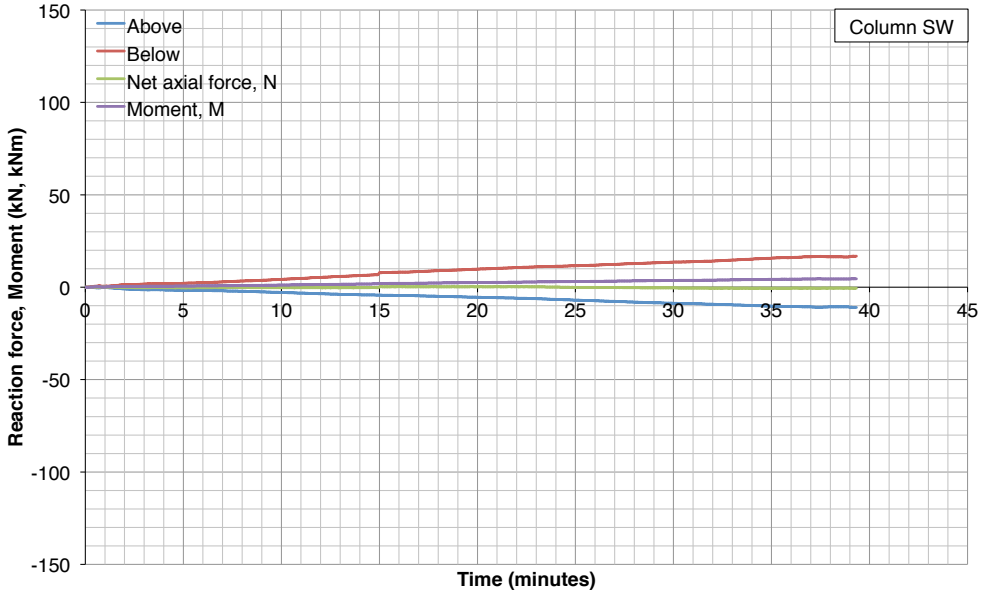

(b) Column SW

Figure 6.81: South reaction frame net axial force, N and moment, M for ambient 50 mm thick, 0.8% reinforced: unrestrained slab

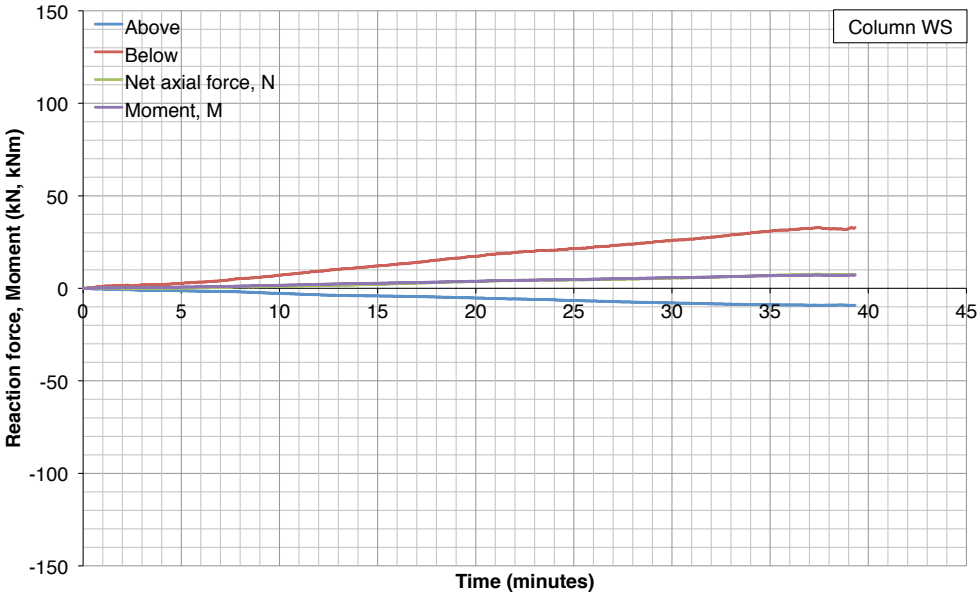

(a) Column WS

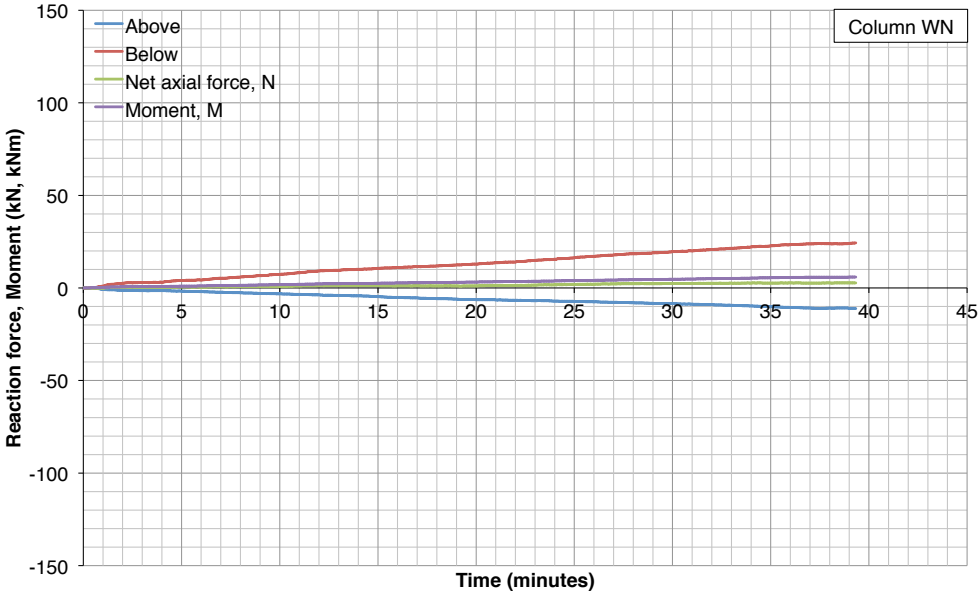

(b) Column WN

Figure 6.82: West reaction frame net axial force, N and moment, M for ambient 50 mm thick, 0.8% reinforced: unrestrained slab

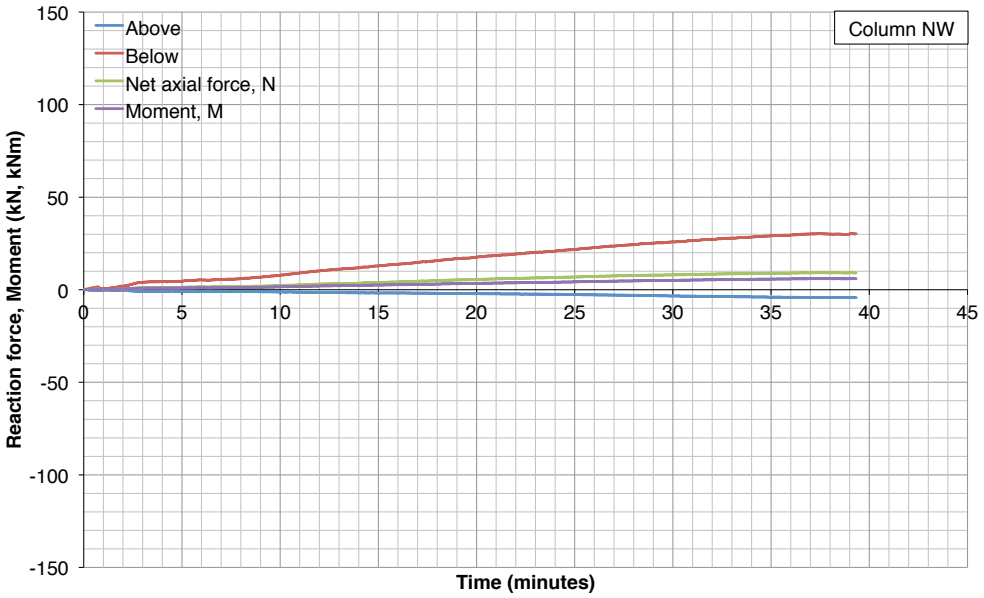

(a) Column NW

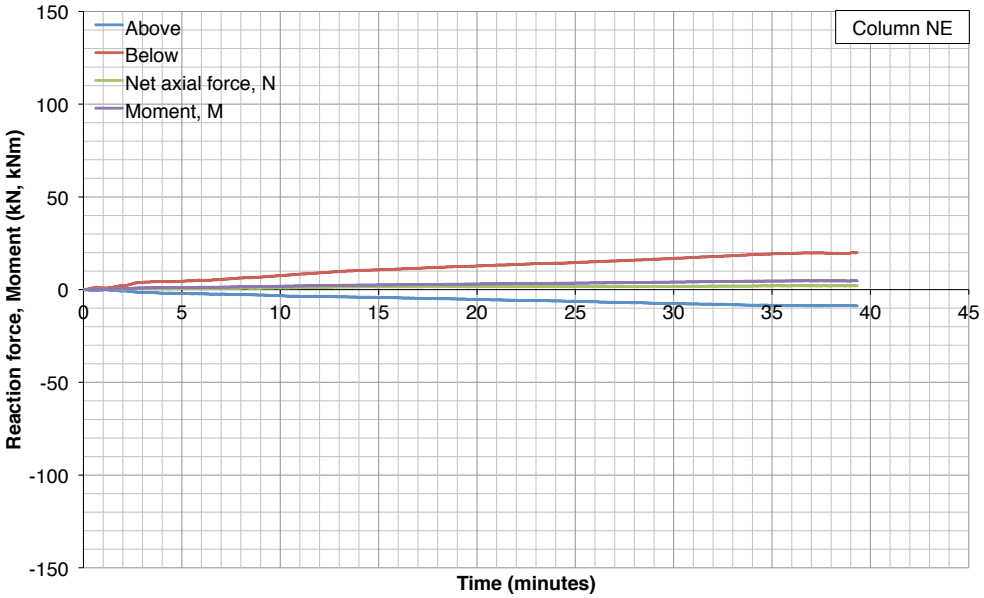

(b) Column NE

Figure 6.83: North reaction frame net axial force, N and moment, M for ambient 50 mm thick, 0.8% reinforced: unrestrained slab

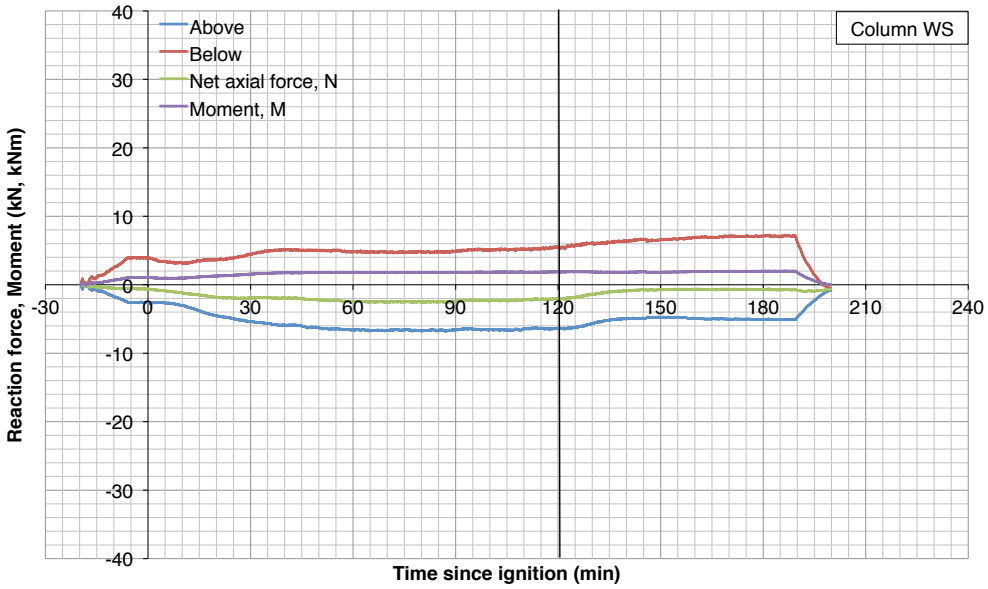

(a) Unrestrained

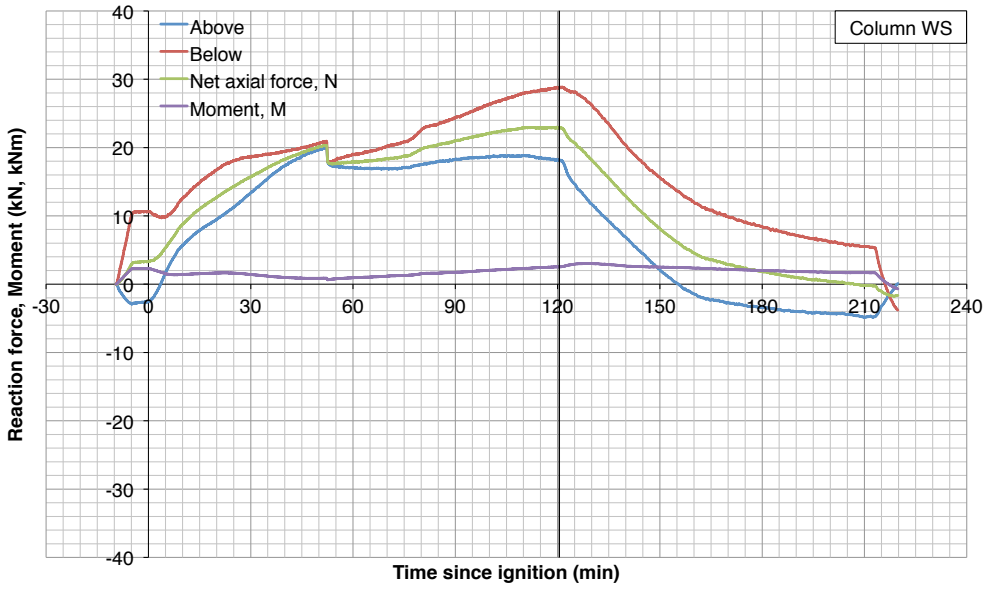

(b) Restrained

Figure 6.84: Column WS net axial force, N and moment, M for heated 50 mm thick, 0.8% reinforced slabs

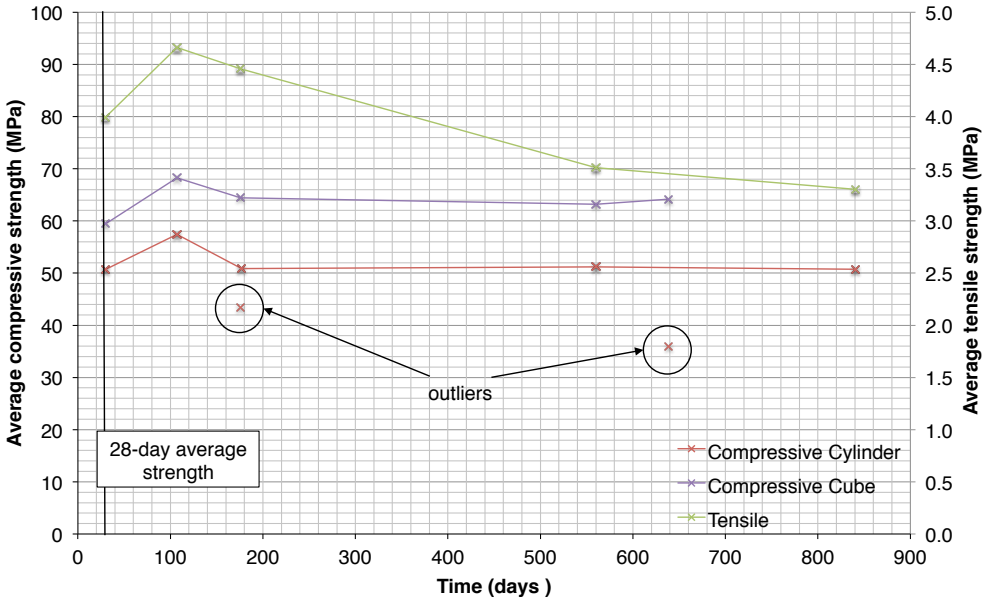

Figure 6.85: Concrete compressive and tensile strength

perature throughout the slabs thickness decreased to below 150°C. The slab contracts and is in negligible compression after 210 minutes, though this could have been caused by experimental error.

Section 7.1.5 assesses the quality of the net average in-plane reaction force, N and moment, M results.

6.13 STRENGTH OF MATERIAL SPECIMENS

6.13.1 *Concrete*

Cube and cylinder concrete strength specimens were tested at ambient temperature to determine the compressive and tensile strengths of the concrete used in the slab-column specimens. Table 6.3 presents the results of the cube and cylinder specimen strength tests relative to the timing of the slab-column specimen testing. Figure 6.85 shows that the ambient characteristic compressive cylinder concrete strength was measured to be an average of 51 MPa at 28 days.

6.13.2 *Steel*

Three types of flexural steel were used in the shear block and punching slab-column testing, as detailed in Table 6.4. These steels were tested to determine their ambient and elevated temperature properties. The steady-state tensile testing procedure, at elevated temperature is shown in Figure 6.86. During

TIME TESTED AFTER CAST (DAY)	SPECIMEN ID	AVERAGE COMPRESSIVE STRENGTH (MPA)		AVERAGE TENSILE STRENGTH (MPA)
		CYLINDER	CUBE	CYLINDER
30		50.7	59.4	4.0
107		57.4	68.3	4.7
176		(43.4)	64.5	4.5
177		50.9	-	-
421	AU100-0.8			
504	AU100-0			
516	AU100-1.5			
525	AU50-0.8			
532	AU75-0.8			
560		51.2	63.2	3.5
577	HR50-0.8			
599	HU50-0.8			
613	HU75-0.8			
629	HR75-0.8			
639		(35.9)	64.2	-
671	HR100-0.8			
689	HR100-0			
704	HU100-0			
731	HU100-0.8			
738	HU100-1.5			
746	HR100-1.5			
841		50.7	-	3.3

() OUTLIERS

Table 6.3: Slab-column specimen concrete strength

EXPERIMENT TESTING	BAR DIAMETER (MM)	BAR SURFACE TYPE	PRODUCTION METHOD
shear block	6	smooth	hot rolled
punching shear	6	ribbed	cold worked
punching shear	8	ribbed	hot rolled

Table 6.4: Steel reinforcement properties

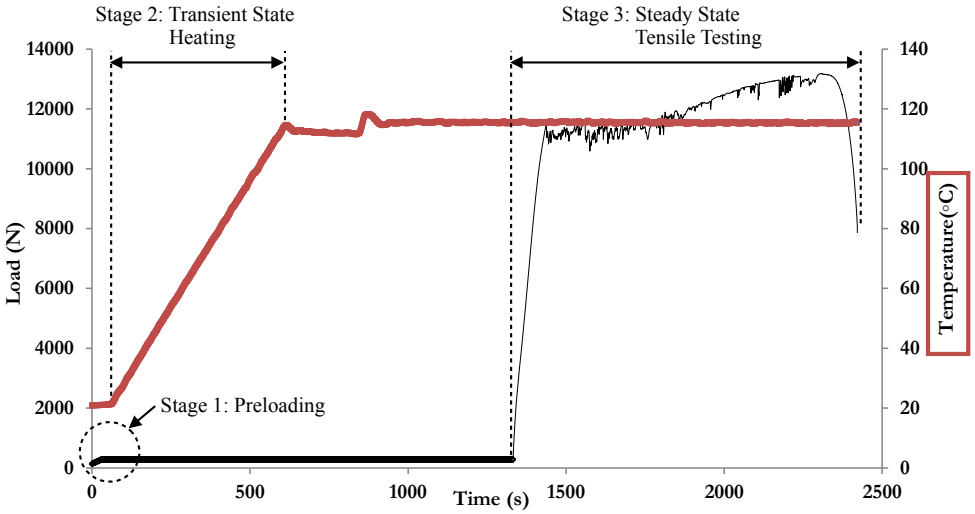

Figure 6.86: Stages in steady-state reinforcement tensile testing, reproduced from Batson (2013)

stage 1, the specimens were loaded with a preload to decrease potential damage to the Instron test machine grips during stage 2. Stage 2 was transient state heating of the specimens up to the target maximum temperature. The elevated temperature causes the specimens to expand slightly during stage 2 and if by accident there had been contraction due to a differential heat gradient and no preload was applied, then the test machine grips could have been damaged. Stage 3 was a steady state tensile test of the specimen to failure.

The specimens were 560 mm in length and tested under strain control at a rate of 2 mm/min until failure. Each test was repeated twice at temperatures of; 19, 112, 191, 390, 475 and 590°C. Bath (2013); Batson (2013), who undertook an MEng thesis project under my supervision, describe the full test methodology.

Batson (2013) reports stiffness correction factors of 245 and 141 for smooth and ribbed steel bars, respectively. These factors were required to account for slippage of the specimens in the Instron test machine grips.

Furthermore, Batson (2013) used the 0.2% proof stress method to find the yield strength of the specimens with curved yield points (denoted in brackets

in Table 6.5). The ambient cold worked ribbed, 6 mm diameter steel and most of the elevated temperature tests also, required the use of the proof stress method. Table 6.5 gives the experimentally found yield strength, $f_{sy,\theta}$ and Young's modulus, $E_{s,\theta}$ of the three steels.

The experimental reduction factors for the yield strength, $f_{sy,\theta}$ and Young's modulus, $E_{s,\theta}$ at the elevated temperatures of 19, 112, 191, 390, 475 and 590°C are shown in Table 6.6. The EC2 linearly interpolated class N and class X reduction factors for the yield strength and Young's modulus, at the elevated temperatures of 19, 112, 191, 390, 475 and 590°C, are shown in Table 6.7 and Table 6.8, respectively.

6.14 SUMMARY

This section summarises the main slab-column punching shear test results from Chapter 6:

- The heating curves were different between different slab-column tests.
- The temperature profiles of the HU50-0.8 test show the radiant panel array did not produce an even heat flux across the top surface, though this was not seen in all the tests.
- The maximum concrete near surface temperature was not consistent between comparative supported tests, due to propane gas flow rate decrease at different times after ignition.
- Where specimens did not fail during the heating phase, the bottom unheated surface reached a maximum temperature during the cooling phase, as the heat front penetrates the slab.
- The 50 mm and 75 mm slabs all failed residually in flexure-shear mechanisms. The thicker 100 mm reinforced slabs failed in a punching shear mode, whereas the unreinforced failed in flexure. Both the restrained 0.8% and 0%, 100 mm thick slabs were tested residually.
- The support condition had a large impact on the punching shear failure of the 100 mm thick heated slabs. The unrestrained (HU100-1.5, HU100-0.8 and HU100-0) failed soon after ignition, whereas the restrained (HR100-0.8 and HR100-0) sustained 120 and 99 minutes heating, respectively and had a high comparative residual strength. Additionally, the restrained support condition significantly decreased the central vertical displacement.

TEMPERATURE	YIELD STRENGTH, $f_{sy,\theta}$, (MPA)			YOUNG'S MODULUS, $E_{s,\theta}$, (GPA)		
	6 mm SMOOTH	6 mm RIBBED	8 mm RIBBED	6 mm SMOOTH	6 mm RIBBED	8 mm RIBBED
(°C)	HOT ROLLED	COLD WORKED	HOT ROLLED	HOT ROLLED	COLD WORKED	HOT ROLLED
19	426.5	(549.6)	571.1	204	200	222
112	401.8	(579.7)	(528.7)	205	194	209
191	388.9	(547.2)	(508.7)	202	186	203
390	(293.9)	(514.3)	(459.0)	181	174	191
475	(241.8)	(439.6)	(398.2)	158	155	158
549	(184.5)	(325.7)	(276.0)	139	123	139

() FOUND BY 0.2% PROOF STRESS METHOD

Table 6.5: Steel reinforcement properties, reproduced from Batson (2013)

TEMPERATURE	YIELD STRENGTH, $f_{sy,\theta}$, (MPA)			Young's modulus, $E_{s,\theta}$, (MPa)		
	6 mm SMOOTH	6 mm RIBBED	8 mm RIBBED	6 mm SMOOTH	6 mm RIBBED	8 mm RIBBED
(°C)	HOT ROLLED	COLD WORKED	HOT ROLLED	HOT ROLLED	COLD WORKED	HOT ROLLED
19	1.00	1.00	1.00	1.00	1.00	1.00
112	0.94	1.05	0.93	1.00	0.97	0.94
191	0.91	1.00	0.89	0.99	0.93	0.91
390	0.69	0.94	0.80	0.89	0.87	0.86
475	0.57	0.80	0.70	0.77	0.78	0.71
549	0.43	0.59	0.48	0.68	0.61	0.62

Table 6.6: Yield strength, $f_{sy,\theta}$ and Young's modulus, $E_{s,\theta}$ reduction factors from experimental values

Temperature	Class N			Class X		
	6 *mm* smooth	6 *mm* ribbed	8 *mm* ribbed	6 *mm* smooth	6 *mm* ribbed	8 *mm* ribbed
(°C)	hot rolled	cold worked	hot rolled	hot rolled	cold worked	hot rolled
19	1.0000	1.0000	1.0000	1.0000	1.0000	1.0000
112	1.0000	1.0000	1.0000	1.0000	1.0000	1.0000
191	1.0000	1.0000	1.0000	1.0000	1.0000	1.0000
390	1.0000	0.9460	1.0000	0.9100	0.9100	0.9100
475	0.8350	0.7375	0.8350	0.7500	0.7500	0.7500
549	0.6281	0.5377	0.6281	0.5873	0.5873	0.5873

Table 6.7: Yield strength, $f_{sy,\theta}$ reduction factors from EC2 linearly interpolated class N and X

TEMPERATURE	Class N			Class X		
	6 *mm* SMOOTH	6 *mm* RIBBED	8 *mm* RIBBED	6 *mm* SMOOTH	6 *mm* RIBBED	8 *mm* RIBBED
(°C)	HOT ROLLED	COLD WORKED	HOT ROLLED	HOT ROLLED	COLD WORKED	HOT ROLLED
19	1.0000	1.0000	1.0000	1.0000	1.0000	1.0000
112	0.9880	0.9844	0.9880	0.9940	0.9940	0.9940
191	0.9090	0.8817	0.9090	0.9545	0.9545	0.9545
390	0.7100	0.5760	0.7100	0.7650	0.7650	0.7650
475	0.6250	0.4400	0.6250	0.6375	0.6375	0.6375
549	0.4579	0.3216	0.4579	0.4579	0.4579	0.4579

Table 6.8: Young's modulus, $E_{s,\theta}$ reduction factors from EC2 linearly interpolated class N and X

- The heavily reinforced restrained, 100 mm heated slab (HR100-1.5) failed on cooling. This is the first recorded punching shear failure during the cooling phase of an elevated temperature test and may also be the first recorded test specimen ever to have failed during the cooling phase of an elevated temperature test.

- All the specimens deflected away from the heat source (in the direction of loading) during the whole test, irrespective of support condition. Only the lightly reinforced, unrestrained 50 mm thick, heated specimen (HU50-0.8) recovered central displacement during the cooling phase. Additionally, the heated unrestrained, unreinforced 100 mm thick slab (HU100-0) slightly deflect towards the heat source, soon after ignition and prior to failure at 6 minutes. This behaviour indicates that the degradation in concrete properties and non-linear material behaviour dominates over the expansion of the slabs due to heat.

- The central vertical deflection of all the specimens showed a distinctive increase in displacement rate on initiation of the cooling phase. The sharp increase in deflection rate is consistent with the heated surface cooling down, whilst the heat front propagates deeper into the slab.

7

ANALYSIS AND DISCUSSION

This chapter presents a comparative analysis and discussion of the slab-column results presented in Chapter 6. Section 7.1 presents an assessment of the experimental methodology to outline strengths, weaknesses and future test design considerations. Section 7.2 presents DIC vertical displacement profiles across the lower (unheated) surface of the slabs at 10 minute intervals throughout the tests. Section 7.3 compares the experimental test results to both EC2 design values and Muttoni's CSCT.

7.1 EXPERIMENT METHODOLOGY VERIFICATION

The experimental setup is assessed to outline its strengths and limitations. Section 7.1.1 examines the post-failure flexural reinforcement positioning within the slab-column specimens and compares them to the initial design. This allows the specimen tolerances to be quantified and further analyses to be undertaken with measured rather than design values. Section 7.1.2 compares the thermocouple data between tests to investigate how reproducible the radiant heating was. Section 7.1.3 evaluates the hydraulic jack friction losses and the impact on the test load readings. Section 7.1.4 compares the LP and DIC vertical displacement readings. The DIC readings from the three digital cameras are compared to assess their accuracy. Section 7.1.5 initially presents an assessment of the net average in-plane reaction force, N and moment, M for the five ambient, unrestrained tests. The N and M values are compared for the two support conditions. Section 7.1.6 presents an assessment of the support condition functionality, by calculating the horizontal displacement of the structural reaction frame.

7.1.1 *Specimen dimensional tolerances*

The slab-column specimens were constructed by hand with a ready mix concrete. Post-failure measurements were taken of the flexural reinforcement spacing, flexural concrete cover and column concrete cover to assess their accuracy compared to design and report measured values for further analyses. Figure 7.1 shows the comparison of the flexural reinforcement initial design and measured spacing. The measured spacing is calculated as an average in mm for each

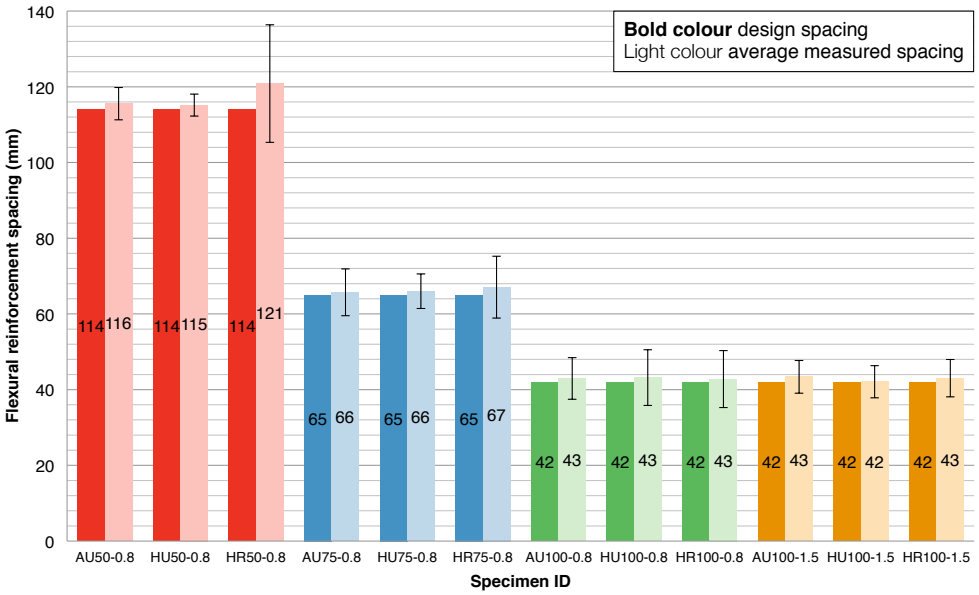

Figure 7.1: Flexural reinforcement spacing: design and measured (with one standard deviation)

slab-column specimen and has one standard deviation error bars to show the variation in the measurements.

The average flexural reinforcement spacings in all the slab-column specimens are shown to be mainly within 2 mm of the design values, except for the spacing in HR50-0.8. The average spacing in HR50-0.8 and HR75-0.8 was greater then the design by 7 mm and 2 mm, respectively. The one standard deviation shows that the measured spacings also had a large variation. As mentioned in the steelwork description of Section 5.2.1, both the 50 mm and 75 mm thick restrained slabs had their edge bar spacings adjusted to ensure there was one bar out with the restraining tubes to provide anchorage. The adjustment of the edge bar spacings will have caused an increase in the average bar spacing calculation and also added to the high one standard deviation plotted. The 50 mm thick slab is affected more due to there only being 11 spaces between bars, compared to 20 spaces in the 75 mm thick slabs.

Figure 7.2 shows the average measured flexural concrete cover compared to the initial design cover, with one standard deviation plotted to show the measured cover variation. The experimental measured cover was always greater than the initial design value, with the exception of two slabs, AU75-0.8 and HU100-1.5. The average measured cover was less then the initial design values by small margins of 2 mm and 1 mm, respectively. The one standard deviation shows a high variation of cover for the AU75-0.8 and HU100-1.5 slabs with 3 mm and 4 mm. The standard deviations are especially high when the measured covers are only 7 mm and 6 mm, respectively. However, most of the slab-column specimens had greater flexural concrete covers than initially de-

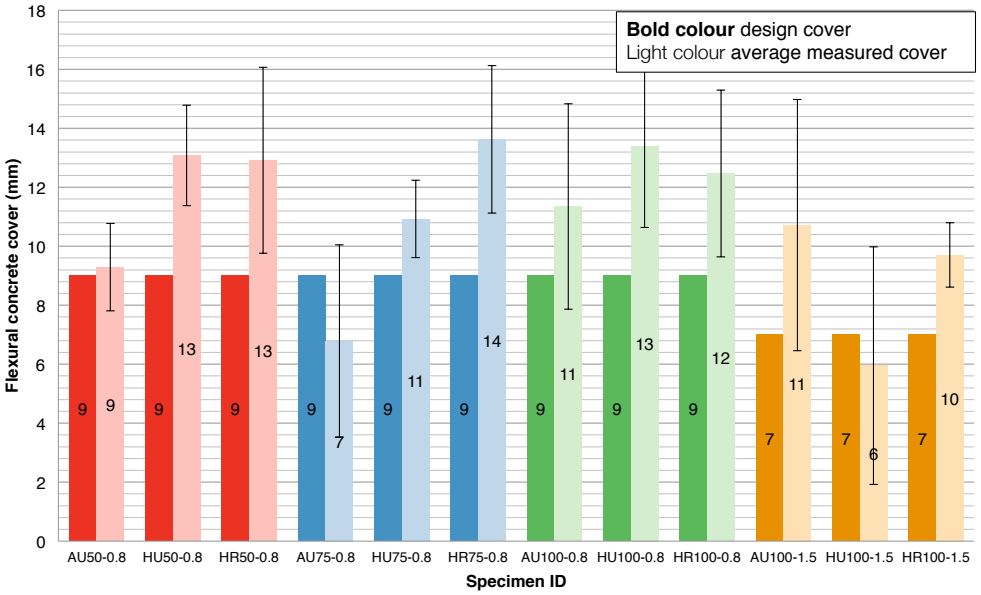

Figure 7.2: Flexural concrete cover: design and measured (with one standard deviation)

signed, making them conservative. The large variation in standard deviation for all the concrete cover measurements, indicates the importance of checking the concrete cover in future steelwork construction.

Figure 7.3 shows the average measured column stub concrete cover compared to the initial design cover, again with one standard deviation plotted to show the measured cover variation. The column concrete cover initial design was 16 mm for all specimens. The average measured cover shows a consistent trend, however the one standard deviation shows a different picture of high variation. The measurement standard deviation ranged from 3 to 13 mm, which corresponds to a normalised standard deviation percentage error of 19 to 90% (where normalised standard deviation is calculated as $\frac{\text{standard deviation}}{\text{mean}} \cdot 100$). This high variation was caused by the difficulty of casing the column stub directly into the slab. As mentioned in the fabrication description of Section 5.2.1, where there was exposed steel reinforcement around the column stubs, it was patched with mortar 78 days post-casting.

7.1.2 *Heat application reproducibility*

From the temperature curves in Chapter 6 the thermocouple readings showed a high degree of variation.

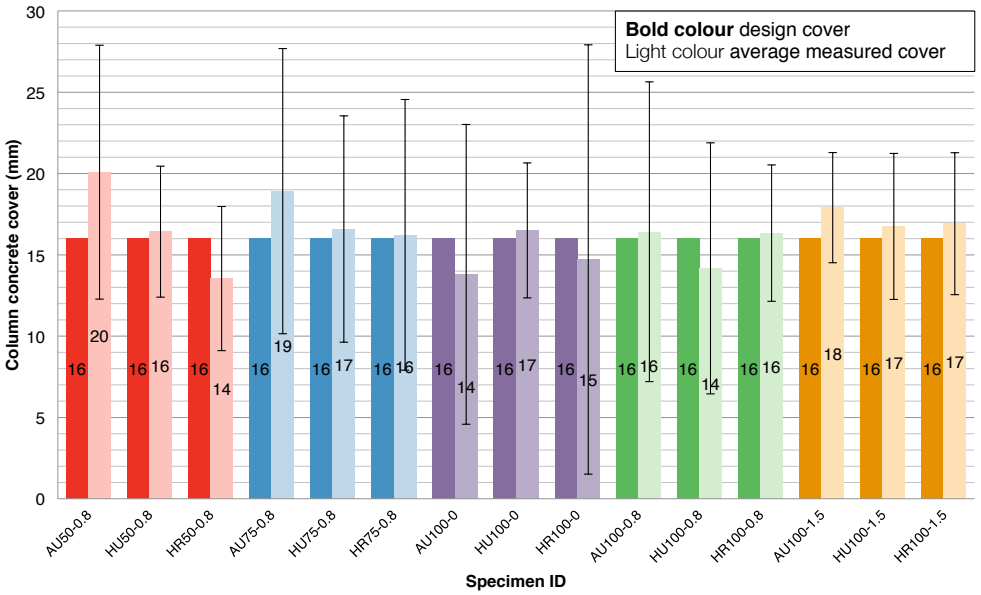

Figure 7.3: Column concrete cover: design and measured (with one standard deviation)

Variation during a single test

This section compares the thermocouple data to investigate if the radiant panels produced an even heat application across the upper surface of the specimens. Differences in thermocouple heating curves during a single test could potentially be caused by:

- the as-built position of the thermocouples not being the same as the designed position; and
- non-uniform heating by the array of radiant heat panels.

Appendix J gives a table of the post-failure measured thermocouple depths in each test. Initial visual interpretation of the thermocouple heating curves has highlighted suspect readings, which have been written in brackets in Appendix J, as described in for example Section 6.2.2. Suspect thermocouple readings need to be ignored before assessing the radiant panel application (refer to Section 6.2.3). Suspect readings have been ignored for the remainder of the analyses. Further analyses have been undertaken with measured rather than design thermocouple depths.

Figure 7.4 compares the heating array uniformity, by comparing thermocouple tree location readings (annotated relative to frame positions S, N, and W), for approximately the same slab depth from the heated surface. Assuming the difference in frame insulation with slab support condition had a minimal impact on the heating uniformity, the thermocouple data for similar slab

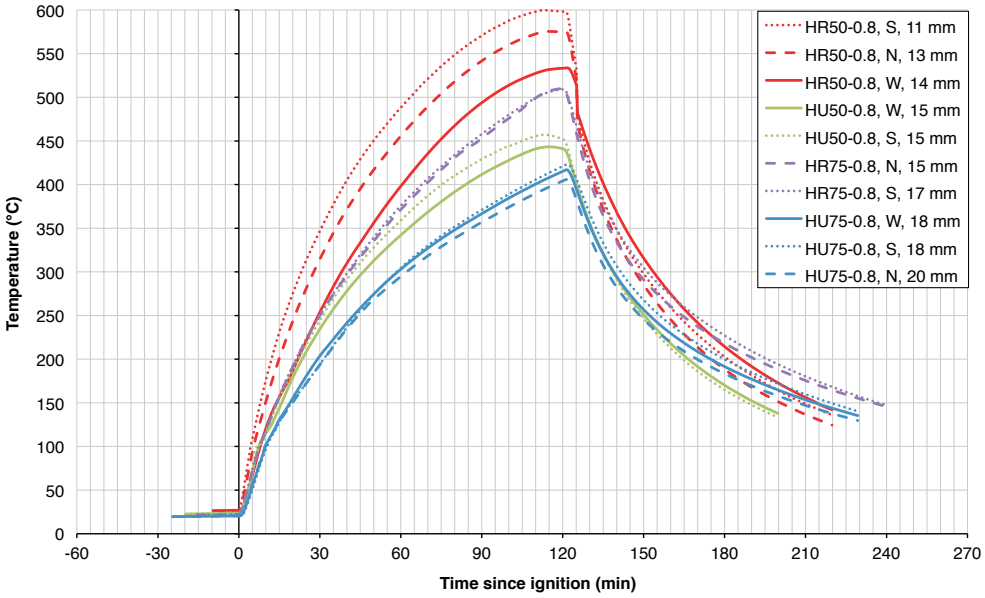

Figure 7.4: Temperature curves at different frame positions, for approximately the same slab depth

thicknesses can be compared. Readings from tests; HR50-0.8, HU50-0.8 and HR75-0.8, HU75-0.8 are compared.

In each test with the exception of HR50-0.8, the temperature readings were similar at comparable slab depths, even at different thermocouple tree locations. As discussed in Section 6.14 the 50 mm thick slab again had the largest variation. This indicates that the array of radiant panels produced an approximate even distribution of heating assault on the upper surface of each slab at radii of 175 mm and 188 mm away from the column edge (50 mm and 75 mm thickness thermocouple tree positioning, respectively). Figure 5.16 showed the thermocouple positioning in the 100 mm thick slabs was at 200 mm away from the column edge. The even radiant heating is assumed to extend to this radii.

The specimens can therefore be assumed to have been uniformly heated through their thickness at axi-symmetrical locations. Therefore any unsymmetrical failure crack patterns seen in Chapter 6 were not caused by non-uniform heating.

Variation between tests

The repeatability of the applied fire scenario for 50 mm and 100 mm thick slab tests is investigated. Figure 7.5 shows a large variation in temperature curves at approximately similar depths, in the range 31 mm to 36 mm from the heated surface. Curves are plotted for three of the six 100 mm thick, heated tests, as the data from the N thermocouple in HR100-0 test was suspect (shown in Appendix J) and the remaining thermocouples were at different depths.

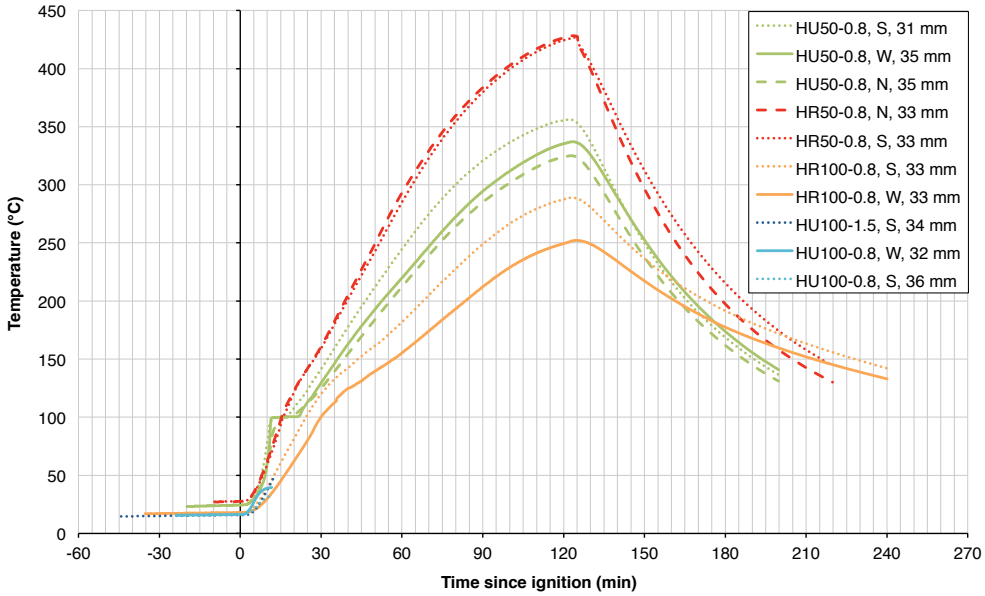

Figure 7.5: Temperature curves for approximately similar slab depths of 31 mm to 36 mm from the heated surface of the 50 mm and 100 mm thick slabs

Differences in thermocouple heating curves between tests could potentially be caused by a change in propane gas flow rate during a test, causing tests to have different applications of heating. The test notes in Chapter 6 indicated that the propane gas flow rate decreased during many of the heated tests. Table 7.1 gives approximate test observation times at which the propane gas flow rate decreased. This complicates the direct comparison of the radiant heating on slab-column specimens with the same thickness. Future analysis, perhaps by inverse heat transfer modelling is required to directly compare the temperatures in the slabs at consistent depths.

7.1.3 *Friction in 600 kN jack*

Chapter 6 highlighted jack friction might have affected the load readings in some tests, including HU75-0.8 shown in Figure 6.36 and HU100-0 similarly shown in Figure 6.70a. This was checked by reacting the jack against a calibrated load cell.

Figure 7.6 show the load readings from the Instron load cell, pressure transducer in the hydraulic pipe line near the 600 kN jack (as positioned during the slab-column tests) and Avery load cell.

SPECIMEN ID	TIME SINCE IGNITION (MIN)	HEATING PHASE LENGTH (MIN)
HU50-0.8	75	120
HR50-0.8	112	121
HU75-0.8	≈106	121
HR75-0.8	106	120
HU100-0.8	NA	4
HR100-0.8	<107	120
HU100-1.5	NA	14
HR100-1.5	68	105
HU100-0	NA	6
HR100-0	49	99

Table 7.1: Approximate observation time the propane gas flow rate decreased during testing

The differences between the three load readings show:

$$\text{Instron} - \text{Pressure transducer} = \text{friction in 250 kN jack and connecting hoses}$$
$$\text{Pressure transducer} - \text{Avery} = \text{friction in 600 kN jack and connecting hoses}$$

The Instron load was the controlled load when testing the specimens, whereas the pressure transducer load was used to measure the actual load on the specimens (this is plotted as load in the graphs). The first relationship is important, because if the slab reacts against the 250 kN jack, the friction in the jack and connecting hoses needs to be overcome prior to the Instron load cell being affected. The second relationship is important because the pressure transducer was used to measure the load on the specimens and it has an approximate 2 kN difference caused by friction in the 600 kN jack and connecting hoses (see Figure 5.14 for jack positioning).

This 2 kN is significant, up to 7% of the constant load applied, for the specimens with lower capacities. The 2 kN represents a difference in constant load applied to the slabs in the range of approximately 1-7%. With respect to the maximum, failure and residual loads this represents a difference in the range of approximately 0.7-5%.

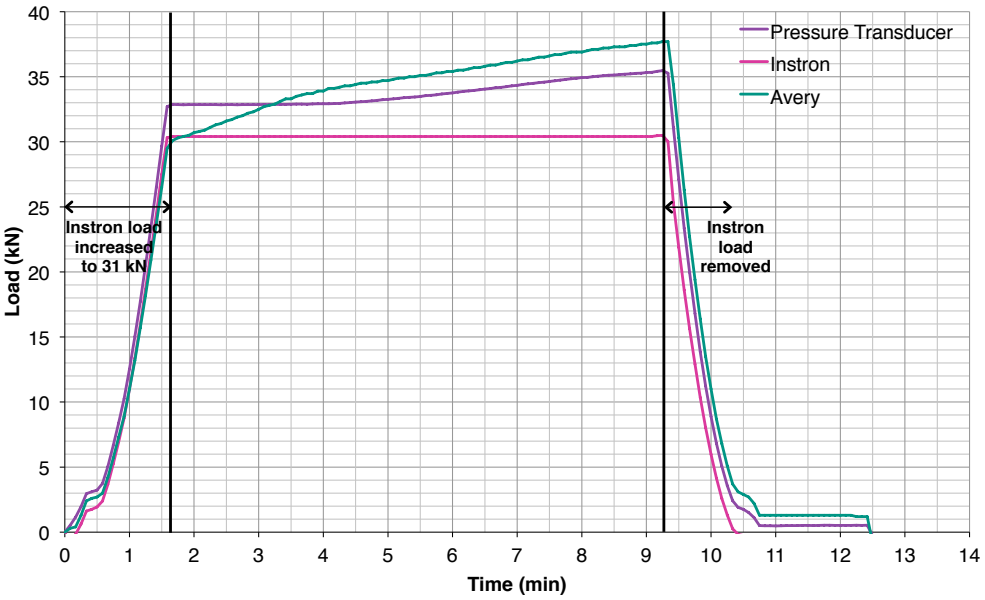

Figure 7.6: Load comparison during hydraulic friction test

7.1.4 *Vertical displacement instrumentation*

Digital camera comparison

An analysis to compare DIC accuracy between the three cameras was undertaken with data from the unrestrained heated, 75 mm thick slab with 0.8%. Two twin Canon 650D cameras were positioned at the S and W frame sides, whereas an older model 450D was positioned on the E frame side.

Figures 7.7 – 7.9 show a coarse analysis of the vertical displacement across the slab, at 10 minute intervals from 25 minutes prior to ignition. The loading and heating phases can be distinguished by the blue and red colours, respectively. The dashed profiles show the the cooling phase deflection response. The DIC analysis is coarse as there were only 6-7 patches analysed for each 10 minute interval test image. Figure 7.7 has no data for the time intervals 156 and 166 minutes, as the E camera failed to take images at these time intervals.

The E and W camera displacement plots shown in Figures 7.7 and 7.9, respectively, are along the same axis of the slab. The central axis is plotted, spanning from frame N at the left to the frame S at the right, with comparable distances across the slab. Figure 7.8 shows the S camera displacement plot, which is at a perpendicular axis to the other cameras. It spans from the frame W at the left to the frame E at the right. A direct comparison of the DIC vertical displacement for the E and W cameras is shown in Figure 7.10. The E and W cameras do not show exactly the same vertical displacements, however they are similar except for a patch 900 mm across the slab. This may be caused due to a DIC analysis patch tracking error.

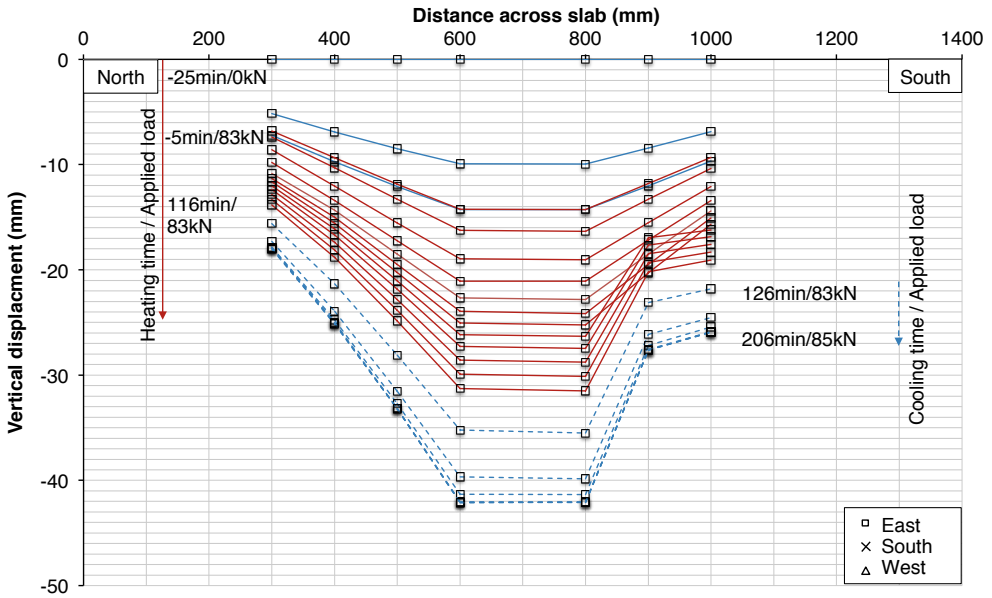

Figure 7.7: East camera DIC vertical displacement across the heated 75 mm thick, 0.8% reinforced: unrestrained slab

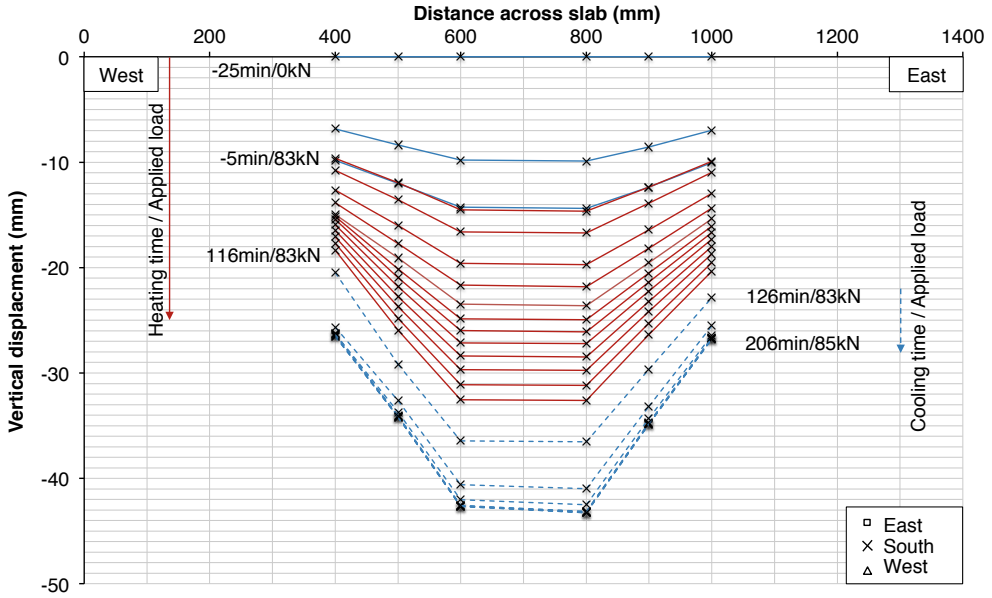

Figure 7.8: South camera DIC vertical displacement across the heated 75 mm thick, 0.8% reinforced: unrestrained slab

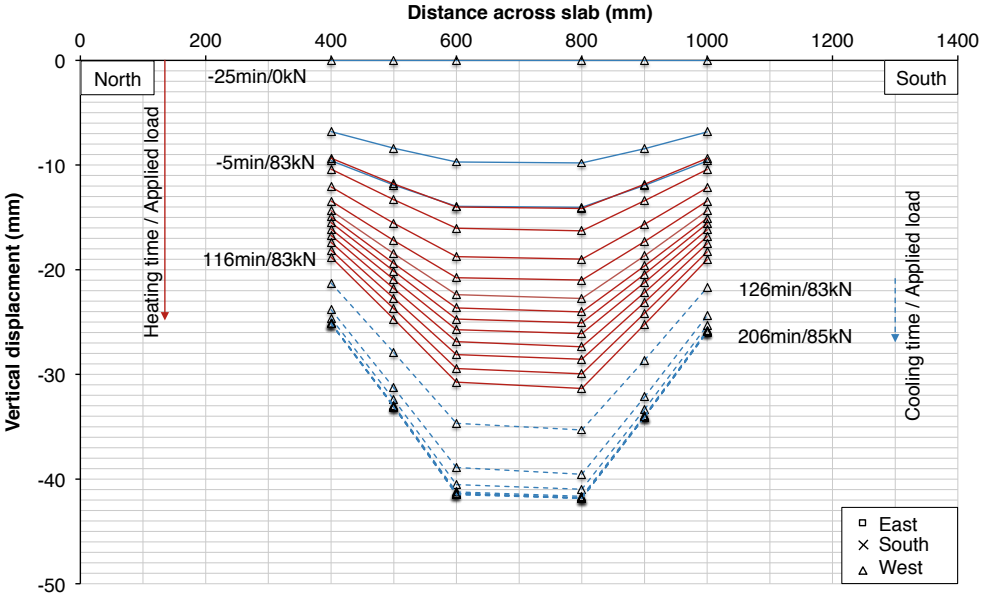

Figure 7.9: West camera DIC vertical displacement across the heated 75 mm thick, 0.8% reinforced: unrestrained slab

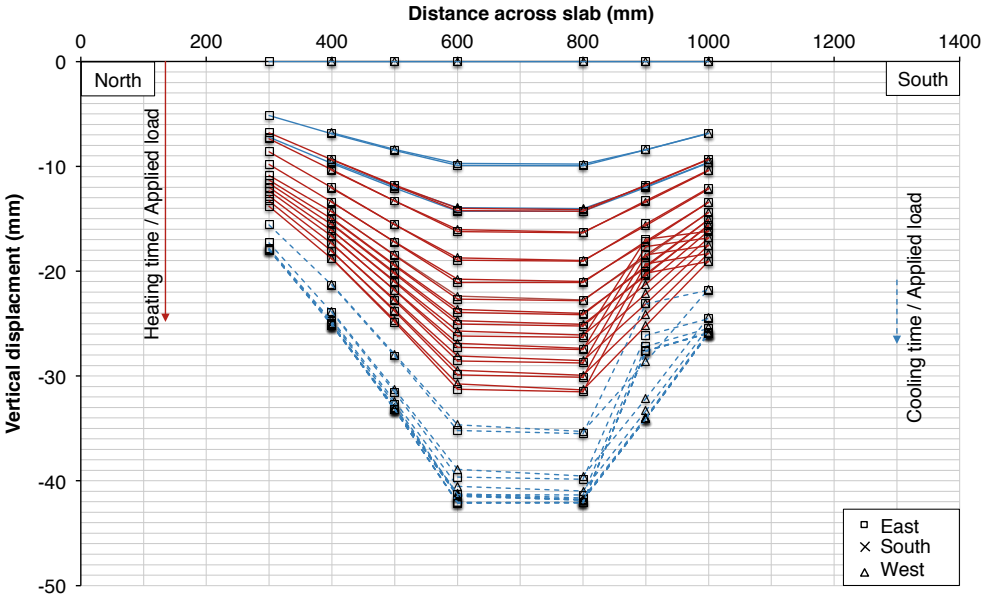

Figure 7.10: Comparison of West and East cameras, DIC vertical displacement across the heated 75 mm thick, 0.8% reinforced: unrestrained slab

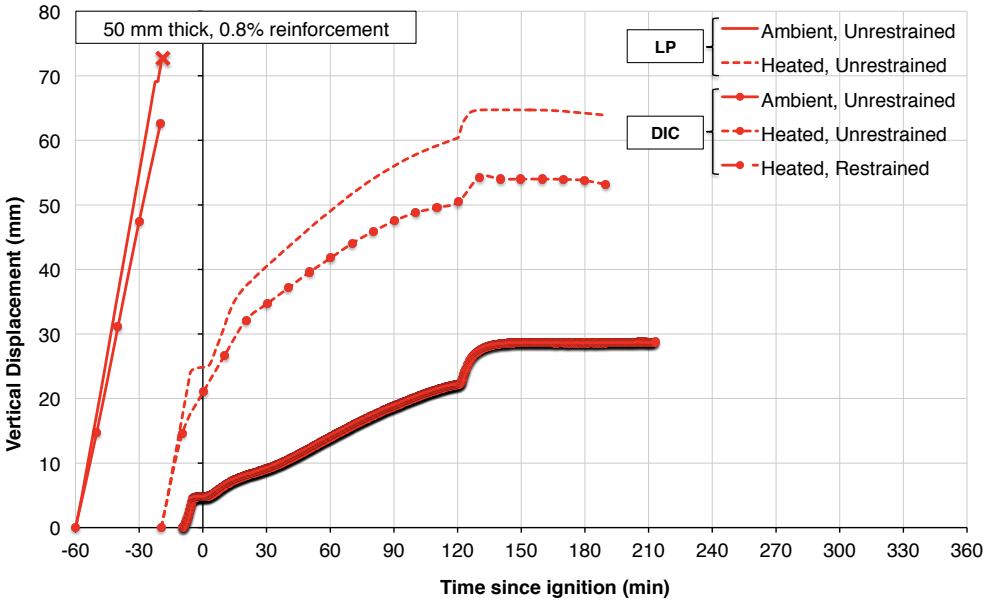

Figure 7.11: Vertical deflection comparison of LP and DIC average for 50 mm thick, 0.8% reinforced slabs

The vertical displacements of the S camera are similar to those of the other two, even though it is in a perpendicular axis. This is contrary to the visual observations of the flexure-shear failure, in Section 6.3.3, which show the shear cone to have been larger on the N frame side in both heated tests.

Displacement Transducer (LP) compared to Digital Image Correlation (DIC)

Section 6.2.6 showed a consistent relationship between the displacement recorded by the LP and the DIC displacement for the 50 mm thick slab. As described in Section 6.2.6, the displacement for 50 mm thick, heated restrained test is plotted by DIC. The DIC vertical displacements were consistently less than the LP. Figures 7.11 – 7.15 compare the vertical displacements determined using LP and DIC for the other specimens. The DIC vertical displacement curves are coarsely sampled with images analysed at 10 minute intervals throughout testing. This is in contrast to the aforementioned restrained heated, 50 mm thick slab in which images were analysed at 10 second intervals during loading and heating phases, and 20 second intervals during the cooling phase. As with the 50 mm thick slab, the other specimens DIC displacements were also consistently less than the LP readings.

Figure 7.16 shows the difference between the LP and DIC vertical displacement readings with respect to time. Specimen thickness does not seem to influence this behaviour. All the heated tests show a relatively consistent difference in the vertical displacement measurements when the load is held constant (after ignition). The ambient temperature tests, which were loaded until

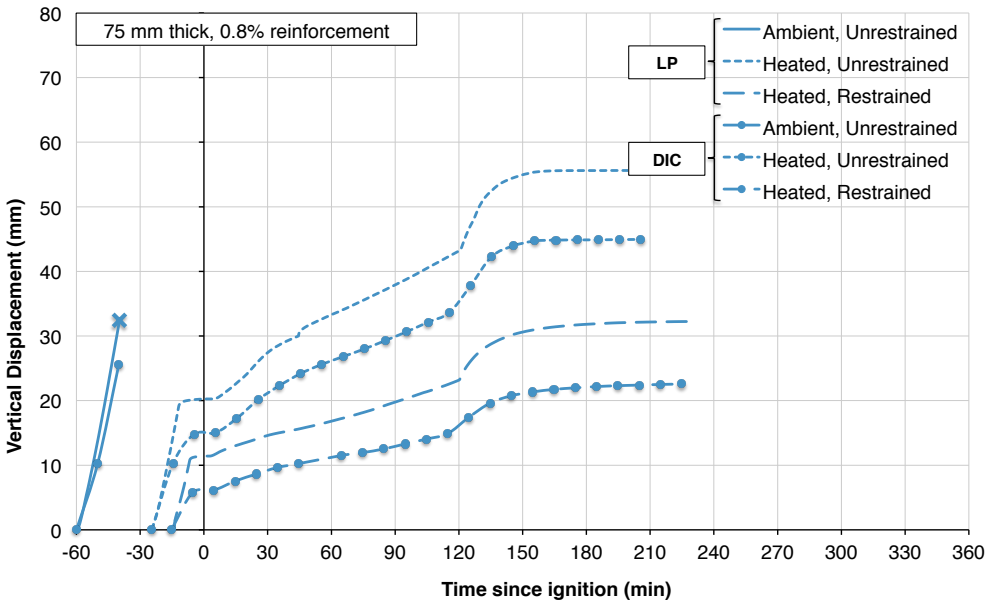

Figure 7.12: Vertical deflection comparison of LP and DIC average for 75 mm thick, 0.8% reinforced slabs

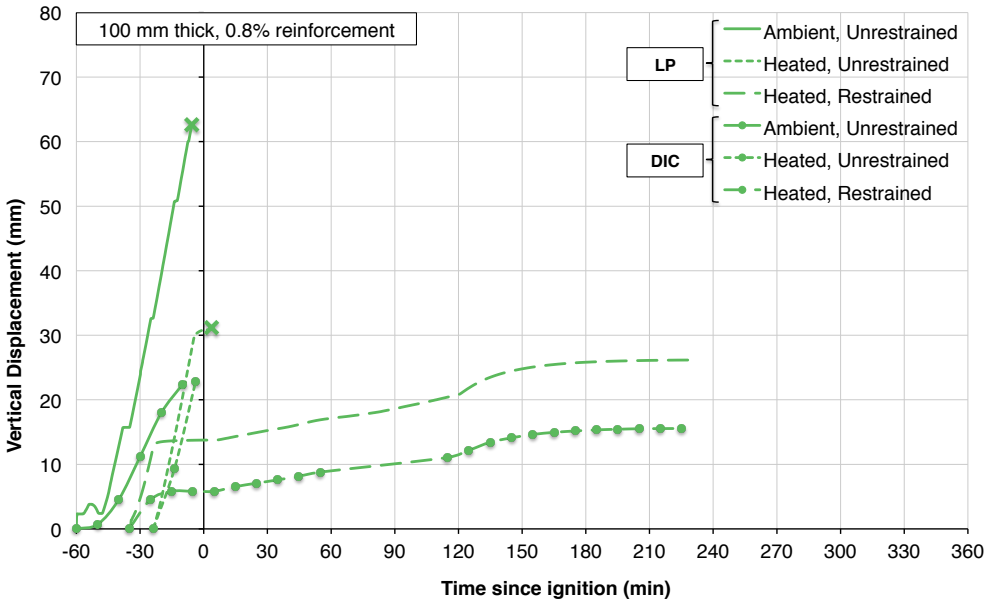

Figure 7.13: Vertical deflection comparison of LP and DIC average for 100 mm thick, 0.8% reinforced slabs

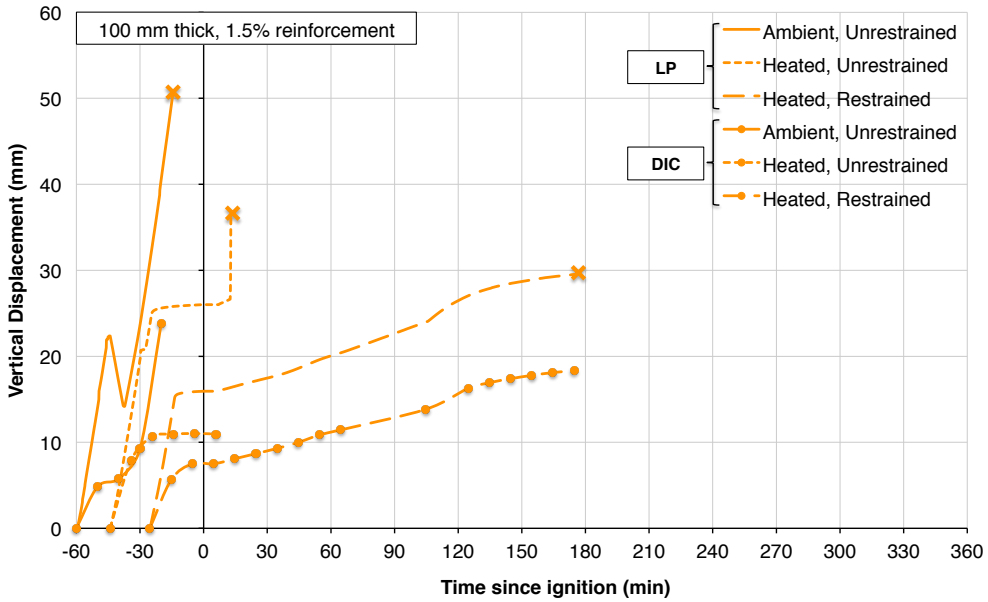

Figure 7.14: Vertical deflection comparison of LP and DIC average for 100 mm thick, 1.5% reinforced slabs

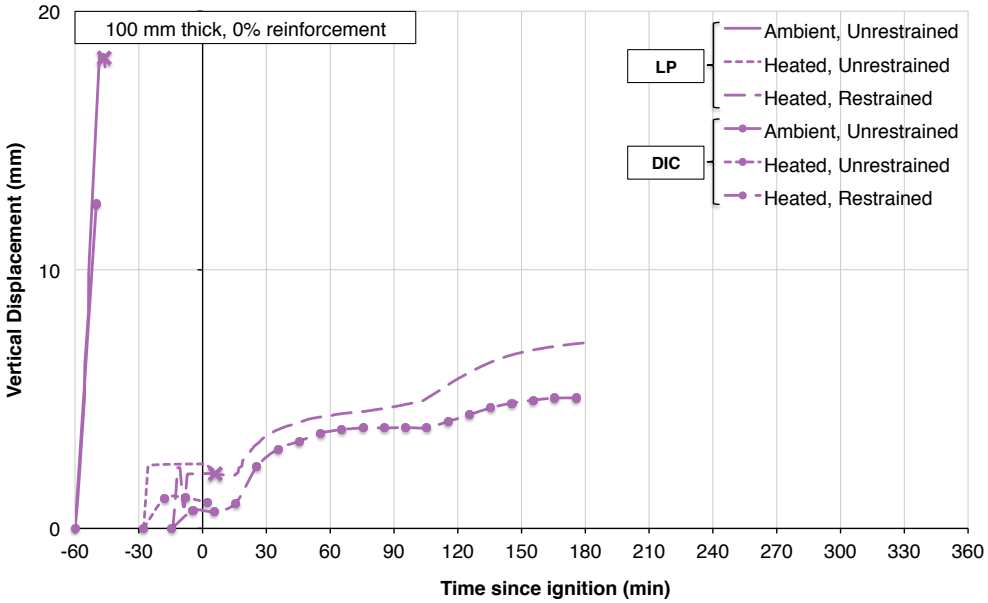

Figure 7.15: Vertical deflection comparison of LP and DIC average for 100 mm thick, 0% reinforced slabs

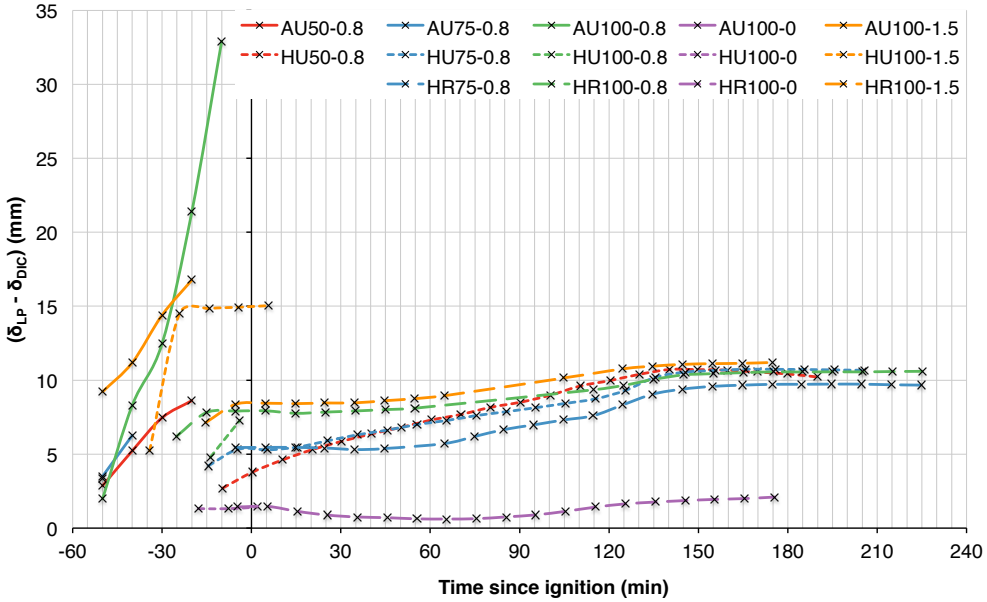

Figure 7.16: Vertical deflection difference between LP and DIC with time

failure, show a constant increase in the displacement difference. These two observations indicate the difference in displacement measurements is related to applied load.

There are three possible causes for the LP displacement readings being higher than the DIC readings: localised crushing of the concrete around the column stub, extension of the loading rod due to the elevated temperature, tension loading or reaction frame movement. These three possible causes are proposed, due to the difference in where the vertical displacements are measured in relation to. The DIC displacement readings were measured on the lower (unheated) surface of the slab. The LP measured the jack extension (Section 5.7.3), which was assumed to be equal to the column stub displacement.

The DIC vertical displacement readings are assumed to be more accurate than the LP measurements. The load-deflection plots in Chapter 6 were graphed with the LP vertical displacement readings as they were finely sampled and allow behaviour analysis. DIC deflection was used for deflection profile analyses in Section 7.2.

7.1.5 *In-plane reaction force and moment accuracy*

The net average in-plane reaction force, N and moments, M were calculated for all the tests, by averaging all the column data in each test. Many strain gauge readings were suspect, which highlights the need to improve the measurement of the in-plane reaction force and moment for future tests. In order to make qualitative comparisons, suspect data was excluded in the net aver-

age in-plane reaction force and moment calculation. Suspect data was assessed by the percentage ratio between the net in-plane force, N and applied load, P, shown in Appendix K. Column data values higher than 20% for the unrestrained tests or that did not follow the trend were assumed to be suspect. Table K.1 in Appendix K gives an overview of the column net in-plane force and moment data for each test and highlights which data was deemed suspect and has been ignored in the average calculation.

As presented in Appendix E, the unrestrained test net in-plane force and moment data needed to be corrected for eccentricity. Figure 7.17 shows that the eccentricity correction has a large impact on the net in-plane force (Figure 7.17a) of the unrestrained test results and not on the net moment (Figure 7.17b).

Figure 7.18 compares the ambient and elevated temperature corrected net average in-plane reaction force, N for the unrestrained tests. Unexpectedly, the net average in-plane force increases during the loading of all the unrestrained, ambient tests. Figure 7.19 shows that there is a linear relationship between the corrected net average in-plane reaction force and the load applied to the column stub during the test. As the ambient, unrestrained strain gauge readings are influenced by the applied load, it is assumed that all the strain gauge readings are similarly affected. This strain gauge analysis highlights that the data should be disregarded for the rest of the thesis, as the readings are falsely affected by the applied load.

Figure 7.20 shows the restrained elevated temperature test net average in-plane force, N and moment, M. Though the quantitative N and M results are to be disregarded, qualitative comparisons can be made. Both the N and M are greater in the restrained tests compared to the unrestrained. There is a clear behaviour change on cooling in the restrained tests, which is also perceiveable in the unrestrained, HU50-0.8 and HU75-0.8 tests.

7.1.6 *Specimen support condition functionality*

The restraint frame allowed the slab-column specimens to be tested under different restraint conditions; restrained and unrestrained. Section 5.3 presents the structural reaction frame design. The stiffness of the structural reaction frame is investigated to assess the effectiveness of the restrained support condition in providing restraint against in-plane forces (caused by thermal expansion) and bending moments.

The lateral structural frame displacement was calculated using stiffness measurements undertaken by Fox (2013), shown in Table 7.2. Fox (2013) gives no explanation for the magnitude increase in the column C4 stiffness. The struc-

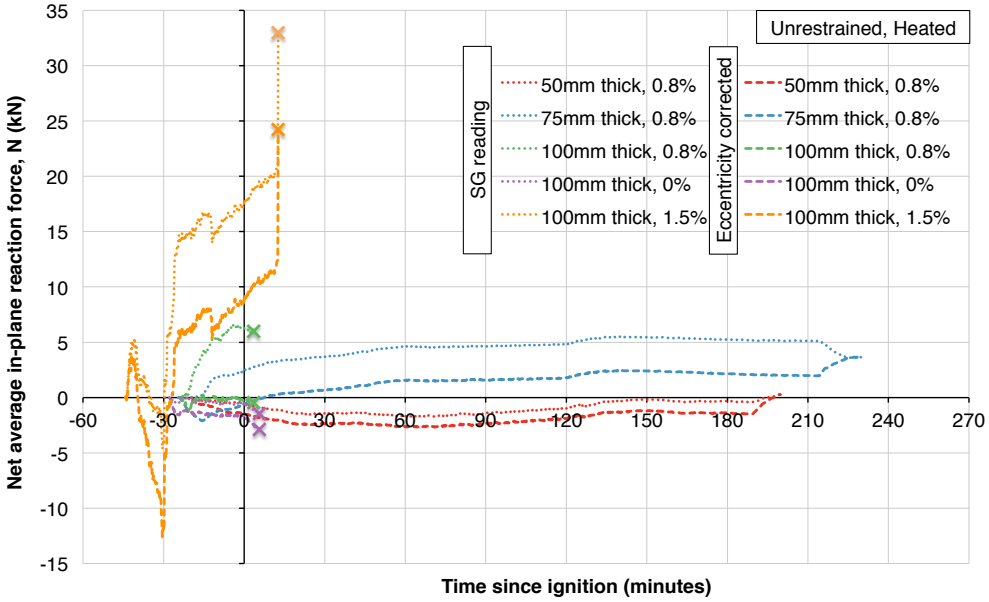

(a) Net average in-plane reaction force, N

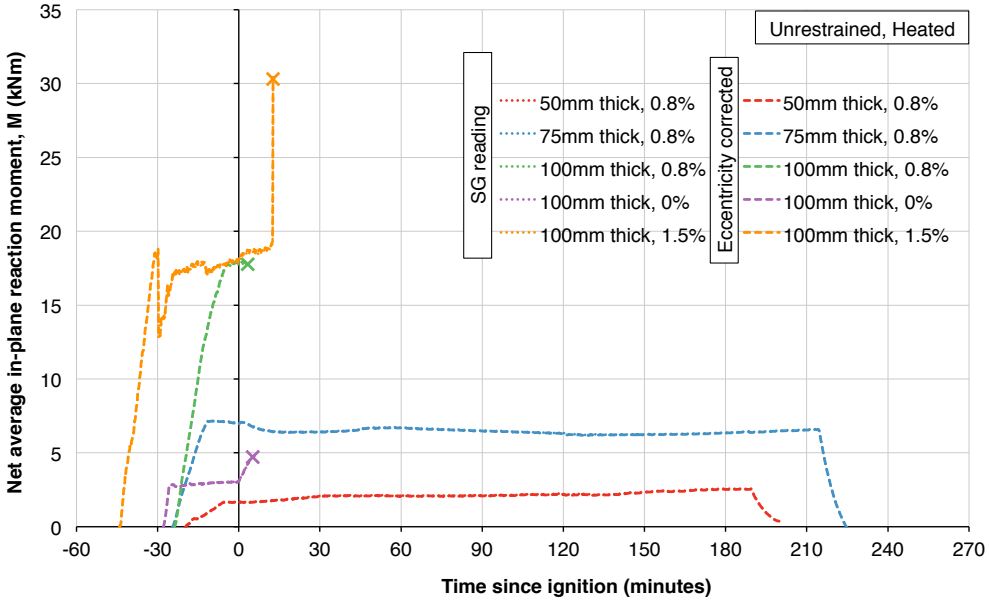

(b) Average net moment, M

Figure 7.17: Impact of eccentricity correction on net average in-plane force and moment unrestrained test graphs

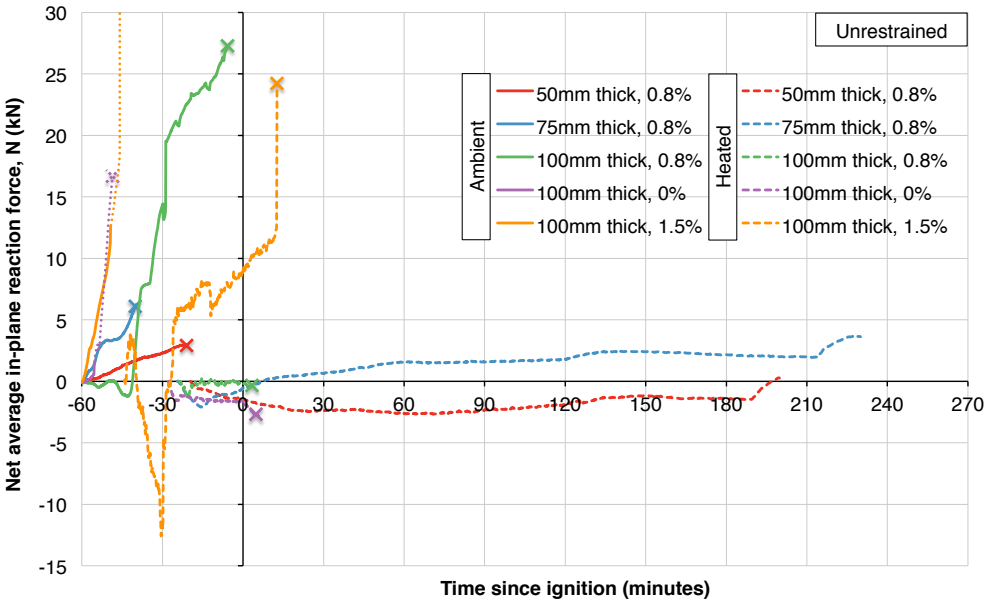

Figure 7.18: Net average in-plane reaction force in the unrestrained ambient and heated tests

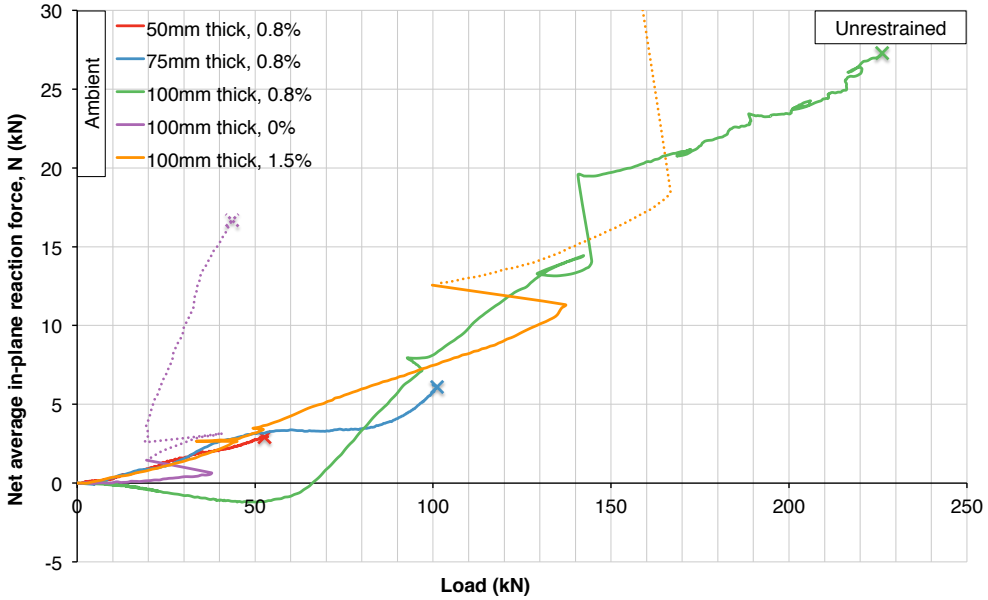

Figure 7.19: Ambient unrestrained tests, net average in-plane reaction force with applied load

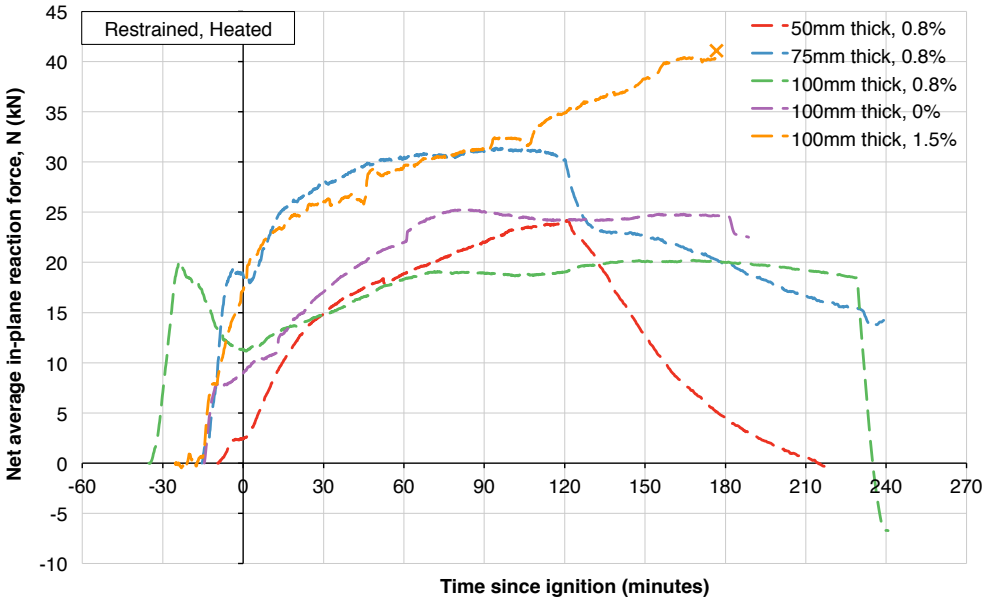

(a) Net average in-plane reaction force, N

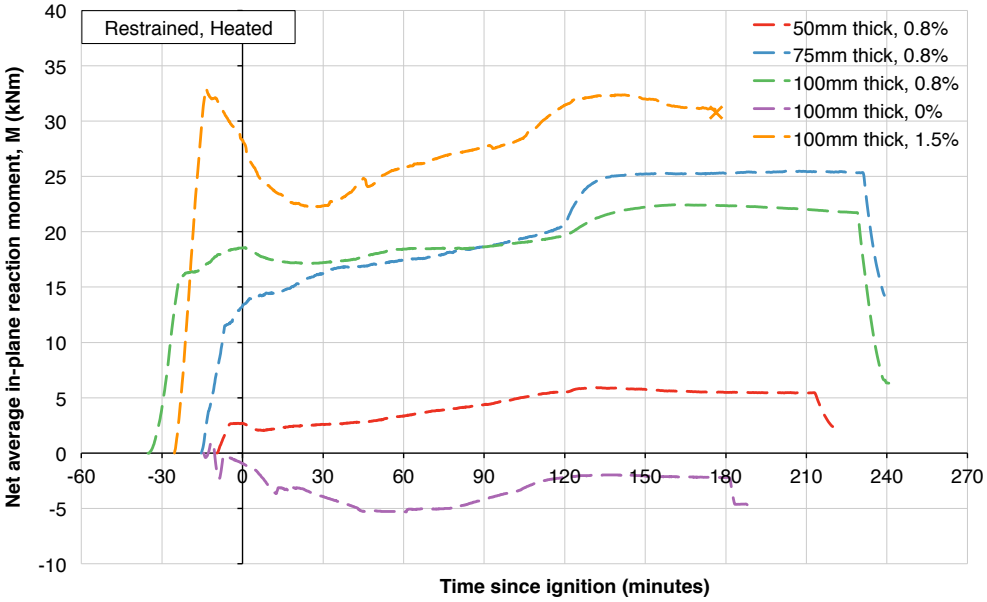

(b) Average net moment, M

Figure 7.20: Restrained ambient and heated test reactions

tural reaction frame strain gauge data was not conclusive (Section 7.1.5), however in order to give an upper bound to the horizontal frame displacement, a reading must be used here. The maximum and hence conservative, net average in-plane force measured by the restrained 100 mm thick, 1.5% reinforced specimen (HR100-1.5), reaction frame strain gauges was approximately 20.5 kN on each column. The maximum potential horizontal displacement in the tests could have been approximately 32 mm. This proves that the restrained support condition was not perfectly fixed.

FOX (2013) COLUMN ID	COLUMN REFERENCE	STIFFNESS (KN/MM)	R^2 FIT FOR STIFFNESS
C5	EN	72.298	0.9504
C6	ES	95.996	0.8690
C7	SE	83.134	0.9624
C8	SW	71.480	0.6484
C1	WS	62.412	0.8846
C2	WN	88.967	0.9464
C3	NW	73.465	0.9925
C4	NE	328.59	0.7764

Table 7.2: Horizontal structural frame stiffness, reproduced from Fox (2013)

7.1.7 *Summary*

The main bullet points summarising the experiment methodology verification, Section 7.1 are presented here:

- An analysis of the post-failure specimen tolerances, showed that the smaller 50 mm and 75 mm thick specimens had higher errors of flexural reinforcement spacing and concrete cover.
- There was little variation in heating application across the upper surface of each individual specimen. The heating application was not repeatable between tests, there was great variation in the temperature curves. Variations are attributed to changes in propane gas flow rates, which were noted during experimental testing.
- Jack friction was proven to have a high influence of up to 7% of the load readings, for specimens with low capacities.
- A direct comparison of the three digital image camera analyses show good vertical displacement agreement. The consistently lower DIC ver-

tical displacement readings, compared to the LP were attributed to: localised crushing of the concrete around the column stub, extension of the loading rod due to elevated temperature, tension loading or reaction frame movement.

- The strain gauge readings were falsely affected by the applied load and quantitative readings were disregarded. Qualitative analyses showed the restrained tests to have greater readings compared to the unrestrained supported case. Additionally, a clear behaviour change was seen at the onset of the cooling phase in the restrained tests and was also seen in the unrestrained 50 mm and 75 mm thick specimens.
- The structural reaction frame stiffness showed that the restrained support condition was not perfectly fixed.

7.2 DEFLECTION PROFILES ACROSS THE SLAB-COLUMN SPECIMENS

Chapter 6 gave vertical displacement at the centre of the slab. However, DIC allows the vertical displacements to be determined anywhere on the lower (unheated) surface of the slabs. Vertical displacement profiles across the slabs are presented here, as they give more information than just the central displacement. This required additional post-test analysis, which is presented here. Only the W camera data is used, as it was shown in Section 7.1.4 to be a good representation of all the cameras, has images for all the tests and has the least missing images during the tests (caused by camera errors). The deflection profiles of the residually tested specimens have not been plotted.

The DIC deflections support the results in Sections 6.8 and 6.10, which show the restrained supported specimens are stiffer, with lower central displacements, compared to similar unrestrained specimens. A comparison of DIC central vertical displacement at the end of slab-column testing, prior to residual testing is shown in Table 7.3, whereas Table 7.4 shows the DIC central vertical displacement at ignition for the heated tests.

FIRE SCENARIO / SUPPORT CONDITION	SLAB THICKNESS (MM) - REINFORCEMENT RATIO (%)				
	50-0.8	75-0.8	100-0	100-0.8	100-1.5
AU	63	26	12	24	28
HU	53*	45*	1	61	21
HR	28*	23*	5*	15*	27

* RESIDUALLY TESTED

Table 7.3: DIC central slab-column vertical displacement at the end of testing

FIRE SCENARIO / SUPPORT CONDITION	SLAB THICKNESS (MM) - REINFORCEMENT RATIO (%)				
	50-0.8	75-0.8	100-0	100-0.8	100-1.5
HU	21*	15*	1	23	11
HR	0*	6*	1*	6*	8

* RESIDUALLY TESTED

Table 7.4: DIC central slab-column vertical displacement at ignition

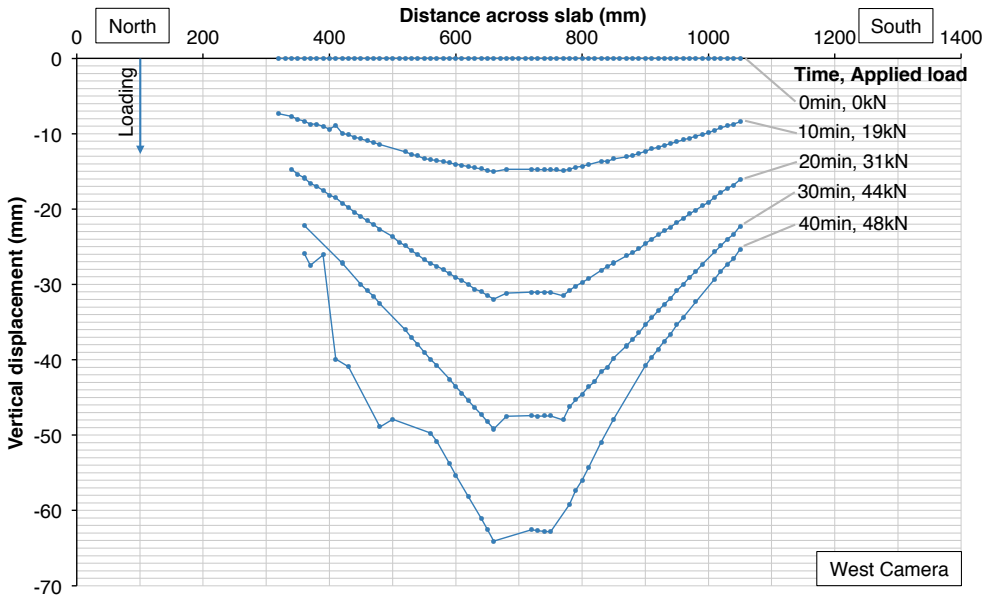

Figure 7.21: DIC vertical displacement across the ambient 50 mm thick, 0.8% reinforced: unrestrained slab at 10 minute intervals

A direct comparison between the ambient and elevated temperature unrestrained tests gives no clear trend in the thermally induced deflection.

7.2.1 *50 mm thick, 0.8% reinforced*

Figures 7.21 – 7.23 show the ambient unrestrained, heated unrestrained and heated restrained DIC deflection profiles, for the 50 mm thick slabs reinforced with 0.8% steel, respectively. The DIC displacement profiles are plotted at 10 minute intervals relative to ignition. Negative deflection is downwards, in the direction of loading and away from the heat source.

In Figures 7.21 – 7.23, the initial profiles with a solid blue colour distinguish the loading, prior to the ignition phase of the test. The red colour denotes the deflection profiles, after ignition when the applied load is held constant. The maximum blue, dashed deflection profiles, show the cooling phase deflection response. A few annotations show the time interval relative to ignition and load applied, P. The plots have been grouped to compare similar slab thicknesses

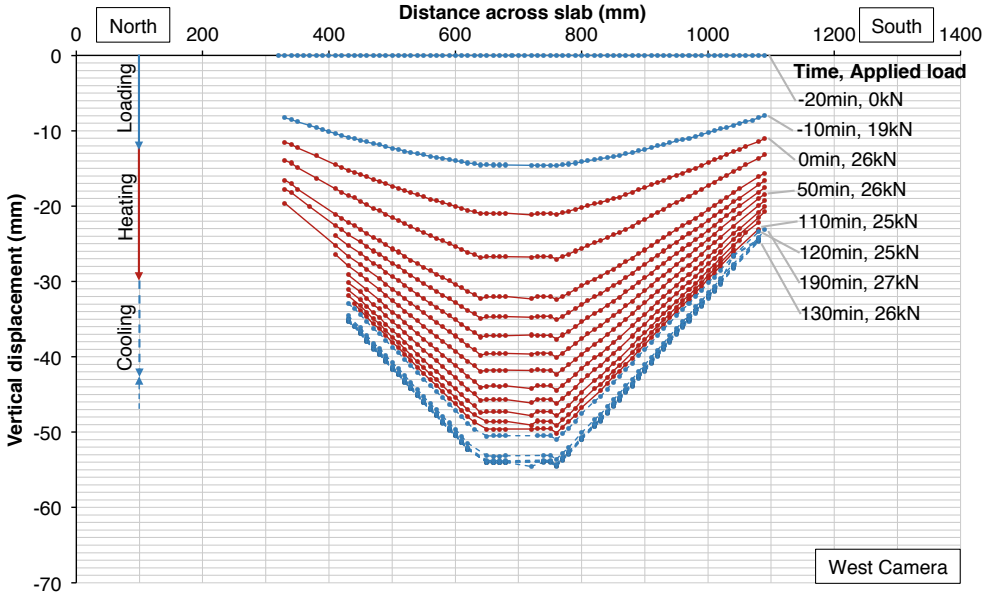

Figure 7.22: DIC vertical displacement across the heated 50 mm thick, 0.8% reinforced: unrestrained slab at 10 minute intervals

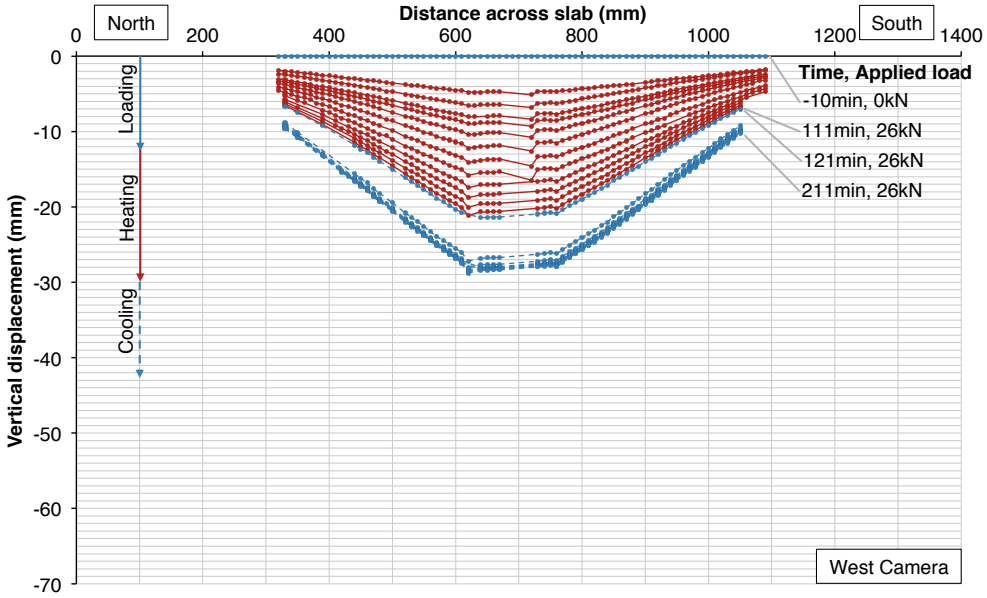

Figure 7.23: DIC vertical displacement across the heated 50 mm thick, 0.8% reinforced: restrained slab at 10 minute intervals

and reinforcement ratios, therefore the fire and support conditions vary. Note that similar y-axis scales have been used for each comparison grouping.

DIC confirms that the central cross-sectional surface of all the slabs, continually deflected away from the heat source, as discussed in Section 6.8. The central linear deflection in all the 50 mm thick deflection profiles is assumed to be caused by the column stub, which approximately agrees with the column stub width of 120 mm.

The impact of heating is assessed by comparing the ambient (Figure 7.21) and heated (Figure 7.22), unrestrained deflection profiles. Section 6.8 discussed the difference in the central deflection of the 0.8% reinforced slabs, however the DIC displacement profiles here can quantify that the heated slab (HU50-0.8) had a small approximate deflection recovery of 1 mm during the cooling phase. Figure 7.22 shows that during the initial cooling phase, the 120 and 130 minute deflection is away from the heat source, however thereafter it reverses. The slab-column material properties have therefore been shown to recover during the cooling phase as the applied load is held constant.

The impact of the support condition is clearly visualised with the DIC deflection profile. The difference in vertical deflection between 10 minute profiles in Figures 7.22 and 7.23 is clearly reduced by the restrained supports. It is important to remember that the restrained support box sections were 100 mm wide, therefore restrained the slab edges at 0–100 mm and 1300–1400 mm with respect to the x-axis. The deflection profiles could not be analysed all the way to the supports, as the digital images only captured a large proportion of the slab surface, but not its entirety. This however could later be extrapolated if required.

7.2.2 *75 mm thick, 0.8% reinforced*

Figures 7.24 – 7.26 show the ambient unrestrained, heated unrestrained and heated restrained DIC deflection profiles, for the 75 mm thick slabs reinforced with 0.8% steel, respectively.

A comparison of the support condition with the thicker, 75 mm slabs, reveals clearly that the angle of rotation of the unrestrained slabs (Figure 7.25) is much greater than that of the restrained (Figure 7.26). The rate of change in vertical displacement across the surface of the slab indicates the rotation of the slab, and the formation of cracks. Figure 7.26 shows the restrained support condition causes hogging moments near the support, with a similar sagging in the centre. Additionally, the failure mode of the heated, restrained test looks unsymmetrical in the N–S frame axis. The maximum displacement is closer to the S frame side, which is perhaps caused by a crack near the S edge of

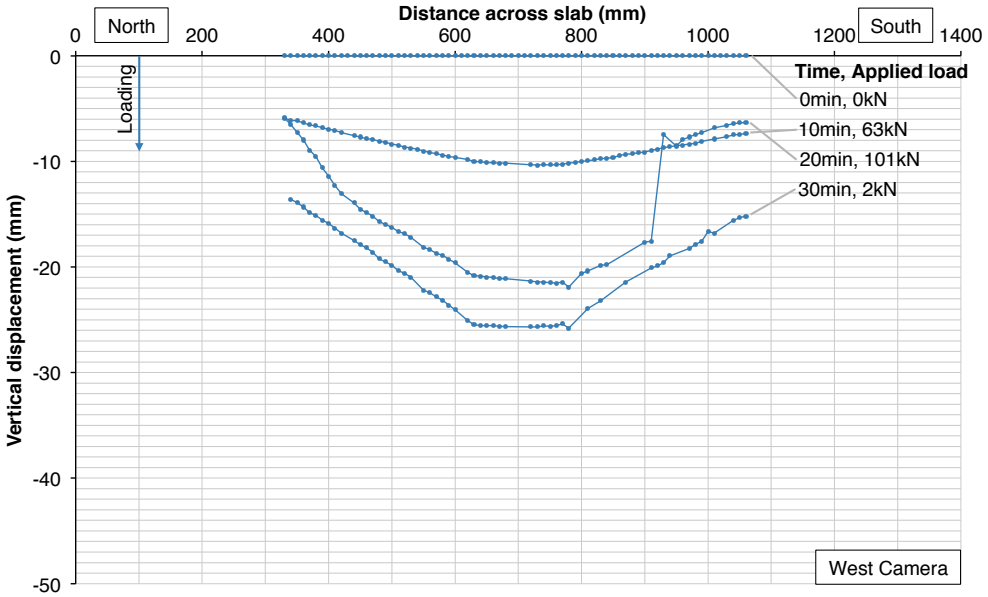

Figure 7.24: DIC vertical displacement across the ambient 75 mm thick, 0.8% reinforced: unrestrained slab at 10 minute intervals

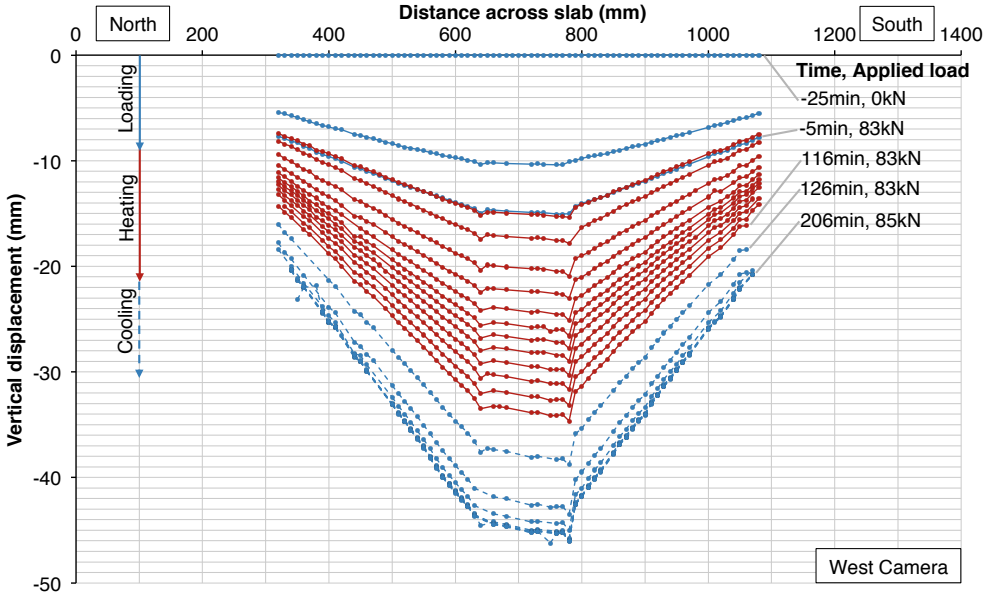

Figure 7.25: DIC vertical displacement across the heated 75 mm thick, 0.8% reinforced: unrestrained slab at 10 minute intervals

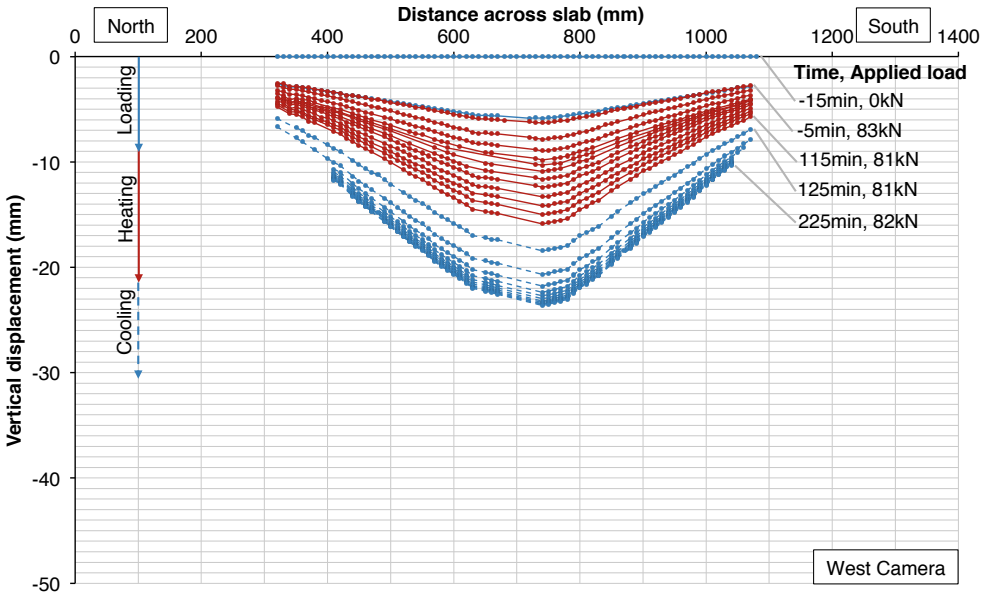

Figure 7.26: DIC vertical displacement across the heated 75 mm thick, 0.8% reinforced: restrained slab at 10 minute intervals

the column stub, seen in the failure cross-section in Figure 6.33c, causing it to rotate.

7.2.3 *100 mm thick, 0.8% reinforced*

Figures 7.27 – 7.29 show the ambient unrestrained, heated unrestrained and heated restrained DIC deflection profiles, for the 100 mm thick slabs reinforced with 0.8% steel, respectively.

The ambient test deflection profiles shown in Figure 7.27 are incomplete. There were many DIC analysis errors, potentially due to this having been the first slab-column test undertaken. The limited data shown in Figure 7.27 makes it difficult to decern the deflected shape.

A support type comparison between the unrestrained (Figure 7.28) and the restrained (Figure 7.29) shows a stark behaviour difference. Aside from the almost magnitude difference in displacement readings (commented on in Section 6.8), crack development can be seen in the restrained profiles, whereas the unrestrained test failed in a brittle, punching shear mode with no pre-warning. Cracks at distances of for example approximately 530 mm, 550 mm and 830 mm across the restrained slab can be seen in Figure 7.29. Future assessment of individual cracks could be undertaken with a higher density of DIC patches.

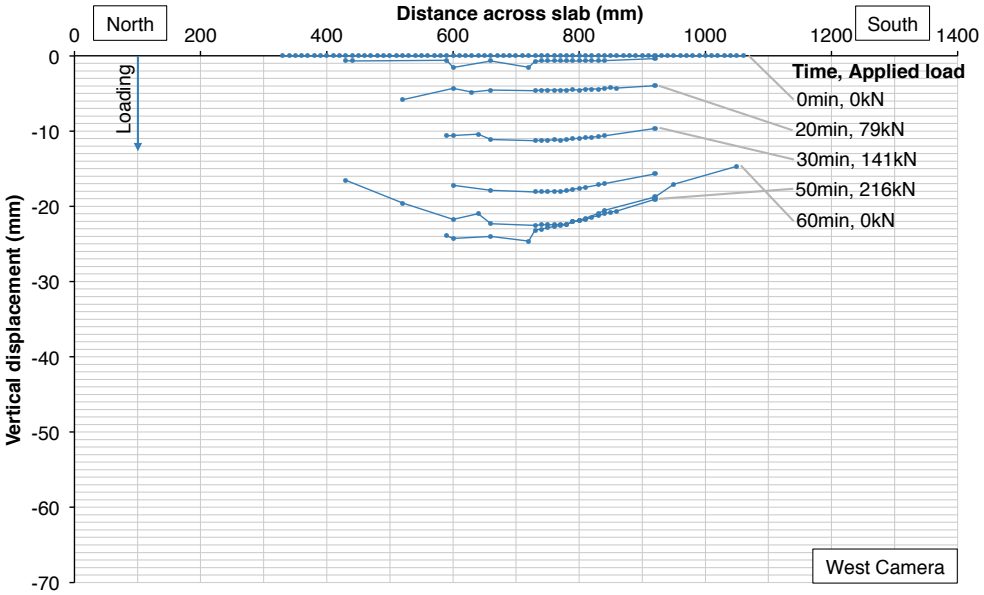

Figure 7.27: DIC vertical displacement across the ambient 100 mm thick, 0.8% reinforced: unrestrained slab at 10 minute intervals

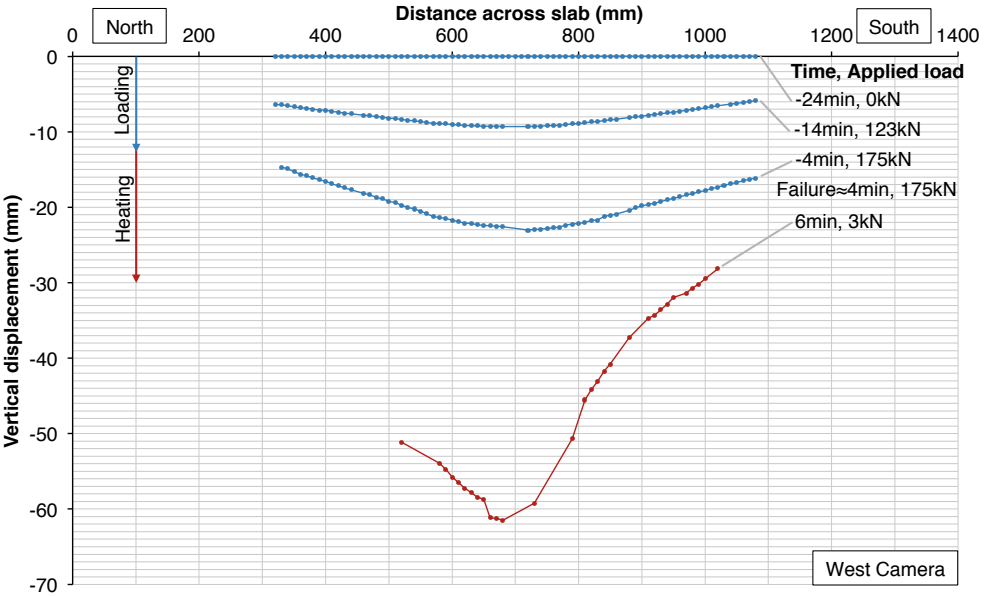

Figure 7.28: DIC vertical displacement across the heated 100 mm thick, 0.8% reinforced: unrestrained slab at 10 minute intervals

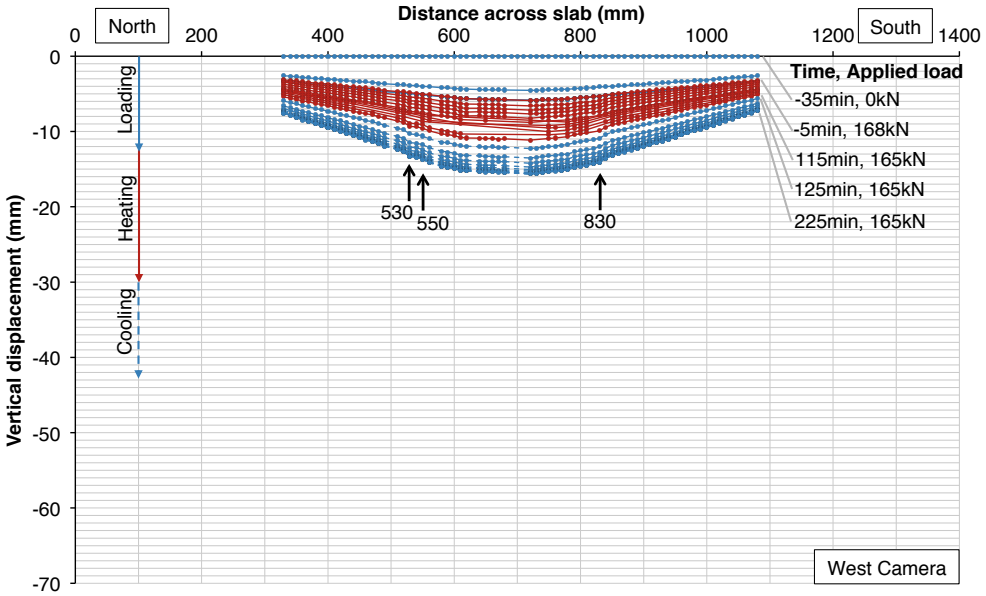

Figure 7.29: DIC vertical displacement across the heated 100 mm thick, 0.8% reinforced: restrained slab at 10 minute intervals

7.2.4 *100 mm thick, 1.5% reinforced*

Figures 7.30 – 7.32 show the ambient unrestrained, heated unrestrained and heated restrained DIC deflection profiles, for the 100 mm thick slabs reinforced with 1.5% steel, respectively.

The deflection profiles of the 100 mm thick and most heavily reinforced slabs, 1.5% show the crack development with time clearly. The punching shear cone is shown in both the unrestrained tests, in Figures 7.30 and 7.31. The ambient unrestrained cone can be seen in the 40 and 50 minute profiles, at 590 and 880 mm across the slab. Cracks are seen in the heated unrestrained test at 570 and 820 mm across the slab, at -24 minutes (prior to ignition). Further cracks develop prior to failure, for example at approximately 470 and 870 mm across the slab.

As with previous tests, the unrestrained support condition shows a sagging deflection profile, whereas the restrained support condition shows the change from hogging near the supports and sagging in the centre.

7.2.5 *100 mm thick, 0% unreinforced*

Figures 7.33 – 7.35 show the ambient unrestrained, heated unrestrained and heated restrained DIC deflection profiles, for the 100 mm thick unreinforced slabs, respectively.

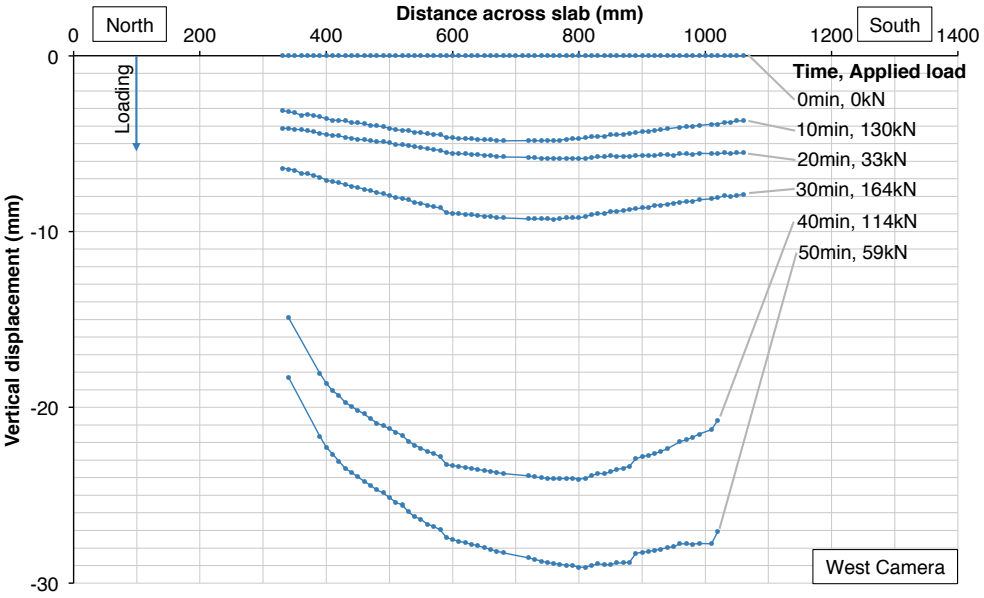

Figure 7.30: DIC vertical displacement across the ambient 100 mm thick, 1.5% reinforced: unrestrained slab at 10 minute intervals

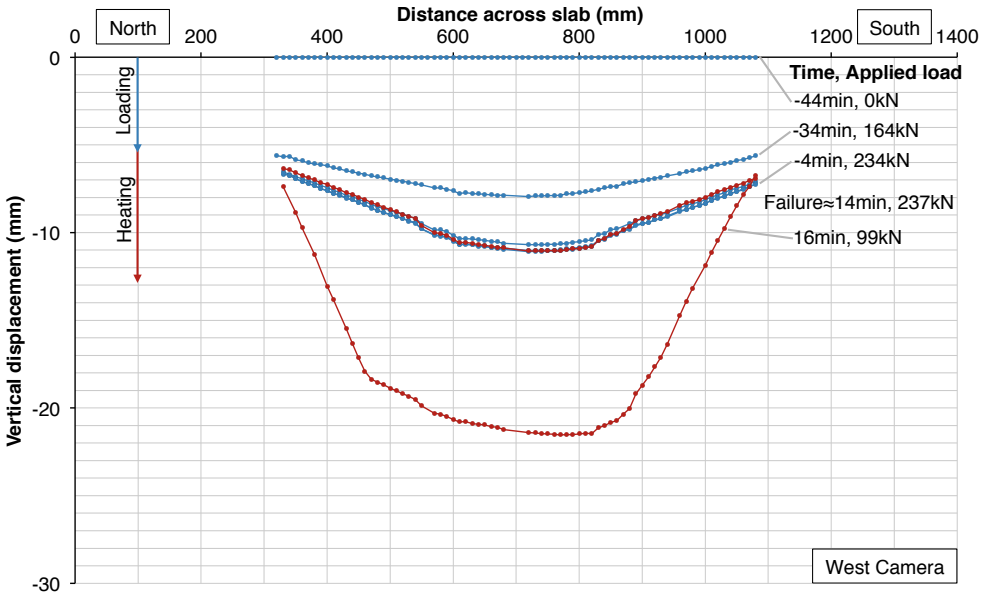

Figure 7.31: DIC vertical displacement across the heated 100 mm thick, 1.5% reinforced: unrestrained slab at 10 minute intervals

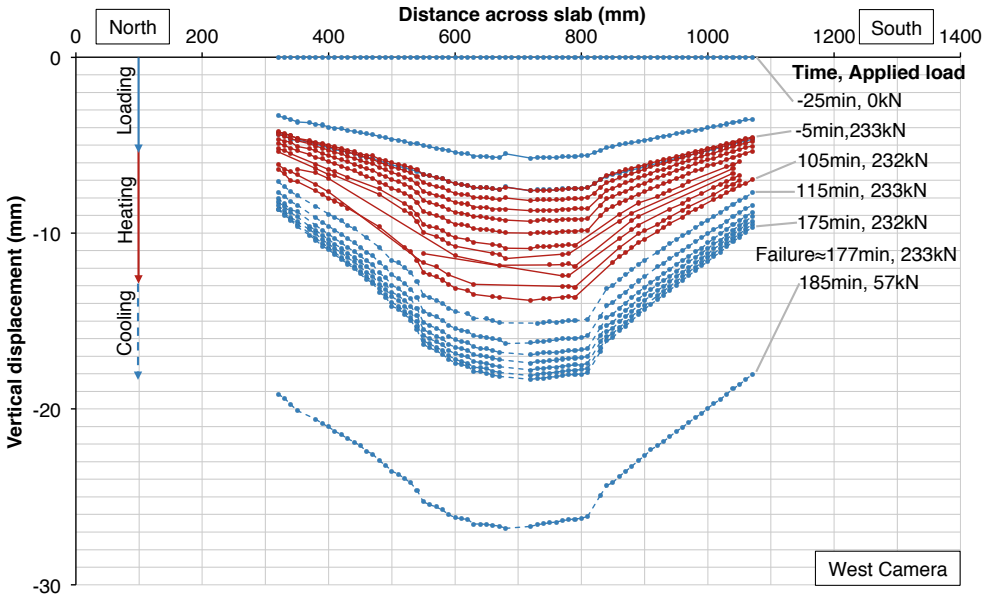

Figure 7.32: DIC vertical displacement across the heated 100 mm thick, 1.5% reinforced: restrained slab at 10 minute intervals

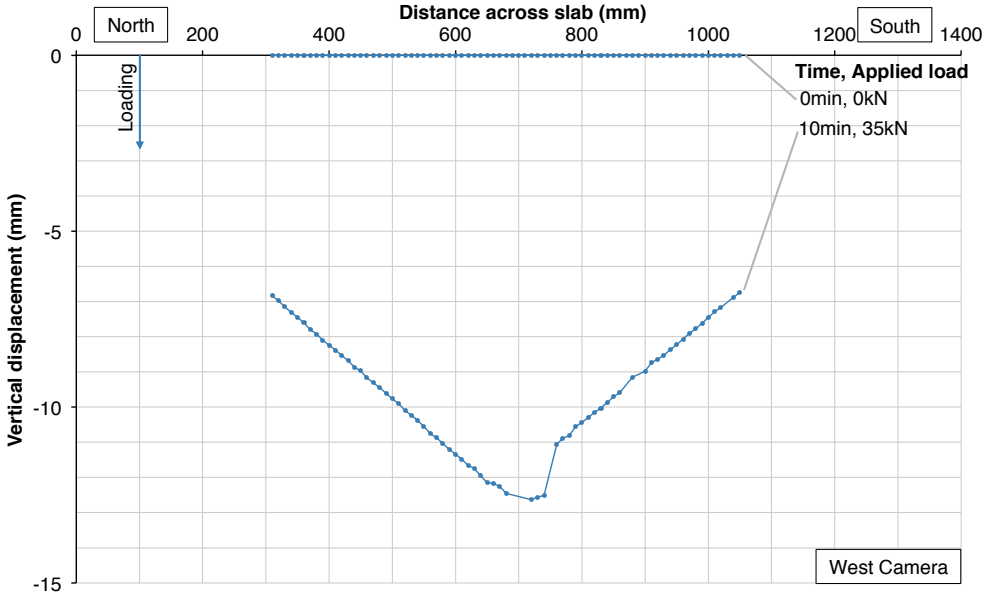

Figure 7.33: DIC vertical displacement across the ambient 100 mm thick, 0% reinforced: unrestrained slab at 10 minute intervals

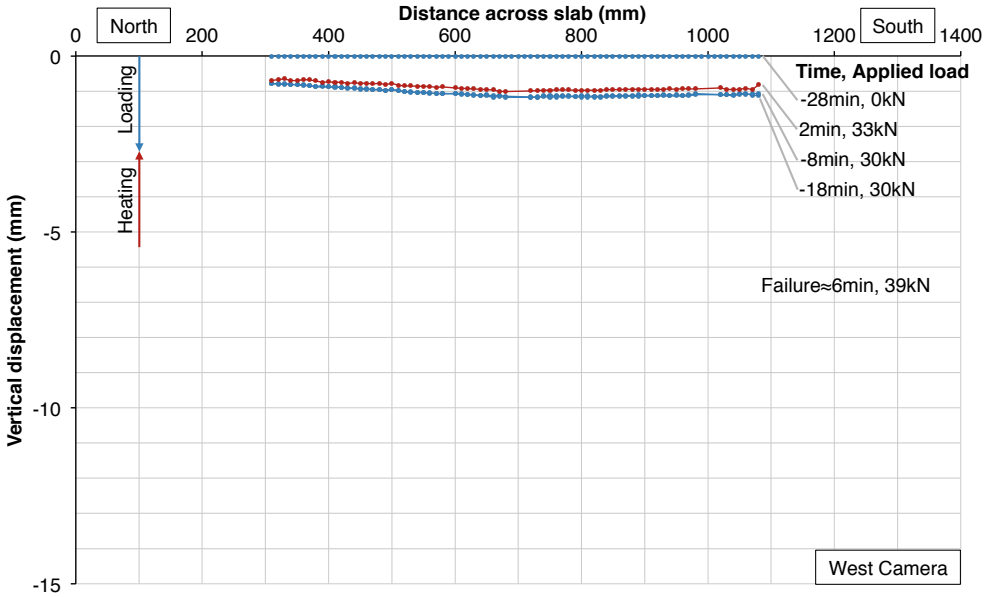

Figure 7.34: DIC vertical displacement across the heated 100 mm thick, 0% reinforced: unrestrained slab at 10 minute intervals

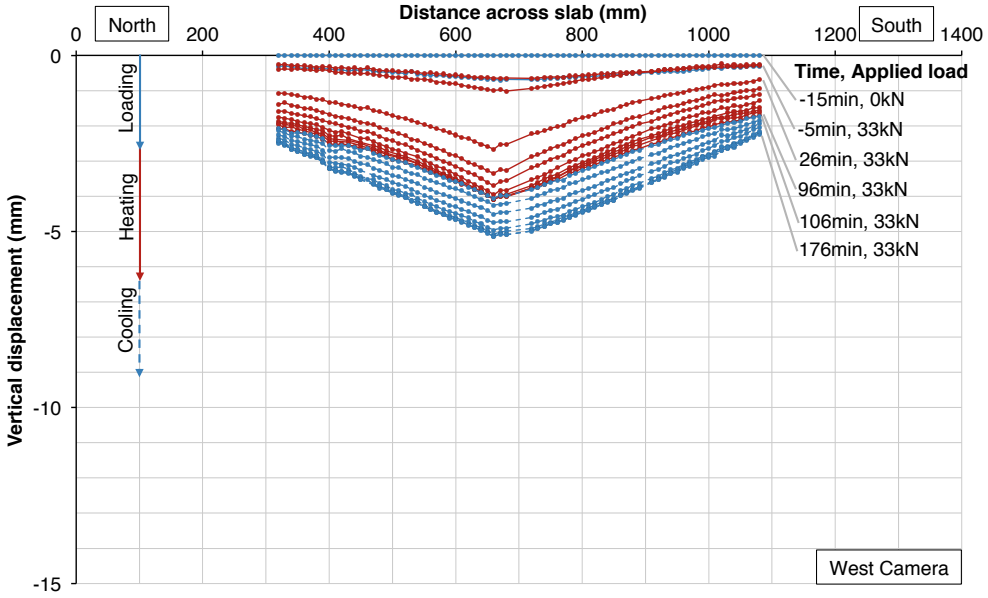

Figure 7.35: DIC vertical displacement across the heated 100 mm thick, 0% reinforced: restrained slab at 10 minute intervals

The displacement profiles of the unreinforced slabs, in Figures 7.33 and 7.35 show the flexural failure modes well. The unrestrained, ambient failure occurred quickly, therefore there is only one profile prior to failure at 10 minutes into the test. The displacement profile shows the expected central crack with symmetrical linear displacement of the slab pieces about the crack. The slab pieces about the heated restrained flexural crack have a curvature to them.

The heated unrestrained displacement profile in Figure 7.34 does not capture the failed deflection as it occurs only 6 minutes after ignition. The vertical displacement is seen to recover very slightly (0.2 mm) during the heating phase. This recovery is also shown in the LP readings, used to plot the load-deflection behaviour in Figure 6.70a of Section 6.6.5.

7.2.6 *Summary*

The main bullet points summarising the deflection profiles across the slab-column specimens in Section 7.2, are presented here:

- DIC vertical displacement profiles across the lower (unheated) surface, showed the deflection to continuously be away from the heat source, in the direction of loading, throughout the heating and cooling phases.
- The unrestrained lightly reinforced heated, 50 mm thick slab (HU50-0.8) and unrestrained unreinforced heated, 100 mm thick slab (HU100-0) were the only specimens which recovered their deflection slightly. HU50-0.8 recovered 1 mm during the cooling phase, whereas HU100-0 recovered approximately 0.2 mm during the heating phase.
- DIC allows the change in curvature to be visualised, from hogging moment near the restrained supports to sagging moment under the applied load. Similarly, the continual slab sagging behaviour in the unrestrained support condition is shown.
- DIC shows the rotation of the slab and the formation of cracks. The angle of rotation near the unrestrained support condition is greater than that of the restrained slab supports. The crack development, including the punching shear cone can be visualised throughout the loading, heating and cooling phases.
- DIC technique is an effective displacement measurement tool for structural fire testing.

7.3 PUNCHING SHEAR FAILURE COMPARISON TO SHEAR DESIGN

Section 7.3.1 analyses the degraded concrete and steel material properties due to elevated temperature, using EC2. Section 7.3.2 compares the experimental results with the design values from EC2, including failure loads, and the shape of the shear cracks. The results are also compared to the Muttoni's Critical Shear Crack Theory (CSCT) in Section 7.3.3.

7.3.1 *Material properties at elevated temperature*

This section describes how the concrete and steel material properties were degraded due to elevated temperature, according to EC2 design. For conservatism, the maximum recorded elevated temperature in each test was used to reduce the material properties of that respective test.

Concrete

Section 5.2.4 stated that the aggregate used was siliceous aggregate, which determines the factors used to degrade the properties at elevated temperatures. Figure 2.36 in Section 2.5.2 showed the EC2 stress-strain relationship for a uniaxial, siliceous aggregate concrete, in compression at different elevated temperatures. The ambient characteristic compressive cylinder concrete strength, f_{ck} was measured as an average of 51 MPa at 28 days (Section 6.13.1). Table 7.5 shows the degraded concrete parameters, characteristic compressive cylinder strength, $f_{c,\theta}$ and ultimate strain, $\varepsilon_{cu1,\theta}$, at each test maximum elevated temperature. The reduction factors are quoted to four decimal places, as in EC2.

Steel

Figure 2.37b shows the class N values used to decrease the steel properties with respect to the elevated temperature. However, EC2 states that class X values shown in Figure 7.36 can be used if the strength at elevated temperatures is tested. Section 6.13.2 details experimental tests undertake by (Bath, 2013; Batson, 2013) under my guidance. An analysis is undertaken to assess which class factor reduction values are more conservative for the comparison.

Table 6.6 - 6.8 (Section 6.13.2) presented the experimental and class N and X reduction factors for the yield strength, $f_{sy,\theta}$ and Young's modulus, $E_{s,\theta}$ at the elevated temperatures of 19, 112, 191, 390, 475 and 590°C. Figure 7.37 shows a factor comparison to analyse if the class N or X factors more closely match the experimental results. Both Figures 7.37a and 7.37b for yield strength, $f_{sy,\theta}$ and Young's modulus, $E_{s,\theta}$, respectively, show the experimental factors to be

SPECIMEN ID	MAXIMUM TEMP (°C)	CHARACTERISTIC COMPRESSIVE STRENGTH REDUCTION FACTOR	ULTIMATE STRAIN REDUCTION FACTOR	CHARACTERISTIC COMPRESSIVE CYLINDER STRENGTH $f_{c,\theta}$, (MPA)	ULTIMATE STRAIN $\varepsilon_{cu1,\theta}$
HU50-0.8	500	0.6000	0.0325	30.6	0.000114
HR50-0.8	630	0.4050	0.0358	20.7	0.000125
HU75-0.8	480	0.6300	0.0320	32.1	0.000112
HR75-0.8	560	0.5100	0.0340	26.0	0.000119
HU100-0.8	130	0.9850	0.0233	50.2	0.000081
HR100-0.8	435	0.6975	0.0309	35.5	0.000108
HU100-1.5	208	0.9420	0.0252	48.0	0.000088
HR100-1.5	510	0.5850	0.0328	29.8	0.000114

Table 7.5: Siliceous concrete material parameters at elevated temperature

Steel Temperature θ[°C]	$f_{sy,\theta}$ / f_{yk} hot rolled and cold worked	$f_{sp,\theta}$ / f_{yk} hot rolled and cold worked	$E_{s,\theta}$ / E_s hot rolled and cold worked
20	1,00	1,00	1,00
100	1,00	1,00	1,00
200	1,00	0,87	0,95
300	1,00	0,74	0,90
400	0,90	0,70	0,75
500	0,70	0,51	0,60
600	0,47	0,18	0,31
700	0,23	0,07	0,13
800	0,11	0,05	0,09
900	0,06	0,04	0,07
1000	0,04	0,02	0,04
1100	0,02	0,01	0,02

Figure 7.36: Class X values for either hot rolled or cold worked reinforcing and prestressing steel stress-strain relationships at elevated temperature, reproduced from BS EN 1992-1-2:2004 (2010) (notations: p =prestressing, s =reinforcing steel)

more closely matched by the EC2 class X factors. The EC2 class X factors have therefore been used here to reduce the steel properties.

Table 7.6 shows the maximum temperature in the slab-column flexural reinforcement, which was extrapolated from the temperature profiles in Chapter 6 and factor reduced yield strength, $f_{sy,\theta}$ and Young's modulus, $E_{s,\theta}$.

7.3.2 *EC2 ambient and elevated temperature*

This section compares the experimental results to the EC2 design punching shear capacity, crack diameter and crack angle for both ambient and elevated temperature.

Punching shear capacity

Equation 2.5 in Section 2.5.1 gives the ambient temperature punching shear stress design resistance of slabs without shear reinforcement. The elevated temperature punching shear capacity is calculated by using the reduced characteristic compressive cylinder strength, $f_{c,\theta}$ in Table 7.5.

Though EC2 design does not explicitly assess for varying support conditions, it is assumed that the second term, σ_{cp} in Equation 2.5 is sufficient to make a comparison for both support conditions, restrained and unrestrained. The boundary reaction forces are considered by using the unrestrained and

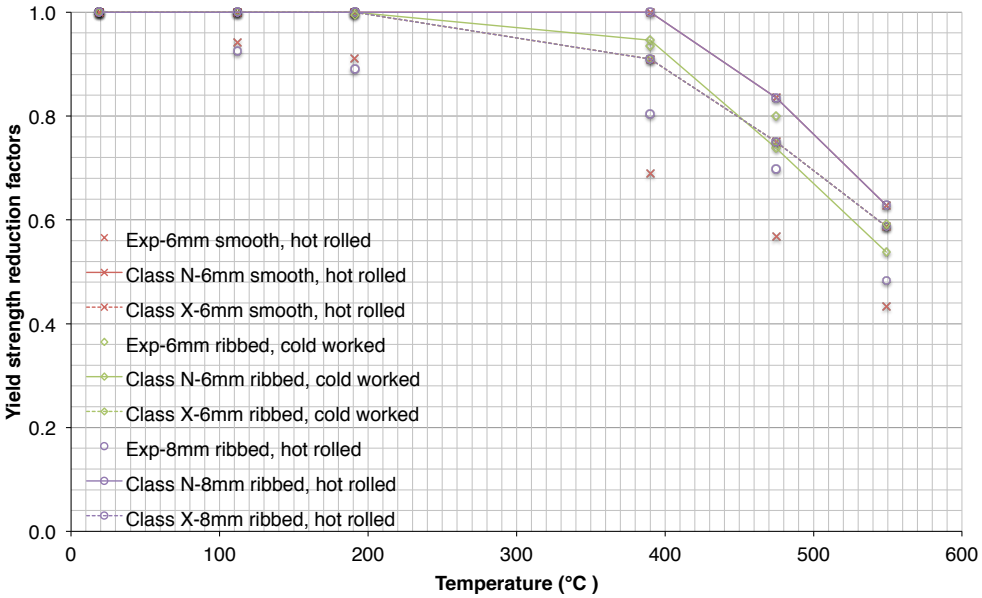

(a) Yield strength, $f_{sy,\theta}$, (MPa)

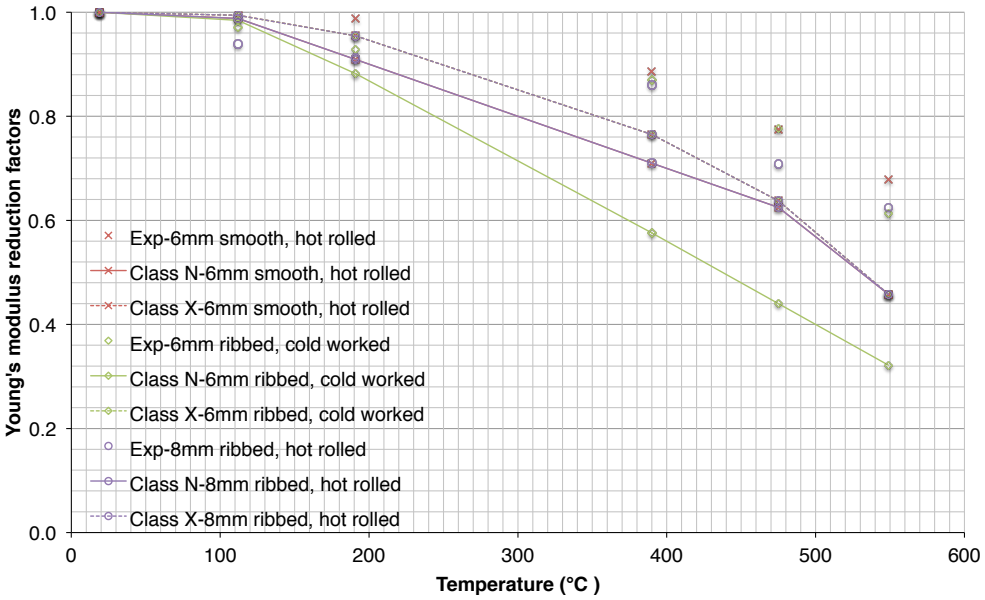

(b) Young's modulus, $E_{s,\theta}$, (MPa)

Figure 7.37: Elevated temperature reduction factors from experimental values and EC2 class N and X

SPECIMEN ID	MAXIMUM TEMP ($^\circ$C)	CLASS X REDUCTION FACTORS YIELD STRENGTH $f_{sy,\theta}$, (MPA)	CLASS X REDUCTION FACTORS YOUNG'S MODULUS $E_{s,\theta}$, (MPA)	CLASS X REDUCED YIELD STRENGTH $f_{sy,\theta}$, (MPA)	CLASS X REDUCED YOUNG'S MODULUS $E_{s,\theta}$, (GPA)
HU50-0.8	350	0.95	0.8250	522	165
HR50-0.8	445	0.81	0.6825	445	136
HU75-0.8	245	1.00	0.9275	549	185
HR75-0.8	290	1.00	0.9050	549	181
HU100-0.8	18	1.00	1.0000	549	200
HR100-0.8	170	1.00	0.9650	549	193
HU100-1.5	22	1.00	1.0000	571	222
HR100-1.5	148	1.00	0.9760	571	216

Table 7.6: Reinforcing steel material parameters at elevated temperature

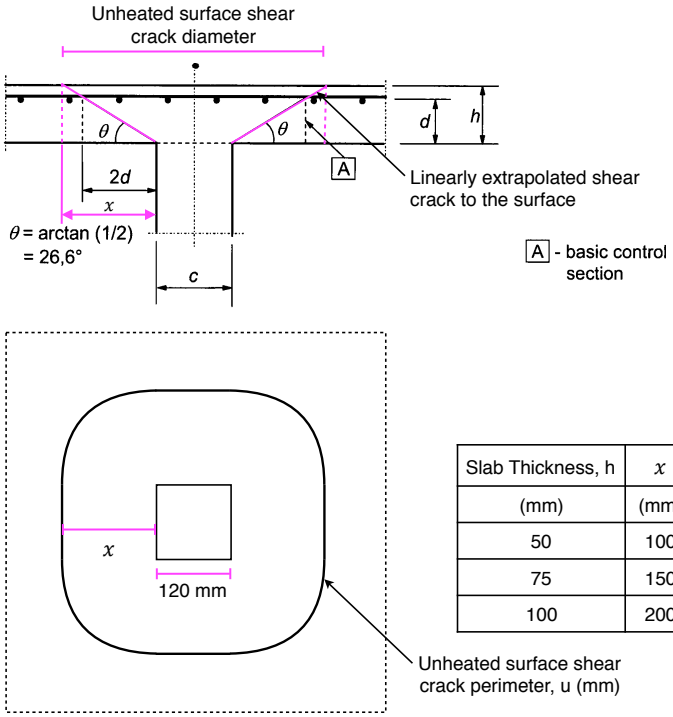

Slab Thickness, h	x	u
(mm)	(mm)	(mm)
50	100	1107
75	150	1421
100	200	1735

Figure 7.38: EC2 ambient square column, punching shear crack diameter and perimeter, adapted from BS EN 1992-1-1:2004 (2008)

restrained experimental boundary reaction forces, presented in Section 7.1.5. It is important to note that Section 7.1.5 concluded that the strain gauge data should be disregarded. The maximum net average in-plane force was used here to give the most conservative EC2 design values to compare to the experimental failure load.

BS EN 1992-1-1:2004 (2008) states that the σ_{cp} sign convention is positive, compression in Equation 2.5. This is similar to what was has been presented in the previous in-plane force graphs. The maximum net average in-plane force, N (tensile or compressive) is taken from Figures 7.18 and 7.20a for unrestrained and restrained tests, respectively. The maximum N is used to calculate the largest σ_{cp} term. Adding the second term in the Equation 2.5 gives comparative EC2 design values.

Tables 7.7 and 7.8 shows the parameters used in the calculation of the punching shear stress design resistance, $v_{Rd,c}$ for each test. The punching shear capacity, V is calculated from the multiplication of the shear stress resistance, $v_{Rd,c}$ in Equation 2.5 and the area over which the stress is applied. The area is defined by the slab thickness and the punching shear perimeter, u. The EC2 basic control section was linearly extrapolated to the unheated surface as in Figure 7.38, to find the perimeter. As in EC2, the unheated surface shear crack perimeter accounts for the square column stub shape.

SPECIMEN ID	SLAB THICKNESS (MM)	AVERAGE CONCRETE COVER (MM)	REINFORCEMENT DIAMETER (MM)	AVERAGE EFFECTIVE DEPTH (MM)	k	AVERAGE REINFORCEMENT SPACING (MM)	ρ_l
AU50-0.8	50	9	6	35	3.39	116	0.007
AU75-0.8	75	7	6	62	2.80	66	0.007
AU100-0.8	100	11	6	83	2.55	43	0.008
AU100-1.5	100	11	8	81	2.57	43	0.014
HU50-0.8	50	13	6	31	3.54	115	0.008
HU75-0.8	75	11	6	58	2.86	66	0.007
HU100-0.8	100	13	6	81	2.57	43	0.008
HU100-1.5	100	6	8	86	2.52	42	0.014
HR50-0.8	50	13	6	31	3.54	121	0.008
HR75-0.8	75	14	6	55	2.91	67	0.008
HR100-0.8	100	12	6	82	2.56	43	0.008
HR100-1.5	100	10	8	82	2.56	43	0.014

Table 7.7: EC2 punching shear resistance parameters

SPECIMEN ID	f_{ck} (MPA)	N_{Ed} (N)	A_c (MM^2)	σ_{cp} (MPA)	$v_{Rd,c}$ (MPA)	u (MM)	v_{min} CHECK (MPA)	$(v_{min} + k_1\sigma_{cp})$ CHECK (MPA)	V (KN)
AU50-0.8	51.0	2960	70000	0.04	1.19	1107	0.71	0.70	66
AU75-0.8	51.0	6250	105000	0.06	1.19	1421	0.71	0.70	126
AU100-0.8	51.0	27300	140000	0.20	1.25	1735	0.71	0.69	218
AU100-1.5	51.0	12600	140000	0.09	1.52	1735	0.71	0.70	263
HU50-0.8	30.6	-2680	70000	-0.04	1.04	1107	0.55	0.55	57
HU75-0.8	32.1	3670	105000	0.03	1.04	1421	0.56	0.56	111
HU100-0.8	50.2	-1270	140000	-0.01	1.24	1735	0.70	0.70	215
HU100-1.5	48.0	24200	140000	0.17	1.48	1735	0.69	0.67	256
HR50-0.8	20.7	24200	70000	0.35	0.93	1107	0.45	0.42	52
HR75-0.8	26.0	31400	105000	0.30	1.01	1421	0.50	0.47	107
HR100-0.8	35.5	20200	140000	0.14	1.11	1735	0.59	0.58	193
HR100-1.5	29.8	41100	140000	0.29	1.29	1735	0.54	0.51	223

Table 7.8: Further EC2 punching shear resistance parameters

Similar parameters for all slab-columns:

$\gamma_c = 1$ (partial concrete factor of 1 to allow for comparison to the experimental values)

$C_{Rd,c} = 0.18$

$k = 2,0$ (Note: Calculation in Table 7.7 shows EC2 limit consistently exceeded)

$\rho_{ly} = \rho_{lz}$ (Note: flexural reinforcement spacing axi-symmetrical) (All the slab-columns satisfy the ρ_l check of mean values taking into account column width plus $3d$ each side.)

$N_{Ed,y} = N_{Ed,z}$ (Assume: maximum net average in-plane force, N acts in both directions)

$A_{c,y} = A_{c,z}$

$k_1 = 0.1$

Figure 7.39 compares the shear capacities obtained during the experiments with the EC2 predictions. Upon first inspection, it is concerning that the design code is not consistently conservative. However on closer inspection, EC2 is not conservative for many of the small, thinner specimens. The 50 mm and 75 mm thick specimens failed in flexure-shear mechanisms and the design code does not accurately predict these failure modes. Additionally, the thinner specimens are likely to be smaller than those used in formulating the empirical Equation 2.5, and are potentially affected by size effects. EC2 punching shear design predicts shear capacities similar to the measured failure loads for the 100 mm thick reinforced slabs, which failed in pure punching shear mechanisms. Figure 7.40 shows this more clearly.

Figure 7.40 gives the ratio of the EC2 design calculation to the experimentally measured shear capacity (with unconservative results > 1.0). The EC2 calculated capacities for the 50 mm and 75 mm slabs do not vary greatly between the unrestrained and restrained support conditions in Figure 7.39. All four heated specimens were heated for 120 minutes, however the maximum concrete temperature recorded in the restrained slabs was consistently greater than the unrestrained supported slabs. Large temperature differences of 130° and 80° for the 50 mm and 75 mm thick slabs, respectively, were recorded. The effect of the restrained slabs having a larger concrete strength reduction, thereby making the first term in Equation 2.5 smaller, was balanced by a greater in-plane axial force in the second term.

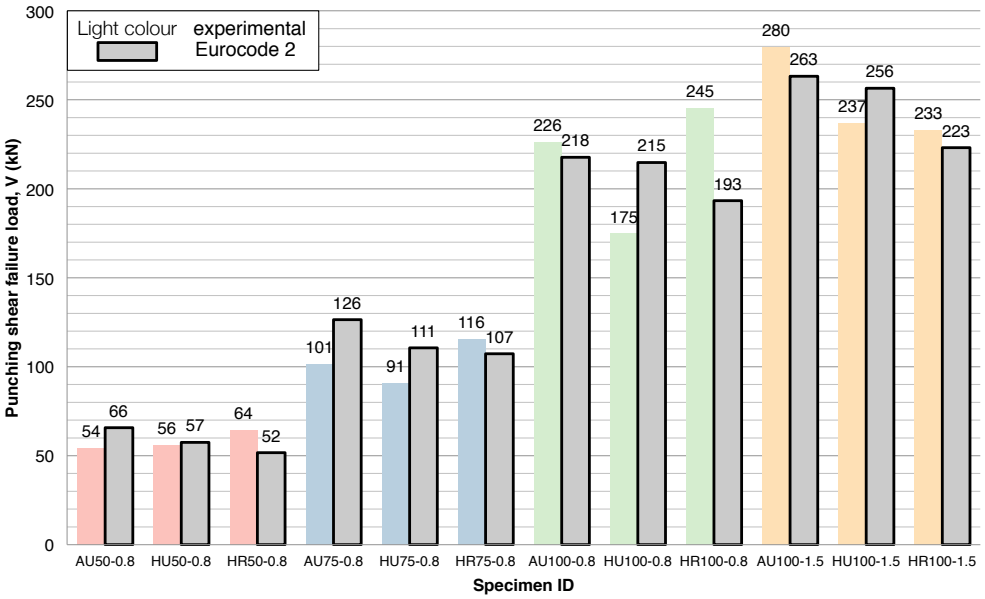

Figure 7.39: Punching shear failure load compared to EC2

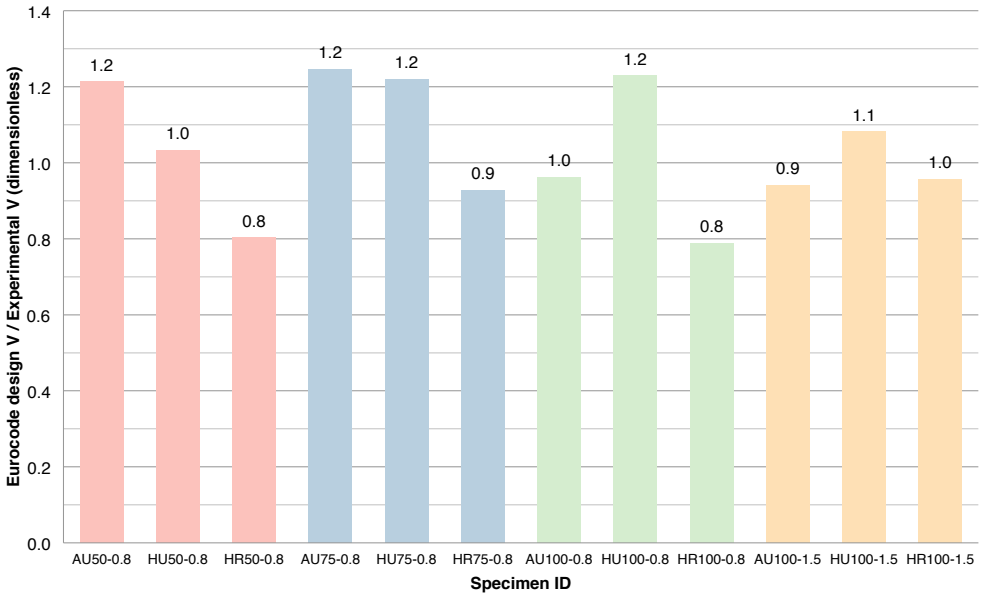

Figure 7.40: Ratio of EC2 design shear capacity to experimental punching shear capacity

The EC2 calculated capacities for the 100 mm thick, unrestrained slabs do not vary greatly between the ambient and elevated temperature conditions in Figure 7.39. This is caused by the heated unrestrained slab-column specimens having failed soon after ignition, therefore the concrete strength is not significantly degraded prior to failure.

Figure 7.40 shows the respective difference between the two support cases when at elevated temperature. The unrestrained are consistently not conservative, whereas the restrained are conservatively predicted by EC2. It is comforting that the restrained supported slabs are conservatively predicted by EC2, as real buildings have supports closer to the restrained case rather than the unrestrained.

Punching shear capacity sensitivity to concrete strength degradation at elevated temperature

EC2 capacities were calculated for both support conditions, with the temperature at the end of the unrestrained and restrained tests. This shows the sensitivity of the punching shear capacity to the concrete strength degradation variable (in the first term of Equation 2.5), which was impacted by propane supply in many of the tests (discussed in Section 7.1.2). The following allows a support condition comparison, though there is no meaning to the quantitative capacities of the:

- heated unrestrained test (HU), calculated with the concrete strength degradation due to temperature at the end of the restrained test (T=R) and
- heated restrained test (HR), calculated with the concrete strength degradation due to temperature at the end of the unrestrained test (T=U)

It is important to note that the strain gauge data, hence in-plane axial force data was recommended to be disregarded. The maximum net average in-plane force from Section 7.1.5, was used here to give the most conservative EC2 design values to compare to the experimental failure load.

Figures 7.41 – 7.44 compares the shear capacities obtained during the experiments with the EC2 predictions. Figures 7.41 – 7.44 show that the support condition (none explicitly considered to impact the second term, σ_{cp} in Equation 2.5) has a small impact on the EC2 punching shear capacity, relative to the variation in concrete strength degradation at elevated temperature. This comparison indicates how the EC2 equation for punching shear capacity lacks in its consideration for whole structural behaviour.

For the EC2 heated unrestrained predictions, the comparison using the restrained concrete strength degradation, to that of the unrestrained, reduces

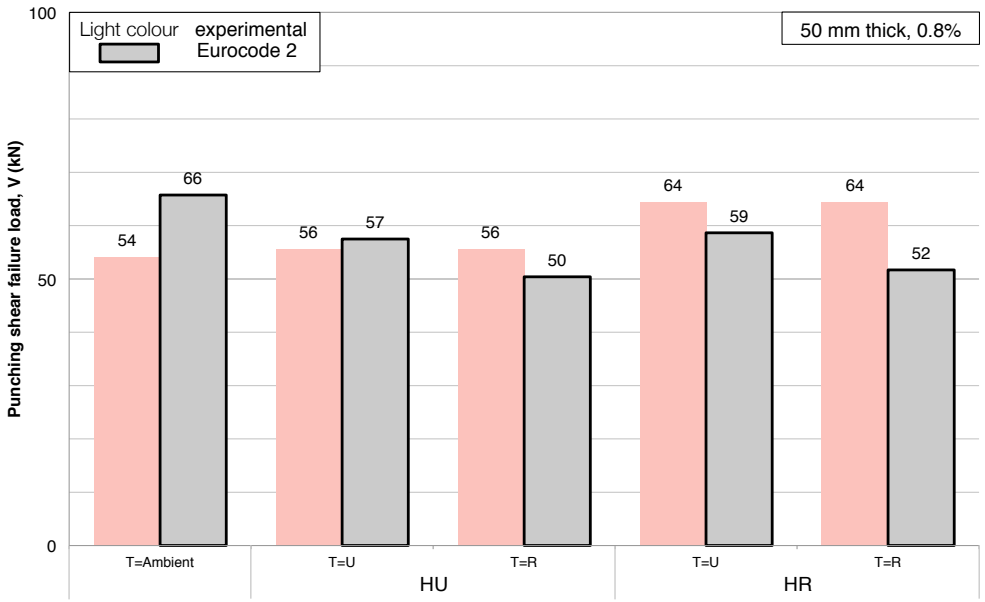

Figure 7.41: EC2 punching shear failure load sensitivity to concrete strength degradation for 50 mm thick, 0.8% reinforced slabs

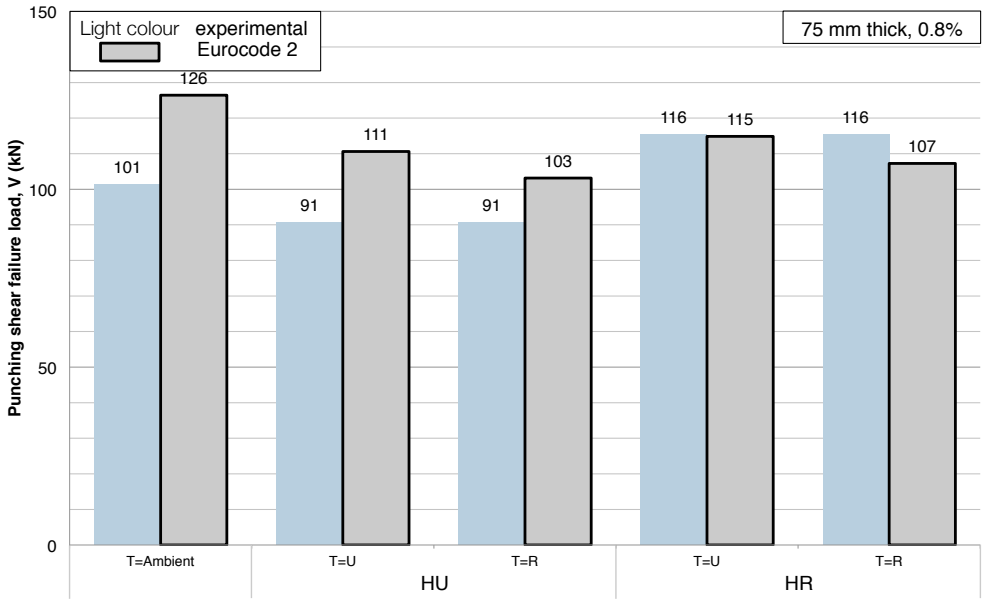

Figure 7.42: EC2 punching shear failure load sensitivity to concrete strength degradation for 75 mm thick, 0.8% reinforced slabs

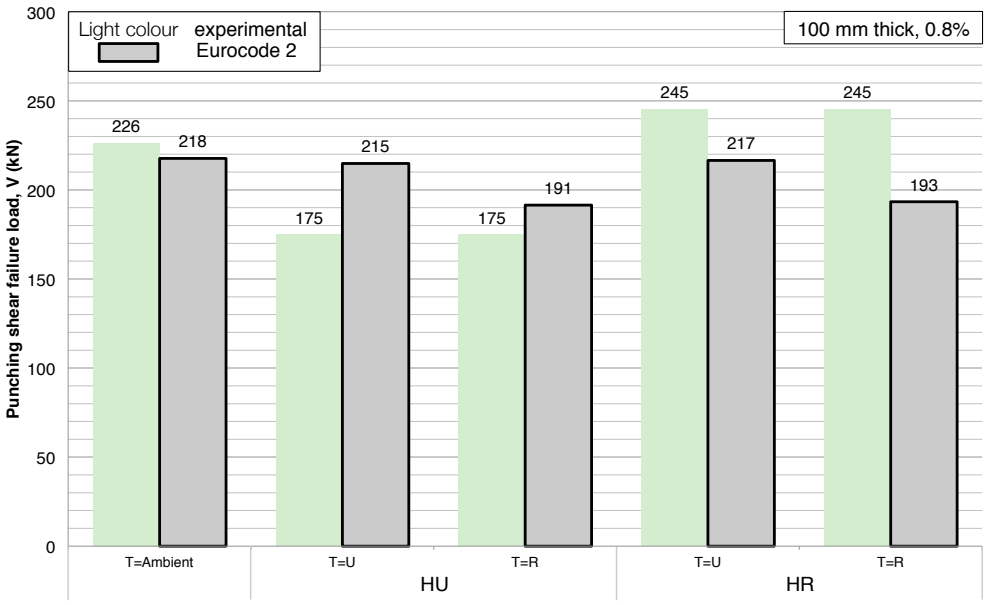

Figure 7.43: EC2 punching shear failure load sensitivity to concrete strength degradation for 100 mm thick, 0.8% reinforced slabs

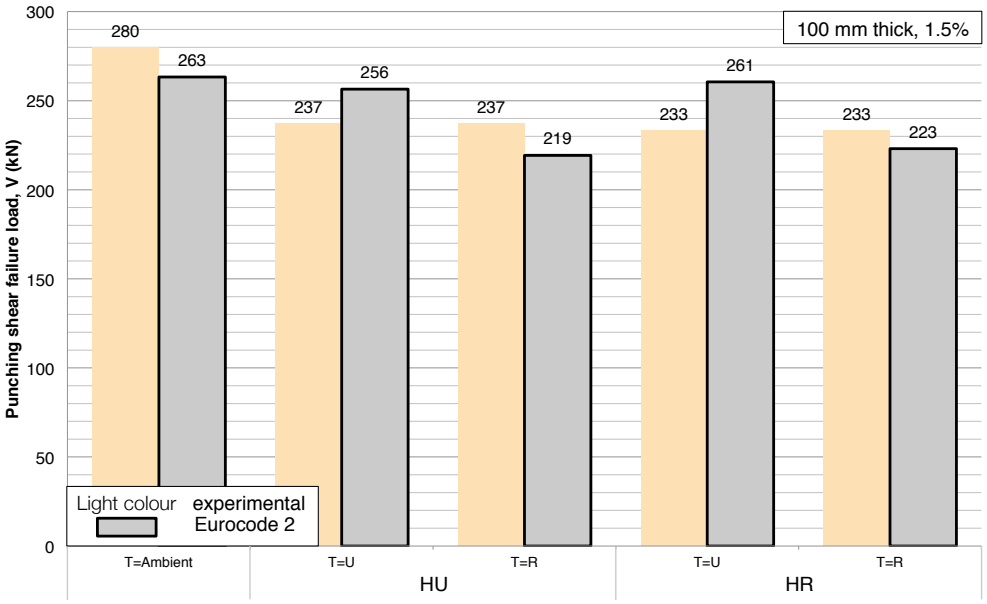

Figure 7.44: EC2 punching shear failure load sensitivity to concrete strength degradation for 100 mm thick, 1.5% reinforced slabs

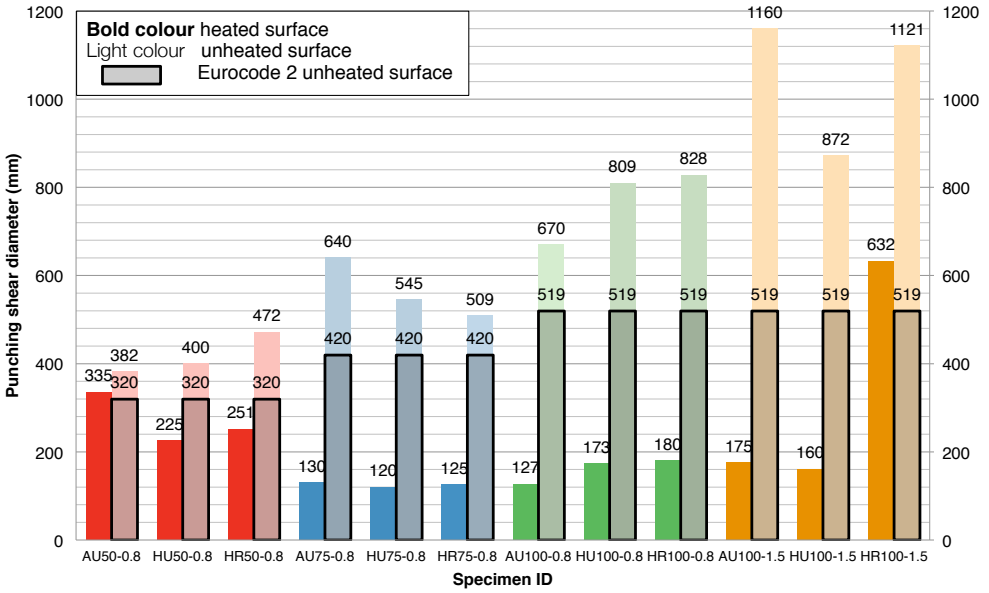

Figure 7.45: Punching shear crack diameter on heated and unheated surfaces compared to EC2

the punching shear capacity (more conservative). This is caused by the concrete temperature degradation in the restrained tests having been high, as they did not fail soon after ignition. Therefore the first term in Equation 2.5 is decreased, causing the punching shear capacity to be less.

Comparing the EC2 heated restrained predictions calculated using the unrestrained concrete strength degradation, to that of the restrained, causes (inversely) the EC2 punching shear capacity to increase (less conservative). The increased punching shear capacity becomes critical compared to the experimental measurements in the most heavily reinforced case (HR100-1.5).

Comparison of shear crack diameter

This section presents a comparison of the experimental punching shear crack diameter to EC2. The affect of the support condition on the punching shear cone is assessed. Figure 7.45 presents the heated and unheated surface punching shear crack diameters of all the slabs. The black outline indicates EC2 ambient design comparisons for the unheated surface shear crack diameter, as shown in Figure 7.38. The unreinforced slabs are not included as they failed in pure flexure.

The experimentally measured average diameters were taken along the profiles at which the slab was cut. This data inherently assumes a perfectly symmetrical failure mode, which was not always applicable as shown with the crack patterns in Chapter 6.

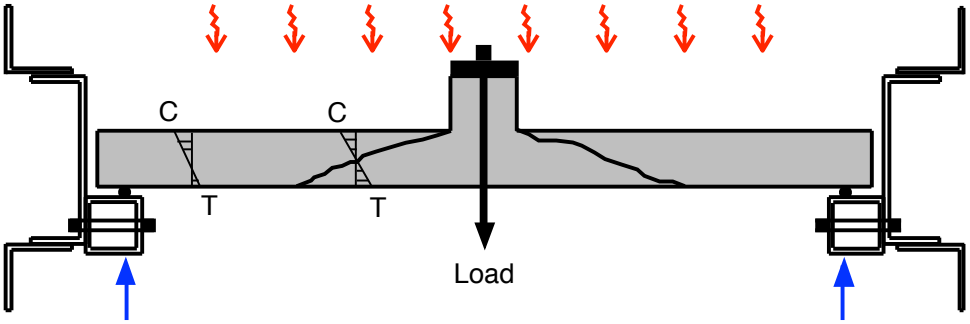

(a) Unrestrained support condition

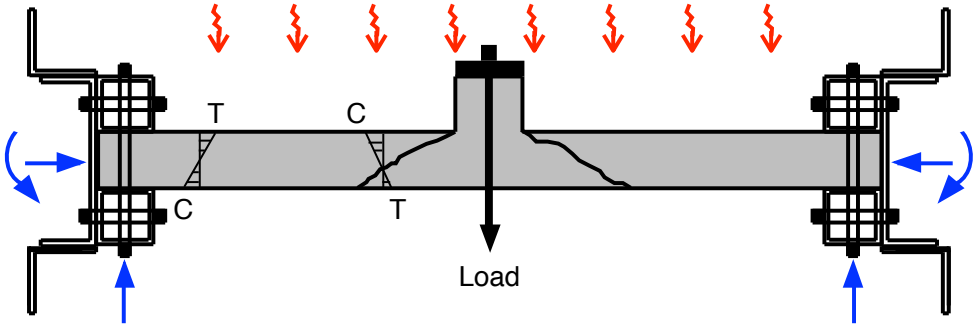

(b) Restrained support condition

Figure 7.46: Theoretical stress profiles in the heated slab-column specimens

The EC2 punching shear diameters are smaller, therefore considering the EC2 design punching shear equation, it is conservative. When comparing all the 0.8% reinforced slabs of thicknesses 50 mm, 75 mm and 100 mm, the punching shear diameter increases with slab thickness, as expected. There is no significant difference in the diameters of the punching shear cones of all the heated 100 mm thick slabs, except for the most heavily reinforced (HR100-1.5), which failed during the cooling phase. The similar punching shear cone diameters indicate that the failure mechanisms are the same, despite different reinforcement ratios.

It was assumed that if compression in-plane forces and bending moments developed in the restrained support case, then the position at which the shear crack formed would be closer to the slab centre. Therefore the shear crack cone would be smaller for the restrained supported slabs, compared to the unrestrained. Figure 7.46b shows the resulting stress profiles in the restrained, heated slab. No clear trend in punching shear diameter with support condition is shown in Figure 7.45.

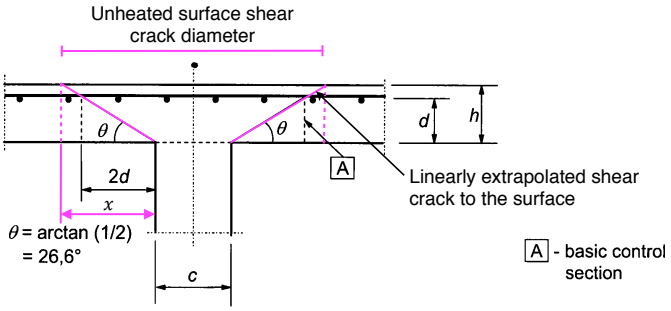

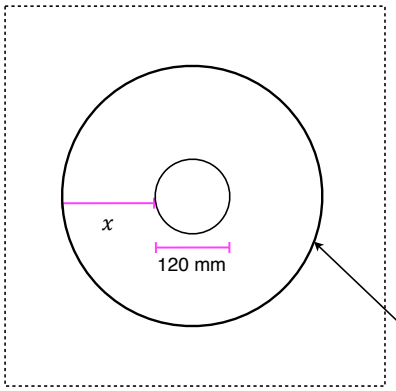

Slab Thickness, h	x	u
(mm)	(mm)	(mm)
50	100	1004
75	150	1318
100	200	1632

Figure 7.47: EC2 ambient circular column, punching shear crack diameter and perimeter, adapted from BS EN 1992-1-1:2004 (2008)

Punching shear capacity sensitivity to shear crack diameter

The experimentally measured punching shear crack diameters in Section 7.3.2 are used to assess the sensitivity of the EC2 punching shear design resistance to the perimeter variable.

The punching shear stress design resistance is calculated using the same method as in Section 7.3.2 and is multiplied by the area over which the stress is applied. The failure is assumed to be circular and symmetrical, therefore the experimentally measured punching shear crack diameter in Figure 7.45, is used to calculate an experimentally derived perimeter. The area over which the stress is applied is defined by the slab thickness and the experimentally derived shear crack perimeter.

The punching shear capacity derived with the experimental perfectly circular shear crack is compared to the EC2 capacity calculated with a similar circular shear crack perimeter, shown in Figure 7.47.

Table 7.7, Table 7.8 and the list of further similar parameters in Section 7.3.2 detail those used in the calculation, with the exception of the punching shear perimeter, u and calculated punching shear capacity, V. Table 7.9 compares the perimeters used to calculate the EC2 punching shear capacity, V.

Figure 7.48 compares the sensitivity of the EC2 punching shear capacity to the unheated surface perimeter variable, showing it as a ratio of the experi-

SPECIMEN SPECIMEN ID	EXPERIMENTAL FAILURE LOAD (KN)	EC2 WITH EXPERIMENTAL SHEAR PERIMETER u (MM)	EC2 WITH EXPERIMENTAL SHEAR PERIMETER V (KN)	EC2 WITH CIRCULAR COLUMN PERIMETER u (MM)	EC2 WITH CIRCULAR COLUMN PERIMETER V (KN)	EC2 WITH SQUARE COLUMN PERIMETER u (MM)	EC2 WITH SQUARE COLUMN PERIMETER V (KN)
AU50-0.8	54.2	1200	71	1004	60	1107	66
AU75-0.8	101.4	2011	179	1318	117	1421	126
AU100-0.8	226.3	2105	264	1632	205	1735	218
AU100-1.5	279.7	3644	553	1632	248	1735	263
HU50-0.8	55.7*	1257	65	1004	52	1107	57
HU75-0.8	90.7*	1712	133	1318	103	1421	111
HU100-0.8	174.8	2542	315	1632	202	1735	215
HU100-1.5	237.0	2793	405	1632	241	1735	256
HR50-0.8	64.4*	1483	69	1004	47	1107	52
HR75-0.8	115.5*	1599	121	1318	99	1421	107
HR100-0.8	245.1*	2601	290	1632	182	1735	193
HR100-1.5	233.2	3522	453	1632	210	1735	223

* RESIDUAL EXPERIMENTAL FAILURE LOADS

Table 7.9: Experimental punching shear loads and EC2 punching shear capacity, calculated with different perimeters

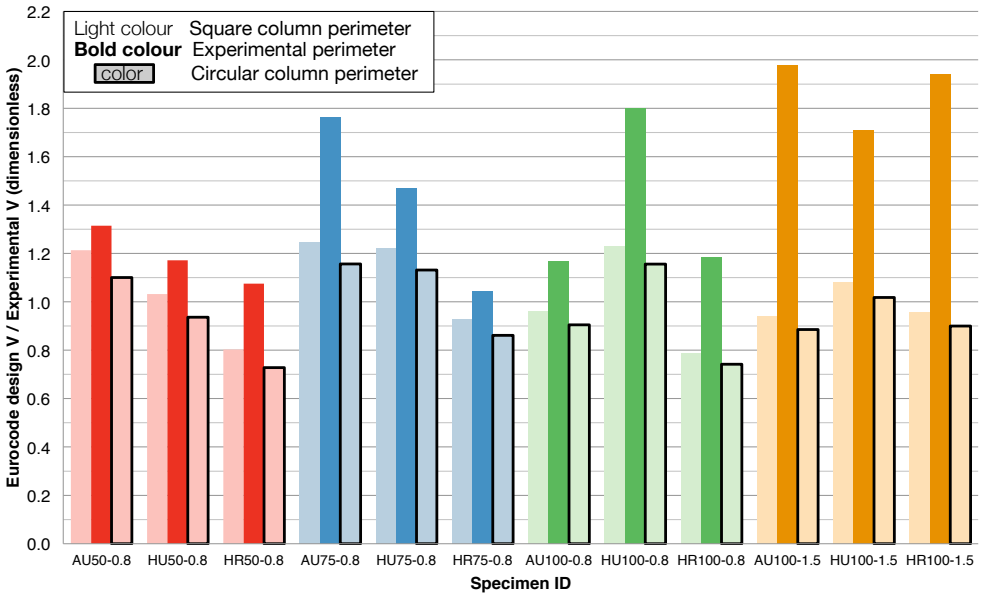

Figure 7.48: Sensitivity of EC2 punching shear capacity to the perimeter variable, as a ratio of the experimental punching shear capacity

mental punching shear capacity. The EC2 punching shear capacity is highly sensitive to the punching shear crack perimeter, showing variations of up to double the capacity with AU100-1.5.

As anticipated, the circular column perimeter is consistently less than the square column perimeter, due to the shorter length over which the shear stress acts. Counter intuitively, both the EC2 punching shear capacities calculated with the square and circular column perimeters agree with the experimental punching shear failure load (shown as 1.0 ratio in Figure 7.48) better than that calculated with the experimentally measured punching shear diameter. This may be caused by the EC2 punching shear capacity equation assuming a fixed crack angle, $\theta = 26.6°$, which experimentally was shown to vary (Section 7.3.2).

Comparison of shear crack angle

Figure 7.49 shows the shear crack angle of all the specimens, on both the N and S frame sides. These angles were measured post-failure, after the specimens were cut through their cross-section. Figure 7.49 shows that the shear crack angle varies between different slab-column specimens, though there is no clear trend. The three 50 mm thick slabs and AU100-0.8 slab, all have large differences between the angles on the two frame sides. The plan failure crack patterns in Chapter 6 showed reasonably symmetrical failure modes. It is therefore assumed that the large differences in crack angle for the thinner 50 mm slabs is caused by measurement error, due to extensive failure cracks and added difficulty in cutting the post-failure, damaged slabs.

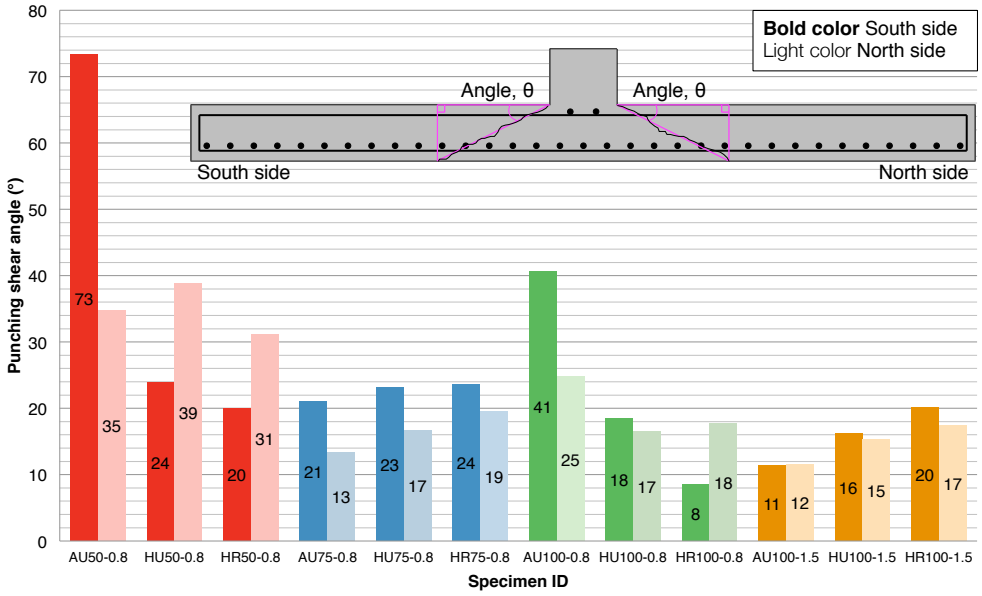

Figure 7.49: Punching shear crack angle on the North and South frame sides

EC2 punching shear design does not consider variable shear crack angles, unlike its consideration of shear in beams.

7.3.3 *Critical Shear Crack Theory (CSCT) ambient and elevated temperature*

This section compares the ambient and elevated temperature experimental punching shear capacity, shear crack diameter and angle results to the Muttoni CSCT. Only unrestrained support condition comparisons are made.

Punching shear capacity

Muttoni (2008) model is based on an unrestrained support condition and a circular slab specimen. The CSCT failure criterion and load-rotation curve for an ambient, unrestrained member are given by Equations 2.1 and 2.2 in Section 2.2.1, respectively (Muttoni, 2008). The punching shear strength is found at the intersection between the CSCT failure criterion and the load-rotation response of the slab.

The load-rotation curve assumes the slab specimens are circular, however Equation 2.2 can be modified for a rectangular specimen. Modification parameters, developed by Guandalini (2005), are used to account for the geometrical difference of the experimentally tested slabs being rectangular in plan rather than circular. Equation 7.1 outline the assumptions made in order to modify the load-rotation response of the slab.

$$r_{a,eq} = \frac{2b}{\pi} \tag{7.1}$$

where:

$r_{a,eq}$ = for this analysis, equal to r_c, which is the radius of an equivalent circular column (mm)

b = column width (mm)

The CSCT variables that are temperature dependant are the concrete characteristic compressive cylinder strength, $f_{c,\theta}$, flexural reinforcement yield strength, $f_{sy,\theta}$ and Young's modulus, $E_{s,\theta}$. The calculated material reduced parameters are presented in Tables 7.5 and 7.6 for concrete and steel, respectively.

Tables 7.10 and 7.11 present the failure criterion and load-rotation response parameters used to calculate the CSCT punching shear capacities, for the unrestrained support condition at ambient and elevated temperatures.

Other variables that were used in Equation 2.2 and Equation 2.3 that were common to all the tests were:

$$\begin{aligned} b &= 120 \text{ mm} \\ r_q &= 655 \text{ mm} \\ r_s &= 700 \text{ mm} \\ r_c &= 76 \text{ mm} \\ d_{g0} &= 16 \text{ mm} \\ d_g &= 10 \text{ mm} \\ \text{width of the slab} &= 1400 \text{ mm} \end{aligned}$$

Figure 7.50 shows the intersecting capacity and load-rotation curves that define the ambient and elevated temperature punching shear capacities. The elevated temperature decreases the steel stiffness, thereby decreasing the shear capacity for equivalent slab rotation angles.

Figure 7.51 compares the CSCT capacities calculated with the unrestrained slab-column experimental values. A comparison to the CSCT shows that it is consistently conservative in comparison to the experimental results. The 100 mm thick specimen comparison shows that the model has large differences when compared to the experimental values. However, these variations are within the scatter shown in Figure 2.23.

SPECIMEN ID	SLAB THICKNESS (MM)	AVERAGE CONCRETE COVER (MM)	REINFORCEMENT DIAMETER (MM)	AVERAGE EFFECTIVE DEPTH (MM)	b_0 (MM)	f_c (MPA)
AU50-0.8	50	9	6	35	590	51.0
AU75-0.8	75	7	6	62	675	51.0
AU100-0.8	100	11	6	83	741	51.0
AU100-1.5	100	11	8	81	734	51.0
HU50-0.8	50	13	6	31	577	30.6
HU75-0.8	75	11	6	58	662	32.1
HU100-0.8	100	13	6	81	734	50.2
HU100-1.5	100	6	8	86	750	48.0

Table 7.10: CSCT failure criterion parameters

SPECIMEN ID	NO. REBARS IN EACH ORIENTATION	ρ	f_y (MPA)	m_R (N)	V_{flex} (KN)	E_s (GPA)
AU50-0.8	12	0.007	550	4,540	34.5	200
AU75-0.8	21	0.007	550	14,100	107	200
AU100-0.8	33	0.008	550	29,500	224	200
AU100-1.5	33	0.015	571	51,100	388	222
HU50-0.8	12	0.008	522	3,730	28.3	165
HU75-0.8	21	0.007	549	12,900	97.8	185
HU100-0.8	33	0.008	549	28,800	219	200
HU100-1.5	33	0.014	571	53,800	409	222

Table 7.11: CSCT load-rotation parameters

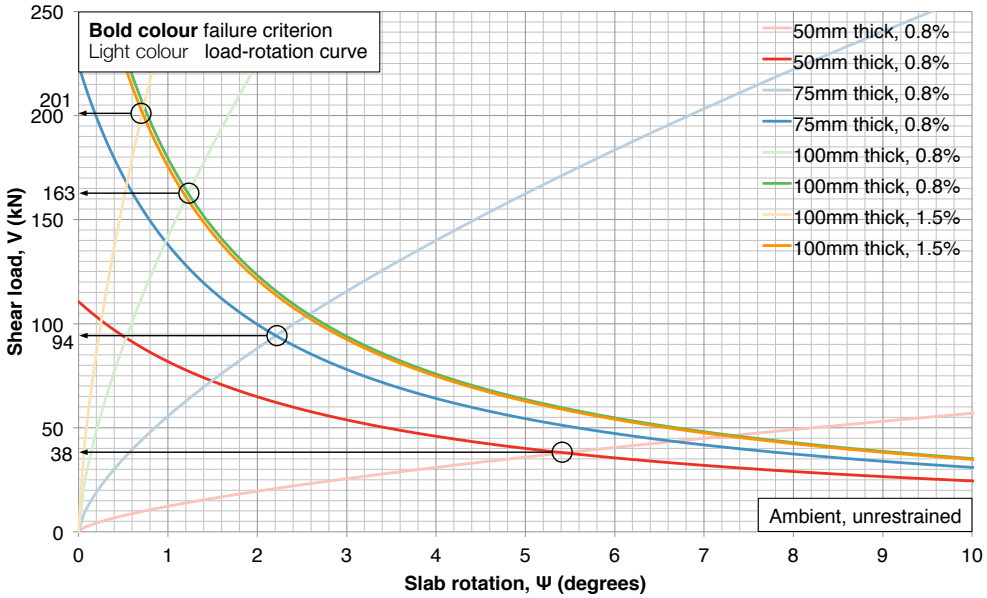

(a) Ambient temperature

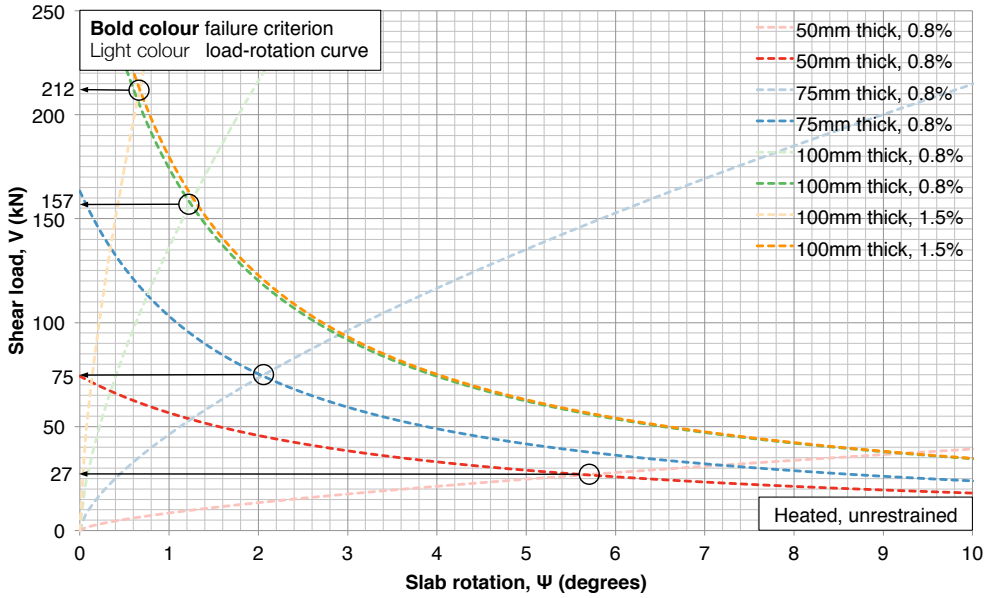

(b) Elevated temperature

Figure 7.50: CSCT punching shear capacity for the unrestrained slab-column parameters

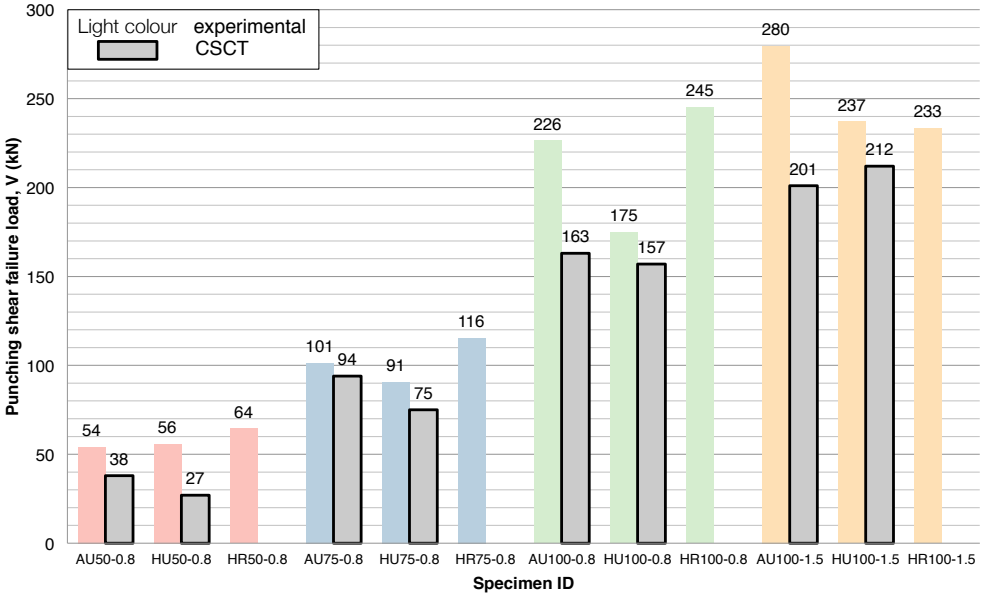

Figure 7.51: Punching shear failure load compared to CSCT

The CSCT has been applied to the heated tests by simply degrading the steel and concrete material properties using the EC2 reduction factors and recorded experimental temperatures. However, this does not consider the restrained thermal stresses and in-plane forces, which require a more detailed re-evaluation of the mechanics in the CSCT at higher temperatures.

Slab rotation

This section compares the experimentally measured slab rotation, found from the DIC vertical displacement slab profiles presented in Section 7.2, to the CSCT slab rotations shown in Section 7.3.3. Figure 7.52 presents the experimental and CSCT predicted punching shear slab rotation angles. Experimental rotations are presented for both the North and South frame sides. Only unrestrained support condition comparisons are made, as in Section 7.3.3.

The DIC slab rotations are measured from the final deflection profile prior to failure, as described in Section 7.2. The experimental heated, unrestrained 50 mm and 75 mm thick slabs are not compared, as they failed residually and the DIC profiles in Figure 7.22 and Figure 7.25, respectively are not representative of the final punching shear slab rotation. Two slab rotations could not be determined from the DIC vertical displacement slab profiles, these included the North and South sides of the 100 mm thick, ambient 0.8% and 1.5%, respectively reinforced slabs.

Though the data set is small, there are some comparison that can be made. Figure 7.52 shows the experimental slab rotations are consistent for the thinner 50 mm and 75 mm slab thicknesses only. The CSCT predicted slab rotations

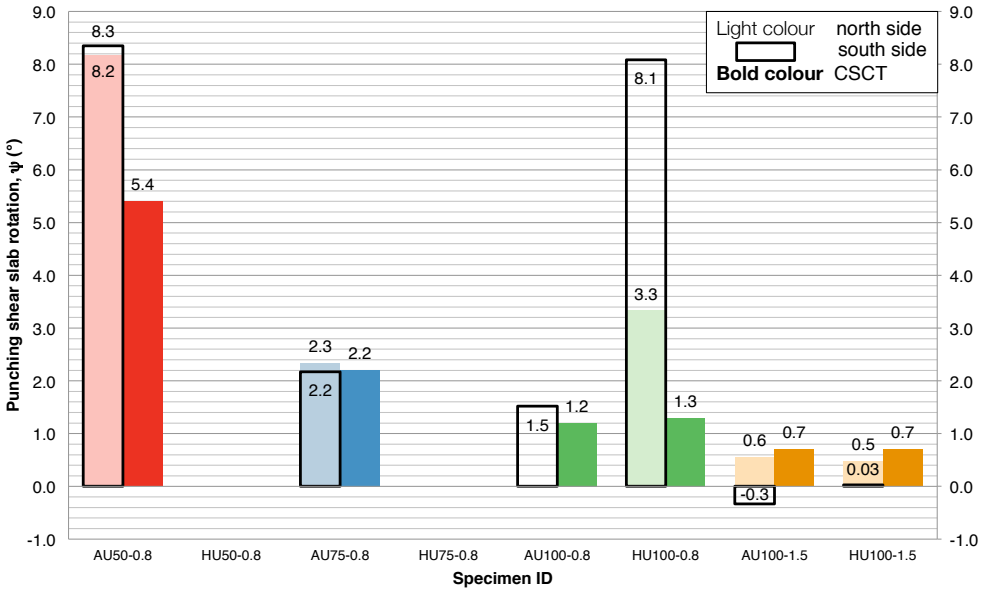

Figure 7.52: Punching shear slab rotation compared to CSCT

are similar to the experimental measurements, with the exception of the 0.8% reinforced, ambient, 50 mm thick and heated, 100 mm thick slabs. The rotations of the heavily 1.5% reinforced slabs are an order of magnitude less than the other slabs.

7.3.4 *Summary*

These bullet points summarise the findings from the experimental punching shear failure compared to both EC2 and CSCT shear design, Section 7.3:

- Comparing EC2 design punching shear capacity to the experimental values, showed EC2 was not conservative for many of the smaller, thinner specimens. This is attributed to the design code not accurately predicting the flexure-shear failure modes that the 50 mm and 75 mm thick specimens demonstrated. Additionally, the formulation of the empirical design equation does not lend itself to the specimen small dimensions, therefore size effect may be an influencing factor.

- The EC2 predicted punching shear capacities of the 50 mm and 75 mm thick, heated slabs do not vary greatly with support condition. The limited variability is attributed to differences in temperature gradient achieved in the unrestrained and restrained tests and the restrained tests having a greater in-plane axial force compared to the unrestrained. These two differences balanced each other out in the EC2 calculation of the capacity, causing there to be limited variability with support condition.

- The EC2 predicted punching shear capacities of the 100 mm thick, unrestrained slab-column specimens do not vary greatly between the ambient and elevated temperature conditions. This is caused by the heated unrestrained specimens having failed soon after ignition, therefore the concrete strength is not significantly degraded prior to failure.
- The slabs that failed in pure punching shear (100 mm thick, reinforced specimens) had similar capacities to those predicted by EC2 design.
- The unrestrained support condition is consistently not conservative, whereas the restrained support condition are conservatively predicted by EC2.
- EC2 punching shear capacity equation is shown to be sensitive to the concrete strength degradation, so much so that the restrained support case for the most heavily reinforced, 100 mm thick slab (HR100-1.5) becomes critical.
- The experimentally measured punching shear diameter increases with slab thickness, though there was no clear trend with support condition.
- The 100 mm thick, heated slabs had similar punching shear cone diameters regardless of the support condition, except for HR100-1.5 which failed on cooling. This indicates that the failure mechanisms are the same and the punching shear capacity does not depend on the shear cone diameter.
- EC2 design punching shear capacity is highly sensitive to the perimeter variable, showing variations of up to double the capacity.
- The shear crack angle is shown to vary between different slab-column specimens, with no clear trend.
- CSCT predicted punching shear capacity is consistently conservative in comparison to the experimental results.
- The CSCT has large capacity variances for the 100 mm thick specimens, which failed in pure punching shear, however these variations are consistent with the original model comparison to data from 99 tests.
- The CSCT predicted slab rotations are similar to the experimental measurements, with the exception of the 0.8% reinforced, ambient, 50 mm thick and heated, 100 mm thick slabs.
- Both the experimental and CSCT predicted heavily 1.5% reinforced slab rotations, which are an order of magnitude less than the other reinforced slabs.

8

CONCLUSIONS AND FURTHER WORK

This thesis has discussed the behaviour of punching shear in RC flat slabs during fire. The implications of punching shear within whole structural behaviour and the broader structural fire engineering discipline have been presented. The fundamental transfer of shear in RC, experimental testing and numerical modelling of punching shear failure at both ambient and elevated temperature have been presented and the role of this research has been placed within the discipline.

Chapter 4 presented the results and analysis of sixteen shear block specimens, four at ambient temperature and twelve tested after being cooled from elevated temperatures. This experimental series have been used to develop an understanding of shear transfer mechanisms and their interactions in RC after being exposed to elevated temperature. These tests were effective in simplifying the shear behaviour, in order to investigate the shear transfer mechanisms. The shear is a two-dimensional shear behaviour. Therefore the pure shear behaviour cannot and have not be directly compared to the three-dimensional punching shear behaviour of the slab-column specimens. The simplified pure shear block tests are representative of the shear behaviour of a column, which may be useful for future researchers.

The results and analysis of fifteen slab-column specimens, five at ambient temperature and ten at elevated temperature, have been used as a means to develop a fundamental understanding of punching shear. This experimental series is the first to test restrained punching shear specimens at elevated temperature and therefore allow a direct support condition (unrestrained vs. restrained), experimental comparison. Previous researchers have shown with modelling techniques the importance of restrained thermal expansion and curvature, caused by restrained support conditions, on the behaviour of punching shear.

This test series increases the current RC punching shear experimental elevated temperature tests by 50%, with 21 previously documented elevated temperature punching shear tests. There have been a total of 51 elevated temperature punching shear tests, where 30 were residual punching shear tests, tested to failure after cooled from elevated temperature to ambient temperature.

The work has touched on the following key points: experimental methodology verification to investigate the whole structural punching shear response un-

der fire conditions, impact of support condition on punching shear behaviour, displacement and cooling behaviour in punching shear testing, current EC2 punching shear design methods are assessed, and the DIC technique has been applied and proven to be reliant in structural fire testing. This final chapter will review the key findings and comment on potential future work.

8.1 EXPERIMENTAL METHODOLOGY VERIFICATION

The fifteen experimental punching shear slab-column tests have been shown to be reliable. The test methodology has been validated and test data error limits have been bounded. The setup yielded flexural (unreinforced slabs), flexure-shear (thinner 50 mm and 75 mm slabs) and punching shear (100 mm reinforced slabs) failure modes, with respective varying parameters. A purpose built reaction frame allowed the three-dimensional punching shear effects of: in-plane actions that result from restrained thermal expansion, large deflection load-carrying mechanisms and degradation of material properties on punching shear in fire to be investigated. This test setup is the first to investigate the whole structural behaviour on punching shear failure, at elevated temperature. Though the support conditions in a real building are unlikely to be at either extreme, the experimental results bound the problem.

Quantitative experimental data are presented, analysed and compared, however the qualitative comparisons are the main research outcomes and have greater value for further research. The quantitative data is impacted by size effect, non-repeatable heating application between tests and jack friction influences on specimens with low capacities. A non-standard fire curve was used, therefore comparisons with other tests are achieved by comparing the temperature distributions from the thermocouple data. The experimental restrained support condition was shown to be not perfectly fixed.

8.2 SUPPORT CONDITION IMPACT

The support condition is shown to have a large impact on the punching shear failure of the 100 mm thick heated slabs. The unrestrained slabs failed soon after heating started, whereas the equivalent restrained slabs endured up to 120 minutes of heating and had a high comparative residual strength. Additionally, the restrained support condition significantly decreased the central vertical displacement.

The punching shear failure of the 100 mm thick reinforced slabs was clearly shown in the failure crack patterns. The critical shear cracks were distinctive and the 100 mm thick slabs had larger shear cones than seen in the thinner

slabs. The restrained, 0.8% reinforced slabs, plan view crack pattern, showed the slab utilised membrane action. The punching shear cone in the heavily reinforced, heated restrained slab was very different compared to all the others. The top and bottom surface crack diameters were larger and the crack propagated along the compression zone further than in all the other tests. This was explained by the slab having failed during the cooling phase, unlike any of the other tests, the slab having the most reinforcement tested and it having a restrained support condition.

8.3 DISPLACEMENT BEHAVIOUR

In all the specimens the central deflection was away from the heat source (in the direction of loading) during the whole test, irrespective of support condition. The unrestrained lightly reinforced heated, 50 mm thick slab (HU50-0.8) and unrestrained, unreinforced heated 100 mm thick slab (HU100-0) were the only specimens which recovered their deflection slightly, by 1 mm during the cooling phase and approximately 0.2 mm during the heating phase, respectively. Similar behaviour was reported by Kordina (1997) in four initial simply supported tests, after 30 minutes of heating.

The test setup was assessed to investigate that the unusual slab-column deflection away from the heat source was not caused by the test setup design. The complex behaviour observed during the tests, cannot currently be explained however. It is assumed that the degradation in concrete properties and non-linear material behaviour dominates over the thermal expansion of the slabs. Further work of a heat transfer analysis may help to evaluate quantitatively what impact the support condition, heating and loading each have on the punching shear behaviour.

8.4 COOLING BEHAVIOUR

This work presents the first recorded punching shear failure during the cooling phase of an elevated temperature test. It may also be the first recorded test specimen ever to have failed during the cooling phase of an elevated temperature test. The heavily reinforced restrained, 100 mm thick heated slab failed on cooling, with temperatures below 150°C throughout its thickness. Cooling behaviour is shown to be important in structural fire testing, however there is currently limited research undertaken to assess the cooling interactions.

Both the vertical displacement and strain gauge data showed a clear behaviour change at the onset of the cooling phase. The central vertical deflection of all the specimens showed a distinctive increase in displacement rate on

initiation of the cooling phase. The sharp increase in deflection rate is consistent with the heated surface cooling down, whilst the heat front propagates deeper into the slab.

8.5 ASSESSMENT OF THE CURRENT PUNCHING SHEAR DESIGN METHODS

8.5.1 *Eurocode 2 design shortcomings*

The current EC2 punching shear prescriptive design is shown to have many shortcomings. The design approach is based on the regression of experimental data available at the time. The ambient punching shear equations are used for elevated temperature, by reducing the temperature-dependant parameters by factors. The reinforcement capacity is not used in the calculation of the punching shear capacity, therefore the reinforcement interaction in carrying shear is not considered by EC2. Most importantly, EC2 design tells the designer not to consider in-plane thermal expansion effects and consequently ignores the premature punching shear failure that can occur.

EC2 performance-based design often utilises modelling techniques, which allow the whole structural interactions to be analysed. However, performance-based design requires a fundamental understanding of the behaviour, which is what this thesis presents for punching shear at elevated temperature.

8.5.2 *Comparison to experimental tests*

EC2 punching shear prescriptive design capacity predictions were similar to those found for the 100 mm thick, reinforced slabs that failed in a pure punching shear mechanism, experimentally. The unrestrained support condition was consistently not conservatively predicted by EC2, whereas the restrained support condition was conservatively predicted by EC2. It is comforting to know that the EC2 design predicts the restrained supported slabs conservatively, as real buildings are more likely to have supports closer to the restrained condition rather than the unrestrained support condition. However, the EC2 punching shear design needs to consider support condition in order to design effectively and safely.

The EC2 variable, σ_{cp} was used to make an experimental comparison for both support conditions, as the boundary reaction forces are not explicitly considered in the EC2 equation. Experimentally, the support condition causes a large difference in behaviour and capacity, but this is not represented in the EC2 capacity equation, even when considering support condition with the

σ_{cp} variable. This direct comparison was masked by the two terms in the EC2 equation. A sensitivity analysis showed the EC2 punching shear capacity equation to be highly sensitive to the concrete strength degradation. When the concrete strength degradation with elevated temperature was considered, the restrained, 100 mm thick 1.5% reinforced heated slab was shown to be critical. The sensitivity analysis indicates that the EC2 equation for punching shear capacity lacks in its consideration for whole structural behaviour.

8.5.3 *Critical Shear Crack Theory punching shear design*

For the experimental test conditions considered, the CSCT was safe in predicting the punching shear capacity. The model had large capacity variances for the 100 mm thick specimens, which failed in pure punching shear, however these variations were consistent with the original model comparison data. The CSCT predicted slab rotations were similar to the experimental measurements, with the exception of the 0.8% reinforced, ambient, 50 mm thick and heated, 100 mm thick slabs. Though Bamonte et al. (2012) expanded the CSCT for elevated temperature, the model requires further validation with experimental restrained thermal expansion tests, in order to make a more compelling elevated temperature comparison. The tests presented in this thesis allow for such a future comparison to be made.

8.6 DIGITAL IMAGE CORRELATION TECHNIQUE FOR STRUCTURAL FIRE TESTING

Finally, the DIC analysis technique yielded repeatable and reliable results in comparison to the two traditional linear potentiometer readings. The linear potentiometer readings were unexpectedly impacted by either local concrete crushing around the column stub, extension of the loading rod due to the elevated temperature and tension loading or reaction frame movement. As with any measurement technique, the associated application specific errors need to be addressed. Further advantages of the DIC technique for this experimental testing included;

- post-processing of test photo stream, therefore regions of interest could be chosen after testing is complete;
- change in curvature was visualised during testing, which allow the points of inflection to be found; and
- angle of slab rotation and formation of cracks during testing were shown.

8.7 FURTHER WORK

Various factors impact the complex punching shear behaviour of the slab-column specimens, which make it difficult to separate and quantify the impact of each. The non-repeatable heating application between tests impact direct comparisons. Further inverse heat transfer modelling would allow direct comparison of the temperature through the slabs at comparative depths. This may yield further understanding of the quantitative impact, that the support condition, loading and heating each have on the punching shear strength.

These tests have presented what may be the first punching shear failure during the cooling phase of an elevated temperature test. Furthermore, the vertical displacement rate showed a clear increase at the onset of cooling. These results shows that the cooling behaviour after an elevated temperature test is important. Further research into the cooling behaviour of RC members needs to be undertaken, in order to understand the fundamental cooling interactions.

The elevated temperature punching shear tests undertaken in this thesis allow for future comparison to Bamonte et al. (2012) expanded elevated temperature CSCT. Furthermore the test results from the restrained supported slab-column specimens may be used to compare to the model also.

Further post-processing of the test photo streams, using DIC may allow more detailed analysis of the slab points of inflection and crack locations. Crack width analysis may also be undertaken with DIC.

Adrian, R. (1991). Particle-imaging techniques for experimental fluid mechanics. *Annual Review of Fluid Mechanics*, 23(1):261–304.

Alam, J., Amanat, K. M., and Seraj, S. M. (2009). An experimental study on punching shear behavior of concrete slabs. *Advances in Structural Engineering*, 12(2):257–265.

Alexander, S. and Simmonds, S. H. (1992). Tests of column-flat plate connections. *ACI Structural Journal*, 89(5):495–502.

Anderberg, Y., Forsén, N. E., Hietanen, T., Izquierdo, J. M., Le Duff, A., Richter, E., Whittle, R. T., Bossenmayer, H., Litzner, H.-U., and Kruppa, J. (2004). Background documents to EN 1992-1-2. Technical report.

Anis, N. N. (1970). *Shear strength of reinforced concrete flat slabs without shear reinforcement*. PhD thesis, Imperial College London.

Annerel, E., Lu, L., and Taerwe, L. (2011a). Analysis of Punching Shear at High Temperatures. In *International Workshop Fire and Explosion Safety in Large Car Parks, 30 May 2011, Ghent Belgium*, page 56.

Annerel, E., Lu, L., and Taerwe, L. (2011b). Punching shear tests on flat concrete slabs at high temperatures. In *2nd International RILEM Workshop on Concrete Spalling due to Fire Exposure. 5-7 October 2011, Delft, The Netherlands*.

Annerel, E., Lu, L., and Taerwe, L. (2012). Punching shear tests on flat concrete slabs exposed to fire. *Fire Safety Journal*, 57:83–95.

Annerel, E., Taerwe, L., Merci, B., D, J., Bamonte, P., and Felicetti, R. (2013). Thermo-mechanical analysis of an underground car park structure exposed to fire. *Fire Safety Journal*, 57:96–106.

Bailey, C. and Khoury, G. (2011). *Performance of Concrete Structures in Fire*. An in-depth publication on the bahaviour of concrete in fire. The Concrete Centre.

Bamonte, P. (2011). Punching shear of R/C slabs in fire conditions. In *University of Edinburgh Lunchtime Seminar, 16 August 2011*, page 47.

Bamonte, P. and Felicetti, R. (2009). Fire scenario and structural behaviour of underground parking lots exposed to fire. *Applications of Structural Fire Engineering, Proceedings, Prague*, pages 60–65.

Bamonte, P., Felicetti, R., and Gambarova, P. (2009). Punching shear in fire-damaged reinforced concrete slabs. *American Concrete Institute*, 265:345–366.

Bamonte, P., Fernández Ruiz, M., and Muttoni, A. (2012). Punching shear strength of R/C slabs subjected to fire. In *7th International Conference on Structures in Fire, Zurich, Switzerland, June 6-8, 2012.*, pages 689–698.

Bath, I. (2013). Punching shear at elevated temperatures. Master's thesis, The University of Edinburgh.

Batson, A. (2013). How does fire affect concrete in shear? Master's thesis, The University of Edinburgh.

Bažant, Z. and Cao, Z. (1987). Size effect in punching shear failure of slabs. *ACI Structural Journal*, 84(1):44–53.

Bisby, L. and Take, W. (2009). Strain localisations in FRP-confined concrete: new insights. *Proceedings of the ICE-Structures and Buildings*, 162(5):301–309.

Bisby, L., Take, W. A., and Caspary, A. (2007). Quantifying strain variation in FRP confined concrete using digital image correlation: proof-of-concept and initial results. In *Asia-Pacific Conference on FRP in Structures (APFIS 2007)*, pages 599–604, Hong Kong, China.

BS EN 12390-3:2002 (2009). *Testing hardened concrete, Part 3: Compressive strength of test specimens.* European Committee for Standardisation.

BS EN 12390-6:2000 (2004). *Testing hardened concrete, Part 6: Tensile splitting strength of test specimens.* European Committee for Standardisation.

BS EN 1992-1-1:2004 (2008). *Eurocode 2: Design of concrete structures, Part 1-1: General rules and rules for buildings.* European Committee for Standardisation.

BS EN 1992-1-2:2004 (2010). *Eurocode 2: Design of concrete structures, Part 1-2: General rules-Structural fire design.* European Committee for Standardisation.

Collins, M., Mitchell, D., Adebar, P., and Vecchio, F. (1996). A general shear design method. *ACI Structural Journal*, 93(1):36–45.

Diederichs, U. and Schneider, U. (1981). Bond strength at high temperatures. *Magazine of Concrete Research*, 33(115):75–84.

Duncryne (2014). Econicboard.

El-Hawary, M., Ragab, A., El-Azim, A., and Elibiari, S. (1997). Effect of fire on shear behaviour of RC beams. *Computers & Structures*, 65(2):281–287.

Ellingwood, B. and Lin, T. (1991). Flexure and shear behavior of concrete beams during fires. *Journal of Structural Engineering*, 117(2):440–458.

Elstner, R. C. and Hognestad, E. (1956). Shearing strength of reinforced concrete slabs. *Journal Proceedings of the American Concrete Institute*, 53(7):29–58.

Enerpac (2014). High pressure hydraulic tools & equipment.

Felicetti, R. and Gambarova, P. (2000). On the residual behaviour of HPC slabs subjected to high temperature. In *PCI/FHWA/FIB International Symposium on High-Performance Concrete, Orlando, FL (USA), September 2000*, pages 598–607.

Fenwick, R. C. and Paulay, T. (1968). Mechanisms of shear resistance of concrete beams. *Proceedings of the American Society of Civil Engineers*, 94(10):2325–2350.

Ferguson, P. (1966). Bond stress - the state of the art. *ACI Journal Proceedings*, 63(11):1161–1190.

Fernández Ruiz, M. and Muttoni, A. (2010). Performance and design of punching shear reinforcing systems. In *3rd fib International Congress - 2010, Washington DC, USA*.

Fox, D. (2013). *The fire performance of restrained polymer-fibre-reinforced concrete composite slabs*. PhD thesis, The University of Edinburgh.

Gales, J. A., Bisby, L., and Stratford, T. (2012). New parameters to describe high-temperature deformation of prestressing steel determined using digital image correlation. *Structural Engineering International*, 22(4):476–486.

Gardner, N. (1990). Relationship of the punching shear capacity of reinforced concrete slabs with concrete strength. *ACI Structural Journal*, 87(1):66–71.

Ghoreishi, M., Bagchi, A., and Sultan, M. A. (2013). Review of the punching shear behavior of concrete flat slabs in ambient and elevated temperature. *Journal of Structural Fire Engineering*, 4(4):259–279.

Ghoreishi, M., Bagchi, A., and Sultan, M. A. (2015). Experimental investigation of concrete flat slabs in elevated temperature. In *5th International Workshop on Performance, Protection & Strengthening of Structures under Extreme Loading, 28-30 June 2015, East Lansing, Michigan*.

Grauers, K., Cederwall, K., and Gylltoft, K. (1994). Anchorage and shear in concrete structures exposed to fire - a literature reveiw, BRANDFORSK - project M.53. Technical report, Swedish National Testing and Research Institute, SP Report 1994:02.

Guandalini, S. (2005). *Poinçonnement symétrique des dalles en béton armé*. PhD thesis, Ecole Polytechnique Fédérale de Lausanne.

Guandalini, S., Burdet, O., and Muttoni, A. (2009). Punching tests of slabs with low reinforcement ratios. *ACI Structural Journal*, 106(10):87–95.

Hamadi, Y. and Regan, P. (1980). Behaviour in shear of beams with flexural cracks. *Magazine of Concrete Research*, 32(111):67–78.

Hawkins, N., Bao, A., and Yamazaki, J. (1989). Moment transfer from concrete slabs to columns. *ACI Structural Journal*, 86(6):705–716.

Hertz, K. (1982). The anchorage capacity of reinforcing bars at normal and high temperatures. *Magazine of Concrete Research*, 34(121):213–220.

Hillerborg, A., Modéer, M., and Petersson, P.-E. (1976). Analysis of crack formation and crack growth in concrete by means of fracture mechanics and finite elements. *Cement and Concrete Research*, 6(6):773–781.

Hofbeck, J., Ibrahim, I., and Mattock, A. (1969). Shear transfer in reinforced concrete. *ACI Journal Proceedings*, 66(2):119–128.

Kani, G. (1964). The riddle of shear failure and its solution. *Journal of the ACI*, 61(4):441–467.

Khan, M., Prasad, J., and Abbas, H. (2010). Shear strength of RC beams subjected to cyclic thermal loading. *Construction and Building Materials*, 24(10):1869–1877.

Khan, M. R. and Royles, R. (1986). Post heat exposure behaviour of reinforced concrete beams. *Magazine of Concrete Research*, 38(135):59–66.

Khoury, G. (2000). Effect of fire on concrete and concrete structures. *Progress in Structural Engineering and Materials*, 2(4):429–447.

Kim, W. and White, R. (1991). Initiation of shear cracking in reinforced concrete beams with no web reinforcement. *ACI Structural Journal*, 88(3).

Kordina, K. (1997). *Über das Brandverhalten punktgestützter Stahlbetonplatten (On the Fire Behaviour of Reinforced Concrete Flat Slabs)*. Deutscher Ausschuss für Stahlbeton (DAfStb).

Kotsovos, M. (1983). Mechanisms of 'shear' failure. *Magazine of Concrete Research*, 35(123):99–106.

Kotsovos, M. (1988). Compressive force path concept: basis for reinforced concrete ultimate limit state design. *ACI Structural Journal*, 85(1):68–75.

Kotsovos, M. and Pavlović, M. (1999). *Ultimate limit-state design of concrete structures: A new approach*. Thomas Telford.

Kuang, J. and Morley, C. (1993). Punching shear behaviour of restrained reinforced concrete slabs. *ACI Structural Journal*, 89(1):13–19.

Law, A. and Gillie, M. (2008). Load induced thermal strain: implications for structural behaviour. In *Structures in Fire: Proceedings of the Fifth International Conference*, pages 448–496.

Li, Y. and Franssen, J. (2011). Test results and model for the residual compressive strength of concrete after a fire. *Journal of Structural Fire Engineering*, 2(1):29–44.

Lips, S., Fernández Ruiz, M., and Muttoni, A. (2012). Experimental investigation on punching strength and deformation capacity of shear-reinforced slabs. *ACI Structural Journal*, 109(6):889–900.

Long, A. E. and Bond, D. (1967). Punching failure of reinforced concrete slabs. *Proceedings of the Institute of Civil Engineers*, 37(1):109–135.

Masterson, D. M. and Long, A. E. (1974). The punching strength of slabs, a flexural approach using finite elements. *American Concrete Institute Special Publication*, 42:747–768.

Mattock, A. and Hawkins, N. (1972). Shear transfer in reinforced concrete—recent research. *PCI Journal*, 17(2):55–75.

Mattock, A., Johal, L., and Chow, H. C. (1975). Shear transfer in reinforced concrete with moment or tension acting across the shear plane. *Journal of the Precast/Prestressed Concrete Institute*, 20(4):76–93.

Millard, S. and Johnson, R. (1984). Shear transfer across cracks in reinforced concrete due to aggregate interlock and to dowel action. *Magazine of Concrete Research*, 36(126):9–21.

Millard, S. and Johnson, R. (1985). Shear transfer in cracked reinforced concrete. *Magazine of Concrete Research*, 37(130):3–15.

Mitchell, D. and Collins, M. (1974). Diagonal compression field theory - a rational model for structural concrete in pure torsion. *ACI Journal Proceedings*, 71(8):396–408.

Moe, J. (1961). Shearing strength of reinforced concrete slabs and footings under concentrated loads. Technical report, Portland Cement Association-Research and Development Laboratories.

Mohamed Ali, M. S., Oehlers, D., and Griffith, M. (2008). Shear transfer across cracks in FRP strengthened RC members. *Journal of Composites for Construction*, 12(4):416–424.

Morley, P. and Royles, R. (1980). The influence of high-temperature on the bond in reinforced-concrete. *Fire Safety Journal*, 2(4):243–255.

Morley, P. and Royles, R. (1983). Response of the bond in reinforced-concrete to high-temperatures. *Magazine of Concrete Research*, 35(123):67–74.

Mörsch, E. (1909). *Concrete-Steel Construction*. The Engineering News Publishing Company.

Muttoni, A. (2008). Punching shear strength of reinforced concrete slabs without transverse reinforcement. *ACI Structural Journal*, 105(4):440–450.

Muttoni, A. and Fernández Ruiz, M. (2008). Shear strength in one-and two-way slabs according to the critical shear crack theory. *fib*, pages 559–563.

Muttoni, A., Fürst, A., and Hunkeler, F. (2005). Deckeneinsturz der tiefgarage am Staldenacker in Gretzenbach, Gutachten zur einsturzursache.

National Annex to BS EN 1992-1-1:2004 (2009). *UK National Annex to Eurocode 2: Design of concrete structures - Part 1-1: General rules and rules for buildings*. European Committee for Standardisation.

Naus, D. (2005). The Effect of Elevated Temperature on Concrete Materials and Structures - A Literature Review, (Milestone 2.4). Technical report, Oak Ridge National Laboratory.

Neves, I., Rodrigues, J., and Loureiro, A. (1996). Mechanical properties of reinforcing and prestressing steels after heating. *Journal of Materials in Civil Engineering*, 8(4):189–194.

Nielsen, M., Braestrup, M., and Bach, F. (1978). Rational analysis of shear in reinforced concrete beams. In *IABSE Proceedings*, volume 15, pages 1–16.

Rankin, G. I. and Long, A. E. (1987). Predicting the punching strength of conventional slab-column specimens. *Proceedings of the Institution of Civil Engineers. Part 1, Design and Construction.*, 82(2):327–346.

Regan, P. (1986). Symmetric punching of reinforced concrete slabs. *Magazine of Concrete Research*, 38(136):115–128.

Regan, P. (1993). Research on shear: a benefit to humanity or a waste of time? *The Structural Engineer*, 71:337–347.

Reineck, K. (2001). Punching of structural concrete slabs. Technical report, FIB - Fédération Internationale du Béton.

Ritter, W. (1899). Die Bauweise Hennebique (Hennebiques Construction Method). *Schweizerische Bauzeitung*, 33(7).

Robertson, A. F. (1982). Development of an improved radiant heat source for fire testing. *Fire and Materials*, 6(2):68–71.

Sagaseta, J. and Vollum, R. J. (2011). Influence of aggregate fracture on shear transfer through cracks in reinforced concrete. *Magazine of Concrete Research*, 63(2):119–137.

Salem, H., Issa, H., Gheith, H., and Farahat, A. (2012). Punching shear strength of reinforced concrete flat slabs subjected to fire on their tension sides. *Housing and Building National Research Center Journal*, 8(1):36–46.

SiG (2013). Ceraboard 100.

Sigrist, V. (2010). Shear and punching shear in RC and FRC elements. Technical report, Salò, Italy.

Smith, H. (2010). Using digital imagery to understand concrete in shear. Master's thesis, The University of Edinburgh.

Smith, H., Reid, E., Beatty, A. A., Stratford, T., and Bisby, L. (2011). Shear strength of concrete at elevated temperature. In *Applications of Structural Fire Engineering, Proceedings, Prague, Czech Republic, 29th April 2011.*, pages 133–138.

Stratford, T. (2001). *The Shear of Concrete with Elastic FRP Reinforcement.* PhD thesis, Jesus College, University of Cambridge.

Stratford, T. (2007). Behaviour and design of structures 3 lecture notes. *Miscellaneous*, pages Lectures 1–3.

Stratford, T. and Burgoyne, C. (2003). Shear analysis of concrete with brittle reinforcement. *Journal of Composites for Construction*, 7(4):323–330.

Taylor, R. and Hayes, B. (1965). Some tests on the effect of edge restraint on punching shear in reinforced concrete slabs. *Magazine of Concrete Research*, 17(50):39–44.

Tepfers, R. (1979). Cracking of concrete cover along anchored deformed reinforcing bars. *Magazine of Concrete Research*, 31(106):3–12.

Tepfers, R. (2000). Bond of reinforcement in concrete. Technical report, FIB - Fédération Internationale du Béton.

Vecchio, F. and Collins, M. (1986). The modified compression-field theory for reinforced concrete elements subjected to shear. *ACI Journal*, 83(2):219–231.

VITCAS (2011). Thermal ropes, tapes and adhesives.

Walraven, J. (1981). Fundamental analysis of aggregate interlock. *ASCE Journal of Structural Engineering*, 107(11):2245–2270.

White, D. and Take, W. (2005a). Discussion on "Application of particle image velocimetry (PIV) in centrifuge testing of uniform clay". *International Journal of Physical Modelling in Geotechnics*, 4:27–31.

White, D. and Take, W. (2005b). *GeoPIV 8.01 - Particle Image Velocimetry Software*.

White, D., Take, W., and Bolton, M. (2003a). Discussion of "Accuracy of Digital Image Correlation for Measuring Deformations in Transparent Media" by Samer Sadek, Magued G. Iskander, and Jinyuan Liu. *Journal of Computing in Civil Engineering ASCE*, pages 217–222.

White, D., Take, W., and Bolton, M. (2003b). Soil deformation measurement using particle image velocimetry (PIV) and photogrammetry. *Géotechnique*, 53(7):619–631.

A

HEALTH AND SAFETY CONSIDERATIONS

Safe System of Work
Residual Shear Block Testing

Overview

The aim of these tests is to investigate shear residual mechanisms and their interactions in reinforced concrete after cooled from high temperatures.

The concrete shear block specimens are 100×160×320 mm, and are supported by steel loading plates. The blocks will be heated in an annealing oven and left to cool to room temperature prior to testing. The blocks will be tested to failure in pure shear, by a load applied to the loading plates by the Avery 7104 test machine. Displacement will be measured by a single displacement gauge and two DSLR cameras (for DIC). One thermocouple each will measure the internal concrete and internal oven temperature during heating.

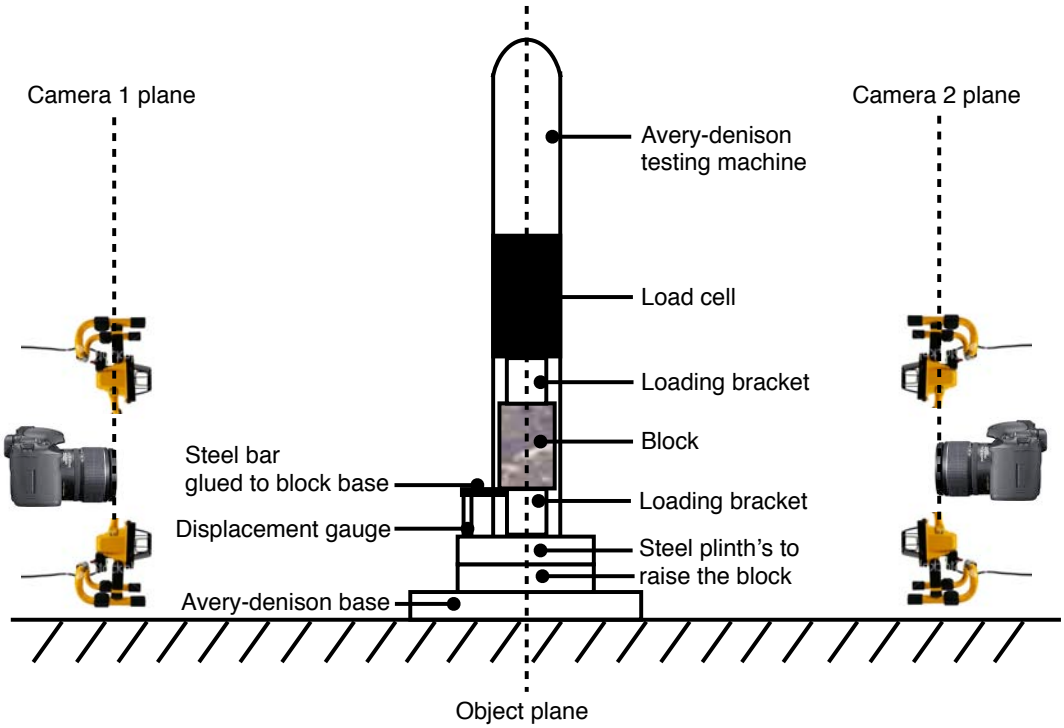

Key Watchpoints

- Heavy test specimens.
- Heated test specimens.
- Large applied forces; potential sudden failure of test specimen.
- Trip hazards such as trailing cables.

This document is intended for use by the University *of* Edinburgh staff and students only
The University of Edinburgh is a charitable body, registered in Scotland, with registration number SC005336

Required PPE

Safety boots and glasses are required at all times. Riggers gloves are required when handling materials. A hard hat is required when working underneath items, and during testing.

Specimen Fabrication

1. **Assembling formwork and reinforcement cages.** This requires the formwork to be drilled and screwed together. The steel reinforcement requires cutting with a circular saw and shear stirrups require bent into shape using a jig and cantilever bending tool. Take care when cutting, use protective clothing on arms, gloves and safety googles.

2. **Casting shear blocks and cube and cylinder specimens.** This requires a concrete slump test, formwork and moulds to be filled with ready-mix concrete. Tamping rods and electric vibrator will be used to compact the specimens. Take care when working with concrete as it is a eye and skin irritant, see separate SSW for Making standard cube and cylinder specimens, Vibratory poker and Emptying cube and cylinder moulds. Dust masks must be worn and skin covered. Take special care in lifting heavy objects.

Test

3. **Heat and cool specimens** in the annealing oven. Take care not to injure back or drop specimens onto toes when inserting and removing them from the oven. Wear heat protective gloves when removing items from the oven.

4. **Lift specimen into place.** Lift specimens with bent knees to protect back.

5. **Position displacement gauges**. LP displacement gauges will be positioned under the block, out of view of the cameras.

6. **Position DIC cameras and lights**. Check that the cameras are not in danger due to failure of the block or overheating from the lights. Route power supply and timing cables to avoid trip hazards.

7. **Test cube and cylinder specimens** to determine strength using Avery 7104 test machine (refer to separate SSW).

During Testing

8. **Inform other lab users** that a test is about to take place, and ensure everyone is wearing the necessary PPE (safety boots, eye protection, hard hats, lab coat and gloves).

This document is intended for use by the University *of* Edinburgh staff and students only
The University of Edinburgh is a charitable body, registered in Scotland, with registration number SC005336

9. **Start the camera systems recording**.

10. **Apply load** until failure

11. **Monitor test progress.** Monitor the load, and deflection of the block during the test. Keep notes of significant test events (such as cracking) so that they can be cross-referenced to the test data. When it appears that failure is about to occur, all observers must be told to keep clear.

12. **After block failure,** unload the specimen. Turn off Avery 7104 and cameras. Back up data to a safe place as soon as is practicable.

After Testing

13. **Remove cameras, displacement gauges, and loading plates.**

14. **Closely inspect the block** on both sides and photograph cracks and deflection, taking care to identify location and orientation (using arrow on the concrete) of the photographs.

15. **Clean the Avery 7104 and surrounding area of the lab.**

16. **Return lab equipment to the cupboards.**

17. **Specimen storage and disposal.** All specimens will be stored in the basement laboratory of the William Rankine Building until individual blocks are tested in the structures laboratory. Specimens will be disposed in the skip outside the structures laboratory.

Prepared by

Researcher: Holly Smith (PhD Student)	
Signature:	Date:

Approved by

PhD Supervisor: Tim Stratford	
Signature:	Date:

Lab Manager: Tim Stratford	
Signature:	Date:

This document is intended for use by the University *of* Edinburgh staff and students only
The University of Edinburgh is a charitable body, registered in Scotland, with registration number SC005336

General Risk Assessment

Form RA1

(Refer to Notes for Guidance before completing this form)

School Assessment No:	NA
Title of Activity:	Residual Reinforced-Concrete Shear Block Testing
Location(s) of Work:	Structures Laboratory, The University of Edinburgh, The King's Buildings, Mayfield Road, Edinburgh, EH9 3JL
Brief Description of Work: Small reinforced concrete specimens (100×160×320mm) will be constructed and then subjected to elevated temperature in the annealing oven in the structures laboratory. Once cooled, the specimens will be tested to failure in the Avery loading machine.	

Hazard Identification: Identify all the hazards; evaluate the risks (low / medium / high); describe all existing control measures and identify any further measures required. Specific hazards should be assessed on a separate risk assessment form and cross-referenced with this document. Specific assessments are available for hazardous substances, biological agents, display screen equipment, manual handling operations and fieldwork. See http://www.ed.ac.uk/schools-departments/health-safety/risk-assessments-checklists/risk-assessments for details.

Hazard(s)	**Present Risk** **Evaluation** L/M/H	**Control Measures** (i.e., alternative work methods / mechanical aids / engineering controls, etc.)	**Risk** **Evaluation after control** L/M/H
FABRICATION			
Tying steel reinforcement together with wire	M - fingers or hands cut from wire, steel or wire cutters - wire offcuts could damage eyes	- wear riggers gloves - ensure exposed skin covered - wear safety glasses	L
Readymix concrete cast specimens and	M - wet concrete is a skin, respiratory system	- wear impermeable gloves	

This document is intended for use by the University *of* Edinburgh staff and students only
The University of Edinburgh is a charitable body, registered in Scotland, with registration number SC005336

undertaking slump test	and eye irritant - can cause burns when in direct contact - trapped fingers or feet if filled mould are dropped - tripping over filled mould	- ensure exposed skin covered - wear safety glasses - wear face mask - wear safety boots - place formwork on pallet prior to casting	L
Removing formwork and storing specimens	M - trapped fingers or feet - dropping specimens or moulds onto feet - fingers trapped - back injury from lifting specimens	- wear riggers gloves - wear safety boots - wear safety glasses - bend knees when lifting heavy objects and lift in increments, Ex. Table	L
TESTING			
Heating specimens in oven	M - burns from hot specimens - burns from oven when removing specimens	- wear high temperature gloves - wear safety boots - wear safety glasses - ensure exposed skin covered	L
Load application	H - fingers trapped in Avery - feet trapped as Avery platen lowered - flying debris from specimen failure	- wear safety boots - wear riggers gloves - wear safety glasses - ensure exposed skin covered	L

**Continue on separate sheet if necessary*

This document is intended for use by the University *of* Edinburgh staff and students only
The University of Edinburgh is a charitable body, registered in Scotland, with registration number SC005336

Engineering Controls: *Tick relevant boxes*

Guarding		Extraction (LEV)		Interlocks		Enclosure	
Other relevant information (incl. testing frequency if appropriate):							

Personal Protective Equipment (PPE): Identify all necessary PPE.

Eye / Face	✔	Hand /Arm	✔	Feet / Legs	✔	Respiratory	✔
Body (clothing)	✔	Hearing		Other (Specify)			
Specify the grade(s) of PPE to be worn: • Safety boots with toe and sole protection • Goggles and safety glasses with side protection							
Specify when during the activity the item(s) of PPE must be worn: • Clothing protection, safety boots and eye protection at all times.							

Non-disposable items of PPE must be inspected regularly and records retained for inspection

Persons at Risk: Identify all those who may be at risk.

Academic staff	✔	Technical staff	✔	P'Grad students	✔	U'Grad students	✔
Maintenance staff		Office staff		Cleaning staff		Emergency personnel	
Contractors		Visitors		Others			

Additional Information: Identify any additional information relevant to the activity, including supervision, training requirements, special emergency procedures, requirement for health surveillance etc.

NA

Prepared by

Researcher: Holly Smith (PhD Student)	
Signature:	Date:

This document is intended for use by the University *of* Edinburgh staff and students only
The University of Edinburgh is a charitable body, registered in Scotland, with registration number SC005336

Approved by

Supervisor: Tim Stratford	
Signature:	Date:

Lab Manager: Tim Stratford	
Signature:	Date:

Verification by Users

Sign below to indicate you have read and understood the safe system of work.

Signature:	Date:

This document is intended for use by the University *of* Edinburgh staff and students only
The University of Edinburgh is a charitable body, registered in Scotland, with registration number SC005336

Safe System of Work
Slab/Column Punching Shear at High Temperature Testing

Overview

The aim of these tests is to investigate punching shear mechanisms and their interactions at high temperature in reinforced concrete.

The concrete slab/column specimens are 1.4m square, and are supported by a steel test frame. The slabs will be tested to failure under a load applied to the column, and heated from above using a gas radiant panel array. Displacement will be measured by displacement gauges placed below the slab and digital cameras. Strain gauges will measure reaction forces in the steel frame and thermocouples will measure the internal concrete and external temperature.

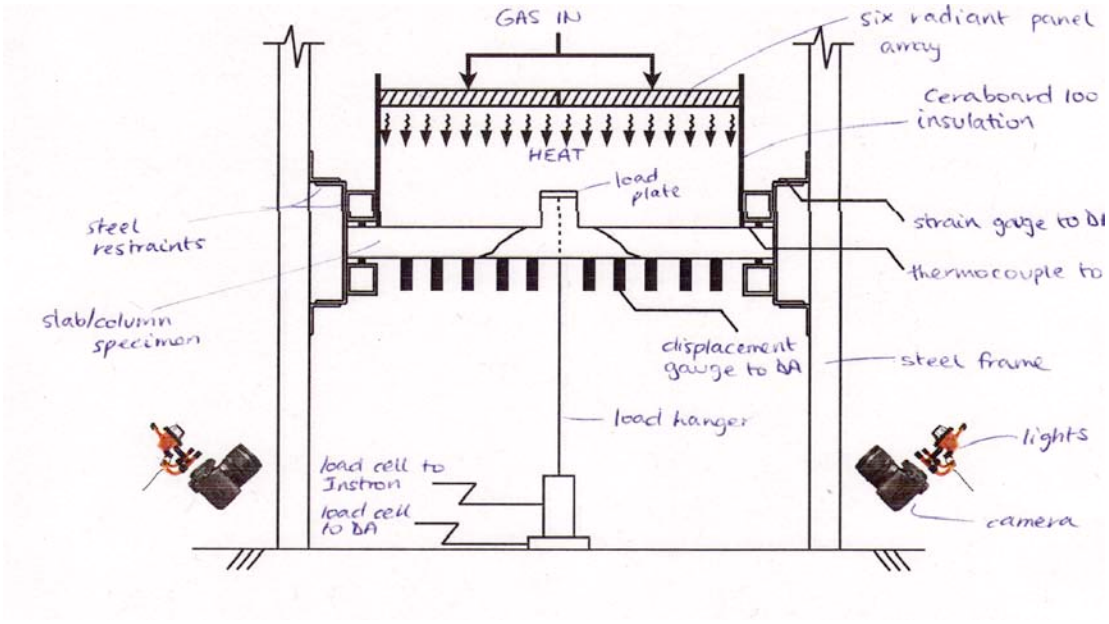

Key Watchpoints

- Large, heavy test specimens and equipment.
- Large applied forces; potential sudden failure of test specimen.
- Use of propane in the lab: leaks of gas, fire, and ventilation during burning.
- Trip hazards such as trailing cables.

This document is intended for use by the University *of* Edinburgh staff and students only
The University of Edinburgh is a charitable body, registered in Scotland, with registration number SC005336

Required PPE

Safety boots and glasses are required at all times. Riggers gloves are required when handling materials. A hard hat is required when working underneath items, and during testing.

Test Setup

1. **Remove Ceraboard insulation** from the existing test frame and radiant panels. Ceraboard must be handled with care (refer to the MSDS on the structures lab wiki) to avoid inhalation and contact with skin. Dust masks and coveralls essential. Old board should be immediately bagged and placed in skip for disposal.

2. **Modify the steel restraint frame.** This requires new slots and holes to be drilled in the test frame. Take special care in lifting heavy objects. Follow the SSW for the magnetic clamp drill.

3. **Install loading arrangement.** Load will be applied to the slab by a high tensile steel rod through the centre of the column, which passes through an Enerpac jack anchored to the lab strong floor. The design must ensure that all components can carry the required load. Take care when lifting heavy steelwork into place. Refer to the Enerpac SSW.

4. **Strain gauge installation, testing and calibration.** Refer to SSW for strain gauge installation. Strain gauge cables to be bundled in trunking to keep cabling neat. The strain gauges will be calibrated by applying load using an Enerpac jack and comparing to the strain gauge reading. Applying load will require jack and loading arrangement to be lifted into place. Consider using crane to support the jack. Refer to Enerpac SSW.

5. **Install, test and calibrate gas radiant panel system**, including gas and air distribution systems, ignition and flame detection systems, and insulation for steel test frame. The gas radiant panels run off the lab propane supply, and use high voltage ignition system. Refer to the radiant panel SSW. The high voltage ignition system must be isolated from the test frame to avoid damage to sensitive instrumentation, refer to the electronics box for radiant panel array ignition SSW.

6. **Thermocouple testing and connection of lead wires.** The thermocouple wires and extension cables will be routed neatly to the data acquisition using cable trunking.

7. **DIC camera support.** Install supports for cameras, to give solid support in positions where they are unlikely to be damaged, and where the cameras or cables do not present a trip hazard.

This document is intended for use by the University *of* Edinburgh staff and students only
The University of Edinburgh is a charitable body, registered in Scotland, with registration number SC005336

Prior to each Test

8. **Lift specimen into place.** Use forklift to move specimen from WRB into place in test frame (only persons with forklift training can do this). Slab orientation should always be with arrow (drawn on concrete) at West (columns 1 +2) side of the load frame. Apply mortar layer between slab and test frame, fit restraining steelwork, fit and tighten bolts. This work involves heavy and large, concrete and steel items.

9. **Install the west side of the test frame.**

10. **Install catch mesh** beneath the slab to catch large pieces of concrete that might fall on instrumentation.

11. **Set up Enerpac loading with Instron actuator.** Load will be applied to the Enerpac system using the Instron 250kN actuator. Ensure that the actuator and Enerpac jack are properly aligned. A test programme will need to be created for the Instron, and this must be double-checked by an independent and experienced user of the system. Run the test programme against a dummy specimen before the real test. The load reading from the Instron will be fed to the DA using the Instron 10V output. Care is required to check that the wiring is properly grounded to avoid overloading the DA.

12. **Position displacement gauges**. LP displacement gauges will be positioned under the slab, beneath a protective catch mesh.

13. **Connect instrumentation to DA.** Connect the strain gauges, thermocouples, and displacement gauges to the System 7000 DA. All cabling must be tidily routed to avoid snags and trip hazards. Low voltage and high voltage cables should be separated to avoid noisy signals.

14. **Position DIC cameras and lights**. Check that the cameras are not in danger due to failure of the slab or overheating from radiant panel array. Route power supply and timing cables to avoid trip hazards.

15. **Ensure working area is clear.** Before testing, all tools and equipment must be returned to cupboards, Debris must be swept and vacuumed away. The area around the tests must be clear and clean, and there must be clear access routes towards and away from the test frame. Ensure that fire extinguishers are in place and accessible.

16. **Test cube and cylinder specimens** to determine strength using Avery-Denison test machine (refer to separate SSW).

During Testing

17. **Inform other lab users** that a test is about to take place, and ensure everyone is wearing the necessary PPE (safety boots, eye protection, hard hats, lab coat and gloves). **Lab access** should be restricted to only those who need to be present during the test. Spectators are not allowed, to avoid unnecessary distraction. Barriers and notices should be placed across doors.

18. **Turn on the lab fans.** Use lab fans to provide forced ventilation during the tests.

19. **Start the Instron, DA, and camera systems recording**.

This document is intended for use by the University *of* Edinburgh staff and students only
The University of Edinburgh is a charitable body, registered in Scotland, with registration number SC005336

20. **Apply load** by starting the Instron test program. For the ambient temperature tests, the test will be conducted under displacement control, with an initial loading cycle to ensure that the specimen has bedded in. The heated tests will be subjected to a sustained load that is 60% of the ambient slab capacity.

21. **Ignite the radiant panels.** Follow the SSW for the radiant panels and electronics box for radiant panel array ignition. Ensure that insulation is in place to protect the test frame and instrumentation from heat. Make sure the magnetised emergency stop to shut off the gas and radiant panels is positioned next to someone with a view of the radiant panel array.

22. **Monitor test progress.** Monitor the load, temperature, and deflection of the slab during the test. Keep notes of significant test events (such as cracking) so that they can be cross-referenced to the test data (on paper or by audio recording). Shout out values so that everybody is aware of the test progress. Nobody is to get close to the test unless the person monitoring test progress confirms that it is safe to do so. When it appears that failure is about to occur, all observers must be told to keep clear.

23. **After slab failure,** turn off the radiant panels and unload the slab. Turn off Instron, DA, and cameras. Back up data to a safe place as soon as is practicable. Take care over hot parts of the test; leave warning notices if the specimen is left unattended.

After Testing

24. **Wait until slab and frame have cooled down** before dismantling.

25. **Remove cameras, displacement gauges, catch mesh, loading rod and connections from DA.**

26. **Closely inspect the slab** on both sides and photograph cracks and deflection, taking care to identify location and orientation (using arrow on the concrete) of the photographs.

27. **Undo the restraining steelwork, remove the west side of the frame, and remove the slab** from the test frame in as much of a whole piece as possible (only persons with forklift training can do this). Store each slab on a pallet to allow for plan photo in the lower fire lab.

28. **Clean the frame and surrounding area of the lab.**

29. **Return lab equipment to the cupboards.** Do an inventory of the restraining nuts and bolts, and carefully check the frame, loading arrangements, and instrumentation for damage. Repair as necessary.

30. **Take plan photos** in lower fire lab to compare cracks to previous reinforcement location photos. Take photos with arrow at the top of the image (see previous images for correct orientation).

31. **Cut the slab along two orthogonal directions** using a diamond tipped stone saw. (Wear dust mask, gloves, goggles, and safety boots). Record the as-built position of the reinforcement. Photograph the cut surfaces. Also break open along other cracks as appropriate and record. Store in the lab on a pallet until end of test series. Slabs can be disposed of in skip after the end of the test programme.

This document is intended for use by the University *of* Edinburgh staff and students only
The University of Edinburgh is a charitable body, registered in Scotland, with registration number SC005336

Prepared by

Researcher: Holly Smith (PhD Student)	
Signature:	Date:

Approved by

PhD Supervisor: Tim Stratford	
Signature:	Date:

Lab Manager: Tim Stratford	
Signature:	Date:

This document is intended for use by the University *of* Edinburgh staff and students only
The University of Edinburgh is a charitable body, registered in Scotland, with registration number SC005336

General Risk Assessment

Form RA1

(Refer to Notes for Guidance before completing this form)

School Assessment No:	STR0012
Title of Activity:	Slab/Column Punching Shear at High Temperature Testing
Location(s) of Work:	Structures Laboratory, The University of Edinburgh, The King's Buildings, Mayfield Road, Edinburgh, EH9 3JL

Brief Description of Work:

Slab/column specimens are 1.4m square, and are supported by a steel test frame. The slabs will be tested until failure under a load applied to the column using Enerpac jacks and 250kN Instron actuator, and heated from above using a gas radiant six panel array. Displacement will be measured by displacement gauges placed below the slab and three digital cameras at the corners of the frame. Strain gauges will measure the reaction forces in the steel frame and thermocouples will measure the internal concrete and external temperature.

This Risk Assessment should be read along with the corresponding Safe System of Work.

Hazard Identification: Identify all the hazards; evaluate the risks (low / medium / high); describe all existing control measures and identify any further measures required. Specific hazards should be assessed on a separate risk assessment form and cross-referenced with this document. Specific assessments are available for hazardous substances, biological agents, display screen equipment, manual handling operations and fieldwork. See http://www.ed.ac.uk/schools-departments/health-safety/risk-assessments-checklists/risk-assessments for details.

Hazard(s)	**Present Risk Evaluation** L/M/H	**Control Measures** (i.e., alternative work methods / mechanical aids / engineering controls, etc.)	**Risk Evaluation after control** L/M/H
TESTING SETUP:			
Insulation board (Ceraboard)	M - irritation to upper respiratory system when inhaling particles/fibres - irritation to skin and eyes - carcinogen classification by E.U.	- users must read and follow the Ceraboard MSDS. - replace board if charring present or used for multiple tests - wear face mask at all times when moving and cutting material	L

This document is intended for use by the University *of* Edinburgh staff and students only
The University of Edinburgh is a charitable body, registered in Scotland, with registration number SC005336

		- wear safety glasses with side shields - wear rigger gloves - wear disposable full body suit to decrease transfer of particles/fibres when moving and cutting material - cut material outside and away from people - when moving material work with ventilation on - dispose of insulation board in sealed bags - clean workspace post removal with vacuum cleaner fitted with high efficiency filter (HEPA)	
Modifications to the steel restraint frame	H - cut hands on rough cut edges - inhaling fine steel particles could lead to respiratory difficulties - back injury from lifting drill - serious cuts/loss of digits - burns due to steel heating up - sharp shards of steel could damage eyes	- wear rigger gloves - ensure exposed skin covered - wear face mask - wear safety glasses - bend knees when lifting heavy objects and lift in increments, Ex. Table - get drill instruction from experienced laboratory technician - check equipment prior to work to ensure in good working order	L
Install loading arrangement	M - back injury from lifting heavy steelwork	- bend knees when lifting heavy objects and lift in increments, Ex. Table - use structures lab crane where possible (only trained persons)	L
Strain gauge installation, testing and calibration	H - NP50 strain gauge Drug A is flammable, acutely toxic (oral), skin and eye irritant and hazardous to the aquatic environment - NP50 strain gauge Drug B is flammable explosive, corrosive to metals, acutely toxic, skin and eye irritant, hazardous to the aquatic environment	- read and follow MSDS for NP50 adhesive - keep away from heat, sparks and open flames - wear protective gloves (be cautious of glove type and wear extra layers) - wear safety glasses - wear face mask - wear protective clothing to ensure exposed skin covered - wash hands after handling - use ventilation fans	L
Install, test and calibrate gas radiant panel system	H - baking-in of insulation between 180°C to 600°C causes gases and fumes - refer to heating samples with radiant panel risk assessment	- refer to gas radiant panel risk assessment	L
Propane Gas (orange hose colour)	H - highly flammable - can cause cold burns - asphyxiation if it has	Refer to SSW and RA for Gas Radiant Panels	L

This document is intended for use by the University *of* Edinburgh staff and students only
The University of Edinburgh is a charitable body, registered in Scotland, with registration number SC005336

	displaced the normal oxygen level in air (heavier than air, therefore collects in low-lying areas)		
Thermocouple testing and connection of lead wires DIC camera support	M - trip hazards from instrumentation connections to DA	- use trunking around loading frame - use anti-trip cable protectors when cables need to be routed on the floor	L
PRIOR TO EACH TEST:			
Lift specimen into place	H - trapping body and or limbs under specimen, if dropped which could lead to broken bones	- only experienced laboratory technician to handle forklift transportation (forklift training required) - keep eye contact with forklift driver so location of people in the vicinity is known	L
Install west side of the test frame	M - fingers trapped in steel fixings - back injury from lifting steel sections	- wear riggers gloves - bend knees when lifting heavy objects and lift in increments, Ex. Table	L
Install catch mesh	M - cuts from sharp mesh edges - cut finger with angle grinder - sharp shards of steel could damage eyes	-wear riggers gloves -wear safety glasses -ensure exposed skin covered -wear face mask	L
Set up Enerpac loading with Instron actuator	M - fingers trapped in actuator	- wear riggers gloves - have safety stop near actuator frame	L
Connect instrumentation to DA	M - trip hazards from cable connections to DA	- use rubber trip guards when running cables across workspace walkways - make sure workspace is kept clear	L
Position DIC cameras and lights	M - burns from lights getting hot during usage	- wear rigger gloves to handle lights after testing	L
Test cube and cylinder specimens	H - fingers and feet trapped in Avery-Dension loading and under platen - flying debris from specimen failure	- Refer to concrete standard cube and cylinder testing risk assessment	L
DURING TESTING:			

This document is intended for use by the University *of* Edinburgh staff and students only
The University of Edinburgh is a charitable body, registered in Scotland, with registration number SC005336

Load application	H - Fingers trapped in actuator - Malfunction of Inston loading system	- Read and follow the SSW and RA for the Instron actuator system. - Have remote emergency stop near actuator frame	L
Ignite the radiant panels	H - refer to heating samples with radiant panel risk assessment and electronics box for radiant panel array ignition risk assessment	- refer to heating samples with radiant panel risk assessment and electronics box for radiant panel array ignition risk assessment	L
Monitor test progress	H - unexpected sudden failure of the specimen will be catastrophic and there could be flying debris - heat from the radiant panels will be great and could cause burns	- wear safety glasses - wear rigger gloves - ensure exposed skin covered - steel mesh should protect from larger pieces of flying debris - stand at a safe distance from failure	L
High voltage cabling	H - electrocution - refer to electronics box for radiant panel array ignition risk assessment	- Refer to electronics box for radiant panel array ignition risk assessment - Electricity cables are channelled overhead and are in copex trunking near ground level	L
AFTER TESTING:			
Wait until slab and frame have cooled down	- burns from hot reinforced concrete specimen - as specimen cooling, further concrete cracking can occur which may lead to flying debris	- wear safety glasses - wear rigger gloves - ensure exposed skin covered - don't move specimen until completely cool	L
Closely inspect the slab	H - slab debris fall down from remaining cool specimen	- wear safety glasses - ensure exposed skin covered - stay outside load frame	L
Undo the restraining steelwork, remove the west side of the frame, and remove the slab	M - refer to installing west side of the test frame above	- refer to installing west side of the test frame above	L
Cut the slab along two orthogonal directions	H - serious cuts/loss of digits - specimen dropping onto feet, limb, etc.	- get saw instruction from experienced laboratory technician - work near the floor and ensure broken specimen pieces are adequately supported	L

This document is intended for use by the University *of* Edinburgh staff and students only
The University of Edinburgh is a charitable body, registered in Scotland, with registration number SC005336

Engineering Controls: *Tick relevant boxes*

Guarding		Extraction (LEV)	✔	Interlocks		Enclosure	
Other relevant information (incl. testing frequency if appropriate): Do not use compressed air for clean up of particles/fibres of insulation							

Personal Protective Equipment (PPE): Identify all necessary PPE.

Eye / Face	✔	Hand /Arm	✔	Feet / Legs	✔	Respiratory	✔
Body (clothing)	✔	Hearing		Other (Specify)			
Specify the grade(s) of PPE to be worn: • Safety boots with toe and sole protection • Goggles or safety glasses with side protection.							
Specify when during the activity the item(s) of PPE must be worn: • A disposable full body protective suit must be worn during insulation removal, cutting and replacement. A new suit should be worn and disposed of each time. • Hard hat required during all lifting operations, when working beneath the test or test frame, and during the test. • Clothing protection, safety boots and eye protection at all times.							

Non-disposable items of PPE must be inspected regularly and records retained for inspection

Persons at Risk: Identify all those who may be at risk.

Academic staff	✔	Technical staff	✔	P'Grad students	✔	U'Grad students	✔
Maintenance staff		Office staff		Cleaning staff	✔	Emergency personnel	
Contractors		Visitors	✔	Others			

This document is intended for use by the University *of* Edinburgh staff and students only
The University of Edinburgh is a charitable body, registered in Scotland, with registration number SC005336

Additional Information: Identify any additional information relevant to the activity, including supervision, training requirements, special emergency procedures, requirement for health surveillance etc.

All laboratory and cryogenic gas users must hold a compressed gases safety passport. Users: (Issue No, Issue Date, Renewable Date) Holly Smith, 11129110, 02 December 2011, January 2015 Dr Tim Stratford, 11129102, 02 December 2011, January 2015 Jim Hutcheson, 11129096, 2 December 2011, January 2015 Michal Krajcovic, NA, 24 November 2010, NA

Prepared by

Researcher: Holly Smith (PhD Student)	
Signature:	Date:

Approved by

PhD Supervisor: Tim Stratford	
Signature:	Date:

Lab Manager: Tim Stratford	
Signature:	Date:

This document is intended for use by the University *of* Edinburgh staff and students only
The University of Edinburgh is a charitable body, registered in Scotland, with registration number SC005336

Safe System of Work
Slab Specimen Storage in Construction Materials Lab

School SSW number: STR0034

Overview

Fifteen slab/column specimens (1.4m square) are stored in three stacks with a maximum of five slabs per stack. The slabs are supported with stacked bricks and wooden blocks on a pallet in the centre of the lab. Steel box sections and wooden planks spread the slab load along two edges of the slabs.

The slabs are stored together with cube and cylinder specimens, which are part of the test series. The humidity in the lab is controlled using a dehumidifier, the exterior door is sealed with duck tape, and the internal door is kept closed at all times. There is limited access to this lab to keep the environmental conditions as controlled as possible.

Key Watchpoints

- Large heavy test specimens (each slab 500kg approx.)
- Slab stacks could become unstable if pushed.
- Moving the slabs requires expert forklift truck driver. A maximum of two 100mm depth specimens can be moved at a time, due to forklift weight restrictions and unsteadiness

Required PPE

Safety boots and glasses are required at all times. Riggers gloves are required when handling materials.

This document is intended for use by the University *of* Edinburgh staff and students only
The University of Edinburgh is a charitable body, registered in Scotland, with registration number SC005336

Working within the Lab

1. **Keep a safe distance** from the slab stacks, and take care when moving around the slabs not to knock or lean on them.

2. **Do not place anything on the slab stacks** as this can unpset their balance. We have also found that the wooden spacer blocks creep, which could cause instability.

3. **Always make sure somebody knows you are in the lab.** The lab is isolated and it is rare for anybody to pass by or look in to the lab, consequently an accident will not be noticed. Always tell a UoE colleague that you are going to be working in the lab, and make sure they know to come and find you if you do not report back after an agreed time. Lone working in this lab is to be avoided whilst the slabs are in storage.

Removing Specimens

4. **Forklift specimens moving out of the lab.** Use forklift to move specimen from Construction Materials lab into the structures lab (only persons with forklift training can do this). Maximum of two 100mm depth specimens can be moved at a time with the forklift, due to weight restrictions and unsteadiness of the load.

Prepared by

Researcher: Holly Smith (PhD Student)	
Signature:	Date: 11 JUNE 2013

Approved by

PhD Supervisor: Tim Stratford	
Signature:	Date:

Lab Manager: Tim Stratford	
Signature:	Date:

Review required 11 June 2014

This document is intended for use by the University *of* Edinburgh staff and students only
The University of Edinburgh is a charitable body, registered in Scotland, with registration number SC005336

Verification by Lab Users

Sign below to indicate you have read and understood the safe system of work.

Signature:	Date:

This document is intended for use by the University *of* Edinburgh staff and students only
The University of Edinburgh is a charitable body, registered in Scotland, with registration number SC005336

General Risk Assessment

Form RA1

(Refer to Notes for Guidance before completing this form)

School Assessment No:	STR0034
Title of Activity:	Slab Specimen Storage in the Construction Materials Lab
Location(s) of Work:	Construction Materials Lab, William Rankine Building

Brief Description of Work:

Fifteen slab/column specimens (1.4m square) are stored in three stacks with a maximum of five slabs per stack. The lab humidity is controlled using a dehumidifier. There is limited access to this lab to keep the environmental conditions as controlled as possible.

This Risk Assessment should be read along with the corresponding Safe System of Work.

Hazard Identification: Identify all the hazards; evaluate the risks (low / medium / high); describe all existing control measures and identify any further measures required. Specific hazards should be assessed on a separate risk assessment form and cross-referenced with this document. Specific assessments are available for hazardous substances, biological agents, display screen equipment, manual handling operations and fieldwork. See http://www.ed.ac.uk/schools-departments/health-safety/risk-assessments-checklists/risk-assessments for details.

Hazard(s)	**Present Risk Evaluation** L/M/H	**Control Measures** (i.e., alternative work methods / mechanical aids / engineering controls, etc.)	**Risk Evaluation after control** L/M/H
WORKING WITHIN THE LAB			
Lone working	H Lab is isolated so an accident would go unnoticed.	- Operate buddy system when entering the lab alone.	L
Trip hazards (cable and hose from dehumidifier)	L Dehumidifier is placed on bench to avoid any trip hazard	- None required	L
Unstable slab stacks (maximum	H - Slabs unsteady if knocked. Toppling of slab stacks	- Lab users have been limited (sign posted on the lab door)	L

This document is intended for use by the University *of* Edinburgh staff and students only
The University of Edinburgh is a charitable body, registered in Scotland, with registration number SC005336

of five)	could lead to broken bones, trapped body and or limbs under specimen.	- Limited users have been warned of slab unsteadiness and danger. They have been warned to keep a safe distance, not put anything down on the slabs and never work in the lab alone. -	
REMOVING SPECIMENS:			
Forklift removal of specimens	H - broken bones, trapping body and or limbs under specimen, if specimen falls during moving	- only experienced laboratory technician to handle forklift transportation (forklift training required) - maximum of two 100mm depth specimens can be moved using the forklift at a time, due to weight restrictions and unsteadiness - keep eye contact with forklift driver so location of people in the vicinity is known	L

Engineering Controls: *Tick relevant boxes*

Guarding		Extraction (LEV)		Interlocks		Enclosure	
Other relevant information (incl. testing frequency if appropriate):							

Personal Protective Equipment (PPE): Identify all necessary PPE.

Eye / Face	✔	Hand /Arm	✔	Feet / Legs	✔	Respiratory	
Body (clothing)	✔	Hearing		Other (Specify)			
Specify the grade(s) of PPE to be worn: • Safety boots with toe and sole protection							
Specify when during the activity the item(s) of PPE must be worn: • Clothing protection, safety boots and riggers gloves at all times.							

Non-disposable items of PPE must be inspected regularly and records retained for inspection

Persons at Risk: Identify all those who may be at risk.

Academic staff	✔	Technical staff	✔	P'Grad students	✔	U'Grad students	
Maintenance staff		Office staff		Cleaning staff	✔	Emergency personnel	
Contractors		Visitors		Others			

This document is intended for use by the University *of* Edinburgh staff and students only
The University of Edinburgh is a charitable body, registered in Scotland, with registration number SC005336

Additional Information: Identify any additional information relevant to the activity, including supervision, training requirements, special emergency procedures, requirement for health surveillance etc.

Prepared by

Researcher: Holly Smith (PhD Student)	
Signature:	Date: 11 JUNE 2013

Approved by

PhD Supervisor: Tim Stratford	
Signature:	Date:

Lab Manager: Tim Stratford	
Signature:	Date:

Review required 11 June 2014

This document is intended for use by the University *of* Edinburgh staff and students only
The University of Edinburgh is a charitable body, registered in Scotland, with registration number SC005336

Verification by Lab Users

Sign below to indicate you have read and understood the safe system of work.

Signature:	Date:

This document is intended for use by the University *of* Edinburgh staff and students only
The University of Edinburgh is a charitable body, registered in Scotland, with registration number SC005336

Safe System of Work
Radiant Panel Array

School SSW number: STR0018

Overview

This document describes the safe use of the Flammaire Gas Radiant Panels in the structures laboratory. They are typically used to heat specimens during combined structural and fire testing.

The gas radiant panel array comprises:

- **one or more gas radiant panels;**
- **a mixer valve for each panel;**
- **air supply (using one or more fans);**
- **gas supply (from the lab propane line); and**
- **electric ignition and flame protection system (depending upon the application).**

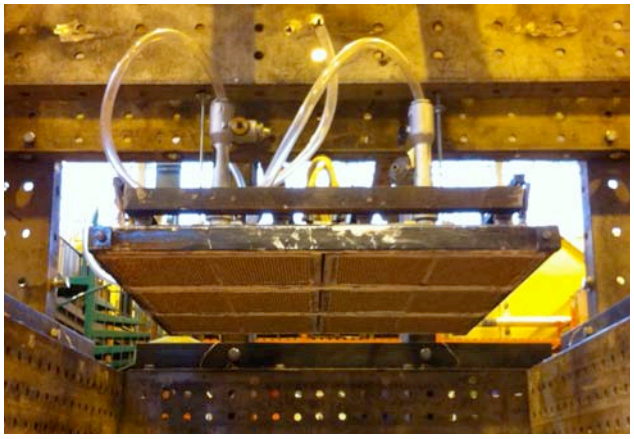

This following documents should be read alongside this safe system of work:

- **the radiant panel array risk assessment;**
- **the safe system of work for the Gas Emergency Stop Valve;**
- **the safe system of work for the Electric Control System; and**
- **the MSDS for propane.**

This document is not an instruction manual for use of the radiant panels.
All users must be trained, and authorised to use the equipment.

The list of authorised users is maintained on the structures lab wiki.

This document is intended for use by the University *of* Edinburgh staff and students only
The University of Edinburgh is a charitable body, registered in Scotland, with registration number SC005336

Key Watchpoints

- Lone working is not allowed with the gas radiant panels.
- The panels must always be used with the Emergency Stop Gas Solenoid Valve.
- Read and understand the MSDS for propane. It is highly flammable and explosive, but can also cause cold burns and asphyxiation (it is heavier than air).
- Gas bottles and connections must only be changed by authorised users who have attended the Gas Safety Course.
- Incorrect use of the panels can lead to dangerous blowback. Only use the panels if you understand what this is and how to avoid it.
- Be aware of hot surfaces: the panels heat the vicinity by convection, conduction and radiation.
- Keep the area clear of combustible materials.
- The correct shutdown procedure (described below) must be followed so that excess gas is not left in the supply pipes.
- All specimens and any other materials that will be heated must be risk assessed separately. For example, fumes developed during heating and the degradation of insulation materials must be addressed.
- Tests that produce substantial amounts of smoke, fumes or other combustion products must not be carried out in the structures lab.

Required PPE

The following PPE is required at all times when using the radiant panels. Other PPE may be required for a particular test, and must be assessed on a case by case basis:

A lab coat is required because it provides a protection barrier against burns and electrical shock (from the ignition system).

A full face mask must be used if the gas radiant panels are ignited manually.

This document is intended for use by the University *of* Edinburgh staff and students only
The University of Edinburgh is a charitable body, registered in Scotland, with registration number SC005336

Handling the Radiant Panels

The Flammaire radiant panels are made from ceramic refractory blocks held in a cast iron chamber. The ceramic is delicate and must be handled with care. Do not knock the panels, and protect the heating surface whenever it is vulnerable. If the panels need to be laid face down, rest them on expanded polystyrene or a similar soft material.

Test Setup

1. Check that there is sufficient gas in the bottles for the test to be conducted. (Bottles must only be changed by someone who has attended the gas safety training course).

2. Check the correct operation of the mass flow meter.

3. Inspect the panels, valves and pipes for damage before every test.

4. Check the whole gas system for leaks. A gas radiant panel array should be pressure tested when it is first assembled, and leak checks should also be carried out prior to each use. The person carrying out the leak checks must be experienced and have received appropriate training.

5. The gas supply lines must not be left in a vulnerable position, or a position where they will cause a trip hazard. Place them in an overhead conduit, or protect them using a steel section if they must be placed on the ground.

6. Check the correct operation of the air supply fan. Check that the power supply to the fan is correct and that its connection to the panels is sound.

7. Check the ratio of gas to air supplied to the panels (set using the mixer valve). If you do not understand the gas:air mix supply requirements, you should not be using the panels.

8. Position the remote Emergency Gas Stop Button so that it can easily be accessed in the case of emergency. Check the operation of the two Emergency Gas Stop Buttons. (Refer to the separate SSW).

9. Check the presence of and clear access to fire extinguishers.

10. Ensure that the immediate area around the radiant panels is clear of all combustible materials. Ensure that the surrounding area is free of clutter and trip hazards, and that routes of access and egress are completely clear.

11. Ensure that there are no distractions during a test. If other lab activity could cause a distraction it should be stopped. Depending upon the nature of the tests, anybody not directly involved in the tests should leave the lab. Spectators are not allowed to avoid unnecessary distraction. Place notices and barriers on the doors to prevent people entering the lab. Consider moving the fork lift truck out of the lab in case it is required elsewhere.

12. Before starting a test, those involved should agree upon their roles during the test. Check that everyone is familiar with the lab layout and egress routes, first aid kit and fire extinguisher location, first aider and emergency numbers etc, emergency stop procedures, expected test outcomes and procedures etc. Identify the chain of command to avoid mis-communication during the test.

This document is intended for use by the University *of* Edinburgh staff and students only
The University of Edinburgh is a charitable body, registered in Scotland, with registration number SC005336

Test Start Up

13. Make sure all lab users know that you are about to start a test, and that everyone in the lab is wearing the required PPE.

14. Switch the laboratory fans on to ventilate the laboratory. (NB: these fans only provide background ventilation and as noted above specimens that produce substantial fumes or smoke must not be tested in the structures lab).

15. Turn on the power to the air supply fan.

Ignition *with* the Electrical Control Box

16. Refer to the SSW for the Electrical Control Box.

17. Immediately after starting the electrical ignition control box for the array, open two yellow propane gas valves to introduce gas to the panels.

18. If the panels ignite, check that the electric ignition stops sparking. This indicates that the flame failure detection probes are working correctly.

19. If the panels do not ignite, turn off the gas by closing the yellow propane supply valves after sparking has stopped. Leave the air supply fan on for 1 minute to dissipate the excess propane before following the restart procedure described in the Electric Control Box SSW.

Ignition *without* the Electrical Control Box

20. The radiant panels should normally be used with the Electrical Control Box because this automatically shuts off the gas supply in the event of flame failure.

21. If the electrical control box is not being used, open the two yellow propane gas valves to introduce gas to the panels, and simultaneously ignite the gas with handheld torch or electric spark. The person operating the propane valves must be ready to shut them off if the panels do not ignite quickly.

Operation of the Panels with or without the Electrical Control Box

22. Visually check that all the panels in an array are burning correctly and equally. Users must have received training to understand correct combustion of the panels, and to understand how to spot the symptoms of combustion within the panel, which can lead to dangerous blowback.

23. Never leave the radiant panel array unattended during operation. An experienced radiant panel user must always be watching, listening and smelling for possible blowback, burning, or open flames.

24. Strike an Emergency Gas Stop Button in the event of an emergency such as a blowback event. Follow the correct restart procedure (described in the separate SSW) if the emergency stop is used.

This document is intended for use by the University *of* Edinburgh staff and students only
The University of Edinburgh is a charitable body, registered in Scotland, with registration number SC005336

Test Shutdown

25. After specimen failure, close the two yellow propane gas valves before the mass flow meter to reduce the amount of propane in the line as much as possible.
26. If the electrical control box is being used, turn off the control box according to the method described in its SSW.
27. Leave the air supply fan on for 30 minutes to cool down radiant panels, which will extend their life.
28. Close all gas valves and bottles.

Assessment carried out by:

Name:	Michal Krajkovic Revised Tim Stratford	Date:	26/9/14
Signature:			

Review required 1 September 2015

Verification by users

Sign below to indicate you have read and understood the safe system of work.

Signature:	Date:

This document is intended for use by the University *of* Edinburgh staff and students only
The University of Edinburgh is a charitable body, registered in Scotland, with registration number SC005336

This document is intended for use by the University *of* Edinburgh staff and students only
The University of Edinburgh is a charitable body, registered in Scotland, with registration number SC005336

General Risk Assessment

Form RA1

(Refer to Notes for Guidance before completing this form)

School Assessment No:	STR0018
Title of Activity:	Heating Samples with Radiant Panel
Location(s) of Work:	Structures Laboratory, The University of Edinburgh
Brief Description of Work: Use of radiant panel assembly to heat samples during testing. Propane and air mixture supplied to panels and ignition source from sparkers operated by electronics control box or blow torch.	

Hazard Identification: Identify all the hazards; evaluate the risks (low / medium / high); describe all existing control measures and identify any further measures required. Specific hazards should be assessed on a separate risk assessment form and cross-referenced with this document. Specific assessments are available for hazardous substances, biological agents, display screen equipment, manual handling operations and fieldwork. See http://www.ed.ac.uk/schools-departments/health-safety/risk-assessments-checklists/risk-assessments for details.

Hazard(s)	**Present Risk** **Evaluation** L/M/H	**Control Measures** (i.e., alternative work methods / mechanical aids / engineering controls, etc.)	**Risk** **Evaluation after control** L/M/H
Propane gas (orange hose colour)	H - highly flammable - can cause cold burns - asphyxiation if it has displaced normal oxygen level in air (heavier than air, therefore collects in low-lying areas)	- check for leaks if gas smell detected - whole gas system should be check for leaks along line prior to testing by experienced technician - inform experienced technician when testing - prior to testing check sufficient gas for	L

This document is intended for use by the University *of* Edinburgh staff and students only
The University of Edinburgh is a charitable body, registered in Scotland, with registration number SC005336

		experiment - users should attend gas safety training course, or receive supervision by someone who has attended the course.	
Explosions	H	- check gas lines for leaks - only trained persons can change gas bottles or adjust gas bottle settings	L
Open flames	H - panel blow back - combustibles	- use emergency gas shut off if blowback of flames occurs, as flames can damage equipment and cause injury - individual mixer for each panel reduces risk of flame propagation upstream - watch that small combustibles burn themselves out, and look for smoke	L
Hot surfaces	H - conductive heat into frame - radiation effects from panels - convection from hot gases	- prior to testing check that all combustibles are away from the vicinity - wear rigger gloves (be cautious of glove type) - wear laboratory coat - hair tied back - be cautious of burning smells	L
Gases/fumes	M - poor air quality - respiratory difficulties for persons with such as asthma	- ventilation from fans - all combustibles away from heat and flames - specimens that give off substantial fumes or smoke should not be	L

This document is intended for use by the University *of* Edinburgh staff and students only
The University of Edinburgh is a charitable body, registered in Scotland, with registration number SC005336

		carried out in the structures lab	
Safety of persons wanting lab access	M	- warning signage on lab entrances nearby test area, that test is in progress - place safety barriers across lab entrances nearby test area - consider moving the fork lift truck out of the lab in case it will be needed elsewhere.	L
Failure of specimen	M - sudden specimen failure	- close the yellow valves that are in the gas supply before the mass flow meter. This reduces the volume of propane left in gas line as much as possible. - refer to individual user radiant panel SSW for full radiant panel shut down procedure	L
Trip hazard	M - gas line and power cables	- place gas lines and cables under a channel section or in overhead channel	L
Safety of lab users	M	- all users must be familiar with the lab layout and egress routes, first aid kit location, fire extinguisher location, etc. Identify who has ultimate say in test procedure and who needs to be present during test.	L
Ignition electrical control box	M	- check sparking stops after ignition - warn nearby lab users sparking in progress - refer to SSW and RA for	L

This document is intended for use by the University *of* Edinburgh staff and students only
The University of Edinburgh is a charitable body, registered in Scotland, with registration number SC005336

		electronics box for radiant panel array ignition	

Engineering Controls: *Tick relevant boxes*

Guarding		Extraction (LEV)	✔	Interlocks		Enclosure	
Other relevant information (incl. testing frequency if appropriate):							

Personal Protective Equipment (PPE): Identify all necessary PPE.

Eye / Face	✔	Hand /Arm	✔	Feet / Legs	✔	Respiratory	✔
Body (clothing)	✔	Hearing		Other (Specify): Hard hat			
Specify the grade(s) of PPE to be worn: Full face mask required for manual ignition of panels.							
Specify when during the activity the item(s) of PPE must be worn: To be worn at all times							

Non-disposable items of PPE must be inspected regularly and records retained for inspection

Persons at Risk: Identify all those who may be at risk.

Academic staff	✔	Technical staff	✔	P'Grad students	✔	U'Grad students	
Maintenance staff		Office staff		Cleaning staff		Emergency personnel	
Contractors		Visitors		Others			

Additional Information: Identify any additional information relevant to the activity, including supervision, training requirements, special emergency procedures, requirement for health surveillance etc.

Assessment carried out by:

Name:	John Gales/Michal Krajcovic/Holly Smith	Date:	17 AUG 2012
Signature:		Review Date:	

This document is intended for use by the University *of* Edinburgh staff and students only
The University of Edinburgh is a charitable body, registered in Scotland, with registration number SC005336

Review required 1 July 2014

Verification by users

Sign below to indicate you have read and understood the safe system of work.

Signature:	Date:

This document is intended for use by the University *of* Edinburgh staff and students only
The University of Edinburgh is a charitable body, registered in Scotland, with registration number SC005336

Safe System of Work
Structures Lab Gas Supply Shutoff Valves and Emergency Shutoff Buttons

School SSW number: STR0048

Overview

This document describes the gas control valves in the Structures Lab. The Emergency Gas Stop Buttons provide an easy and quick way to turn off the gas supply in the event of an emergency.

- **During a test, gas is supplied through the solenoid valve.**
- **Two emergency stop buttons are provided which shut off the solenoid valve in case of emergency.**
- **Manual valves are also provided to shut off the gas supply.**

Any lab user can strike one of the Emergency Stop Buttons in case of emergency.

After an Emergency Stop Button has been struck, only approved users should reset release the Emergency Stop and reset the system. A list of approved users is maintained of the structures lab wiki.

All users must receive training.
This document is not an instruction manual for use of the device.

Emergency gas shutoff (wall mounted)

Gas Supply Solenoid Valve

This document is intended for use by the University *of* Edinburgh staff and students only
The University of Edinburgh is a charitable body, registered in Scotland, with registration number SC005336

Remote Emergency Gas Shutoff Button

One of the emergency gas shutoff buttons is mounted on the wall next to the gas supply. A second emergency stop button is fitted with a long cable and magnetic base so that it can be positioned remotely, for example for easy access by a test operator.

Key Watchpoints

- In the event of an emergency, either of the Emergency Stop Buttons can be struck to stop the gas supply. The gas bottles outside the back door of the structures lab should also be turned off.
- Propane gas is highly flammable and explosive, can cause cold burns and asphyxiation. Refer to the MSDS for Propane.
- All gas users must have attended a Gas Safety Training course.

Required PPE

The following PPE is required at all times when using the propane gas system. Other PPE may be required for a particular test, and must be assessed on a case by case basis:

A lab coat should be worn at all times to provide protection from burns and electric shock.

This document is intended for use by the University *of* Edinburgh staff and students only
The University of Edinburgh is a charitable body, registered in Scotland, with registration number SC005336

Prior to Testing

1. Check the gas bottles to ensure sufficient gas is available for the test.
2. Check the mass flow meter to ensure it is working properly.
3. An experienced technician should visually check the whole gas system for leaks, including the connection to the test rig. Leak detect spray should be used to check connections.
4. Gas lines from the gas supply must be protected from accidental damage and to avoid a trip hazard. They can be placed in an overhead channel, or within a protective steel section when on the ground.
5. Check that the Emergency Stop Buttons and solenoid valve are fitted with a Residual Circuit Device (R.C.D.), and test the device.
6. Check the correct operation of the two gas Emergency Stop Buttons.
7. Position the remote Emergency Stop Button (with the magnetic base) where it can be easily accessed by the test operator and other lab users.

In the Event of an Emergency – Evacuation Required

8. Strike either Emergency Stop Button to stop the gas flow.
9. Follow normal evacuation procedures.
10. Close all gas valves and gas bottles outside the back door of the structures lab.

In the Event of an Emergency – Evacuation NOT Required

11. Strike either Emergency Stop Button to stop the gas flow.
12. Close the two yellow propane gas shut off valves (#1 and #2, shown below) to the right of the mass flow meter.
13. Close all gas valves and gas bottles outside the back door of the structures lab.

Resetting the Gas Supply after an Emergency Stop

14. If an Emergency Stop Button is pressed, the gas supply must only be reset by an experienced technician.
15. The emergency gas shutoff solenoid valve is not designed to be a perfectly closed valve, therefore there will be small amount of propane leaking through.
16. Close all valves (#1-5) in the system.
17. Release the Emergency Stop Buttons.

This document is intended for use by the University *of* Edinburgh staff and students only
The University of Edinburgh is a charitable body, registered in Scotland, with registration number SC005336

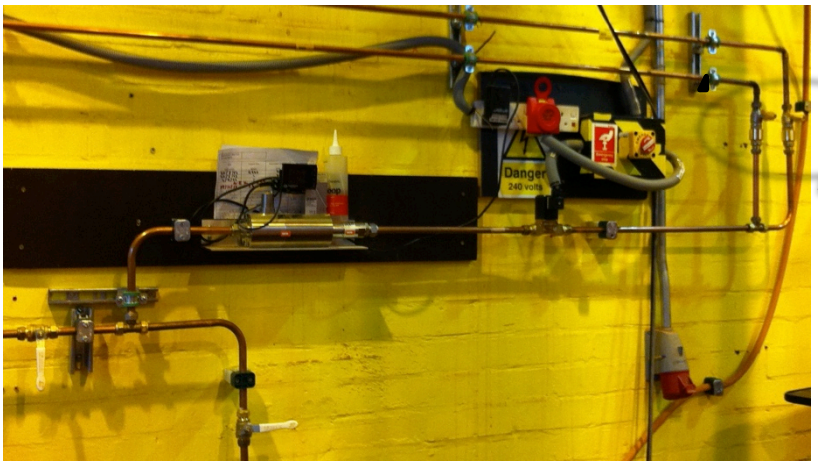

After the test – close these valves

(#1 and #2)

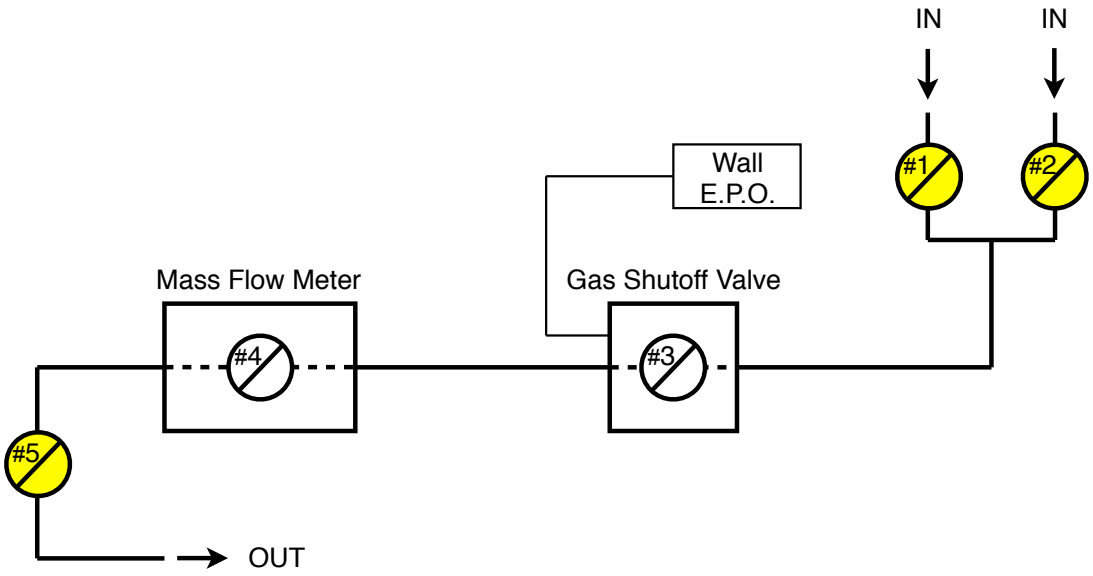

After Testing

18. Once the testing apparatus has extinguished, close the two yellow propane gas shut off valves to the right of the mass flow meter (#1 and #2).

19. Close all gas valves and bottles outside the back door of the structures lab.

This document is intended for use by the University *of* Edinburgh staff and students only
The University of Edinburgh is a charitable body, registered in Scotland, with registration number SC005336

Review required 1 July 2014

Verification by users

Sign below to indicate you have read and understood the safe system of work.

Signature:	Date:

This document is intended for use by the University *of* Edinburgh staff and students only
The University of Edinburgh is a charitable body, registered in Scotland, with registration number SC005336

Safe System of Work
Electrical Control System for
Radiant Panel Array Ignition

School SSW number: STR0017

Overview

This document is designed to give an overview of the mode of operation of the electrical control box for gas radiant panels. The control system provides electric ignition and automatic shut off of the gas in the event of flame failure.

It is imperative that all users receive training before using the device. Only approved users (named on the structures lab wiki) are allowed to use this equipment.

This document is not an instruction manual for use of the system.
It is not a substitute for training.

A separate safe system of work describes use of the gas radiant panels. As noted there, lab access is restricted during use of the radiant panels to ensure safe operation.

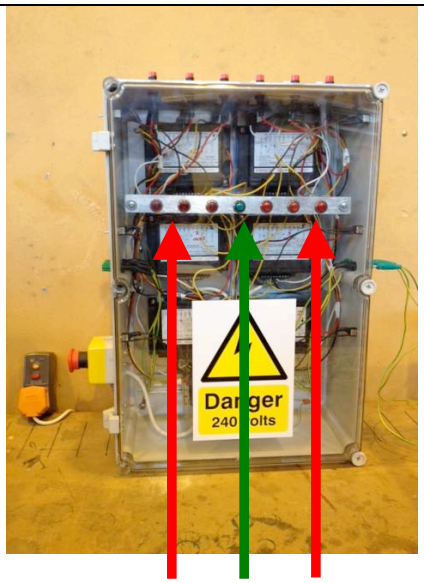

Green neon in centre – lit when box is live

6 Red neons – lit sequentially when individual panel probe(s) are live

Key Watchpoints

- The system has one Emergency Power Off button (E.P.O.), which should be struck in the event of emergency. All users must be familiar with safe use of the E.P.O.s.
- The ignition probes and other equipment must only be installed by qualified users. Incorrect installation will lead to dangerous stray current, which is both potentially lethal and can cause serious damage to equipment (such as data loggers). If you do not fully understand the importance of “arcing” and “earthing”, you must not install or use this equipment.
- Danger of electric shock and burns (mains voltage 240V and high voltage 20kV ignition system).
- All users personnel MUST stay clear/keep clear of the RED high voltage outputs

This document is intended for use by the University *of* Edinburgh staff and students only
The University of Edinburgh is a charitable body, registered in Scotland, with registration number SC005336

Required PPE

The following PPE is required at all times when using the Electrical Control Box. Other PPE may be required for a particular test, and must be assessed on a case by case basis:

A lab coat should be worn at all times to help protect against electric shock.

Equipment Safety Features

1. This control box must always be used with a residual current device (RCD).

2. This equipment has an Emergency Power Off Button (E.P.O.). The E.P.O. on the left side of the control box turns off all power and the gas supply to the radiant panels during an emergency.

3. This equipment should always be used the Emergency Gas Supply Shutoff E.P.O. button. This is a separate system, which closes a valve on the lab gas supply when the emergency power off button is struck. This second E.P.O. button is on a remote lead that can be positioned near your work. See the separate Safe System of Work.

Description of the Electrical Control System

4. The electrical control system provides remote control of the radiant panels. Each of six radiant panels can be controlled individually. It incorporates:
   - electric ignition
   - control of gas supply
   - automatic shutdown of gas supply in the event of flame failure

5. To use this system, each radiant panel must be fitted with a solenoid valve to control its gas supply, an ignition spark (two probes: earth and 20kV), and a flame detect probe. The panel must also be independently earthed.

6. Connections from the box are colour coordinated 4mm banana plug extension sockets mounted on the box top:

   Red - 20 kV supply to ignition probe.
   Black - 240 V on/off switch Valve 1 (pilot gas supply).
   White - 240 V on/off switch Valve 2 (main gas supply).
   Yellow - flame sensor probe.

This document is intended for use by the University *of* Edinburgh staff and students only
The University of Edinburgh is a charitable body, registered in Scotland, with registration number SC005336

Green - return and earth.

7. Connections between the radiant panels and the control box are by means of the appropriate colour coded and labelled cables. These extensions must be protected in appropriate sheathing, overhead cable run channels, or within ground level anti-trip cable protectors.

8. Six On/Off switches on the side of the control box provide automated control of the six individual panels.

Connection of one Radiant Panel to the Electrical Control Box

Ignition probe connection

9. The panel ignition is by means of two probes that must be held with a gap of 2 to 3mm gap between their tips. A ceramic terminal block can be used to adjust the gap between the probes. The probes must be rigidly mounted onto the support structure so that there is no danger of them moving or being knocked.

10. Ceramic spine beads are used to ensure that the ignition spark occurs only at the tip of the probe, and that the spark does not leak to the mounting frame. Feed ceramic spine beads onto the two ignition probes and secure onto probe with a single metal terminal block at the probe end.

11. Set the gap between the probe tips to 2 to 3mm (for example, use an appropriate size of drill bit to check the gap size). If the gap is incorrect, high voltage can leak within the electrical control box (between the right of the individual black box(s) and the electrical control box back plate).

12. Connect the red 20 kV firmly / hand tight to the end of a long probe using a spade or bullet terminal and a securing nut.

13. Connect the green earth firmly / hand tight to the end a second long probe using a spade or bullet terminal and a securing nut.

14. The radiant panels and the radiant panel support frame must be fitted with an independent earth wire, which is a separate earth back to the control box. This earth wire provides a second safe route for high voltage in case of failure of the return from the ignition probes. It should be checked for continuity using an appropriate meter.

15. The high voltage system must be electrically isolated from data logging equipment (such as the Vishay System 7000). Stray kilovolts are very likely to cause irreparable and expensive damage the data logger, which is designed to measure millivolts. The gas radiant panel can be isolated from the remainder of a test frame using ceramic washers and ceramic tubes. Do not rely only on the earth system. Electrical isolation will also avoid the risk of the main test frame becoming live due to stray voltage. Check that radiant panel assembly and the main test frame are electrically isolated using an appropriate meter.

Flame failure probe connection

16. Mount the flame sensor securely so that it will not move or be knocked during operation.

17. Connect the yellow flame sensor firmly/hand tight to the end of a short probe using a spade terminal and a securing nut

This document is intended for use by the University *of* Edinburgh staff and students only
The University of Edinburgh is a charitable body, registered in Scotland, with registration number SC005336

Operation of the Electrical Control Box During a Test

Before each Test

18. Make sure all lab users know that you are about to start a test, and that everyone in the lab is wearing appropriate PPE (including safety boots and glasses). Check that everyone in the lab knows the location and purpose of the E.P.O. button.

19. Unwanted noise and other activity can distract from the test and distract from safe conduct of the test. The radio must be turned off, any noisy activities (such as hammering or angle grinding) stopped, and spectators asked to leave.

20. Carefully check that the probes and connections are correctly set up (refer to the previous section) before every use. In particular, check the gap between the red and green ignition probes is between 2 and 3mm.

Lighting the Panels

21. Switch on mains power and press Reset to activate the R.C.D. The labelled central green neon light shows that the box has mains power.

22. Turn on the air supply (refer to the SSW for the radiant panels).

23. Switch each individual panel using the On/Off switches on the side of the electrical control box. The labelled red neon light(s) indicate power to the respective panels.

24. The start up sequence when a panel is turned on is as follows:

    - The flame sensor probe is active as soon as the panel is turned on.
    - There is a 5 to 7 second purge time after power is provided to the panel.
    - Immediately, valve 1 (the pilot gas supply) opens in conjunction with ignition sparking for 14 seconds or until the flame is sensed. The red neon will be off while sparking is in progress.
    - If a flame is sensed and ignition is successful, valve 1 (the pilot supply) stays open and valve 2 * (the main gas supply) opens to increase the gas flow to the radiant panel. Sparking will stop once a flame is detected.
    - If ignition does not occur within 14 seconds, the start up sequence is aborted, the control box shuts down, and the gas is turned off to that panel. Turn off the individual panel using the individual On/Off switch on the side of the box and repeat the steps above to light the panel.

    * It may be possible to run the gas panel using only the pilot gas supply with the agreement of the fire lab technician.

During Use of Panels

25. Never leave the control unit or panels unattended whilst they are burning. The control unit operator should be watching, listening and smelling for electrical

This document is intended for use by the University *of* Edinburgh staff and students only
The University of Edinburgh is a charitable body, registered in Scotland, with registration number SC005336

'arcing'.

26. If the panel stops burning, the gas supply will be automatically turned off. If it is safe to re-ignite the panel turn the individual panel switch off, then repeat the steps above.

To Turn Off an Individual Panel

27. An individual radiant panel can be turned off using the On/Off switch on the side of the control box. This will turn off the gas supply to that panel.

Turning Off the Panels at the End of a Test

28. Use the two yellow gas shut off valves in the propane supply (to the right of the mass flow meter) to turn off the gas supply. The radiant panels will extinguish. (NB: This method of turning off the panels will use up the gas held within the length of pipe from the valves to the radiant panels, which will not happen if the panels are turned off using the switches on the control box).

29. After the radiant panels have extinguished, turn off the control box by striking the E.P.O. button. Then turn off the individual panel switches, and turn off mains power.

Review required 1 July 2014

Verification by users

Sign below to indicate you have read and understood the safe system of work.

Signature:	Date:

This document is intended for use by the University *of* Edinburgh staff and students only
The University of Edinburgh is a charitable body, registered in Scotland, with registration number SC005336

General Risk Assessment

Form RA1

(Refer to Notes for Guidance before completing this form)

School Assessment No:	STR0017
Title of Activity:	Electronics Box for Contorl of Radiant Panel Array
Location(s) of Work:	Structures Laboratory, The University of Edinburgh, The King's Buildings, Mayfield Road, Edinburgh, EH9 3JL

Brief Description of Work:

The Electronic Control System Box provides the semi-automated control of the gas radiant panels:

- spark ignition using 20kV
- gas supply using solenoid valves
- gas shut off in the event of flame failure or if the panels fail to ignite.

Hazard Identification: Identify all the hazards; evaluate the risks (low / medium / high); describe all existing control measures and identify any further measures required. Specific hazards should be assessed on a separate risk assessment form and cross-referenced with this document. Specific assessments are available for hazardous substances, biological agents, display screen equipment, manual handling operations and fieldwork. See http://www.ed.ac.uk/schools-departments/health-safety/risk-assessments-checklists/risk-assessments for details.

Hazard(s)	**Present Risk Evaluation** L/M/H	**Control Measures** (i.e., alternative work methods / mechanical aids / engineering controls, etc.)	**Risk Evaluation after control** L/M/H
Electric Shock	H	- Signage for overhead electricity cables (for the attention of crane users in particular). - All cables must have secondary sheathing (Copex tubing or similar, or other cable protectors). - Residual current device (RCD)	L

This document is intended for use by the University *of* Edinburgh staff and students only
The University of Edinburgh is a charitable body, registered in Scotland, with registration number SC005336

		must always be fitted to the mains supply for this equipment. - EPO fitted to electronic box and magnetic EPO on spiral for placement near experiment users - Electronics contained in IP67 Class box. - Electrical insulation tape around side of individual black box(s) to stop spark leakage inside the electrical control box. - Nearby lab users warned of sparking between individual panel probes - Spark probe testing undertaken in quiet area of lab, where people will not walk past and brush against live probes - The radiant panel support frame will be electrically isolated from the main support frame by means of ceramic spacers in case of stray voltage. - The radiant panels and the radiant panel support frame will be earthed with an earth cable that runs to the control box and is separate to the return from the ignition probes.	
Trip Hazard	M	- All electrical cables to be gathered within sheathing, and will be carried at high level to avoid trip hazards.	L
Malfunction of control equipment (for example, leading to incorrect gas supply).	H	- A list of approved users is kept on the lab wiki, and only these users may use the equipment. - The equipment must be carefully checked before every use, including correct operation of the solenoid valves, and the ignition probe gap.	L

This document is intended for use by the University *of* Edinburgh staff and students only
The University of Edinburgh is a charitable body, registered in Scotland, with registration number SC005336

		- The gas supply is fitted with an independent solenoid shut off valve, as well as an independent manual shut off valve. - An Emergency Power Off button is provided to shut down the system in the event of malfunction. - The panels and control system will never be left unattended, and must be observed (visually, by sound, and by smell) at all times.	
Conduction of electricity through frame. As well as physical injury, this can cause serious damage to data logging equipment.	H	- Electrical isolation of radiant panel support frame from main test frame (check with an appropriate meter), and provision of an independent earth cable from the radiant panel assembly back to the control box (check with an appropriate meter). - Ceramic spline insulation on spark probes. - Ceramic electrical blocks used to keep sparking probe gap at required 2-3mm, to stop spark leakage at other connections - RCD fitted to mains	L

**Continue on separate sheet if necessary*

Engineering Controls: *Tick relevant boxes*

Guarding		Extraction (LEV)		Interlocks		Enclosure	
Other relevant information (incl. testing frequency if appropriate): Signage posted on overhead electricity cables							

This document is intended for use by the University *of* Edinburgh staff and students only
The University of Edinburgh is a charitable body, registered in Scotland, with registration number SC005336

Personal Protective Equipment (PPE): Identify all necessary PPE.

Eye / Face	✔	Hand /Arm	✔	Feet / Legs	✔	Respiratory	
Body (clothing)	✔	Hearing		Other (Specify)			
Specify the grade(s) of PPE to be worn: • safety glasses with side protection • gloves • safety boots • lab coat							
Specify when during the activity the item(s) of PPE must be worn: To be worn at all times during use and installation.							

Non-disposable items of PPE must be inspected regularly and records retained for inspection

Persons at Risk: Identify all those who may be at risk.

Academic staff	✔	Technical staff	✔	P'Grad students	✔	U'Grad students	✔
Maintenance staff		Office staff		Cleaning staff		Emergency personnel	
Contractors		Visitors		Others			

Additional Information: Identify any additional information relevant to the activity, including supervision, training requirements, special emergency procedures, requirement for health surveillance etc.

Assessment carried out by:

Name:	Kevin Tierney/Holly Smith	Date:	17 AUG 2012
Signature:		Review Date:	17 AUG 2013

This document is intended for use by the University *of* Edinburgh staff and students only
The University of Edinburgh is a charitable body, registered in Scotland, with registration number SC005336

Review required 1 July 2014

Verification by users

Sign below to indicate you have read and understood the safe system of work.

Signature:	Date:

This document is intended for use by the University *of* Edinburgh staff and students only
The University of Edinburgh is a charitable body, registered in Scotland, with registration number SC005336

B

CONCRETE MOISTURE CONTENT WITH TIME

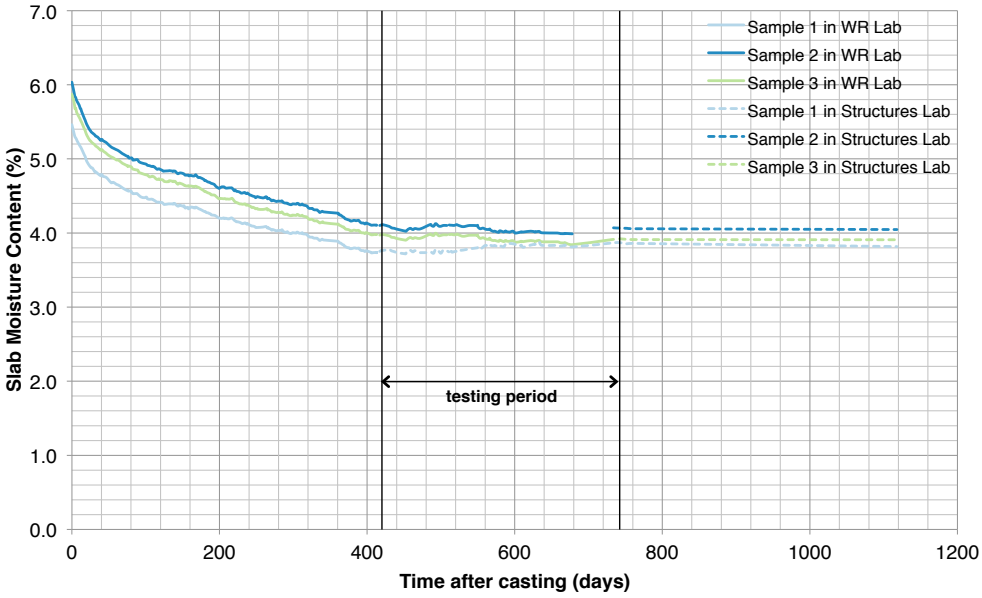

Figure B.1: Graph of slab-column concrete moisture content

C

SLAB CONCRETE DESIGN CERTIFICATE

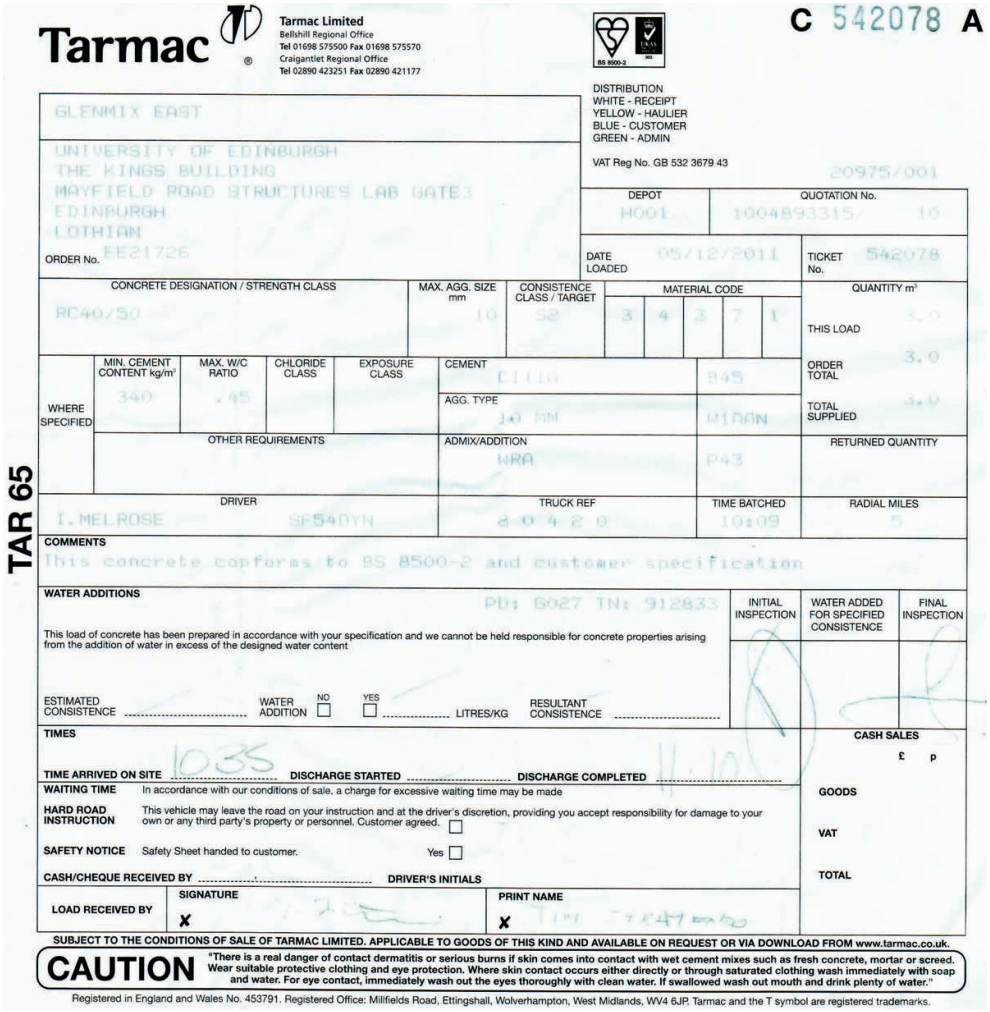

Tarmac

Tarmac Limited
Bellshill Regional Office
Tel 01698 575500 Fax 01698 575570
Craigantlet Regional Office
Tel 02890 423251 Fax 02890 421177

C 542078 A

DISTRIBUTION
WHITE - RECEIPT
YELLOW - HAULIER
BLUE - CUSTOMER
GREEN - ADMIN

VAT Reg No. GB 532 3679 43

GLENMIX EAST

UNIVERSITY OF EDINBURGH
THE KINGS BUILDING
MAYFIELD ROAD STRUCTURES LAB GATE3
EDINBURGH
LOTHIAN

ORDER No. EE21726

20975/001

DEPOT H001 | QUOTATION No. 1004893315/ 10

DATE LOADED 05/12/2011 | TICKET No. 542078

TAR 65

CONCRETE DESIGNATION / STRENGTH CLASS	MAX. AGG. SIZE mm	CONSISTENCE CLASS / TARGET	MATERIAL CODE	QUANTITY m³
RC40/50	10	S2	3 4 3 7 1	THIS LOAD 3.0

WHERE SPECIFIED	MIN. CEMENT CONTENT kg/m³	MAX. W/C RATIO	CHLORIDE CLASS	EXPOSURE CLASS	CEMENT		ORDER TOTAL 3.0
	340	.45			CEM1	P45	
					AGG. TYPE		TOTAL SUPPLIED 3.0
					14 MM	WIGAN	
	OTHER REQUIREMENTS				ADMIX/ADDITION		RETURNED QUANTITY
					WRA	P43	

DRIVER	TRUCK REF	TIME BATCHED	RADIAL MILES
I.MELROSE SE54DYN	8042O	10:09	5

COMMENTS
This concrete conforms to BS 8500-2 and customer specification

WATER ADDITIONS
PO: 6027 TN: 912833

This load of concrete has been prepared in accordance with your specification and we cannot be held responsible for concrete properties arising from the addition of water in excess of the designed water content

ESTIMATED CONSISTENCE ..... WATER ADDITION NO ☐ YES ☐ ..... LITRES/KG RESULTANT CONSISTENCE .....

INITIAL INSPECTION	WATER ADDED FOR SPECIFIED CONSISTENCE	FINAL INSPECTION

TIMES

TIME ARRIVED ON SITE 1035 DISCHARGE STARTED ..... DISCHARGE COMPLETED 11.10

CASH SALES £ p

WAITING TIME In accordance with our conditions of sale, a charge for excessive waiting time may be made

HARD ROAD INSTRUCTION This vehicle may leave the road on your instruction and at the driver's discretion, providing you accept responsibility for damage to your own or any third party's property or personnel. Customer agreed. ☐

SAFETY NOTICE Safety Sheet handed to customer. Yes ☐

CASH/CHEQUE RECEIVED BY ..... DRIVER'S INITIALS .....

GOODS

VAT

TOTAL

LOAD RECEIVED BY	SIGNATURE	PRINT NAME
	✘	✘

SUBJECT TO THE CONDITIONS OF SALE OF TARMAC LIMITED. APPLICABLE TO GOODS OF THIS KIND AND AVAILABLE ON REQUEST OR VIA DOWNLOAD FROM www.tarmac.co.uk.

CAUTION "There is a real danger of contact dermatitis or serious burns if skin comes into contact with wet cement mixes such as fresh concrete, mortar or screed. Wear suitable protective clothing and eye protection. Where skin contact occurs either directly or through saturated clothing wash immediately with soap and water. For eye contact, immediately wash out the eyes thoroughly with clean water. If swallowed wash out mouth and drink plenty of water."

Registered in England and Wales No. 453791. Registered Office: Millfields Road, Ettingshall, Wolverhampton, West Midlands, WV4 6JP. Tarmac and the T symbol are registered trademarks.

Figure C.1: Tarmac readymix concrete receipt

CONCRETE DESIGN CERTIFICATE

GLEN MIX

Mix Design Certificate 1004901818 **Quotation Number** 1004893315
Dated 15.12.2011 **Your Ref.**

Tarmac Limited
PO Box 8720
Bellshill
ML4 3WB
Tel 01698 575 500
Fax 01698 575 570
Web www.tarmac.co.uk

To: SCHOOL OF ENGINEERING STORES
UNIVERSITY OF EDINBURGH
FINANCE DEPARTMENT
9-16 CHAMBER STREET
EH1 1HT

Site DELIVERED 1-10 RADIALS
EDINBURGH
LOTHIAN
.

Our Representative: TQM CUST SERVICES NORTH & SCOT

Specification	**Our Ref.:**
Plant	Glenmix East East
Concrete Grade	RC40/50
Cement Type	CIIIA 42.5L
Maximum Aggregate Size (mm)	10
Target Slump (mm)	S2
Minimum Cement Content	340
Max Water / Cement Ratio	0.45

Mix Design: Materials & Mix Proportions: kg/m^3 at SSD

CEM I 52.5N	214
GGBS BS 6699	214
4/10mm Single Size Conc Agg	1061
0/4mm Washed Conc Sand MP	727
MIRA 71 Water Reducer Grace (C P) - Warrington	1.28
Water	177
Aggregate/ Cement Ratio	4.18
Water/ Cement Ratio	0.41
Percentage Fines	40.66

Please Note:

HEALTH & SAFETY
There is a real danger of contact dermatitis or serious burns if skin comes into contact with wet cement mixes such as fresh concrete, mortar or screed. Wear suitable protective clothing and eye protection. Where skin contact occurs either directly or through saturated clothing wash immediately with soap and water. For eye contact, immediately wash out the eyes thoroughly with clean water. If swallowed wash out mouth and drink plenty of water.

For and on behalf of
Tarmac Limited

This design is relevant to the above quotation of which it is a part thereof and subject to our Standard Conditions of Sale
This certificate is for illustrative purposes only, the materials and mix design(s) are those in current production, these may be changed and/or modified when material properties vary or supply sources change.

BS 8500-2 UKAS PRODUCT CERTIFICATION 003

Technical Services Department

Glenmix is a trading name of Tarmac Limited.
Registered in England and Wales No. 453791.
Registered Office: Millfields Road, Ettingshall, Wolverhampton, West Midlands, WV4 6JP.
A member of the Anglo American plc Group

Figure C.2: Tarmac readymix design certificate

LAFARGE TARMAC

Product Data Sheet

Lafarge Tarmac - North & Scotland Region

Ravelrig Quarry

Address -

Typical Aggregate properties					Typical Chemical Analysis		
Particle Density	Oven Dried	2.61		EN 1097-6	Iron	% as FE_2O_3	10.03
	Saturated Surface Dry	2.70			Calcium	% as CaO	6.54
	Apparent	2.86			Silicon	% as SiO_2	53.55
Water Absorption		3.3	%	EN 1097-6	Magnesium	% as MgO	4.56
Aggregate Abrasion Value (AAV)		6.3		EN1097-8	Aluminum	% as Al_2O_3	15.12
Polished Stone Value (PSV)		55		EN1097-8	Phosphorus	% as P_2O_5	0.15
Los Angeles Coefficient (LA)		20		EN1097-2	Titanium	% as TIO_2	2.15
Micro-Deval Coefficient (M_{DE})		21		EN1097-1	Potassium	% as K_2O	1.1
Magnesium Sulfate Soundness		9	%	EN1267-2	Sodium	% as Na_2O	1.98
Water Soluble Chloride		<0.001	%	EN1744-1			
Water Soluble Sulphate		<0.01	%	EN1744-1			
Acid Soluble Sulphate		<0.01	%	EN1744-1	Loss on Ignition	@ 1000C	1.3
Total Sulfur		0.057	%	EN1744-1	**Additional Information :**		
Carbon Dioxide Content		0.4	%	EN196-21	Ten percent Fines Value		250kN
Drying Shrinkage		0.042	%	EN1367-4	Modified ten percent Fines Value		230kN
Resistance to Breakage		88	Mpa	EN1926			
Proportion of Crushed/Broken Surfaces		100	%	EN13383-1			
Resistance to Freeze Thaw		NPD	%	EN13383-2			
Water Absorption		NPD	%	EN13383-2			
Sonnenbrand		None		EN13383-2			
Resistance to Fragmentation (Track Ballast)		NPD		EN1097-2			
Resistance to Wear (Track Ballast)		NPD		EN1097-2			

Issued By :

Christopher Abbott
Technical Systems Manager

Date of Issue : 30/05/2013

Notes
1. The above data is provided in good faith as a guide to typical values and does not constitute a specification
2. The company reserves the right to revise the data at any time
3. Individual Certification available on request

Figure C.3: Tarmac concrete product data sheet

D

OPTIMUM MIX VALVE SETTINGS FOR THE RADIANT PANELS

Table D.1 presents the calibrated optimum radiant panels mix valve settings. Figure D.1 shows the orientation of the numbered radiant panels in Table D.1.

PANEL NO.	MIX VALVE SETTING
1	4.5-4.75
2	4.25
3	7.75-8
4	4
5	5.25-5.5
6	7

Table D.1: Slab testing optimum mix valve settings

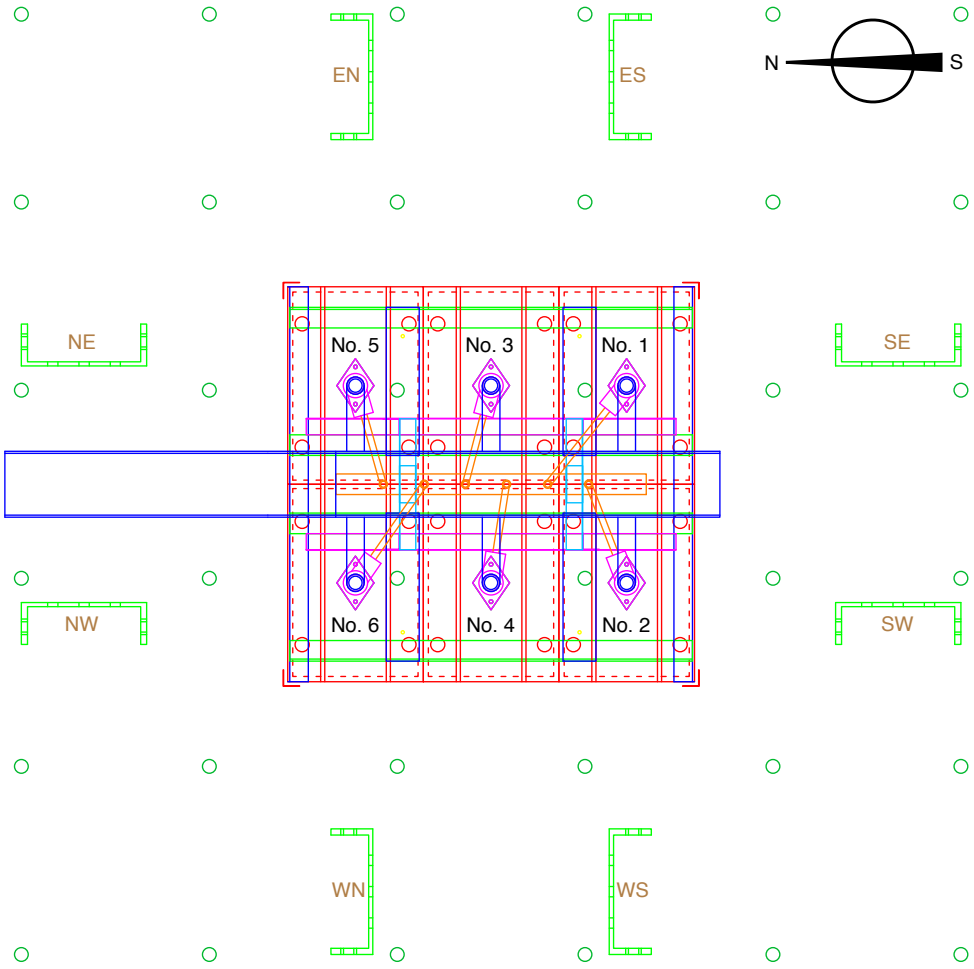

Figure D.1: Schematic of the radiant panel array from plan view

E

STRAIN GAUGE CALIBRATION

The strain gauges were not used to measure a meaningful value of strain, rather they acted as load cells. Calibration factors were found for each strain gauge bridge to convert the measured strain into a load. The calibration was undertaken 3 times throughout slab testing series as some gauge bridges and wiring required fixing or replacement. Where multiple calibrations were undertaken for a gauge bridge, an average calibration factor was used.

Figure E.1 shows that the calibration setup of the N–S strain gauges. A known force, N was applied across the frame and the strain from the gauges was recorded. The N–S and E–W frame sides were calibrated separately. The known calibration force was always applied half way between the above (A) and below (B) gauge pairs and in the centre of the columns. The gauge bridges recorded a linear elastic increase in strain proportional to the load applied.

Figures E.2–E.5 show the known loads applied to the gauge pairs plotted against the recorded gauge pair strain readings. The strain gauge calibration factors were found as the gradient of the best fit line.

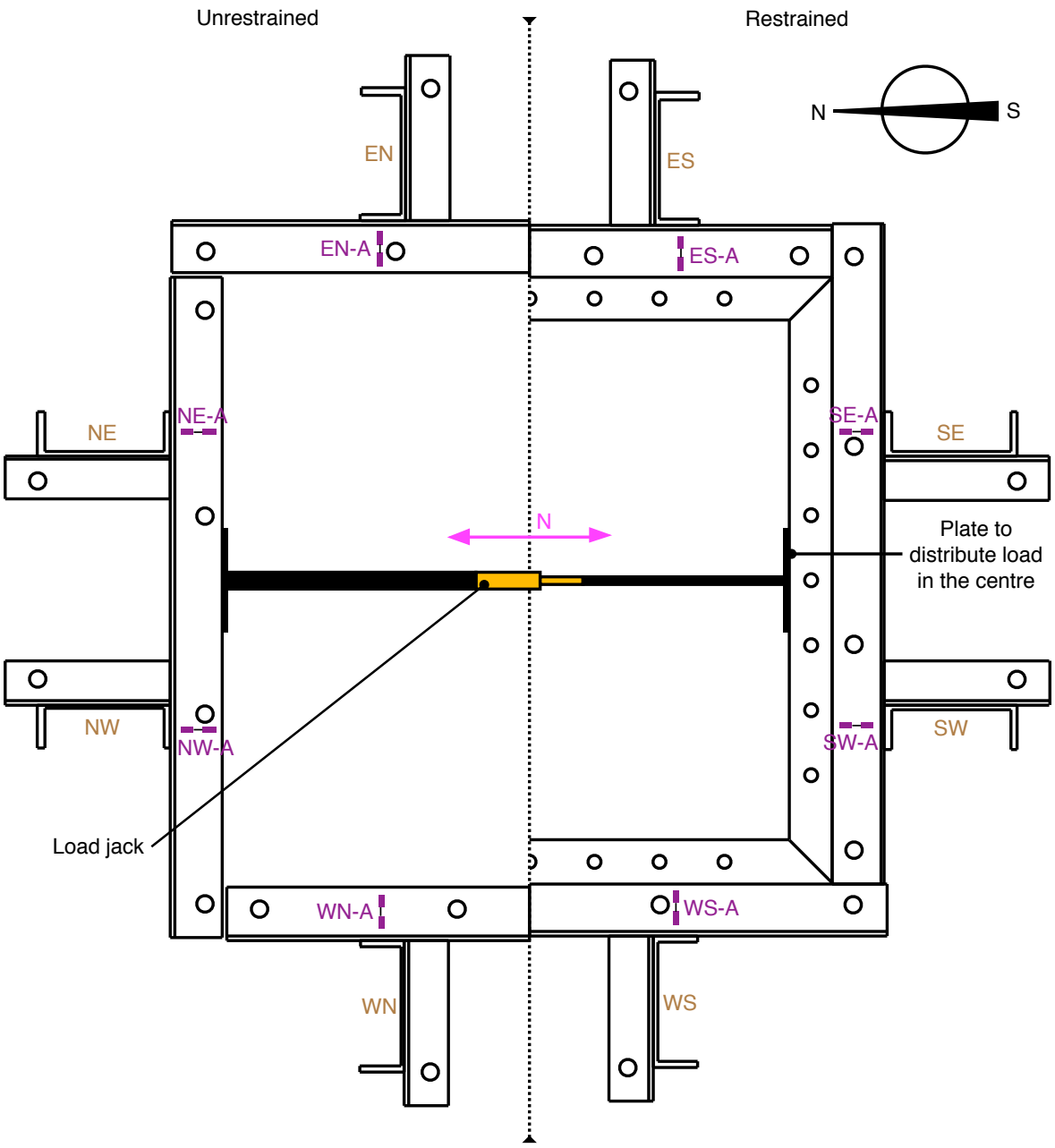

Figure E.1: Plan view schematic of strain gauge calibration setup

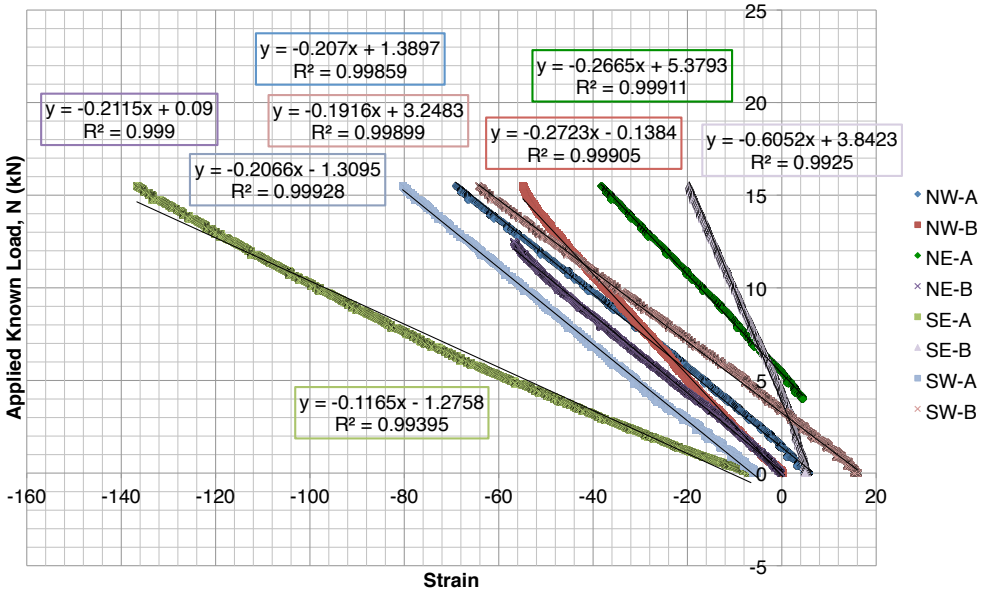

(a) 08 August 2012 calibration

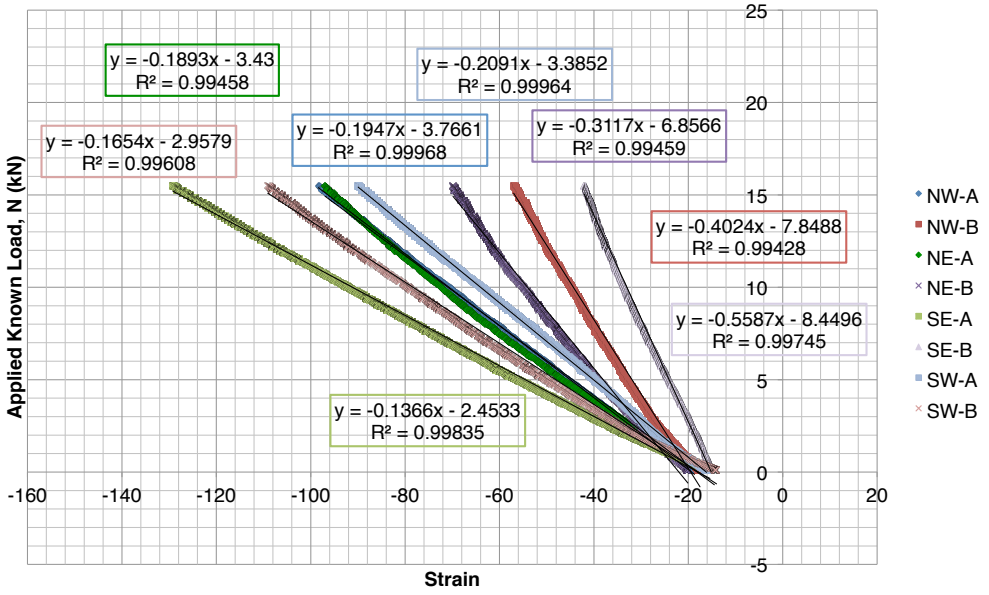

(b) 15 August 2012 calibration

Figure E.2: N–S strain gauge calibration graphs

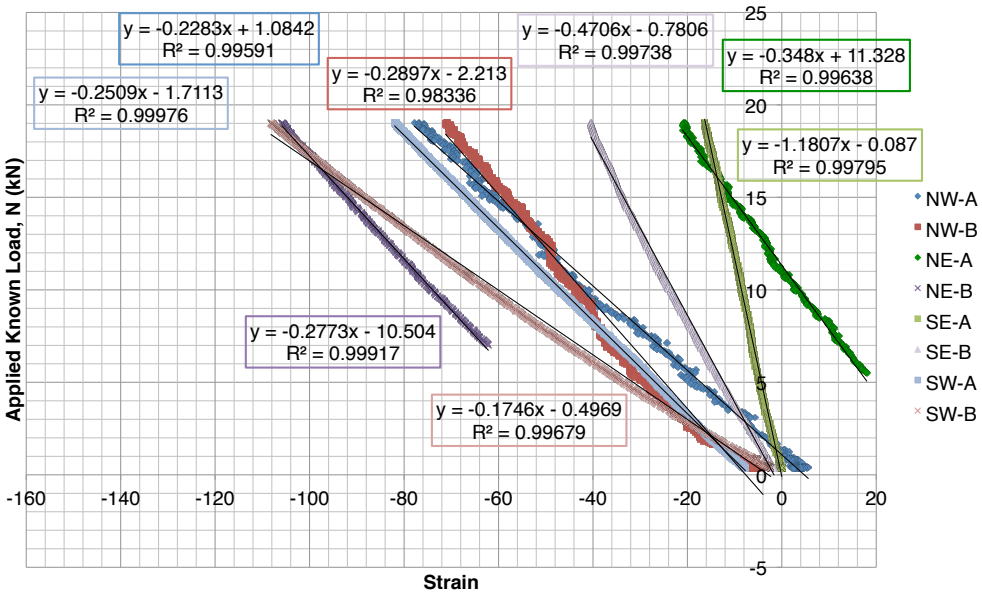

(a) 06 February 2014 calibration

Figure E.3: N–S strain gauge calibration graphs

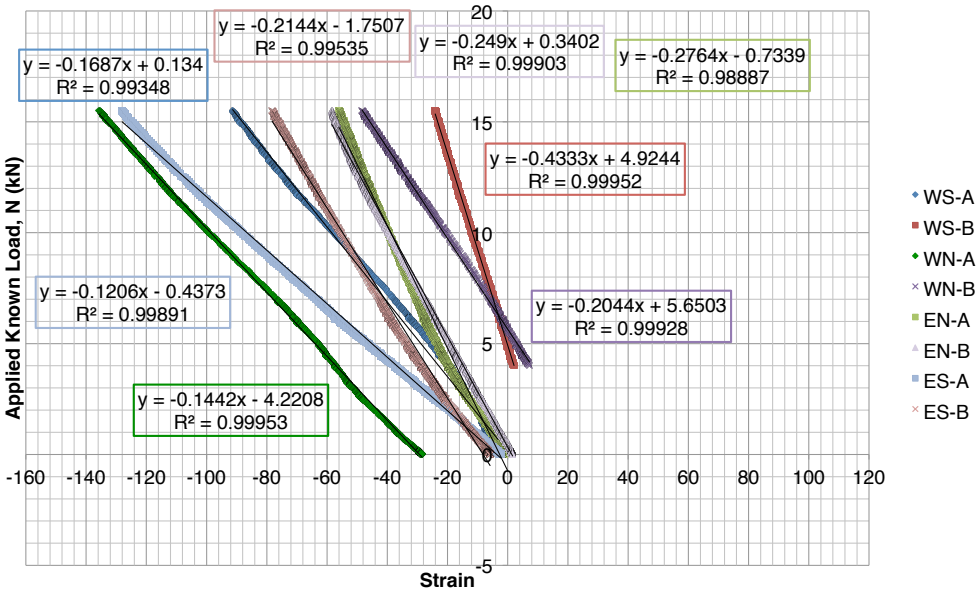

(a) 15 August 2012 calibration

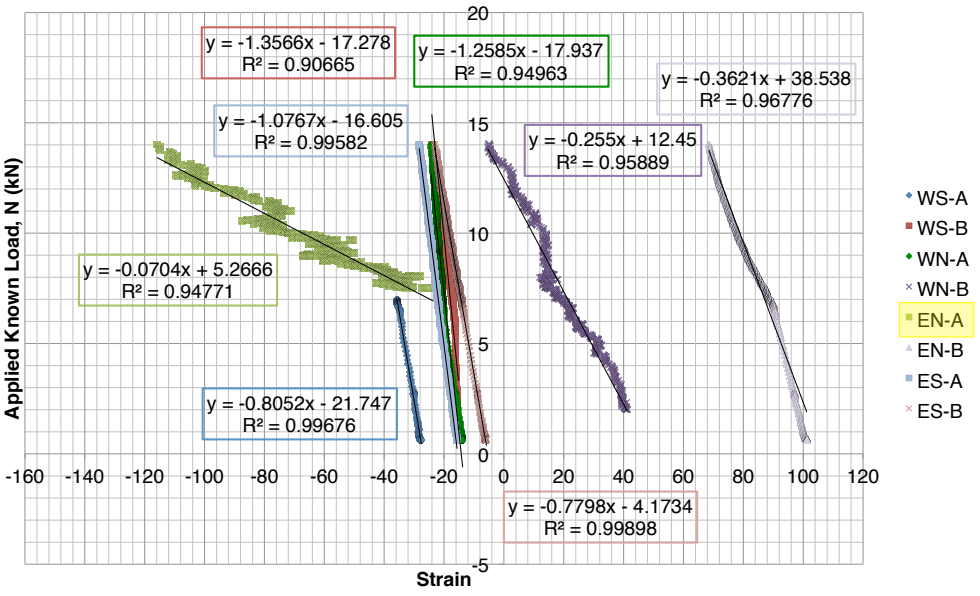

(b) 22 November 2013 calibration

Figure E.4: E–W strain gauge calibration graphs

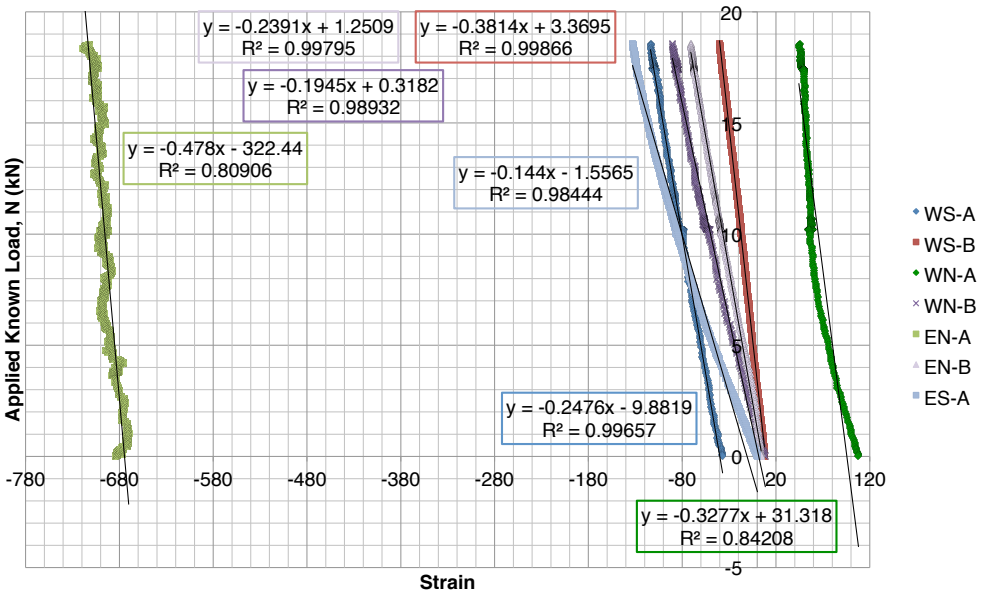

(a) 06 February 2014 calibration

Figure E.5: E–W strain gauge calibration graphs

The strain gauge calibration factors used for each slab test are given in Tables E.1 and E.2. Calibration data from E–W frame on 22 November 2013, as shown in Figure E.4b was deemed unreliable. However, calibration data from gauge EN–A was required to be used as there was no other data available for this gauge for 11 of the slab tests. It was not required for tests AU100-0.8 and HR100-1.5, where there was other calibration data available.

The structural frame reaction forces on the slab specimen were calculated for each column by multiplying the gauge bridge readings by the calibration factors in Tables E.1 and E.2. The strain gauge calibration factors were used to calculate the above and below slab level reaction force, F_A and F_B respectively. These structural frame reaction forces were used in force and moment equilibrium equations to find the in-plane reaction forces, N and moments, M imparted by the slab on the four sides of the reaction frame.

Figure 5.15 shows the lever arm distances for the moment calculation for the 100 mm slab thickness. The lever arm distances for all 3 slab thickness cases are given in Table E.3.

The in-plane reaction forces and moments (highlighted in pink in Figure 5.15) are calculated from force and moment equilibrium:
Case 100 mm slab thickness:

$$\begin{aligned} N &= \frac{31}{65}F_A + \frac{34}{65}F_B, \\ M &= 0.155F_B - 0.17F_A \end{aligned} \tag{E.1}$$

Case 75 mm slab thickness:

$$\begin{aligned} N &= \frac{67}{130}F_A + \frac{63}{130}F_B, \\ M &= 0.1675F_B - 0.1575F_A \end{aligned} \tag{E.2}$$

Case 50 mm slab thickness:

$$\begin{aligned} N &= \frac{36}{65}F_A + \frac{29}{65}F_B, \\ M &= 0.18F_B - 0.145F_A \end{aligned} \tag{E.3}$$

where:

N = in-plane reaction force of the slab on the frame (kN)
M = reaction moment of the slab on the frame (kNm)
F_A = above (A) stain gauge reaction force on the slab (kN)
F_B = below (B) strain gauge reaction force on the slab (kN)

SPECIMEN ID	STRAIN GAUGE ID							
	NW-A	NW-B	NE-A	NE-B	SW-A	SW-B	SE-A	SE-B
AU50-0.8	-0.21000	-0.33735	-0.26793	-0.26683	-0.25090	-0.17720	-1.18070	-0.54483
AU75-0.8	-0.21000	-0.33735	-0.26793	-0.26683	-0.25090	-0.17720	-1.18070	-0.54483
AU100-0	-0.21000	-0.33735	-0.26793	-0.26683	-0.20785	-0.17720	-1.18070	-0.54483
AU100-0.8	-0.21000	-0.33735	-0.26793	-0.26683	-0.20785	-0.17720	NA	-0.54483
AU100-1.5	-0.21000	-0.33735	-0.26793	-0.26683	NA	-0.17720	-1.18070	-0.54483
HU50-0.8	-0.21000	-0.33735	-0.26793	-0.26683	-0.25090	-0.17720	-1.18070	-0.54483
HU75-0.8	-0.21000	-0.33735	-0.26793	-0.26683	-0.25090	-0.17720	-1.18070	-0.54483
HU100-0	-0.21000	-0.28970	-0.26793	-0.26683	-0.25090	-0.17720	-1.18070	-0.54483
HU100-0.8	-0.21000	-0.28970	-0.26793	-0.26683	-0.25090	-0.17720	-1.18070	-0.54483
HU100-1.5	-0.21000	-0.28970	-0.26793	-0.26683	-0.25090	-0.17720	-1.18070	-0.54483
HR50-0.8	-0.21000	-0.33735	-0.26793	-0.26683	-0.25090	-0.17720	-1.18070	-0.54483
HR75-0.8	-0.21000	-0.33735	-0.26793	-0.26683	-0.25090	-0.17720	-1.18070	-0.54483
HR100-0	-0.21000	-0.28970	-0.26793	-0.26683	-0.25090	-0.17720	-1.18070	-0.54483
HR100-0.8	-0.21000	-0.33735	-0.26793	-0.26683	-0.25090	-0.17720	-1.18070	-0.54483
HR100-1.5	-0.21000	-0.28970	-0.26793	-0.26683	-0.25090	-0.17720	-1.18070	-0.54483

Table E.1: Calibration factor (kN) for N–S frame strain gauges in each slab test (NA specified where no gauge data was recorded)

SPECIMEN ID	STRAIN GAUGE ID							
	WN-A	WN-B	WS-A	WS-B	EN-A	EN-B	ES-A	ES-B
AU50-0.8	-0.23595	-0.19945	-0.20815	-0.40735	-0.07040	-0.24405	-0.12060	-0.21440
AU75-0.8	-0.23595	-0.19945	-0.20815	-0.40735	-0.07040	-0.24405	-0.12060	-0.21440
AU100-0	-0.23595	-0.19945	-0.20815	-0.40735	-0.07040	-0.24405	-0.12060	-0.21440
AU100-0.8	-0.23595	-0.19945	-0.20815	-0.40735	-0.27640	-0.24405	-0.12060	-0.21440
AU100-1.5	-0.23595	-0.19945	-0.20815	-0.40735	-0.07040	-0.24405	-0.12060	-0.21440
HU50-0.8	-0.23595	-0.19945	-0.20815	-0.40735	-0.07040	-0.24405	NA	-0.21440
HU75-0.8	-0.23595	-0.19945	-0.20815	-0.40735	-0.07040	-0.24405	NA	-0.21440
HU100-0	-0.23595	-0.19945	-0.20815	-0.40735	-0.07040	-0.24405	-0.14400	NA
HU100-0.8	NA	-0.19945	-0.20815	-0.40735	NA	-0.24405	-0.14400	NA
HU100-1.5	-0.23595	-0.19945	-0.20815	-0.40735	NA	-0.24405	-0.14400	NA
HR50-0.8	-0.23595	-0.19945	-0.20815	-0.40735	-0.07040	-0.24405	-0.12060	-0.21440
HR75-0.8	-0.23595	-0.19945	-0.20815	-0.40735	-0.07040	-0.24405	NA	-0.21440
HR100-0	-0.23595	-0.19945	-0.20815	-0.40735	-0.07040	-0.24405	-0.14400	NA
HR100-0.8	-0.23595	-0.19945	-0.20815	-0.40735	-0.07040	-0.24405	-0.14400	-0.21440
HR100-1.5	NA	-0.19945	-0.20815	-0.40735	-0.47800	-0.24405	-0.14400	–

Table E.2: Calibration factor (kN) for E–W frame strain gauges in each slab test (NA specified where no gauge data was recorded)

SLAB DEPTH (MM)	DISTANCE FROM A STRAIN GAUGE TO SLAB CENTER (MM)	DISTANCE FROM B STRAIN GAUGE TO SLAB CENTER (MM)
50	145	180
75	157.5	167.5
100	170	155

Table E.3: Lever arm distances for the moment calculation of different slab thicknesses

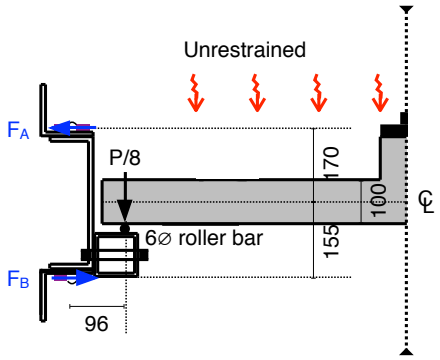

Figure E.6: Unrestrained test setup with applied load eccentric to the strain gauges

The net average in-plane reaction force, N and moments, M were calculated for all the tests, by averaging all the column data in each test.

The unrestrained test results of net axial force, N and moment, M were corrected for eccentricity. The load path in the unrestrained tests was as shown in Figure E.6. The eccentricity corrected net axial force and moment required the subtraction of $\frac{12}{325}P$ from both the above (F_A) and below (F_B) structural frame reaction forces. The restrained arrangement did not need this correction.

F

POST-PROCESSING MATLAB SCRIPT FOR HU75-0.8

```
% Script to plot displacement-position
%
% Holly Smith
% 25/11/2014

clear all, clc

% Go to folder for containing data from test
path='/Users/hols/Dropbox/SlabTesting/';
test='B2_HU75_075';
path=strcat(path,test,'/');
cd(path);

% User input constants
slab_height_stronghold = mean([1190 1190 1190 1195]); %mm

% Cameras - 'W' 'S' 'E', if only running for W then deete
    S and E, but
% cannot run for either S or E without W
cameras = {'W' 'S' 'E'};
camera_height_stronghold = [95 125 140]; %mm
horiz_dist_to_slab_centroid = [(1143.1+363) (1143.1+345)
    (1143.1+345)]; %mm

max_res_450D = [4272 2848]; % pixels
sensor_size_450D = [22.2 14.8]; % mm
max_res_650D = [5184 3456]; % pixels
sensor_size_650D = [22.3 14.9]; %mm

% Generate real X/Y coordinates
grid_size = [11 11]; % Number dots along square grid
grid_dim = 500;
% grid_size = [121 13]; % Number dots along square grid
% grid_dim = 600;
realX = repmat(linspace(-grid_dim,grid_dim,grid_size(2)),
    grid_size(1),1);
realY = repmat(linspace(grid_dim,-grid_dim,grid_size(1))
    ',1,grid_size(2));
```

```
% Get data to map patches to entire grid
cd(path)
map_coord_data = xlsread('DotCoord.xls',1);

% Basic structure for analysis
camera.patch=struct('pixelX',[],'pixelY',[],'theta',[]);

for n=1:length(cameras)
    cd(strcat(path,cameras{n})); % Goto camera folder

    switch cameras{n}
        case 'W'
            tmp = reshape(map_coord_data(:,2),grid_size(1)
               ,grid_size(2));
            camera(n).data_exist = logical(tmp);
        case 'S'
            tmp = reshape(map_coord_data(:,4),grid_size(1)
               ,grid_size(2));
            camera(n).data_exist = logical(tmp);
        case 'E'
            tmp = reshape(map_coord_data(:,6),grid_size(1)
               ,grid_size(2));
            camera(n).data_exist = logical(tmp);
    end

    % Load patch positions in pixels (x & y vectors) from
       'data.mat' file generated by consolidate7
    load('data.mat');
    num_patches = size(x,1);

    for m=1:num_patches
        [row, col] = find(camera(n).data_exist); % Get row
            and column indices where there is data from
           specific camera
        camera(n).patch(m).row = row(m);
        camera(n).patch(m).col = col(m);
        camera(n).patch(m).realX = realX(row(m),col(m)); %
            Translate row and column indices into real i.e
           . mm x-coord
        camera(n).patch(m).realY = realY(row(m),col(m)); %
            Translate row and column indices into real i.e
           . mm y-coord

        camera(n).patch(m).pixelX = x(m,2:end); % Extract
           x-pixel data into structure - add (*
           pixels_to_mm(n)) later
```

```
        camera(n).patch(m).pixelY = y(m,2:end); % Extract
           y-pixel data into structure - add (*
           pixels_to_mm(n)) later

        switch cameras{n}
            case 'W'
                theta = atand((slab_height_stronghold -
                   camera_height_stronghold(n)) / ...
                    sqrt((horiz_dist_to_slab_centroid(n) +
                        realX(row(m),col(m)))^2 + realY(
                       row(m),col(m))^2));
                camera(n).patch(m).theta = theta;
                pixels_to_mm(1) = [(sensor_size_650D(1)/
                   max_res_650D(1)) * (sqrt((
                   horiz_dist_to_slab_centroid(n) + realX(
                   row(m),col(m)))^2 + realY(row(m),col(m)
                   )^2)/50)];
            case 'S'
                theta = atand((slab_height_stronghold -
                   camera_height_stronghold(n)) / ...
                    sqrt((horiz_dist_to_slab_centroid(n) +
                        realY(row(m),col(m)))^2 + realX(
                       row(m),col(m))^2));
                camera(n).patch(m).theta = theta;
                pixels_to_mm(2) = [(sensor_size_650D(1)/
                   max_res_650D(1)) * (sqrt((
                   horiz_dist_to_slab_centroid(n) + realY(
                   row(m),col(m)))^2 + realX(row(m),col(m)
                   )^2)/50)];
            case 'E'
                theta = atand((slab_height_stronghold -
                   camera_height_stronghold(n)) / ...
                    sqrt((horiz_dist_to_slab_centroid(n) -
                        realX(row(m),col(m)))^2 + realY(
                       row(m),col(m))^2));
                camera(n).patch(m).theta = theta;
                pixels_to_mm(3) = [(sensor_size_450D(1)/
                   max_res_450D(1)) * (sqrt((
                   horiz_dist_to_slab_centroid(n) - realX(
                   row(m),col(m)))^2 + realY(row(m),col(m)
                   )^2)/50)];
        end

        camera(n).patch(m).dispX = (camera(n).patch(m).
           pixelX - camera(n).patch(m).pixelX(1)) *
           pixels_to_mm(n);
```

```
        camera(n).patch(m).dispY = (camera(n).patch(m).
            pixelY - camera(n).patch(m).pixelY(1)) *
            pixels_to_mm(n);

        camera(n).patch(m).realdispY = camera(n).patch(m).
            dispY / cosd(camera(n).patch(m).theta);
        xlstmp(m,:) = camera(n).patch(m).realdispY;
    end
    filename = strcat('camera',cameras{n},'_realdispY.csv'
        );
    [status message] = xlswrite(filename,xlstmp);
    clear xlstmp
end
```

G

CAMERA TEST SETTINGS

FUNCTION	SETTING	REASON
Aperture	F-22	Small aperture allows greater depth of field and more use of the centre of the lens
Shutter speed	Varied	Time the shutter is open and therefore amount of light into camera
ISO speed	Varied	Higher value in low light
Autofocusing	Off	Manually focussed using computer view
Auto stabilisation	Off	When on, autofocuses
Picture style	Standard	For vivid colours and sharp images
White balance	Auto	
AF operation	One shot	Lens focus mode for still subjects
Drive mode	Remote control	
Metering mode	Spot metering	
Resolution	Large	18M 5184×3456 pixels
Lens aberration	Off	

Table G.1: Camera test settings

H

SLAB-COLUMN TEST SCHEDULE

H.1 STRUCTURAL REACTION FRAME

All slabs were inserted into the frame by removing the whole S side of the structural reaction frame. The slabs were positioned 260 mm below the radiant panel surface so that the loading rod could be raised through the slabs' thickness.

When assembling a restrained slab test, the upper and lower box section supports were tightly bolted flush to the N, E and S slab sides. The upper box section was attached with mortar below it to ensure a sound bedding on the uneven heated slab surface. The reaction frame channel section was loosened, so that once the slab was in position the horizontal bolts through the box section supports could tighten the channel section flush to the slab edge. The reaction frame N, E, and S channel sections were thereafter tightened into position. The W side box section supports were attached in a similar way to the other sides and the W side channel section and columns were tightened into position.

The unrestrained support condition was achieved by supporting the slab on a 6 mm diameter steel bar. Prior to assembly the channel sections were recessed as close to the reaction frame columns as possible to allow an approximate 5 mm gap around all the slab edges. This additional width within the frame allowed for the slab to be supported and free to expand. The steel bar was positioned with Blu-tack onto the lower box sections and each sides lower box section was raised using props at each end. The box section was tightened into position once the steel bar was in contact with the unheated slab surface.

H.2 SPECIMEN

An optimised texture for DIC analyses was found by varying the initial slab test texture. The optimum texture was imparted onto the unheated slab surface of all the tested slabs as they were in-situ in the structural reaction frame.

H.3 RADIANT PANEL HEATING

Prior to testing, the gas lines and connections were all leak tested. Upgrades to the laboratories gas supply were undertaken, including installation of gas arrest/flame protect valves on the propane bottles, two gas emergency shut-off valves with stop buttons (one at the wall and a second portable one), mass flow meter in the gas line.

H.4 CAMERAS

The cameras were setup using Canon EOS Utility to increase accuracy. The larger computer view rather than camera display allowed for more accurate manual lens focussing. The cameras were initially set to aperture priority mode, which allowed the desired aperture to be set and the shutter speed to be found automatically as the subject was automatically focussed on. A note of the optimum shutter and ISO speed was taken for each cameras largest F-number. For testing, the cameras were adjusted to manual mode and the previous noted optimum shutter and ISO settings were selected. The cameras were manually re-focussed for the single calibration board photo and again for testing. Small blue-tac pieces were attached to the lens focus ring to stop if from sliding out of focus. As the cameras were in an inverted orientation, early practise tests found the lens focus ring slid out of focus as the camera shutter opened and closed to take a photo. Appendix G lists the camera settings used during testing.

A camera remote control was used to take photos with all the cameras at the same 10 second constant interval. During the cooling phase of the heated tests, the photo interval was increased to every 20 seconds to limit the number of photos taken.

I

SLAB-COLUMN REACTION FORCES AND MOMENTS ON THE REACTION FRAME

I.1 50 mm thick, 0.8% reinforced tests

I.1.1 *Ambient unrestrained test*

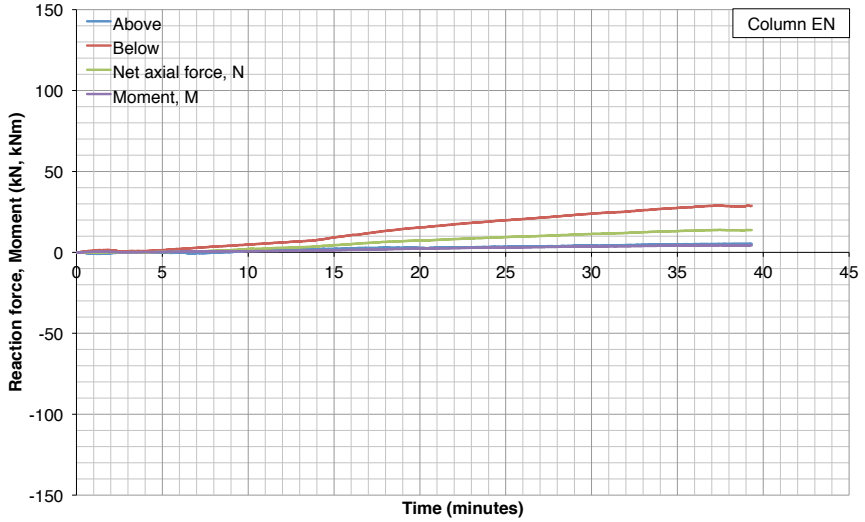

(a) Column EN

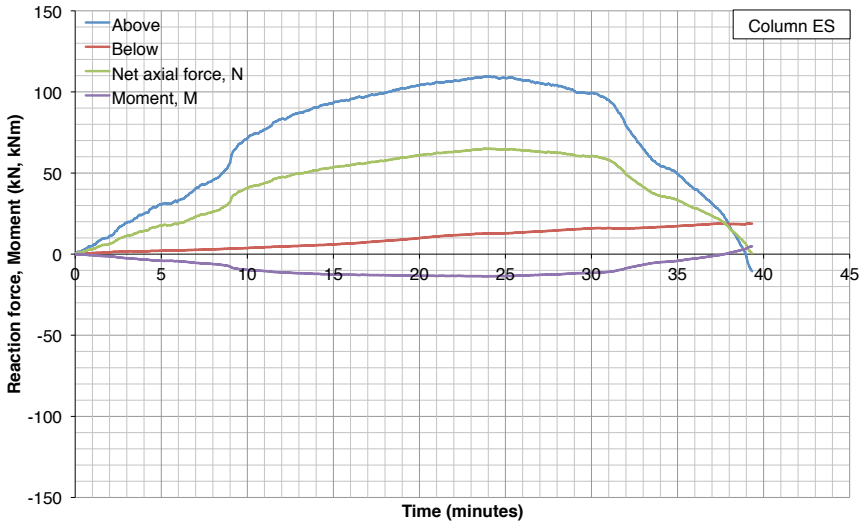

(b) Column ES

Figure I.1: East reaction frame net axial force, N and moment, M for ambient 50 mm thick, 0.8% reinforced: unrestrained slab

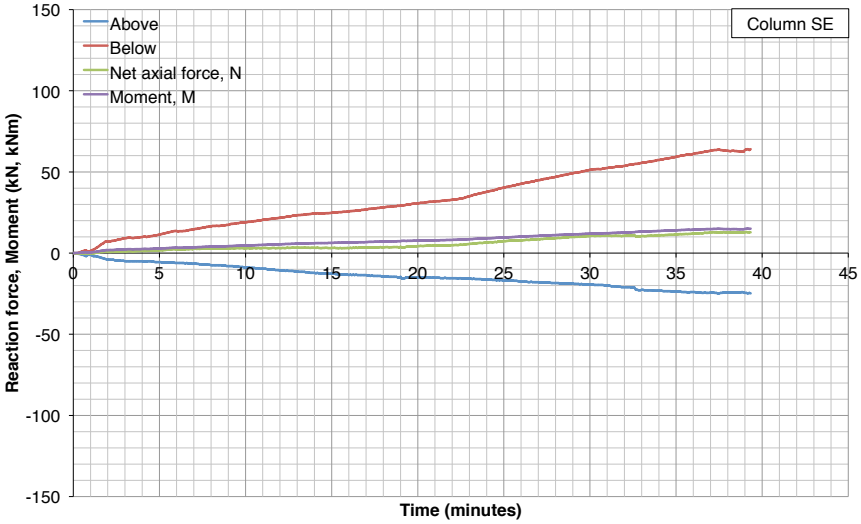

(a) Column SE

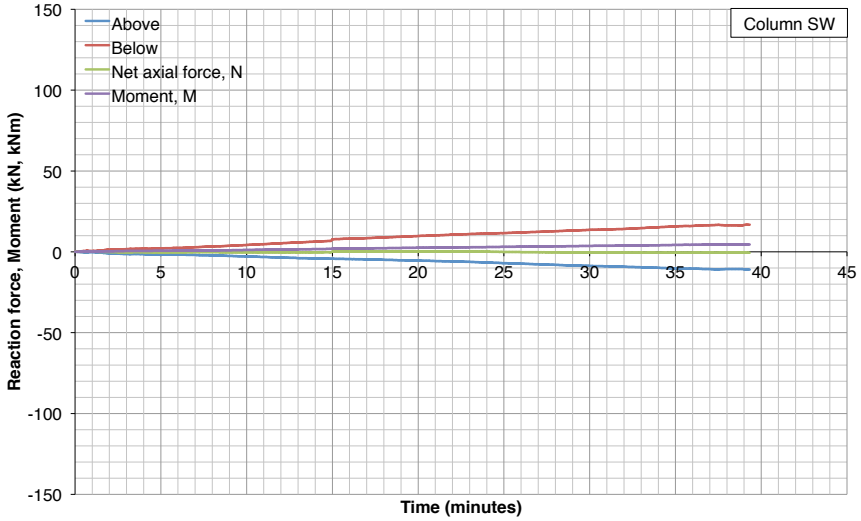

(b) Column SW

Figure I.2: South reaction frame net axial force, N and moment, M for ambient 50 mm thick, 0.8% reinforced: unrestrained slab

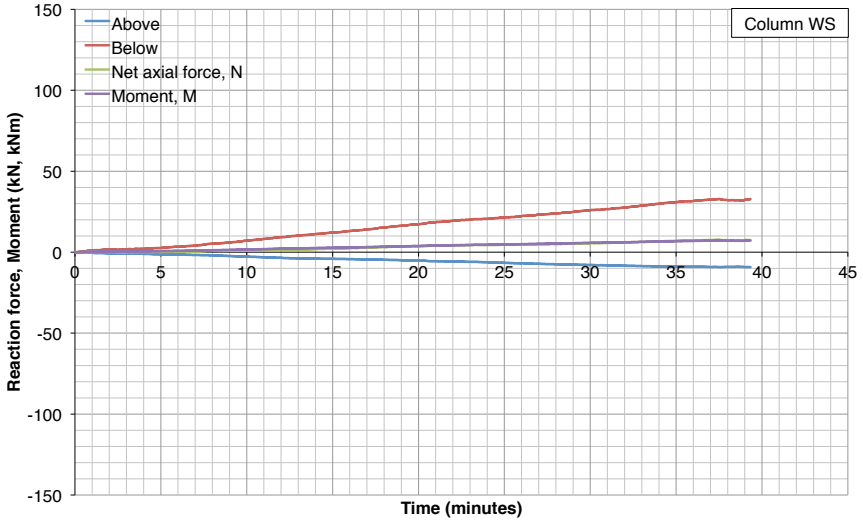

(a) Column WS

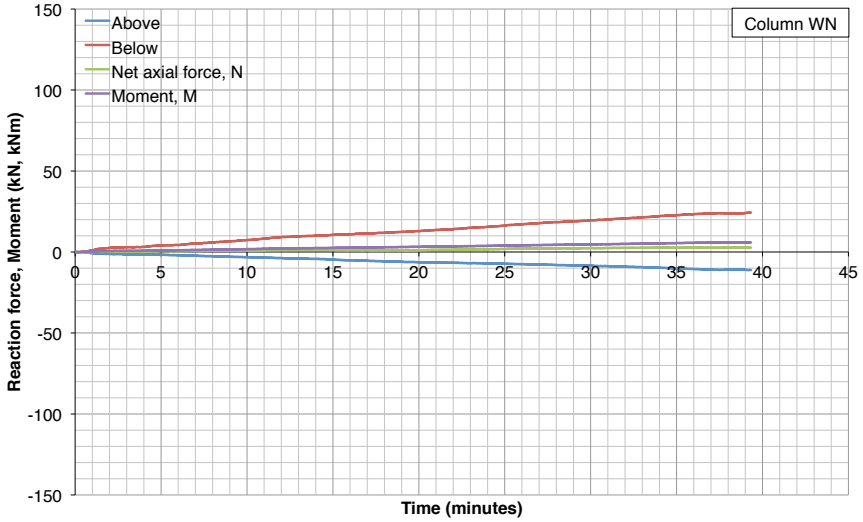

(b) Column WN

Figure I.3: West reaction frame net axial force, N and moment, M for ambient 50 mm thick, 0.8% reinforced: unrestrained slab

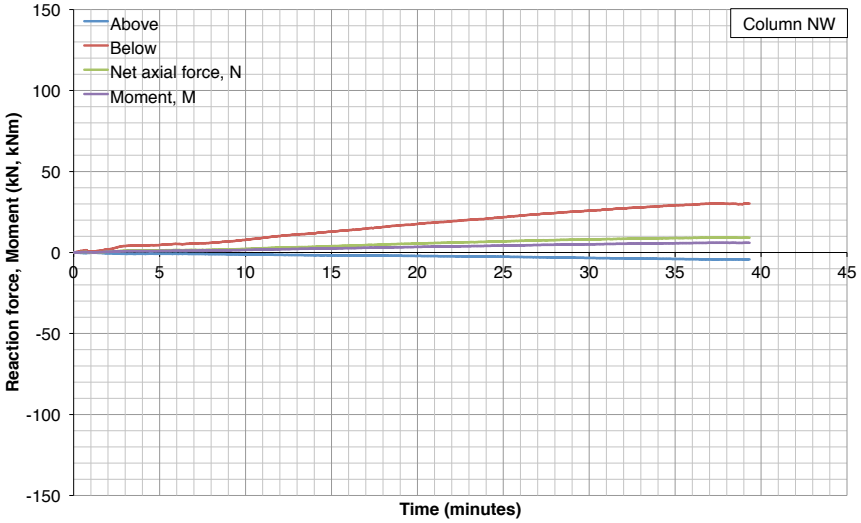

(a) Column NW

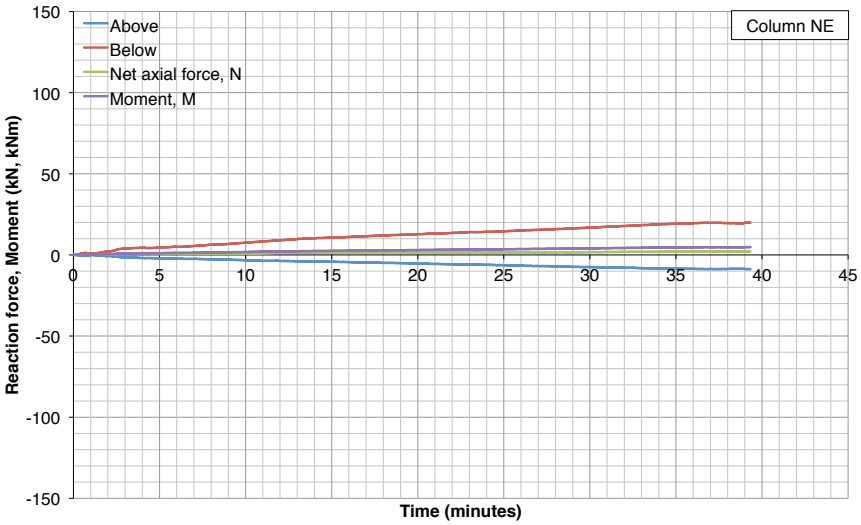

(b) Column NE

Figure I.4: North reaction frame net axial force, N and moment, M for ambient 50 mm thick, 0.8% reinforced: unrestrained slab

I.1.2 *Heated unrestrained test*

[ht]

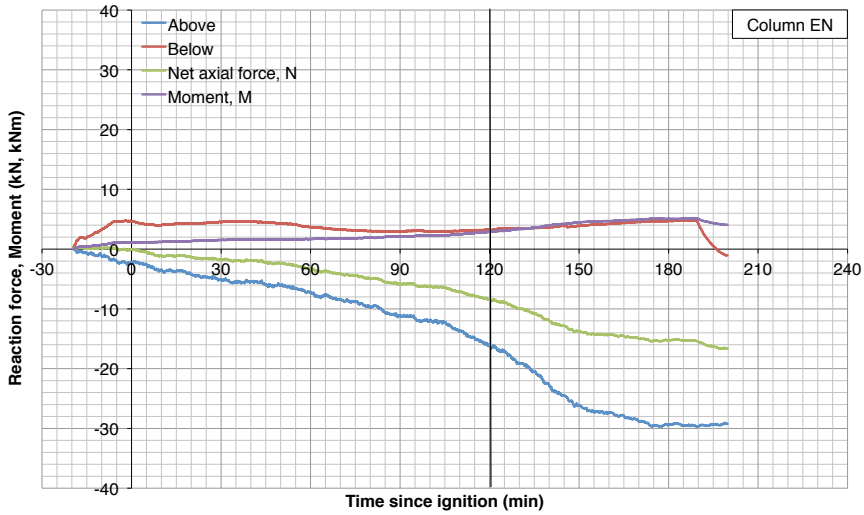

(a) Column EN

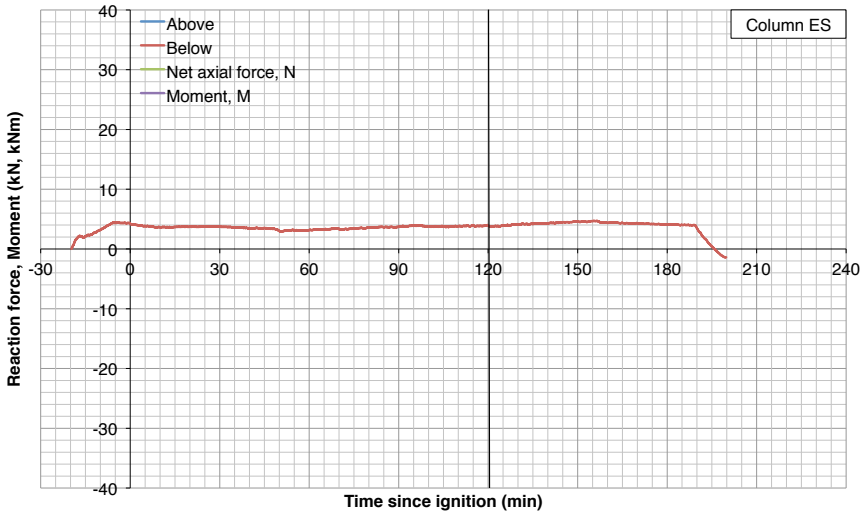

(b) Column ES

Figure I.5: East reaction frame net axial force, N and moment, M for heated 50 mm thick, 0.8% reinforced: unrestrained slab

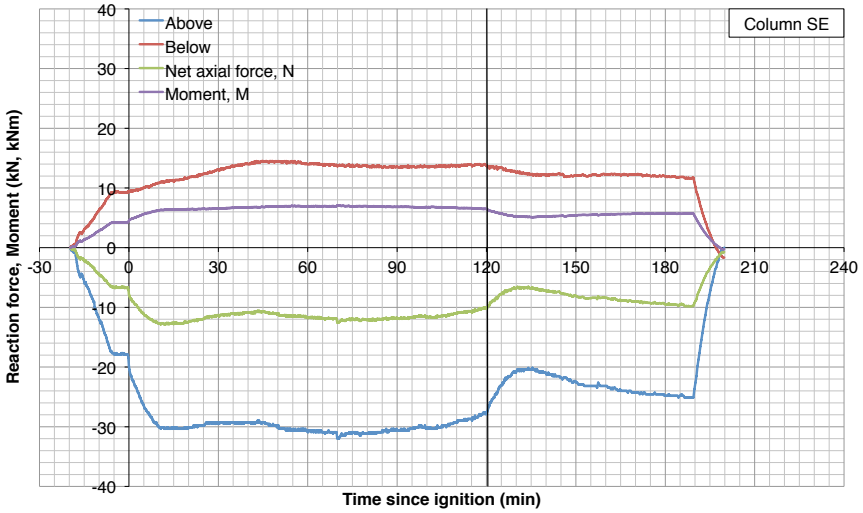

(a) Column SE

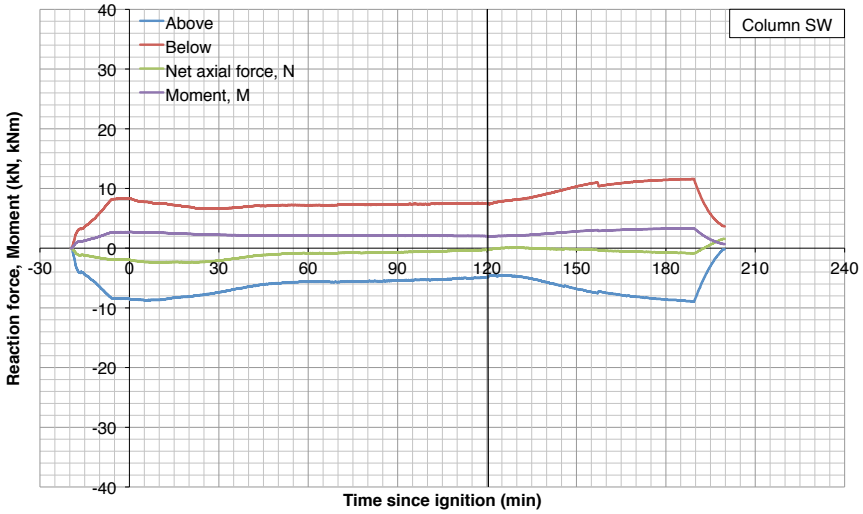

(b) Column SW

Figure I.6: South reaction frame net axial force, N and moment, M for heated 50 mm thick, 0.8% reinforced: unrestrained slab

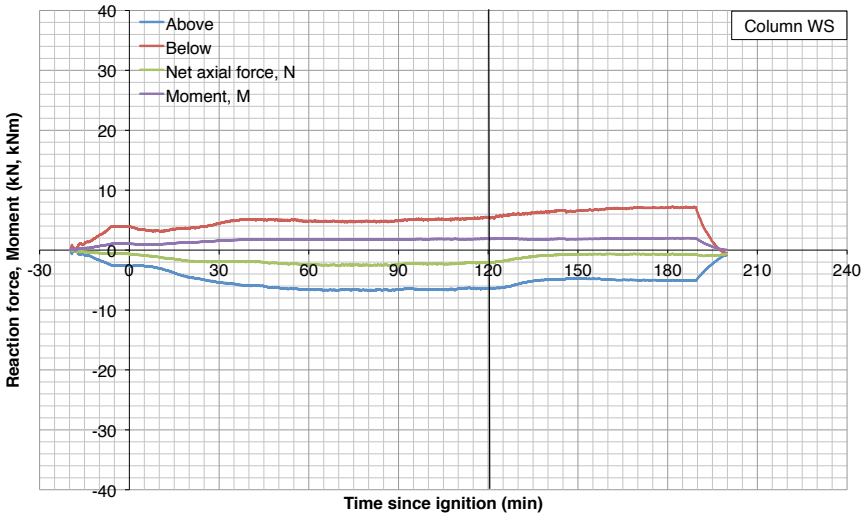

(a) Column WS

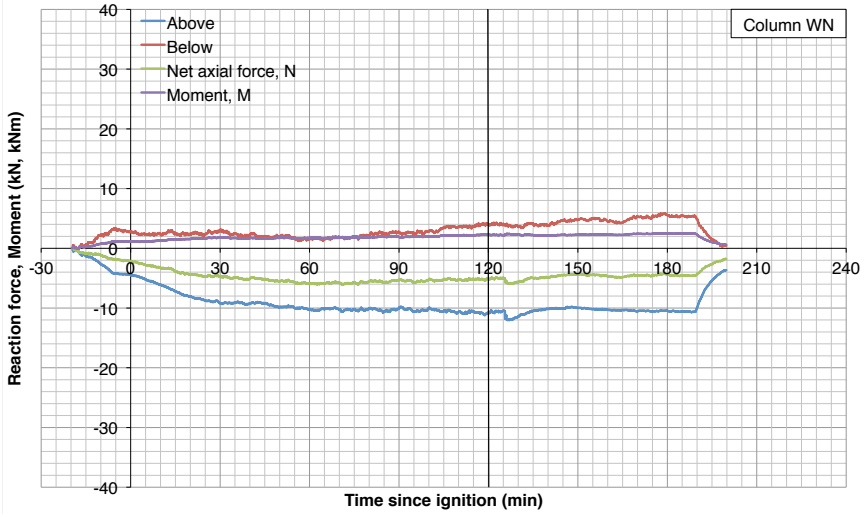

(b) Column WN

Figure I.7: West reaction frame net axial force, N and moment, M for heated 50 mm thick, 0.8% reinforced: unrestrained slab

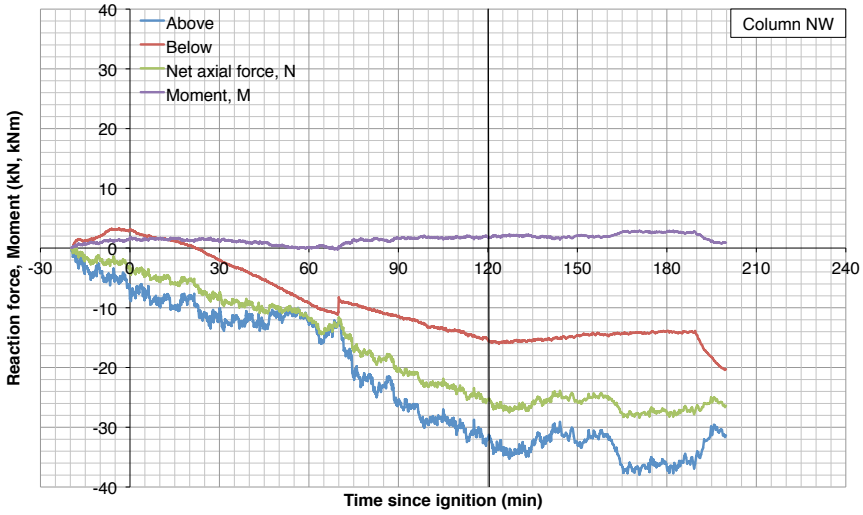

(a) Column NW

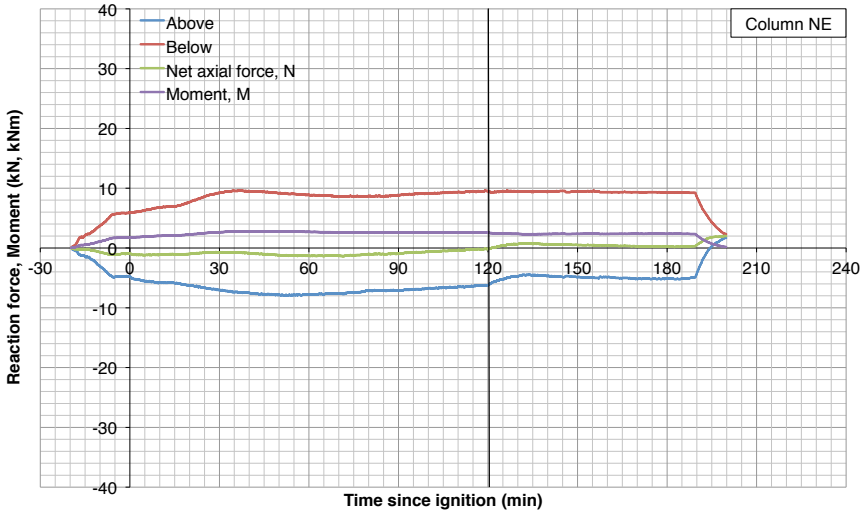

(b) Column NE

Figure I.8: North reaction frame net axial force, N and moment, M for heated 50 mm thick, 0.8% reinforced: unrestrained slab

I.1.3 *Heated restrained test*

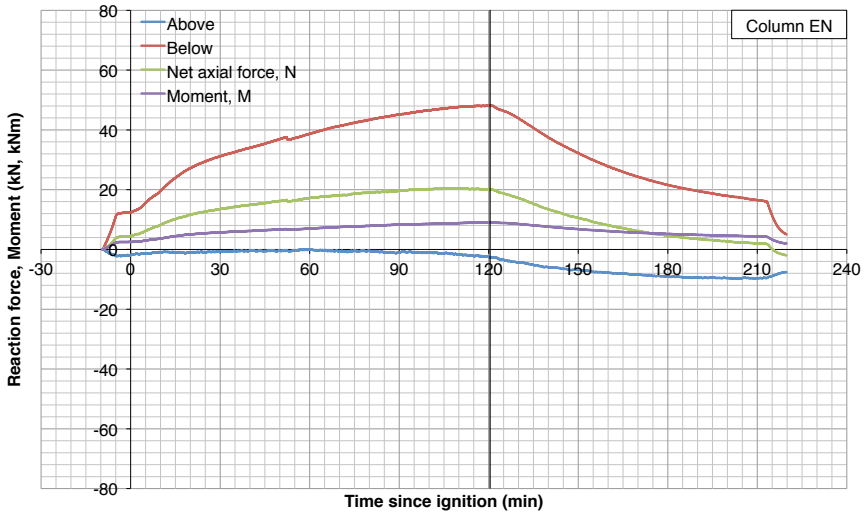

(a) Column EN

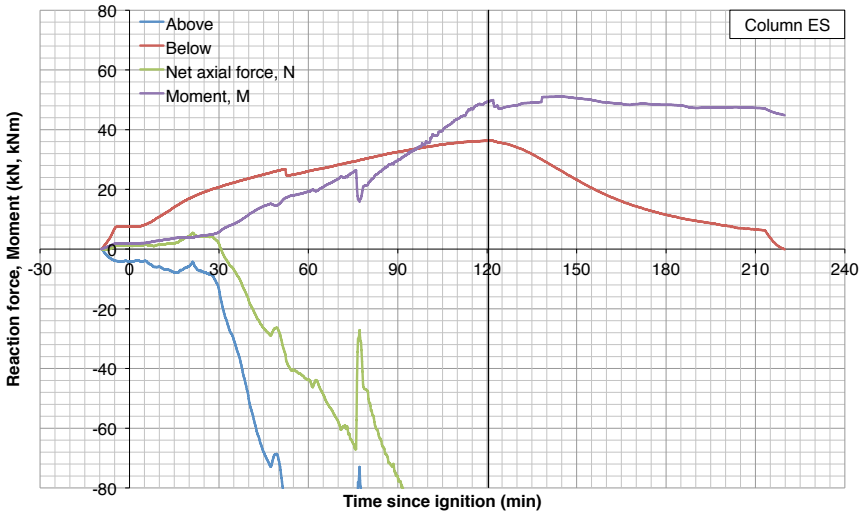

(b) Column ES

Figure I.9: East reaction frame net axial force, N and moment, M for heated 50 mm thick, 0.8% reinforced: restrained slab

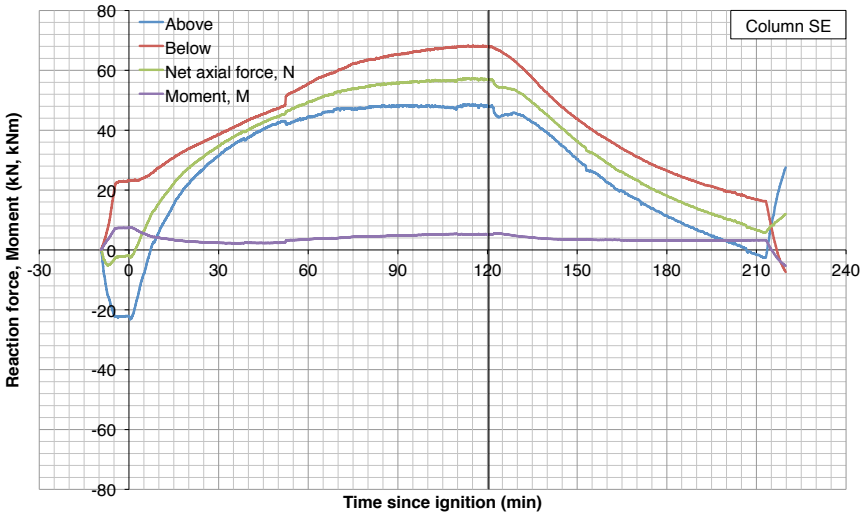

(a) Column SE

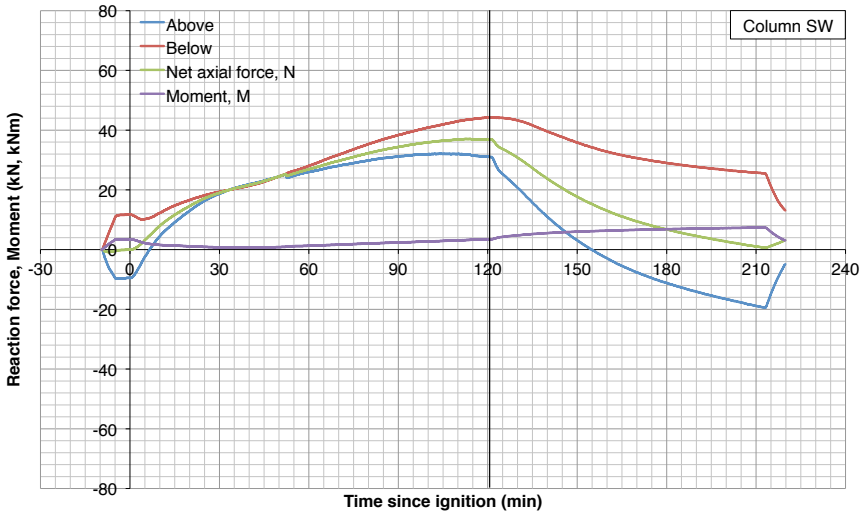

(b) Column SW

Figure I.10: South reaction frame net axial force, N and moment, M for heated 50 mm thick, 0.8% reinforced: restrained slab

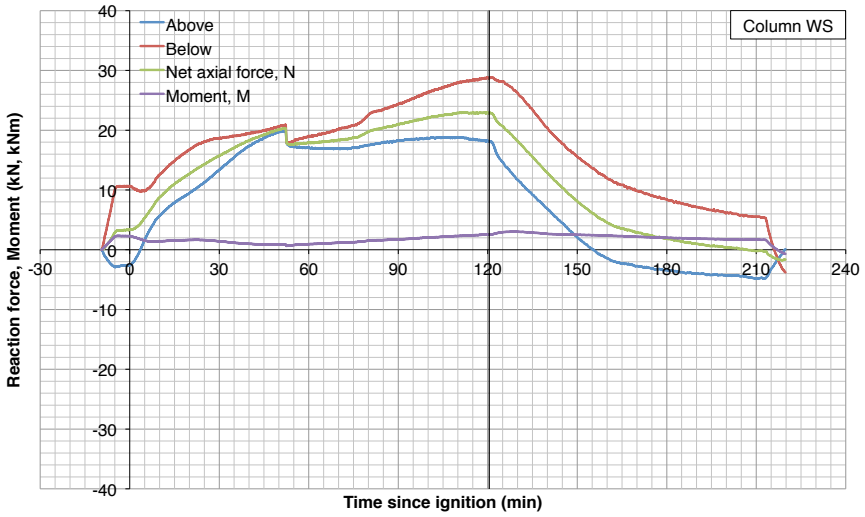

(a) Column WS

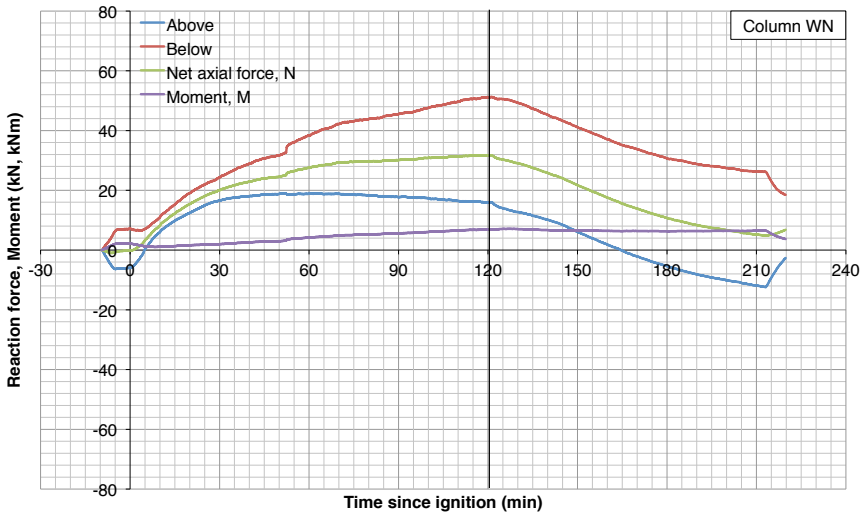

(b) Column WN

Figure I.11: West reaction frame net axial force, N and moment, M for heated 50 mm thick, 0.8% reinforced: restrained slab

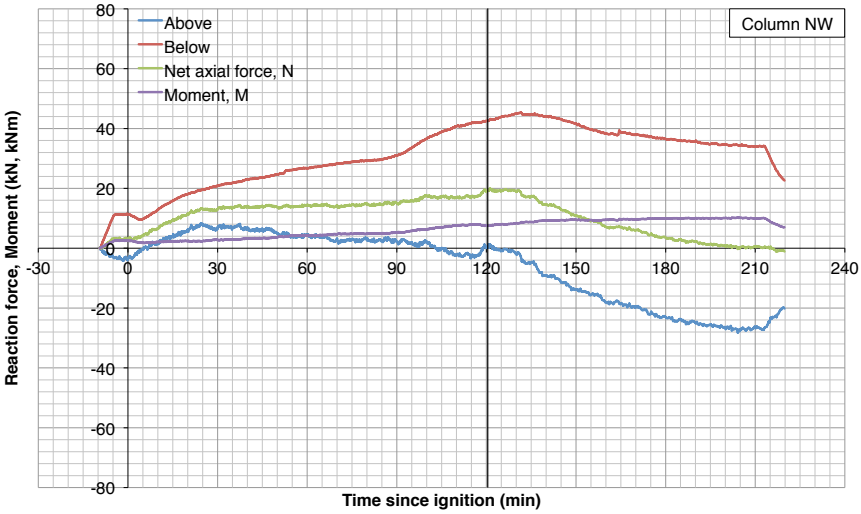

(a) Column NW

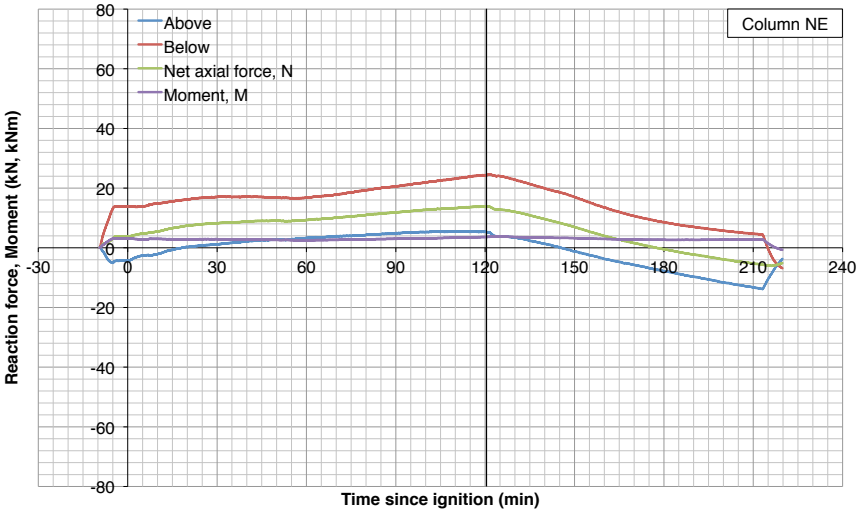

(b) Column NE

Figure I.12: North reaction frame net axial force, N and moment, M for heated 50 mm thick, 0.8% reinforced: restrained slab

I.2 75 mm thick, 0.8% reinforced tests

I.2.1 *Ambient unrestrained test*

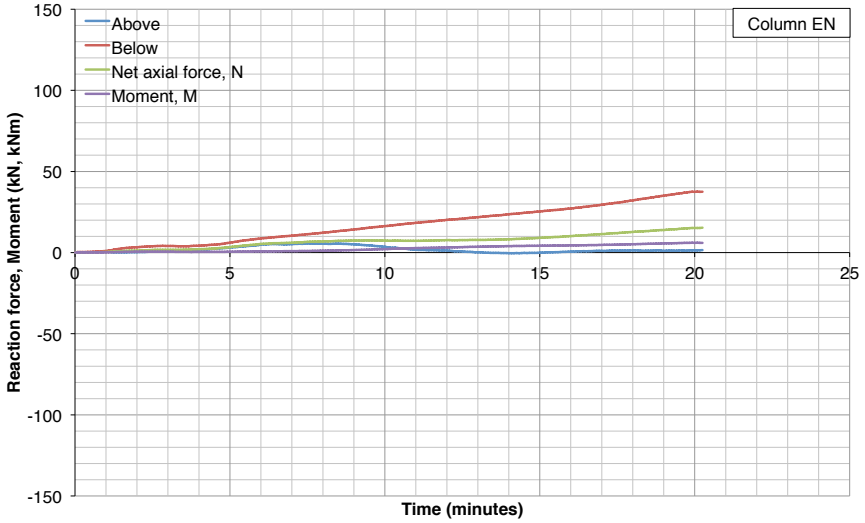

(a) Column EN

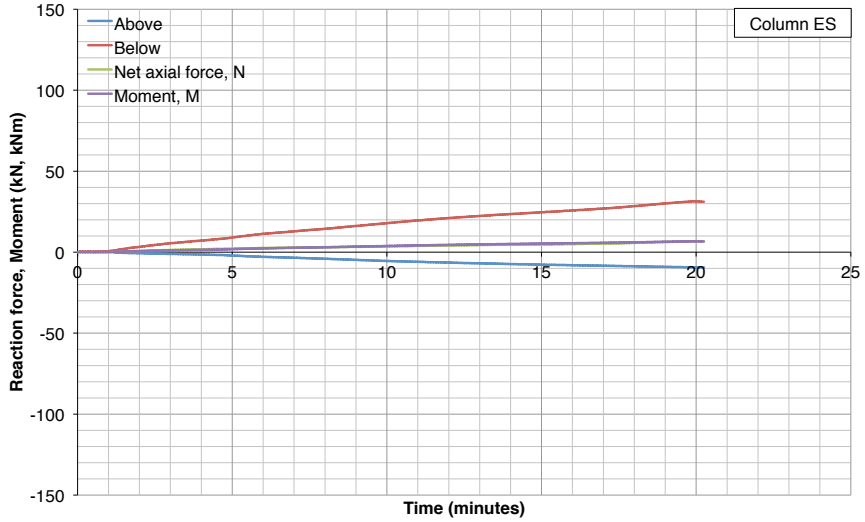

(b) Column ES

Figure I.13: East reaction frame net axial force, N and moment, M for ambient 75 mm thick, 0.8% reinforced: unrestrained slab

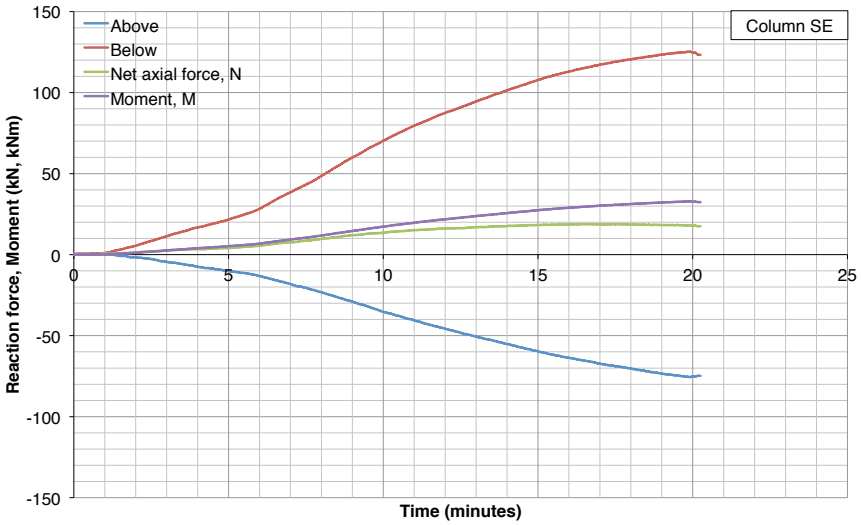

(a) Column SE

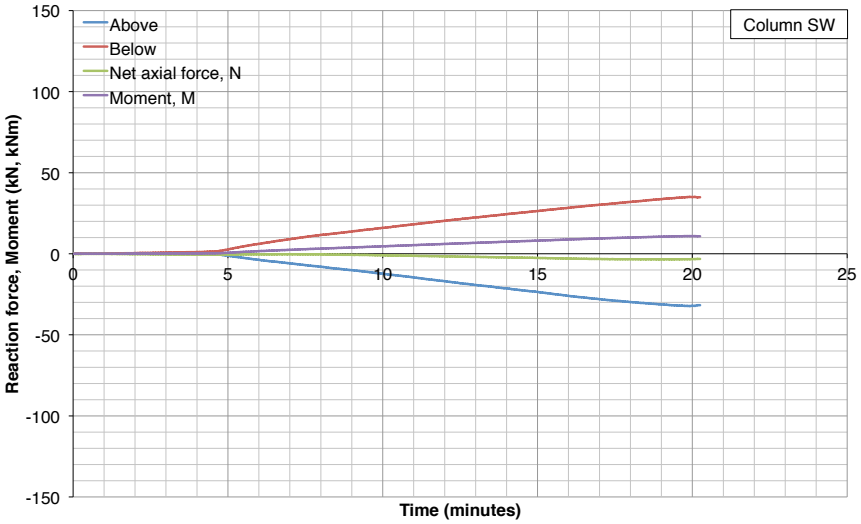

(b) Column SW

Figure I.14: South reaction frame net axial force, N and moment, M for ambient 75 mm thick, 0.8% reinforced: unrestrained slab

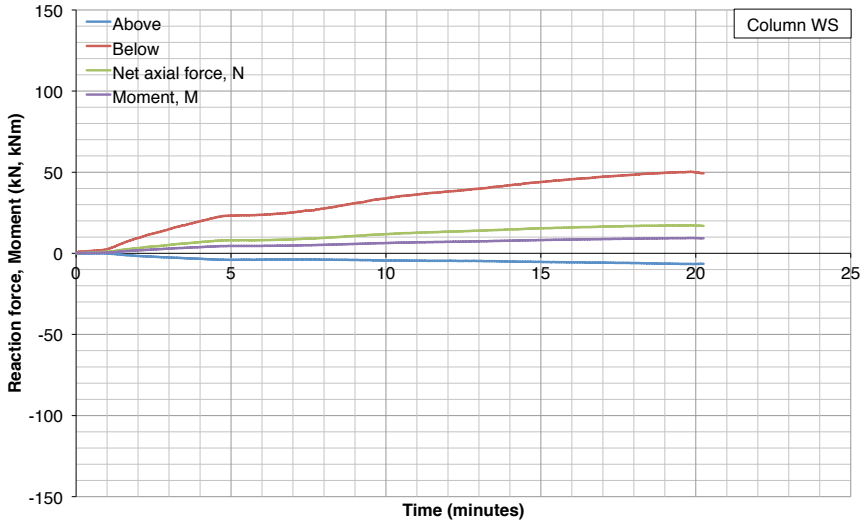

(a) Column WS

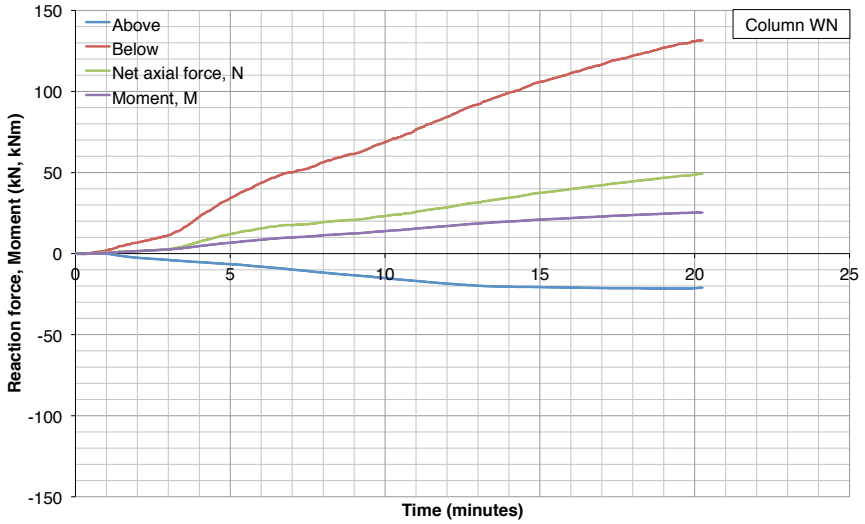

(b) Column WN

Figure I.15: West reaction frame net axial force, N and moment, M for ambient 75 mm thick, 0.8% reinforced: unrestrained slab

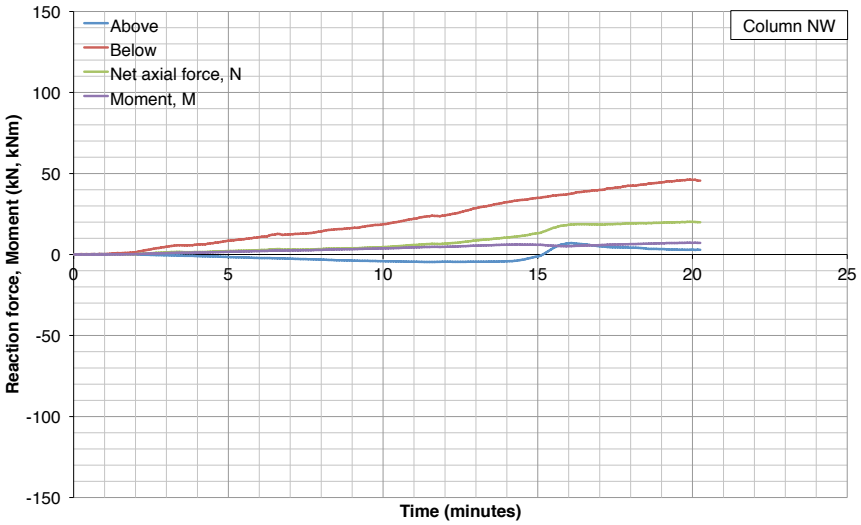

(a) Column NW

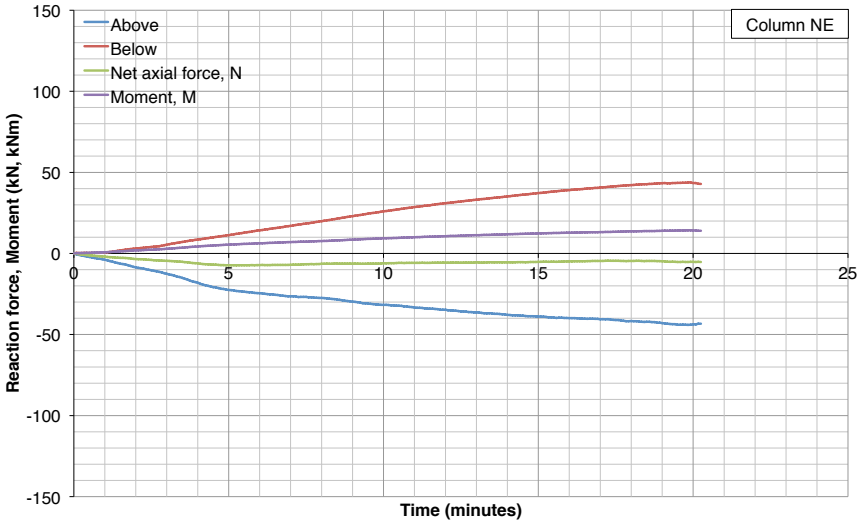

(b) Column NE

Figure I.16: North reaction frame net axial force, N and moment, M for ambient 75 mm thick, 0.8% reinforced: unrestrained slab

I.2.2 *Heated unrestrained test*

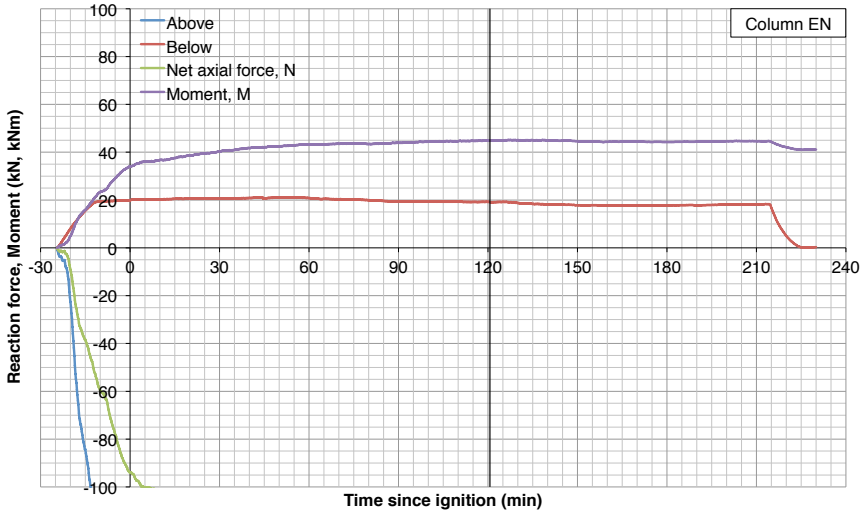

(a) Column EN

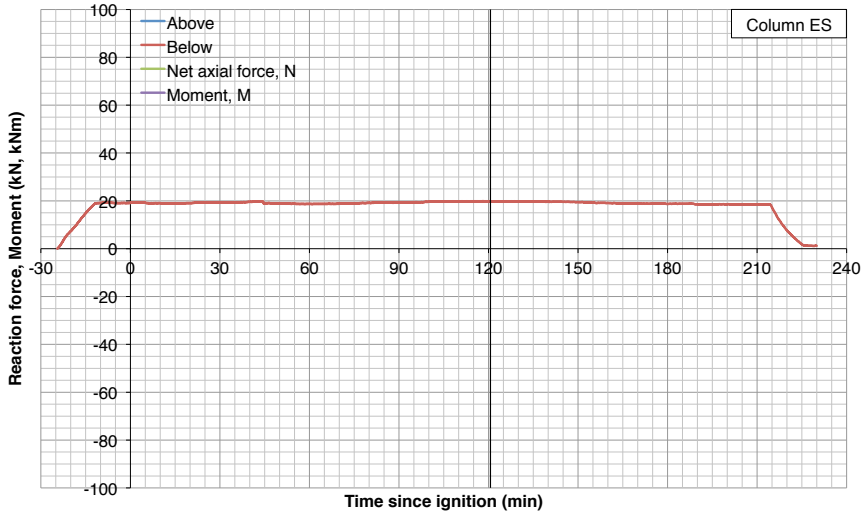

(b) Column ES

Figure I.17: East reaction frame net axial force, N and moment, M for heated 75 mm thick, 0.8% reinforced: unrestrained slab

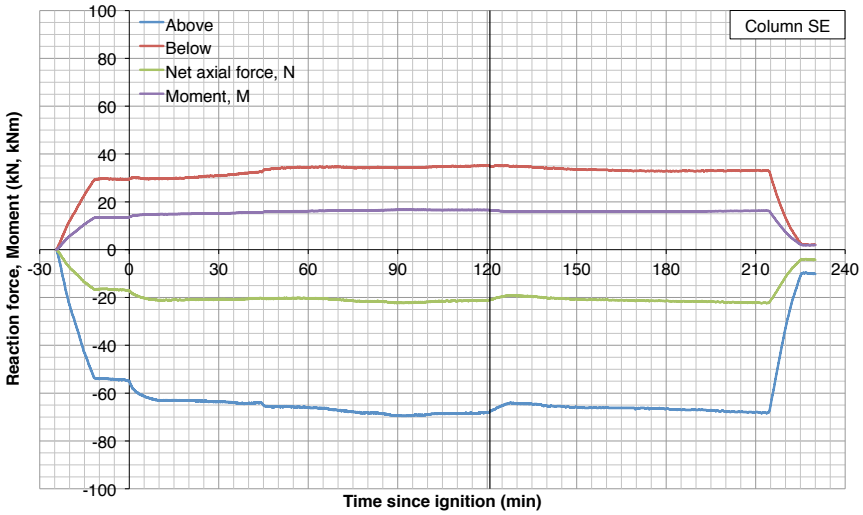

(a) Column SE

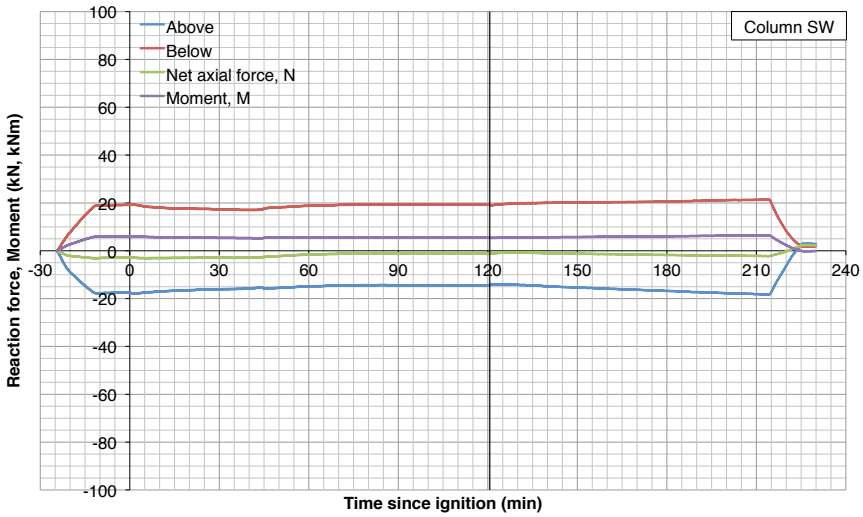

(b) Column SW

Figure I.18: South reaction frame net axial force, N and moment, M for heated 75 mm thick, 0.8% reinforced: unrestrained slab

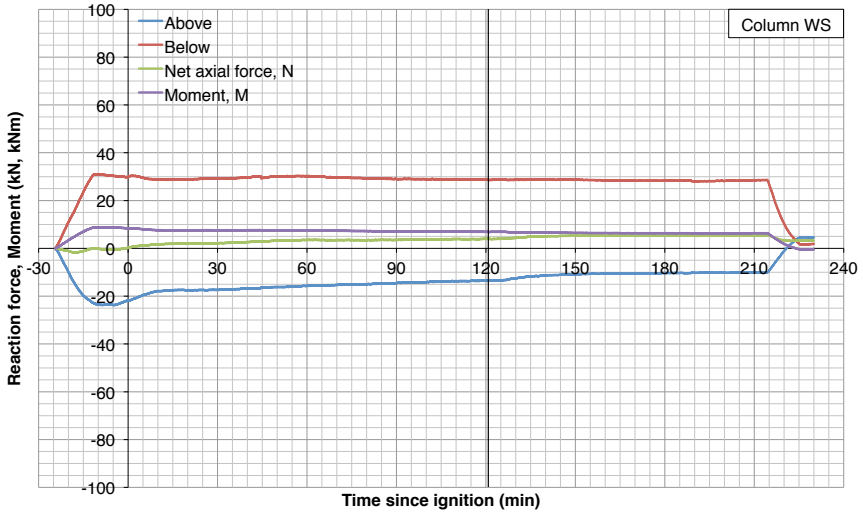

(a) Column WS

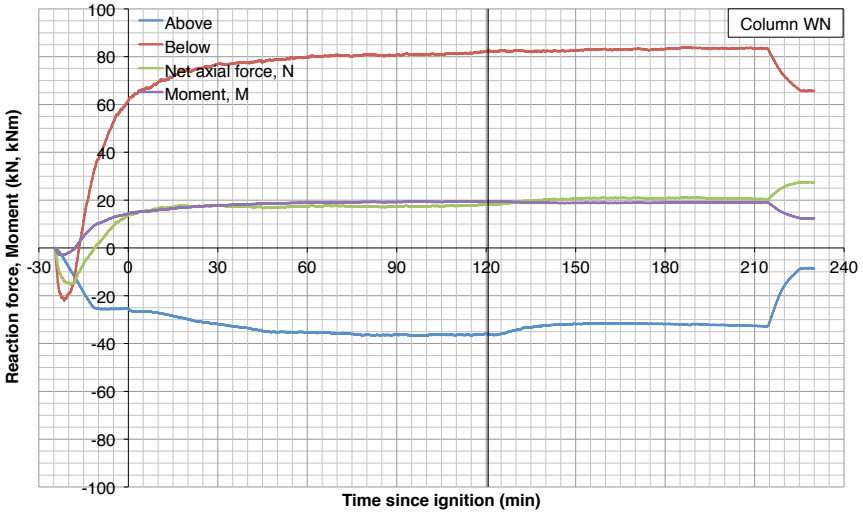

(b) Column WN

Figure I.19: West reaction frame net axial force, N and moment, M for heated 75 mm thick, 0.8% reinforced: unrestrained slab

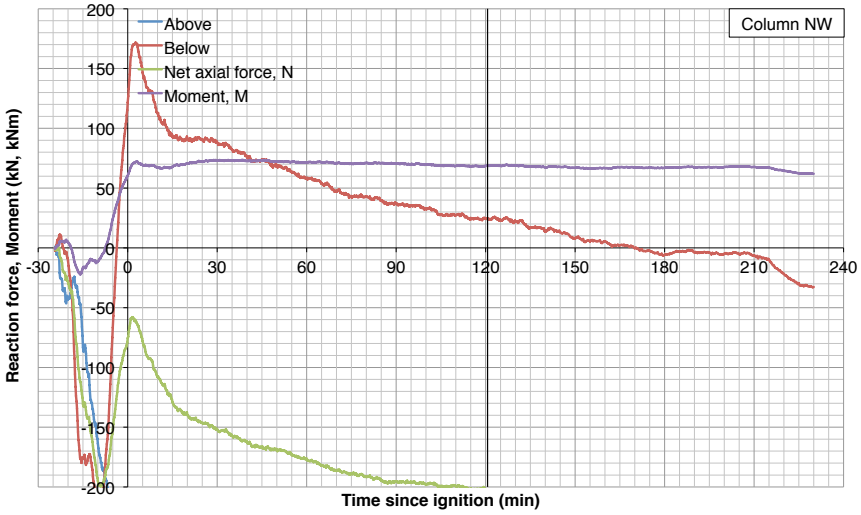

(a) Column NW

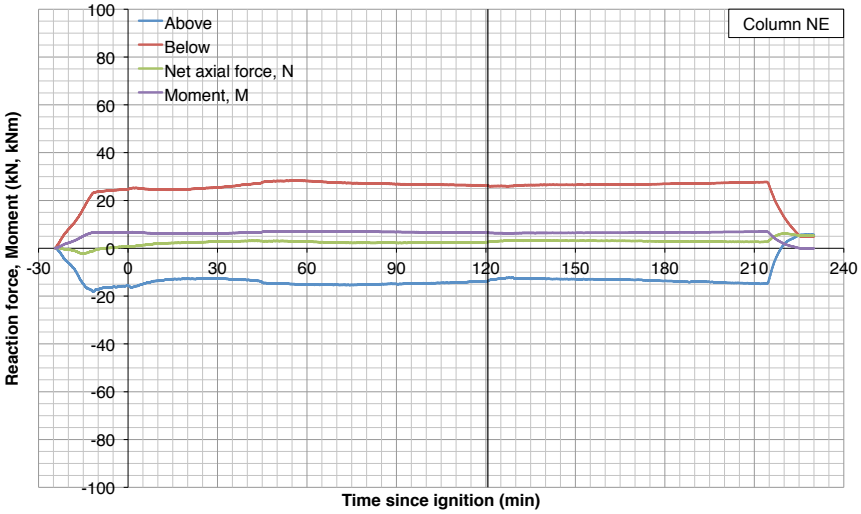

(b) Column NE

Figure I.20: North reaction frame net axial force, N and moment, M for heated 75 mm thick, 0.8% reinforced: unrestrained slab

I.2.3 *Heated restrained test*

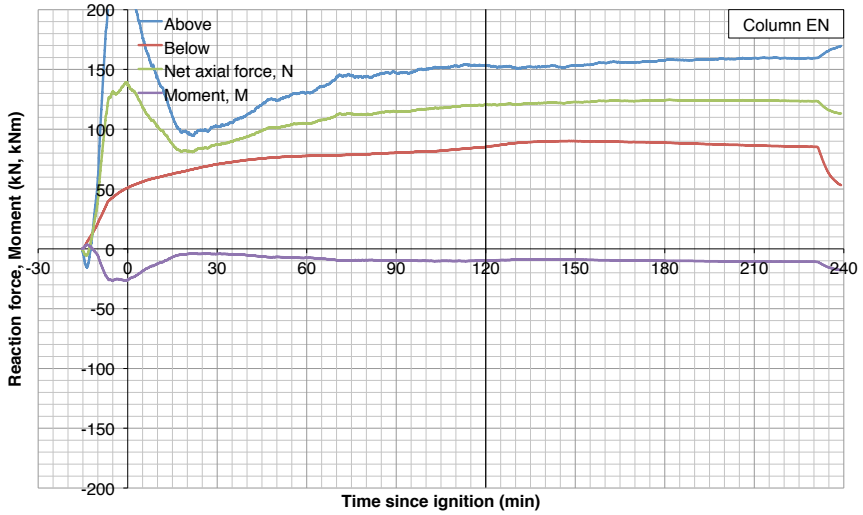

(a) Column EN

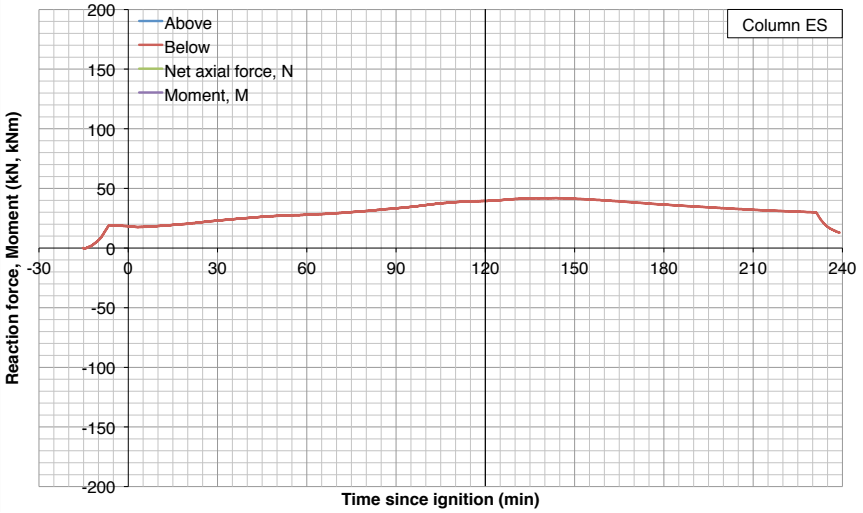

(b) Column ES

Figure I.21: East reaction frame net axial force, N and moment, M for heated 75 mm thick, 0.8% reinforced: restrained slab

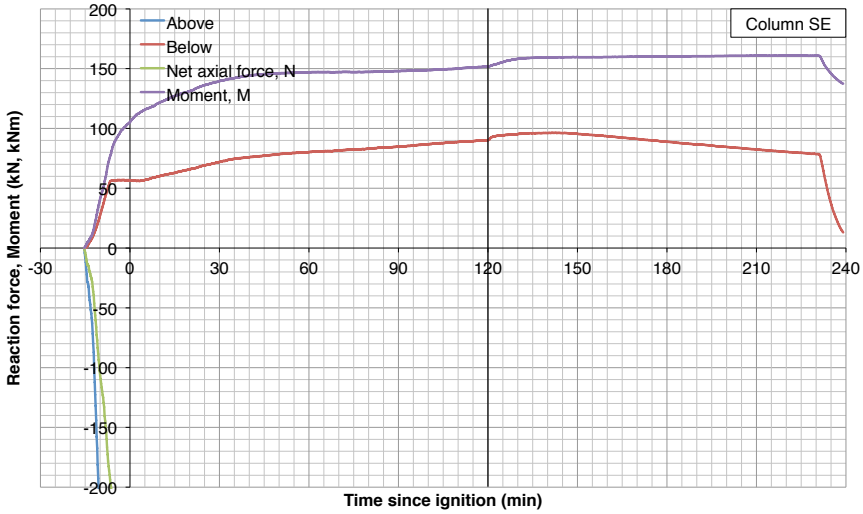

(a) Column SE

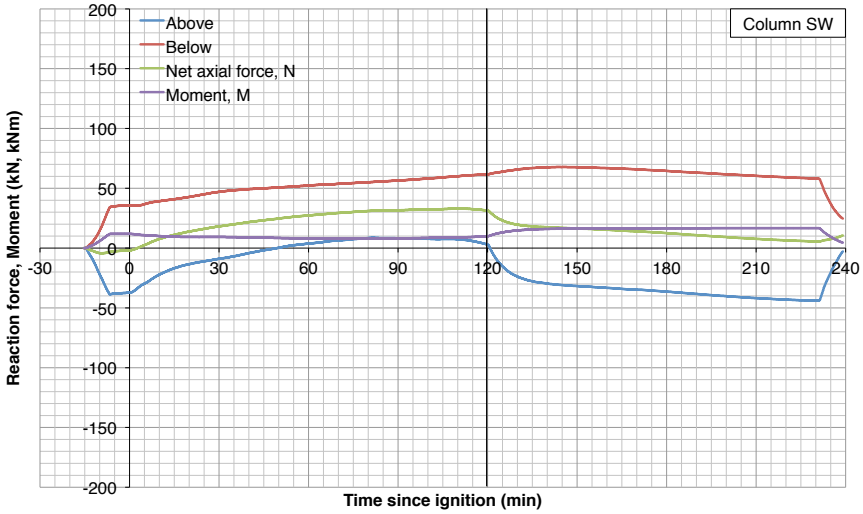

(b) Column SW

Figure I.22: South reaction frame net axial force, N and moment, M for heated 75 mm thick, 0.8% reinforced: restrained slab

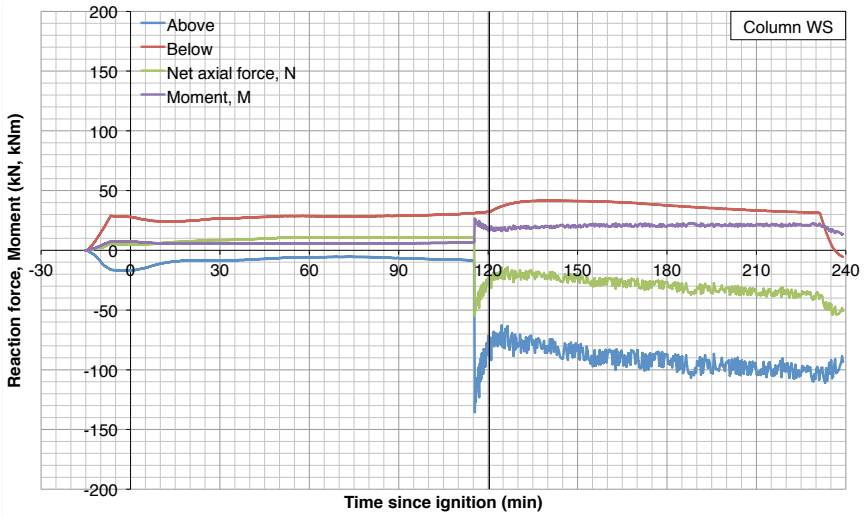

(a) Column WS

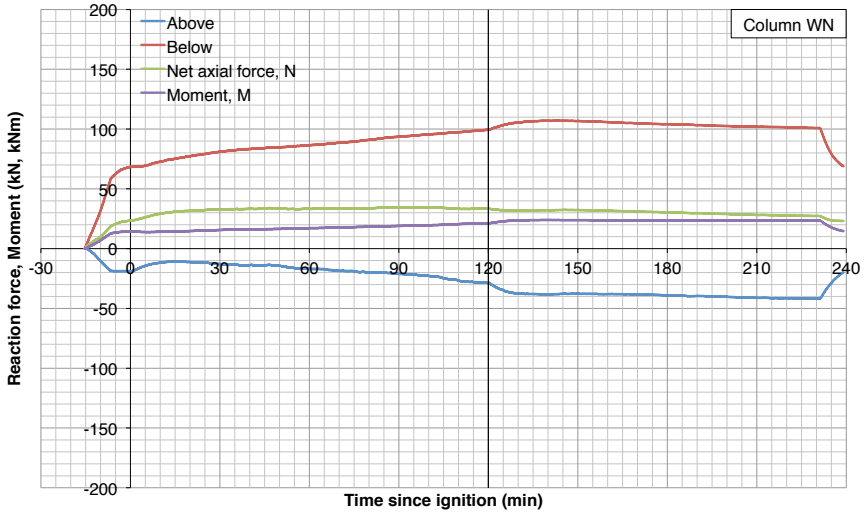

(b) Column WN

Figure I.23: West reaction frame net axial force, N and moment, M for heated 75 mm thick, 0.8% reinforced: restrained slab

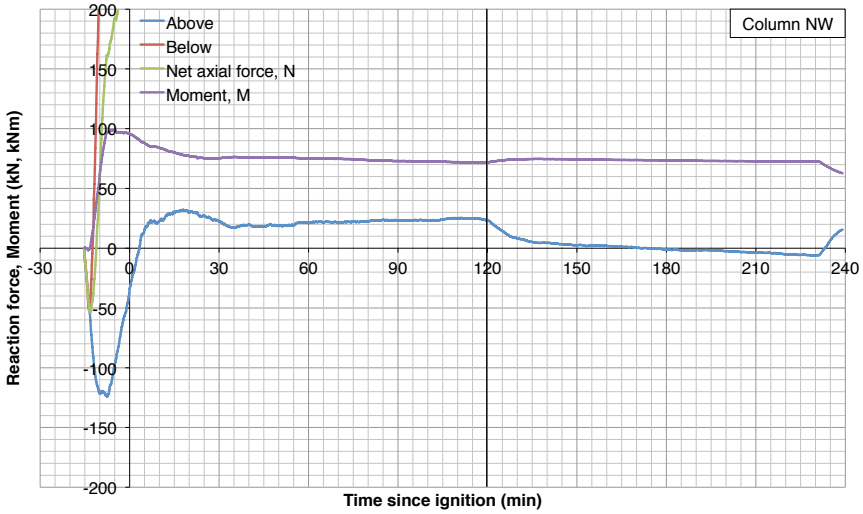

(a) Column NW

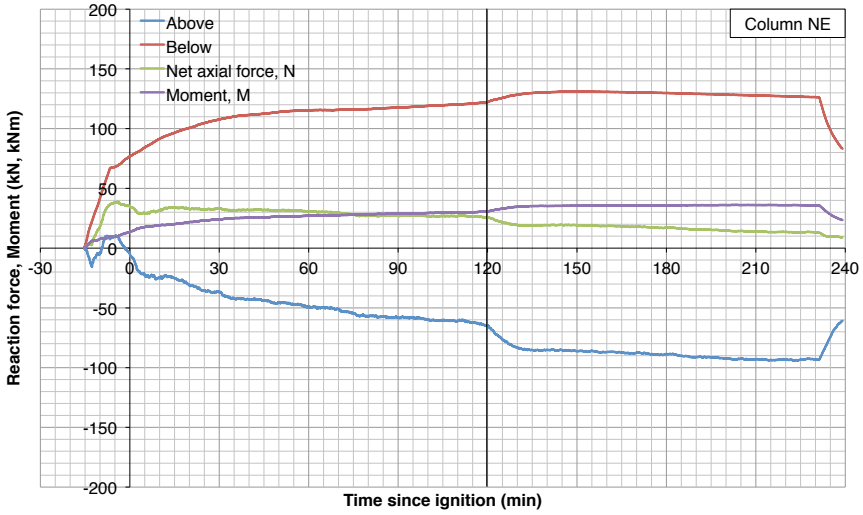

(b) Column NE

Figure I.24: North reaction frame net axial force, N and moment, M for heated 75 mm thick, 0.8% reinforced: restrained slab

I.3 100 MM THICK, 0.8% REINFORCED TESTS

I.3.1 *Ambient unrestrained test*

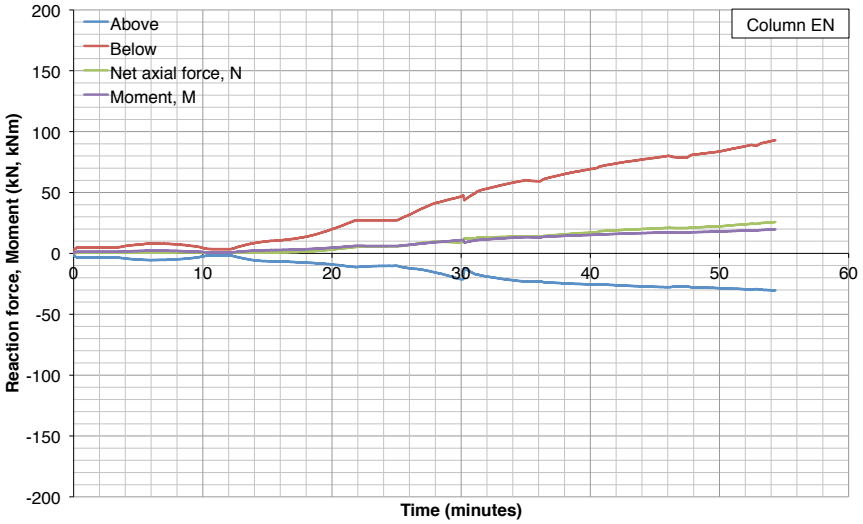

(a) Column EN

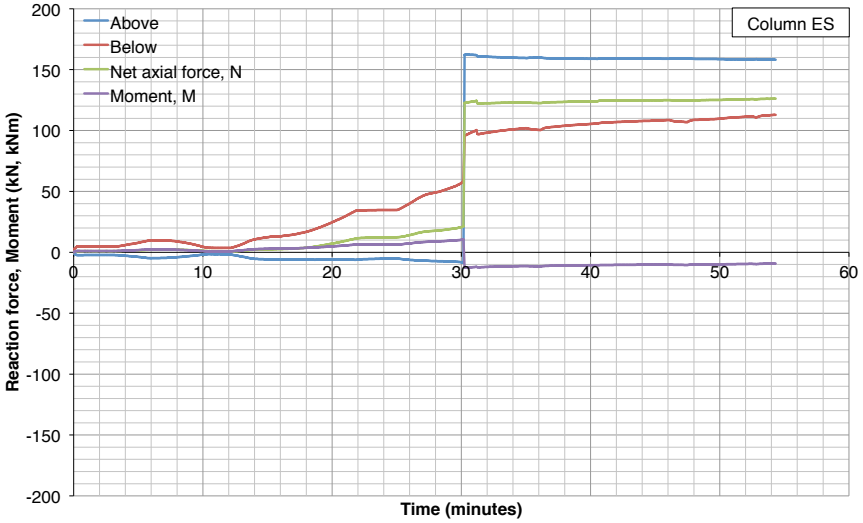

(b) Column ES

Figure I.25: East reaction frame net axial force, N and moment, M for ambient 100 mm thick, 0.8% reinforced: unrestrained slab

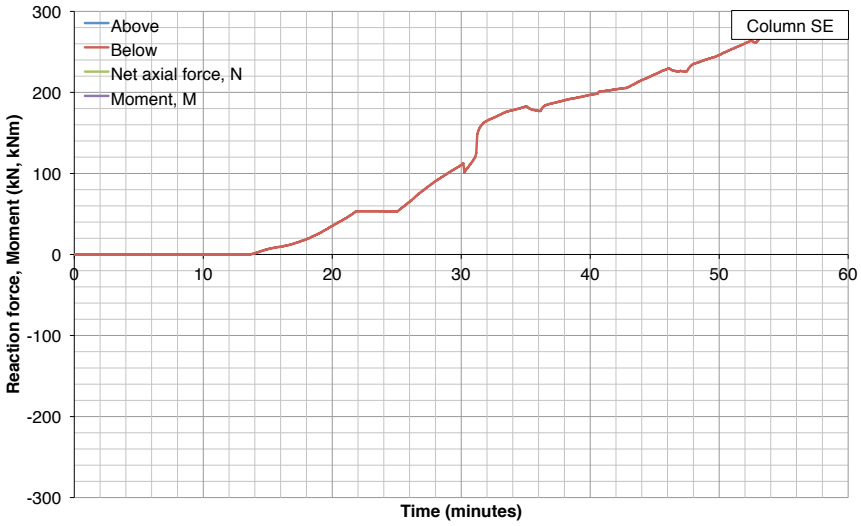

(a) Column SE

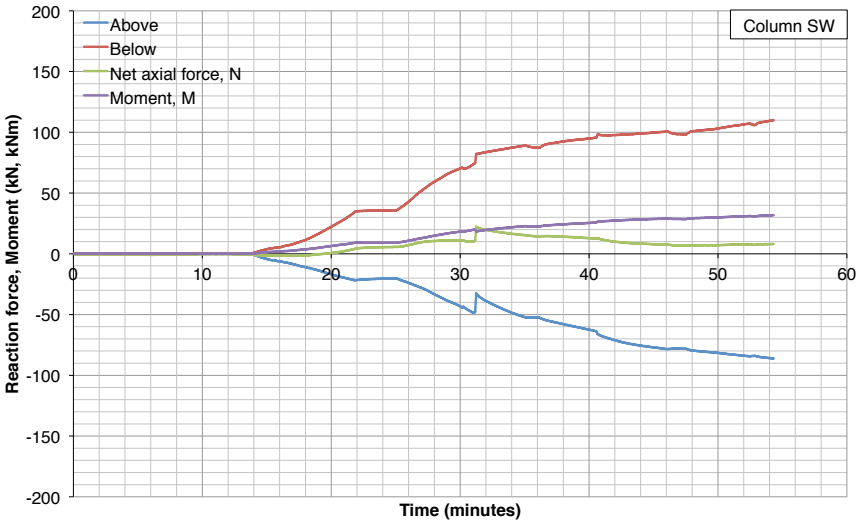

(b) Column SW

Figure I.26: South reaction frame net axial force, N and moment, M for ambient 100 mm thick, 0.8% reinforced: unrestrained slab

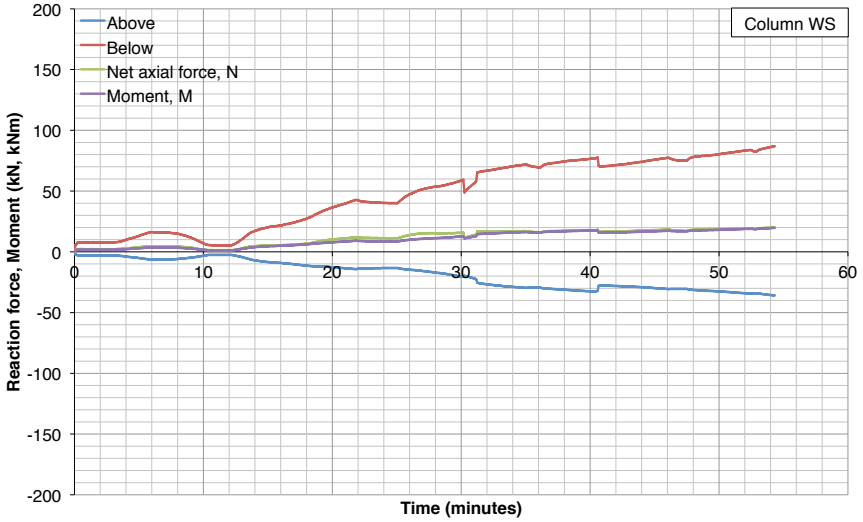

(a) Column WS

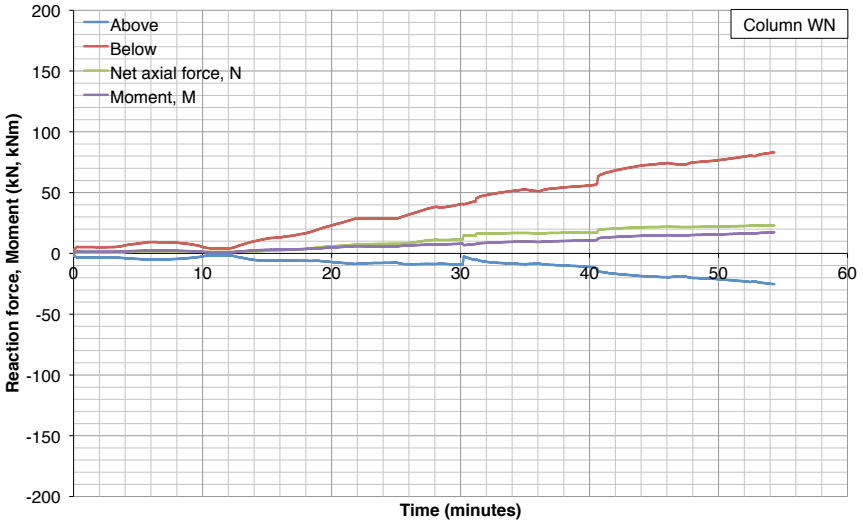

(b) Column WN

Figure I.27: West reaction frame net axial force, N and moment, M for ambient 100 mm thick, 0.8% reinforced: unrestrained slab

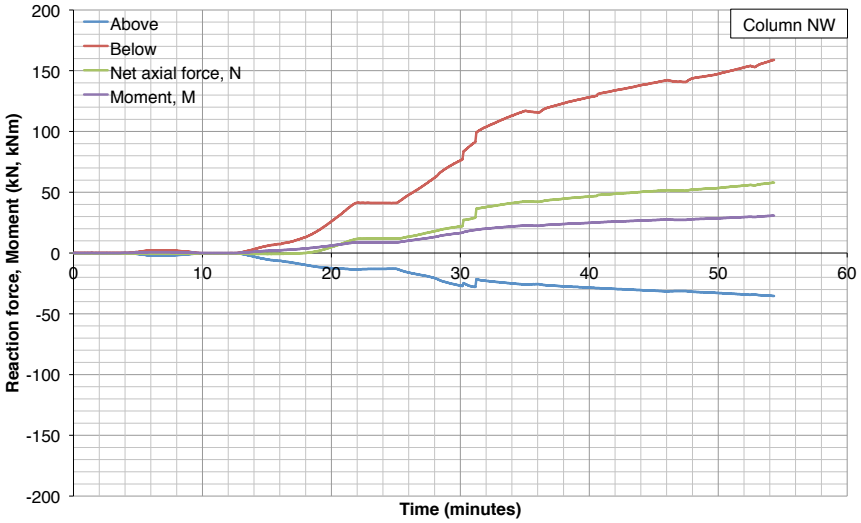

(a) Column NW

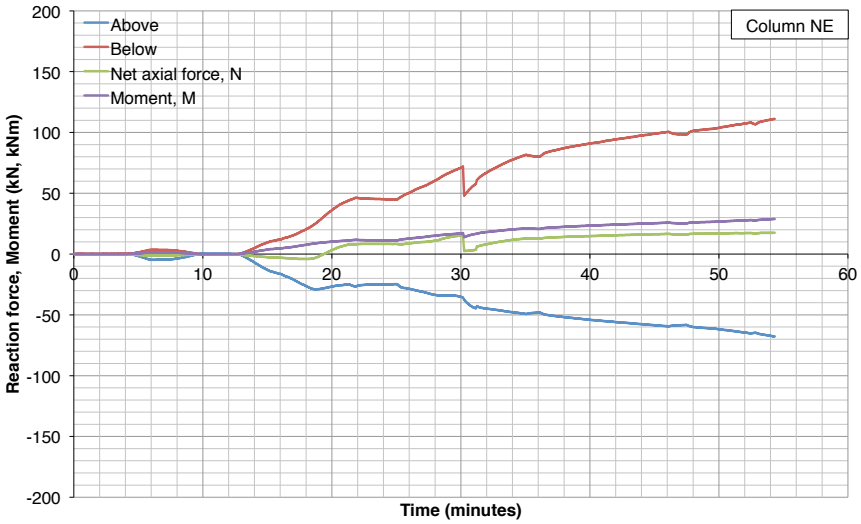

(b) Column NE

Figure I.28: North reaction frame net axial force, N and moment, M for ambient 100 mm thick, 0.8% reinforced: unrestrained slab

I.3.2 *Heated unrestrained test*

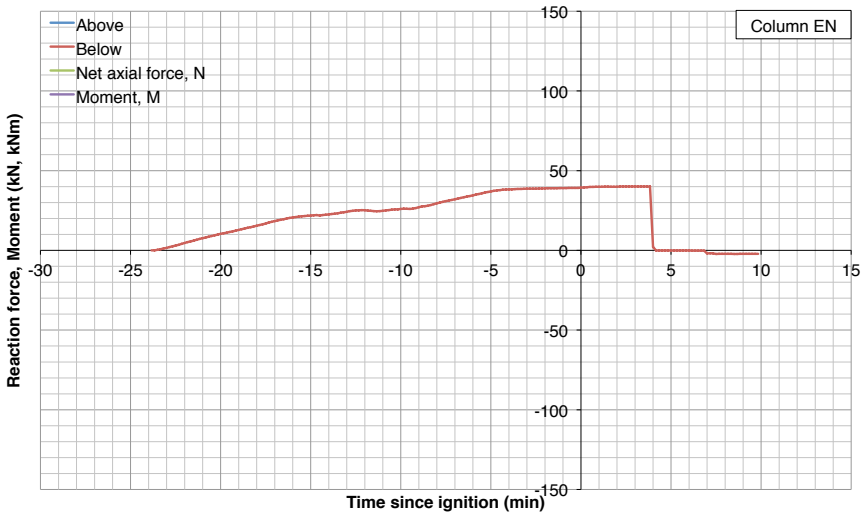

(a) Column EN

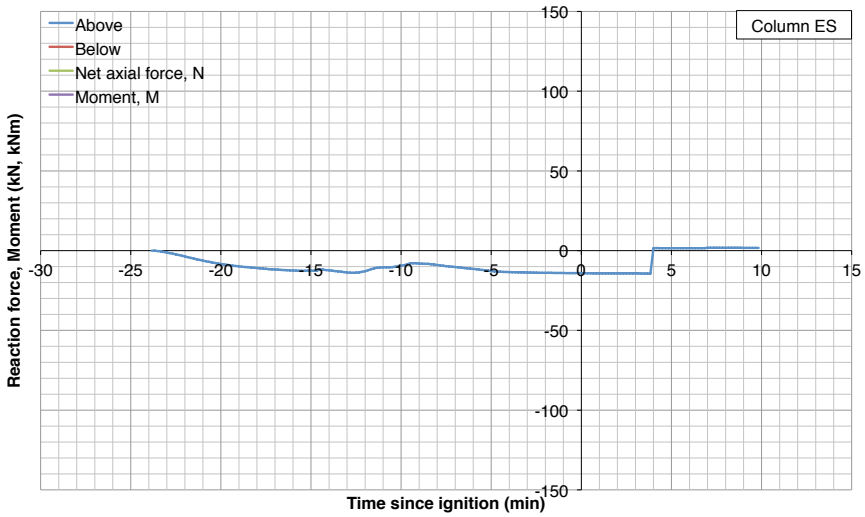

(b) Column ES

Figure I.29: East reaction frame net axial force, N and moment, M for heated 100 mm thick, 0.8% reinforced: unrestrained slab

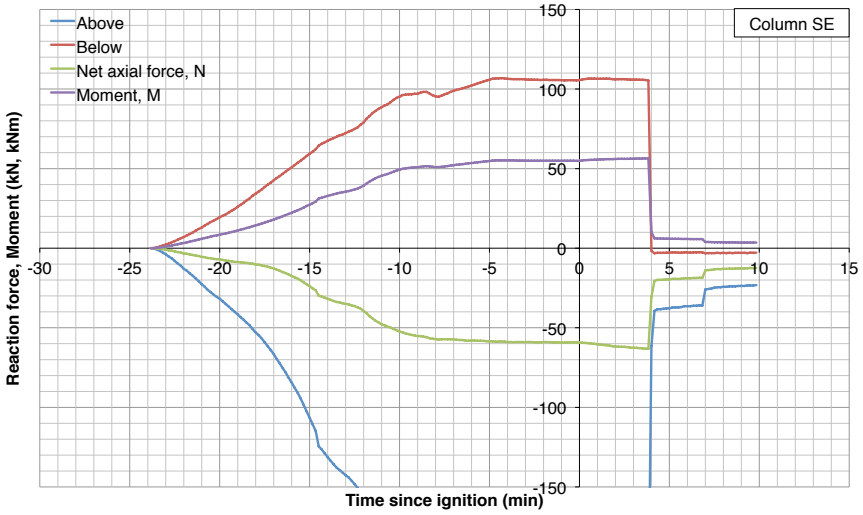

(a) Column SE

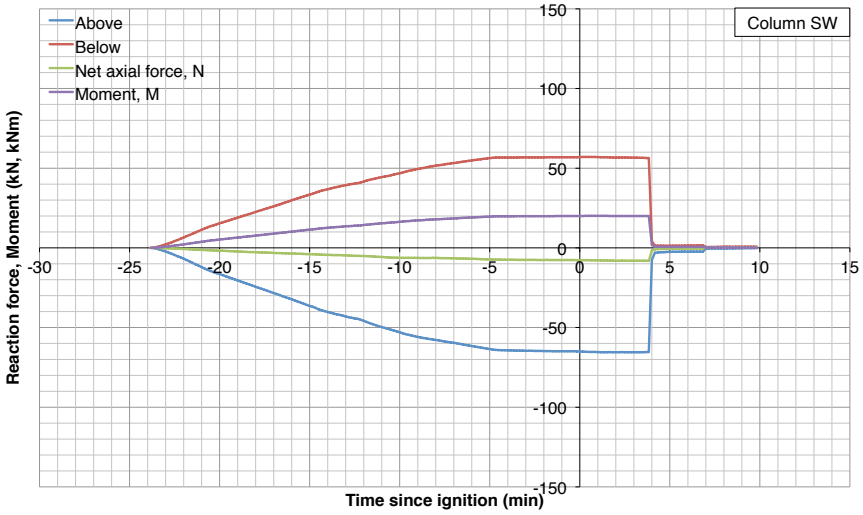

(b) Column SW

Figure I.30: South reaction frame net axial force, N and moment, M for heated 100 mm thick, 0.8% reinforced: unrestrained slab

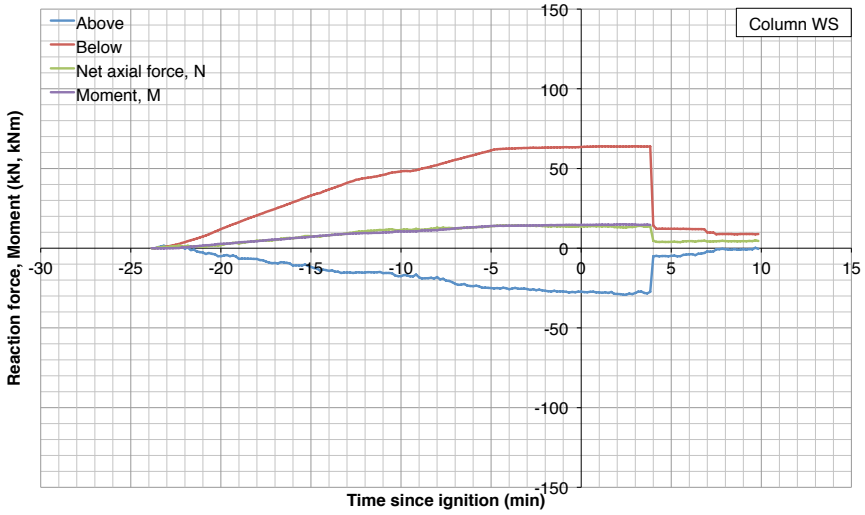

(a) Column WS

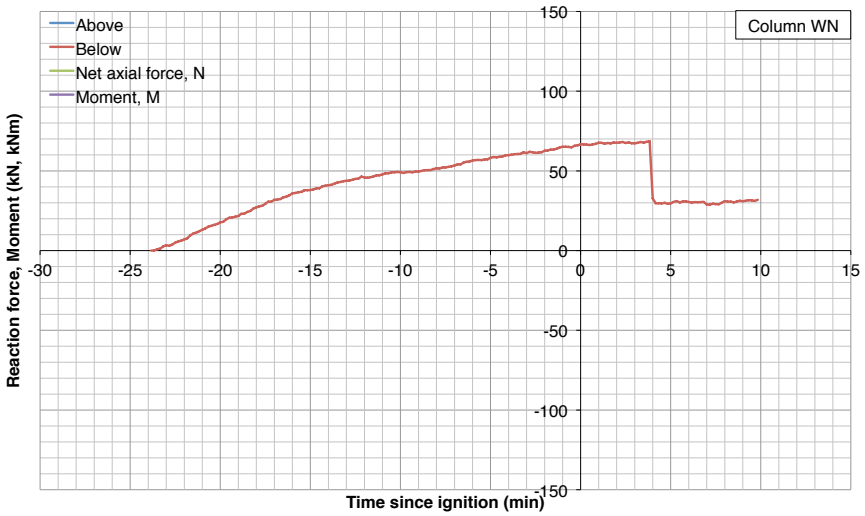

(b) Column WN

Figure I.31: West reaction frame net axial force, N and moment, M for heated 100 mm thick, 0.8% reinforced: unrestrained slab

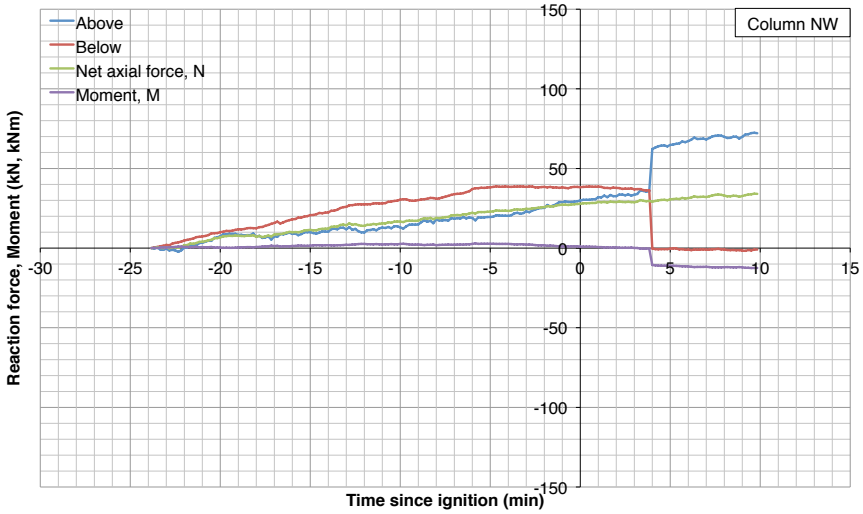

(a) Column NW

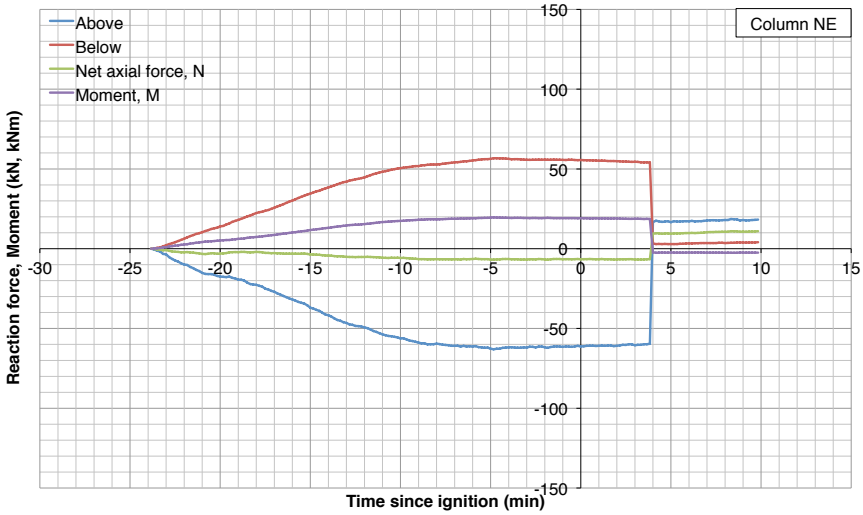

(b) Column NE

Figure I.32: North reaction frame net axial force, N and moment, M for heated 100 mm thick, 0.8% reinforced: unrestrained slab

I.3.3 *Heated restrained test*

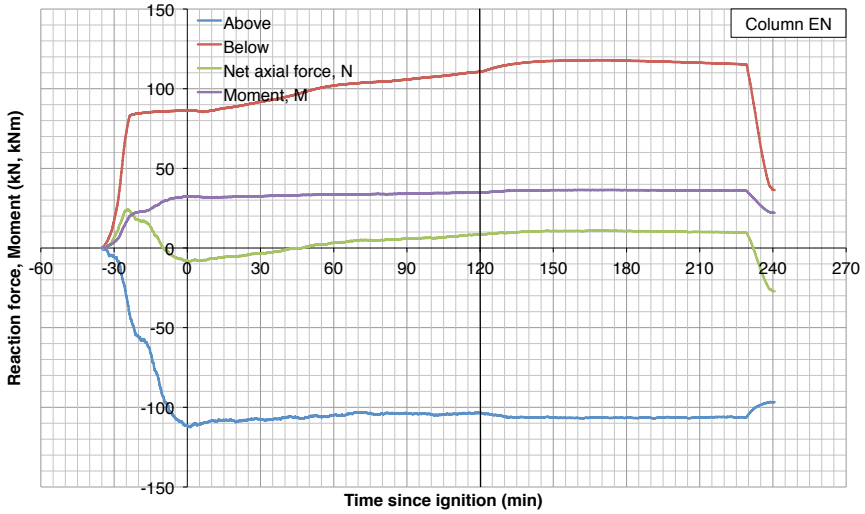

(a) Column EN

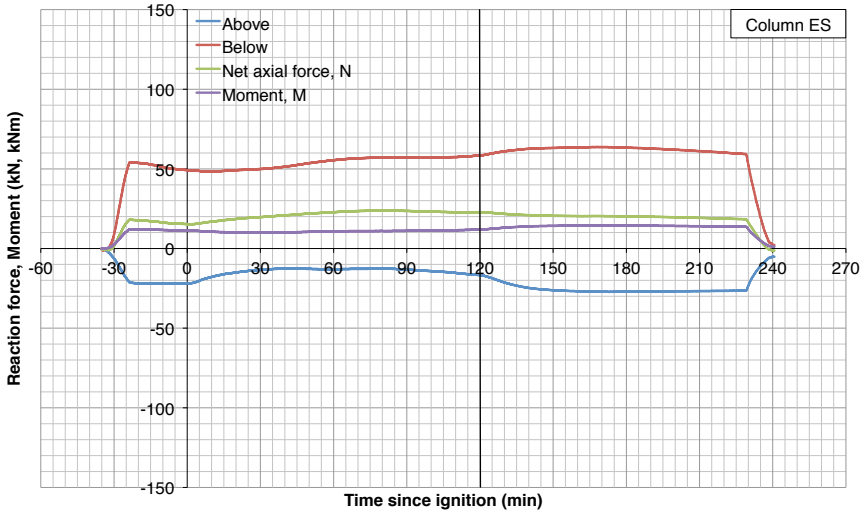

(b) Column ES

Figure I.33: East reaction frame net axial force, N and moment, M for heated 100 mm thick, 0.8% reinforced: restrained slab

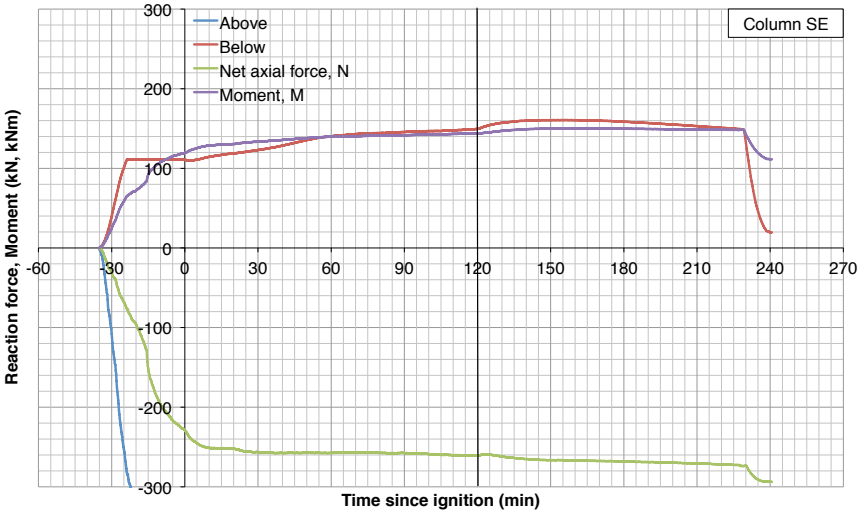

(a) Column SE

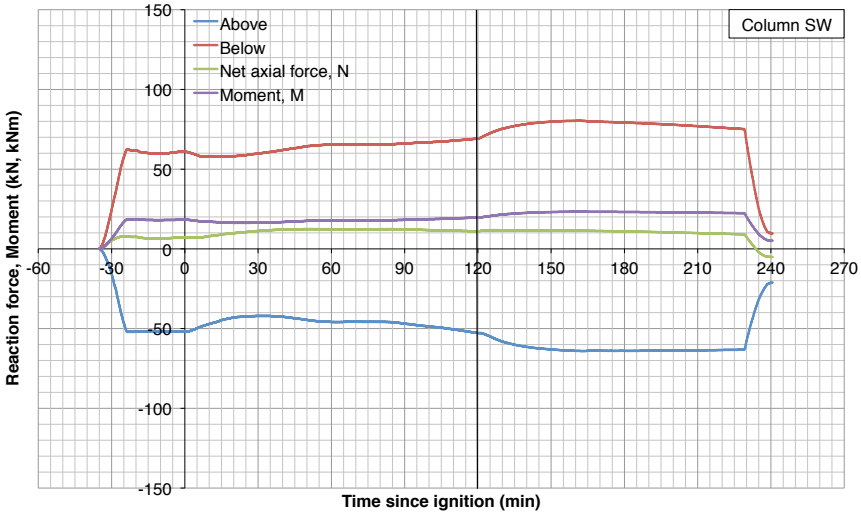

(b) Column SW

Figure I.34: South reaction frame net axial force, N and moment, M for heated 100 mm thick, 0.8% reinforced: restrained slab

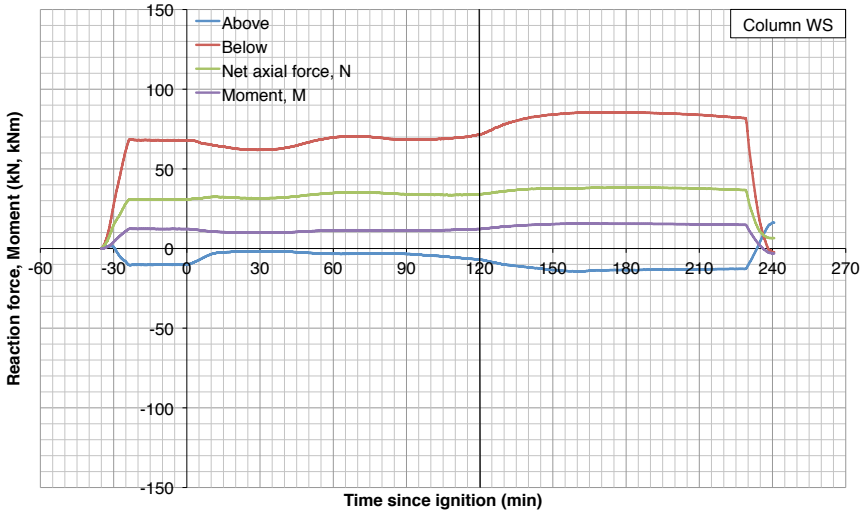

(a) Column WS

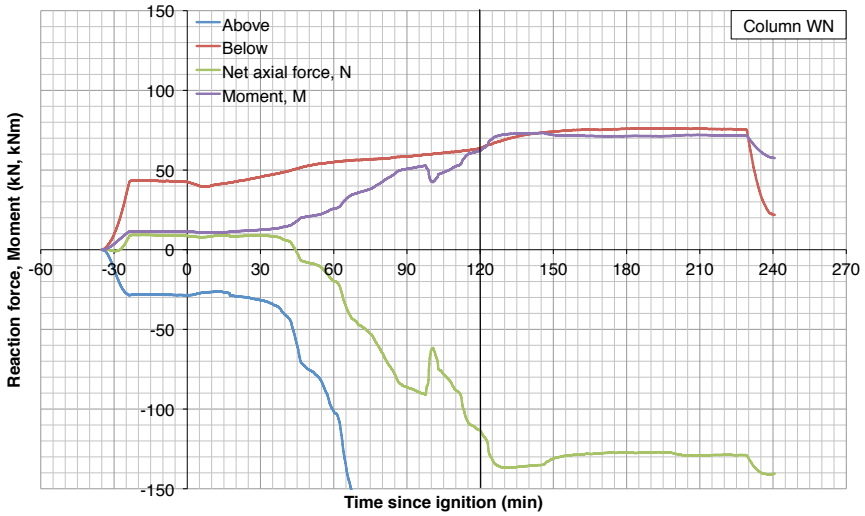

(b) Column WN

Figure I.35: West reaction frame net axial force, N and moment, M for heated 100 mm thick, 0.8% reinforced: restrained slab

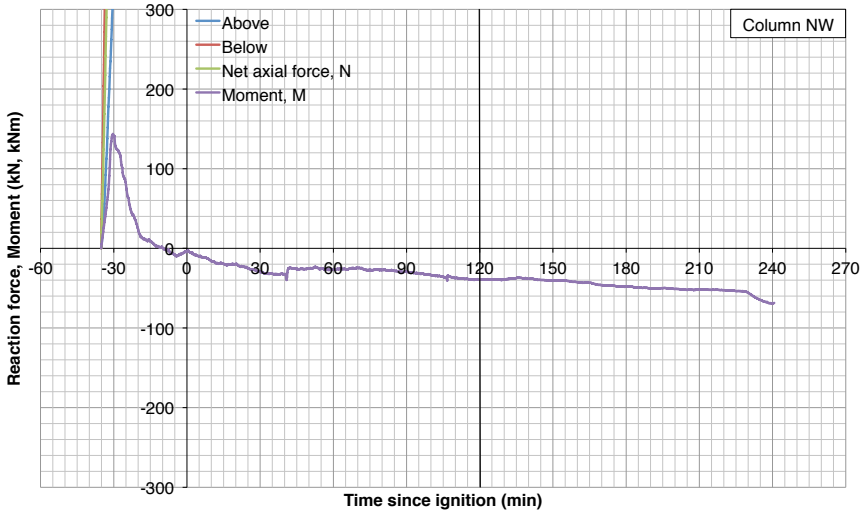

(a) Column NW

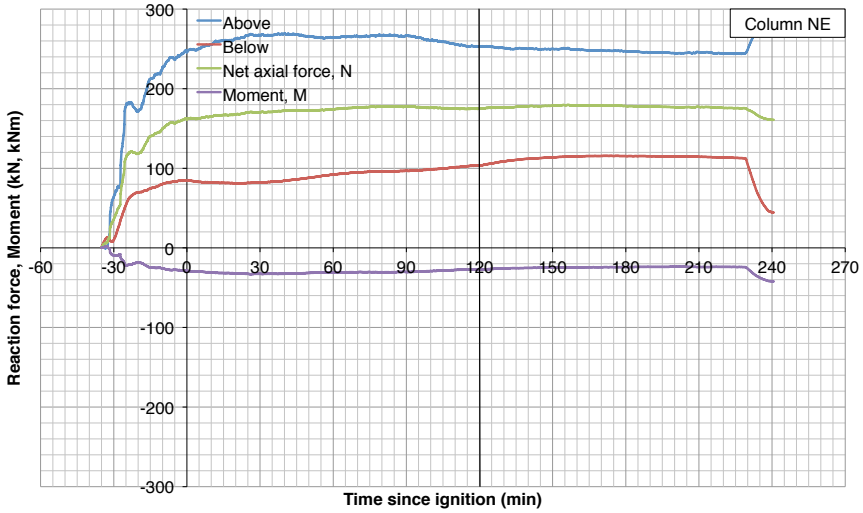

(b) Column NE

Figure I.36: North reaction frame net axial force, N and moment, M for heated 100 mm thick, 0.8% reinforced: restrained slab

I.4 100 MM THICK, 1.5% REINFORCED TESTS

I.4.1 *Ambient unrestrained test*

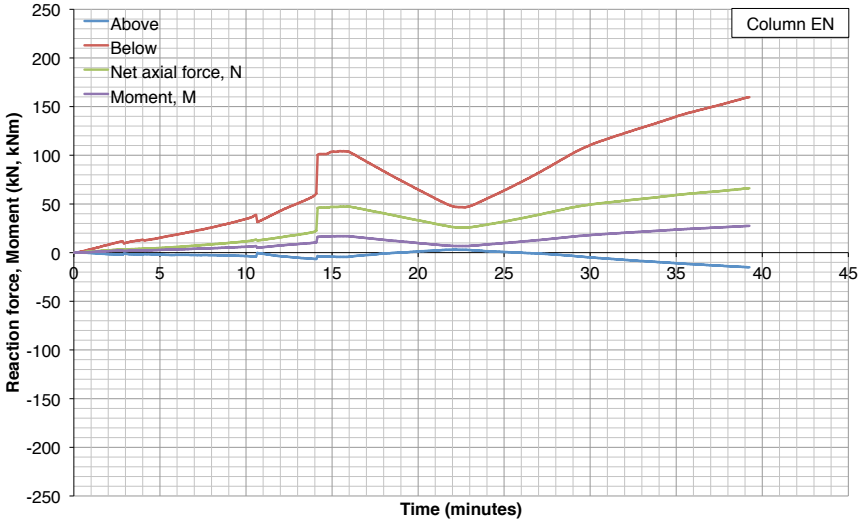

(a) Column EN

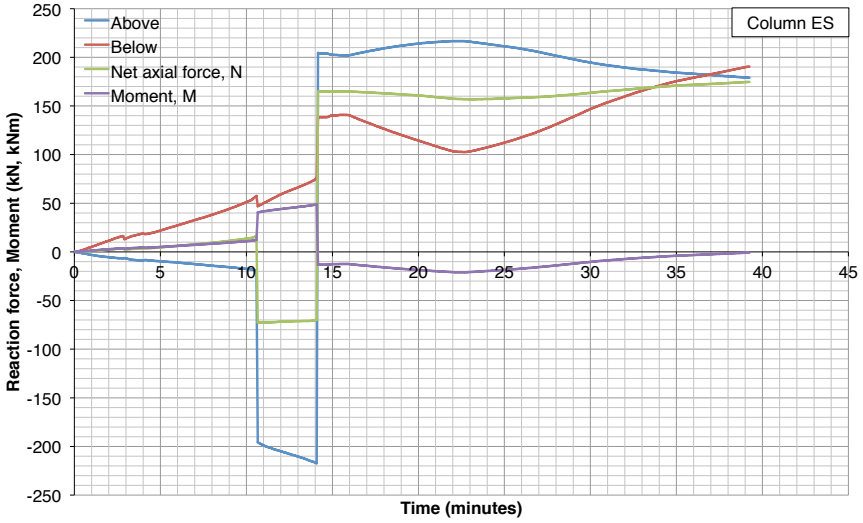

(b) Column ES

Figure I.37: East reaction frame net axial force, N and moment, M for ambient 100 mm thick, 1.5% reinforced: unrestrained slab

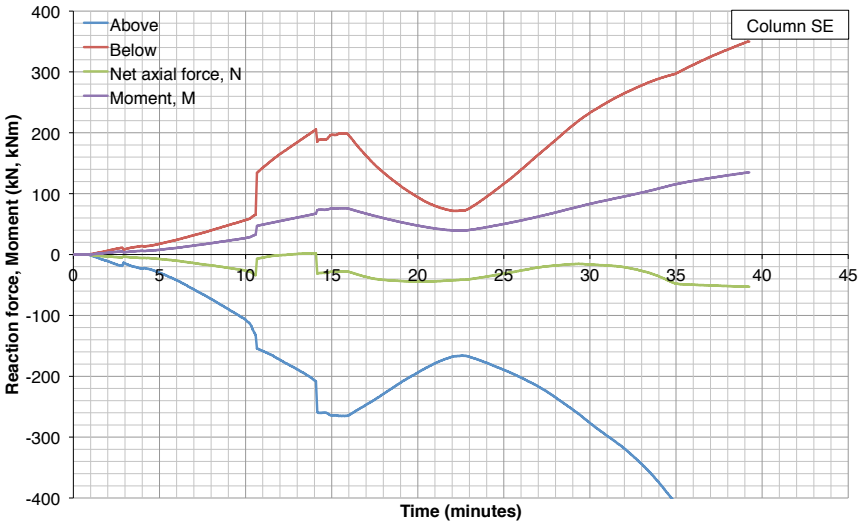

(a) Column SE

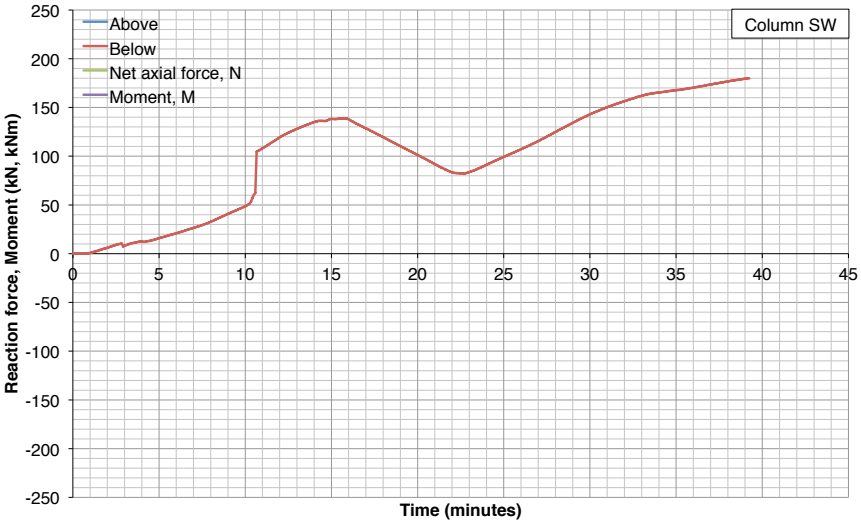

(b) Column SW

Figure I.38: South reaction frame net axial force, N and moment, M for ambient 100 mm thick, 1.5% reinforced: unrestrained slab

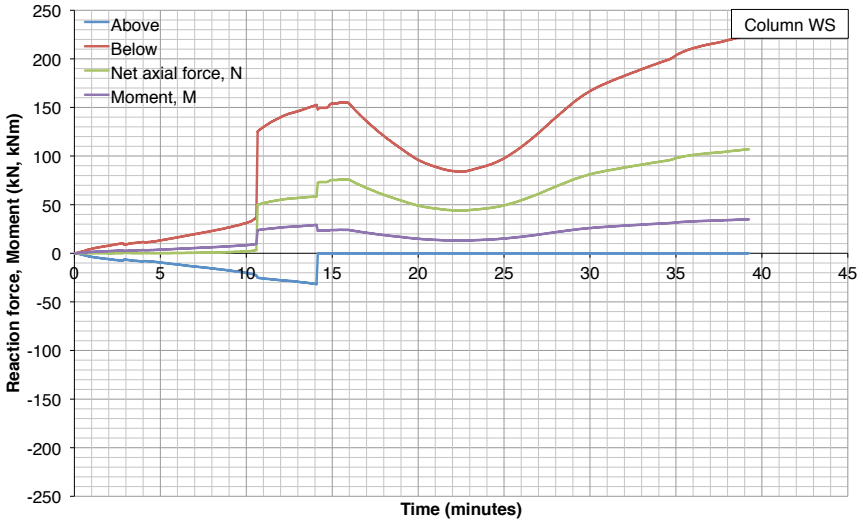

(a) Column WS

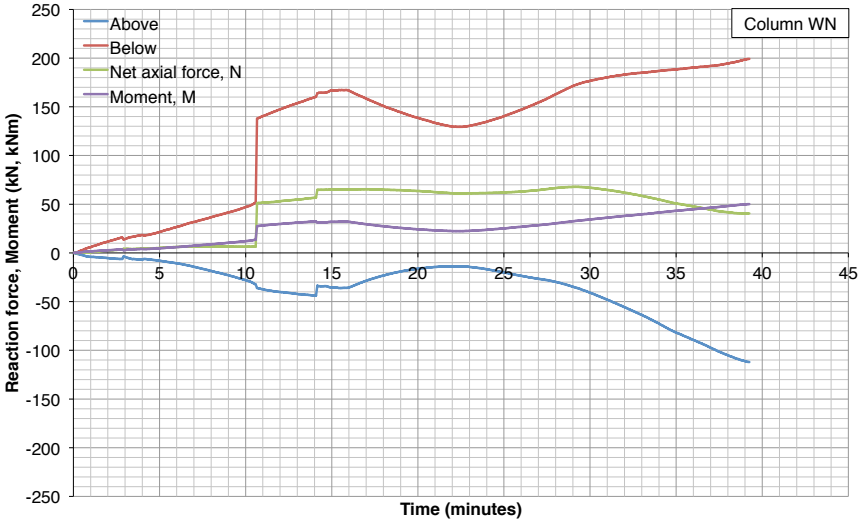

(b) Column WN

Figure I.39: West reaction frame net axial force, N and moment, M for ambient 100 mm thick, 1.5% reinforced: unrestrained slab

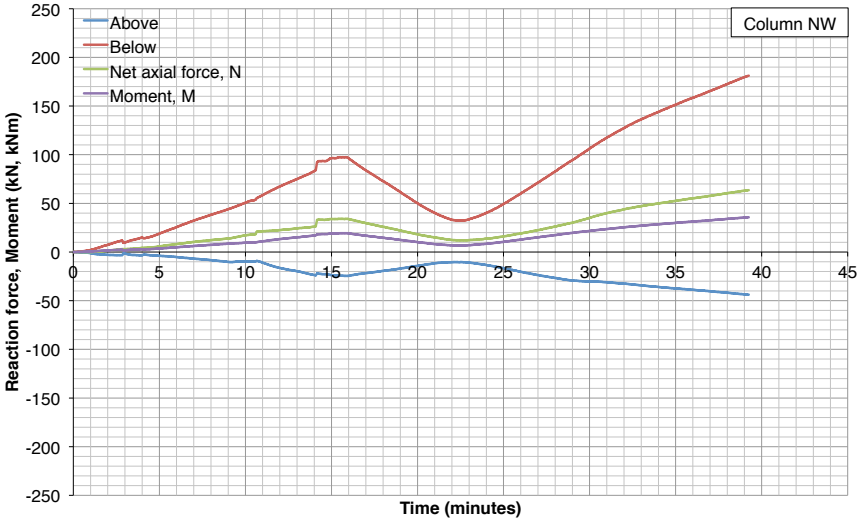

(a) Column NW

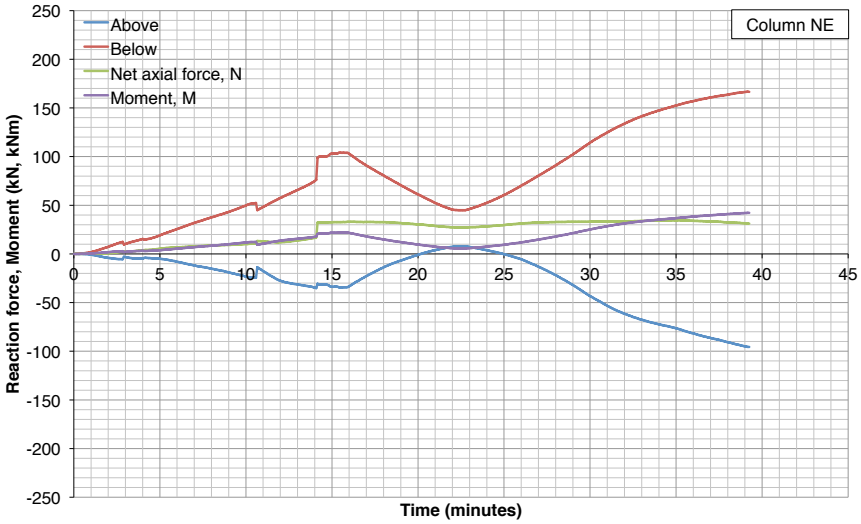

(b) Column NE

Figure I.40: North reaction frame net axial force, N and moment, M for ambient 100 mm thick, 1.5% reinforced: unrestrained slab

I.4.2 *Heated unrestrained test*

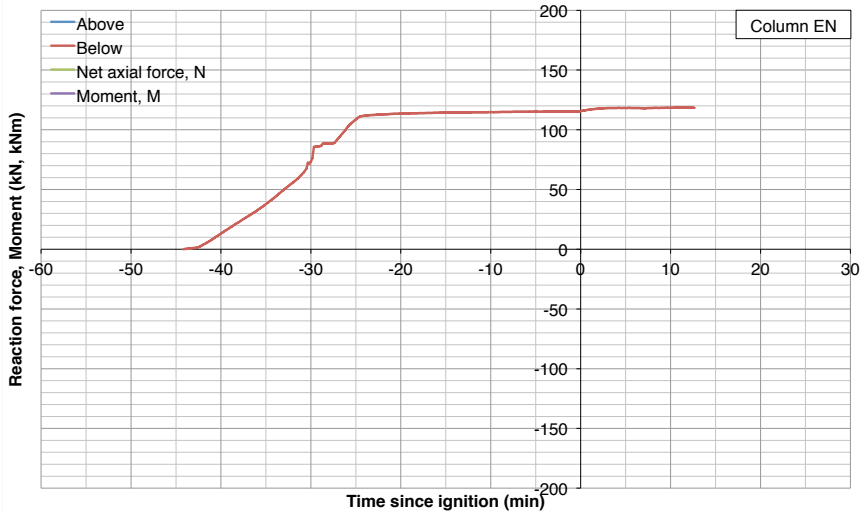

(a) Column EN

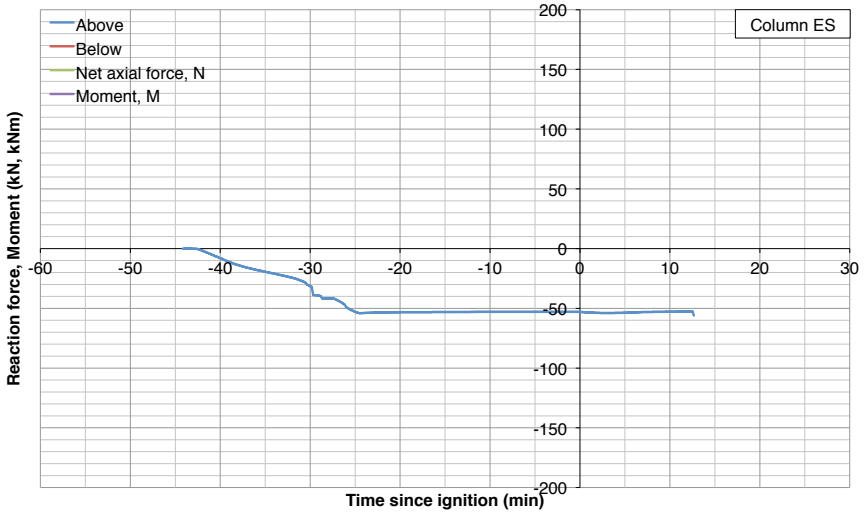

(b) Column ES

Figure I.41: East reaction frame net axial force, N and moment, M for heated 100 mm thick, 1.5% reinforced: unrestrained slab

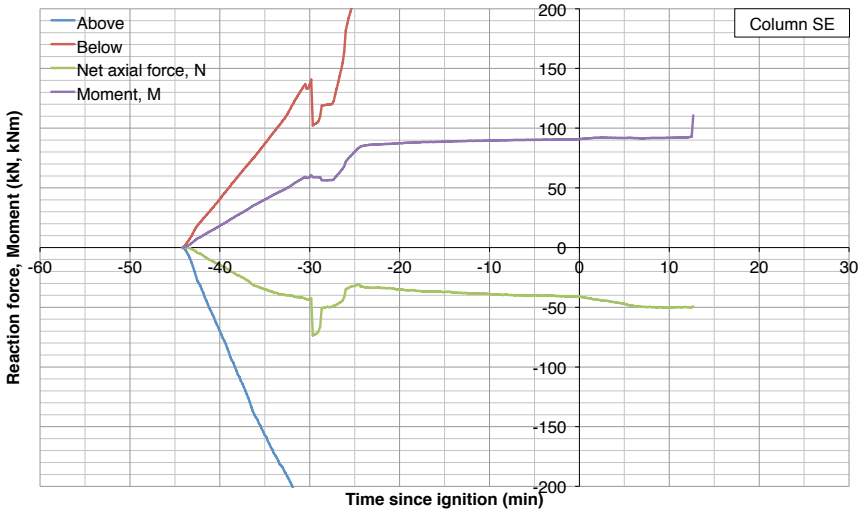

(a) Column SE

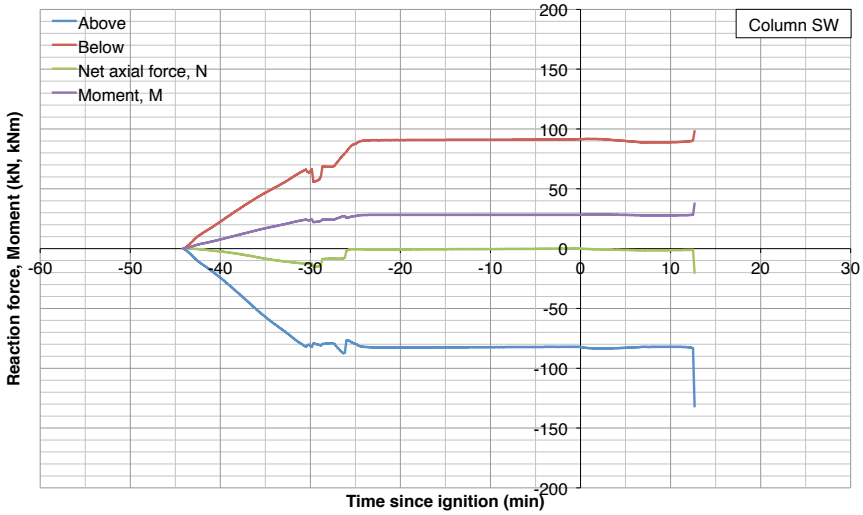

(b) Column SW

Figure I.42: South reaction frame net axial force, N and moment, M for heated 100 mm thick, 1.5% reinforced: unrestrained slab

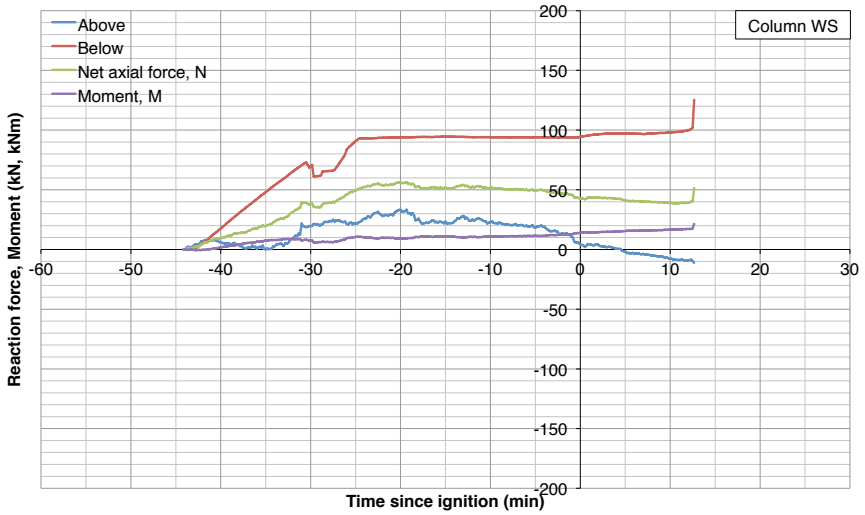

(a) Column WS

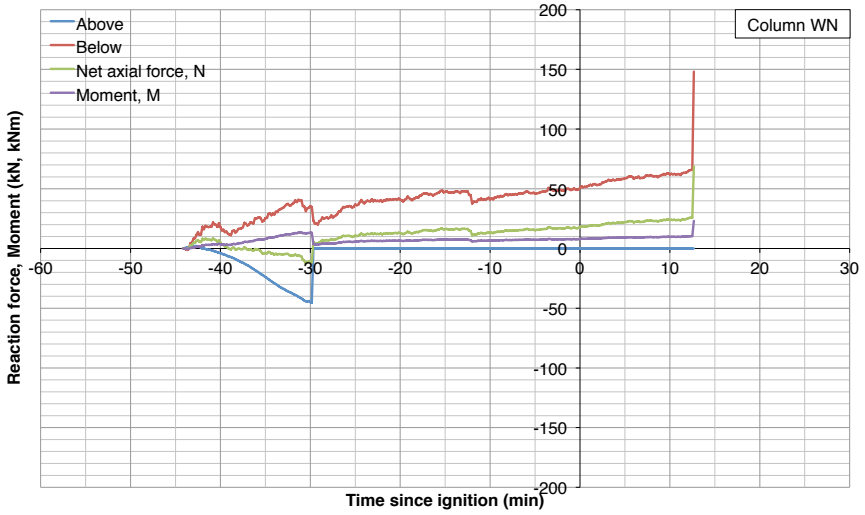

(b) Column WN

Figure I.43: West reaction frame net axial force, N and moment, M for heated 100 mm thick, 1.5% reinforced: unrestrained slab

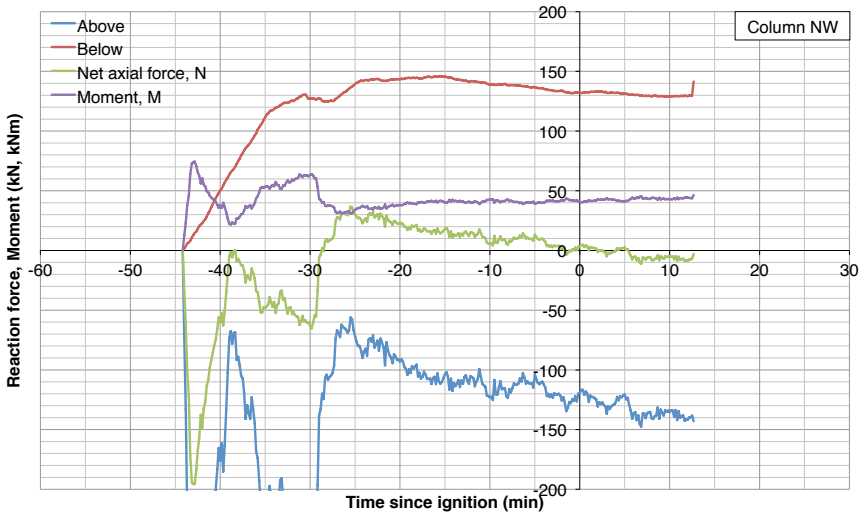

(a) Column NW

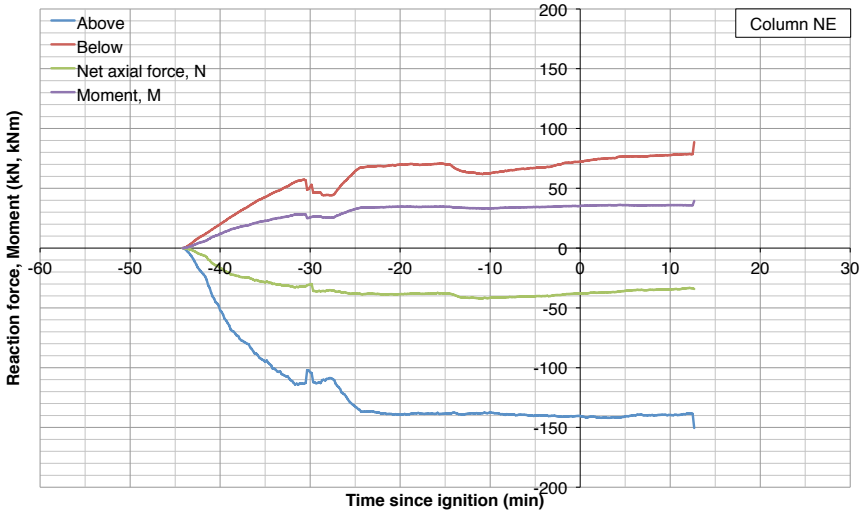

(b) Column NE

Figure I.44: North reaction frame net axial force, N and moment, M for heated 100 mm thick, 1.5% reinforced: unrestrained slab

I.4.3 *Heated restrained test*

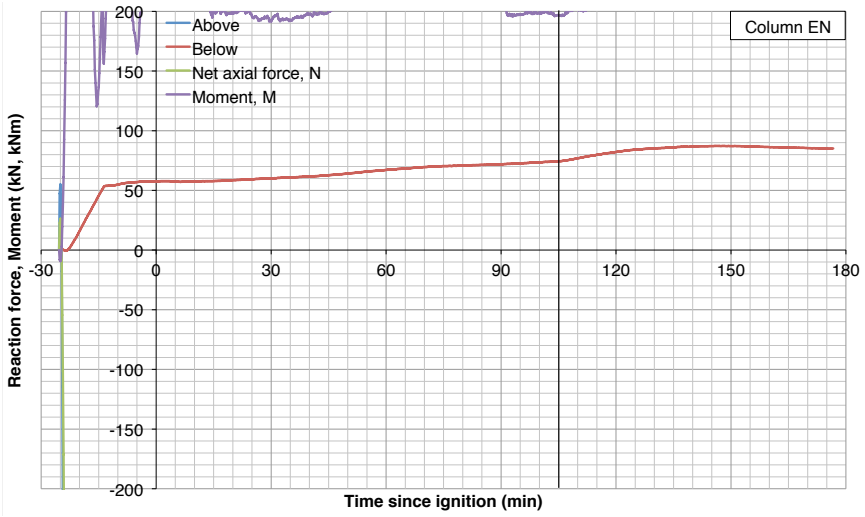

(a) Column EN

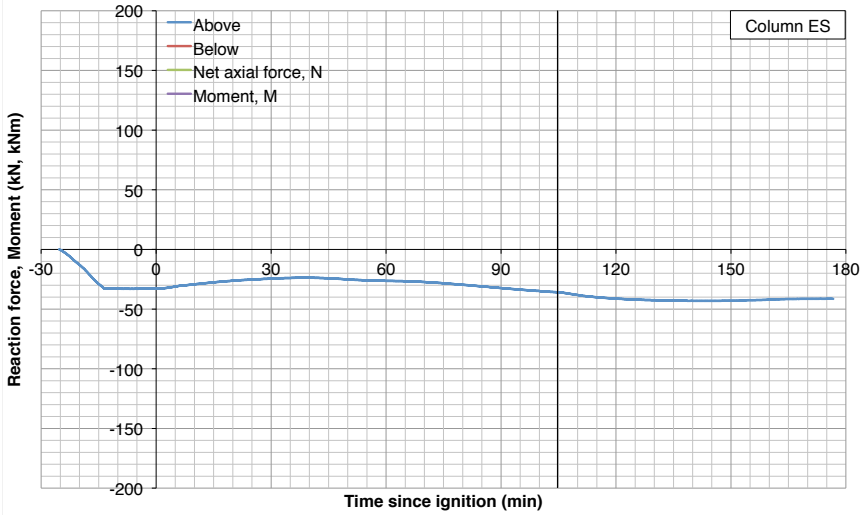

(b) Column ES

Figure I.45: East reaction frame net axial force, N and moment, M for heated 100 mm thick, 1.5% reinforced: restrained slab

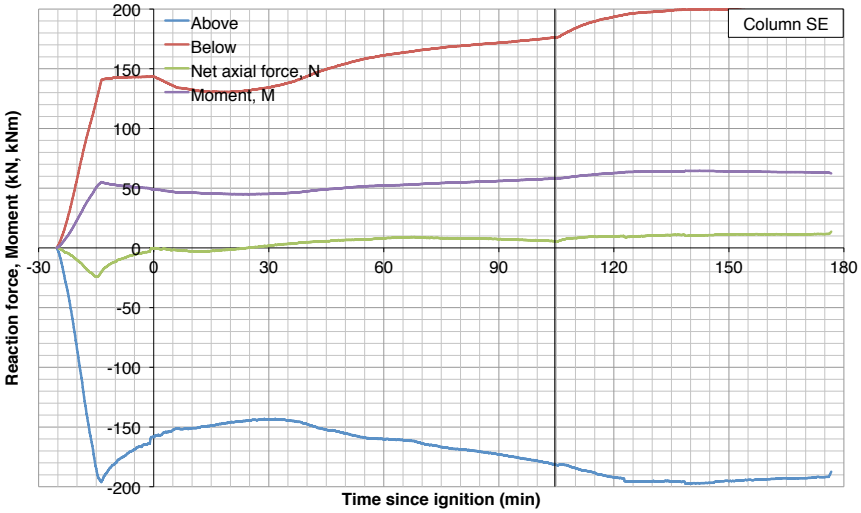

(a) Column SE

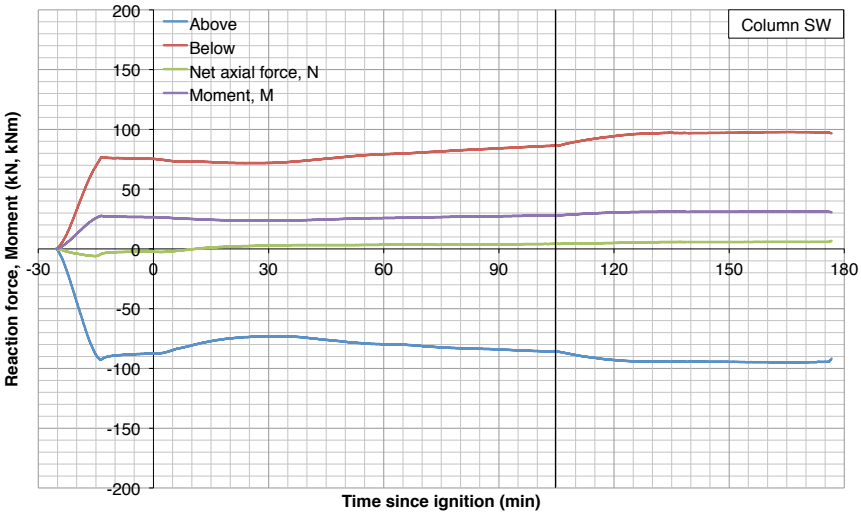

(b) Column SW

Figure I.46: South reaction frame net axial force, N and moment, M for heated 100 mm thick, 1.5% reinforced: restrained slab

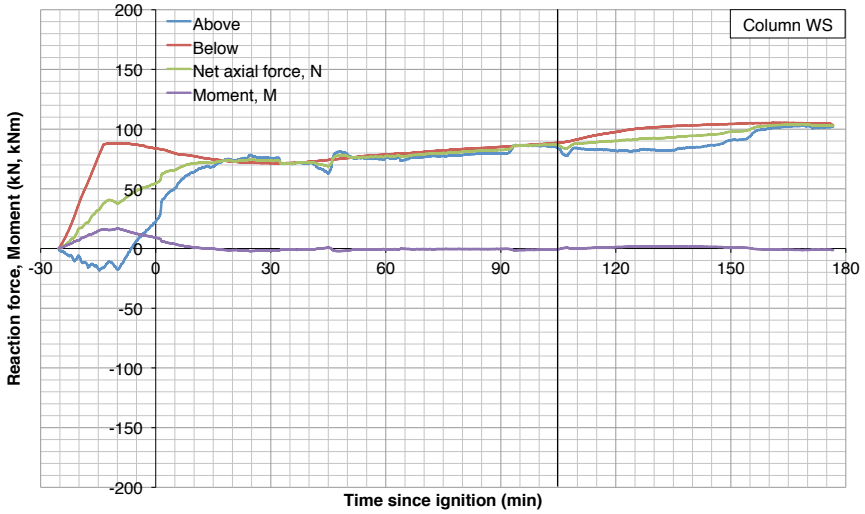

(a) Column WS

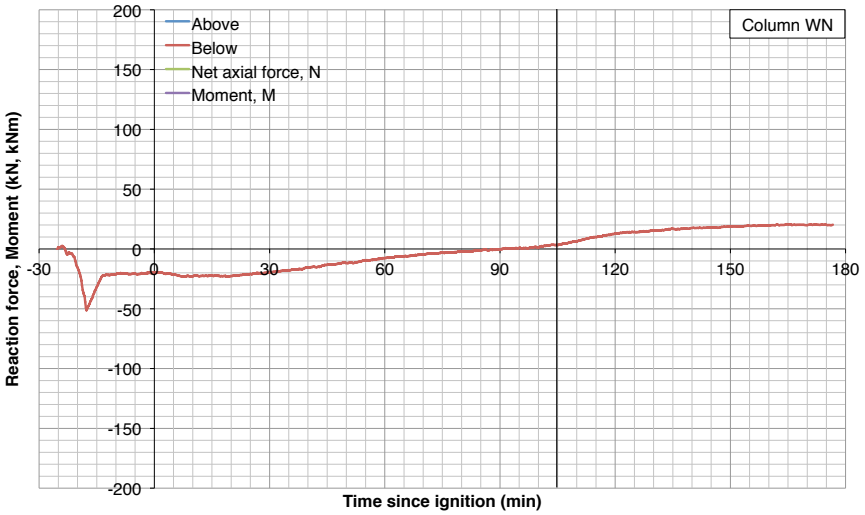

(b) Column WN

Figure I.47: West reaction frame net axial force, N and moment, M for heated 100 mm thick, 1.5% reinforced: restrained slab

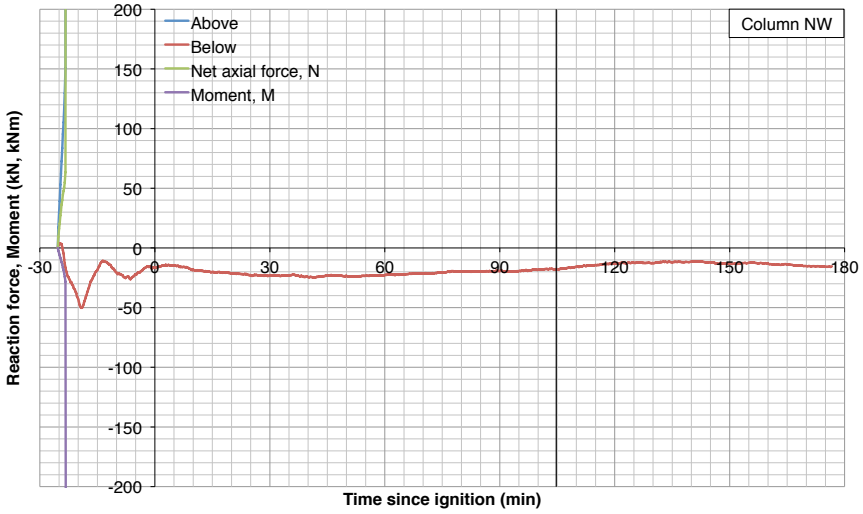

(a) Column NW

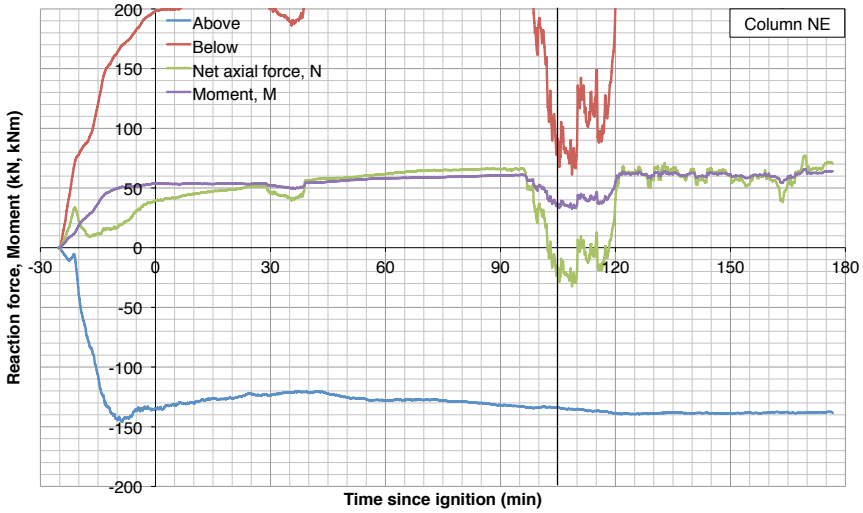

(b) Column NE

Figure I.48: North reaction frame net axial force, N and moment, M for heated 100 mm thick, 1.5% reinforced: restrained slab

I.5 100 MM THICK, 0% REINFORCED TESTS

I.5.1 *Ambient unrestrained test*

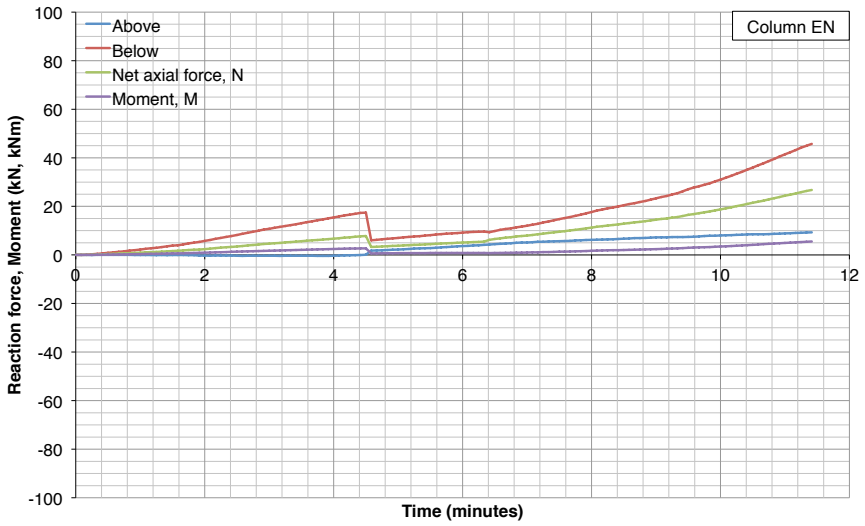

(a) Column EN

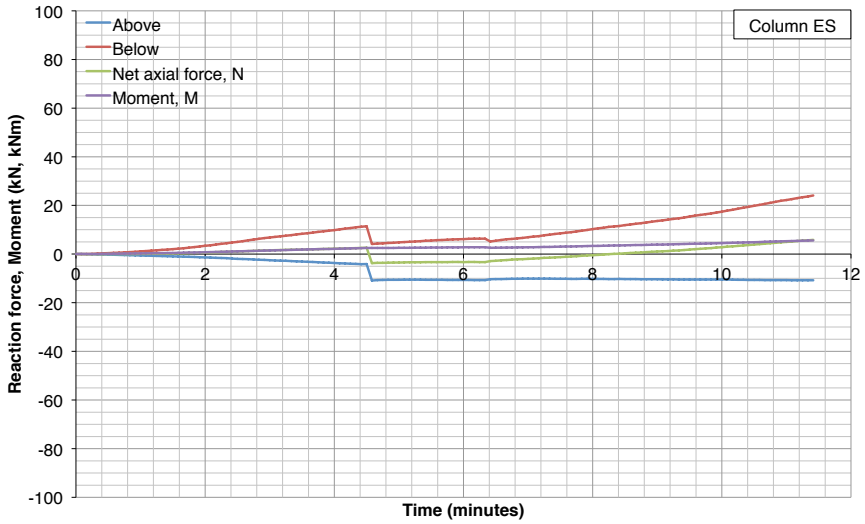

(b) Column ES

Figure I.49: East reaction frame net axial force, N and moment, M for ambient 100 mm thick, 0% reinforced: unrestrained slab

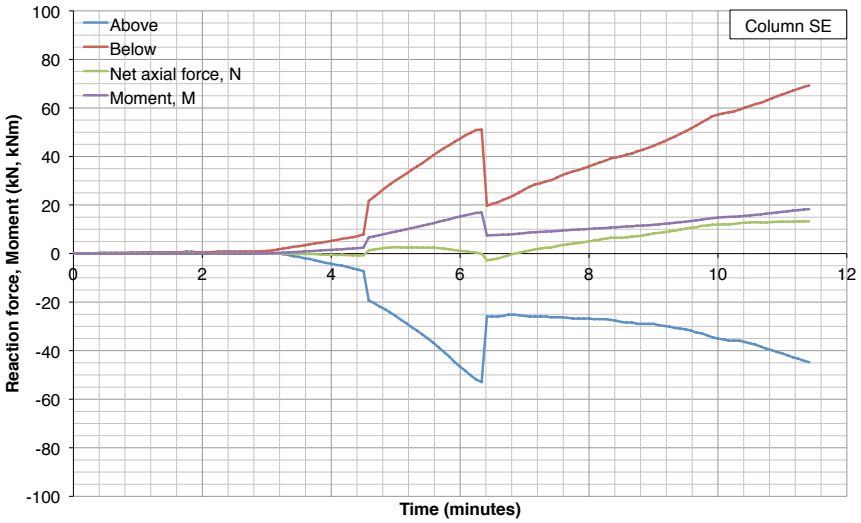

(a) Column SE

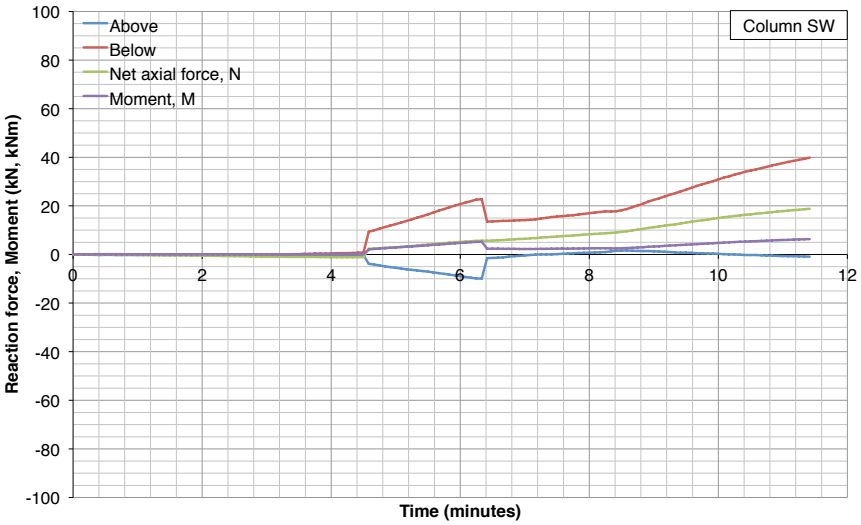

(b) Column SW

Figure I.50: South reaction frame net axial force, N and moment, M for ambient 100 mm thick, 0% reinforced: unrestrained slab

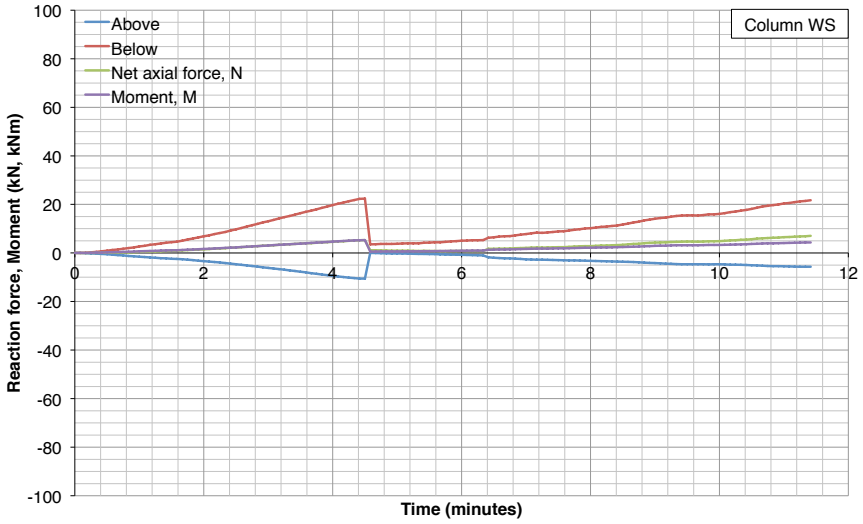

(a) Column WS

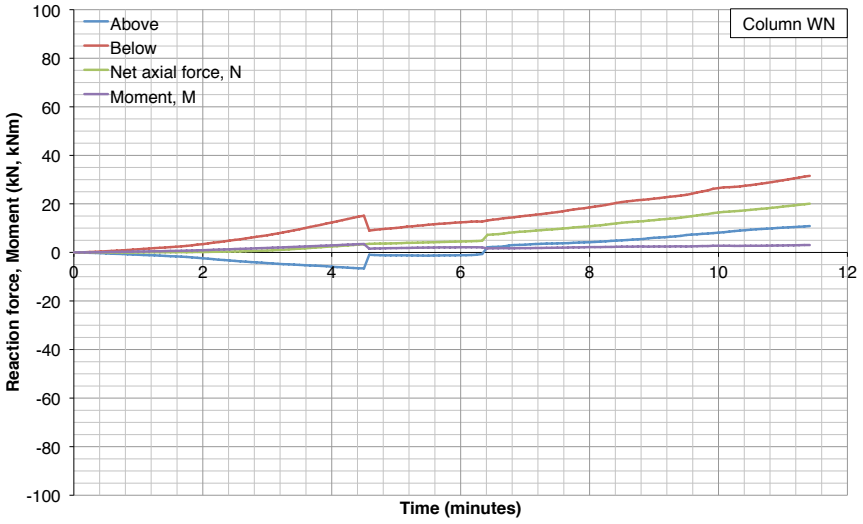

(b) Column WN

Figure I.51: West reaction frame net axial force, N and moment, M for ambient 100 mm thick, 0% reinforced: unrestrained slab

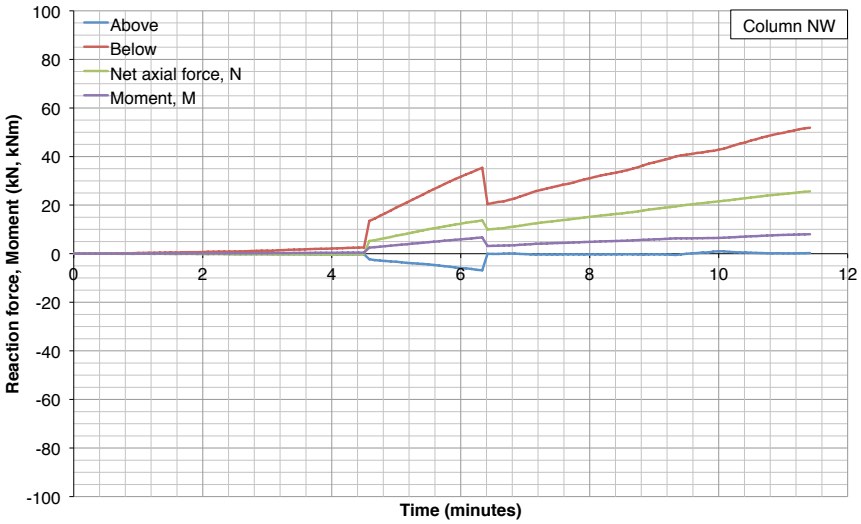

(a) Column NW

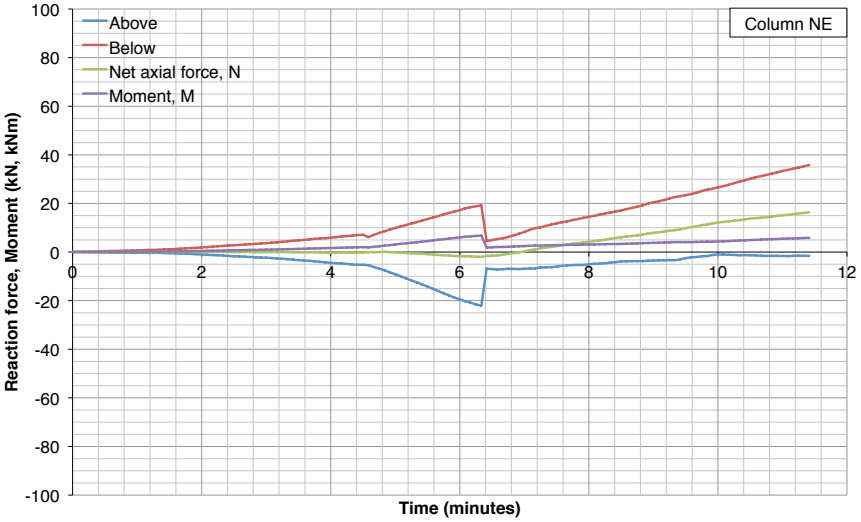

(b) Column NE

Figure I.52: North reaction frame net axial force, N and moment, M for ambient 100 mm thick, 0% reinforced: unrestrained slab

I.5.2 *Heated unrestrained test*

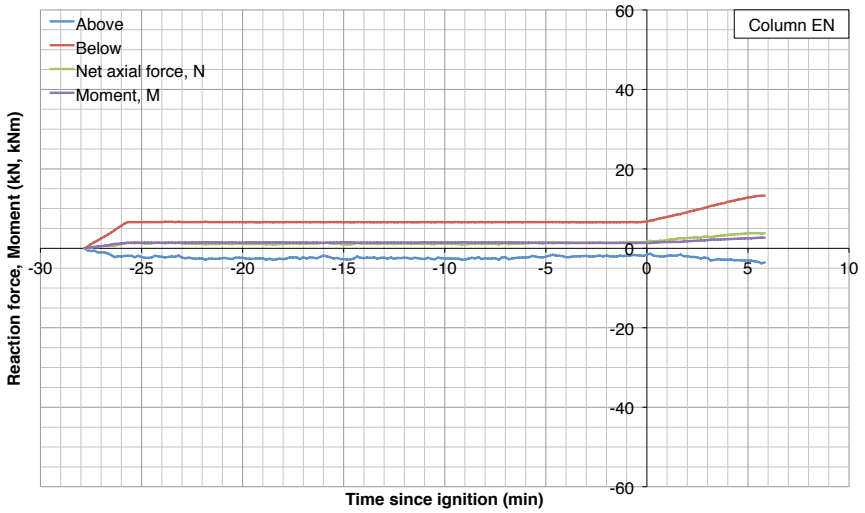

(a) Column EN

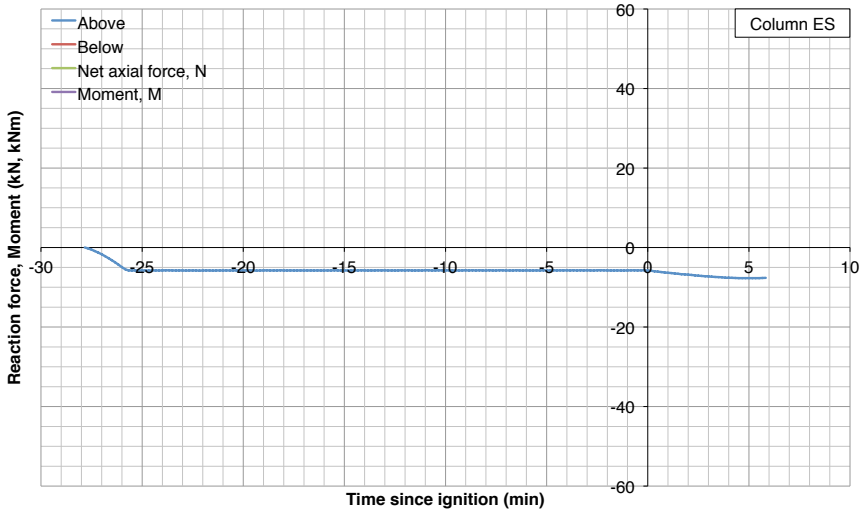

(b) Column ES

Figure I.53: East reaction frame net axial force, N and moment, M for heated 100 mm thick, 0% reinforced: unrestrained slab

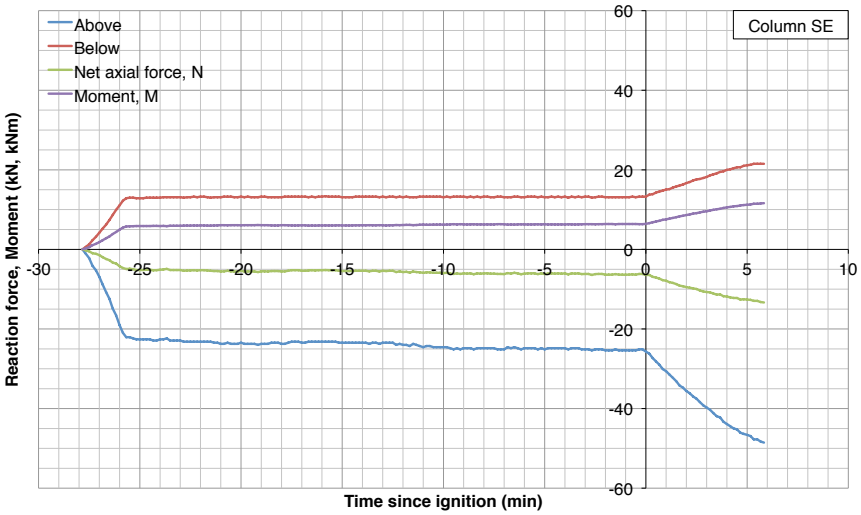

(a) Column SE

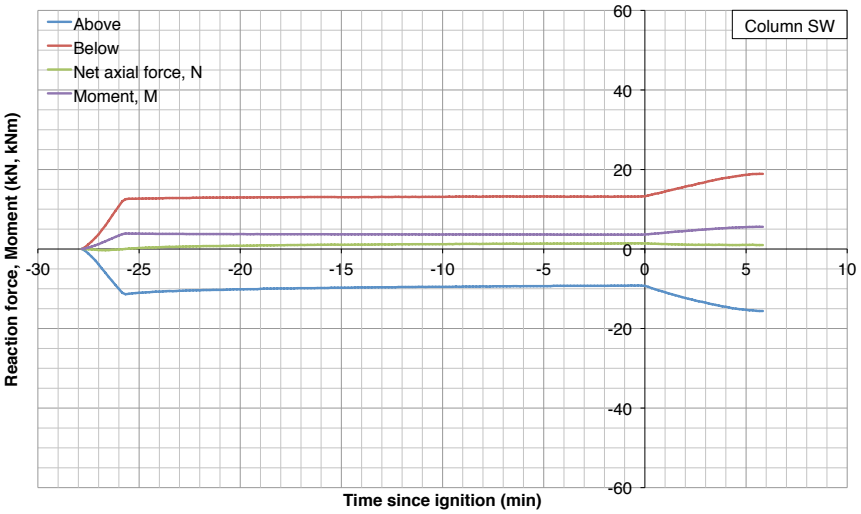

(b) Column SW

Figure I.54: South reaction frame net axial force, N and moment, M for heated 100 mm thick, 0% reinforced: unrestrained slab

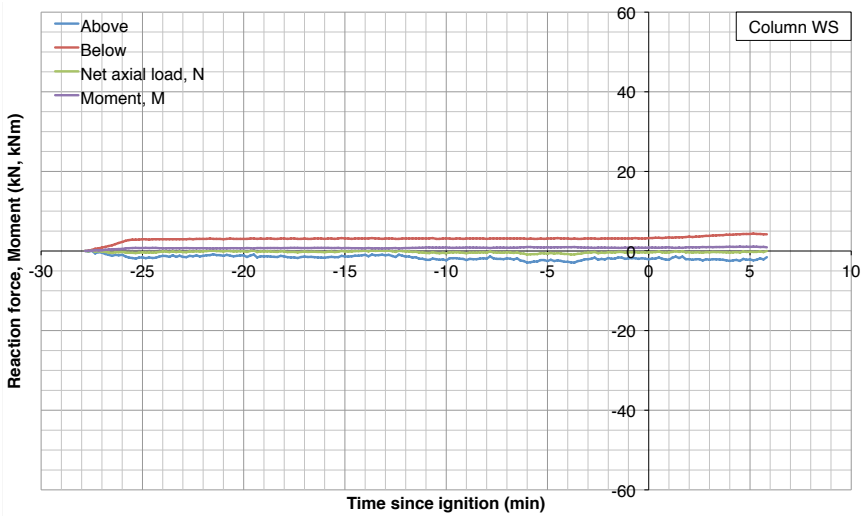

(a) Column WS

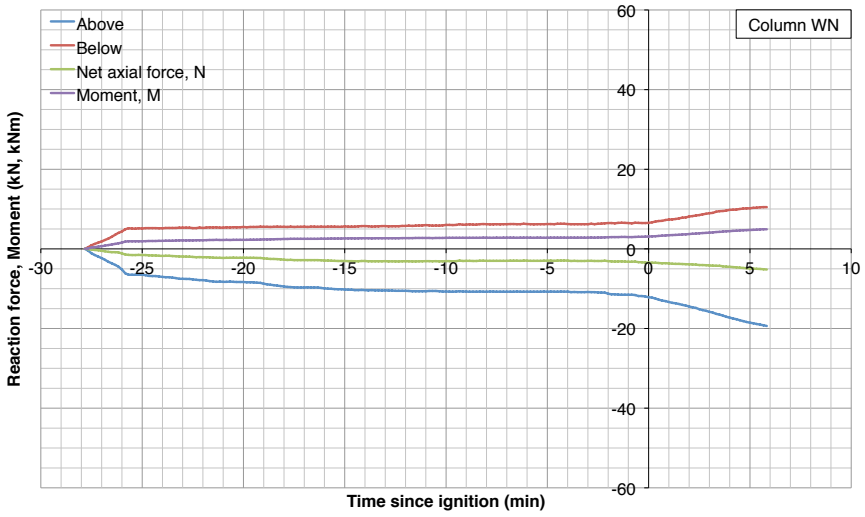

(b) Column WN

Figure I.55: West reaction frame net axial force, N and moment, M for heated 100 mm thick, 0% reinforced: unrestrained slab

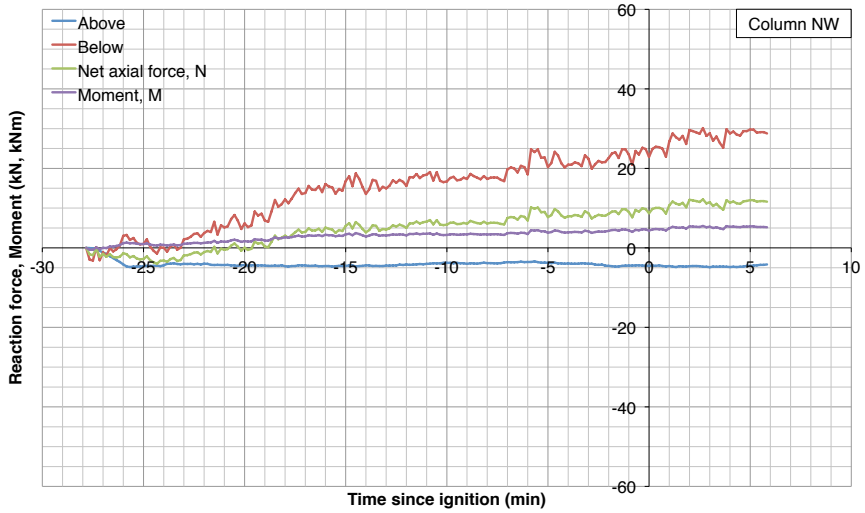

(a) Column NW

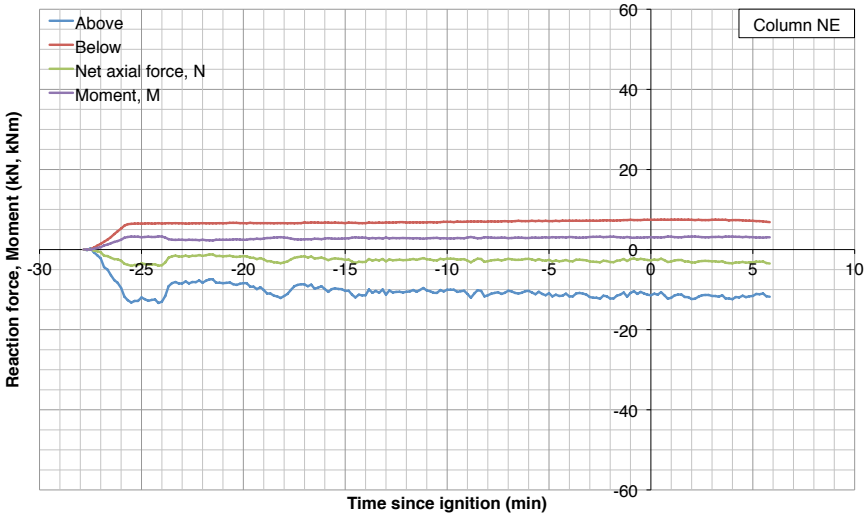

(b) Column NE

Figure I.56: North reaction frame net axial force, N and moment, M for heated 100 mm thick, 0% reinforced: unrestrained slab

I.5.3 *Heated restrained test*

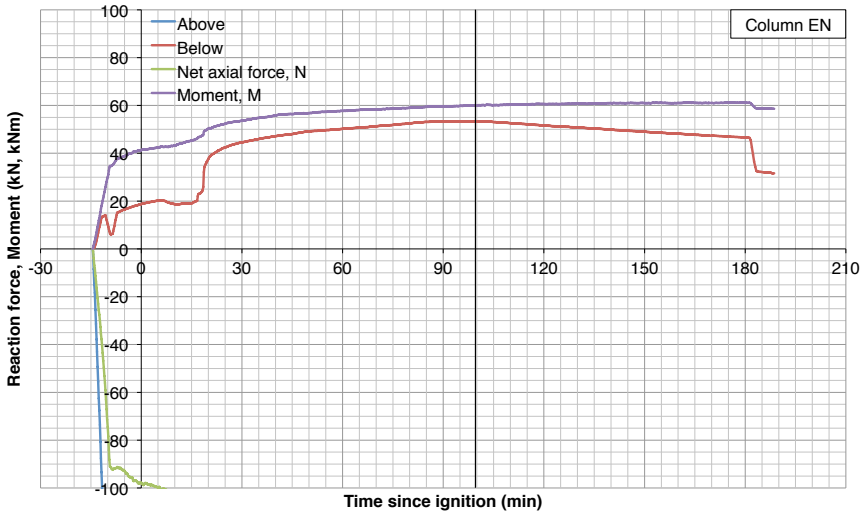

(a) Column EN

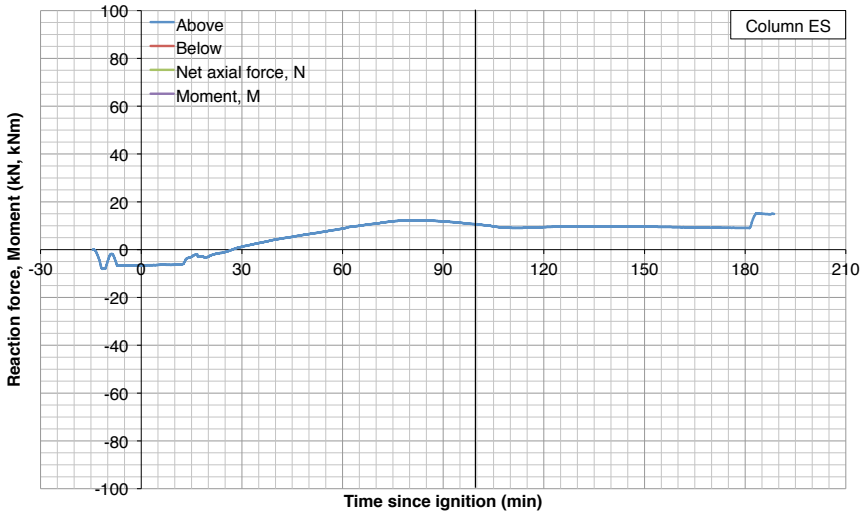

(b) Column ES

Figure I.57: East reaction frame net axial force, N and moment, M for heated 100 mm thick, 0% reinforced: restrained slab

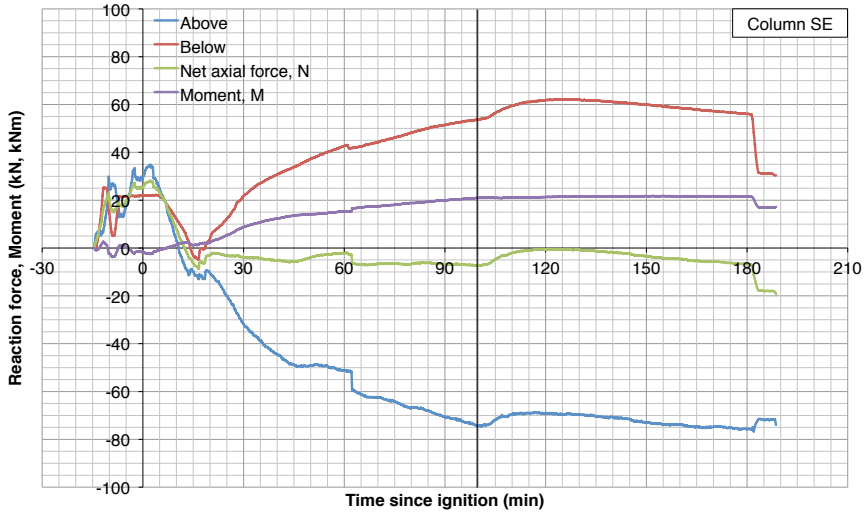

(a) Column SE

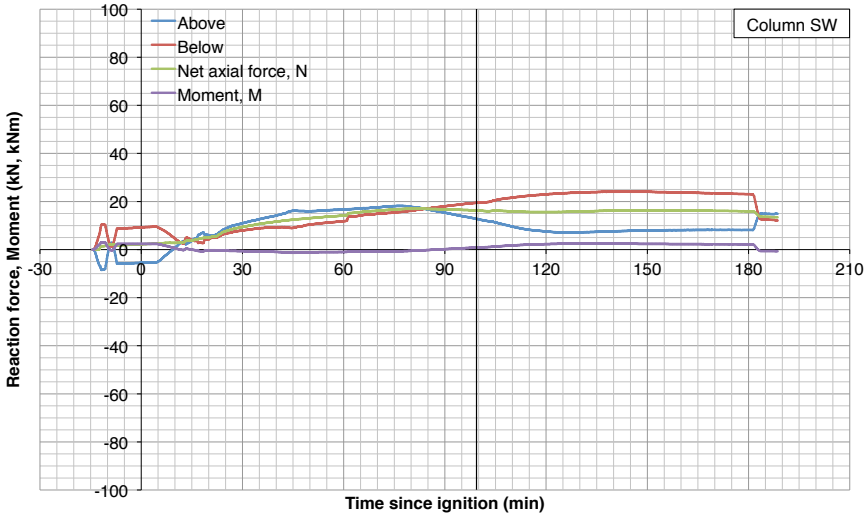

(b) Column SW

Figure I.58: South reaction frame net axial force, N and moment, M for heated 100 mm thick, 0% reinforced: restrained slab

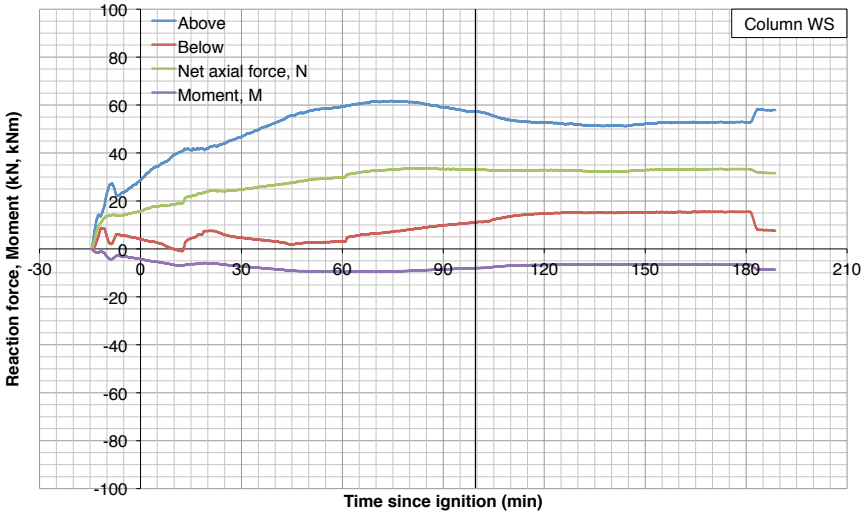

(a) Column WS

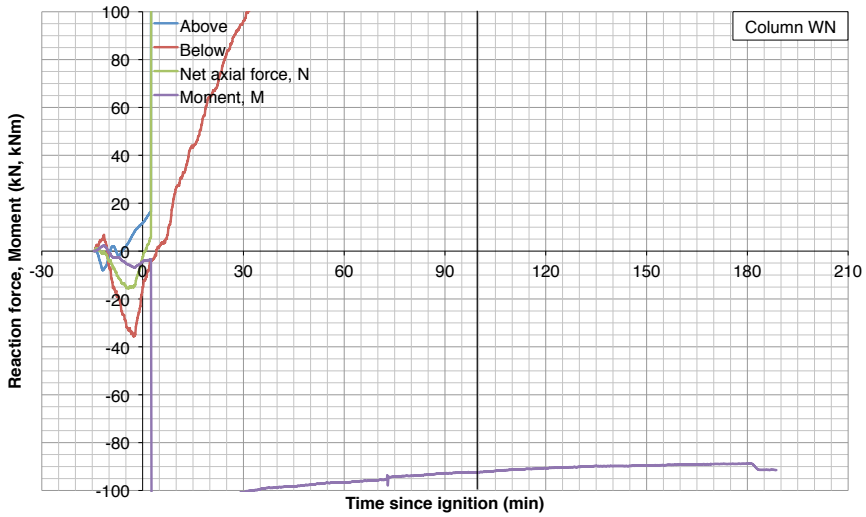

(b) Column WN

Figure I.59: West reaction frame net axial force, N and moment, M for heated 100 mm thick, 0% reinforced: restrained slab

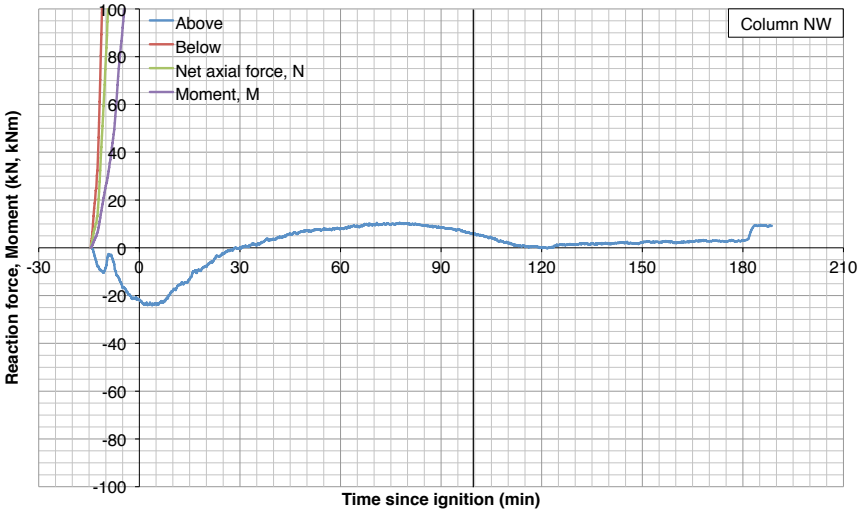

(a) Column NW

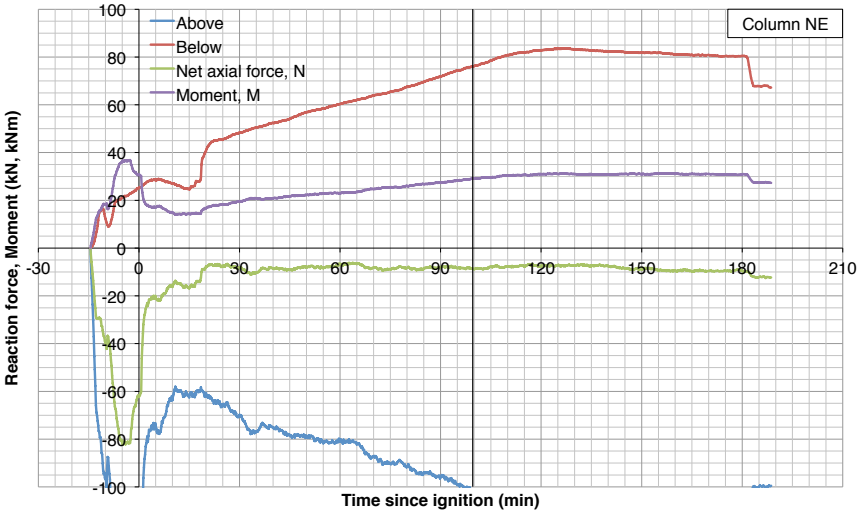

(b) Column NE

Figure I.60: North reaction frame net axial force, N and moment, M for heated 100 mm thick, 0% reinforced: restrained slab

J

POST-FAILURE MEASURED THERMOCOUPLE DEPTHS FROM THE HEATED SURFACE

FRAME POSITION	NORTH					SOUTH					EAST					WEST				
HU50-0.8	5	7	35	50	-	1	15	31	46	-						(7)	15	35	40	-
HR50-0.8	1	13	33	47	-	1	11	33	48	-						(6)	14	38	50	-
HU75-0.8	11	20	36	57	75	10	18	39	55	75						9	18	45	54	75
HR75-0.8	8	15	(35)	57	75	7	17	(34)	53	68	11	19	47	57	75					
HU100-0.8						18	36	61	73	100	0	27	49	79	99	9	32	72	85	92
HR100-0.8						(16)	33	65	88	107	(11)	41	67	85	111	(10)	33	65	82	101
HU100-1.5						(17)	34	53	69	100	3	22	53	76	101	(1)	(12)	58	73	98
HR100-1.5						8	26	66	79	100	(13)	26	52	74	100	0	18	63	79	98
HU100-0	3	27	65	84	98						7	23	59	88	100	(9)	25	62	80	100
HR100-0	(22)	(30)	70	87	105						0	20	59	87	105	1	23	61	89	99

() SUSPICIOUS THERMOCOUPLE DATA, ASSUME WRONG

Table J.1: Post-failure measured thermocouple depths from the heated surface

K

OVERVIEW OF THE COLUMN NET AXIAL FORCE AND MOMENT DATA FOR EACH TEST

SPECIMEN ID	COLUMN STRAIN GAUGE PAIR ID							
	WS-A/ WS-B	WN-A/ WN-B	NW-A/ NW-B	NE-A/ NE-B	EN-A/ EN-B	ES-A/ ES-B	SE-A/ SE-B	SW-A/ SW-B
AU50-0.8	✓	✓	✗	✓	✗	✗	✗	✓
AU75-0.8	✗	✗	✗	✗	✓	✓	✗	✓
AU100-0	✗	✓	✓	✓	✗	✓	✓	✓
AU100-0.8	✗	✗	✓	✓	✓	✗	(✗)	✓
AU100-1.5	✓	✓	✓	✓	✓	✓	✗	(✗)
HU50-0.8	✓	✓	✗	✓	✗	(✗)	✗	✓
HU75-0.8	✓	✗	✗	✓	✗	(✗)	✗	✓
HU100-0	✓	✓	✗	✓	✓	(✗)	✓	✓
HU100-0.8	✓	(✗)	✗	✓	(✗)	(✗)	✗	✓
HU100-1.5	✗	✓	✗	✗	(✗)	(✗)	✗	✓
HR50-0.8	✓	✓	✓	✓	✓	✗	✗	✓
HR75-0.8	✗	✓	✗	✓	✗	(✗)	✗	✓
HR100-0	✓	✗	✗	✗	✗	(✗)	✗	✓
HR100-0.8	✓	✗	✗	✗	✓	✓	✗	✓
HR100-1.5	✓	(✗)	✗	✗	✗	(✗)	✓	✓

✗ SUSPICIOUS STRAIN GAUGE NET AXIAL FORCE, ASSUME WRONG
(✗) DATA FROM EITHER -A OR -B STRAIN GAUGE ONLY

Table K.1: Overview of strain gauge column net axial force and moment data assessment

K.1 AMBIENT

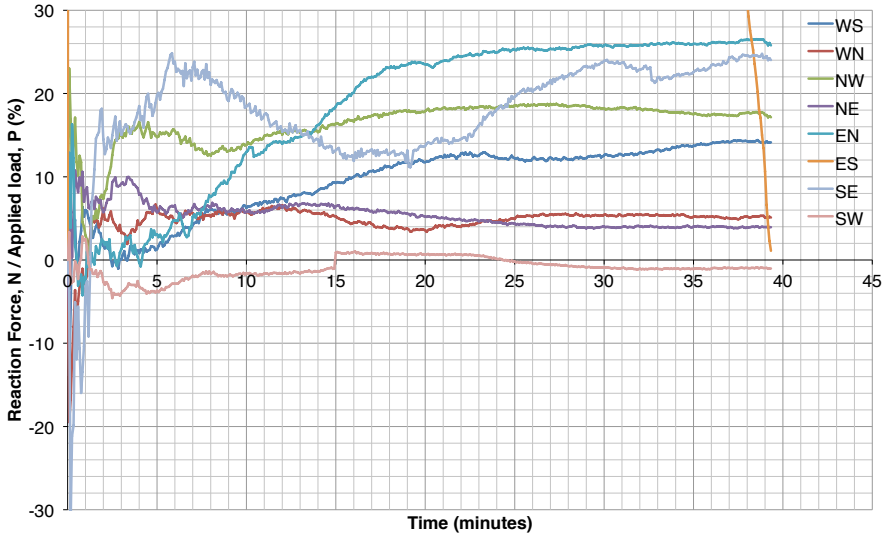

Figure K.1: Percentage ratio between net axial force and applied load for all columns in the ambient 50 mm thick, 0.8% reinforced: unrestrained test

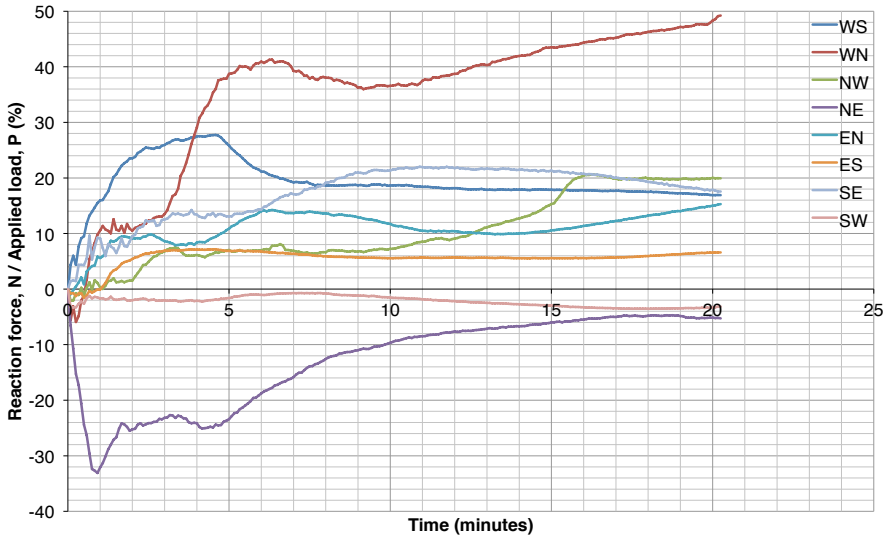

Figure K.2: Percentage ratio between net axial force and applied load for all columns in the ambient 75 mm thick, 0.8% reinforced: unrestrained test

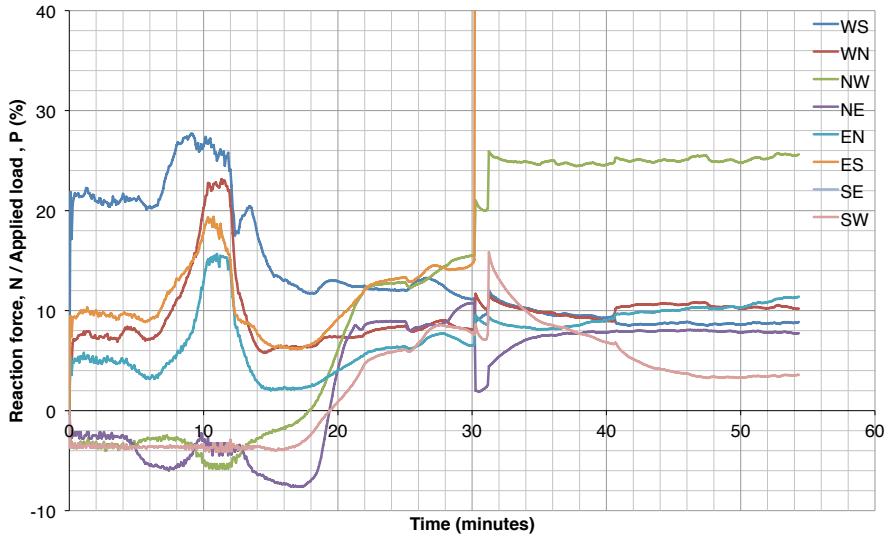

Figure K.3: Percentage ratio between net axial force and applied load for all columns in the ambient 100 mm thick, 0.8% reinforced: unrestrained test

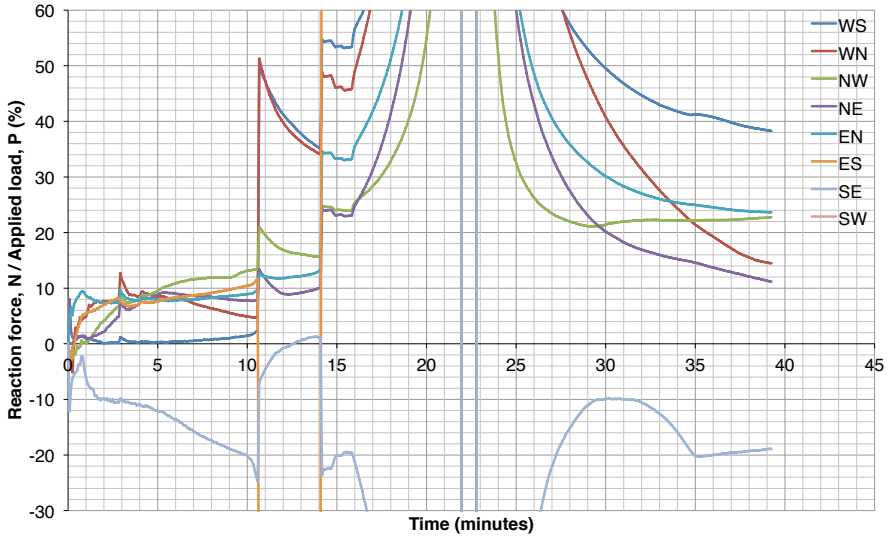

Figure K.4: Percentage ratio between net axial force and applied load for all columns in the ambient 100 mm thick, 1.5% reinforced: unrestrained test

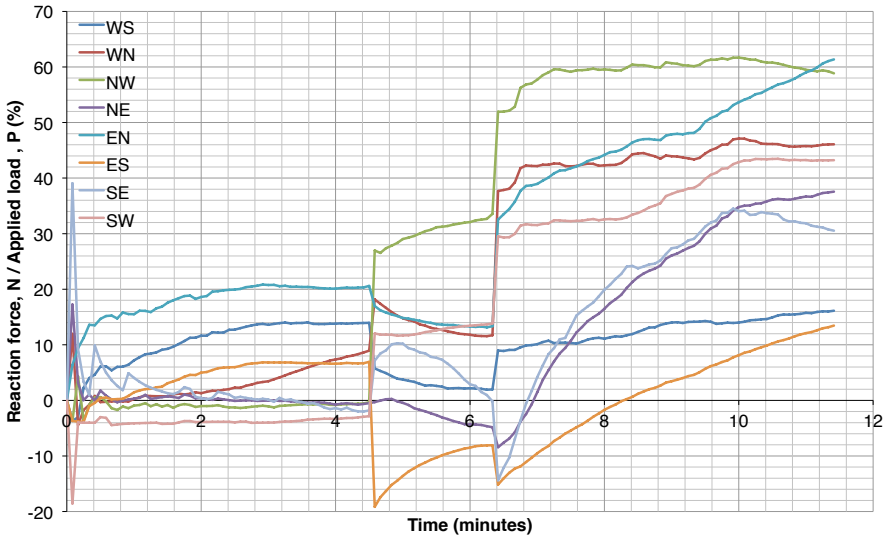

Figure K.5: Percentage ratio between net axial force and applied load for all columns in the ambient 100 mm thick, 0% reinforced: unrestrained test

K.2 50 MM THICK, 0.8% REINFORCED

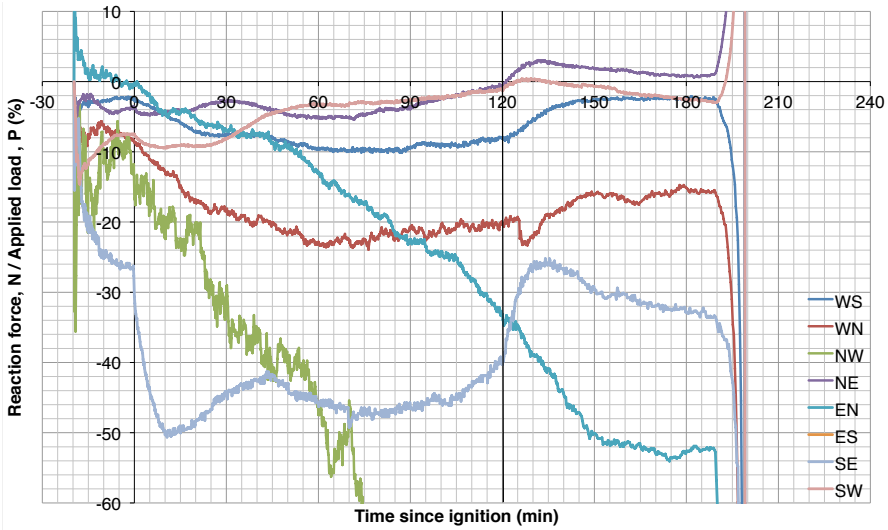

Figure K.6: Percentage ratio between net axial force and applied load for all columns in the heated 50 mm thick, 0.8% reinforced: unrestrained test

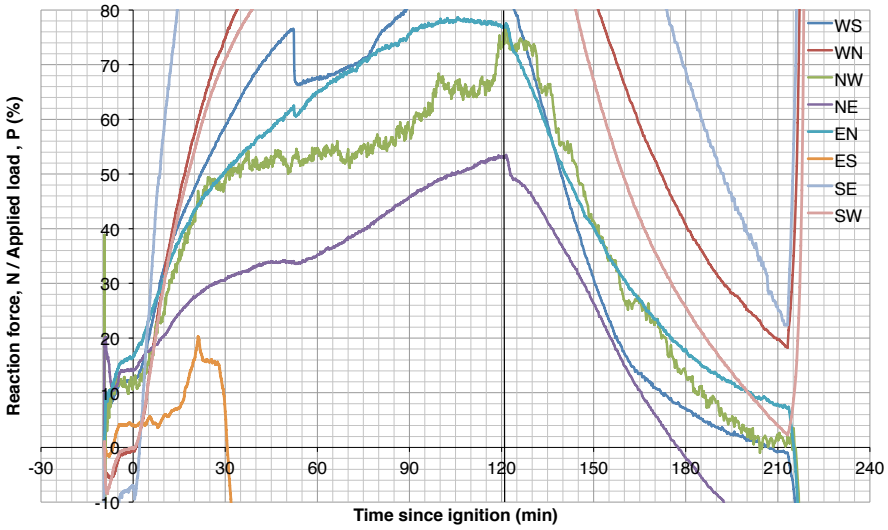

Figure K.7: Percentage ratio between net axial force and applied load for all columns in the heated 50 mm thick, 0.8% reinforced: restrained test

K.3 75 MM THICK, 0.8% REINFORCED

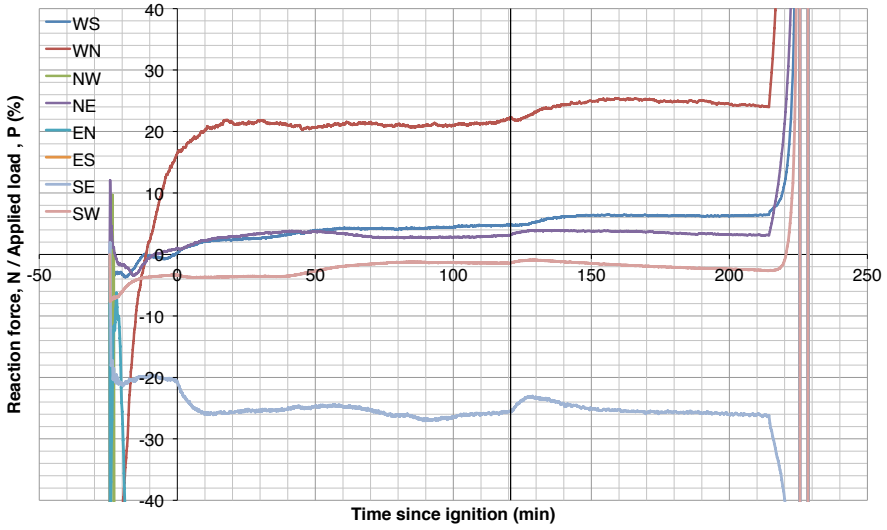

Figure K.8: Percentage ratio between net axial force and applied load for all columns in the heated 75 mm thick, 0.8% reinforced: unrestrained test

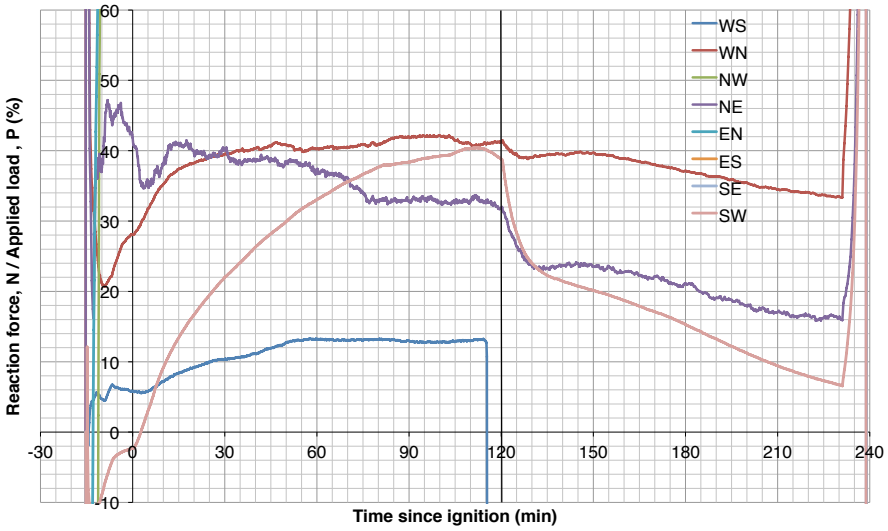

Figure K.9: Percentage ratio between net axial force and applied load for all columns in the heated 75 mm thick, 0.8% reinforced: restrained test

K.4 100 MM THICK, 0.8% REINFORCED

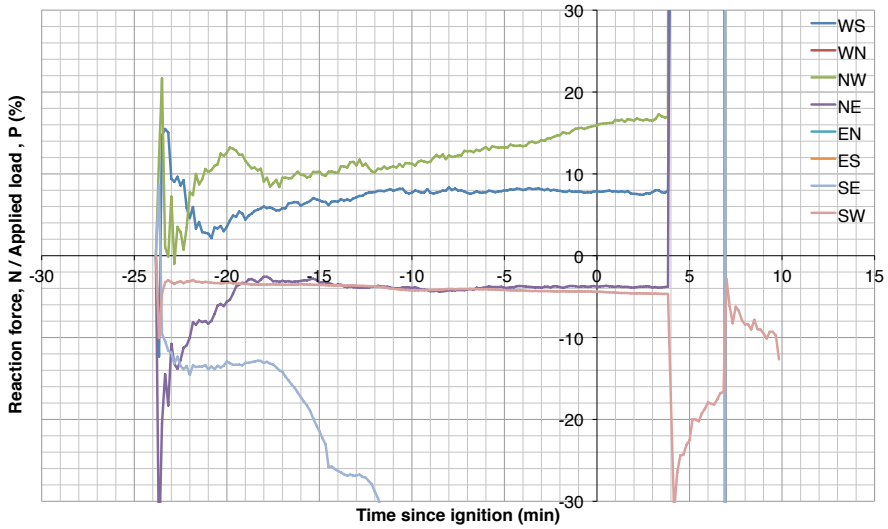

Figure K.10: Percentage ratio between net axial force and applied load for all columns in the heated 100 mm thick, 0.8% reinforced: unrestrained test

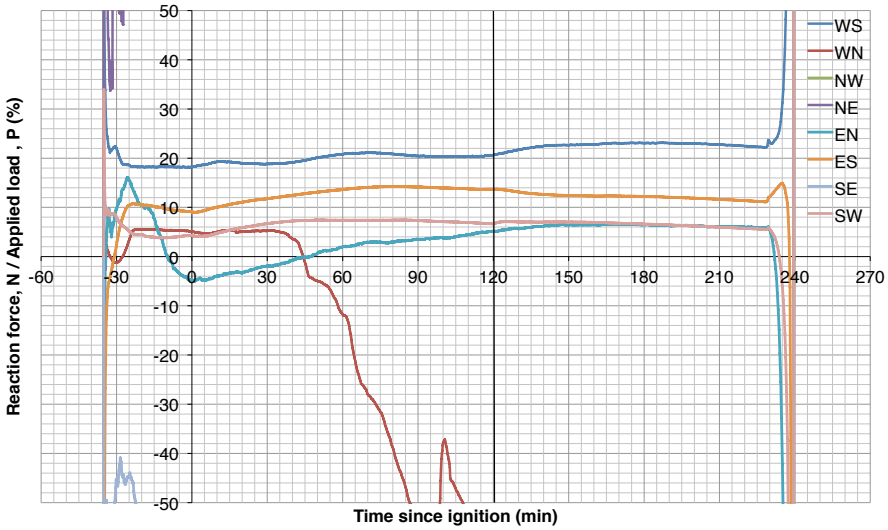

Figure K.11: Percentage ratio between net axial force and applied load for all columns in the heated 100 mm thick, 0.8% reinforced: restrained test

K.5 100 MM THICK, 1.5% REINFORCED

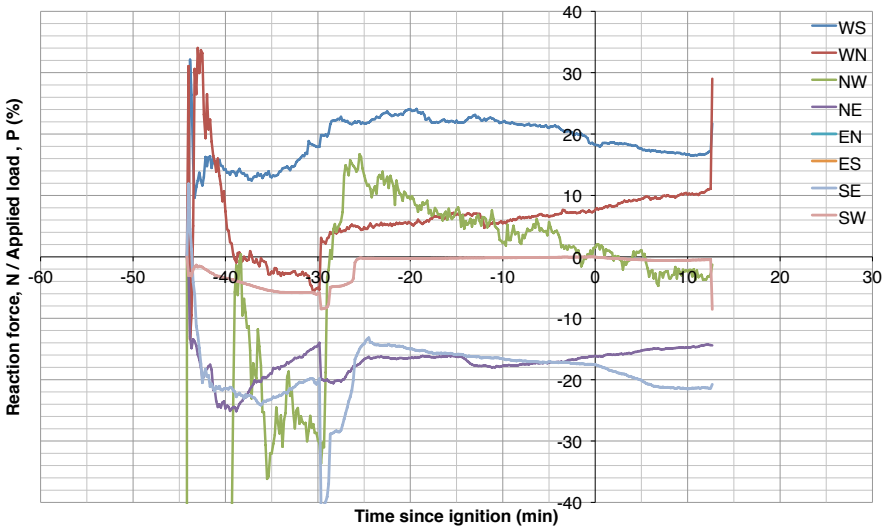

Figure K.12: Percentage ratio between net axial force and applied load for all columns in the heated 100 mm thick, 1.5% reinforced: unrestrained test

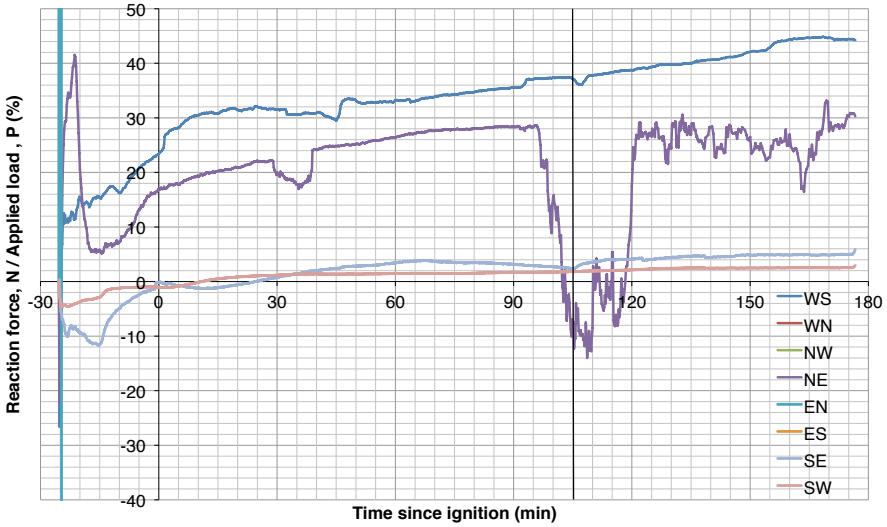

Figure K.13: Percentage ratio between net axial force and applied load for all columns in the heated 100 mm thick, 1.5% reinforced: restrained test

K.6 100 MM THICK, 0% REINFORCED

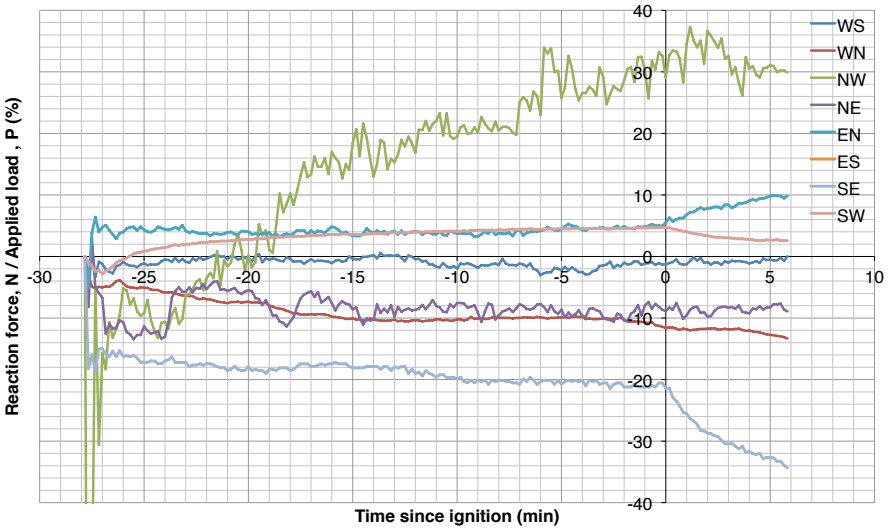

Figure K.14: Percentage ratio between net axial force and applied load for all columns in the heated 100 mm thick, 0% reinforced: unrestrained test

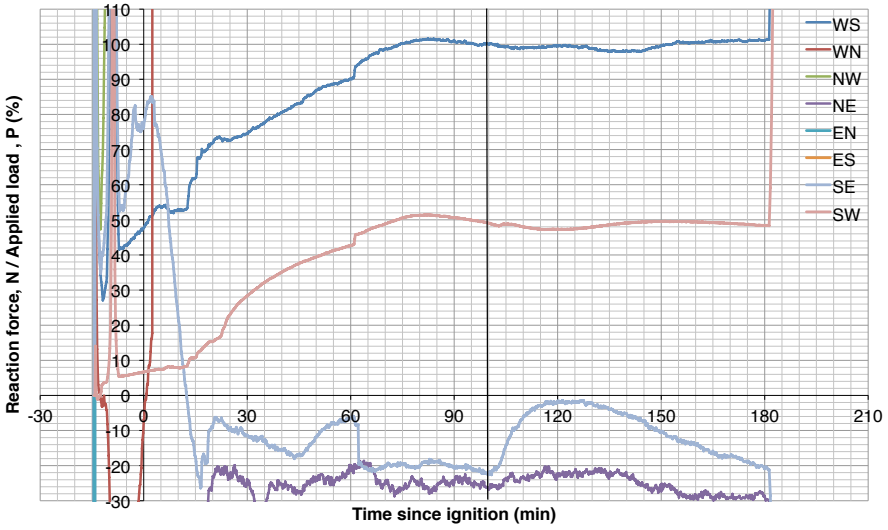

Figure K.15: Percentage ratio between net axial force and applied load for all columns in the heated 100 mm thick, 0% reinforced: restrained test